M E T E O R - B E R I C H T E

00-3

Östliches Mittelmeer - Nördliches Rotes Meer 1999

Cruise No. 44
22 January - 16 May 1999

Edited by:

Jürgen Pätzold, Peter E. Halbach, Gotthilf Hempel, Horst Weikert

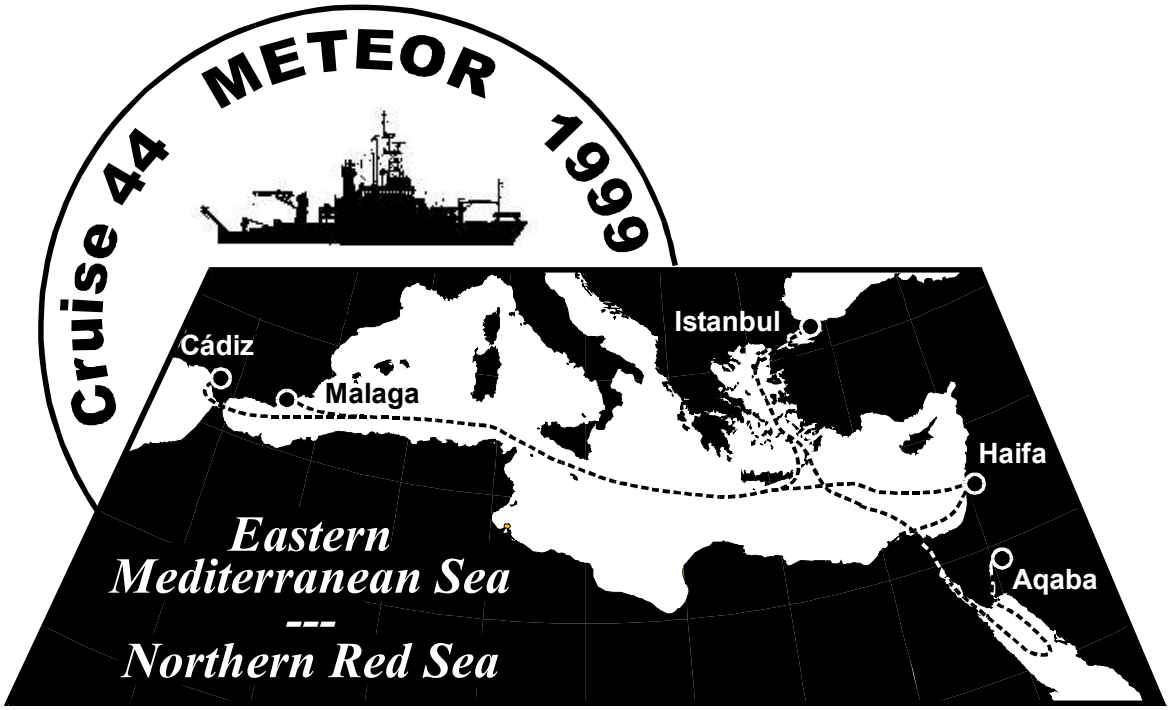

Editorial Assistance:

Frank Schmieder
Fachbereich Geowissenschaften, Universität Bremen

Leitstelle METEOR
Institut für Meereskunde der Universität Hamburg

2000

The **METEOR-Berichte** are published in an irregular sequence. They are working papers for people who are occupied with this specific expedition and are intended as reports for the funding institutions. The opinions expressed within the **METEOR-Berichte** are only those of the authors. They are obtainable at:

Leitstelle METEOR
Institut für Meereskunde
Troplowitzstr. 7
22529 Hamburg
Germany

The METEOR expeditions are funded by the Deutsche Forschungsgemeinschaft and the Bundesministerium für Bildung und Forschung.

Addresses of the editors:

Dr. Jürgen Pätzold
Universität Bremen
FB 5 - Geowissenschaften
Postfach 330440
28334 Bremen

Prof. Dr. Peter E. Halbach
Fachrichtung Rohstoff- und Umweltgeologie
Freie Universität Berlin
Malteserstr. 74-100 (Haus B)
12249 Berlin

Prof. Dr. Gotthilf Hempel
ZMT - Zentrum für Marine Tropenökologie
Fahrenheitstr. 1
28359 Bremen

Dr. Horst Weikert
Institut für Hydrobiologie und Fischereiwissenschaft
Universität Hamburg
Zeiseweg 9
22765 Hamburg

Quotation:

Pätzold, J., P.E. Halbach, G. Hempel and H. Weikert (2000): Östliches Mittelmeer - Nördliches Rotes Meer 1999, Cruise No. 44, 22 January - 16 May 1999. METEOR-Berichte, Universität Hamburg, 00-3, 240 pp.

ISSN 0936-8957

M E T E O R - B E R I C H T E

00-3

Östliches Mittelmeer - Nördliches Rotes Meer 1999

Cruise No. 44
22 January - 16 May 1999

Edited by:

Jürgen Pätzold, Peter E. Halbach, Gotthilf Hempel, Horst Weikert

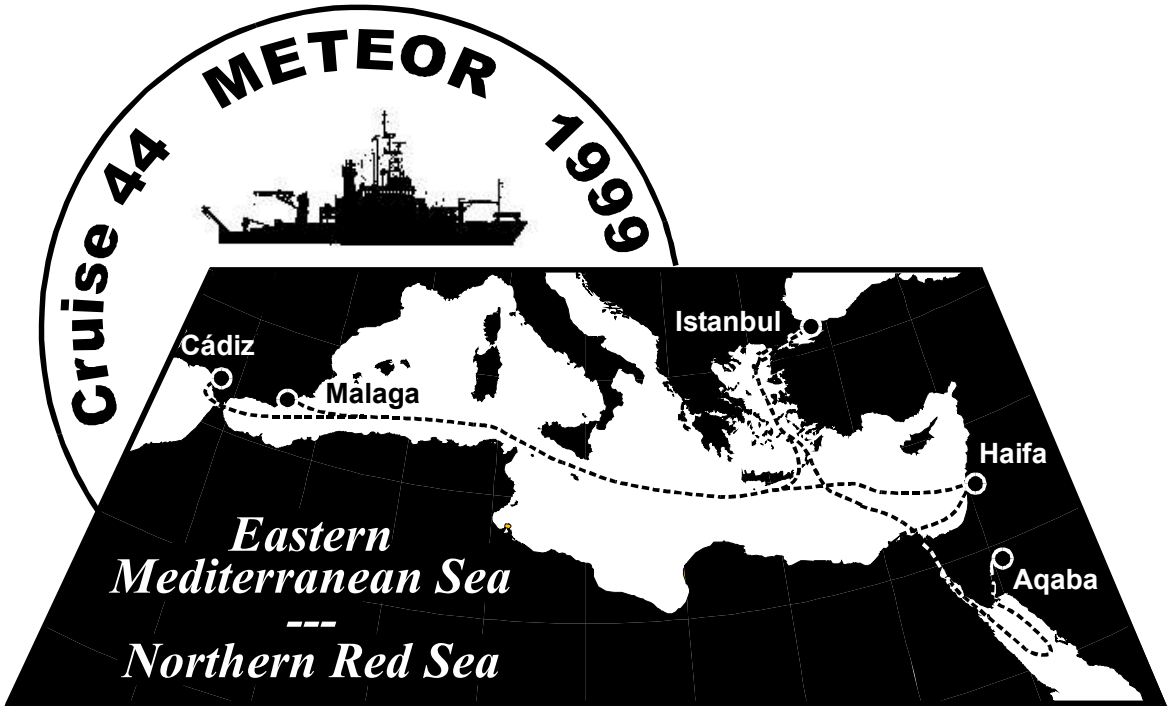

Editorial Assistance:

Frank Schmieder
Fachbereich Geowissenschaften, Universität Bremen

Leitstelle METEOR
Institut für Meereskunde der Universität Hamburg

2000

Table of Contents

Abstract

From January 22, to May 16, 1999 the German research vessel Meteor performed cruise M 44, which was divided into four different legs. Two of them were carried out in the eastern Mediterranean and two in the northern Red Sea. The cruise started in Cádiz (Spain) and continued with stops in Istanbul (Turkey), Aqaba (Jordan), Safaga (Egypt), Port of Dubá (Saudi Arabia), and Haifa (Israel) to its final destination Malaga (Spain). This expedition was conducted by scientists from different German institutions including a large number of guest scientists from the countries visited. The research projects in the Mediterranean focussed on geoscientific studies in the Marmara Sea and on oceanographic and biological studies in the eastern Mediterranean. The two legs in the northern Red Sea were closely linked and dealt with biological and oceanographic studies on one hand and geophysical, geological, and geochemical surveys on the other hand. This report summarizes the main goals of the different working groups, a complete list of all stations and gears employed on each leg and the preliminary results as obtained during the cruise. The cruise was funded by the Deutsche Forschungsgemeinschaft (German Science Foundation).

Zusammenfassung

Vom 22. Januar bis zum 16. Mai 1999 fand die Reise M 44 des Forschungsschiffes Meteor mit insgesamt vier Fahrtabschnitten statt. Zwei Fahrtabschnitte wurden im östlichen Mittelmeer und zwei im nördlichen Roten Meer durchgeführt. Die Expedition begann in Cádiz (Spanien) und setzte mit Stopps in Istanbul (Türkei), Aqaba (Jordanien), Safaga (Ägypten), Port of Dubá (Saudi Arabien), Haifa (Israel) bis zum Zielhafen Malaga (Spanien) fort. Die Reise wurde von Wissenschaftlern aus verschiedenen deutschen Instituten unter der Beteiligung einer Reihe von ausländischen Gastwissenschaftlern der besuchten Länder durchgeführt. Die Arbeiten im Mittelmeer konzentrierten sich auf geowissenschaftliche Untersuchungen im Marmara Meer und aktuelle ozeanographische und biologische Prozesse im östlichen Mittelmeer. Die beiden Fahrtabschnitte im nördlichen Roten Meer waren eng verknüpft und hatten zum einem biologische und ozeanographische zum anderen geowissenschaftliche Fragestellungen zum Ziel. Dieser Bericht fasst die wichtigsten Arbeitsziele und die ersten, an Bord erzielten Ergebnisse der einzelnen Arbeitsgruppen zusammen. Er enthält weiterhin eine vollständige Übersicht über die bearbeiteten Stationen und die dabei eingesetzten Geräte. Die Expedition wurde durch die Deutsche Forschungsgemeinschaft gefördert.

1 Research Objectives

The first leg of METEOR cruise M44 mainly concentrated on geoscientific studies in the Marmara Sea. The Marmara Sea is located in the west of the 1.500 km striking North Anatolian Fault Zone (NAF). It can be described as an epicontinental marginal sea between the Black Sea and the Aegean Sea. It is separated into three small, but deep pull-apart basins and two push-up structures which are generated by shear stress or transpression. On the basis of the tectonic situation cool fluid and gas (mainly methane) emanations were expected particularly in the deep regions of the Marmara Sea because of the availability of fault zones as conductors for fluid migration. One scientific objective of the research project was to sample the fluids and gases both within the porewater and the benthic water layer in order to investigate their interrelations with the solid substance of the sediments.

Due to the position of the Sea of Marmara between the Black Sea and the Aegean Sea its palaeoceanographic evolution is clearly controlled by both marine realms. The quarternary development is characterized by several changes between marine and limnic or brackish habitats. Furthermore, intervals of stagnation with anoxic and sapropelitic environments were probable. For that reason a further scientific objective was to examine the quarternary palaeoceanographic evolution of this marginal sea by studying the geochemical and micropalaeontological characteristics of sediments from long piston cores. On the way towards the Sea of Marmara some sediment sampling and bathymetric profiling was carried out in the Urania Basin in the Ionian Sea and a sediment trap system consisting of two sediment traps and a releasing system was deployed in the Ierapetra Deep.

The research objectives of the second leg of cruise 44 center on the investigation of production processes at the beginning of the spring stratification and their physical and biological control mechanisms.

The Gulf of Aqaba and the adjacent waters of the Red Sea were considered as an ideal place for a kind of time station for the following topics to be studied in detail and with adequate attention to the temporal and spatial variability in the observation area and the water column over the period of 15 days:

- Analysis of the intensity, depth and regional distribution of winter mixing in the Gulf of Aqaba and circulation of water masses as well as the study of physical and biological exchanges between the Gulf and the Red Sea
- Description of the distribution, adaptations and photosynthetic performance of the phytoplankton during the early stage of succession
- Experimental determination of the grazing control of phyto- and bacterioplankton development by nano-, micro- and mesoplankton
- Analysis of the importance of the microbial loop under extreme oligotrophic conditions
- Description of the distribution, adaptations and production of the zooplankton.

The third leg of METEOR Cruise M 44 started on March 12, 1999 in Aqaba, Jordan. The scientific program included geoscientific studies in the Gulf of Aqaba, the northern Red Sea, and in the eastern Mediterranean. The goal of the paleoceangraphic studies in the Gulf of Aqaba were to reconstruct the climate history, the circulation, and water mass exchange during the late Quaternary. The impact of sea level changes, variations in productivity, changes in the carbonate budget and terrigeneous input were considered. The geophysical programme aimed to carry out continuous seismic and hydroacoustic profiling of the sea floor. Evaluation and interpretation will give detailed descriptions of the development of the tectonic and sedimentological history within the Gulf of Aqaba. The Shaban Deep in the central northern Red Sea was sampled for geochemical investigations to determine the geochemical budget of the brines in the northern Red Sea. High resolution sampling from the water column/brine interface to the sediment were carried out. The

geochemical project intended to measure the hydrocarbon concentrations and their isotopic composition in order to determine the processes ruling the formation and oxidation of hydrocarbons in the Red Sea. Elemental exchange rates between the brines and the water column will be analysed and the elemental and isotopic compositions will be used to assign the origin of the geochemical budget. Also, collection of sediment cores for paleoclimatic and paleoceanographic studies was carried out in the northern Red Sea, as well as in the eastern Mediterranean. These studies are directed towards the reconstruction of deep water formation and productivity and their changes through time in both distinct marine environments. An extensive collection of sediment cores will be completed by this expedition to construct a geoscientific section from the Indian Ocean continuing through the entire Red Sea to its utmost northern end and linking the eastern Mediterranean. A comprehensive data set will be summarized to reconstruct the environmental changes during the late Quaternary and to determine climatic teleconections between the oceans.

The fourth cruise leg M 44/4 starting in Haifa, Israel, on April 10 and ending in Malaga, Spain, on May 16 was substantial part of a joint ship programme in the Levantine and Ionian Seas. The topic of the combined hydrographical and biological research was the transient change of the Eastern Mediterranean ecosystem which is strongly influenced by the long term variability in the atmosphere. The study is based on a substantial data set which is available from previous cruises (see METEOR cruises 5, 25, 31, 40). The hydrographical project focussed on the Aegean deep water outflow into the Levantine and Ionian Seas which likely started in 1990, with the aim to understand the evolution of the thermohaline circulation and water mass structure during the intervening time.

One subproject of the ecological study aimed to qualitatively and quantitatively estimate the composition and standing crops of pelagic organismens (microbes, metazoans), based on the concomitant hydrographical study. The question is posed whether the documented change in the zooplankton of the Levantine deep-sea is caused by the change of the hydroclimate. The second subproject's aim was for the first time to estimate the vertical carbon flux into the western Levantine deep-sea. The assessment of the particle distribution and fluxes by means of particle traps was combined with the determination of production and metabolic rates of the microbial biota and zooplankton.

Table 1: Legs and chief scientists of METEOR cruise no. 44

Leg M44/1 22 January 1999 - 13 February 1999 Cádiz (Spain) – Istanbul (Turkey) Chief Scientist: Prof. Dr. P. E. Halbach	**Leg M 44/2** 16 February 1999 - 9 March 1999 Istanbul (Turkey) – Aqaba (Jordan) Chief Scientist: Prof. Dr. G. Hempel
Leg M44/3 12 March 1999 - 7 April 1999 Aqaba (Jordan) – Haifa (Israel) Chief Scientist: Dr. J. Pätzold	**Leg M44/4** 10 April 1999 - 16 May 1999 Haifa (Israel) – Malaga (Spain) Chief Scientist: Dr. H. Weikert

2 Participants

Table 2: Participants of METEOR cruise no. 44

Leg M44/1

Name	Discipline	Institution	Leg*
Halbach, Peter, Prof. Dr. (Chief Scientist)	Geology	FUB	B
Algan, Oya, Dr.	Sediment Geochemistry	IMSMUI	B
Arndt, Christine	Hydrogeochemistry	FUB	B
Behr, Hein Dieter, Dr.	Meteorology	DWD	AB
Bindseil, Tatjana	Sediment Sampling	GPITü	B
Büsing, Jörg	HBS electronics	FUB	B
Cagatay, Namik, Dr.	Sediment Geochemistry	IMSMUI	B
Cremer, Arno	Biogeochemistry	IBMC	A
Gochmen, Cemal	Structural Geology	MTA	B
Grossmann, Rico	Sediment Sampling, HBS	FUB	AB
Halbach, Margret, Dr.	Geology, Bathymetry	FUB	B
Hübner, Andreas	Hydrogeochemistry	FUB	B
Hübner, Hagen	Sediment Sampling	GPITü	B
Inthorn, Maik	Sediment Geochemistry	FUB	B
Jennerjahn, Tim, Dr.	Biogeochemistry	IBMC	A
Karagoz, Sahin	Structural Geology	MTA	B
Knappe, Andrea	Hydrogeochemistry	FUB	B
Koschinsky-Fritsche, Andrea, Dr.	Hydrogeochemistry	FUB	B
Kuhn, Thomas, Dr.	Sediment Geochemistry Organization	FUB	AB
Kuscu, Ismail	Structural Geology	MTA	B
Moche, Ralf	Hydrogeochemistry	FUB	B
Mühlstrasser, Thomas	Micropaleontology	GPITü	B
Ochsenhirt, Wolf-Tilo	Meteorology	DWD	AB
Pekdeger, Asaf, Prof. Dr.	Hydrogeochemistry	FUB	B
Richter, Steffen	Sediment Geochemistry	FUB	B
Schmaljohann, Rolf, Dr.	Microbiology	IfM	B
Schmale, Oliver	Hydrogeochemistry	IBMC	B
Schmiedl, Gerhard, Dr.	Micropaleontology	GPITü	B
Seifert, Richard, Dr.	Hydrobiochemistry	IBMC	AB
Winkler, Andreas, Dr.	Hydrogeochemistry	FUB	B

*Participation: AB 23.01. – 13.02.1999
A 23.01. – 31.01.1999
B 31.01. – 13.02.1999

Table 2: continued

Leg M44/2

Name	Discipline	Institution	Leg*
Al-Qutob, Mutaz	Primary Productivity	PCG/Bar Ilan Uni	AB
Al-Tabarin, K.	Chemistry	MSS	B
Badewien, Thomas	Phys. Oceanography	IOW	AB
Badran, Mohammed	Phys./Chem. Oceanography	MSS	AB
Beese, Bärbel	Prim. Productivity/Phytoplankton	UniKo	AB
Berger, Andreas	Ass. Camera	NDR	B
Berninger, Ulrike-Gabriele	Protozooplankton	IfM	AB
Burmeister, Karl-Heinz	Camera man	NDR	B
Dowidar, Magdi	Mesozooplankton	NIOF	AB
Dray, Murielle	Prim. Product./Phytoplankton	IUI	A
Elbrächter, Martina	Phys. Oceanography	IOW	AB
El-Deek, Moh. Sedik	Trace Metals	NIOF	AB
Grossart, Hans-Peter	Bacterioplankton	ICMB	AB
Häse, Clivia	Prim. Product./Phytoplankton	ZMT	AB
Hagen, Wilhelm	Mesozooplankton	UniBr, FB 2	AB
Hansen, Thomas	Grazing	IfM	AB
Hassan, Yaser Sadek	Chemistry	EEAA	AB
Hempel, Gotthilf	Chief Scientist	ZMT	AB
Kirndörfer, Georg	Filmproducer	NDR	B
Kroon, Bernd	Phytoplankton	AWI	B
Manasreh, Riyad	Phys. Oceanography	MSS	A
Melegy, Mandouh	Observer	Navy, Egypt	AB
Omar, O.M.	Observer	Navy, Egypt	AB
Plähn, Olaf	Phys. Oceanography	IOW	AB
Post, Anton	Prim. Productivity/Phytoplankton	IUI	A
Richter, Claudio	Mesozooplankton	ZMT	A
Sangok, Yaser Kamel	Trace Metals	NIOF	AB
Schiel, Sigrid	Mesozooplankton	AWI	AB
Selje, Natascha	Bacterioplankton	ICBM	AB
Simon, Meinhard	Bacterioplankton	ICBM	A
Sommer, Ulrich	Grazing	IfM	AB
Stambler, Noga	Prim. Product./Phytoplankton	IUI	AB
Stibor, Herwig	Grazing	LMU, München	AB
Walter, Maren	Phys. Oceanography	IOW	AB

*Participation: AB 16.02. - 09.03.1999
A 16.02. – 01.03.1999
B 01.03. – 09.03.1999

Table 2: continued

Leg M44/3

Name	Discipline	Institution	Leg*
Abd El-Wahab Farha, Osama	Marine Geophysics	NIOF	B
Abu-Ouf, Mohammed	Micropaleontology	KAU/DMG	C
Al Hazmi, Yahia Mohd. M.	Observer	MDA/MSD	D
Al-Rousan, Saber A.	Marine Geology	MSS	B
Arz, Helge W.	Marine Geology	GeoB	A
Bagabas, Khalid A. A.	Geology	KAU/FES	C
Bassek, Dieter	Meteorolgy	DWD	A
Blaschek, Heike	Marine Geochemistry	IfGK	D
Böke, Wolfgang	Marine Geophysics	GeoB	B
Donner, Barbara	Micropaleontology	GeoB	A
Eder, Wolfgang	Microbiology	UniRe	D
Felis, Thomas	Marine Geology	GeoB	A
Gayed, Hany Yehia K.	Marine Sciences	EEAA	B
Gutowski, Martin	Marine Geophysics	GeoB	A
Hemleben, Christoph	Marine Geology	GPITü	E
Hübner, Hagen	Marine Geology	GPIGö	E
Hübscher, Christian	Marine Geophysics	IfG/ZMK	A
Kadi, Khalid A.	Geology	MPMR	C
Kästner, Rudolf	Marine Geophysics	Martini	B
Klauke, Sonja	Marine Geochemistry	IfGK	D
Körner, Sven Olaf	Meteorology	DWD	A
Kuhlmann, Holger	Marine Geology	GeoB	A
Lützeler, Thurid	Marine Geology	GeoB	A
Meier, Sebastian	Micropaleontology	GeoB	A
Melegy, M.M.		Egypt. Obs.	B
Moammar, Mustafa O.	Marine Sciences	KAU/MCD	D
Mohamuda, Amr Zakarie	Marine Sciences	NIOF	B
Mokhtar, Talal A.	Geophysics	KAU/FES	C
Moos, Christopher .	Marine Geology	GeoB	B
Omar, O.M., Lieu		Egypt. Obs.	B
Pätzold, Jürgen (Chief Scientist)	Marine Geology	GeoB	A
Rasheed, Mohammed	Marine Geochemistry	MSS	B
Rosiak, Uwe	Marine Geology	GeoB	A
Salem, Mohammed	Marine Geophysics	GeoB	B
Schmidt, Mark	Marine Geochemistry	IfGK	D
Schmitt, Manfred	Marine Geochemistry	GCA	D
Shata, Aly Mohammed	Marine Geology	NIOF	B
Stoffers, Peter	Marine Geochemistry	IfGK	D
Themann, Sören	Marine Geology	GPITü	E
Weldeab, Syee	Marine Geology	GPITü	E

*Participation:
A Aqaba - Haifa, 12.03. - 07.04. 1999
B Aqaba - Safaga, 12.03. - 25.03.1999
C Safaga - Dubá, 26.03. - 01.04.1999
D Safaga - Suez, 26.03. - 04.04.1999
E Safaga - Haifa, 26.03. - 07.04.1999

Table 2: continued

Leg M44/4

Name	Discipline	Institution
Weikert, Horst, Dr. (Chief Scientist)	Planktology	IHF
Abel, Mirko, Student	Planktology	IHF
Bassek, Dieter, Technician	Meteorology	DWD
Blümel, Martina, Student	Microbiology	IfMK
Blume, Bodo, Student	Planktology	IHF
Bulsiewicz, Klaus, Technician	Tracer Chemsitry	TCUB
Deponte, Davide, Elec. Technician	Physical Oceanography	OGST
Fabian, Heiner, Student	Planktology	IHF
Gollembiewski, Renate, Technician	Physical Oceanography	IHF
Grabbert, Sabine, Student	Planktology	IHF
Hoffmann, Detlef Uwe, Technician	Microbiology	IfMK
Kämper, Stephan, Dipl. Phys.	Tracer Chemistry	TCUB
Karsten, Gudrun, Dr.	Microbiology	IfMK
Klein, Birgit, Dr.	Tracer Chemistry	TCUB
Koppelmann, Rolf, Dr.	Planktology	IHF
Kress, Nurit, Dr.	Chemical Oceanography	IOLR
Krischker, Petra, Technician	Microbiology	IfMK
Lappe, Frank, Technician	Microbiology	IfMK
Manca, Beniamino, Dr.	Physical Oceanography	OGST
Miske, Volker Christian, Dipl. Biol.	Zoology	ZUR
Montella, Elena, Student	Planktology	STAZN
Neugebohrn, Liesel, Technician	Planktology	IHF
Neumann, Kirsten, Student	Biogeochemistry	IBMC
Plep, Wilfried, Technician	Tracer Chemistry	TCUB
Schroll, Gunnar, Student	Biogeochemistry	IBMC
Strüfing, Meinhard, Dipl.-Met.	Meteorology	DWD
Süling, Jörg, Dr.	Microbiology	IfMK
Walter, Sylvia, Student	Microbiology	IHF
Zimmermann-Timm, Heike, Dr.	Planktology	IHF
Zervoudaki, Soultana, M.Sc.	Planktology	NCMR

Table 3: Participating Institutions

AWI	Alfred-Wegener-Institute for Polar and Marine Research Columbusstraße, D 27515 Bremerhaven, Germany
Bar Ilan Uni	Bar Ilan University, Ramat Gan, Israel
DWD	Deutscher Wetterdienst, Geschäftsfeld Seeschiffahrt Bordwetterwarte FS Meteor, Bernhard Nocht-Straße 76 D 20359 Hamburg, Germany
EEAA	Egyptian Environmental Affairs Agency, National Parks of Egypt Protectorates Development Programmes, Area Management Unit, P.O. Box 19 46619 Sharm El Sheikh, Egypt
FUB	Fachbereich Geowissenschaften, Freie Universität Berlin Malteser Str. 74-100, Haus A, D 12249 Berlin, Germany
GCA	Geochemische Analysen, Glückaufstr. 50, D 31319 Sehnde-Ilten, Germany
GeoB	Fachbereich 5 – Geowissenschaften, Universität Bremen Klagenfurter Strasse, D 28359 Bremen, Germany
GPIGö	Institut und Museum für Geologie und Paläontologie Georg-August-Universität Göttingen Goldschmidtstr.3, D 37077 Göttingen, Germany
GPITü	Institut und Museum für Geologie und Paläontologie, Universität Tübingen Sigwartstraße 10, D 72076 Tübingen, Germany
IBMC	Institut für Biogeochemie und Meereschemie, Universität Hamburg Grabenstr. 27, D 20359 Hamburg, Germany
ICBM	Institut für Chemie und Biologie des Meeres Carl von Ossietzky Universität Oldenburg Carl-von-Ossietzky-Straße 9-11, D 26111 Oldenburg, Germany
IfGK	Institut für Geowissenschaften, Universität Kiel Olshausenstr. 40, D 24118 Kiel, Germany
IfG/ZMK	Institut für Geophysik, Zentrum für Meeres- und Klimaforschung Universität Hamburg, Bundesstraße 55, D 20146 Hamburg, Germany
IfM	Institut für Meereskunde, Christian-Albrechts-Universität Kiel Düsternbrooker Weg 20, D 24105 Kiel, Germany
IHF	Institut für Hydrobiologie und Fischereiwissenschaft, Hydrobiologische Abt. Universität Hamburg, Zeiseweg 9, D 22765 Hamburg, Germany

Table 3: continued

IMSMUI	University of Istanbul, Institute of Marine Science Management Müsküle Sok. 1, 34470 Istanbul, Turkey
IOLR	Israel Oceanographic & Limnological Research Ltd. P.O.Box 8030, 31080 Haifa, Israel
IOW	Institut für Ostseeforschung Warnemünde, Universität Rostock Seestraße 15, D 18112 Rostock, Germany
IUI	Interuniversity Institute Eilat, P.O. Box 469, Eilat 88103, Israel
KAU/DMG	Ministry of Higher Education, King Abdulaziz University Faculty of Marine Sciences, Department of Marine Geology P.O. Box 1540, Jeddah 21441, Kingdom of Saudi Arabia
KAU/FES	Ministry of Higher Education, King Abdulaziz University Faculty of Earth Sciences P.O. Box 1744, Jeddah 21441, Kingdom of Saudi Arabia
KAU/MCD	Ministry of Higher Education, King Abdulaziz University Faculty of Marine Sciences, Marine Chemistry Department P.O. Box 15389, Jeddah 21444, Kingdom of Saudi Arabia
LMU	Ludwig-Maximilian Universität, Karlstraße 25 D 80333 München, Germany
Martini	Reederei Martini GmbH, Niederlassung Bremerhaven Barkhausenstraße 37, D 27568 Bremerhaven, Germany
MDA/MSD	Ministry of Defence and Aviation, General Staff Headquarters Military Survey Department P.O. Box 8652, Riyadh 11492, Kingdom of Saudi Arabia
MPMR	Ministry of Petroleum and Mineral Resources Deputy Ministry for Mineral Resources P.O. Box 345, Jeddah 21191, Kingdom of Saudi Arabia
MSS	Marine Science Station, P.O. Box 195, Aqaba, Jordan
MTA	General Directorate of Mineral Research and Exploration 06520 Ankara, Turkey
NCMR	National Centre for Marine Research, Athens, Greece
NDR	Norddeutscher Rundfunk Betriebsstätte Lokstedt (Fernsehen) Gazellenkamp 57, D 22504 Hamburg, Germany

Table 3: continued

NIOF	National Institute of Oceanography and Fisheries Ministry of Scientific Research 101 Kasr El-Einy St., Cairo, Egypt
OGST	Osservatorio Geofisico Sperimentale TriesteBorgo Grotta Gigante 42/C, 34016 Trieste, Italy
PCG	Palestine Consultancy Group, P.O. Box 19322, Jerusalem, Israel
STAZN	Laboratorio di Oceanografia Biologica, Stazione Zoologica A. Dohrn 80121 Napoli / Italy
TCUB	Tracer Chemie, Institut für Umweltphysik, Universität Bremen D 28359 Bremen, Germany
UniBr	Fachbereich 2 – Marine Zoologie, Universität Bremen D 28359 Bremen, Germany
UniKo	Fakultät Biologie, Universität Konstanz J. Burckhardt Straße 25, D 78457 Konstanz, Germany
UniRe	Lehrstuhl für Mikrobiologie, Universität Regensburg Universitätsstr.31, D 93053 Regensburg, Germany
ZMT	Zentrum für Marine Tropenökologie Fahrenheitstraße 1, D 28359 Bremen, Germany
ZUR	Zoologie, Universität Rostock Universitätsplatz 5, D 18051 Rostock, Germany

3 Research Programme

3.1 Research Programme of Leg M44/1

With respect to the recent knowledge about the target area in the Marmara Sea (Fig. 1b) our research work has focussed on the following main points:

a) Bathymetric mapping incl. PARASOUND to investigate the local tectonics and morphologic conditions;
b) study of the seafloor micromorphology and finding of gas emanating sites;
c) sampling and geochemical analysis of the tectonically influenced solid and fluid budgets of the recently to subrecently formed deep regions of the Sea of Marmara; a special aspect is the study of the porewater and near-bottom water geochemistry;
d) investigation of the quarternary evolution under aspects of palaeoceanography and regional geology with the help of long sediment cores.

In order to realize these scientific objectives the following single working steps were necessary:

- Bathymetric and sediment thickness mapping of the working areas using HYDROSWEEP and PARASOUND.
- Video mapping of selected tectonically active areas in the basins and elevated zones; identification of sites of fluid and gas emanation.
- Fluid sampling (incl. short sediment cores) within the first meter above seafloor at sites of fluid emanation.
- Physical and chemical measuring of parameters of the water column (temperature, Eh, pH, salinity etc.) and geochemical analysis (heavy metals, anions, dissolved gases) of the fluid samples in the onboard laboratory; particularly the redox-sensitive elements have been measured immediately after sampling.
- Identification of microbiologically active sites which are probably associated with fluid emanations.
- Sediment sampling with piston corer (max. length 15 m) in the different basins as well as on the respective push-up structures.
- Preliminary study of the mineralogical and geochemical composition of the solid phases as well as of micropalaeontologically important fossils.
- Description of samples, data storage and documentation of the ship-born observations and results.

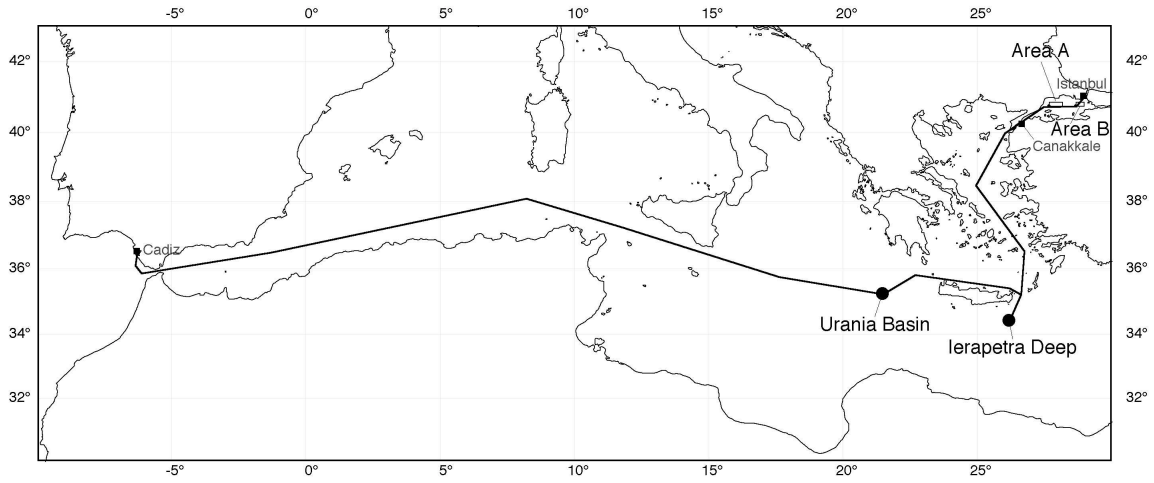

Fig. 1a: Cruise track in the Mediterranean during RV METEOR Cruise M44/1.

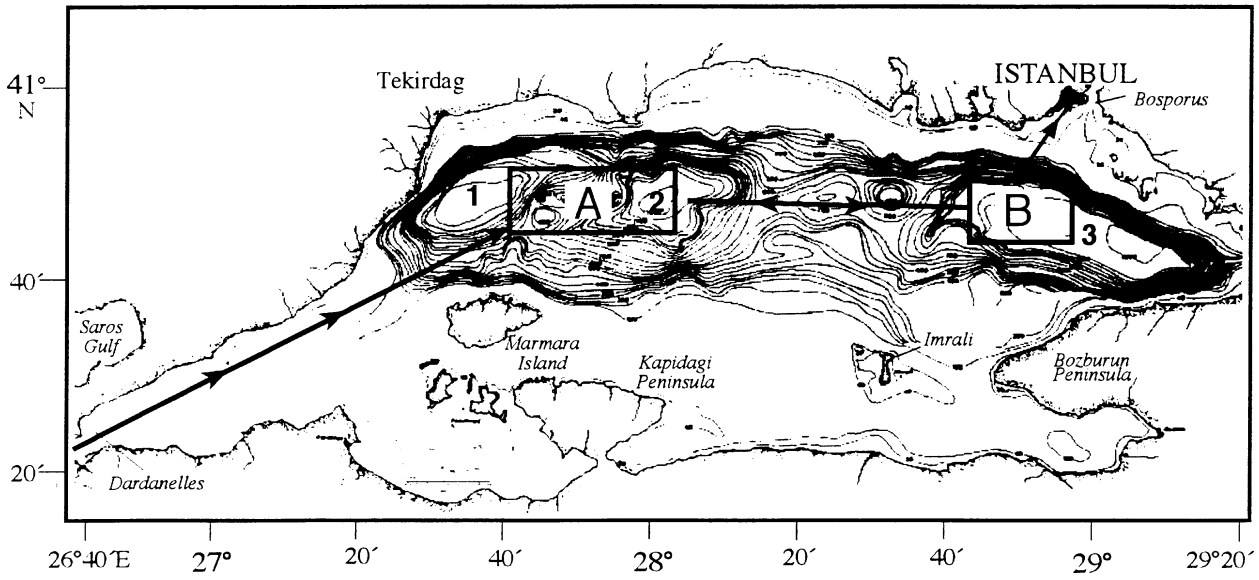

Fig. 1b: Bathymetry of the Sea of Marmara with the three deep basins (1: Tekirdag Basin, 2: Central Marmara Basin, 3: Çýnarcýk Basin), the working areas A and B, and the ship's track during the M 44/1 cruise.

On the way towards the Sea of Marmara some sediment sampling and bathymetric profiling was carried out in the Urania Basin in the Ionian Sea (Fig. 1a). A sediment trap system consisting of two sediment traps and a releasing system was deployed in the Ierapetra Deep to collect settling particles from 700 m and 2700 m water depth in scheduled time intervals by T. Jennerjahn and A. Cremer from the University of Hamburg.

3.2 Research Programme of Leg M44/2

The first of the two legs into the Gulf of Aqaba focuses on the biological and physical processes in the water column during the transition from the winter to spring. The Gulf of Aqaba is rather unique in its weak vertical stratification compared to other subtropical waters. The immediate vicinity of more „normal" water bodies in the adjacent Red Sea make the study of the Gulf of Aqaba very attractive. The northernmost part of the Gulf has been studied already for some time particularly under the Red Sea Program, while a comprehensive and integrated study of the physical and biological oceanography with modern methods was highly wanted. The time window between late February and mid-March seemed particularly promising for the understanding of regional and general questions related to the biological adaptations on the molecular, cellular, organism and community level.

The area of observation of the cruise leg 44/2 consisted of the western half and the northern corner of the Gulf of Aqaba and a small region of the Northern Red Sea near to the Strait of Tiran (Fig. 2). A series of six positions (Pos. I-VI) were chosen 10-15 miles apart along the axis of the Gulf of Aqaba between 28°20' N and its northern end at Eilat and Aqaba. The Red Sea part consisted of further six stations (Pos. VII-XII) mainly on a meridional and a longitudinal section.

The observation period was divided into two parts of 8 days each before and after a port call in Aqaba, where five participants were exchanged. The Gulf was sampled four times on 21-23 February, 25-27 February, 1-3 March and 5-8 March, the Red Sea was visited three times on 24-25 February, 27-28 February and 3-4 March (Fig. 3). Meteorological data as well as sea surface temperature,

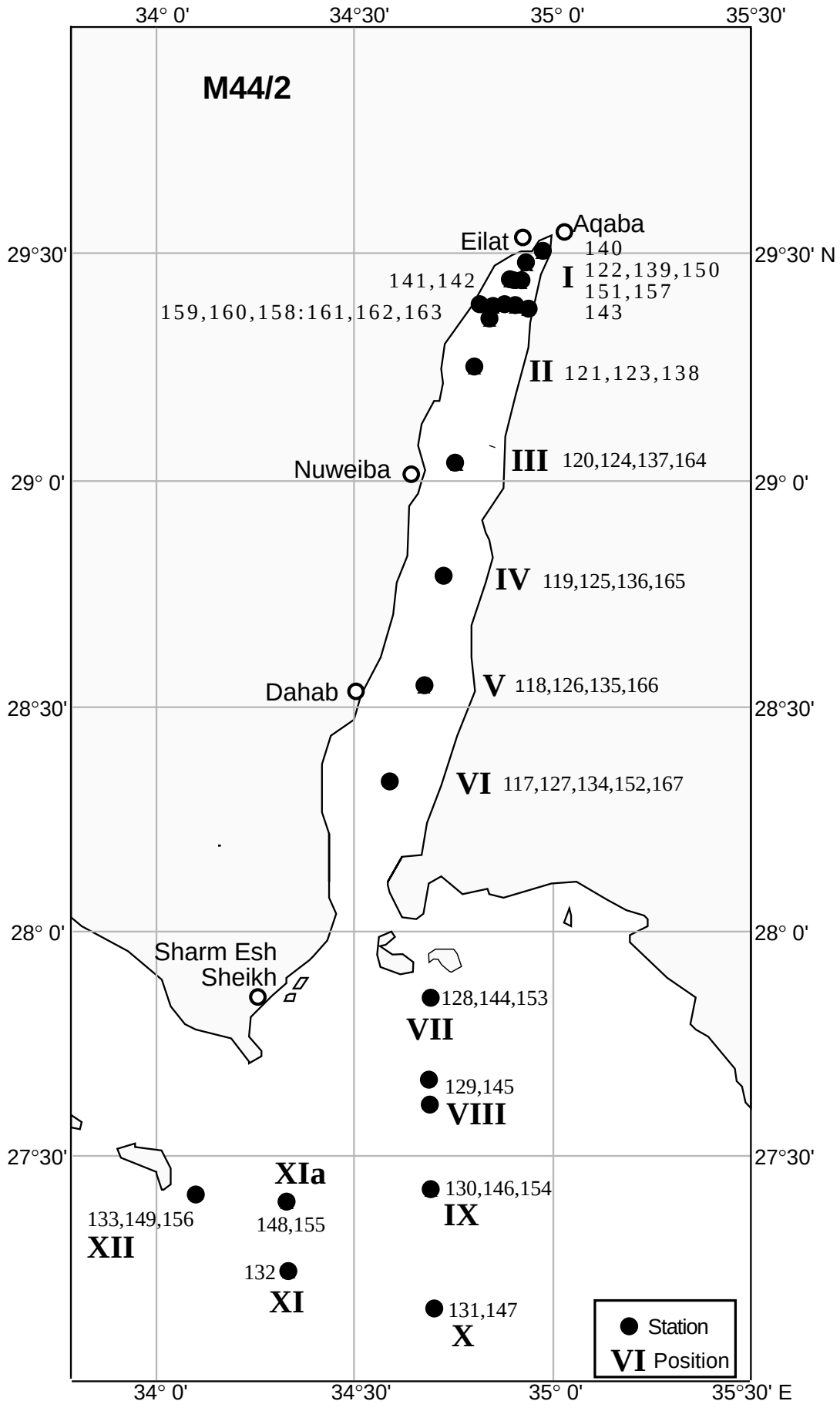

Fig. 2: Area of observation of the cruise leg 44/2.

salinity, and currents (by ADCP) were recorded en route. In some long profiles bottom topography was scanned by Hydrosweep. At the end of the cruise leg a complete bathymetric map was prepared for those areas of the Gulf of Aqaba, which were open to 'Meteor'.

The physical research program focused on a detailed analysis of the water masses in the Gulf, their vertical stratification, their short-term dynamics and their age by tracer chemistry. As direct measurements except for surface observations en route in the Straits of Tiran and their surroundings were not permitted, the exchange with the Red Sea had to be assessed indirectly. Especially the overflow of dense water from the Gulf of Aqaba into the northern Red Sea is important for the formation of the Red Sea Water (RSW).

The biomass distribution of the different size categories of phyto- and bacterioplankton and their variability in space and time were described. Experimental studies in the photosynthetic performance and in the adaptations to low nutrient levels were carried out.

What are the limiting factors controlling phytoplankton biomass, size structure, and taxonomic composition under the special conditions in the Gulf versus the Red Sea? Particular attention was given to the dominance of picoplankton (over 95% of biomass) and to the extreme scarcity of planktonic algae in the intermediate size range which are usually the main food source of crustacean zooplankton. A whole array of shipboard experiments was carried out to see the relative importance of nutrients and of different size categories of grazers as limiting factors for the development of pico- and nanoplankton. Protists' grazing on picoplankton was studied by dilution experiments. The impact of protists' grazing versus nutrient limitation on pico- and nanoplankton was studied in a factorial combination of release from nutrient stress and release from grazing pressure. Metazoan grazing and size selectivity were studied by feeding experiments with labeled phytoplankton. The dual influence of grazing and nutrient regeneration by metazoa was analyzed by double chamber experiments.

Solar radiation and light penetration are particularly high in the Gulf of Aqaba, so phenomena of light inhibition and light limitation of various types of phytoplankton can be studied here very successfully. Two different instruments for measuring the underwater light climate were employed.

The role of the bacterioplankton in the Gulf and the Red Sea was to be analyzed by measuring the biomass of bacteria, the pool size of potential substrates (DOM), as well as their uptake by bacteria both by incubation experiments.

Major emphasis was put on a detailed analysis of the horizontal and vertical distribution of zooplankton in both study areas and on its variations in the course of the day and with the development of the phytoplankton. The resolution in space and time of the plankton sampling during the cruise was much higher than in most other programs and will provide insights in the diurnal movements and the population dynamics of planktonic crustacea. The developmental stages and the nutritional status of key species like *Rhincalanus nasutus* were studied on detail. Further sampling was directed to very small copepods of the genus *Oncaea* and to material for various kinds of grazing experiments.

Only once it was possible to study the exchange of neritic resp. oceanic zooplankton between the narrow stretch of shallow waters along the coasts and the open Gulf. This was done by the cooperation between 'Meteor' and the small research boat of the Marine Science Station in Aqaba.

The biological program was closely related to the work of the Red Sea Program (RSP) in which Egyptian, German, Israeli, Jordanian and Palestinian scientists participate. All five nationalities were also represented on board.

The Israeli, Jordanian and Palestinian participants had been engaged in RSP already for a long time and used the cruise for extension of their current work while the Egyptian experts in zooplankton

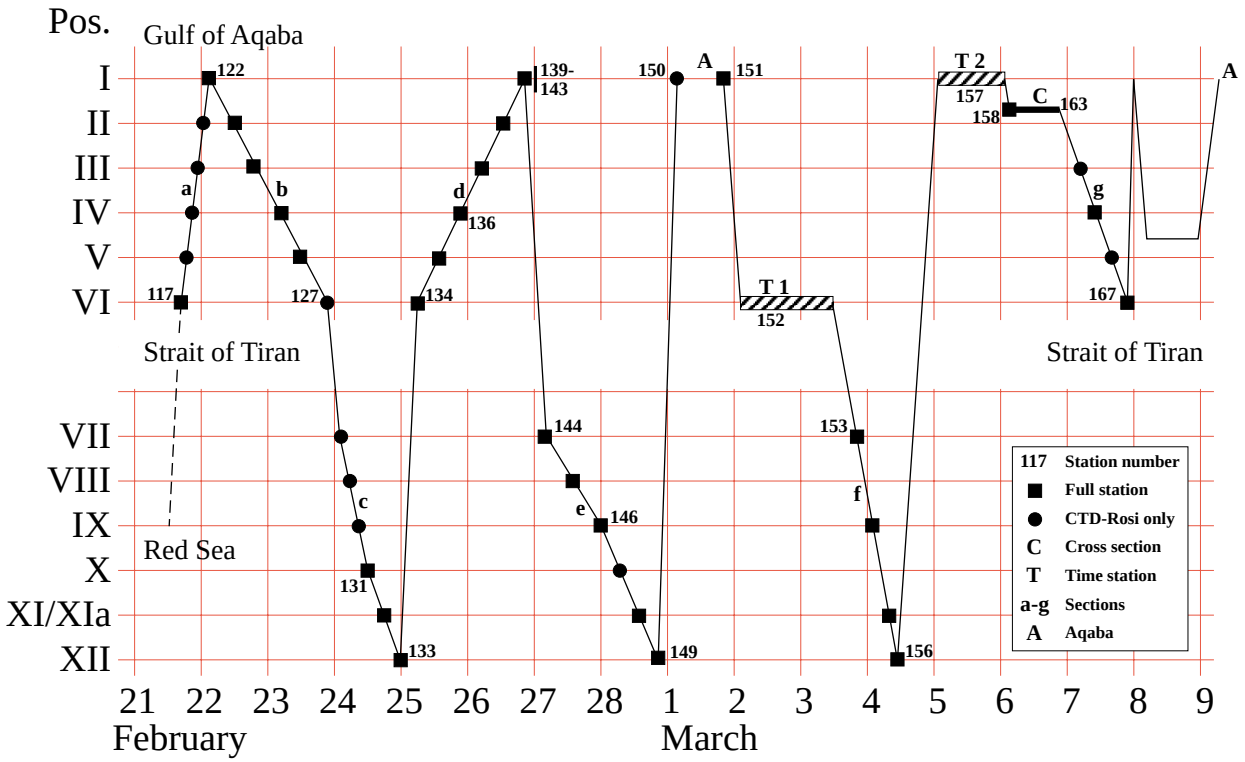

Fig. 3: Route and position of stations of the cruise leg 44/2

work and chemical oceanography were new to RSP. The exchange of ideas and the sharing of data and samples went well beyond the legal obligations for research work in foreign waters and will lead to closer cooperation within the region and between the scientists of the region and their German colleagues.

The following notes by the Head of the Jordanian team, Dr. M. Badran, describes parts of the integration of scientists of the region into the cruise program:

Plans for the Marine Science Station of Jordan (MSS) to participate in the 'Meteor' cruise have been initiated during the RSP Third General Assembly in Bremen, March 1998. The plans included participation in both the oceanography and the geology legs. For this purpose Dr. M. Badran headed a team of young scientists: Riyad Mansreh, Mohammed Rasheed and Saber Al-Rousan, who are working for Ph.D. degrees in the RSP. The team included also the lab technician Khalid Al Tabarin.

R. Manasreh has completed his MSc thesis on circulation of near shore Jordanian waters of the Gulf of Aqaba. Now he aims to develop a simulation model of water circulation in the entire Gulf of Aqaba. For testing the model, current data and CTD profiles will be generated for 15 to 18 months in the northern part of the Gulf. This cruise provided for M. Mansareh a great opportunity to participate in real oceanographic work on a large, well equipped research vessel and to collect an intensive data set regarding the water dynamics of the entire Gulf of Aqaba and the northern Red Sea during this late mixing-early transitional period of the year. These data will be analyzed by M. Mansreh at Rostock University, where he will be registered as a Ph.D. student.

The data of nutrient analyses carried out mainly by the Jordanian team (see 5.2.1.2) will be used by all scientists engaged in studies on primary production, biogeochemical cycles and the microbial loop. A particularly close cooperation developed by the combination of the east/west section of Meteor in the deep Egyptian and Jordanian waters with near shore work on a 23m boat of MSS. This project found a strong support of the team and administration of MSS and of the responsible authorities in Jordan.

Aim of these cross section studies was to compare the physical, chemical and biological characteristics of the near shore waters overlaying the coral reef with the offshore waters. A young Jordanian scientist, T. Al-Najjar who works for his Ph.D. degree at the University of Kiel and Bremen on zooplankton grazing, studied the size fraction distribution of zooplankton.

The 'Meteor' cruise provided the opportunity to initiate collaboration with the Egyptian team interested in heavy metal analysis. The samples obtained on Meteor shall be analyzed in Suez. The results may lead to a proposal for a Ph.D. thesis of an Egyptian student to work on the interaction of heavy metals – nutrient minerals in relation to primary production in the oligotrophic waters of the Gulf of Aqaba and northern Red Sea. This will lead to a closer cooperation between Egyptian and Jordanian oceanographers.

Together with Dr. Anton Post, IUI, we also looked into the possibility of having a Palestinian student to work in Eilat and Aqaba on the problem of the primary production critical depth.

Scientists of the region discussed with their German colleagues the possibility of initiating further research on the comparative oceanography of the Gulf of Suez, the Gulf of Aqaba and the northern Red Sea. The scientists pointed to the fact that most major oceanographic cruises to the Gulf of Aqaba and northern Red Sea have taken place during the winter mixing season. Therefore the present cruise needs to be complemented by another cruise during the summer stratification period.

3.3 Research Program of Leg M44/3

Marine Geology in the Gulf of Aqaba and the northern Red Sea

The aim of the marine geological and paleoceanographic programme was to reconstruct the late Quaternary climate history of the northern Red Sea and the Gulf of Aqaba. This marine environment suffered extreme oceanographic changes due to its restricted location. The late Quaternary oceanographic changes will be reconstructed from sediment cores and will be compared to the history of sea level changes and tectonic development.

Salinity in the Red Sea is influenced by the exchange of water masses with the Indian Ocean and is driven by sea level changes. Amplified climatic signals are recorded in the Red Sea. Stable oxygen isotope chronologies reveal enhanced signals compared to the global isotopic record. Focus was given to different periods of climatic change. High- resolution studies will be performed to reveal the deglacial history and the Holocene record. The terrestrial climate history from northeast Africa and the Middle East is well documented. Wet periods are known from the early Holocene. A comparison between marine and terrestrial records will give clues to the climatic interactions between land and ocean.

A second focus of interest was the reconstruction of environmental conditions during the last glacial maximum. Prior to this climatically extreme event many planktic and benthic organisms lost their habitat due to a lethal salinity increase. Later, during deglaciation, marine conditions became more favorable again during sea level rise. The succession of marine organisms during this extreme period will be analysed. The fate of reef organisms during this period is unknown.

A third primary focus was the high-resolution reconstruction of isotopic stage 3. Rapid climatic change is well known from ice cores and marine sediment records from various oceans. The present studies aim to analyse this period in the northern Red Sea. Lake sediments from the precursor of the modern Dead Sea display sedimentary chronologies for comparison. The development of the Lisan

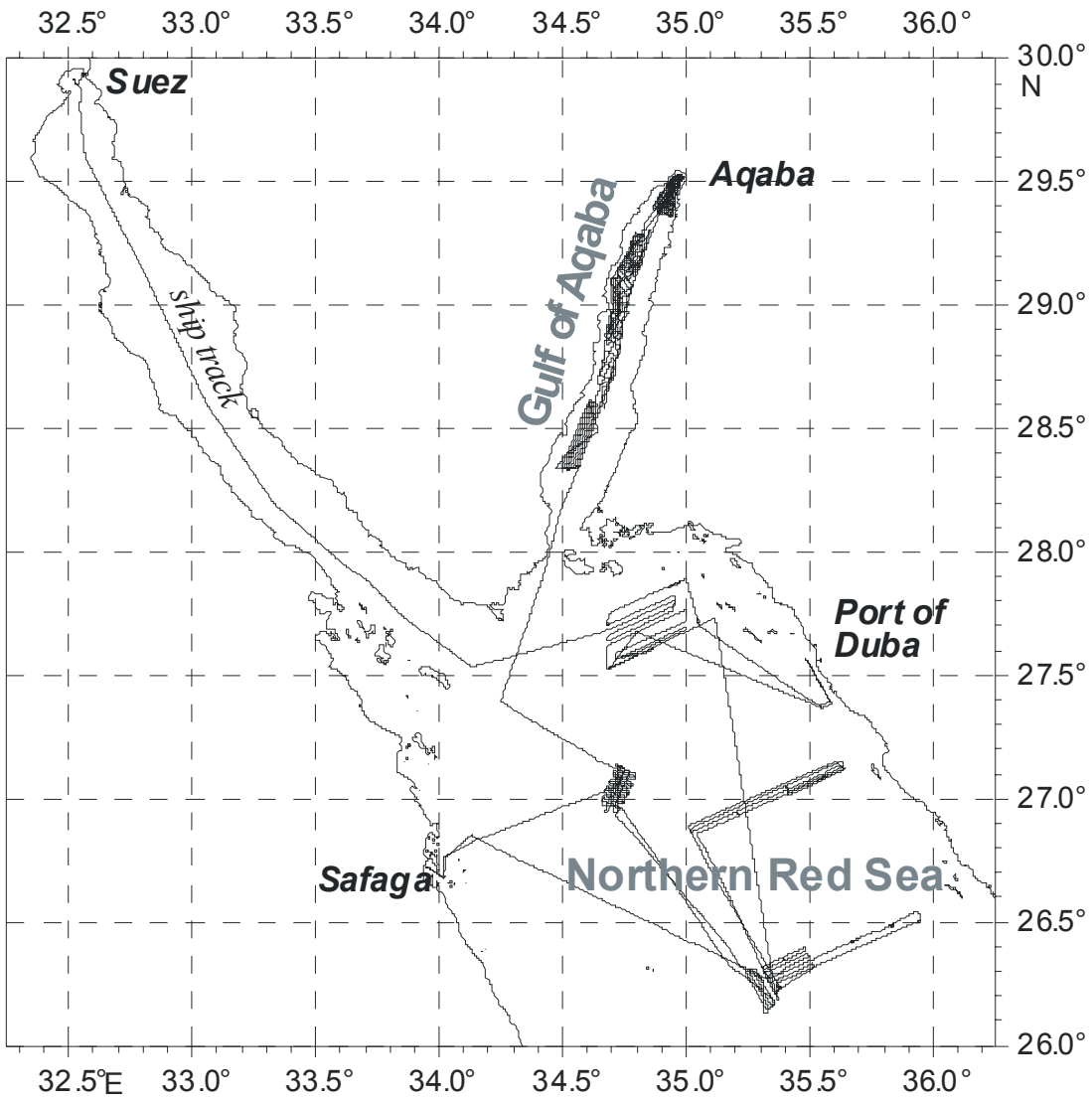

Fig. 4: Cruise track in the Gulf of Aqaba and the northern Red Sea during R/V METEOR Cruise M 44/3.

Formation dates back to between 20,000 to 70,000 years before present and represents a terrestrial analogue to marine isotopic stage 3. It is of international interest to study and understand the processes of climate variability during this period.

Changes in circulation have a great impact on the material budget and productivity of the northern Red Sea and Gulf of Aqaba. The variable production of carbonate and organic material will be studied during glacial and interglacial times. The paleoceanographic results will be used for a synoptic analysis, which will describe the exchange processes between the Indian Ocean and the Red Sea and the impact on the Gulf of Aqaba. A comparison with oceanographic changes in the Mediterranean will also help to clarify the impact of the monsoon system during the late Quaternary.

The geological studies included sampling of the water column, the surface sediments and the sediment column. It was planned to sample the Gulf of Aqaba on various profiles along the main axis and across the sediment basin. In addition, different surveys and sampling were intended in selected areas in the northern Red Sea. Each profile was selected to provide a set of stations in different water depths. At each station a similar sampling procedure was carried out. The water column was sampled by plankton tows for planktic organisms. Water samples were analysed from

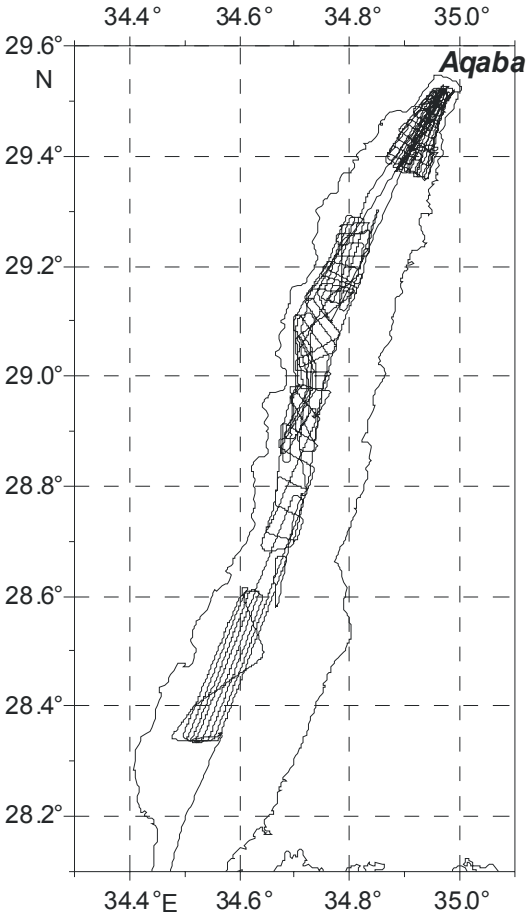

Fig. 5: Cruise track in the Gulf of Aqaba during R/V METEOR Cruise M 44/3.

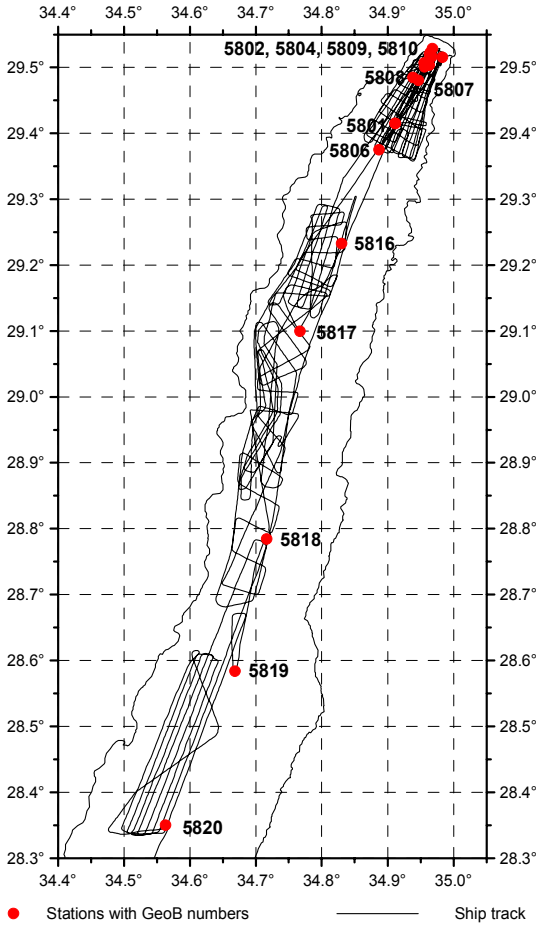

Fig. 7: Cruise track and sampling locations (multi-net and water samples) in the Gulf of Aqaba during R/V METEOR Cruise M 44/3.

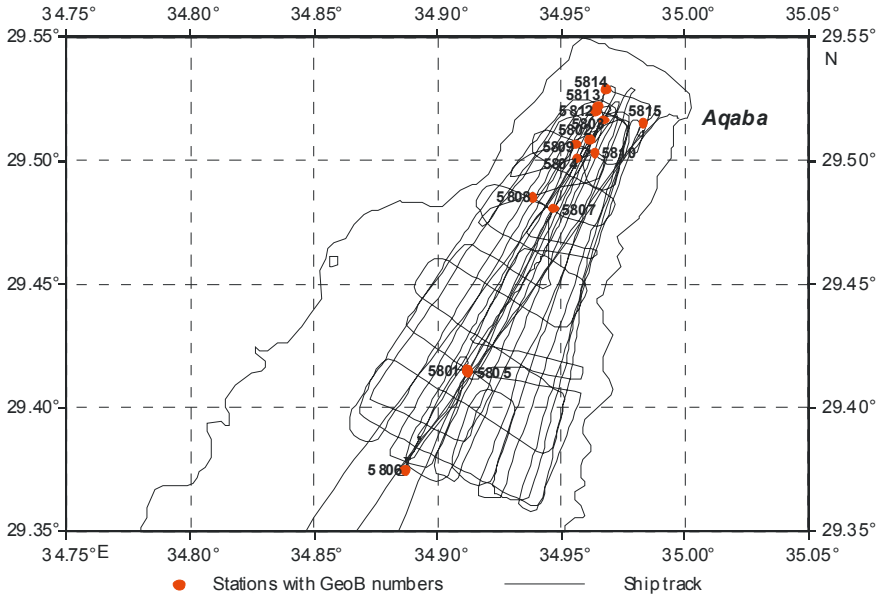

Fig. 6: Cruise track and sampling locations (gravity corer and multicorer) in the northern Gulf of Aqaba during R/V METEOR Cruise M 44/3.

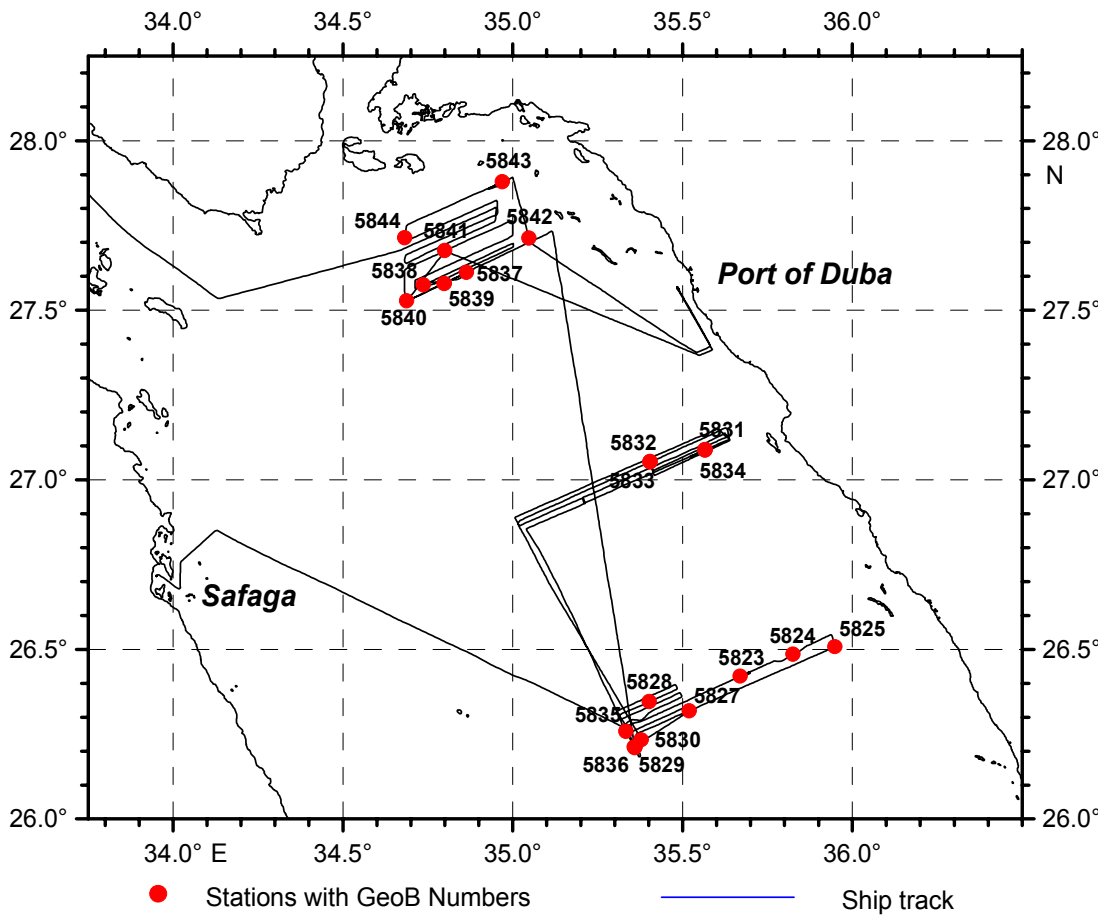

Fig. 8: Cruise track and sampling locations (gravity corer and multicorer) in the northern Red Sea during R/V METEOR Cruise M 44/3.

depth profiles for stable oxygen and carbon isotopic composition for comparison to the profiles of temperature, salinity and oxygen content.

Samples of surface sediments by grab sampler, box corer and multi-corer were used to map the recent sedimentation on the sea floor, and for revealing undisturbed surface layers. Surface sediments document the modern sedimentation and are important references for paleoceanographic reconstructions. Sediment cores up to 18 m in length were recovered. Most of them were opened, documented, described, and sampled. A comprehensive sampling procedure was carried out on the cores for later detailed analyses (biostratigraphy, stable isotope stratigraphy, physical properties, biology and micropaleontology, sedimentology, isotope geology, and geochemistry). A preliminary stratigraphy was established by the abundance of planktic foraminifera and color variations in the sediment cores.

Geophysical investigations in the Gulf of Aqaba and the northern Red Sea

The geophysical program included profiling seismic and hydro-acoustic measurements. The goal was the 2-dimensional imaging of the sea floor and its sedimentary cover. Measurement of bathymetry with the swath sounder HYDROSWEEP and imaging of the uppermost sediments with the narrow beam echosounder PARASOUND were carried out continuously throughout the cruise, while multi-channel seismics were planned just for certain areas. Data analysis and interpretation should provide a detailed characterization of the tectonic and sedimentary history of the survey areas.

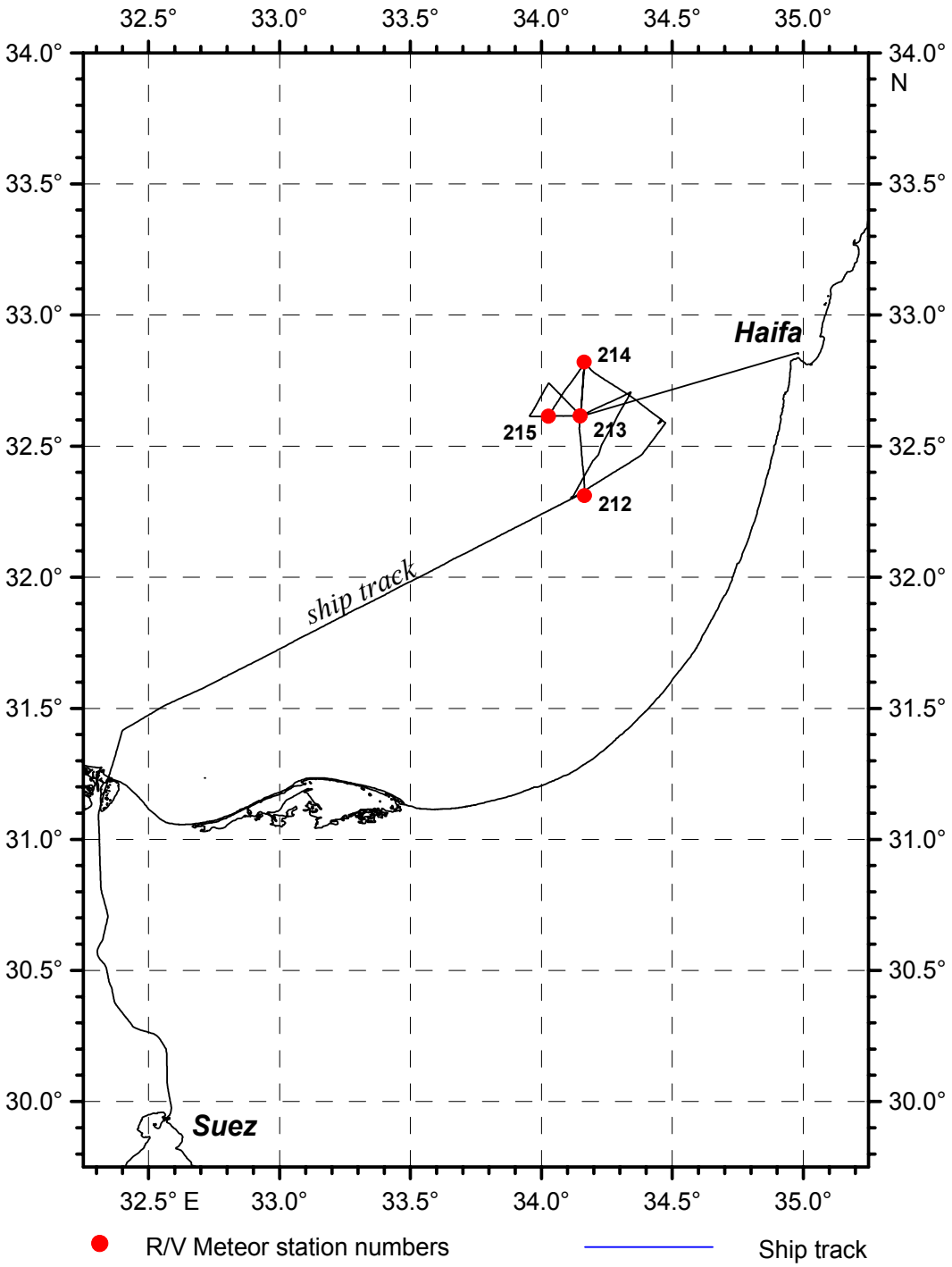

Fig. 9: Cruise track and sampling locations (piston corer and multicorer) in the eastern Mediterranean Sea (Levantine Sea) during R/V Meteor Cruise M44/3.

Detailed studies were mainly planned for the Gulf of Aqaba: internal structures, sea floor topography, and budget calculations of the large subaqueous sedimentary fans in front of the wadis Watir, Dahab, and Kid. The sediment input results from rare rainfall on the Sinai Peninsula. The growing pattern reflects the impact of sea level and climatic fluctuations on sediment input and depositional processes. Problems of the reconstruction of the tectonic history will be tackled in the very north at the crossing of the Shlomo Graben and the Elat Fault. Another important target was the Aragonese Deep, a proposed pull-apart basin.

In the northern Red Sea, the focus was given to fluid migration and exchange between young oceanic crust and seawater column through the sedimentary cover. Fluid migration paths have been recently observed in high-resolution seismic data in the east Pacific. The closest link between geology and geophysics will result from an integrated interpretation of sediment cores and ultra-high resolution seismo-acoustic data, since these data provide information about the structural context of each core.

Exchange processes at brine-seawater interfaces in Red Sea deeps

One goal of the ongoing research in the Red Sea was to characterize genetic processes of trace gases in the sediments, water columns and brines of Red Sea deeps. Isotopic compositions of hydrocarbon gases, in particular, should give us better information about thermal degradation processes of buried organic compounds in deeper sediments. Furthermore, bacterial methanogenesis or oxidation should be characterized by isotopic measurements.

The main objective during this cruise was to understand the complex mixing and oxidation processes of hydrocarbons in the brine-seawater interface. Furthermore, high-resolution sampling (<1m, without disturbance of the layered water structure) and isotope measurements of various trace gases were performed. Microbial investigations will uncover hydrocarbon formation and/or oxidation processes by microorganisms. Inorganic chemistry investigations (e.g. elemental composition and isotope ratios of trace elements) of brine layers will provide information about fluid sources. Detailed investigations of concentration gradients at brine-seawater interfaces will provide better understanding of exchange processes and complex redox cycles.

Hydrographic data of the water column in Shaban and Oceanographer Deep in the northern Red Sea were measured by CTD. Brine-seawater interfaces were identified by temperature and salinity increases. These interfaces were sampled by a newly designed interface-sampler. With this special device we were able to take undiluted water samples from biogeochemically active water layers with a high resolution. Water samples were planned to be degassed and onboard gaschromatographic analyses should give information about the gaseous compositions. Isotope ratios of hydrocarbons will be measured after the cruise at BGR (Hannover).

It was planned to sample the steep gradients of inorganic trace elements at the brine seawater interface with a special interface sampler (IS-1, DeLange), if possible. This device fills 10 syringes (50ml) simultaneously at the selected water depth over a 3m interval. Water samples will be measured onboard under anoxic conditions. Brine bodies and Red Sea deep waters will be sampled using a Hydrobios water sampler (5l Niskin bottles, CTD-device). Oxygen, alkalinity and pH will be measured onboard. It was planned to perform cation- and anion-measurements at Kiel University.

For microbial investigations (University Regensburg) water samples were taken from the same water depth of geochemical interest. The influence of microbial activity on inorganic/organic redox processes should be characterized by the abundance of specific organisms, which will be selected and cultivated in the land laboratory. This combined microbial and geochemical research will give us new information about microbial activities under extreme environmental conditions and the geochemical characteristics of related trace gases and elements (only known by empirical assumptions).

Reconstruction of the Pleistocene and Holocene paleoenvironment in the Levantine Sea and the Gulf of Suez by means of benthic and planktic foraminifera

The main objective of this study is to reconstruct the history of intermediate- and deep-water circulation and paleoproductivity in the Levantine Sea, the northern Red Sea and the Gulf of Suez during the late Pleistocene. Previous paleoceanographic studies have shown that past climatic changes are clearly recorded in sediments from the eastern Mediterranean and the Red Sea. These climatic fluctuations can be reconstructed from the species composition and stable isotope signals of both planktic and benthic foraminifera. However, the significance of the individual environmental parameters (salinity, temperature, productivity, deep water circulation) and their connection to the regional and global climate is still controversial. To solve these questions, high-resolution studies are required to record short-term paleoclimatic events, and more information is necessary to document the present marine environment and circulation patterns for comparison to the past. Finally, we want to characterize the impact of Quaternary climatic changes on both oceanic environments that are divided in terms of oceanography and biogeography.

During the cruise it was planned to sample surface sediment and sediment cores at different stations by means of a multicorer and a piston corer. Prior to coring the site would be intensively investigated using Parasound and Hydrosweep to find the best spot to core. The recovered sediment samples will be investigated for temporal and spatial changes in the compositions of planktic and benthic foraminiferal faunas and the stable oxygen and carbon isotope signals of their tests. Since we will mainly concentrate on high-resolution studies we expect to gain information not only on long-term glacial to interglacial cycles but also on high frequency fluctuations of the past climate and deep-water circulation. The surface sediment samples will be studied to describe the ecology of the faunal assemblages and the relationship between the stable isotope signal and various environmental parameters. These results will serve as a modern analogue for the reconstruction of the paleoceanographic history of the different regions. This new data set will close the gap between our existing results from the Mediterranean Sea, Red Sea, and Gulf of Aden.

3.4 Research Program of Leg M44/4

The thermohaline circulation of the Eastern Mediterranean has entered a transient phase since about 1990 triggered by the start of deep water production in the Aegean Sea and the novel outflow of this very dense water into the Levantine Basin. In line with previous investigations the combined hydrographical and biological survey in the Levantine an Ionian Seas aimed at the evolution of the transient and is effect on the pelagic biota. Biological implications of intraannual variability shall be discrimininated against longer term climatic changes in relation to physical processes which govern the abundance and production of the plankton biota and the flux of particles in the deep water column. Thus, the drastic change in the deep thermohaline circulation of the Eastern Mediterranean is of particular interest of the hydrographers and biologists as well. The results will enhance our knowledge of the reaction of deep-living pelagic communities to physical and chemical signals of different time scales and, thus, the resilience of the deep-sea ecosystem. Apart from changes in the vicinity of the deep water formation sites in the Adriatic and Aegean Seas, the formation of the Levantine Intermediate Water was investigated together with biological processes in simultaneous regional surveys by Italian and Zypriotic ships in cooperation with R/V Meteor.

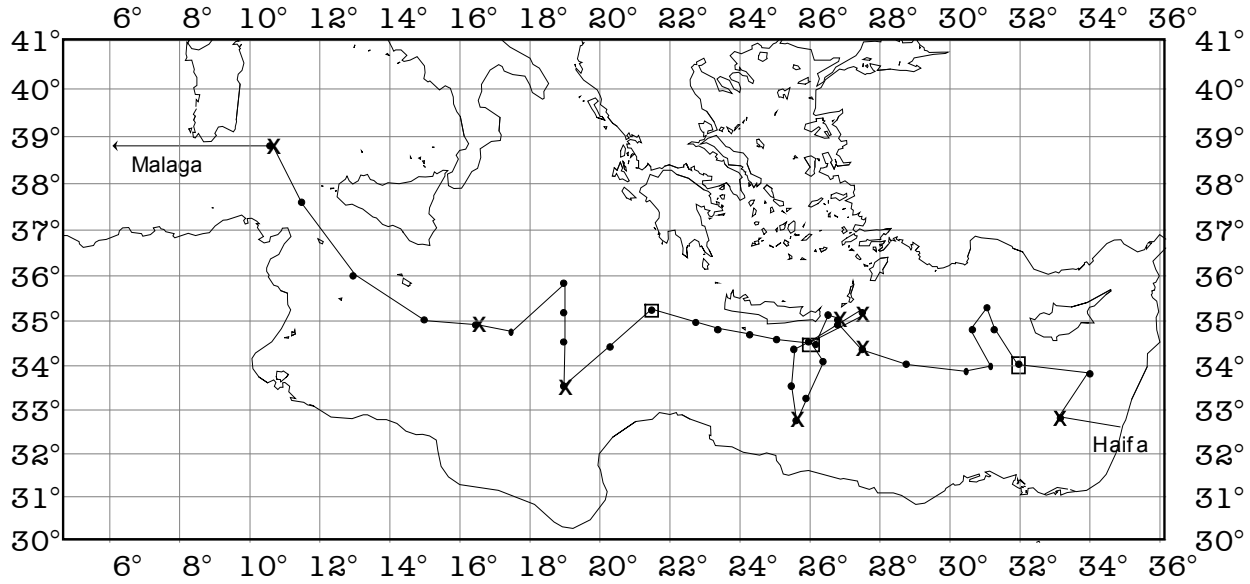

Fig. 10: R/V METEOR, cruise no 44, leg 4: Research areas and main tracks.

The hydrographical and tracerchemical survey of R/V METEOR was done along an east-west transect across the Levantine and Ionian Seas. The embedded plankton programme which included diversity studies on microbial and metazoan plankton owned intensified assays at three sites situated of SW-Cyprus, SE-Crete and in the west off Crete above the Urania Deep (Fig. 10).

Tracer chemistry and hydrography

The purpose of the investigation is to monitor the transition of the system from a quasi-steady state to a transient one. It is of general interest to find out whether the circulation in the Eastern Mediterranean will eventually drift back to the previous equilibrium state or whether a new equilibrium will be established, and also whether the new equilibrium will be characterized by two deep water formation sites, like presently.

The survey provided another snapshot of the transient state of the circulation and water mass properties in the Eastern Mediterranean with sufficient spatial resolution by means of full depth casts with a CTD/Rosette. High precision measurements of transient tracers (CFCs: F-11, F-12, F-113 and CCl_4; tritium) are especially useful to detect these processes because of their time dependent input into the mixed layer. The tracer distributions will be used to investigate the effects of the additionial deep water source on the system and will document changes in the dense water formation rates in the key areas, i.e. the Adriatic and Aegean. These measurements complemented by hydrographic and nutrient/oxygen measurements will therefore provide information on the temporal evolution of the spreading of Aegean derived deep water and document possible changes in the availabilty of nutrients and their possible effects on the ecosystem. The zonal section through the Levantine Basin, the Cretan Passage, the southern Ionian and the Strait of Sicily has been chosen because it monitors the continuous advance of bottom water of Aegean origin into the adjoining basins and the associated changes in the vertical water mass distribution. The measurements will also focus on changes in the Levantine Intermediate Water because of its importance as a precoursor water mass in the deep water formation.

Microbial production and diversity

In connection with recent changes of the hydrological system in the Eastern Mediterranean Sea it is of special interest to determine whether different water bodies harbour characteristic bacterial communities or bacterial key species which can be used to identify these water bodies. The effect of nutrient input and pressure on the phylogenetic structure of the bacterial and archaeal communities is a further research topic. The study was centered on the three stations south-west off Cyprus, south-east off Crete (Ierapetra Basin) and west off Crete in the Urania Basin. A special aspect of the study dealt with bacterial abundances, activities, and diversity in the hypersaline deep waters of the Urania Basin. Sampling of water was performed with sterile bag samplers, deep sea *in-situ*-pumps, but mainly with the CTD/rosette. Samples from the latter were used for the determination of the vertical distributions of primary production (*in-situ*-incubation), bacterial abundances and biomass (fluorescence microscopic determinations), bacterial secondary production (incorporation of ^{3}H-leucine), and bacterial diversity (fluorescence-*in-situ*-hybridization, and denaturing gradient gel electrophoresis). Additionally, these samples will be used for pigment analysis.

Comparisons of data of this expedition with those of former cruises (Meteor-expeditions M 25/2 and M 40/3) into this region shall give information on the temporal variability of the examined parameters.

Structures and dynamics of zooplankton and micronekton

Spectacular changes in the deep-sea zooplankton have been observed during the last decade in the Levantine Sea. One aim of the forth cruise therefore is to assess the acting temporal and spatial scales of variability, i.e. to discriminate longer term, basin-wide effects from shorter term (interannual, seasonal), sub-basin scale effects on abundance and diversity. For this purpose, and based on the concomitant oceanographical survey, the composition and dynamics of zooplankton and micronekton in the water column and near-bottom zone off Crete and SW-Cyprus were investigated in line with earlier expeditions (M5/1, M25/2, M40/3). The second aim is to estimate the carbon demand of the zooplankton and micronekton faunas. These results together with the findings obtained from the microbiological and biogeochemical working groups shall answer the question, if changes in the taxonomical and trophical structure in the deep and near-bottom water column modify the vertical flux of particles to the abyssal sea floor. The zooplankton assay is based on a variety of structural, functional and biochemical parameters which were obtained from samples collected with three types of multiple-opening-and-closing nets and a neuston catamaran.

Biogeochemical fluxes in the deep water

The sediment trap system deployed in the Ierapetra Deep SE of Crete during leg M44/1 had to be recovered. Major goal of the sediment trap experiment is to investigate the variation of fluxes and composition of particles settling to the deep sea in space and time, i.e. (i) during transit through the water column and (ii) throughout the sampling period from the end of January until the end of April, respectively. Detailed analyses of organic compounds will provide information on the sources, transport paths and transport processes of the organic matter. These investigations carried out for the first time in the western Levantine Basin are closely linked to the microbiological and planktological investigations of leg 4 and contribute to the understanding of externally forced material fluxes and its relevance for deep sea biology.

4 Narrative of the cruise

4.1 Narrative of Leg 44/1

(P. Halbach, R. Seifert, T. Kuhn)

The METEOR cruise M 44/1 was divided into two legs. The first one from Cadiz to Canakkale, the second one from Canakkale to Istanbul. The first leg started on January 23, 1999 in Cadiz (Spain). The scientific crew under chief scientist Dr. R. Seifert consisted of six scientists from the Free University of Berlin and the University of Hamburg. R/V METEOR left Cadiz on the early morning of January 23 heading for the Urania Basin. This basin is situated in the Ionian Sea at 35°15' N and 21°28'E which is about 1410 nm away from Cadiz. R/V METEOR arrived at the Urania Basin on January 28. Bathymetric profiling and sediment stations (two box cores) were carried out there.

Afterwards R/V METEOR steamed to 35° 50'N, 22° 40'E to take a 7.5 m long piston core. R/V METEOR continued to 35°25.9'N, 26°10.8'E. On January 29 a sediment trap system consisting of two sediment traps and a releasing system could be deployed despite strong winds (Beaufort 7/8). At about 4 pm station work was finished and R/V METEOR started to cross the Aegean Sea and arrived in Canakkale on the very early morning of January 31.

In Canakkale two scientists from the University of Hamburg left the ship and 22 new scientists (from the Free University of Berlin, the Universities of Hamburg, Kiel, Greifswald, Tübingen and Göttingen) including five Turkish guest scientists embarked. At about 10 a.m., January 31, 1999, the second leg of cruise M 44/1 began. R/V METEOR left Canakkale and continued to the main working area, the Sea of Marmara, under the new chief scientist Prof. Dr. P. Halbach (Free University of Berlin).

It took six hours to steam to the central Sea of Marmara. This part is called the working area A (Fig. 1). The corner coordinates of area A are as follows: 40°52'N, 27°40'E; 40°52'N, 28°10'E; 40°45'N, 27°40'E; 40°45'N, 28°10'E. To get detailed information about the bathymetry of the working area a HYDROSWEEP mapping was started on the evening of January, 31. Vertical resolution of the system is within meters, horizontal resolution depends on the availability of dGPS or GPS. Due to bad weather conditions mapping had to be interrupted several times since the system can properly work only up to Beaufort 6/7. Eventually, we got the first bathymetric map of this deep part of the Sea of Marmara which yielded a lot of new information with respect to the bathymetry in relation to active tectonics. Combined with the HYDROSWEEP system another echosounder system was used: PARASOUND. It measures sediment structures and sediment thickness up to about 100 m sediment depth depending on the physical parameters of the sediments, the slope angle, the ship velocity, and the sea state.

After finishing the bathymetric mapping, sediment, water and video stations were carried out. Sediment stations included multicorer to get the uppermost 10 to 20 cm, piston corer and gravity corer to recover long cores (up to 13 m). Water stations were run with a CTD/rosette system which is equipped with conductivity, temperature, and depth sensors for on-line measurements as well as twelve 10 l Niskin Bottles to collect water samples in the water column. A total of 37 sediment stations, 20 water stations, 12 video stations (with the Hydro-Bottom-Station), and four current meter deployments to measure bottom water velocity and direction were carried out in working area A.

Station work in area A was finished on February 10, 1999. R/V METEOR steamed to area B (Fig. 1), the Çýnarcýk Basin with the following coordinates: 40°45'N, 28°40'E; 40°52'N, 28°40'E; 40°52'N, 28°58'E; 40°45'N, 28°58'E. Station work in area B included bathymetric mapping, the

recovery of six piston cores, two multicores, one CTD station and one current meter station in the deep Çýnarcýk Basin.

On the morning of February 13 R/V Meteor moved to Istanbul and arrived at Istanbul harbour at 3 p.m.

The main part of the scientific crew disembarked on February 14, 1999. The M 44/1 cruise ended on February 15 with a reception onboard the research vessel housing guests from different administrative and scientific Turkish and German organizations.

4.2 Narrative of Leg 44/2

(G. Hempel)

The second leg of the cruise started in the evening of 16 February in Istanbul. The next morning the vessel passed the Dardanelles and proceeded southbound through the eastern Aegean Sea. Supported by strong northwesterly winds Meteor reached Port Said on 19 February and completed the passage through the Suez Canal by the following evening. Six Egyptian scientists and observers came on board, together with four scientists from Eilat and two from Aqaba. At two test stations in the Mediterranean all major sampling gear had been successfully employed, so work could start without technical delays on 21 February in the southern Gulf of Aqaba with a quick CTD survey from South to North (section a) followed by two days of intensive station work in the Gulf which included all disciplines on board (section b). The vessel then went into the Red Sea, again first for a CTD reconnaissance along the eastern profile and then by three full stations on the western profile (section c). On 25 February we were back in the Gulf for the second series of six full stations (section d). In the evening of 26 February when working the northernmost station we encountered an unexpected deep mixing which prompted us to work a short meridional section with high spatial resolution. The next two days were devoted to the Red Sea again moving there from NE to SW. In the night to 1 March Meteor sailed to Aqaba, where five scientists disembarked and two others plus three members of a television team entered.

The six hours' visit to Aqaba was framed by one CTD cast in the morning and a full station in the evening, both at Pos. I. Overnight we moved to the first time station (T1) on Pos. VI where we stayed for about 30 hours. The following section f on 3-4 March in the Red Sea consisted of four stations only. The second time station (T2) at the northern tip of the Gulf took place on 5 March, it was slightly shortened in order to meet sampling needs of the zooplankton group and to reach the starting point of the cross section (C) south of Taba in the early morning of 6 March. At the eastern end of the cross section we met the boat of the Marine Science Station and took samples on board. Finally Meteor revisited briefly Pos. III - VI in the Gulf for a further look at the development of the plankton bloom (section g) and for a Hydrosweep survey. 8 March we spent with no station work near Pos. V for packing, reporting and other activities. Another northbound Hydrosweep survey brought Meteor back to Aqaba. There the cruise leg 44/2 ended in the morning of 9 March, but various public relations activities had been scheduled for 9 and 10 March including an official visit to the vessel by the German ambassador to Jordan, foreign diplomats, Jordanian dignitaries, administrators and scientists as well as the Scientific Steering Committee of the Red Sea Program.

During most of the observation period strong northerly winds prevailed but did not impede our work. The air temperature was around pleasant 20°C. Only during the last days of the cruise the wind calmed down and the temperature increased. We had no rain and saw only few clouds.

4.3 Narrative of Leg 44/3

(J. Pätzold)

After three days in port, R/V METEOR left Aqaba on the morning of Friday, March 12, 1999, beginning the third leg of Cruise M44. During the first part of the cruise, from Aqaba to Safaga, the scientific program included marine geological and geophysical studies primarily in the Gulf of Aqaba, but also in the northern Red Sea, in Jordanian, Israeli, and Egyptian waters (Figs. 4 and 5). The new scientific shipboard party included 14 colleagues from German institutes. The group of guest scientists on board from countries neighboring the Red Sea consisted of two young colleagues from Jordan and seven participants from Egypt, including two naval observers.

Extensive hydro-acoustic studies were carried out initially in the northernmost Gulf of Aqaba, within the territorial waters of Jordan and Israel, by HYDROSWEEP and PARASOUND. Geological sampling of the sea floor by multicorer, box corer, and gravity corer provided a set of sediment cores in water depths ranging from 135 to 838 m (Fig. 6). The northern Eilat Deep was also successfully sampled by sediment cores. The cores reveal records with high temporal resolution from the latest Quaternary, characterized by high siliciclastic input and multiple sets of turbidites. The shallower cores contain greater abundances of pteropods and both benthic and planktonic foraminifera. On the evening of March 16, the geological sampling of sediments was completed in this area with a box corer directly in front of Aqaba harbour. All the sediment cores from this survey area were opened and documented, and some were also sampled on board at high resolution for further studies in the home institutes. The comprehensive sampling program during the early days of the cruise also included the collection of plankton and water samples from the water column using multinets and the pumping of surface waters, respectively, as well as the monitoring of oceanographic conditions with CTD profiles.

Multi-channel seismic surveys in the Gulf of Aqaba were initiated on the evening of April 13 in Jordanian and Israeli waters, and were continued later in Egyptian waters. The first area of interest was the northern end of the Gulf of Aqaba. Problems relating to the reconstruction of tectonic history were tackled in the southwestern Eilat Deep near Ras Burka, to improve the understanding of structures at the crossing of the Shlomo Graben with the Eilat Fault. The submarine fans of the wadi deposits from Wadi Watir off Nuweiba and at Wadi Dahab were two other primary targets of the geophysical survey (Fig. 7). Data analysis and interpretation are aimed at a detailed characterization of the tectonic and sedimentary history of the survey areas. In particular, the growth patterns of the large subaqueous sedimentary fans reflect the impact of sea level and climatic fluctuations on sediment input and depositional processes.

Sampling and monitoring of the water column at five stations along the main axis of the Gulf, which had also been covered during leg M44/2, completed the sampling program down to 28°21´N (Fig. 8). On the afternoon of March 22, R/V METEOR left the Gulf of Aqaba through the Strait of Tiran. The sampling program continued with a multinet station at 27°24´N / 34°14,9´E to complete the plankton profile linking the Gulf of Aqaba with the northern Red Sea. Geophysical surveys were continued in the northern Red Sea in Egyptian waters, concentrating on two small, isolated, deep basins along the axial depression zone of the northern Red Sea. The Conrad Deep, at about 27°03´N / 34°43´E, surprisingly exhibited a brine body that could be identified in the seismic profiles. The western part of Shaban Deep around 26°15´N / 35°19´E, where a previously known dense brine body also exists, was also covered by a set of seismic lines. Altogether, 90 profiles comprising of about 1000 miles of geophysical survey lines were carried out during this initial stage of the cruise M44/3.

On March 25, 1999, part of the scientific crew was exchanged in the port of Safaga. Now the crew comprised of 20 German scientists from eight different institutes and a group of six Saudi Arabian guests, including one military observer. The scientific program of the second stage of the cruise, beginning on the morning of March 26, concentrated on marine geochemical, geological, and sediment-acoustic studies in the eastern sector of the northern Red Sea.

The initial focus of this stage was on geochemical studies in the Shaban Deep, consisting of four basins filled with high-saline brines. Here, the southern, eastern, and northern sub-basins were studied. One major task was a detailed sampling of the brine bodies and the brine interfaces of the Shaban Deep to better understand the geochemical cycles of trace elements and other inorganic compounds in, and between, the convecting brine layers and the overlying Red Sea Deep Water. The aim of trace-gas analysis was to clarify the genesis of gases dissolved in the brine layers and their exchange with the overlying water mass. Stable isotope compositions of the gases should provide evidence on thermal degradation mechanisms of organic matter buried in the sediments, and also on mantle-derived fluid input. Secondary degradation processes of hydrocarbons may also be unravelled by these investigations. Clues to the formation and degradation of organic carbon in this extreme environment are expected. The deployment of a newly designed Interface Water Sampler rendered high-resolution results of the steep concentration gradient of dissolved and particulate compounds in the upper brine interface. In addition, sediment material was sampled using the multicorer and gravity corer. A microbiological procedure was carried out on multicorer surface sediments to enrich and isolate microbial communities from the extreme saline and anaerobic brine sediments.

The collection of surface sediments and long sediment cores for paleoceanographic studies was carried out by a gravity and piston corer during the following days. Three sampling profiles extending from the Saudi Arabian coast to the central axis of the northern Red Sea were carried out succcessfully at about 26°24´N, 27°00´N, and 27°42´N (Fig. 8). Core descriptions and initial stratigraphic analyses indicate continuous sediment records to study paleoceanographic changes during the glacial and interglacial cycles of the late Quaternary in the northern Red Sea.

On the morning of April 2, four Saudi Arabian scientists disembarked in the port of Duba carrying multicorer sample material and samples from the first gravity cores. To make the most efficient use of allocated shiptime, sampling was continued on the same day on the northern sediment profile near the Strait of Tiran. Sediment- and water-column sampling and all profiling measurements in the Red Sea were concluded on April 3 at 05:25 a.m. at 27°41,0´N / 34°40,9´E. The vessel entered the Strait of Gubal heading toward the port of Suez where the second stage of the cruise ended with the departure of two Saudi Arabian guests and the German geochemical group.

On Sunday, April 4, R/V Meteor passed through the Suez Canal and entered the Mediterranean, approaching the final working area of the cruise (Fig. 9). Geological sampling on the continental slope off Israel bordering the eastern Levantinian Basin was successfully performed at four sediment stations using a multicorer and piston corer. Prior to the sampling, a Hydrosweep and Parasound survey had been carried out to identify suitable sampling locations on the steep continental slope. The main objective of this study is to reconstruct the history of intermediate- and deep-water circulation and productivity in the Levantine Sea during the late Pleistocene. This research also aims to characterize the impact of Quaternary climatic changes on the eastern Mediterranean and the northern Red Sea, which are separated in terms of oceanography and biogeography. A last piston corer of 12 m length and a final deployment of the multicorer concluded the scientific work of the Meteor Cruise M44/3 on April 6 at 5 p.m. at 32°37´N / 034°02´E at a water depth of about

1450 m. R/V METEOR sailed northeast towards Haifa, where the third leg of cruise M44 ended safely on the morning of April 12, 1999.

Hydro-acoustic measurements with the shipboard narrow-beam echosounder PARASOUND and the swath sounder HYDROSWEEP were continuously carried out in the survey areas of the cruise to record and study high-resolution bathymetric and sediment echosounding profiles. Sample material from the different marine regions recovered during R/V METEOR Cruise 44/3 will be distributed among the national institutions represented by the scientists on board, as well as to other scientists from each nation visited. Analyses of the samples will be performed in laboratories of various national institutions as stated in the scientific program of the cruise. Data will be exchanged and the results published and presented to the funding agencies and the national authorities of the countries bordering the survey areas in the Gulf of Aqaba, the northern Red Sea, and the eastern Mediterranean.

4.4 Narrative of Leg M44/4

(H. Weikert)

METEOR sailed with fine weather from Haifa/Israel at 1006 local time Saturday 10 April, 1999. Seven and a half hours later, the first station was reached and the clocks were put two hours prior to UTC. The test haul of the 1m^2-Double Mocness throughout the 1500 m water column was successful as were the first shallow and deep cast of the CTD/Rosette.

After a second station with the CTD/Rosette at 034^o eastern longitude, the first of the three main biological research sites, the area of the West Cyprus Cyclonic Gyre, was reached on Monday, at 1700 (Fig. 10). The sea-floor was mapped with the HYDROSWEEP system for two hours prior to the beginning of sampling.

The standard work with the CTD/Rosette, which was also deployed along the ship's track together with continuous current measurements by means of the the ship-mounted ADCP vertical profiler, included the following: hydrography, optics and *in situ*-flourescence (OGS); tracer chemistry (TCUB), nurients, oxygen (IOLR); chlorophyll, bacteria (IfMK), ultraplankton (STAZN) and protozoans (IHF).

Water samples were taken from selected depths in the water column by up-casts starting from the near bottom. Subsamples and/or replicates of the material were used to determine (a) the inorganic nutrient concentrations in the ambient environment, (b) the abundance, diversity and secondary production of microbial organisms, and (c) chloroplastic pigments. For batch cultures, three profiles were obtained by means of sterile butterfly samplers to study the effect of nutrients onto microbial communities. In addition, bacteria were enriched on filters with *in situ*-pumps in the deep-sea for fatty acid analyses. The studies on bacterial abundance and composition were completed by sediment records obtained from a single multi-corer. Subsamples of sediment will be analysed for biogeochemical parameters in the home lab (IBMC).

Shallow casts with the CTD/Rosette were performed in the upper 200 m for two *in situ* -C-14 incubation experiments, supplemented by light measurements with a Secchi disc. A particular 26-hours time series experiment restricted to the area off SW Cyprus was conducted in the upper 1000 m by lowering the CTD/Rosette every three hours (a) to evaluate the fluctuation of the water masses and the short-time scale variability due to internal waves, (b) to study *in situ*-growth rates of ultraplankton (cyanobacteria, prochlorophytes, picoeucaryotes) in the upper 250 m. Finally, assays on the role of protozoans as consumers and prey organisms were made.

On April 15, at 1530 Meteor met the Cypriotic R/V Edt Argonaut for a designated intercalibration of the CTD probes used by both parties. After the repairment of the conducting cable of the R/V Edt Argonaut by the Chief Electronical Engineer of Meteor, the test series were successfully completed. Dr. Zodiatis, chief scientist, together with two colleagues and the 2nd officer came to a one and a half hours visit on board Meteor. At 2000, both ships set about continuing their routine work.

Meteor 's remaining wire time at this main site was exclusively devoted to the gathering of medium- and larger-sized metazoan zooplankton and micronekton by stratified 0.333 mm mesh size tows for taxonomical, structural and functional analyses as well as biogeographical studies (IHF). The latter included an assay on cephalopods (ZUR). The oblique tows with a 1m^2-Double-Mocness, equipped with 20 nets and environmental sensors, usually commenced at 5 to 10 m above bottom (a.b.). In addition, the 10 to 100 m layer a.b. was subsampled by three distinct horizontal depth intervals to catch benthopelagic animals. A hyperbenthic sledge yielded three to five consecutive samples from the 50 to 150 cm-layer a.b.. Sampling of zooplankton was completed by surface tows with a neuston sledge. In a special study, abundant copepods were selected from epipelagic and mesopelagic Mocness samples and stored deep frozen in order to estimate species specific ingestion rates by the gut fluorescence method (NCMR). Later on, starting in the Ierapetra-Deep, the study was supplemented by assays on the egg production of copepods.

On April 17 at 0810, the „stationary" work off SW Cyprus was successfully completed, and Meteor headed towards the Caso Strait. En route, seven full-depth profiles with the CTD/Rosette and seven neuston tows were performed, supplemented by sampling of chlorophyll with the surface water sampler. Station work near and at Caso Strait from April 19 to April 20 consisted of two Mocness hauls, two CTD/Rosette profiles and one *in situ*-primary production assay. On April 20 at 1200, Meteor reached the area of the Ierapetra-Basin and sucessfully recovered the deep-sea sediment trap assembly, which had been deployed with traps at 700 m and 2700 m in January during M44, Leg 1. However, due to malfunction, only the deep trap had collected sediment.

After a deep haul with the 1m^2-Double-Mocness in the basin's area, Meteor sailed towards the coast of Libya taking casts with the CTD/Rosette and surface samples of chlorophyll and zooplankton with the surface water sampler and the neuston net, respectively. On April 21 at 0050, the ship had arrived at 32^{o}43'N, 025^{o}40'E. The CTD/Rosette cast at this southernmost position was followed immediately by a full depth zooplankton profile consisting of two hauls with the double Mocness system when steaming back to the Ierapetra-Deep. Along the track, sampling of neuston and chlorophyll from the surface was repeated.

Station work in the Ierapetra-Deep, from April 22 till May 5, started in the evening with two 10 m^2-Mocness tows for the collection of micronekton. They were followed by a CTD/Rosette early the next day to collect water for the measurement of *in situ*-primary production. Until May 5, in total eleven CTD/Rosette casts, three *in situ* primary production casts, two butterfly sampler casts, one station with *in situ*-pumps in the deep-sea and four tows with the hyperbenthic sledge were carried out. Two multiple corers had been scheduled: The haul at the position of the former sediment trap mooring just outside the deep trough was successful, but sediment sampling in the middle of the basin needed a second attempt. The high number of hauls with the 10 m^2-Mocness (14), the 1m^2-Double-Mocness (11) and the neuston net (21) allows for a statistical treatment of zooplankton samples. Different from previous cruises into the Ierapetra Basin, the long-lastening deep tows

with the Mocness systems and the epipelagic sledge were hampered by long-line fishery. Often, the courses above smooth areas of the seabed were blocked and risky tracks had to be chosen.

On May 2, the intrinsic distortion of the one-core cable had worsened so that 10 km of cable of the deep-sea winch had to be paid out at a ship's speed of 10 knots. The resulting eight hours' break of research activities in the field gave the opportunity to head eastward to carry out a CTD/Rosette cast off Karpathos Island. The measurements completed the hydrographical data set for a better assessment of the source of very high values of salinity which were conspicuous at intermediate depths throughout the investigated area. A full depth Mocness haul and three neuston tows were added before heading back to the Ierapetra-Deep which was reached the same day at 2200. In the morning of May 4, after having paid out 73 m of the deep-sea cable with the epibenthic sledge, the conducting cable was distorted again and had slipped out of guide-unit of the winch. After about eighty minutes the sledge was successfully retrieved, but the twisted cable with a number of hitches had to be shortened by about 690 m. During the about four hours of restoration of the winch system, Meteor made a scheduled CTD/Rosette cast at a site contiguous to the Ierapetra-Deep. Upon return to the Deep, the deployment of the epibenthic sledge was repeated, but only three of the five nets could be closed. In the following, all fishing systems were deployed on the shorter cable of winch no. 9 which, however, was sufficient in its lengths for the investigated depths of the forthcoming sites.

On May 5 at 0422, Meteor set out for the Urania-Deep, performing hydrocasts and surface sampling of chlorophyll and zooplankton along the eastward course track. The deep at 35°14'N, 021°28'E was reached on May 6 at about noon. All sampling systems were deployed in this third main area of biological research except for the 10 m^2-Mocness and the hyperbenthic sledge. Extra water samples with the CTD/Rosette and the butterfly sampler were taken close to and within the highly saline brine and also in the brine/sea-water interface, supplementing a sediment record with the multiple corer. On May 7, northeasterly winds force 7, causing rough sea for 36 hours, the only period of noticable wave action, led to the loss of the *in situ* primary production assembly so that no data on carbon production will be available from this area.

In the morning of May 8, Meteor started for the second track towards the Libyan cost, repeating the sampling routine of the first section situated further to the east. On May 11 at 1200 local time, the last station along the track was finished (1m^2-Double-Mocness, CTD/Rosette), and Meteor entered the Strait of Sicily. En route, three sites were sampled by means with the CTD/Rosette, the surface water sampler and the neuston net. Early in the morning of May 13, the last working position east of Sardinia was reached. A 1m^2-Double-Mocness haul, two neuston tows and a CTD/Rosette cast were carried out. At 0900 the station work was finished. After a smooth voyage Meteor arrived at port of Malaga/Spain on Sunday morning, 16 May 1999.

5 Preliminary Results

5.1 Preliminary Results of Leg M44/1

5.1.1 Oceanography

(T. Jennerjahn, A. Cremer)

A mooring system consisting of two PARFLUX MARK 7G-21 sediment traps was deployed in the Ierapetra Deep off Crete (34°25.90'N, 26°10.75'E, 3750 m water depth). It was designed to collect settling particles from 700 m and 2700 m water depth in preprogrammed time intervals of 3.5 days from January 30 to April 13, 1999 (Tab. 4, Fig. 11). Initial filling of the sampling cups was deionized water with 35 g l^{-1} NaCl and 3.3 g l^{-1} $HgCl_2$ added to avoid organic matter decomposition. It was planned to recover the mooring during cruise M44/4.

Major goal of the project is to investigate externally forced material fluxes to the deep eastern Mediterranean and its relevance for deep sea biology. Analyses of bulk composition and organic compounds of settling particles will provide information on the sources, alteration, transport paths and transport processes of the organic matter. Moreover, it will allow to quantify carbon fluxes to the deep Mediterranean.

Tab. 4: Rotation schedule mooring system MID (Mediterranean Ierapetra Deep). Sampling interval 3.5 days, sampling period 73.5 days.

Cup	Open		Close	
No.	Date	Time (h)	Date	Time (h)
1	30.1.99	0.01	2.2.99	12.01
2	2.2.99	12.01	6.2.99	0.01
3	6.2.99	0.01	9.2.99	12.01
4	9.2.99	12.01	13.2.99	0.01
5	13.2.99	0.01	16.2.99	12.01
6	16.2.99	12.01	20.2.99	0.01
7	20.2.99	0.01	23.2.99	12.01
8	23.2.99	12.01	27.2.99	0.01
9	27.2.99	0.01	2.3.99	12.01
10	2.3.99	12.01	6.3.99	0.01
11	6.3.99	0.01	9.3.99	12.01
12	9.3.99	12.01	13.3.99	0.01
13	13.3.99	0.01	16.3.99	12.01
14	16.3.99	12.01	20.3.99	0.01
15	20.3.99	0.01	23.3.99	12.01
16	23.3.99	12.01	27.3.99	0.01
17	27.3.99	0.01	30.3.99	12.01
18	30.3.99	12.01	3.4.99	0.01
19	3.4.99	0.01	6.4.99	12.01
20	6.4.99	12.01	10.4.99	0.01
21	10.4.99	0.01	13.4.99	12.01

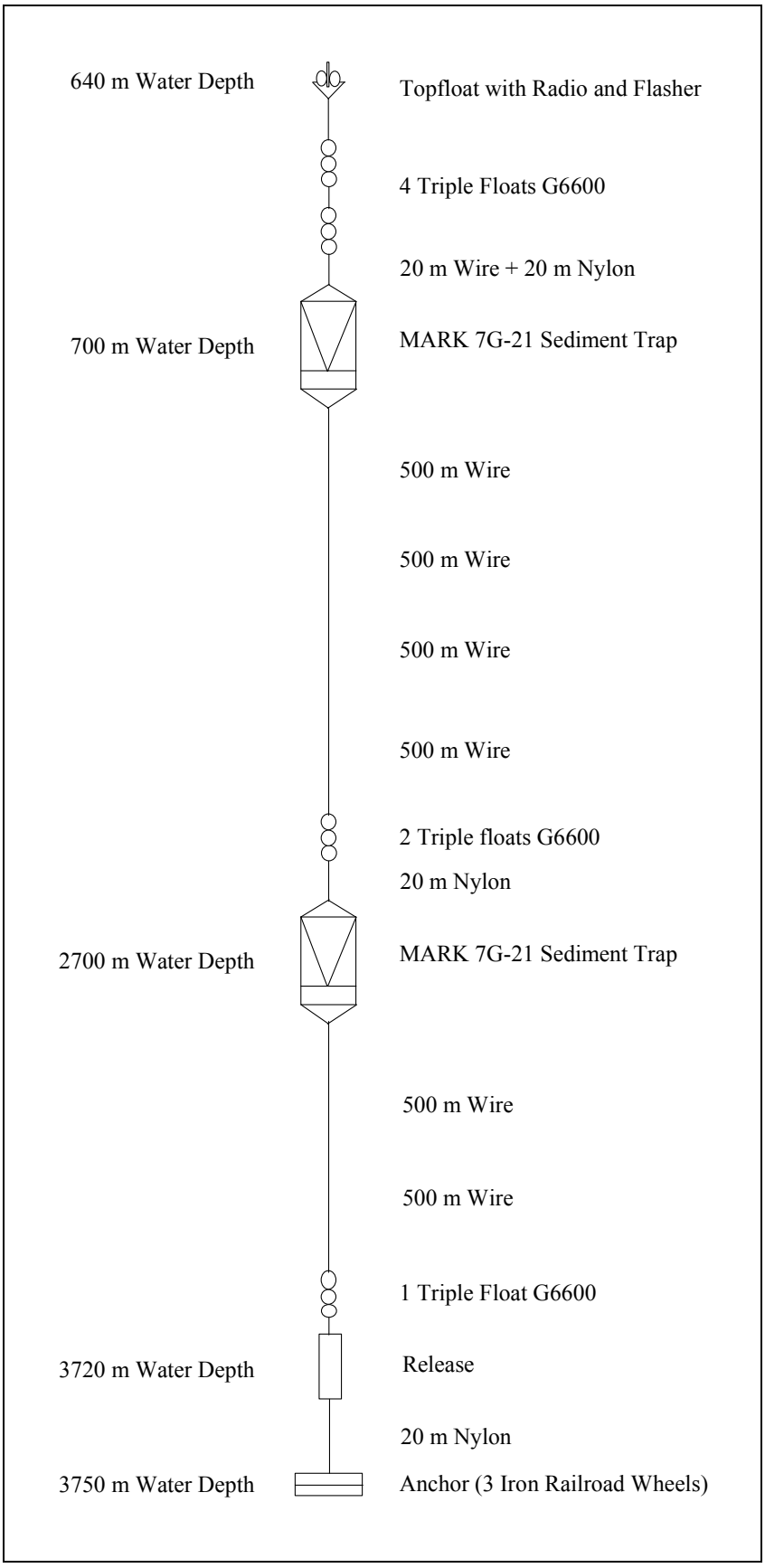

Fig. 11: Mooring system MID (Mediterranean Ierapetra Deep).

5.1.2 Geology

5.1.2.1 Morphology and Structural Geology

(N. Cagatay, I. Kuscu, A. Okay)

The Sea of Marmara is a 270-km long and 80-km wide intracontinental sea on a waterway between the Mediterranean and the Black Seas (Fig. 12). It is connected to the low salinity (S=18‰) Black Sea via the Istanbul (Bosphorus) Strait and to the normal marine (S=38.5‰) Aegean Sea via the Çanakkale (Dardanelles) Strait; these two straits have sill depths of -65 and -35 m, respectively.

The Sea of Marmara Basin has a relatively broad shelf in the south and a narrow one to the north with the shelf break located at a depth of about -100 m (Fig. 12). Between the shelves are three rhomboidal or wedge-shaped, NE-SW trending basins with a maximum depth of 1280 m. They are the Tekirdag , the Central and the Çýnarcýk basins that are separated by bathymetric ridges rising about 600 m above the basins (Barka and Kadinsky-Cade, 1988; Wong et al., 1995). The morphology of the Sea of Marmara is determined by the interaction of the dextral strike-slip tectonics of the North Anatolian Fault (NAF) and the N-S extensional Aegean regime prevailing in northwestern Anatolia (McKenzie, 1972; Dewey and Sengör, 1979; Sengör et al., 1985; Taymaz et al., 1991). As a result of the N-S extension the NAF has splayed in the Sea of Marmara region and formed the three deep strike-slip basins and the intervening bathymetric ridges. According to recent GPS measurements, the dextral displacement with respect to Istanbul along the NAF in the southern Marmara region is about 20 mm/yr, with the slip vectors showing an anticlockwise rotation when going from east to west (Straub and Kahle, 1997)

The Sea of Marmara was formed on a complex basement that consists of various Mesozoic units and the Eocene to Miocene rocks of the Thrace basin (Görür et al., 1997). The onset of its opening is marked by the arrival in the Marmara region of the westward propogating NAF, probably during the latest Miocene-Pliocene, when the Mediterranean waters briefly invaded the future Sea of Marmara along the shear zone of the incipient NAF (Sengör et al., 1985; Görür et al., 1997; Okay et al., 1999). Being on the waterway between the Mediterranean and the Black Sea (and its pre-Quaternary ancestor, Para-Tethys), its paleogeography and paleoceanography have been controlled by its connection with or isolation from the two adjacent basins with contrasting water chemistries (Görür et al., 1997; Çagatay et al., submitted).

The most active northern branch of the NAF is the Ganos Fault, which is responsible for the development of the Tekirdag and the Central basins (Wong et al., 1995; Okay et al., 1999). On land, NE of the Gelibolu Peninsula, it has a 45-km-long transpressive segment, north of which a prominent topographic high, the Ganos Mountain (924m), has developed as an uplifted block (Okay et al., 1999). This fault continues further west forming the southern margin of the Gulf of Saros in the northern Aegean Sea with a switch in its dip towards NW (Çagatay et al., 1998). The Ganos Fault occupies a submarine valley on the western slope of the Tekirdag Basin and forms a 2- to 3-km-wide disturbed zone on the basin floor, where it becomes transtensional and dips north at 70° (Okay et al., 1999).

The three deep Marmara basins are bounded at the shelf break in the north and south by faults (boundary faults) dipping south and north, respectively. The Tekirdag Basin is a 1155-m-deep, rhomb-shaped depression, with an area of 220 km^2. It is bounded by a 1.1-km-high prominent bathymetric escarpment (northern boundary fault) dipping south at 11- 23° (Okay et al., 1999). The southern slope of the basin is less inclined (6-7°) and is intercepted by submarine canyons. The boundary faults are connected at depth below the Tekirdag Basin forming a detachment plane

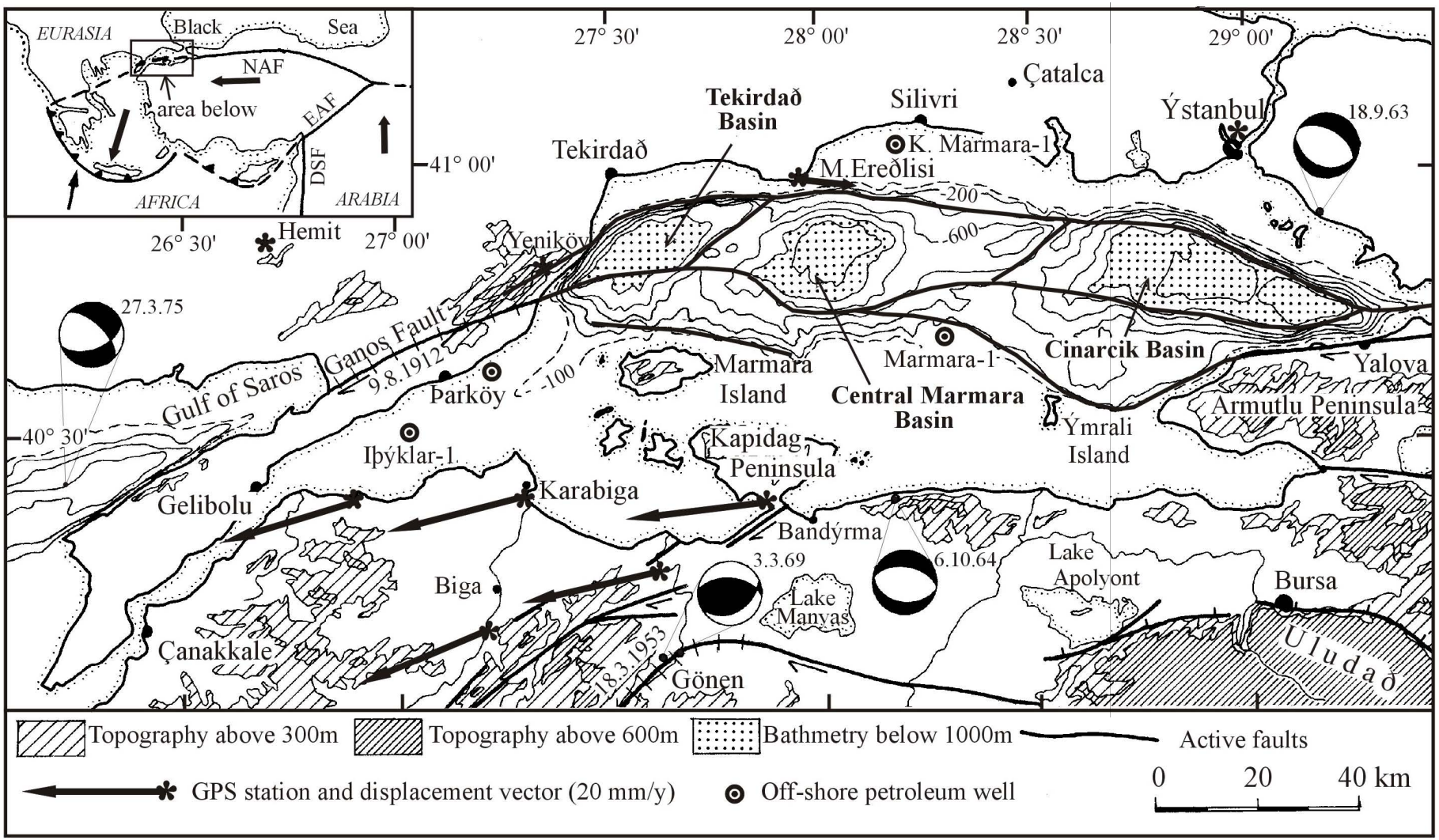

Fig. 12: Structural and bathymetric map of the Sea of Marmara.

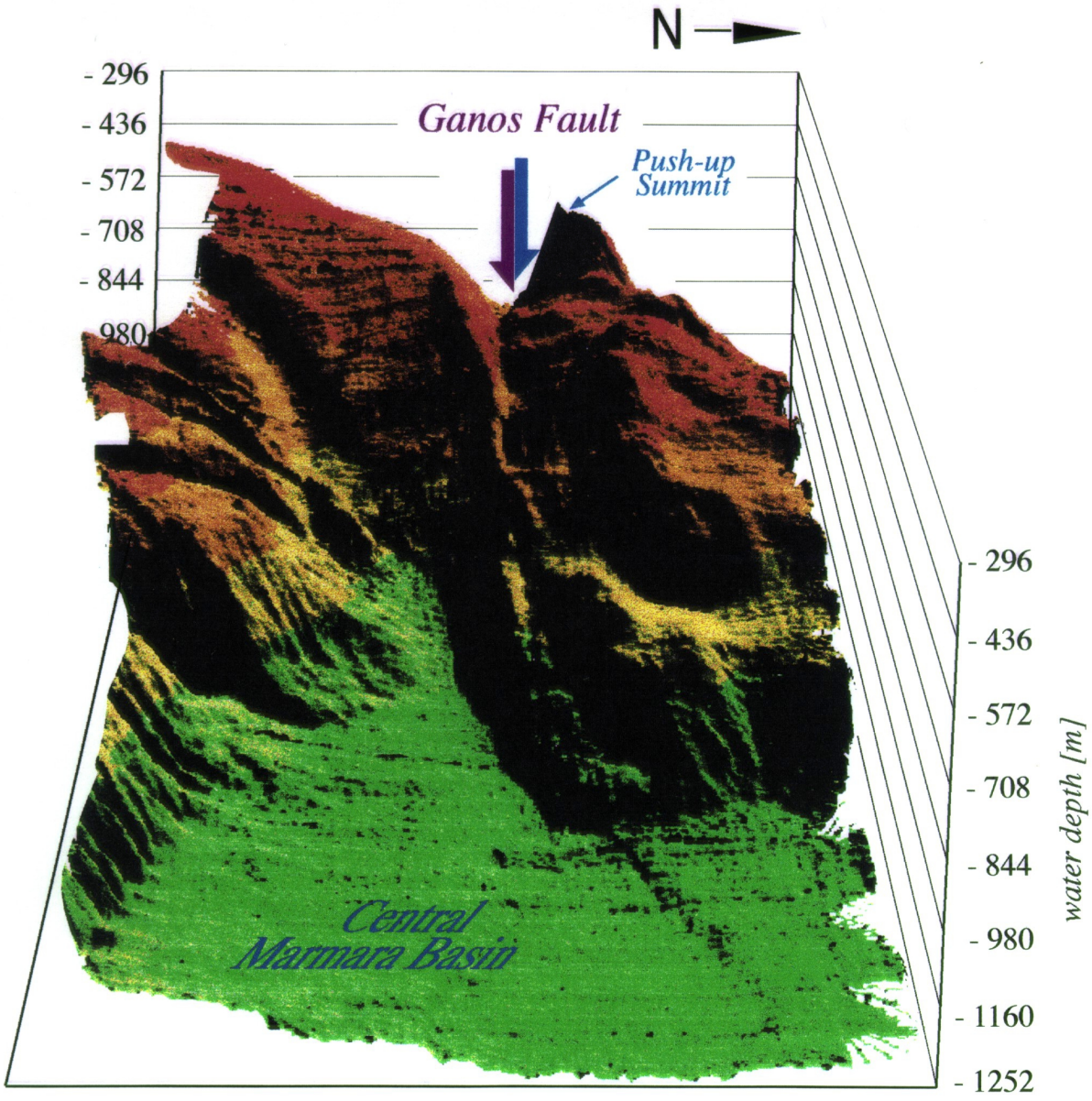

Fig. 13: 3-D view (seen from E to W) of working area A surveyed during Meteor Leg 44/1. Note the prominent furrow in the central push-up structure caused by the Ganos Fault.

beneath the sole of the Plio-Quaternary sediment infill (Okay et al., 1999). The transtensional, sub-vertical segment of the strike-slip Ganos Fault in this basin cuts the detachment plane at depth and, together with the northern boundary fault, forms a negative flower structure.

Eastwards the Ganos Fault splits into E- and NE-trending branches (Okay et al., 1999). The former branch forms the southern boundary of the Central Marmara Ridge between the Tekirdag and the Central Marmara basins, with a deep (-770 m) furrow well marked in the bathymetric map obtained during the Meteor Leg 44/1 (Fig. 13). The Central Marmara Ridge has rather a rugged relief with transpressive structures, such as pressure ridges, folds and thrusts (Wong et al., 1995). This ridge rises up to –440 m and is characterized by a low sedimentation rate compared to the deep basins.

The Central Marmara Basin is a 1280-m-deep, rhomb-shaped depression with an area of about 290 km^2. This basin has a similar structure to that in the Tekirdag Basin, with a transtensional segment of the Ganos fault and the two boundary faults in the north and south. Here, the Ganos

fault appears to form a 500-m-wide and 40-m-deep, young graben structure, as observed in the PARASOUND lines (Fig. 13).

The Çýnarcýk Basin is a wedge-shaped basin between two branches of the NAF in the east of the Marmara Sea. It has a depth of -1276 m and an area of about 810 km^2. The northern margin of this basin is marked by a fault segment striking at about 120°. The southern margin is a coastal fault north of the Armutlu Peninsula. Both faults are believed to have a normal dip-slip as well as a strike-slip component (TAYMAZ ET AL., 1991). This basin is bordered to the west by the transpressive Eastern Marmara Ridge.

The deep basins are filled with up to 2.5-km-thick, syn-transform Plio-Quaternary sediments, showing SW dipping reflectors in the case of the Tekirdag Basin (OKAY ET AL., 1999) and flat lying reflectors in the Central and Çýnarcýk basins (SMITH ET AL., 1995).

The 30-km-wide southern shelf is characterized by E-W to ESE-WNW striking and N dipping normal faults and associated half grabens (SMITH ET AL., 1995). The most notable normal faults are located along the northern coast of the Kapýdag Peninsula, north of the Imralý Island and along the coast between Bandýrma and Gemlik. The greater width of the southern shelf is due to a large catchment area of the Sea of Marmara basin in the south and trapping of the sediments in the half grabens on the shelf. Major rivers (Kocaçay, Gönen and Biga) drain only from the south with their catchment area constituting the major portion of the total catchment area of the Sea of Marmara. These rivers discharge a total of 2.2 x 10^6 t/yr of suspended sediment and 5.80 km^3/yr freshwater to the basin (EÝE, 1993). The onshore area south of the Sea of Marmara is characterized by ENE-WSW trending strike-slip faults and E-W and ESE-WNW trending normal faults.

5.1.2.2 Sea Floor Observations

(T. Kuhn)

Video surveys of the sea floor were carried out along the prominent furrow structure which the Ganos Fault has cut through the central push-up of the central Sea of Marmara (Figs. 12 & 13). The main task was to detect gas or fluid emanation sites. Especially methane emanation sites were concluded from high gas concentrations in the lowermost water column. They were detected in CTD/rosette samples taken and analyzed during the cruise prior to the video survey (see chapter 5.1.4.1).

The sea floor along the Ganos Fault is completely covered by sediments. The most prominent feature of the sea floor is the high density of marks and traces of benthic fauna. They mainly consist of holes more than 10 cm wide and about 10 cm deep which follow close together during all of our surveys (a total of 12 stations).

Methane emanation sites were also detected. They appeared along the Ganos Fault and are characterized by grayish mats some square meters wide which may consist of bacteria and sulfide precipitates (Fig. 14). Outside the Ganos Fault such mats could not be found.

Furthermore, slumping structures occur beneath the steep slope of the push-up summit north of the fault (Fig. 13). Ripple marks due to constant near-bottom currents as they might be concluded from the bathymetry along the Ganos Fault were not discovered.

Fig. 14: Picture of the sea floor taken with the HBS during the cruise M 44/1. The light and black coloured patches are composed of bacterial mats and sulfur. They probably mark the emanation site of methane. The holes around the patches are due to the activity of benthic organisms. The whole sea floor of the Sea of Marmara is characterized by a high density of such benthic traces.

5.1.3 Sediments

5.1.3.1 Core Descriptions

(T. Kuhn, S. Richter, O. Algan)

During the cruise M 44/1 the first long piston cores (up to 13 m lenth) were recovered from the deep basins and the push-ups within the Sea of Marmara (Fig. 15). Multicorer stations were carried out at the locations of the piston corer in order to get undisturbed samples of the uppermost 10 to 30 cm. Moreover, sediment structeres were mapped with the Parasound system (3,5 to 4,5 kHz; 60 km profile length) in order to distinguish between pelagic and turbiditic sequences prior to sediment sampling.

Sediment samples were taken along the Ganos Fault, on the central push-up summit, the push-up plateau, in the deepest parts of the Tekirdag, Central Marmara and Cynarcik Basins as well as beneath the northern and southern continental slopes (Fig. 15). A total of 22 piston corers with 178 m sediment recovery as well as 29 Multicorer samples were recovered during the cruise.

Sediment sampling aims at two scientific objectives: first to analyse the interaction of rising gas and/or fluid fronts within the sediment column along the Ganos Fault, second to examine the paleoceanographic development of the Sea of Marmara in relation to glacial-interglacial changes.

The sediments from the Ganos Fault consist of greenish gray silty clay with grayish olive clasts and graded layers which hint to turbidites. In some parts of the sediment column they are finely laminated (Fig. 16).

Sediment cores for the paleoceanographic examinations were recovered from the Tekirdag Basin (10 KL, 11 KLG[1] (KL: Piston Corer FU Berlin; KLG: Piston Corer Uni Göttingen)), the push-up summit (17 and 18 KL), the plateau northeast of the summit (20 KLG, 21 KL) as well as along a fault structure (33, 40 and 73 KL; Fig. 15).

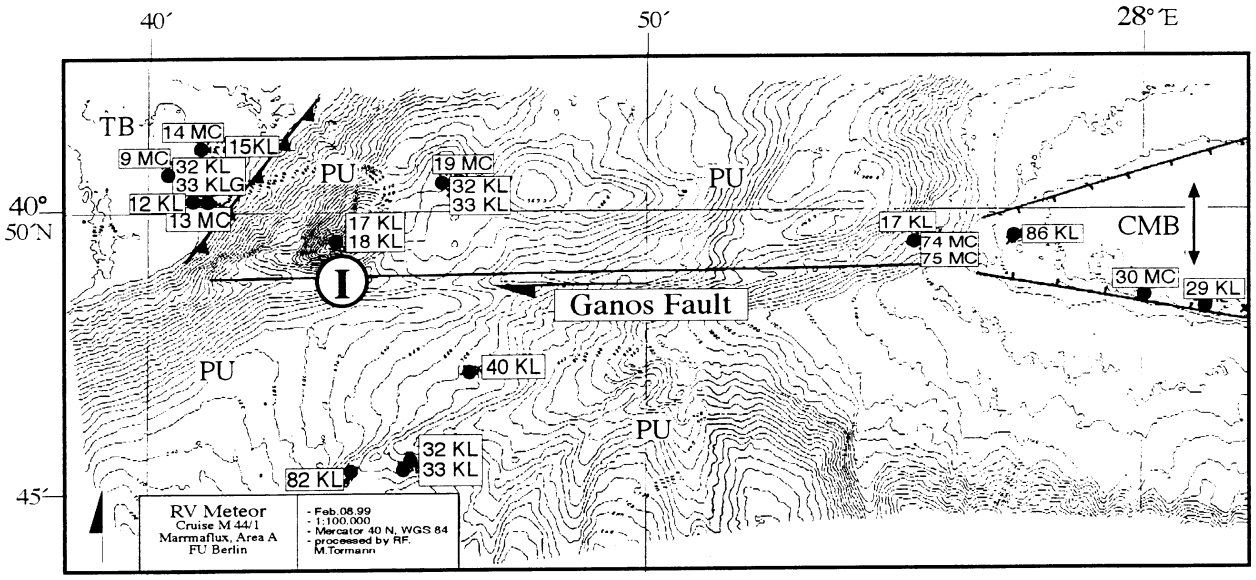

Fig. 15: Locations of the sediment stations carried out during M 44/1 and their relation to the local tectonics of the central Sea of Marmara (working area A - see Fig. 1). Sediment cores were taken along the Ganos Fault (I), on the push-up (PU) summit, the push-up plateau and in the deep basins (CMB: Central Marmara Basin; TB: Tekirdag Basin).

The sediments are mainly composed of silty clay. The sediment surface is characterized by an olive-brownish, oxic layer. The layers following downwards are oliv-gray, olive-black and greenish gray. Blackish-brown laminae (less than 1 mm thick), silty laminae (more than 1 mm thick), black haloes as well as fine-silty lenses appear in the greenish gray sediments (Fig. 16). The cores from the plateau (20 KLG, 21 KL) contain several black horizons consisting of Fe monosulfides, organic components and clay minerals. These horizons could be interpreted as freshwater deposits since they resemble the banded clays from the Black Sea which were formed under pleistocene freshwater conditions. In-between those layers are sediments which are similar to the recent marine deposits of the Sea of Marmara. Thus, there must have been several changes of the paleoceanographic conditions of the Sea of Marmara between a freshwater lake and an epicontinental marginal sea (HALBACH, 1999).

Cores 20 KLG, 21, 33 and 40 KL contain a tephra layer. Microscopically this tephra is similar to the one of the Santorini Y-2 event which happend 18.000 years ago (KELLER ET AL., 1978). If this first interpretation is correct, the cores containing the tephra would surely reach into Pleistocene deposits. However, a detailled examination of the tephra is necessary to prove this first assumption and to exclude possible relocation processes.

In addition to the mentioned features, there are corse-grained partly graded layers in some of the cores (e.g. 33 and 73 KL). They especially occur at core locations beneath the southern and northern continental slope and may be interpreted as turbidites. Some of the coarse-grained layers contain euhedral pyrites which acount for up to 35% of the sand fraction. This pyrite may be a product of early diagenetic reactions of pore water sulfide and Fe^{2+}.

Fig. 16: (opposite) Core logs of some cores taken during the cruise M 44/1. Note the cores from the deep basin (10 KL, 12 KLG) are rather homogenous compared to the other cores. The black layers in 20 KLG and 21 KL are interpreted as freshwater deposits. Marks of gas bubbles occur in some cores from the Ganos Fault (e.g. 23 and 72 KL). Several silty and sandy layers occur in cores beneath the continental slopes (33 and 73 KL).

S. Richter/O. Algan: Sediment profiles, M 44/1, Sea of Marmara

5.1.3.2 Micropaleontology

(G. Schmiedl, T. Mühlstrasser, T. Bindseil, H. Hübner)

The present oceanography of the Sea of Marmara is controlled by both the eastern Mediterranean and the Black Sea. The inflow of high-saline water from the Aegean Sea into the deep basins of the Sea of Marmara and the low-saline surface water of Black Sea origin cause a marked stratification of the water column. Since only little vertical mixing occurs, oxygen concentrations are rather low in the bottom water and show a decrease from the western to the eastern basins (ALAVI, 1988).

The recent benthic foraminiferal fauna of the Sea of Marmara is typical for eutrophic and low-oxygen habitats and resembles faunas that occur adjacent to sapropel layers in late Quaternary sediments of the eastern Mediterranean (MULLINEAUX AND LOHMANN, 1981; ALAVI, 1988; SCHMIEDL ET AL., 1998). This observation suggests that today´s environmental conditions of the Sea of Marmara may be similar to those that occured during times of sapropel formation in the eastern Mediterranean. It can be expected that changes in the oceanographic influence of both the Black Sea and the Mediterranean Sea are reflected in the microfauna of the Sea of Marmara.

Surface samples (multicorer) and long sediment cores (”Meischner” piston corer) were recovered from four stations in the northwestern Sea of Marmara (Tekirdag Basin, Ganos Fault, “Push Up” east of the Tekirdag Basin) and two stations in the northeastern Sea of Marmara (Istanbul Basin) for high resolution studies of late Pleistocene and Holocene planktic and benthic foraminifera (see chapter 7.1.1). The sediments mainly consist of water-rich and bioturbated hemipelagic mud containing numerous and well preserved foraminiferal tests.

The recent foraminiferal faunas from the surface sediments of the Sea of Marmara are characterized by a dominance of benthic taxa. Planktic foraminifera are less important. The benthic foraminiferal fauna is dominated by infaunal species reflecting the eutrophic character of the Sea of Marmara. Studies from different oceans indicate that most of these species flourish in fine-grained organic-rich sediments of eutrophic habitats. Similar faunas occur in sediments of the eastern Mediterranean Sea just before or after the formation of sapropels and therefore also indicate an adaptation to low-oxygen contents.

Using the “Meischner” piston corer a total of 70.5 m of sediment cores were recovered. According to the preliminary stratigraphy, sedimentation rates are very high in the deep basins exceeding 100 cm / kyr. Fluctuations in the species composition of the fossil foraminiferal fauna indicate significant environmental changes during the Holocene.

The foraminiferal faunas of the core catcher samples exhibit higher plankton to benthos ratios and lower benthic diversities when compared to the recent faunas of the same stations. Like in the surface sediment the benthic foraminifera of the Holocene samples comprise predominantly infaunal species that lived in an eutrophic environment. The differences to the Recent samples indicate Holocene changes in organic matter flux rates and oxygenation that are probably related to changes in the inflow of saline water from the Aegean Sea and changes in the fresh water budget. The higher proportion of planktic foraminifera points to a stronger marine influence via the Dardanelles and a reduced fresh water inflow from the Black Sea as it occurs during times of lower sea level (see AKSU ET AL., 1999).

At station 20 (KL71) several meters of glacial sediments and the complete Holocene were recovered including the sapropel S1 and a prominent tephra layer (most likely the Y-2 layer of Santorini). The estimated sedimentation rate is 15 to 20 cm / kyr. The glacial core catcher sample of KL71 lacks any planktic foraminifera. This sample from the “Push up” contains frequent coarse

sand grains of terrigenous origin. The microfauna consists of a few benthic foraminifera and ostracods. Most of the foraminiferal tests are poorly preserved. A number of the occuring species are restricted to shallow marine habitats (Murray, 1991). This suggests that the fauna is allochthonous and consists of reworked tests that were transported into the basin from the surrounding shelf areas. Previous studies suggest that during the sea level lowstand of the last glacial the Sea of Marmara resembled a lacustrine system that was isolated from the surrounding oceans. At the same time the broad shelf areas in the southern Sea of Marmara were exposed and clastic input increased into the deep basins in the north.

5.1.4 Fluid Chemistry

5.1.4.1 Water Column

5.1.4.1.1 Hydrocarbon Concentration and Distribution

(R. Seifert, O. Schmale)

Methodology

120 water samples taken by a CTD (NB1) equipped with a Rosette system (24 x 10 L Niskin bottles), the HBS water sampling device, or a Multicorer (supernatant) were analysed for their content of volatile hydrocarbons applying a purge and trap technique. Gases are stripped from the sample by precleaned He, concentrated on traps and subsequently released into a gaschromatograph (CARLO ERBA GC 6000) equipped with a packed (activated Al_2O_3) stainless steel column and a flame ionisation detector (FID) to separate, detect and quantify individual components. All analytical procedures were performed on board directly after sampling.

Methane

Work in Area A was concentrated along the morphological prominent track of the Ganos Fault at the Marmara High Block (MHB) that is located between the Tekirdag Basin and the Central Marmara Basin (CMB). Focus was laid on the vicinity of the most elevated points located in the western part of the MHB whereat in total 13 CTD stations were realised:

44 CTD, 45 CTD, 46 CTD, and 43 CTD at the northern slope of the Ganos Fault depression; 34 CTD, 35 CTD, 36 CTD, 22 CTD, 37 CTD, 38 CTD, 39 CTD, and 56 CTD at the centre the of the Ganos Fault depression; 47 CTD at the southern slope of the Ganos Fault depression.

Fig. 17 gives an overview of the methane concentrations observed below 500 m water depth, whereby the stations are arranged according to their relative positions. The methane concentrations are strongly increased at most stations with regard to background concentrations < 1 nmol L^{-1}. Highest concentrations of about 45 nmol L^{-1} were found at a water depth of 700 m for stations 34 CTD and 36 CTD. The similar distribution patterns observed at these stations hint to a common source responsible for the enrichment of methane. However, station 35 CTD, performed in between these two stations, reveals a totally different distribution of dissolved methane. Moreover, the water depths whereat highest methane concentrations occurred and the distribution patterns of dissolved methane at the distinct stations are in general quite different taking into account the close vicinity of their positions. Due to the ruff morphology of the investigated region, a complicated current pattern has to be expected for the deeper water. This might at least partly reason the non-uniform distribution of methane in this area.

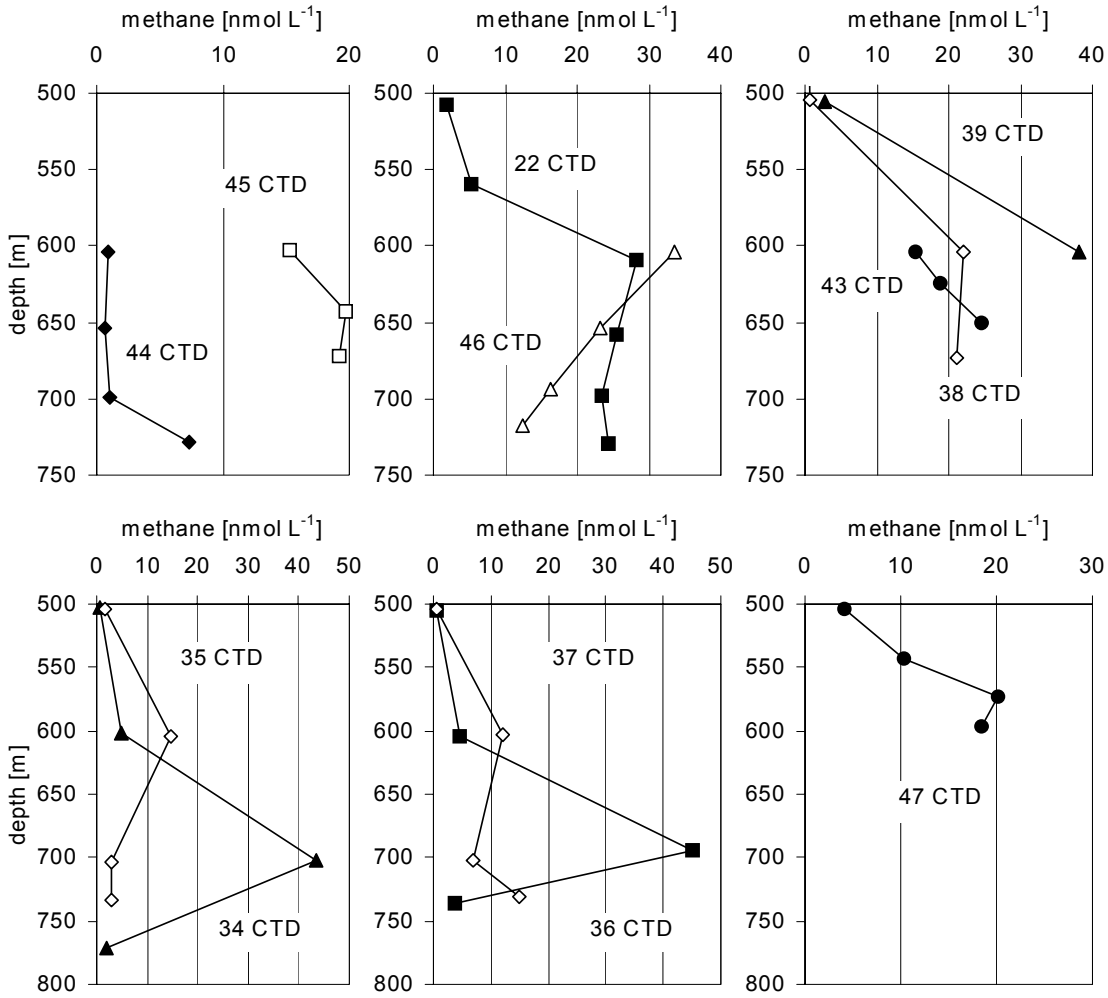

Fig. 17: Methane concentrations vs. water depth in the western part of Area A.

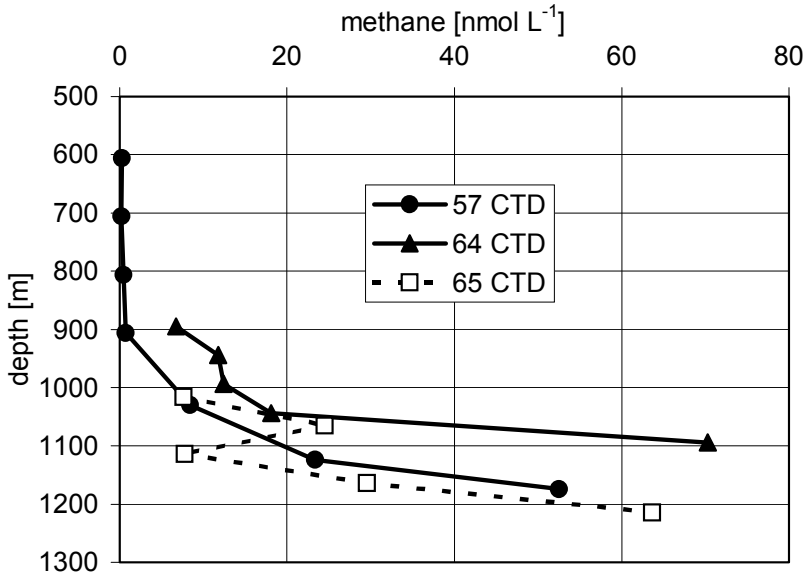

Fig. 18: Methane concentrations vs. water depth above the continuation of the Ganos Fault in the Central Marmara Basin.

Apparently, the western part of Area A is characterised by multiple methane rich seeps, whereby the observed small spatial extension of the distinct methane anomalies argues for a restricted quantity of fluid delivered from the individual sources.

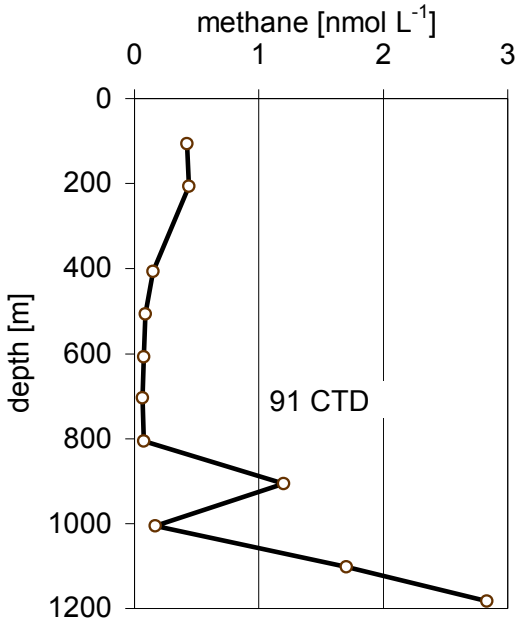

Fig. 19: Methane concentrations vs. water depth, Area B.

Eastern Part of Area A

Three locations were covered by CTD Stations at the eastern rim of the Marmara High Block where the track of the Ganos Fault continues within the Central Marmara Basin, i.e. 57 CTD, 64 CTD, and 65 CTD. All profiles conformably reveal strongly enhanced methane concentrations directly above the seafloor (Fig. 18). 70.3 nmol L^{-1} for the sample from 1094m water depth of 64 CTD are the highest methane concentrations we observed in the deep waters of the Sea of Marmara. As far as we know, equivalent methane enrichments are not reported from this area until now. The height and the relatively wide extension of the methane anomaly indicates the presence of a considerable methane rich vent in the close vicinity of these stations.

Central Marmara Basin

Generally low methane concentrations (< 2.6 nmol L^{-1}) were measured in samples from below 500m water depth of the two stations occupied in the CMB – 26 CTD and 28 CTD. An exception is the increased value of 7.64 nmol L^{-1} found at 700m water depth (26 CTD) that might originate from a source located in the neighbouring MHB. Thus, no indications for considerable methane rich seeps could be observed in the Central Marmara Basin. However, methane concentrations of 5.75 nmol L^{-1} found in surface water at station 28 CTD in the illustrate strong supersaturation with respect to atmosphere of the uppermost about 25m thick water body.

Area B

Only one station was covered by water sampling in Area B. Methane concentrations were found to be relatively low throughout the water column below 25 m depth (Fig. 19) but increase in the deep water column to reach 2.83 nmol L^{-1} directly above the sea floor. Though this concentration appears to be quite low compared to the data from Area A, it indicates recent input of methane from the sediments into the water column also for this part of the Sea of Marmara.

Worth mentioning is the methane content we analysed for the surface water that amounts to 30.2 nmol L^{-1} (not included in Fig. 19), representing an about 15-fold supersaturation with respect to atmosphere. As methane concentrations of the surface layer did not belong to the targets of this expedition, no additional data were raised from the uppermost water body. However, our data indicate that, compared to other regions of the ocean, the Sea of Marmara represents a very strong methane source for the atmosphere.

Non Methane Hydrocarbons (NMHC)

Concentrations of saturated and unsaturated hydrocarbons of carbon chain lengths from 2 to 4 were determined to attain information on the origin of dissolved hydrocarbons. One parameter suitable in this context is the ratio between methane and the sum of NMHC. This ratio has found to be high for microbiological (> 1000) and lower in case of thermogenic methane. However, caution has to be taken using this parameter in the water column. NMHC are known to be produced by photochemical processes. Moreover, high NMHC concentrations have been found below the euphotic zone that might be related to light stressed phytoplankton or microbial activity (SEIFERT ET AL., 1999). Another relevant source of NMHC to be beware of, are mineral oil spills, this especially in areas like the Sea of Marmara that are subject to severe shipping traffic and off shore gas and oil production. Therefore, only data from samples that yield methane concentrations > 20 nmol L^{-1} and for which the above mentioned factors can be regarded as not relevant are included in figure 20. Most of the samples reveal methane/NMHC ratios well below 1000. Highest ratios derive from stations 57 CTD, 64 CTD, and 65 CTD, all located at the transition from MHB to the CMB. Two distinct types of hydrocarbon sources apparently are present in the western part of Area A. One is similar to that observed at the eastern part of Area A and exhibits a relatively low contribution of NMHC (34 CTD and 36 CTD), while the other type is characterised by a high portion of NMHC. The latter is represented by stations 39 CTD, 43 CTD, 46 CTD, and by the investigated HBS and MC stations (52 HBS, 75 MC, 76 MC, 84 MC).

The different hydrocarbon characteristics within the relatively small working area substantiate the above made assumption of multiple seeps. The occurrence of low methane/NMHC ratios indicate an inflow of low temperature thermogenic hydrocarbons, i.e. components cleaved from sedimentary organic matter, into the water column.

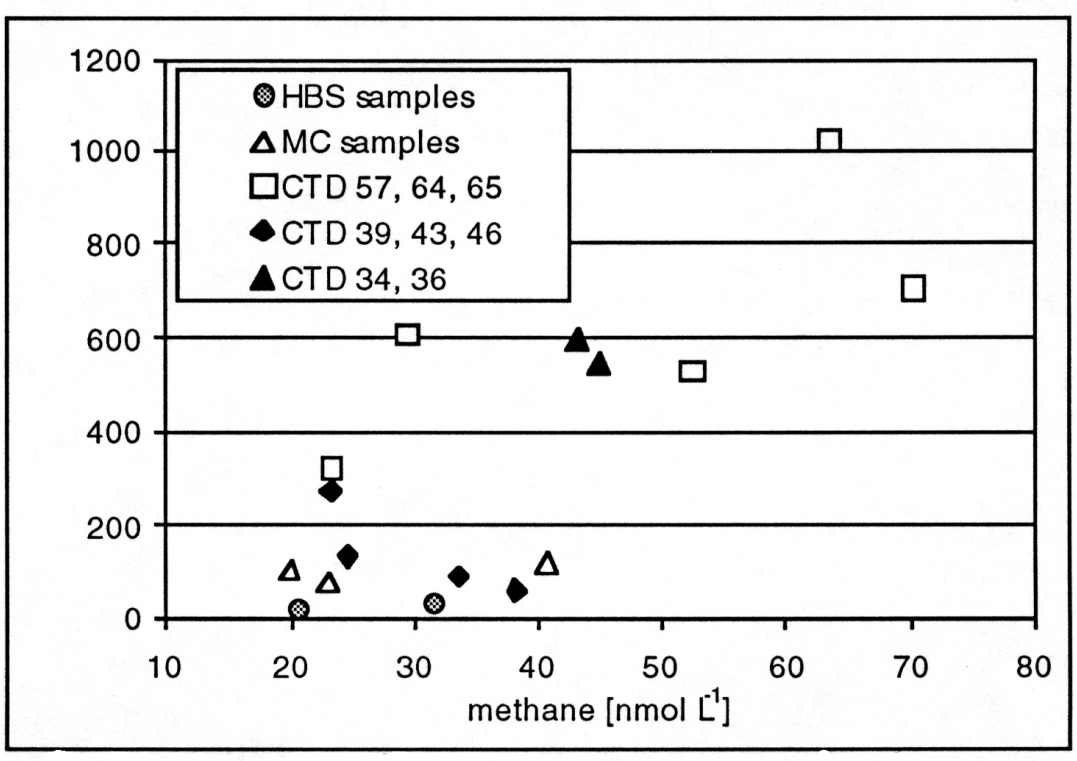

Fig. 20: Methane/NMHC ratio versus methane for selected samples.

5.1.4.1.2 Manganese and Oxygen Measurements

(A. Koschinsky, C. Arndt)

a) Determination of dissolved manganese

The electrochemical method of voltammetry can easily be carried out onboard ship and can yield very low detection limits in the ppb- or sub-ppb-range. However, the analyses are time-consuming (about 20-30 minutes per element and sample), and care has to be taken concerning possible contamination sources during sampling and sample handling. Therefore, only manganese was determined onboard in order to use it as a tracer for diagenetic or hydrothermal signals.

Instrumentation and chemicals

The instrumentation used for the voltammetric analyses and the sample pretreatment is from Metrohm (Switzerland): 693 VA Processor with 694 VA Electrode Stand (Ag/AgCl – 3 M KCl reference electrode and platinum auxiliary electrode) and a 705 UV Digester. For the pH control of the solutions, a WTW 537 microprocessor pH-Meter with an Ingold pH electrode was used. All chemicals used were Suprapure (Merck) or at least analytical grade quality. Nitrogen 5.0 was used for the deairation of the solutions.

Sample pretreatment

The water samples from the CTD and HBS stations were filled into cleaned PE bottles immediately after recovery. First, pH, Eh, dissolved oxygen (when possible), conductivity and alkalinity were determined in an aliquot of the sample. Samples from close to the seafloor were then filtered through 0.2 µm membrane filters. 100 ml of the sample were acidified with 0.2 ml hydrochlorid acid (final pH about 2) and used for onboard Mn analyses and stored in the cool room for further cation analyses in the home laboratories. To destroy interfering organic material, the fresh water samples were digested one hour by UV irradiation. 20 µl hydrochloric acid and 50 µl hydrogen peroxide were added to 10 ml samples in quartz vessels, and the temperature during the irradiation was set to about 85 °C.

Mn^{2+} determination

Depending on the expected concentration, 1-10 ml of the UV-digested water sample were pipetted into the voltammetric cell and eventually made up to 10 ml with Millipore water. 1 ml of 1 M ammonia buffer (pH 10) and 0.5 ml of sodium tetraborate buffer (saturated, pH 9.4) were added to the sample. After purging 5 minutes with nitrogen, the determination procedure was started. Accumulation was done at –1700 mV for 60 seconds, and stripping was done in the differential pulse mode at a scan rate of 12 mV/s. The manganese peak appears around –1450 mV. The measurement was repeated, and then 20-100 µl of a 1 ppm Mn standard solution were added. After a double measurement, a second standard addition was carried out and measured.

b) Results

Dissolved manganese could be detected in most of the CTD samples (between <1 and 6 ppb). At the first 3 stations samples between the surface and the bottom were chosen to get an idea of the general Mn distribution in the water column. Measured concentrations range between 0.5-2 ppb at the surface and up to 6 ppb in the samples closest to the bottom. Stations 26 and 28 CTD in the Central Marmara Basin with a water depth > 1200 m show a strong Mn increase at depth which is

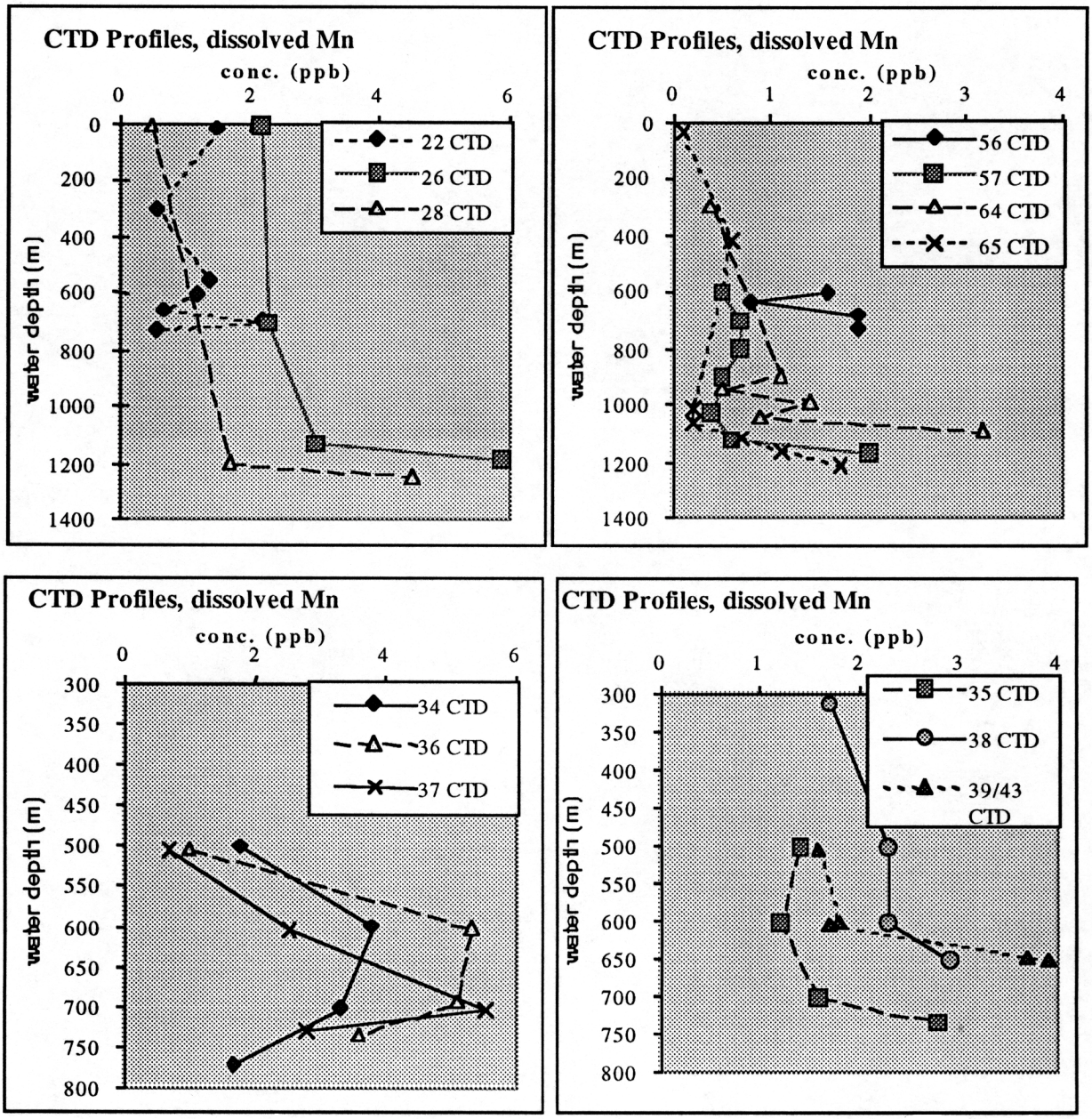

Fig. 21: Dissolved Mn distribution in the water column, as determined at several CTD stations.

typical for diagenetic Mn mobilization from the surface sediment. The somewhat unusual Mn profile of 22 CTD in the western part of the Ganos fault at 730 m maximum depth was confirmed by the higher resolution profile of station 37 CTD at the same location; here the highest Mn value was measured in the sample taken several tens of metres above the seafloor, while the lowermost sample and the ones taken at lower water depth showed significantly smaller Mn concentrations. Similar Mn profiles were observed at stations 34 and 36 CTD, in consistency with the methane profiles (chapter 5.1.4.1.1). In contrast, at stations 35, 38 and 39/43 CTD the highest Mn concentrations (up to 4 ppb) were measured in the lowermost samples, although these stations are located at similar positions and all exhibit a water depth < 800 m. The deeper profiles (< 1000 m) of stations 57, 64 and 65 CTD which are located at the transition of Ganos fault and Central Marmara Basin again show Mn enrichment at depth and low concentrations at the surface, like stations 26 and 28 CTD. This is well in agreement with methane enrichments at depth at these stations (chapter 5.1.4.1.1).

The reason for the two different types of Mn profiles which coexist on a rather small scale within the Ganos fault is not clear. However, we can summarize that no direct hint for hydrothermalism was found; Mn profiles, especially in the Central Marmara Basin, indicate diagenetic Mn enrichment at depth. No sulfide was detected in any of the CTD samples from the water column.

5.1.4.1.3 REE Sampling

(A. Knappe)

Water samples were taken from different depths with the CTD rosette. Sample volumes of about 10 l of seawater were filled into Nalgene bottles and immediately filtered through 0,2 µm cellulose acetate membrane filters. The filters were mounted in a Nalgene filter holder and with a peristaltic pump the water was pressed through with a delivery range of 100 ml/min. The first 0,5 l of each seawater sample were passed through the filter to cause a self contamination of the filter holder. Because of the low particle concentrations in seawater only one or two filters were needed for a 10 l sample.

Tab. 5: Sampling data

Station/ Sample	Pore water	Sea water	Position		Depth (cm)	Depth (m)
			Lat.	Long.	Sediment	Water Column
9 MC		x	40°50,63	27°40,20		1087
14 MC/1	x		40°51,11	27°40,84	7-9	
14 MC/ 2	x		40°51,11	27°40,84	20-50	
22 CTD/ 1		x	40°48,86	27°44,02		13,5
22 CTD/ 2		x	40°48,86	27°44,02		408
22 CDT/ 3		x	40°48,86	27°44,02		609
22 CTD/ 4		x	40°48,86	27°44,02		729
23 KL/ 1	x		40°48,85	27°43,99	50-60	
23 KL/ 2	x		40°48,85	27°43,99	565-585	
40 KL/ 1	x		40°47,12	27°46,31	226-266	
40 KL/ 2	x		40°47,12	27°46,31	460-506	
46 CTD/ 1		x	40°48,71	27°43,98		694
46 CTD/ 2		x	40°48,71	27°43,98		717
47 CTD/ 1		x	40°48,22	27°44,78		573
47CDT/ 2		x	40°48,22	27°44,78		597
71 MC/ 1		x	40°48,83	27°43,98		
71 MC/ 2	x		40°48,83	27°43,98	0-7	
71 MC/ 3	x		40°48,83	27°43,98	37-45	
81 MC/ 1		x	40°45,51	27°43,00		28
81 MC/ 2		x	40°45,51	27°43,00		28

Pore water samples of 70-230 ml volume were collected from oxic and anoxic sediment cores. The pore water samples were filtered to avoid any possible contamination. For this filtration we used 0,2 µm syringe filters mounted on one way polypropylen syringes.

The filtered waters were acidified with 6 M HCl until a final pH between 1,9 and 2,1 was reached. A Thulium-spike was added to each sample to determine the recovery of the rare earth elements. With a method described by BAU & DULSKI (1996) the REE were preconcentrated by passing the water samples with a flow rate of 18 ml / min through Sep-PakâC$_{18}$ cardridges (Millipore corp. USA) loaded with an exchange column. The REE were quantitativlely complexed by the mixture of HDEHP + H_2MEHP.

The loaded cartridges were purged with 15 ml 0,1 M HCl to remove remaining matrix elements and than eluated with 6 M HCl. This solution was evaporated to incipient dryness, again taken up with 1 ml 5 M HNO_3 and filled up to a volume of 10 ml. The elements Ru and Re were added for correction of instrumental drift. Measuring the REE will be carried out with ICP-MS as described by DULSKI (1994).

Only ultrapure reagents were used throughout the complete procedure.

5.1.4.2 Pore Water

5.1.4.2.1 Sampling Procedure and Treatment of Pore Water

(A. Hübner, R. Moche)

The pore waters of both piston corer and multicorer sediments were obtained using a gas pressure pore water squeezer (SCHLÜTER, 1990). This all-PTFE device with a volume of 110 cm^3 of each sample compartment allows one-step pore water squeezing and microfiltration (0.2 µm). To prevent oxidation of sub- or anoxic porewaters, sediments were squeezed in inert gas (Ar) atmosphere and at a room temperature of 10°C.

After core retrieval, multicorer sediments were subsampled and squeezed immediately or within a maximum time of 12 h. Piston corer sections were kept in glove bags under Ar atmosphere and were squeezed subsequently. However, reduced species of S and Mn were obviously oxidized during continuing storage of the section (max. 2 days). A maximum of 12 samples may be squeezed in one run, but since the pore water yield of one squeezer compartment was usually too low, 2 or even 3 squeezer compartments were filled up with the same sediment sample in order to get enough pore water. The remaining sediment was kept and stored under Ar atmosphere for further geochemical investigation in the home laboratories.

Aliquots of pore waters were analysed immediately after squeezing for H_2S, Mn and HCO_3 contents, the remaining volume was stored for anion and cation analysis with the cation sample acidified with HNO_3 to pH 2.

5.1.4.2.2 Vertical Distribution of Eh and pH

(A. Pekdeger, A. Knappe, T. Kuhn)

The sediments recovered along the Ganos Fault are rather homogenous. The decision where to take pore water samples was therefore made on the basis of Eh and pH measurements. Those measurements were carried out with penetration electrodes. The Ganos sediments are characterized by the following Eh profile:

The corrected Eh value of the surface sediment is larger than 100 mV (based on the standard hydrogen electrode). Within the first 100 cm below surface, Eh decreases to about 10 mV (Mn^{4+} reduction zone), between 100 and 200 cm bsf Eh rapidly drops to -150 mV (Fe^{3+} reduction zone) and finally it continually lowers to -250 mV at the bottom of the core (see Fig. 20). This general Eh trend could be detected in all cores from the Ganos Fault.

The pH values showed only small variations within the sediment column ranging between 7.30 and 7.60. There was no clear correlation between the Eh and pH profiles.

5.1.4.2.3 Concentration and Vertical Distribution of Methane and Hydrogen

(R. Schmahljohann)

Sediment subsamples were taken by cut-off 5 ml syringes from piston corer cores immediately after opening. These subcores were injected into 25 ml vials filled with 5 ml of double saturated NaCl solution, which were quickly sealed afterwards. The vials were intensely shaken until the sediment was homogeneously suspended and left for equilibration with the headspace for at least two hours. By the high salt concentration microbial activity was inhibited and the solubility of the gases was reduced nearly completely. Methane and hydrogen in the headspace were separated by gas chromatography on a 3 m x 1/3" Porapak Q, 80-100 mesh column at room temperature, using nitrogen as the carrier gas. The gases were detected using a Figaro TGS 711 solid-state detector. Gas contents per sediment volume were corrected for water content to give gas concentrations in the pore water.

Water content of the sediment:
Sediment subsamples taken with a cut-off 5 ml syringe were weighed, dried for 24 h at 100°C and weighed again. Water content in % (w/w) was calculated from wet weight and dry weight of the samples.

Analysis of bacterial populations:
Water samples of different depths were taken from Niskin bottles. 330 ml samples were fixed with 1 % formaldehyde (final concentration) for the analysis of total bacterial number and biomass by epifluorescence microscopy. Samples of 2 l were filtered for qualitative analysis of the bacterial community by molecular ecological methods.

Sediment samples of selected layers were taken for later investigations of the microbial population.

Examples of the methane and hydrogen concentrations of two cores with different locations are given in Fig. 22. It is obvious that the sediments taken in the Ganos Fault (23 KL) have much higher methane concentrations in the pore water than those taken outside the fault zone (e.g. 12 KLG from the Tekirdag Basin).

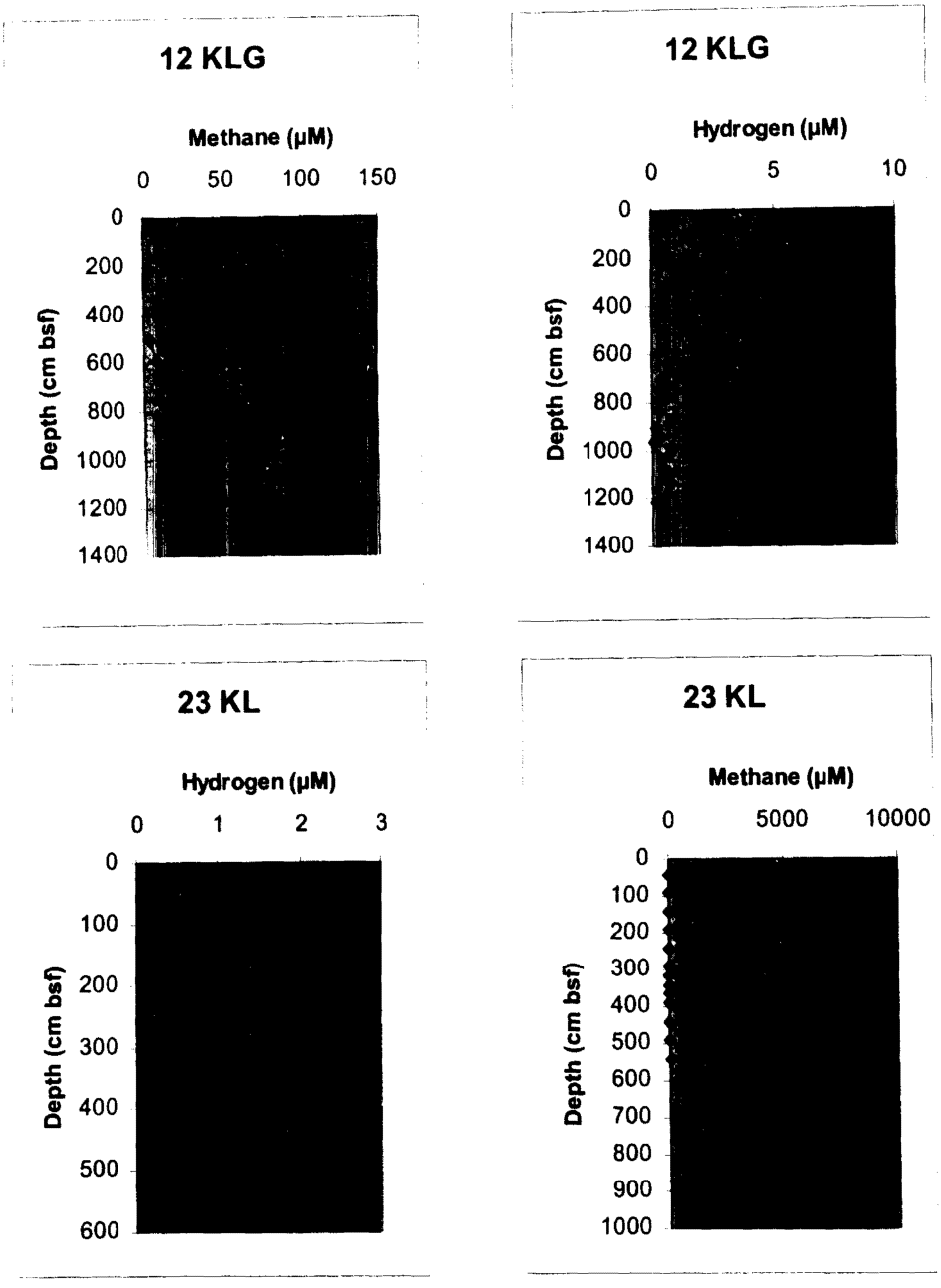

Fig. 22: Methane and hydrogen concentrations in pore water of two sediment cores. Note that the methane conc. in 23 KL (Ganos Fault) is much higher than that in 12 KLG (far away from the fault zone) whereas the hydrogen concentrations are rather similar.

5.1.4.2.4 Bicarbonate Concentrations

(A. Winkler)

A survey on the bicarbonate concentrations was done in order to see if it will serve as an indicator for chemical changes introduced by ascending thermal waters. This kind of survey was done in the water column, using the samples from the CTD log as well as pore waters from the four multi corer stations and two piston core samples. For the determination of the bicarbonate concentration of pore waters a micro device was established to do the measurement in minimalized sample volumes off about 150 µl.

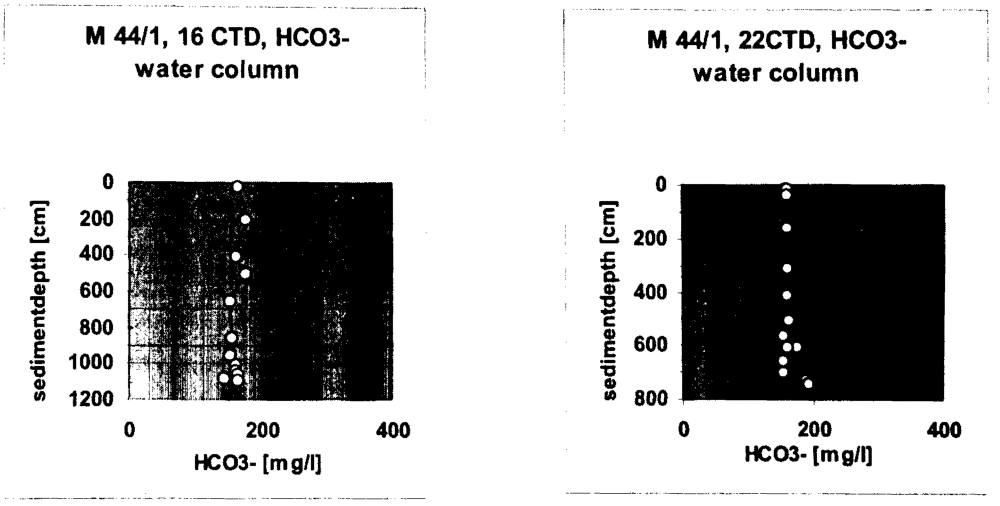

Fig. 23: Bicarbonate concentration in the water column at two CTD stations.

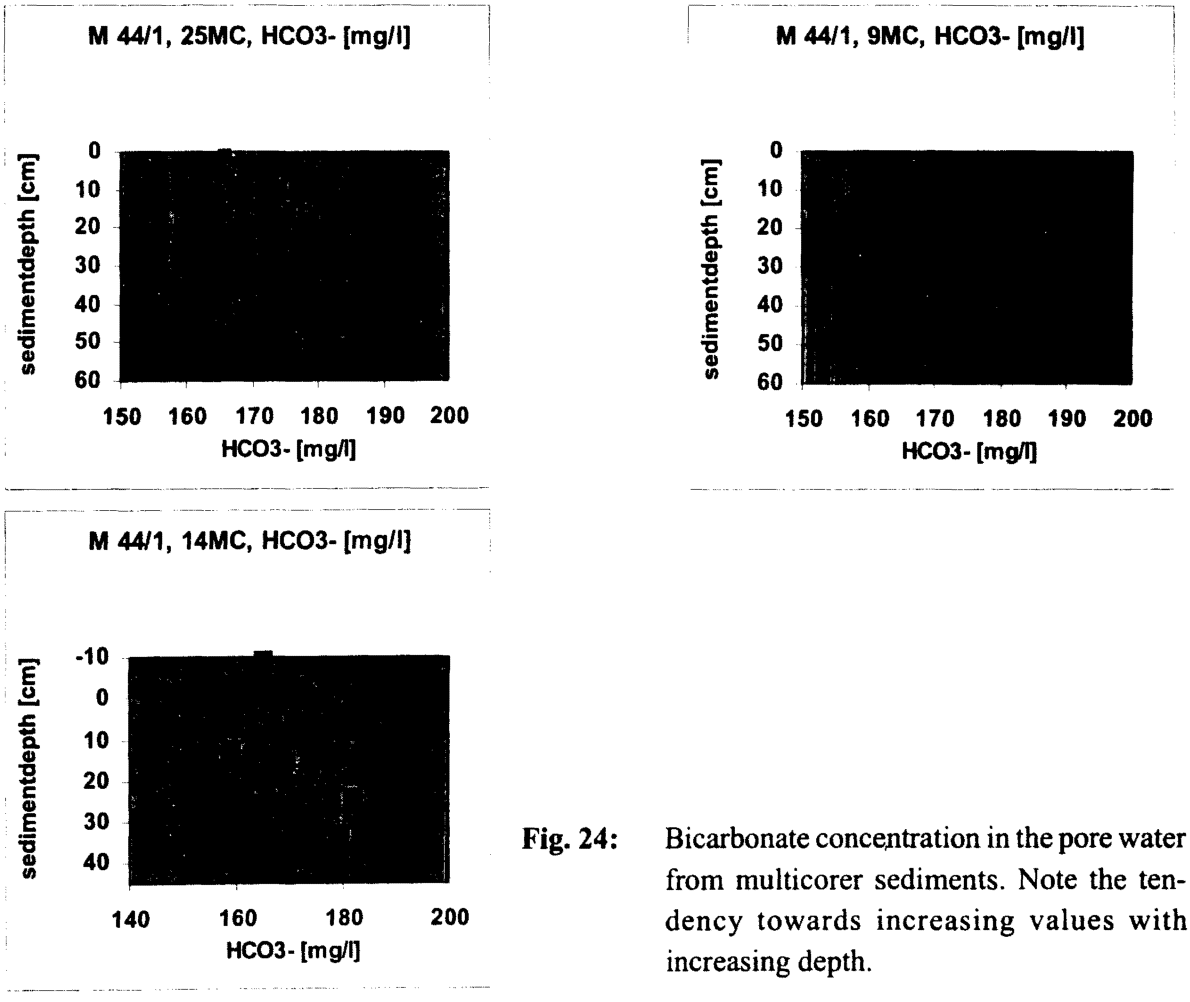

Fig. 24: Bicarbonate concentration in the pore water from multicorer sediments. Note the tendency towards increasing values with increasing depth.

Results

There is no significant hint for chemical changes in the water column regarding the bicarbonate concentration (Fig. 23). This behaviour is true for all the other 15 measurements in the water column.

The cores from the multi corer have a length of about 50 cm. The distribution of HCO_3^- is shown in Fig. 24. A tendency to a higher bicarbonate content with the depth is obvious.

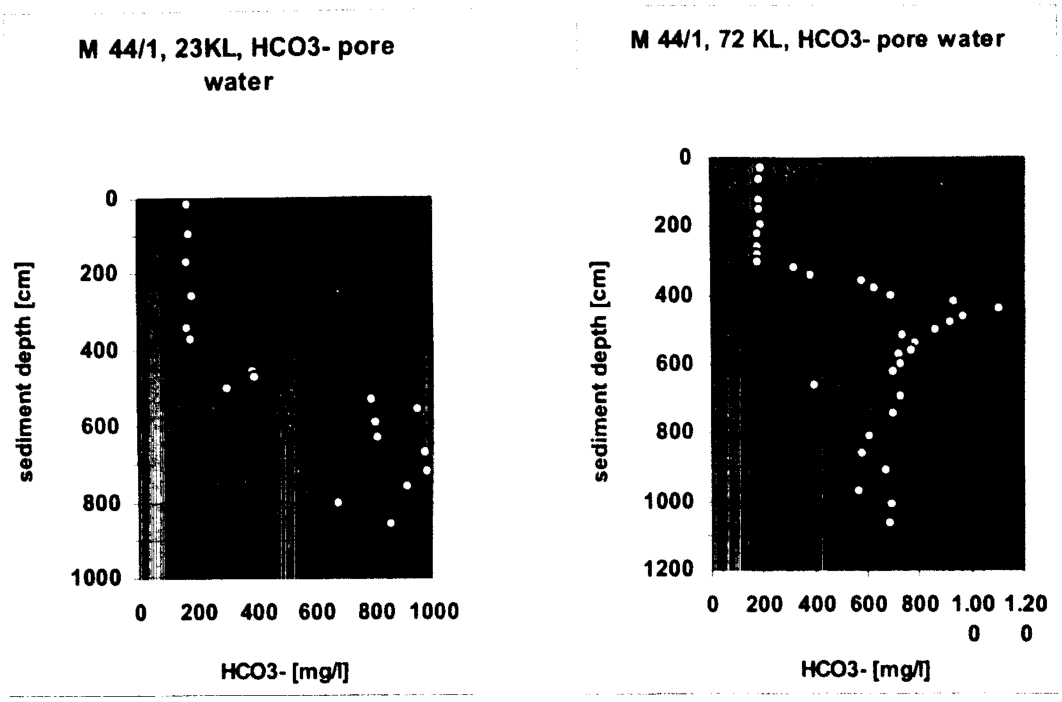

Fig. 25: Bicarbonate concentration profiles of the pore water of sediments from two long piston cores. Both cores were taken from the Ganos Fault zone. The increasing HCO_3^- concentrations in core 23 KL coincide with the methane-sulfide reaction zone (see Fig. 20).

Really significant changes were measured in the pore water of the piston cores from station 23 KL and 72 KL. Down to 4 m depth respectively 3 m (72 KL) the concentration is equal to the amount in the free water column, followed by a 4 to 5 fold concentration increase in the next 1.5 m depth (Fig. 25). The bicarbonate increase is correlated with an increase of the sulfides and the occurrence of methane. In the pore water we find a good correlation of high HCO_3^- and CH_4 content. In the water column the HCO_3^- concentration proved to be a far too poor indicator for the chemical changes which could be detected by the methane concentrations.

5.1.4.2.5 Total Sulfide and Manganese

(A. Koschinsky, C. Arndt)

a) Determination of dissolved manganese and total sulfide

Both dissolved Mn^{2+} and total dissolved S^{2-} were determined by stripping voltammetric methods. Only manganese and sulfide were determined onboard in order to serve as diagenetic or hydrothermal signals; all other trace elements will be analyzed in the home laboratory. Mn determination and the equipment used for the voltammetric analyses is described in chapter 5.1.4.1.3. For photometric sulfide determinations a Perkin Elmer Lamda 2 Spectrometer was available.

Total S^{2-} analyses

Sulfide had to be determined immediately after the sample recovery because a delay caused immediate loss of H_2S by degassing and by oxidation of the samples. In pore water samples with sulfide concentrations in the ppm range, the photometric methylene blue method (GRASSHOFF ET AL., 1983) at 670 nm wavelength was used. Evaluation was done with a calibration curve.

Most samples had to be analyzed with the more sensitive differential pulse cathodic stripping voltammetric method (DPCSV) on the HMDE or SMDE. 10 ml of water containing 3.6 % NaCl at pH 10 were put into the voltammetric cell and deaerated with nitrogen for 5 minutes. Then about 1 ml of the sample was added, and after a short purging the determination procedure was started. The deposition was done at –400 mV for 60 seconds, and the scan range was –400 to –900 mV. The sulfide peak was located at about – 600 mV. Standard addition with a 1 ppm Na_2S standard was used for the evaluation.

Pore water samples were treated immediately after squeezing. A sample aliquot was filled into a small PE bottle, 1 ml was taken for immediate sulfide analyses and stored in the cool room for anion analyses in the home laboratory.

In order to avoid losses of sulfide in the pore water samples due to the long squeezing procedure, we tried an alternative method. Sediment samples were taken immediately after the opening of the core with syringes, and a defined volume (2 ml) of sediment was filled into a small PE bottles filled with 20 ml of deionized water adjusted to pH 10 with ammonia buffer and flushed with argon or nitrogen. A magnetic stirrer was used to extract the pore water into the solution within a few minutes. After filtration, the extract was immediately analyzed for sulfide. Voltammetric measurements in the unfiltered suspension did not give reproducible results, probably because of colloid sorption on the mercury drop electrode.

b) Results

Dissolved manganese could be detected in all pore water samples. In short cores (0-52 cm) from the multicorer the typical diagenetic Mn behaviour was observed: Mn concentrations mostly < 10 ppb in the overlying water and < 100 ppb in the upper centimeters of the core, and then a strong increase (up to 2.5 ppm) below the Mn redox boundary around 10-20 cm depth. The increases in dissolved Mn concentrations correlate well with the drops in redox potential found between 10 and 15 cm depth. Sulfide concentrations were < 10 ppb in all MC pore water samples. No significant difference was found for the cores from the Tekirdag Basin (9 and 14 MC), the Ganos fault (25 and 31 MC) and the Central Marmara Basin (30 MC).

In longer cores, a decrease in Mn with increasing depth was observed below the Mn maximum within the uppermost 50 cm. The profile of core 10 KL (Tekirdag Basin, 1087 m water depth) shows an increase of total sulfide at about 8 m which means that the diagenetic stage of sulfate reduction is located at about 8 m depth; in core 40 KL taken at 700 m water depth south of the Ganos fault the lowermost pore water sample at 7.70 m was still above this boundary.

More detailed pore water profiles were carried out from cores 23 KL and 72 KL, both from the same location in the Ganos fault at 730 m water depth. These profiles confirm the general decrease of Mn below 100 cm; local smaller peaks within the profile may be artefacts from the sampling procedure because the samples were not taken continuously from the surface to the bottom, and we had observed that samples taken at a later time have somewhat lower Mn values due to oxidation. In 23 KL the sulfide peak lies between 5 and 6 m depth and is directly followed by a methane peak (chapter 5.1.4.2.3) with a maximum at about 6 m depth. Below 5 m depth also the HCO_3^- concentrations are significantly increased (chapter 5.1.4.2.4). In 72 KL the whole peak sequence is located about 1 m higher; carbonate increases around 4 m depth (chapter 5.1.3.2.4), the sulfide maximum lies at about 4.5 m, and the highest methane concentrations were determined between 4.5 and 5.5 m depth (chapter 5.1.4.2.3).

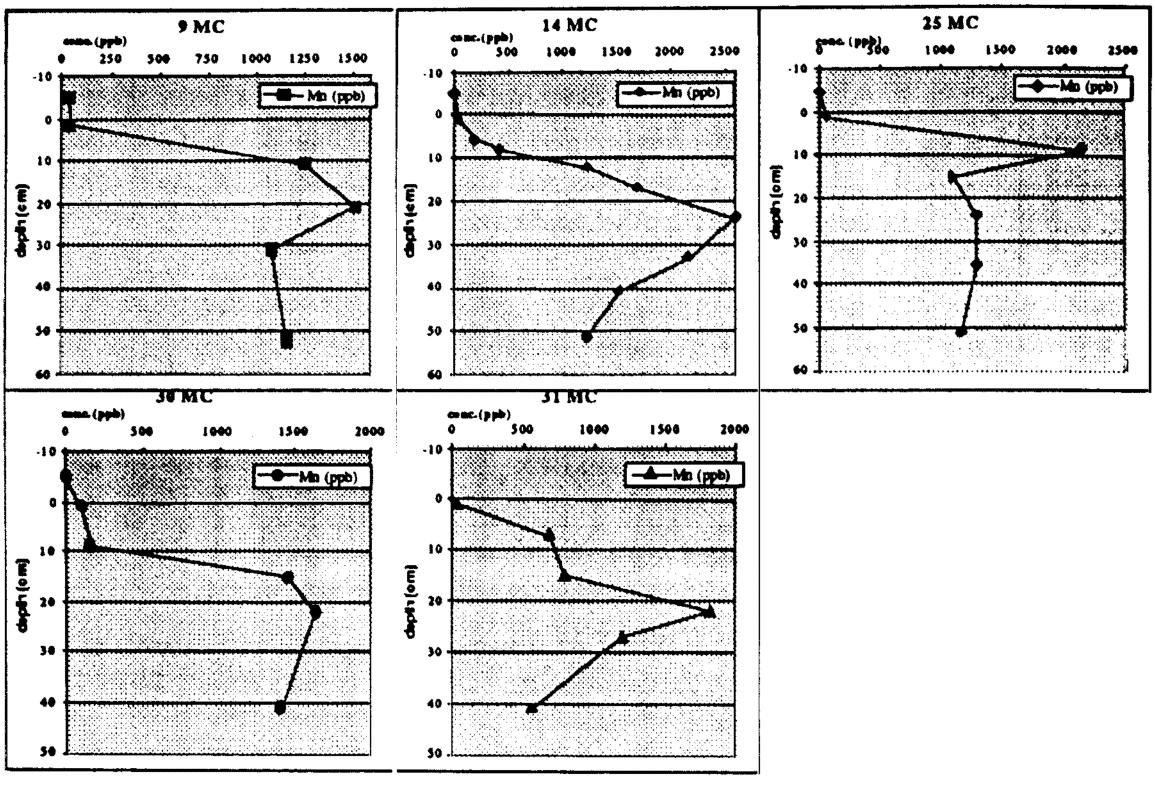

Fig. 26: Dissolved Mn concentrations in pore water samples of some MC surface sediment cores.

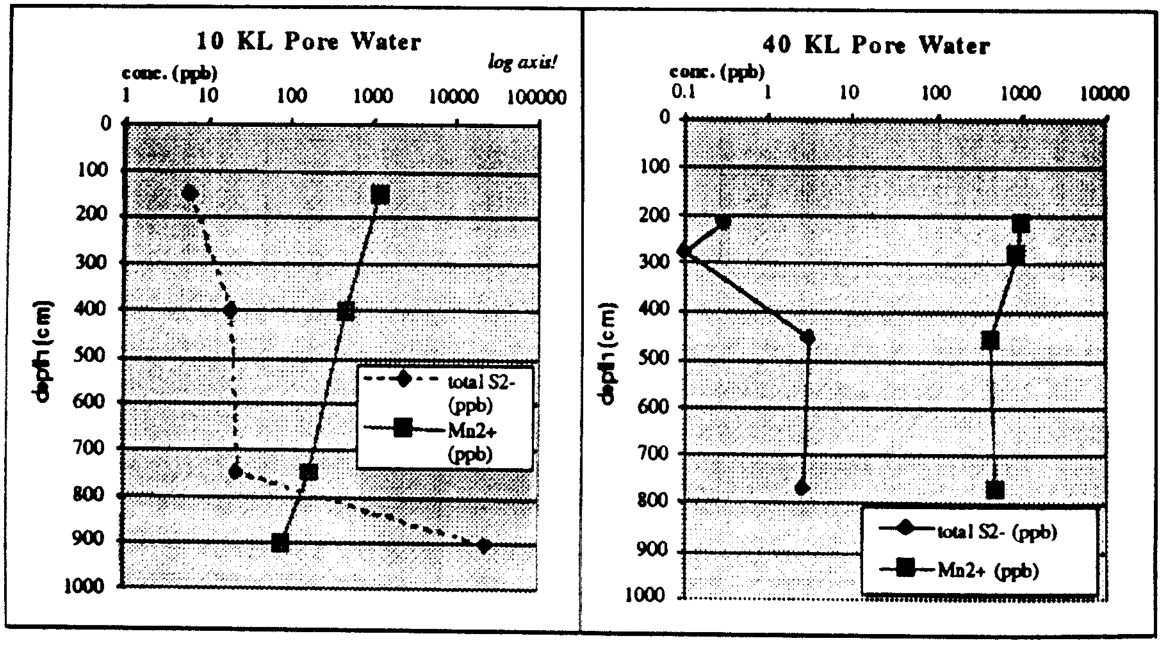

Fig. 27: Pore water concentrations of dissolved Mn and total sulfide in cores 10 KL and 40 KL.

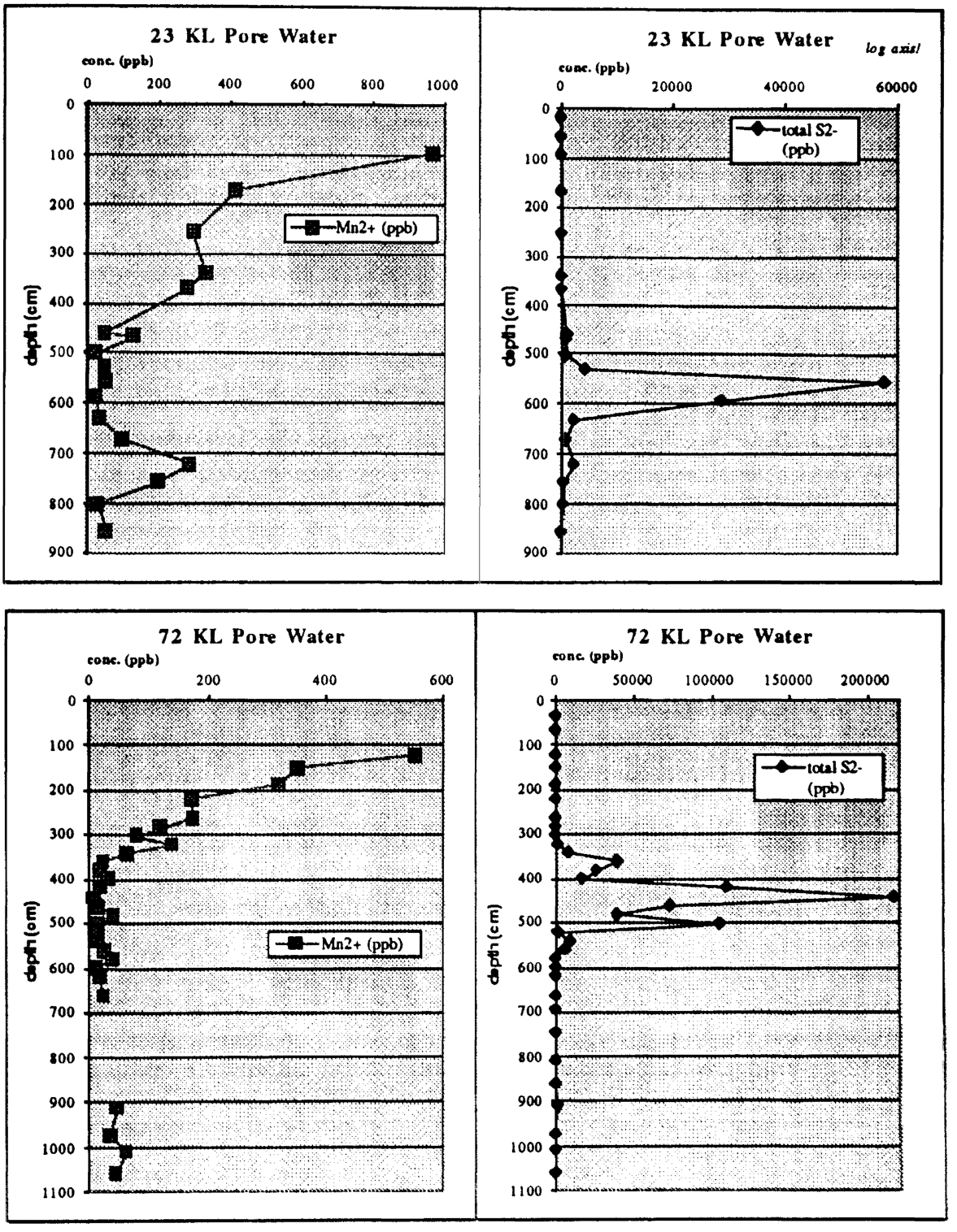

Fig. 28: Pore water concentrations of dissolved Mn and total sulfide in cores 23 KL and 72 KL.

5.1.5 First Conclusions

(P. Halbach, T. Kuhn)

The Sea of Marmara is situated along the North Anatolian Fracture Zone. Since the devastating earthquake around Izmit in August 1999 all scientific results of the M 44/1 cruise have to be seen in a new and actual context. Especially the investigations of the activity of the Ganos Fault (in particular the study of the gas content and gas behaviour), which is suggested to form the active western prolongation of the NAF, are of interest.

As eye witnesses from the earthquake area reported, methane emanations may have preceded the main earthquake (pers. commun. from a Turkish reporter). Thus, our results of the particularly high methane concentrations both in bottom and porewater of sediments along the Ganos Fault could have been a direct hint to the forthcoming earthquake. Therefore, a repeated survey of the Ganos Fault zone with respect to the recent methane concentration in bottom and porewater should be carried out since we are convinced that the gas concentration and gas behaviour is significantly controlled by the active tectonics.

The porewater of the sediment core 23KL contains particularly high methane concentrations. At 600 cm below seafloor they reach up to 4 mmol/dm^3 with a distinct decrease above that depth (Fig. 29). A sulfide maxima occurs slightly above the methane peak. Obviously, the rising methane is quantitively oxidized at that depth by porewater sulfate according to the following reaction (NIEWÖHNER ET AL., 1998):

$$CH_4 + SO_4^{2-} \longrightarrow HS^- + HCO_3^- + H_2O \qquad \text{(at pH > 7)}$$

At pH < 7 the following reaction may take place:

$$2CH_4 + 2SO_4 + 4H^+ \longleftrightarrow 2\,H_2S + 2CO_2 + 4H_2O$$

The anaerobic methane oxidation in the deeper sediment causes an increased sulfate reduction which is kinetically very efficient. Therefore the porewater sulfate which is provided by diffusion from the upper sediment column hardly oxidizes any of the organic material. Thus, the degradation of organic material is mainly controlled by the methanogenesis (NIEWÖHNER ET AL., 1998) and not by sulfate reduction. These processes may lead to the high methane concentrations in the sediments of the Sea of Marmara. However, the Ganos Fault may provide a pathway for the migration of methane whereas the fine-grained sediments outside the Ganos Fault area do not.

The methane-sulfate double peak or, as we call it, the methane front, was found in all sediment cores of the Ganos Fault which were analyzed during the cruise. However, they appear in different depths. In general, an enhanced concentration of H_2 (measured by the headspace-method) exists immediately above the methane peak. This hydrogen is obviously an intermediate product of the above-mentioned overall reaction. At some locations, the methane front even reaches the seafloor, forming Fe sulfides and bacterial mats (as identified by the video survey of the seafloor).

At the moment we do not know if the methane is a pure diagenetic product or if there are some thermogenic contributions from Tertiary layers which contain natural gas. This is one of the scientific aims of the project and can be solved by carbon isotope measurements.

A further step of important investigation considers the porewater chemistry in relation to salinity. First results show (72 KLG) that in a depth of three meters a distinct decrease of chlority-sodium-

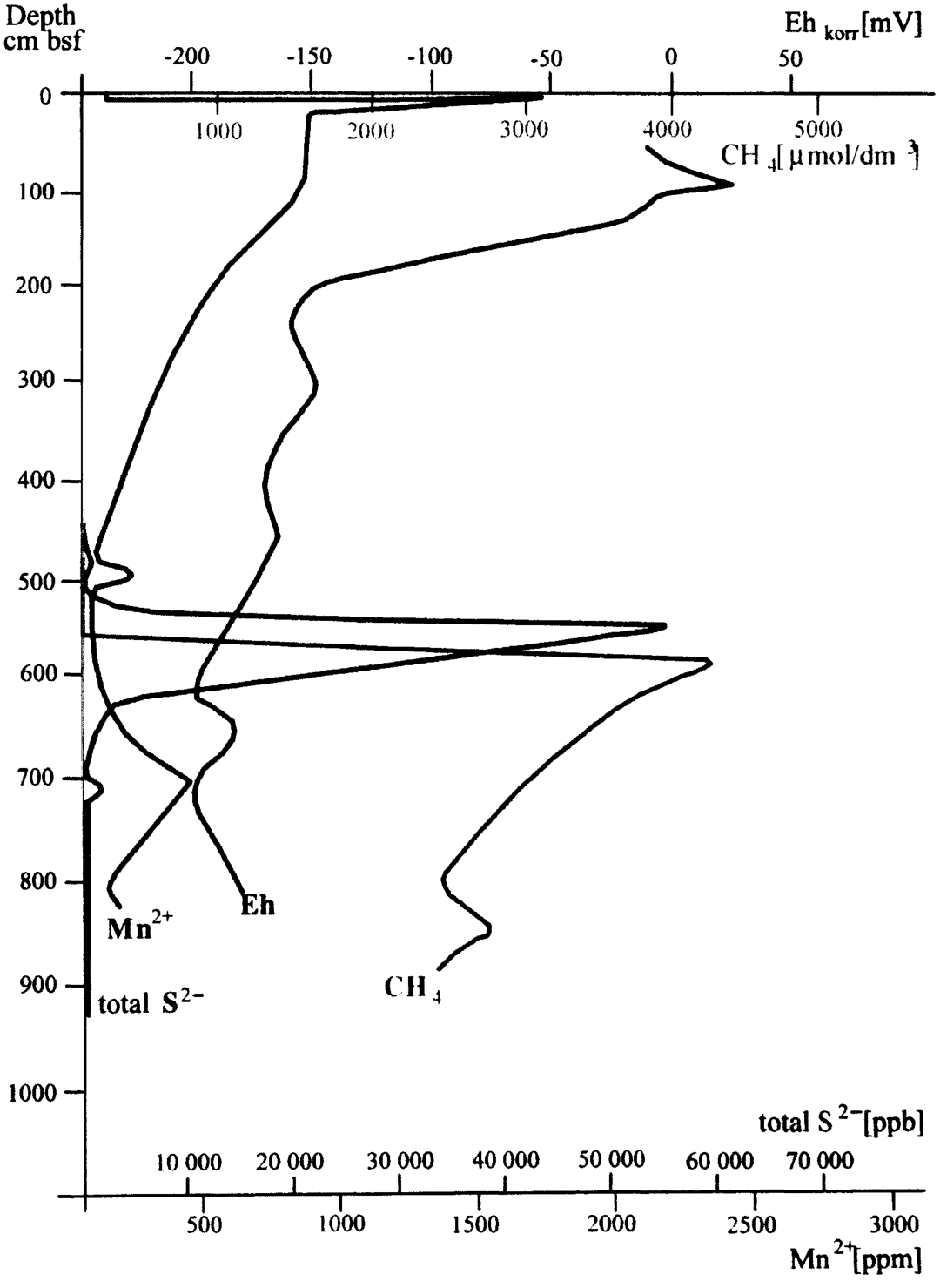

Fig. 29: Concentration vs. depth profiles of the methane, Mn^{2+}- und S^{2-}_{ges} concentrations in core 23KL. For core location see Fig. 15. At a sediment depth of 550 through 600 cm methane and S^{2-} peaks occur slightly separated. They may be interpreted as a reaction zone of the anaerobic methane oxidation and sulfate reduction. Eh values of less than -150 mV below 200 cm depth point to strongly reducing conditions.

strontium-potassium concentrations begins. In a depth of six-seven meters the salinity amounts only 2/3rd of the seawater salinity of the Sea of Marmara. Thus, the question arises wheteher this is controlled by a freshwater input. On the other side Ca does not follow this decreasing concentration and has a clear minimum in the depth where the sulfide concentrations show their maximum. We explain this by a carbonate formation in the depth range above the methane front which is related to consumption of Ca. Further porewater investigations have to be made to clarify this interrelationships.

The long sediment cores taken during the M 44/1 cruise outside the Ganos Fault provide excellent material for the study of the paleoceanographic development of the Sea of Marmara. It could already be proved by the tephra layer that the cores reach down to more than 18.000 years ago. Thus, the sediments of at least one interglacial-glacial change have been sampled. However, the repeated occurrence of freswater deposits in two sediment cores may point towards several of such changes. Furthermore, a condensed sediment column of the push-up summit (2.5 m sediment may represent several 100 000 years) on the one hand and the high resolution cores of the Tekirdag and Central Marmara Basins (more than 10 m sediment represent less than 10.000 years) on the other hand provide material for different paleoceanographic studies.

With the available sample material a detailed study of the development of the Sea of Marmara during the late Pleistocene and Holocene as the connecting body of the Agean and the Black Sea is now possible.

5.2 Preliminary Results of Leg M44/2

5.2.1 Physical and Chemical Oceanography

(O. Plähn, M. Badran, M. El-Deek, Y. Sangok, T. Badewien, M. Elbrächter, R. Manasreh, M. Walter)

5.2.1.1 Hydrography and Tracer Measurements

CTD Measurements and Calibrations

The CTD used was a Neil Brown Mark I. It was attached to a 24 bottle 10 L General Oceanic rosette water sampler. Four of the bottles were equipped with deep-sea reversing electronical thermometers from SIS. When employed, the rosette was lowered and heaved at a speed of 0.5 m/s in the upper 100 m and at 1 m/s thereafter.

At a test station on the second day of the cruise some sporadic disconnections between the CTD and the deck unit were observed. Changing to a different winch, the connection was established without any problems during the whole leg.

Calibration of the pressure and temperature sensors was done previous to the cruise at the IfM Kiel. The thermometer readings were used to check the laboratory calibration of the temperature sensor. The salinity samples, typically three per profile, will be analyzed after the cruise with an Autosal Salinometer in Kiel.

During the cruise M44/2 72 profiles were measured on 52 stations. Additionally, at two 24h stations 30 ‘yoyo’-profiles were carried out.

The CTD-rosette casts were the back bone of the cruise as they provided the ad hoc information on the physical structure of the water column and the Rosette water sampler were the source of many of the chemical and biological studies. Main “customers” were M. Badran, M. El-Deek and Y. Sangok for chemical analyses and U. Sommer, U.-G. Berninger, M. Simon, H.-P. Grossart and Selje for biological work.

Analysis of Chlorofluorocarbons (CFC-11, CFC-12)

Both CFC components CFC-11 and CFC-12 were analyzed during the cruise M44/2. After sampling, 25 ml of water were transferred from precleaned 10 L Niskin bottles to a purge and trap unit. The gases were then separated on a gaschromatographic column and detected with an Electron Capture Detector (ECD). A standard gas was used to convert the ECD signals in concentrations. The efficiency of the ECD was very stable in time, the observed temporal variations were less than 15% for both components.

To correct for the temporal drift of the ECD, a calibration curve with five to seven different gas volumes was taken before and after each station assuming that the temporal change between two calibration curves is linear in time. The mean blank of the sample transfer and the measurement procedure was determined by degassing 25 ml of blankwater. This CFC-free blankwater was created by degassing 10 L of seawater with ECD-pure nitrogen gas.

460 water samples from 36 CTD stations were analyzed. The CFC samples were collected from different depths covering the whole water column. In addition air samples were taken regularly and analyzed. Accuracy was checked by analyzing about 65 water samples at least twice. It was found to be +/-0.65% for CFC-12 and +/-0.85% for CFC-11.

Shipboard ADCP

The shipboard ADCP (acoustic Doppler current profiler) worked very well during the cruise Meteor 44/2. The range of the 150 kHz ADCP was about 350 m, using a binlength of 8 m and a pulselength of 16 m. The number of bins was 60. The profiles were averaged over 2 minutes. In order to study the abundance and distribution of plankton the backscatter of each beam was recorded. To derive the needed absolute backscatter strength, a calibration was done as described in the technical paper of RD Instruments (FST-003, May 1998).

Preliminary Results

Along four different sections, two in the Gulf of Aqaba (a meridional section in the center of the Gulf and a cross-section along about 29°20'N) and two in the northwestern Red Sea (along 34°40'E and along about 27°20'N) CTD and CFC measurements were carried out. Most of the stations were repeated once or twice to study the temporal variability.

The CFC data obtained during this cruise are the first available for the Red Sea and Gulf of Aqaba. The most striking feature in the Gulf of Aqaba is a CFC-12 concentration maximum at about 500 m depth. The highest values were measured in the northern part of the Gulf with saturation above 250% (Fig. 30). This signal decreased southward to a saturation of 130% at 28°20'N. The maxima were three times higher than in the ambient surface water. The CFC-11 component did not show any special signals. The high CFC-12

concentrations measured cannot originate from air-sea gas exchange and they are not caused by contamination of the 10 L Niskin bottles, syringes or of the freon purge and trap system. At present the source of the CFC-12 inflow is still unknown. The same observation could be made three times along the whole Gulf-of-Aqaba-section, but was not seen in the northern Red Sea. The density of the contaminated water is more than 28.8 sigma-units. The densest water observed during this leg in the northern Red Sea was less than 28.6 sigma-units. North of the Strait of Tiran this density can be found at 300 m depth. Thus it is unlikely that the extreme CFC-12 signal cannot leave the Gulf of Aqaba across the Strait of Tiran.

Along the zonal section in the northern Red Sea (between 34°E and 34°42'E) a salinity maximum at about 800 m depth was observed at the western edge. In contrast both Freon components showed a concentration minimum at nearly 600 m along the whole zonal section (Fig. 31). Towards the bottom, the concentrations increased again and reached their largest values at the eastern edge. The high CFC concentrations are caused by the inflow of recently ventilated water masses created by convection processes in the northern part of the Golf of Suez and/or Golf of Aqaba. Because the largest freon concentrations at the bottom were measured in the eastern part of the zonal section, it is supposed that this water came from the Gulf of Aqaba.

An intensive convection event was observed in the northern Gulf of Aqaba on February, 26th, when the profile was homogeneously mixed down to 550 m depth (Fig. 32). Four days before, the mixed layer was only 350 m thick. During these 4 days, the air temperature did not cool down markedly and the wind blew also steady from northern direction. Thus it is supposed that the convection was not primarily caused directly by local atmospheric influences. A large variability in the vertical extension of the thermocline was observed, probably forced by internal waves. The analysis of the 'yoyo' CTD-profiles will lead to a better understanding of the amplitude and frequency of these perturbations.

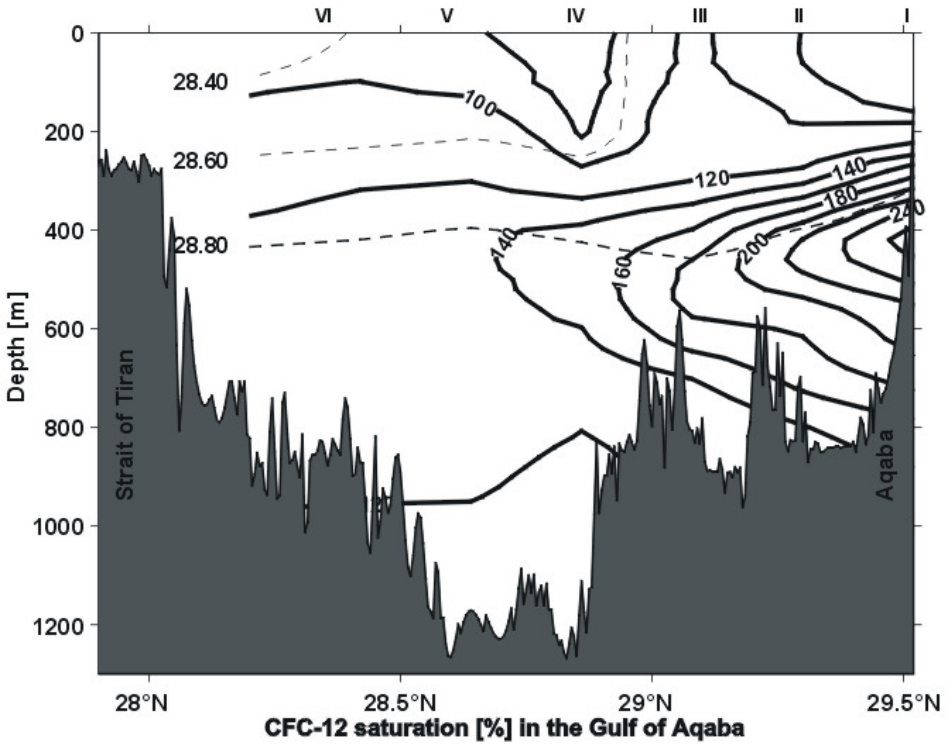

Fig. 30: CFC-12 saturation (%), relative to the atmosphere, in the Gulf of Aqaba including the density distribution (sigma-units).

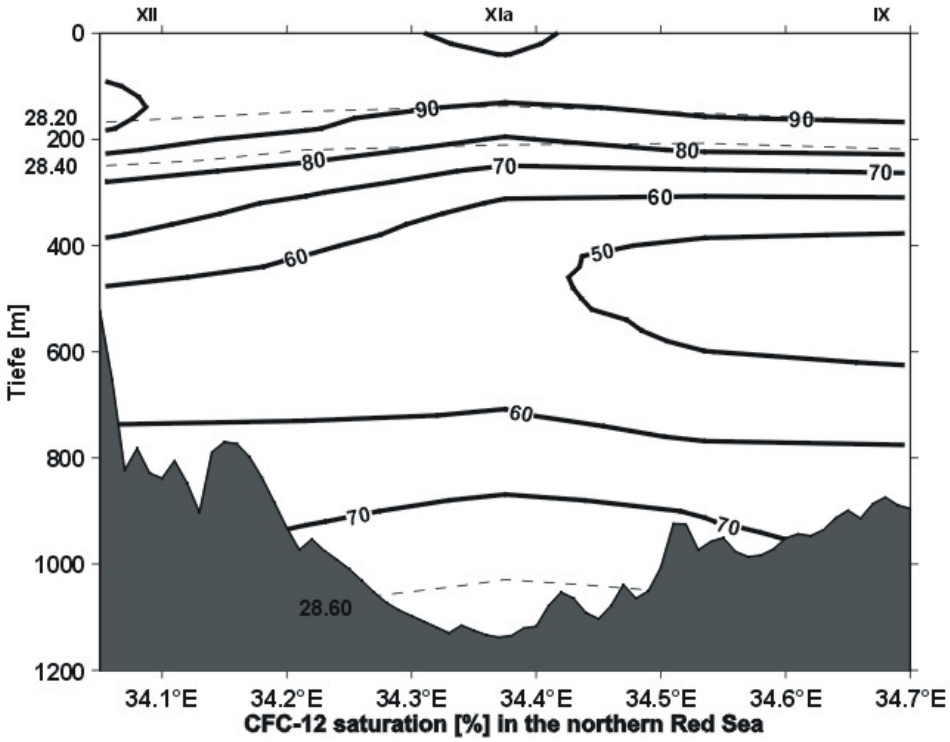

Fig. 31: CFC-12 saturation (%), relative to the atmosphere, in the northern Red Sea, including the density distribution (sigma-units).

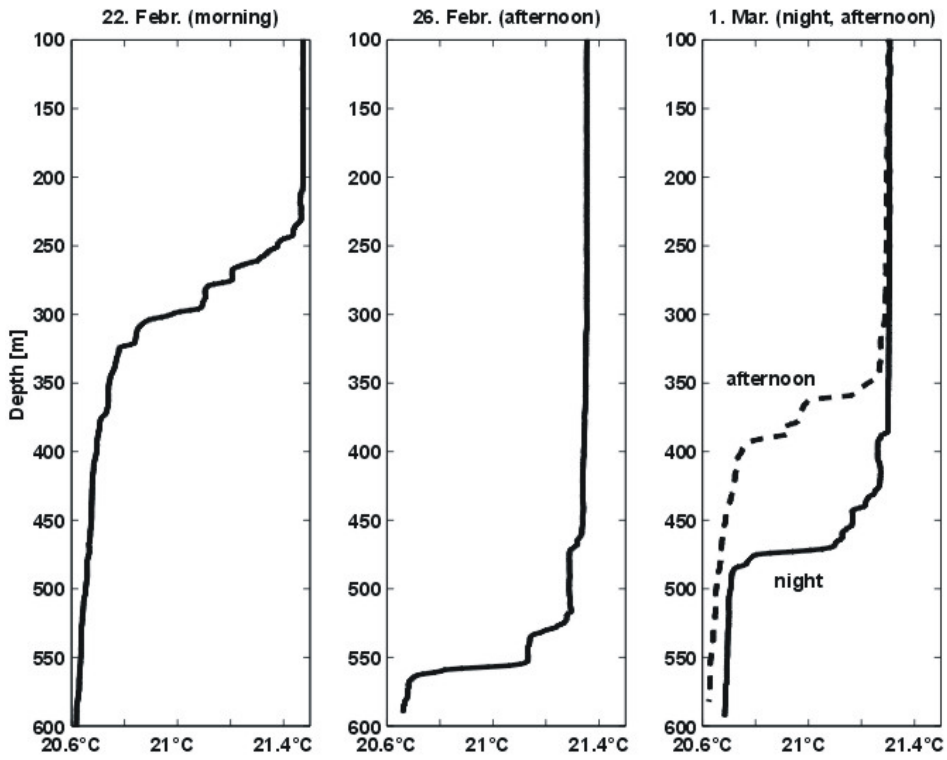

Fig. 32: Temperature profiles measured in the northern Gulf of Aqaba (Position I) during the cruise M44/2 (22.2. / 26.2. / 1.3.1999).

5.2.1.2 Nutrients and Chlorophyll *a* Concentrations

Records of nutrient and chlorophyll *a* concentrations in the northern part of the Gulf of Aqaba are being generated by the MSS on regular basis since 1995. These records have given a fairly clear idea about the mixing and stratification regimes in the northern parts of the Gulf and to soma extent about inter-annual variability there. Our work on the Meteor aims to generate an integrated image of nutrient and chlorophyll *a* concentrations in the Gulf of Aqaba and the Red Sea. Samples have been collected in such a way that enables the analysis of spatial, vertical and temporal variability. A long section of six stations between the Strait of Tiran and the northern tip of the Gulf was collected at the very early stage of the cruise. The same section was also repeated at the latest possible stage. Variations in the depth of the thermocline coupled with variations in the nutrient and chlorphyll *a* concentrations will be used for calculation of the entrainment rate and magnitude within about 16 days of mixing, while the thermocline is still deepening. In additionsamples were collected for analysis of total organic carbon. These samples will be the first to be analysed by the MSS when a shortly expected carbon analyzer is received.

5.2.2 Phytoplankton and Primary Productivity

5.2.2.1 Vertical Distribution of Chlorophyll *a*

(C. Richter)

For measurements of phytoplankton biomass vertical profiles from the surface to 1000 m (or sea bed) were carried out with a multiparameter probe (ADM-Elektronik, Warnau) including a sensor for in-vivo fluorescence (Dr. Haardt, Nettelau).

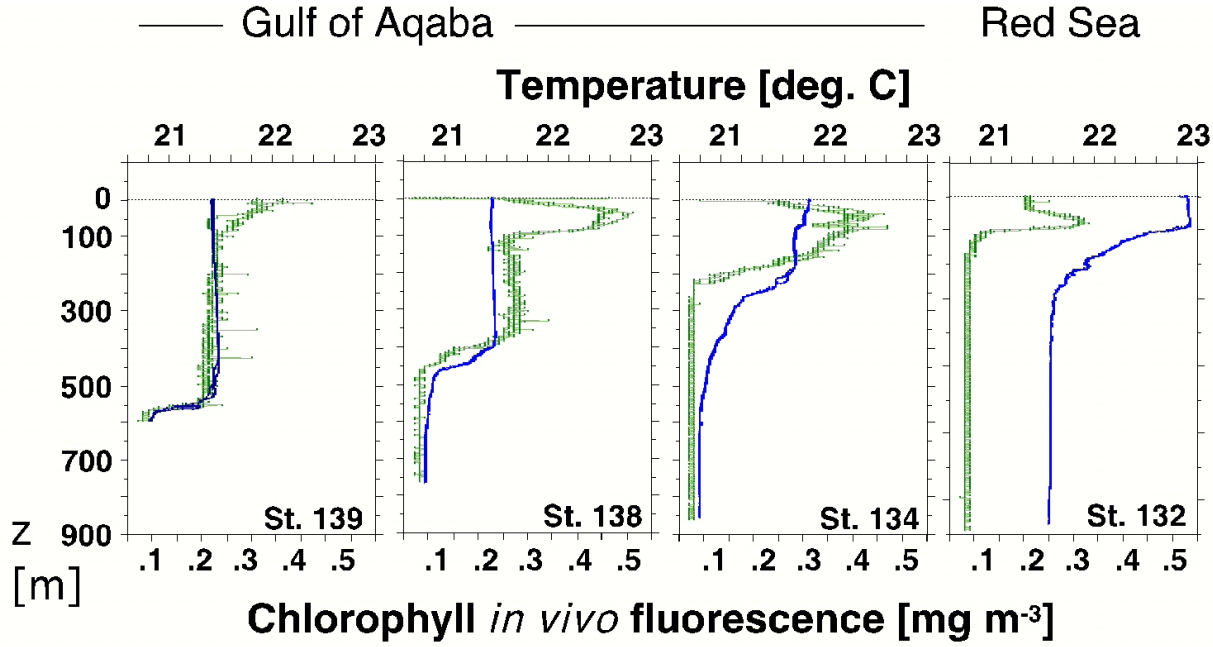

Fig. 33: Vertical profiles of temperature (dark line) and phytoplankton chlorophyll fluorescence (light line) in a north-south section between the Gulf of Aqaba (St. 139 and 138 / 26.02.1999; St. 134 / 25.02.1999) and the Red Sea (St. 132 / 24.02.1999).

We encountered rather different chlorophyll distributions in the Gulf of Aqaba and the Red Sea proper coinciding with differences in vertical stratification of the water masses. In the northern Gulf of Aqaba we encountered a winter situation with a relatively high phytoplankton standing stock of ~120 mg chl m^{-2} mixed down to more than 500 m, with an early phytoplankton bloom discernible at the surface (Fig. 33, St. 139) which developped into a spring bloom towards the end of the cruise. In the southern part of the investigation area, a shallowing mixed layer was accompanied by the development of progressively distinct subsurface chlorophyll maxima. It was accompanied by a marked decline in the total integrated algal biomass over the water column, dropping to ~75 mg chl m^{-2} in the southern Gulf (Fig. 33, St. 134) and to less than 30 mg m^{-2} in the Red Sea proper (Fig. 33, St. 132). Thus we found within 100 nautical miles strikingly different successional stages of phytoplankton development corresponding to a late winter situation in the northernmost Gulf to a mature 'summer' situation in the Red Sea.

5.2.2.2 Primary Productivity and its Control by the Light and Nutrient Regimes: A Comparative Study Between the Gulf of Aqaba and the Northern Red Sea

(C. Häse, N. Stambler, M. Al-Qutob, B. Beese, M. Dray)

The Gulf of Aqaba and the Northern Red Sea were studied as model systems for the control of phytoplankton distribution and primary productivity by the light and nutrient regimes. In the Gulf of Aqaba, nutrients from deep waters are injected into the photic zone by deep vertical mixing in winter/spring triggering a phytoplankton bloom after the onset of stratification. By contrast, the Northern Red Sea is permanently stratified throughout the year. Therefore, we expected that phytoplankton productivity in the Northern Red Sea is based mainly on nutrient recycling

(regenerated production). New production should be of greater importance in the Gulf of Aqaba than in the Northern Red Sea. These hypotheses were tested by two types of experiments: simulated mixing and nutrient enrichment bioassays.

In the Northern Red Sea a deep chlorophyll maximum (DCM) is present all around the year whereas in the Gulf of Aqaba it develops only during stratification in summer. Photosynthetic characteristics of the DCM phytoplankton were studied in comparison to surface phytoplankton in the Northern Red Sea. In the Gulf of Aqaba, where no DCM was present at that time, the photosynthetic potential of the phytoplankton within the mixed water column was investigated.

Measurements and Experiments

Six stations in the Gulf of Aqaba and six in the Northern Red Sea were sampled during the 44/2 cruise with R/V Meteor between 21.2.99 to 8.3.99.

Light measurements:

Light measurements covered the upper 100 m of the water column.

The spectral distribution of the underwater light field, both up and downwelling, was measured using a Biospherical underwater MER-1010 spectroradiometer (nmol quanta m-2 s-1 nm-1). Downwelling irradiance, $E_d(l)$, and upwelling irradiance, $E_u(l)$ were measured within the range of PAR (photosynthetic available radiation) at 12 discrete wavelengths between 410 and 694nm (410, 441, 448, 507, 520, 540, 560, 589, 625, 656, 683, and 694 nm) with 8 nm bandwidth FWHM (full width at half-maximum). These are the same wavelengths measured by the SeaWiFS ocean color satellite. Measurements of downwelling fluxes were performed by using the spectroradiometer facing upward and upwelling fluxes by using it facing downward. During the casts incident PAR was logged by a sensor on deck (QSP100, Biospherical Instruments) to correct underwater readings for variations in incident light during the measurements.

Data were recorded on-line, on a PC on board. Dark values were measured at the beginning of each station, and subtracted from all readings. Attenuation coefficients of downward irradiance, $K_d(l)$, will be determined from the slopes of linear regression lines of the natural logarithmic transformation of $E_d(l)$ as function of depth.

The depth of the euphotic zone (z_{eu}) will be calculated from the light data, and will be compared with the bathymetric distribution of the concentrations of light-absorbing components in the water column, which are mainly the phytoplankton pigments. The upwelling radiation and the chlorophyll concentrations will be used to develop a better algorithm for this region for the interpretation and calibration of the SeaWiFS ocean color satellite images.

In addition, photosynthetically available radiation (PAR) was recorded at each station by an underwater scalar irradiance meter (LiCor, Lincoln, USA) down to 30 m only.

For light measurements within the incubators (simulated *in situ* incubations) a spherical laboratory quantum sensor (Biospherical, San Diego, USA) was used. Different light levels in the incubators were created by spectrally neutral nets of different mesh sizes.

Water chemistry:

Water samples were collected from the 24 bottle rosette (General Oceanics, 12 liters) for:

1. Samples for nutrient analyses (NO_3^-, NO_2^-, NH_4^+, PO_4^{3-}, and Si) were taken in vertical profiles from the surface to the bottom at all of the stations. During the 24-hr sampling, samples for

nutrients were taken every 4 hr at the same location to see the diurnal variation in nutrients, mainly those involved in the nitrogen cycle. Samples were preserved at – 4 °C. Nutrient concentrations will be determined by an autoanalyzer.

2. Chlorophyll *a* concentrations from all depths from the surface to the bottom of the mixed layer from all stations and during the 24-hr stations were determined from 250 ml of water that were filtered onto glass fiber filters (GF/F) with $MgCO_3$, and stored at -80 °C.
3. Oxygen concentrations in samples from the whole water column were measured by the Winkler method. In addition, at all stations oxygen was also measured with a WST electrode.
4. Salinity - samples were taken from all positions and kept at 4 °C for future analysis.
5. Alkalinity samples were also taken from all positions and likewise kept at 4 °C for subsequent analysis.
6. Water samples (3-6 liters) for detailed pigment analysis were filtered onto glass fiber filters (GF/F) and preserved at -80 °C. The samples were taken from all the positions, from the surface to bottom of the mixed layer. The pigments will be extracted with acetone, separated and quantified by HPLC. From the pigment analysis, we shall be able to separate the phytoplankton populations according to their major taxonomic groups. These measurements will be used to calculate the absorption of light in the water column.
7. Samples (1.8ml) were taken from 10-200m depths for optical characterization by flow cytometry, these samples were fixed immediately at room temperature with 20 ml 25% glutaraldehyde (Sigma G-5882) and preserved at -70 °C.
8. Particulate organic carbon (POC) analysis and C:N ratios will be done on material collected from water samples (3-6 liters) that were filtered onto glass fiber filters (GF/F).
9. $\delta^{13}C$ will be measured in 150 ml water samples that were preserved with $HgCl_2$ for future analysis by mass spectrometry.
10. Water samples for analysis of dissolved organic carbon (DOC) were collected from all stations at all depths. Samples were immediately acidified with ultrapure 30 % HCl, sealed in precombusted glass ampoules and stored at –70 °C.

Photosynthetic activity:

The photosynthetic activity of the phytoplankton was measured by the radiocarbon method. After incubation samples were filtered onto GF/F glass fiber filters and counted in a scintillation counter. In some of the experiments also DOC release by phytoplankton was considered.

At three stations in the Gulf of Aqaba (Pos III, V, and VI) and at one station in the Northern Red Sea (Pos X) simulated in situ incubations were carried out in order to estimate photosynthetic profiles in the water column. Vertically integrated photosynthetic rates will be calculated from these profiles.

At two stations in the Northern Red Sea (Pos X and XII) photosynthesis versus irradiance curves were measured for phytoplankton from the DCM layer and from surface waters by simulated in situ incubations.

At three stations in the Gulf of Aqaba (Pos III, V, and VI) the photosynthetic potential of the phytoplankton within the mixed water column was examined. Water samples were collected from various depths within the euphotic zone and beyond throughout the mixed layer and incubated at a saturating light level (30 % of surface light).

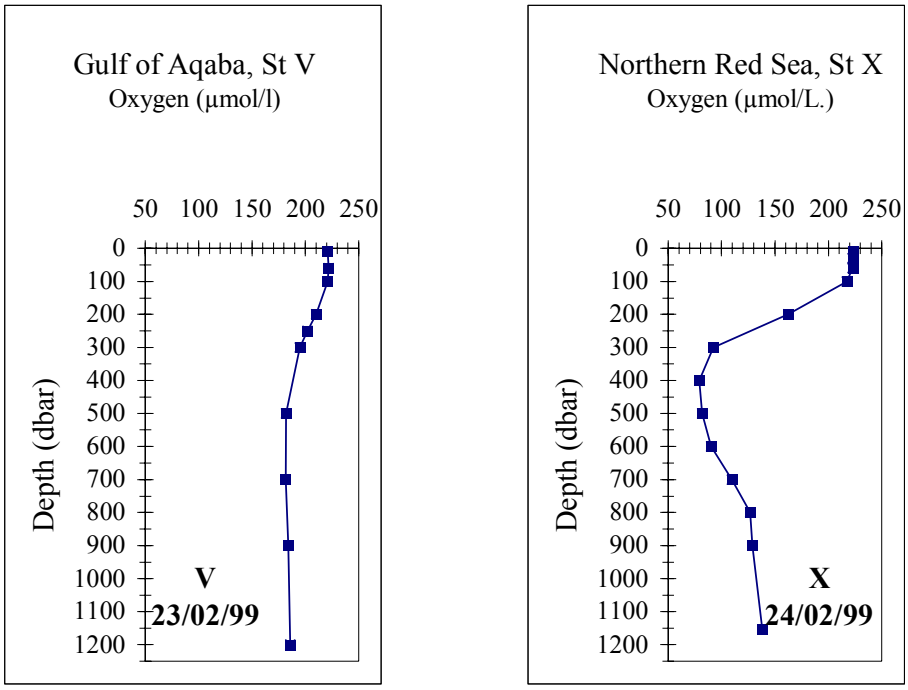

Fig. 34: Oxygen concentrations in the Gulf of Aqaba and the northern Red Sea.

Experiments on Nutrients and Primary Productivity

1. Simulated mixing:

At two stations in the Gulf of Aqaba (Pos I and IV) and in the Northern Red Sea (Pos IX and X), experiments were carried out to simulate a deep mixing event by adding water from ~ 700 m to water samples from two different depths within the photic zone in different ratios (0 %, 1 %, 2 %, 5 %, 10 %, and 50 %). One set of samples was spiked with ^{14}C, the other set of samples was left for nutrient analyses. All samples were incubated on board under saturating light levels (30 % of incident light) and in the dark (as a reference) for 4 hrs and 24 hrs, respectively. In one case, also a set of samples was incubated for analysis of chlorophyll concentrations.

2. Nutrient enrichment:

In order to determine the limiting nutrient for primary productivity in the two different systems, nutrient enrichment bioassays were conducted at two stations in the Northern Red Sea (Pos IX and XII) and at one station in the Gulf of Aqaba (Pos I). The experiments were performed as described above but instead of nutrient-rich deep water known concentrations of different nutrient salts were added to the water samples from two different depths within the photic zone.

Preliminary results

Physical and chemical parameters

During the cruise, the vertical winter mixing reached its maximum of more than 400 m in the northern part of the Gulf of Aqaba. By contrast, at the southern stations in the Gulf of Aqaba vertical gradients of temperature and chlorophyll were observed within the upper 200 m. In the Northern Red Sea, temperatures were generally higher and stratification was more pronounced. A deep chlorophyll maximum was present at all stations.

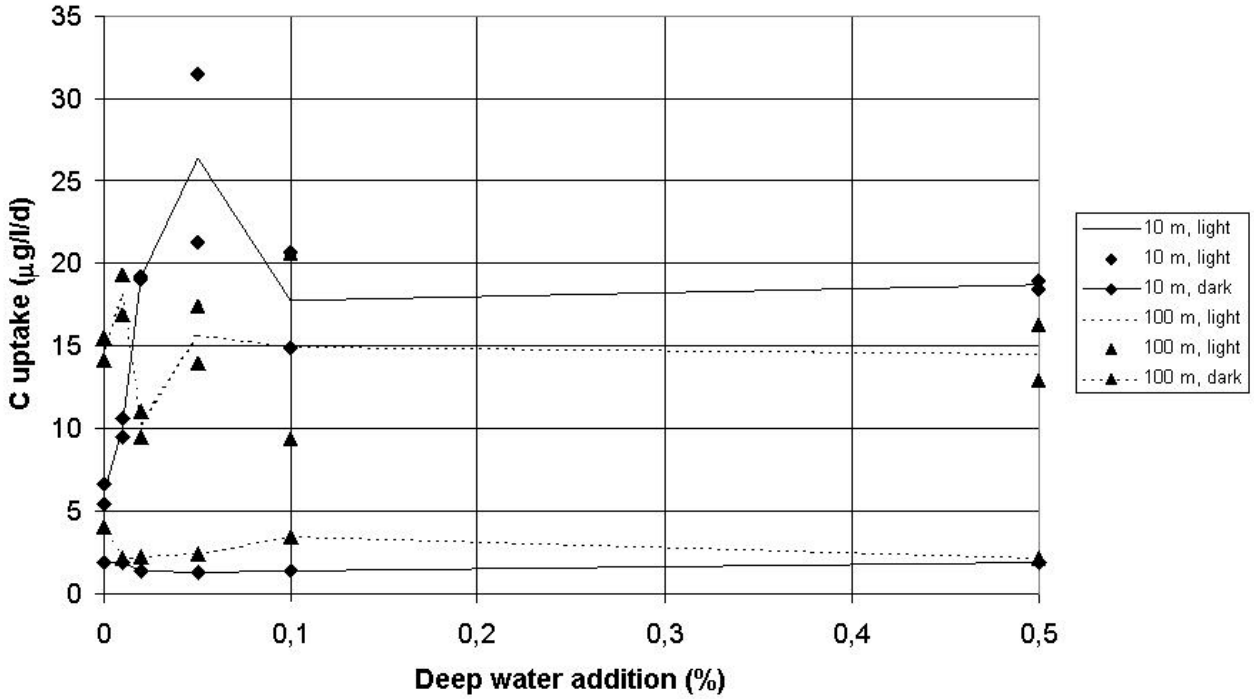

Fig. 35a: Photosynthetic rates in a simulated mixing experiment at position I (Station 151, Gulf of Aqaba, 1/3/1999).

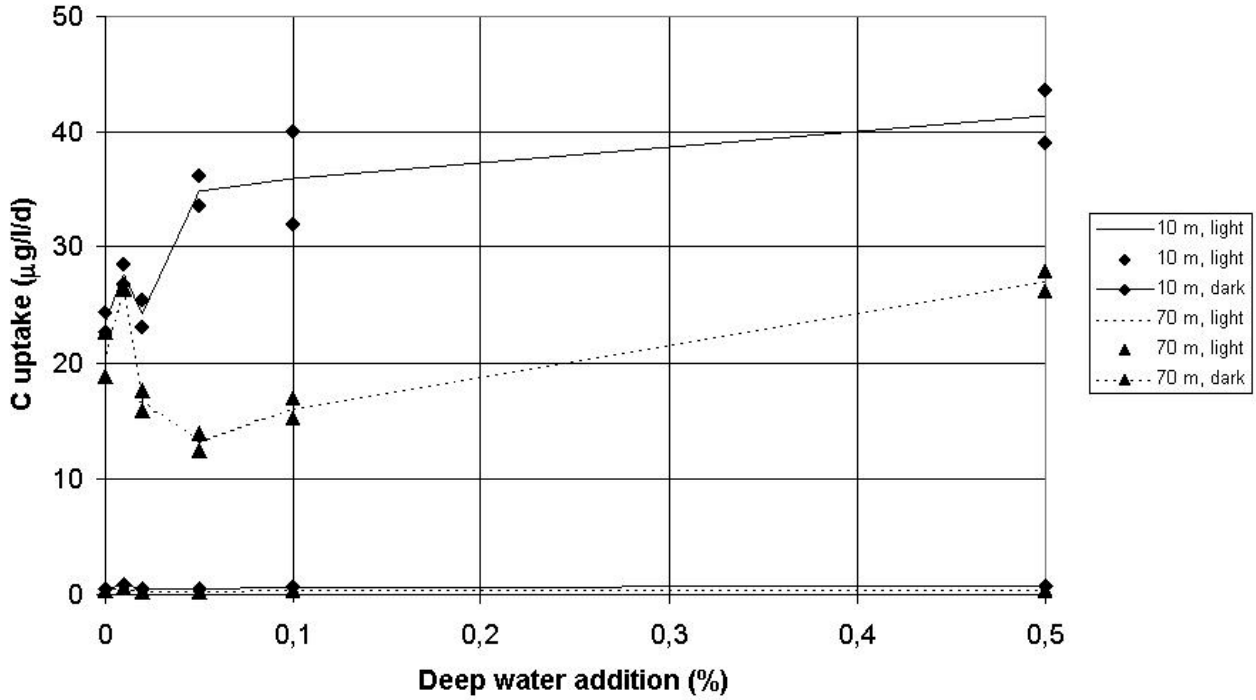

Fig. 35b: Photosynthetic rates in a simulated mixing experiment at position IX (Station 154, Northern Red Sea, 3/3/1999).

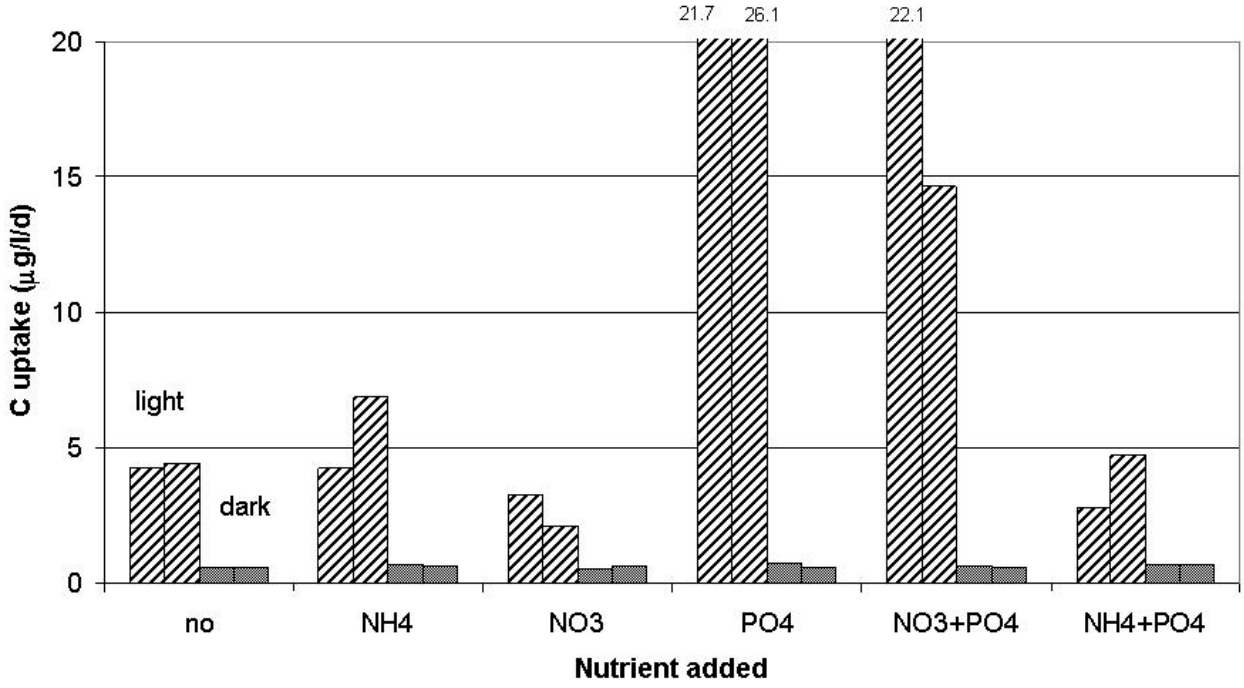

Fig. 36a: Nutrient enrichment in a 10 m sample from position I (Station 143, Gulf of Aqaba, 26/2/1999, 16h incubation in 20 m light level)

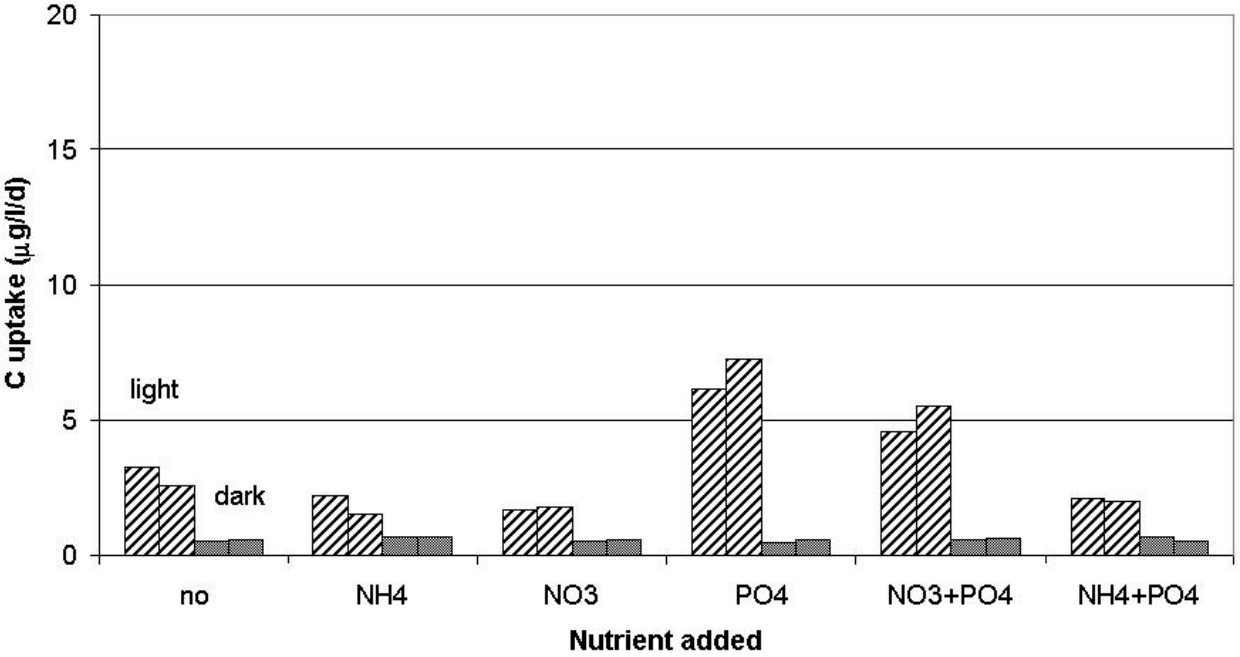

Fig. 36b: Nutrient enrichment in a 100 m sample from position I (Station 143, Gulf of Aqaba, 26/2/1999, 16h incubation in 20 m light level)

In the Northern Red Sea deep oxygen concentrations were much lower than in the Gulf of Aqaba and a local minimum below the photic zone was observed (Fig 34) suggesting oxygen consumption due to decomposition of sinking organic matter.

Nutrients and Primary Productivity

In the 4-hr incubation experiments no significant stimulating effect of neither nutrient additions nor deep water mixing could be observed. Even the 24-hr incubations might have been too short to see clear and pronounced signals of nutrient stimulated carbon uptake rates. However, in some cases a stimulating effect on photosynthetic rates was observed.

In the Gulf of Aqaba (Pos I), photosynthetic rates were stimulated by deep water addition only with phytoplankton from the surface, whereas phytoplankton from 100 m depth did not significantly respond (Fig. 35a). A similar pattern was found in the Northern Red Sea (Pos IX), but the difference between the surface and the deep sample (70 m, from the DCM) was even more pronounced (Fig. 35b).

In the northern part of the Gulf of Aqaba (Pos I), primary productivity was stimulated by the addition of phosphate and a combination of phosphate and nitrate suggesting phosphate limitation (Fig 36). The stimulatory effect was much more pronounced with the surface sample (Fig. 36a) compared to the deep sample (Fig. 36b). One week later at the same position, photosynthetic rates were stimulated significantly only by ammonia addition. In the Northern Red Sea once a stimulatory effect on photosynthetic rates by ammonia and by nitrate was observed but only with phytoplankton from the DCM.

Phytoplankton from the DCM in the Northern Red Sea was much more sensitive to surface light exposure than phytoplankton from the surface.

5.2.2.3 Regulation of Photosynthetic Energy Fluxes in the Gulf of Aqaba and the Red Sea During Winter-Spring Time

(B. Kroon)

Introduction

During winter, the waters in the Gulf of Aqaba and the Red Sea are severely depleted in nutrients. Springtime stratification occurs later in the season in the Gulf compared to the Red. Mixing depths are typically in the order of several hundreds of meters. Overall biomass figures, at all levels in the food chain, are low (typically less than 1 $\mu g\ l^{-1}$ Chl are recorded). The underwater light profiles are dominated by absorption by water and as a consequence, euphotic depth is well beyond 100 meters. The combination of low nutrient levels and – even in winter time – high incident solar radiation without strong light attenuation in the water column, impose an energetic problem for phytoplankton: while sufficient light energy is available to induce significant rates of photochemical activity, the nutrients are lacking to realize matching growth rates. With the beginning of springtime, the nutrients from deeper water masses are entrained within the photic zone, thus allowing for a typical bloom of phytoplankton growth. The Gulf of Aqaba and the Red Sea represent model systems to investigate the regulatory response (in terms of mechanisms and time characteristics) of phytoplankton exposed to high light and low nutrient conditions and the transition to a more nutrient replete situation.

Due to the lack of nutrients in both ecosystems, the phytoplankton absorbs more energy than can be safely channeled into metabolic processes. The excess energy could impair critical photosynthetic

components. The only solution to repair damaged components is to biosynthesize and replace the functionally needed structures. However, at low nutrient concentrations, such repair mechanism is expected to be slow and – in case full repair cannot take place overnight – would further minimize the photochemical potential for forthcoming days. If the irradiance levels were invariant in nature, the overall photochemical activity would slow down and only increase when more nutrients become available. In reality, the irradiance that is available for phytoplankton varies in a sinusoidal pattern, thus providing time windows where the rate of energy absorption matches the instantaneous biosynthetic demand. The short time windows of low irradiance do allow balanced acquisition of nutrients and carbon, provided that active regulatory mechanisms exist to safely dissipate excess light energy, and hence, minimizing long-lasting deteriorating effects of structural damage.

Between March 1 and March 9 samples were analyzed in both ecosystems. Technical problems during the first 3 days limited the experimental activity to observations of biophysical aspects of the energy regulation in photosystem II (PSII) only. The results will be examined in order to describe the regulatory potential of the photosynthetic machinery in phytoplankton from both ecosystems. A technique called 'fluorescence induction' was used to quantify PSII photochemistry (for the reader unfamiliar with this technique, a short introduction is given below).

Short explanation of experimental methodology

This section is not relevant for the preliminary results, but offers some general introduction to the applied methodology.

Photosynthesis is a hierarchical, sequential link of light absorption and electron transfer steps. Schematically, it might be represented as:

PSII -> Qa -> Qb -> PQ ->cyt. b6f -> PC -> PSI -> Fd -> terminal acceptor (e.g. CO_2, NO_3)

After light absorption by the pigments, electrons are transferred from water, through PSII and several other electron carriers, passed on to PSI and ferredoxin (Fd) finally used in metabolic processes. The term photochemistry refers to the successful transfer of electrons from PSII to the first stable electron acceptor Qa. Dark adapted phytoplankton shows a high probability for photochemistry, simply because all Qa is oxidized. Any process that reduces Qa will make photochemistry less likely. At any given light intensity, a fraction of Qa will become reduced. At the same time, Qa may become more reduced if the rate of electron transfer to a final acceptor is less than the rate of electrons transferred to Qa. PSII-complexes that do have their Qa reduced have to dissipate the absorbed light energy in a different way, most prominently as heat, and partly as fluorescence. In consequence, the probability to dissipate absorbed light energy as fluorescence is minimal with all Qa oxidized, and maximal if all Qa is reduced. A simple biophysical analysis of these two fluorescence extrema shows, that the difference between maximal and minimal fluorescence relative to the maximal level is a fairly accurate quantification of the PSII quantum yield (ϕ_{PSII}): the amount of electrons transferred from PSII to Qa for one photon absorbed in the pigment array associated with PSII. This quantum yield is stoichiometrically related to the better known oxygen quantum yield, and similarly to the quantum yield for carbon fixation. Experimentally, the fluorescence extrema are easily measured with a so-called active fluorometer in samples that were poised with diuron (DCMU), which effectively blocks electrons flowing from Qa to Qb (hence, one can easily reduce all Qa).

The time dependent increase in fluorescence after switching on light on a sample poised with DCMU yields information on the number of pigment molecules that are associated with PSII, and on energy flows in and between PSII complexes. The following analogy highlights the interpretation

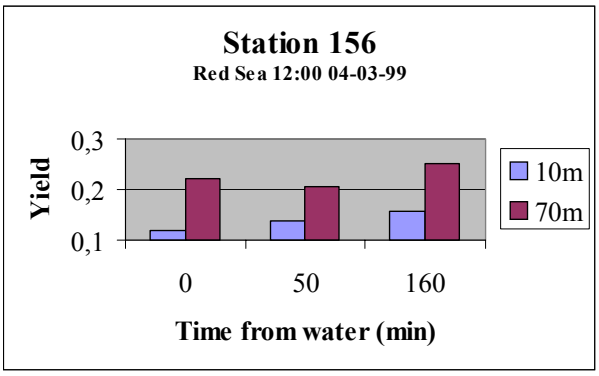

Fig. 37: Quantum yield values at 10 and 70 meter, measured immediately (t=0) or after a dark incubation of 50 and 160 minutes.

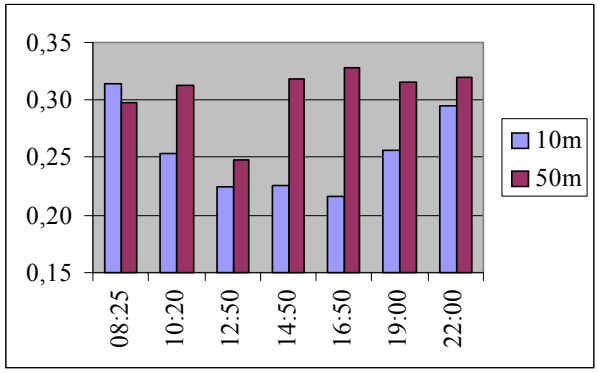

Fig. 38: Quantum yield values for two depths, 10 and 50 meter, taken along a latitudinal cross section in the Gulf of Aqaba. Data were ordered by sampling time.

of fluorescence kinetics: using water (= light) flowing through a funnel (pigments) to fill a container (PSII), one might keep track of the water level by looking at the water flowing out a small leak (fluorescence) of the container.

Preliminary results

Samples from 10 m and 70 m taken in the morning of March 4 from the Red Sea showed very low ϕ_{PSII} values (compared to the theoretical upper limit of around 0.7). The high-irradiance exposure to the surface samples caused a very strong decrease in ϕ_{PSII}. Fifty or 160 minutes of darkness did not increase ϕ_{PSII} even though such treatment allows for a full re-oxidation of Qa (Fig. 37).

On March 6, a latitudinal cross section was examined in the Gulf of Aqaba. The data are plotted as a function of local time, and not ordered by geographical location (Fig. 38). Early morning and late evening yield values were highest for the surface samples, with a typical diurnal decline during midday. Samples from 50 meter did not show a response to the daily irradiance variation, despite the fact that irradiance levels are still high at this depth.

Conclusion

The measured quantum yield values increased with the progression of the cruise, indicating that we witnessed the onset of the early spring phytoplankton bloom development. At the same time, samples from between 50 to 70 meters did not respond to the diurnal changes in solar radiation. Such a response would only be possible if nutrient limited cells decreased their PSII-antennae size during winter. The large changes in qantum yields in surface sample can be explained assuming that the rate constant for heat dissipation is highly variable and maximal during nutrient replete conditions (winter).

5.2.2.4 Grazing Versus Nutrients as Limitating Factors of Phytoplankton Growth

(U. Sommer)

Phytoplankton in the northern Red Sea and in the Gulf of Aqaba is characterized by a low biomass dominated (>95%) by extremely small cells (<5 µm). Only during the summer period also the large, nitrogen fixing cyanobacterium *Trichodesmium* becomes important. Algae of the size range from 5 to several 100 µm are extremely scarce, usually detectable only by plankton nets or by sedimentation of several liters. In this study the question should be answered, whether the scarcity of nanophytoplankton and of microphytoplankton is caused by nutrient limitation or by selective removal by grazers. During the stratified period dissolved N and P are depleted below the detection limit while remaining Si are low but still detectable (ca. 0.5 µM). The resulting high Si:N ratios make the scarcity of diatoms a special surprise. The analysis of grazing in this study is focused on protozoan grazing, while the grazing pressure by metazoa can be calculated from the abundance data obtained in the study on the distribution of mesozooplankton (see Chapter 5.2.4.1) and the grazing rate data on the study mesozooplankton as grazers (see Chapter 5.2.4.2).

The importance of nutrient stress versus grazing pressure was studied by shipboard experiments where algae were released from one or both control factors in a fully factorial combination of manipulations. Nutrient manipulations consisted of controls (no addition), silicate enrichment (4 µM Si) to release diatoms with high Si- but low N- and P-requirements from nutrient stress and a full enrichment (4 µM Si, 4.5 µM N, 0.3 µM P) to release all phytoplankton from nutrient stress. Grazer manipulations consisted of sieving of the sample through net-screens with the mesh sizes 100 µM (removal of metazoa but not of protozoa), 20 µM (removal of larger protozoa) and 10 µM (removal of medium sized protoza). Protozoa <10 µm were not removed because the usually feed on pico- but not on nanoplankton and their removal would have also removed the target algae of this study.

The water samples for the experiments were taken from 10 m depth from two stations in the Gulf of Aqaba (118, 152) and two stations in the open Red Sea (132, 145) in order to compare phytoplankton from a circulating water column (Gulf of Aqaba, >300 m mixing depth) to phytoplankton from a stratified water column (Red Sea, mixing depth <50 m). The manipulated water samples were incubated in 2 l bottles floating in a deck incubator. The deck incubator was cooled by a flowthrough of surface water and shielded against direct sunlight by a cover, which absorbed ca. 50% of incident radiation.

Samples from the incubation bottles were taken at the start, after 2, and after 5 days. The 2 d samples are expected to show the response of species, which are relatively abundant, and/or to respond quickly to nutrient enrichment. The 5 d samples are expected to show the response of rare and/or slowly reacting species. Aliquots of the samples were preserved by Lugol's iodine for identification and cell counts of the nanoplankton species, preserved by glutardialdehyde for identification and cell counts of the picoplankton species, and filtered through GFF-filters for chlorophyll measurements. The response of individual taxa and of bulk biomass to the experimental treatments will be assessed by calculating growth rates from the cell density/biomass data. Protozoa will be identified, counted and checked microscopically for algae in their food vacuoles.

5.2.2.5 Characterization of Prokaryotic Picoplankton in the Northern Red Sea

(A.F. Post)

Background

The northern Red Sea and the Gulf of Aqaba are adjacent waterbodies that differ in their physical properties in winter. Whereas the mixed layer in the northern Red Sea spans only part of the photic zone (<100 m), mixing extent to far below the photic layer in the Gulf of Aqaba (>300 m). The deep convective mixing in the Gulf of Aqaba causes the injection of nutrients from deep waters into the otherwise nutrient depleted photic layer. Throughout the year picophytoplankton (< 2 mm) dominates the phytoplankton community and they contribute more than 95% of the chlorophyll *a* biomass at most if not all locations in the Red Sea. This fraction contributes significantly to the pelagic food web as well as to the coral reef community (Yahel et al., 1998). The picophytoplankton community consists of a number of eukaryotic genera and of only two prokaryotic genera, *Prochlorococcus* and *Synechococcus.*

Picophytoplankton groups undergo a distinct annual succession in the Gulf of Aqaba: Eukaryotic species (10^3-10^4 cells.ml^{-1}dominate the deep mixed water column, whereas *Synechococcus* (10^4-10^5 cells.ml^{-1}) and *Prochlorococcus* (>10^5 cells x ml^{-1}) dominate the thermally stratified waters in early and late summer respectively (Lindell and Post, 1995).

Prochlorococcus numbers decline by four orders of magnitude during deep winter mixing.

For both *Synechococcus* and *Prochlorococcus* it is known that different ecotypes (co)exist. Phycoerythrobilin (PEB) rich, non motile, *Synechococcus* types are common in continental shelf waters and mixed water columns, whereas phycourobilin (PUB) rich, motile *Synechococcus* are found in nutrient deplete, open ocean waters. Differences in pigmentation were also found in *Prochlorococcus* types. The "deep" *Prochlorococcus* types have high chlorophyll b_2/a_2 ratios whereas the "shallow" types have low chlorophyll b_2/a_2 ratios. The PEB-rich *Synechococcus* and the deep *Prochlorococcus* are characteristic for waters with higher nutrient availability while the PUB-rich *Synechococcus* and the shallow *Prochlorococcus* are typical of waters with low nutrient availability.

The different types are distinguished not only in their physiological properties, but also in their clustering in phylogenetic trees based on 16S rRNA sequence similarities.

Different *Synechococcus* and *Prochlorococcus* types are found to co-occur in the Red Sea at various locations (Post et al., in prep.). However, little is known about the population dynamics of these ecotypes drive by the competition for available nutrients and light. We have identified a gene *(ntcA)* the expression of which forms the first step in the response of *Synechococcus* and *Prochlorococcus* to limited supply of combined nitrogen (Lindell et al., 1998), presumably the main limiting factor in primary productivity in the Red Sea. Study of this gene yields information at two levels:

1. The expression of the gene is proportional to the level of N-limitation.
2. Sequence similarities yield phylogenetic trees that are virtually identical to those obtained with 16S rRNA sequences.

The purpose of my work during the Meteor cruise in the northern Red Sea (20February - 1March 1999) was to further characterize prokaryotic picophytoplankton in shallow and deep mixing waterbodies during winter. Samples were taken to test the following hypotheses:

1. *Prochlorococcus* populations do occur in the northern Red Sea, but not in the deeply mixed Gulf of Aqaba and

2. Nutrient deplete waters of the northern Red Sea carry different ecotypes of prokaryotic picophytoplankton than the nutrient replete water of the Gulf despite the open connection between the two areas.

Sampling

Six liter samples were taken at six depths at six stations in the Gulf of Aqaba (Stations I,V,VI (2x); Stations II, III and IV (lx)) and four stations in the northern Red Sea (Stations VIII, XI, X and XI). Sampling depths in the Gulf of Aqaba were 10, 20, 60, 100, 200 and 300 m, whereas in the northern Red Sea sampling depths were 10, 30, 60, 100, 150, 200 m. Water samples were filtered over a 20 mm mesh. Duplicate 1.5 ml samples for flow cytometry analysis were preserved with 0.2% paraformaldehyde, quickly frozen and stored at -80°C. Six liter water samples for DNA analysis were filtered onto 47 mm 0.45 mm Gelman Supor 450 filters, submersed into 4 ml of lysis buffer and stored at -80°C. Ancillary data like temperature and salinity, chlorophyll *a* and inorganic nutrient concentrations were collected by other teams during sampling at the station.

Analyses

Flow cytometry samples will be analyzed at MIT, Cambridge Ma, where flow cytometers are set up for analysis of the especially dim *Prochlorococcus* populations. Flow cytomtery analysis will provide quantitative information on the populations sizes of both *Synechococcus* and *Prochlorococcus,* as well as on the existence of different ecotypes within either genus. DNA extracts will be analyzed at the Interuniversity Institute for Marine Sciences in Eilat. PCR amplification of a 450 bp *ntcA* fragment will yield products, which will be cloned into a pGEM-t vector. Environmental sequences will be obtained from individual clones and compared to sequences from cultured strains and isolates. In addition PCR products will be submitted to degenerating gradient gel electrophoresis (DGGE) or similar techniques for separation of different sequence populations (different ecotypes?). DNA samples from 400 m depths will be used as negative controls.

Prospects

Analyses are expected to provide valuable information on the "make-up" of the prokayotic picophytoplankton in two adjacent water bodies with distinctly different physical and chemical characteristics. Differences in picophytoplankton populations can then be related straightforwardly to the selective pressure that deep convective mixing exerts on prokaryotic picophytoplankton. We expect to find certain genotypes to be dominant (successful) in shallow mixing whereas other genotypes will be dominant in deep mixing water bodies. With knowledge about genotypes we can select laboratory strains to perform lab and field experiments to further analyze the effects of deep mixing on physiology and growth potential.

5.2.3 The Importance of the Microbial Loop

5.2.3.1 Bacterioplankton Dynamics

(M. Simon, H.-P. Grossart, N. Selje)

Introduction

The Gulf of Aqaba is known as a very oligotrophic extension of the Red Sea with a typical dominance of autotrophic picoplankton as primary producers and surface blooms of *Trichodesmium* spp. in

summer. In the food web and trophic structure of such oligotrophic systems based mainly on regenerated production the microbial loop usually dominates the carbon and nutrient flow.

Until today, however, the Gulf of Aqaba has virtually not been studied with respect to the significance of the microbial loop and the growth and substrate dynamics of the heterotrophic bacterioplankton. Therefore, we took the excellent chance during this cruise to do first investigations on this subject in the Gulf and for comparison also in the northernmost Red Sea south of the Strait of Tiran.

Our measurements included the following parameters:

- Bacterioplankton cell numbers
- Bacterioplankton biomass production measured by ^{14}C-leucine incorporation
- Turnover rates of free amino acids and glucose by a radiotracer approach
- Concentrations of dissolved organic carbon (DOC)
- Concentrations of dissolved free and combined amino acids
- Concentrations of dissolved free and combined carbohydrates
- Enzymatic activities of the leucine amino-peptidase, the a- and b-glucosidase and the chitinase (N-acetylglucosaminidase)
- Analysis of the community structure of the bacterioplankton determined by in situ hybridization with rRNA-targeted fluorescently labeled oligonucleotide probes (FISH) and by denaturing gradient gelelectrophoresis (DGGE) of PCR-amplified 16S rRNA gene fragments

In addition, we produced macroscopic aggregates in rolling tanks for further investigations of the microbial colonization of this unique environment in the home lab. Changes in bacterial community structure and activity due to nutrient additions were studied in a mesocosm experiment in which we added starch, agar, peptone and autoclaved organic material from a green algae as bacterial substrates to water samples.

Bacterioplankton numbers, production, and growth

During the entire cruise we sampled 6 profiles in the Gulf (stations 122,125, 139, 151, 152, 157) and 8 in the Red Sea (stations 128, 131, 133, 148, 149, 150, 154, 157). Bacterioplankton numbers ranged between <1 and $4x10^8$ L^{-1}. Rates of bacterioplankton biomass production at 100 and below were between <5 and 35 ng C L^{-1} h^{-1}. At 10 and 50 m rates reached 40-58 ng C L^{-1} h^{-1} with highest values in the Red Sea between 21 and 27 February and at the northernmost station in the Gulf near Aqaba at the end of the cruise (Fig. 38). These rates are low as compared to more productive pelagic systems but typical for oligotrophic oceanic regions. Rates integrated over the upper 150 m increased twofold from the northernmost stations (122, 139, 151) via the southern Gulf (152) to the northern Red Sea between 21 and 27 February (Fig. 39). In contrast, between 28 February and 5 March rates in the Red Sea were lower than at the northernmost station in the Gulf (station 157) where bacterial production had increased twofold since the first visit of this station. Often, biomass production rates in the vicinity of islands and coral reefs were higher than at more distant stations. Bacterioplankton growth rates varied between <0.05 and 0.4 d^{-1} (doubling times of 2-4 days) and thus indicated that the bacterioplankton community was fairly actively growing at the stations with highest production rates. Whenever rates of biomass production were elevated numbers of bacteria were reduced, suggesting an enhanced grazing pressure on the bacterioplankton standing stock as a rapid response by bacterioplankton grazers.

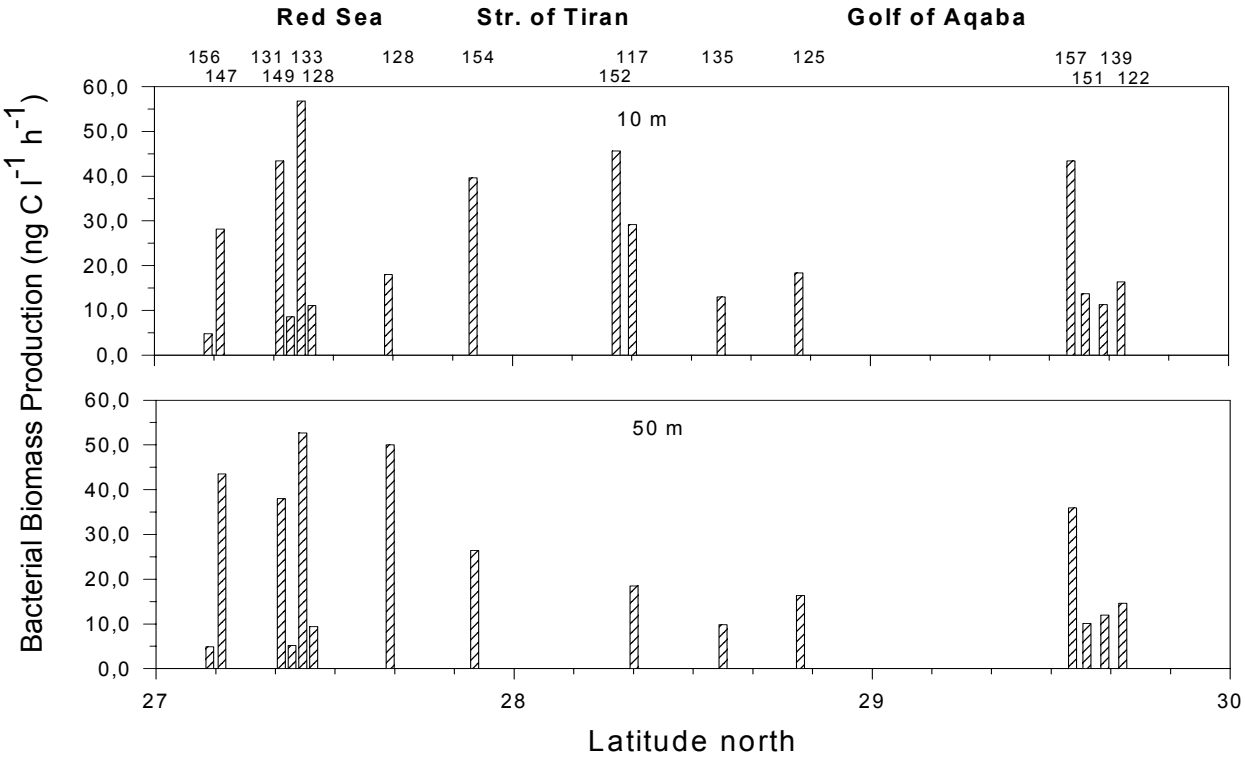

Fig. 38: Bacterioplankton biomass production at 10 and 50 m in the Gulf of Aqaba and the Northern Red Sea between 21 February and 5 March 1999. Stations are indicated by numbers. Measurements were done by the ^{14}C-leucine incorporation technique. Numbers above the upper panel indicate station numbers.

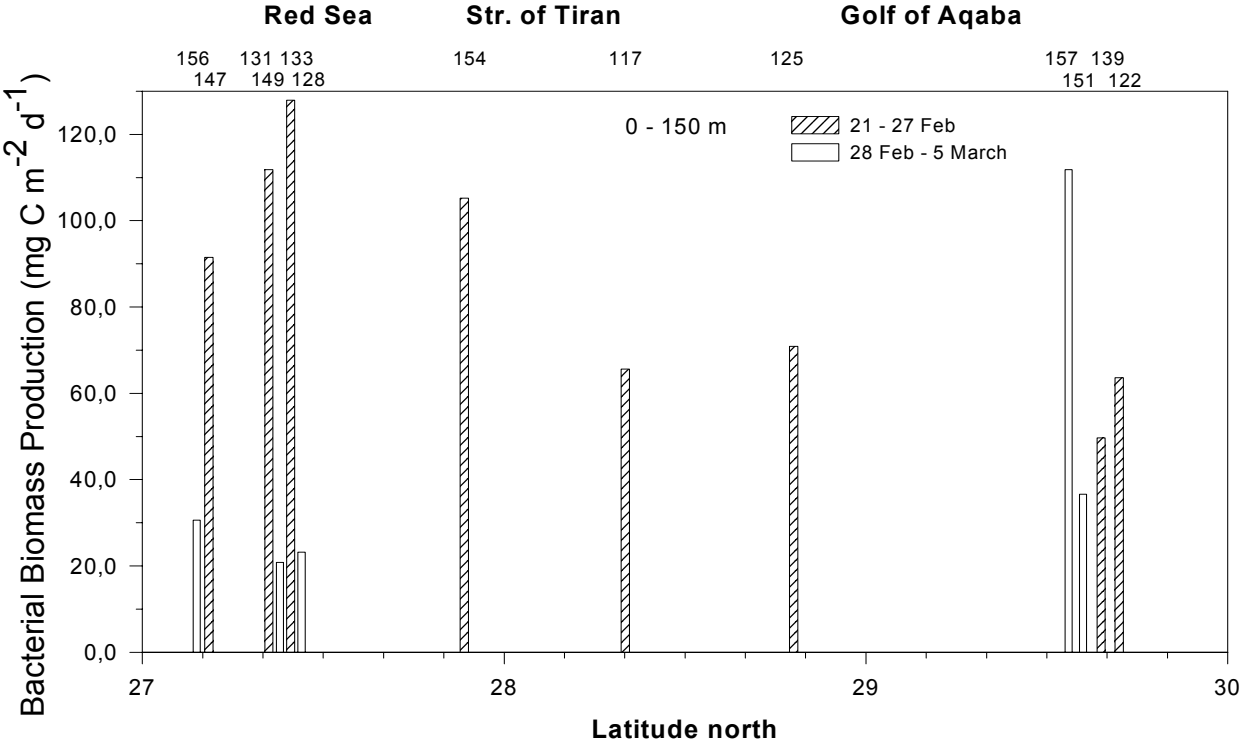

Fig. 39: Bacterioplankton biomass production integrated for the upper 150 m in the Gulf of Aqaba and the Northern Red Sea between 21 February and 5 March 1999. Stations are indicated by numbers. Numbers above the panel indicate station numbers.

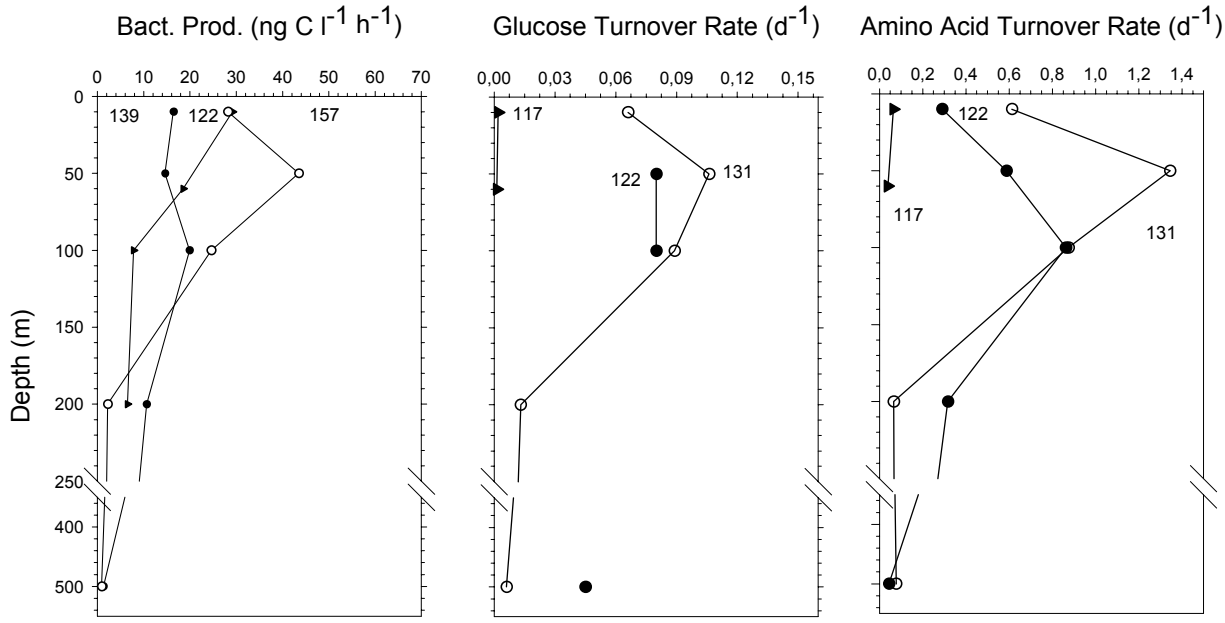

Fig. 40: Bacterioplankton biomass production (BP) and turnover rates of glucose and amino acids at stations 117 and 122 in the Gulf of Aqaba and at station 131 in the Red Sea.

Turnover rates of amino acids and glucose

Turnover rates of free amino acids were in the range of <0.1 to 1.4 d^{-1}. Between 21 and 27 February, rates were higher in the Red Sea than in the Gulf (Fig. 40) whereas thereafter we observed the opposite trend with highest rates at the end of the cruise at the northernmost station (157) where also high rates of bacterial production were measured. Turnover rates of glucose were one order of magnitude lower than those of amino acids and showed no systematic differences between the Gulf and the Red Sea (see example on Fig. 40). After the analyses of dissolved amino acids and carbohydrates, which are not yet finished, we will be able to also determine uptake rates of amino acids and monosaccharides and to calculate the fraction of the biomass production supported by the uptake of these different substrate classes. The analyses of dissolved combined amino acids, carbohydrates, and of DOC will complement our studies on the bacterioplankton substrate turnover.

Measurements of bacterial enzymatic activities

Ectoenzymatic hydrolytic activities of bacteria, determined at saturating substrate concentrations, were usually measured at the same stations and depths as the parameters mentioned above. Rates ranged between <0.1 and 245 nmol l^{-1} h^{-1} and thus were fairly low. In general, activities of the leucine aminopeptidase and b-glucosidase were higher than that of the a-glucosidase and chitinase. As for biomass production, rates at stations close to islands and coral reefs were elevated suggesting an input of polymeric substrates from reefs into the pelagic zone. There were no obvious systematic patterns between stations in the Gulf and the Red Sea and also no systematic vertical distribution (Fig. 41). Often, when bacterial biomass production and amino acid turnover rates exhibited maxima rates of the leucine aminopeptidase were reduced such as at station 131 (Figs. 40 and 41).

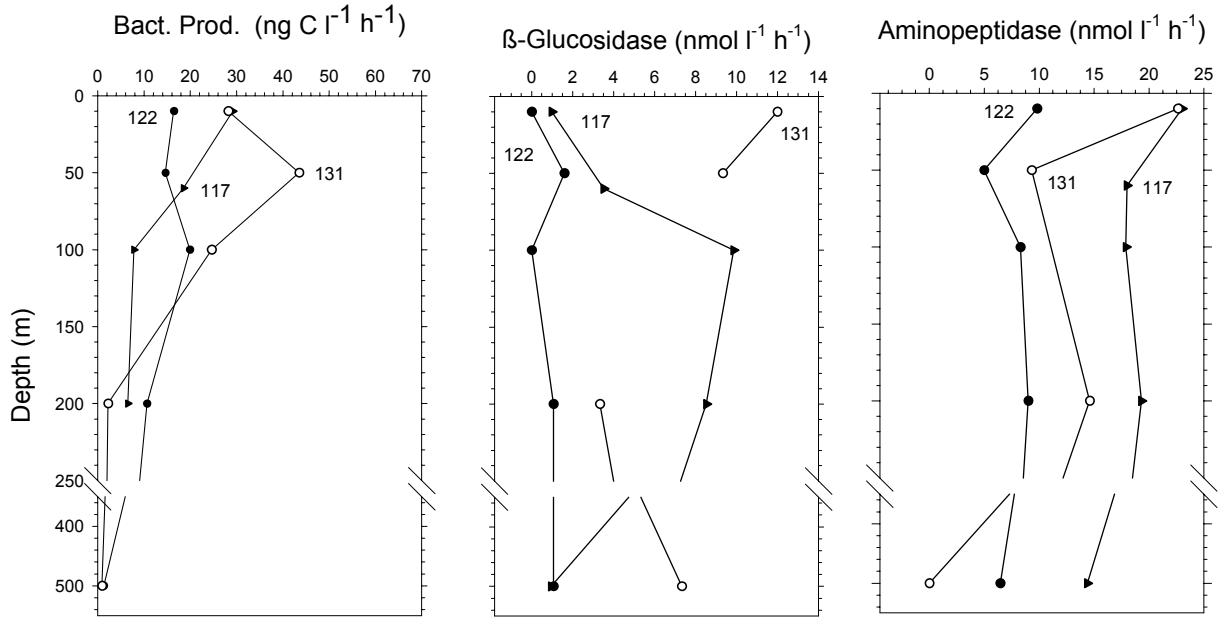

Fig. 41: Bacterioplankton biomass production (BP) and hydrolysis rates of b-glucosidase and leucine aminopeptidase at stations 117 and 122 in the Gulf of Aqaba and at station 131 in the Red Sea.

Mesocosm Experiment

In the mesocosm experiment with substrate enrichments the bacteria responded rapidly to the increased substrate concentrations, most pronounced at the additions of peptone and the green algal concentrate. This effect was evident from highly increased rates of bacterial biomass production, amino acid and glucose turnover, and also from increased enzymatic activities.

Bacterioplankton community structure

Samples for the analysis of the bacterioplankton community structure by FISH with various oligonucleotide probes and DGGE were taken from various depths (10 to 800 m) at 10 stations in the Gulf /117, 122, 125, 137, 139, 145, 152, 157, 165, 167) and 6 stations in the northern Red Sea (131, 144, 147, 149, 154, 156). Each sample was separated into a fraction of particle-associated and free-living bacteria by filtration onto 5 µm and 0.2 µm polycarbonate-filters, respectively. Filters were placed into sterile caps and stored at –20°C until further processing and the final analysis in the lab at home. Preliminary analyses of samples of 10, 100, 200, and 500 m from station 117 by DGGE show distinctly different banding patterns, and thus differences in the community structure, between the particle-associated and free-living bacterial fraction and also between the mixed layer (10-200) and 500 m.

5.2.3.2 Microbial Food Web

(U.-G. Berninger)

Activities and preliminary results

The concept of the microbial food web and the prominent role of heterotrophic protists as key organisms channeling organic carbon from the smallest size fraction (picoplankton) to higher pelagic food webs, have been widely accepted for most aquatic environments. However, there are

surprisingly few data available referring to the Red Sea and the Gulf of Aqaba. Previous studies have shown that the concentrations of heterotrophic nanoflagellates, the main bacterivores in most pelagic systems, are relatively low here, and that the autotrophic community at most times is dominated by very small forms, the so-called autotrophic picoplankton (consisting mostly of cyanobacteria and small eukaryotic algae). The goal of my investigations was to study interactions within the microbial food web and the possible role of protozoan grazing in the mixed surface waters of this system. To this end five on-deck incubation experiments were carried out, using samples collected at five different sites in the study area.

As experimental approach 'dilution experiments', developed by Landry and Hassett (1982) and later refined by Landry et al. (1995) were chosen. This method uses varying dilutions of whole (unfiltered) water with 0.2 µm filtered water to alter the encounter rate of predators with their prey, and therefore alter the net growth rate of the prey. At higher dilutions, the encounter rate between predator and prey will be lower, decreasing the predation rate and increasing the net growth rate of the prey. When the net growth rates are regressed against the proportion of whole water, the intercept (at the theoretical 0% whole water, where predators would be totally absent) gives the growth rate of the prey in the absence of predation, while the slope of the regression gives the grazing rate of the predators. There are three assumptions underlying this method:

(1) the specific growth rate of the prey is not density dependent,
(2) predation is a direct linear function of prey abundance, and
(3) prey growth can be adequately represented by the exponential growth equation.

In order to avoid effects of nutrient limitations during the incubations, samples are supplemented with a mix of nutrients at the beginning of the experiments.

Experiments were conducted using water from stations 123, 132, 147, 152 and 157. Sampling depth was 10 m below the water surface, samples were collected either before or after sunset to avoid light shock to the planktonic organisms. The dilution steps created 100, 90, 80, 60, 50 and 35% whole water. Experimental containers were filled following a randomized design. Duplicate treatments of each dilution were poured into 2.5 l clear polycarbonate bottles and incubated for 36 hours under in-situ conditions in on-deck incubators connected to a sea water flow-through system. The incubators were covered with semi-transparent lids, reducing the incident light level to ca. 50%. Initial samples for the enumeration of picoplankton, nanoplanktonic protists, microzooplankton, planktonic algae, nutrient concentrations and concentrations of chlorophyll a were collected before the incubations were started. At the end of the incubations, subsamples for the quantification of the components mentioned above were collected. Samples for the enumeration of picoplankton and nanoplankton were preserved in 1% (f.c.) glutaraldehyde, samples for microzooplankton and algae were fixed in Lugol's solution, samples for later nutrient analyses were deep-frozen, and 2 l of water were filtered onto GF/F filters for chlorophyll analysis and also frozen.

The quantification and the further analyses will have to be carried out in the home laboratory.

Data that will become available after the processing of the samples will be completed include:
- standing stock of picoplankton, nanoplanktonic protists, microzooplankton, chlorophyll *a* concentration and nutrient concentration
- growth rates of the various groups of potential prey in the system
- predation rates on picoplankton (autotrophic and heterotrophic) and small algae.

5.2.4 Zooplankton

5.2.4.1 Distribution and Ecophysiology of Zooplankton

(S. Schiel, W. Hagen, M. Dowidar and C. Richter)

Objectives

The primary aim of the zooplankton investigations was to describe the transitional period from winter to spring in the Gulf of Aqaba as compared to the northern Red Sea. This included the horizontal and vertical distribution of plankton communities, their effect on phytoplankton biomass as well as seasonal adaptations of the key species. We postulated regional differences between the Gulf of Aqaba and the Red Sea proper, namely an immature state of the pelagic community in the northern Gulf characterized by deep mixing, bottom up control of phytoplankton biomass and a less diverse zooplankton community as opposed to a mature pelagic system in the stratified Red Sea proper characterized by a low biomass species rich community. We also postulated differences in zooplankton distribution between open and near shore waters in the vicinity of coral reefs.

A second aim was to carry out large- and mesoscale surveys of macrozooplankton biomass and to relate biomass changes to differences in developmental state of the pelagic community, vertical migration patterns, hydrographic conditions and topographic effects by the Straits of Tiran and islands, using a combination of ship-borne ADCP and multiple opening-closing nets.

A third goal was to collect material for taxonomic analyses of micro- and gelatinous macrozooplankton by experts from Egypt and Germany (Dr. M. Dowidar, Dr. N. S. Abdel-Rahman, Dr. R. Böttger-Schnack) to be analyzed in Alexandria, Bremen and Kiel.

The final goal was to contribute to a mass-balance estimate of nutrients and plankton exchanged between Gulf of Aqaba and Red Sea across the sill in the Straits of Tiran.

Material and Methods

Major gear employed for the distributional studies of mesozooplankton were the small and the new large Multiple Opening and Closing Net (HYDROBIOS, Kiel. Small net: 5 nets, opening of 0.25 m^2, 55 micron mesh; large net: 9 nets, 0.5 m^2, 150 micron). Stratified vertical hauls covered the entire water column in 100 m and 200 m (bottom strata, deep stations) increments between the surface and about 1300 m. Altogether, 13 hauls were carried out with the small net, they served particularly the studies in small copepods. The backbone of the zooplankton work consisted of 43 hauls with the large net. Both together provided a rich set of more than 400 samples.

To study the distribution of macrozooplankton a BIOMOC (multiple opening closing net, 9 nets, 1 m^2, 330 micron) was trawled behind the ship (2 knots, double oblique haul, 100 m depth increments). As the opening/closing system malfunctioned, BIOMOC was abandoned after 6 casts. For the same reason information on depth affiliation and volume filtered are uncertain. Therefore BIOMOC samples will be analyzed for qualitative purposes only.

All samples were fixed in 4% formaline seawater solution. At selected stations samples were also taken with MultiNet maxi (n=20) and MultiNet mini (n=5) for molecular genetical and biochemical analyses and preserved in ethanol or deep-frozen at -80°C. Zooplankton species as *Rhincalanus* have been sorted out from samples of Nansen Net, MultiNet maxi and MocNess.

In addition to sections along the main axis of the Gulf extending into the Red Sea –but omitting the Straits of Tiran, which is closed for research of stations- we carried out a cross section through the northern Gulf between Egypt and Jordan, which was complemented on its eastern side by near

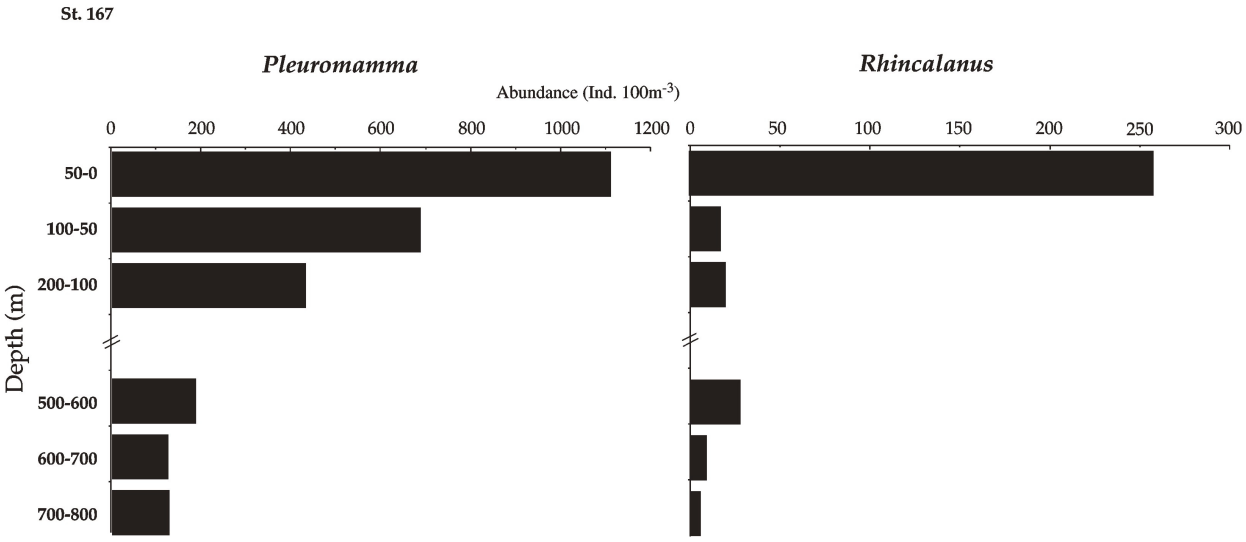

Fig. 42: Vertical distribution of the calanoid copepods *Pleuromamma* sp. and *Rhincalanus nasutus* in the southern Gulf of Aqaba (Station 167) during the second part of the cruise.

shore work from the boat of the Aqaba Marine Science Station inter alia for a study of the effects of coral reefs on the size fraction distribution of zooplankton (Tariq Al-Najjar).

Zooplankton abundances were generally low, particularly in the Red Sea proper. Highest concentrations were found in the top 100 m, coinciding with the phytoplankton maximum. Zooplankton communities were dominated by a diverse assemblage of small calanoid copepods. Other conspicuous groups were cyclopoid copepods, amphipods and large chaetognaths. Gelatinous zooplankton (medusae, siphonophores, salps) and other macrozooplankton (fish larvae, euphausids) were rather scarce, even in the BIOMOC samples. Sorting of zooplankton samples and taxonomic analyses are under way in Alexandria, Bremerhaven and Kiel.

Of the larger calanoid copepods, *Pleuromamma* sp. occurred in moderate numbers with highest concentrations near the surface (Fig. 42a). Abundances increased during the second leg (Fig. 43) when early developmental stages indicated the onset of a new generation (Fig. 44). The very large calanoid *Rhincalanus nasutus* was found in low numbers, initially at depths between 400 and 600 m where it appeared to be in a resting stage with clearly visible oil sacs, but empty guts and unripe gonads. In contrast, a week later these specimens were in an active state near the surface (Figs. 42b and 43)

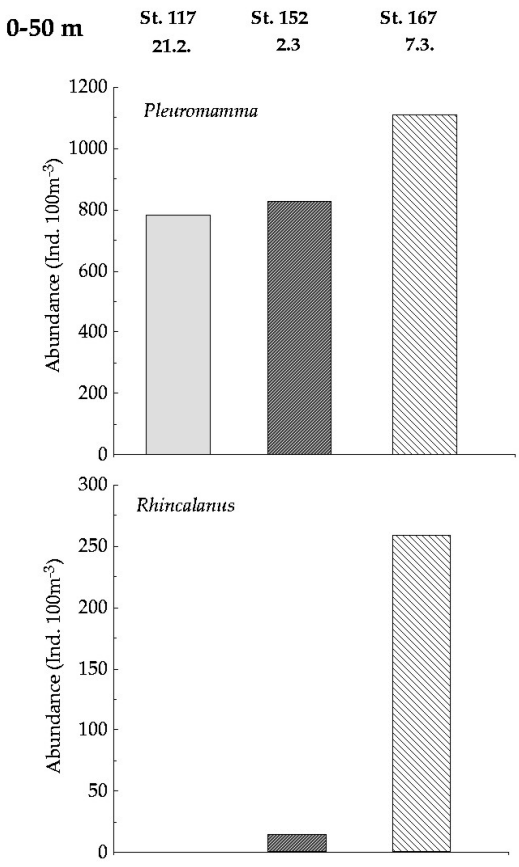

Fig. 43: Temporal variation in the near-surface abundances of the calanoid copepods *Pleuromamma* sp. and *Rhincalanus nasutus* in the southern Gulf of Aqaba during repeated visits of Pos. VI in the course of the study (Stations 117, 152 and 167).

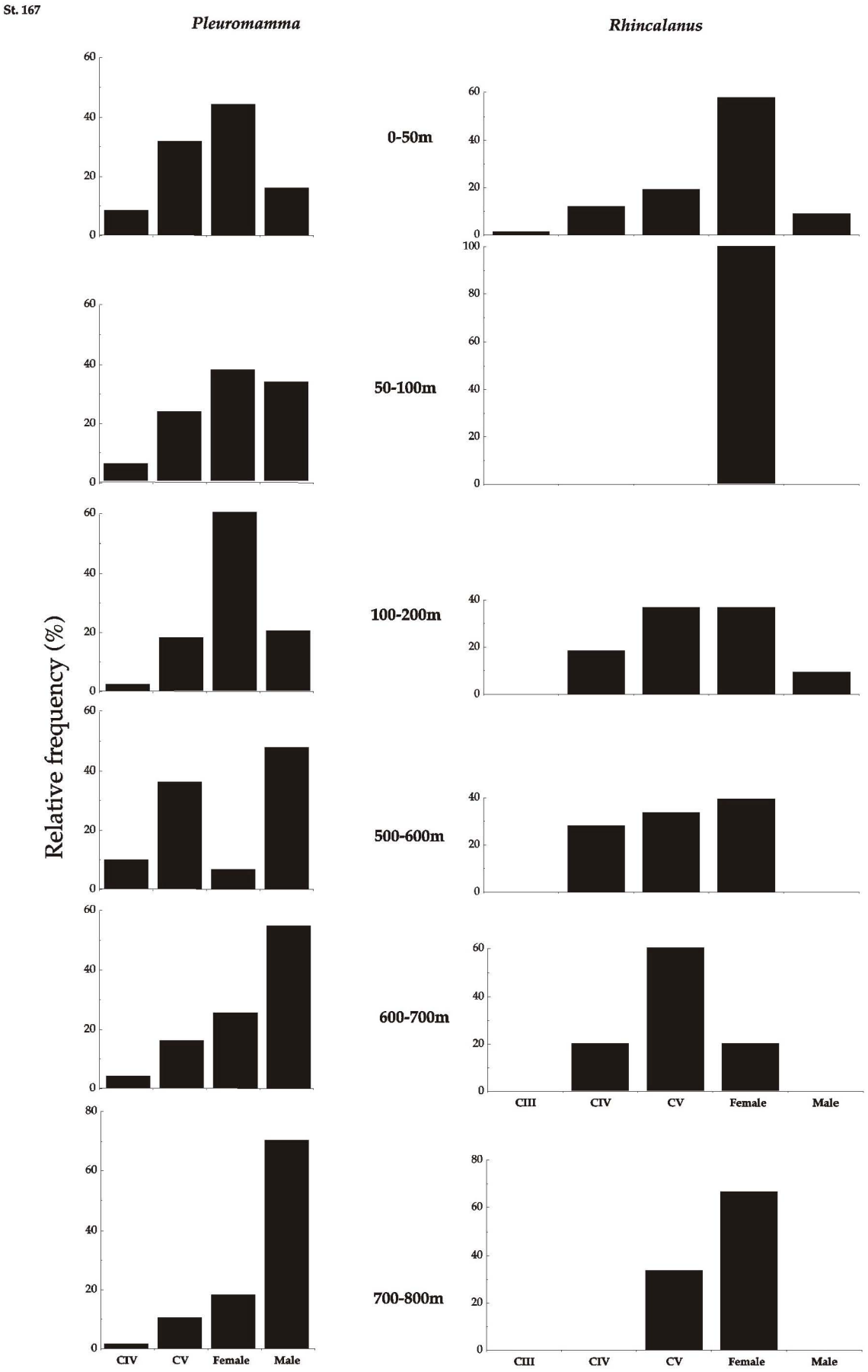

Fig. 44: Vertical distribution of *Pleuromamma* sp. and *Rhincalanus nasutus* copepodite stages in the southern Gulf of Aqaba (Station 167).

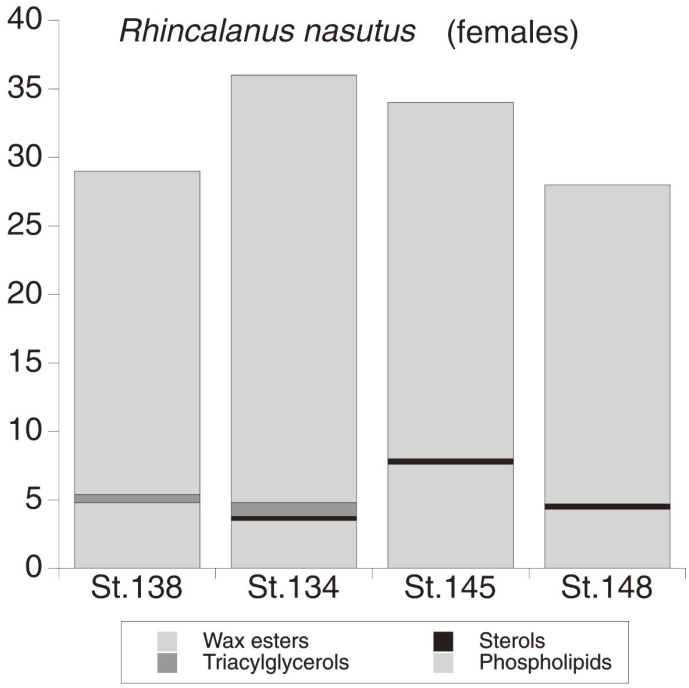

Fig. 45: Total lipid content and lipid class composition in females of *Rhincalanus nasutus* collected during Meteor cruise 44/2 (stations sorted from north to south).

and feeding experiments revealed high ingestion rates of the population dominated by females (Fig. 44), although egg production had not commenced as yet.

Subsequent lipid analyses of late copepodids (CV) and females of *Rhincalanus nasutus* showed high lipid and wax ester levels, usually a characteristic of herbivorous copepods from higher latitudes and very similar to the lipid pattern of *Rhincalanus gigas* from Antarctic waters. Throughout the investigation period lipid contents of *R. nasutus* ranged around 30% of dry mass with the primary depot lipid, wax esters, usually making up 80-90% of total lipids (Fig. 45). Higher concentrations of the fatty acid 16:1(n-7) suggest significant diatom uptake, when these energy reserves were accumulated.

A thorough investigation of the samples will elucidate the development of the zooplankton community in the Gulf and the Red Sea. These data will be discussed with respect to the life strategies of the species and relationships to hydrography and primary production. Additional evidence on the state of the zooplankton, especially *Rhincalanus nasutus*, will be derived from their lipid quantities and compositions. The fatty acid compositions of the particulate matter may be reflected in the copepod lipids revealing trophic relationships by means of these biomarkers.

ADCP-sections revealed diel variations in the backscattering intensity possibly related to zooplankton vertical migration (cf. results, Physical Oceanography Group). ADCP-backscatter echograms will be compared to abundances of zooplankton in different acoustic size classes in order to assess physical and biological effects on the macrozooplankton distribution. Unfortunately, the mass balance of plankton and nutrients between the Gulf and Red Sea is thwarted by the absence of plankton data from the Straits region and by acoustic noise rendering the 30 m layers near surface and bottom useless.

However, with this exception the group's goals could be fulfilled thanks to the good international cooperative spirit within and among the working groups, as well as the sound leadership provided by the Chief scientist, the Master of the vessel and the on board representatives of the competent Egyptian authorities.

5.2.4.2 Mesozooplankton as Grazers

(H. Stibor, Th. Hansen)

Mesozooplankton grazing has two implications: It is the most important cause of algae and protozoan mortality. On the other hand, zooplankton grazing can also influence the growth rate of algae because it provides nutrients via sloppy feeding, excretion and defecation. In marine systems this recycling is sometimes the only source of important plant-nutrients like nitrogen or phosphorus. Additionally, not all algae are grazed by zooplankton with the same efficiency. Therefore, grazing by zooplankton can have also a strong impact on the competition between different algae species.

Not all zooplankton species have the same impact on the above mentioned processes. Different feeding modes, the production of fecal pellets, and selective feeding are some examples of mechanisms that differ between zooplankton groups.

In our study we investigated both sides of zooplankton grazing and its impact on the Red Sea algae community. In short term experiments we estimated the grazing rates of a varity of zooplankton species for different sizes of potential food resources. Long term experiments were planned to elucidate the role of different zooplankton groups for nutrient recycling and for structuring the phytoplankton community in the Red Sea.

Short term experiments

Zooplankton species of different functional groups (filter feeders, size selective capture feeders) and taxonomic groups (copepods, krill, ostracods, salps, appendicularia, polychaetes) were carefully isolated from net hauls with a Nansen net. After some hours of adaptation to laboratory conditions (controlled for temperature and light) we tested the vitality of the organisms (escape responses). Only healthy looking animals were put into experimental jars and fed for about 15 minutes with a natural phytoplankton community. We added radioactive labeled algae as tracers to the natural phytoplankton community and offered those mixtures to the different zooplankton species as a food resource. Our tracers had a size distribution from < 1 µm to about 100 µm and included a variety of possible food organisms for zooplankton ranging from bacteria to large diatoms.

Our experiments will result in estimates of size selective feeding, clearance rates and ingestion rates of important zooplankton groups in the Red Sea.

Long term experiments

We performed these experiments in semicontinous cultures exposed to natural light and temperature conditions in shipboard incubators. A daily exchange of 25% of the water was performed between a grazer unit, a bottle in which different species of zooplankton were incubated together with natural phytoplankton, and a prey unit, a bottle in which natural phytoplankton and protozooplankton was growing under exclusion of large zooplankton. Recycled nutrients and ungrazed (inedible) algae are transported from the grazer unit to the prey unit and influence there the succession of the phytoplankton and protozooplankton community. We investigated the effects of several species of copepods, euphausiids and salps in our experiments. The experiments were done according to a gradient design, i.e. that we increased the density of the specific zooplankton in replicated grazer units. This will allow estimating a possible density dependent influence of the zooplankton on the prey community. These experiments will give insight into differences between important zooplankton species in terms of nutrient recycling and the top down effects of unselective and size selective feeding. Additionally, these experiments will give measurements of the C:N:P ratios of important zooplankton species.

5.3 Preliminary Results of Leg M44/3

5.3.1 Very High-Resolution Multichannel Reflection Seismics

(C. Hübscher, W. Böke, M. Gutowski, R. Kästner, M. Salem)

5.3.1.1 Introduction

Multichannel seismic measurements were carried out with the equipment of the Department of Earth Sciences, Bremen University, utilizing two seismic sources of different volume in an alternating mode for some profiles. A SODERA Inc. S-15 water gun with a frequency range from 200 to 2000 Hz provides information on the upper 100 to 300 m of the sediment column, whereas a GI-Gun (Generator-Injector Gun; SODERA Inc.) with signal energy up to 350 Hz allows seismic imaging of sedimentary layers down to 1500 m below the sea floor. A total of 1680 km of multichannel data were collected along 89 seismic lines.

5.3.1.2 Instruments

The particular components of the entire seismic system are shown in Fig. 46 and will be described in the following sub chapters.

5.3.1.2.1 Trigger Unit

The custom trigger unit controls seismic sources, seismograph, MultiTrak Controller, online-plotter and digital scope (near-field hydrophones). The primary building blocks are an IBM compatible PC, an amplifier unit and a gun amplifier unit. The PC runs a custom software (WindowsNT 4.0 OS), which controls a real-time controller interface card (SORCUS) with 16 I/O channels, synchronized by an internal clock. The program user interface enables the operator to change trigger times of each device online. The amplifier unit converts the controller output to TTL levels, which have to be negative for most of the devices.

The gun amplifier unit was placed in the compressor container to avoid electronic noise in the seismic lab. It generates the required 60V/8 Amp. trigger level for the magnetic valves of the individual seismic sources.

5.3.1.2.2 Seismic Sources and Compressor

For the seismic surveying two different seismic sources, a GI-Gun and a watergun, were available. For some profiles they were triggered in an alternating mode at a time interval of 13 s between sources. If the GI-Gun was the only source, the time interval between shots was 10 s which results in a shot spacing of 25 m owing to an average ship speed of 4.9 kn over ground. Both sources were operated with an air pressure of 145 bar. Ship velocity (through water) during deployment and retrieval was 3 kn and 2 kn, respectively.

Junkers compressors owned by the Alfred-Wegener-Institute of Polar and Marine Research, Bremerhaven provided high-pressure air for gun operation. The compressors were operated according to the requirements of the chosen gun volumes.

The volume of a standard GI-Gun was reduced to 2 x 0.41 l by two special titanium volume reducers. It was towed starboard by a wire from the A-crane about 20 m behind the ship. The

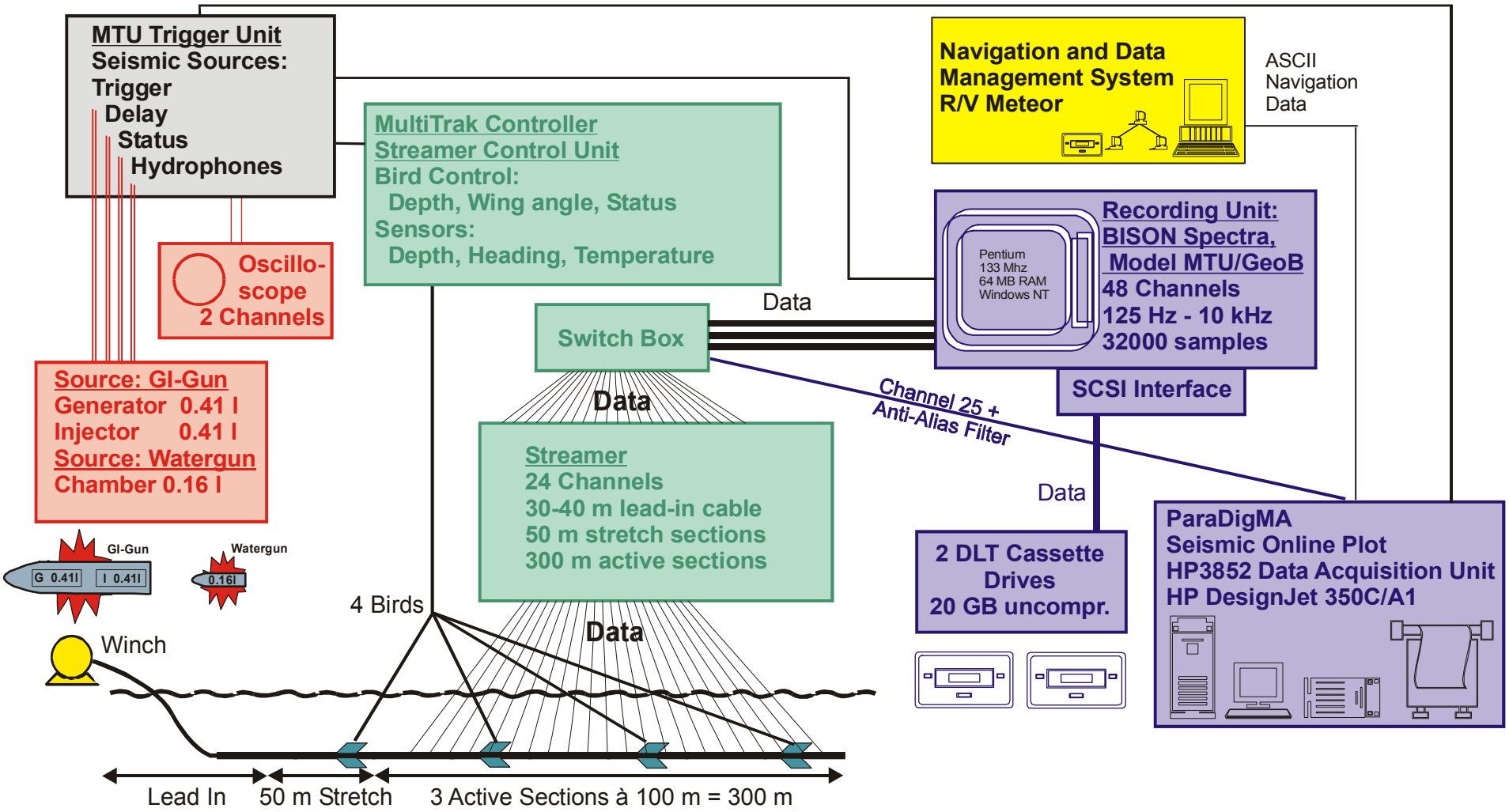

Fig. 46: Multichannel seismic instrumentation used during R/V METEOR cruise M44/3.

towing wire was connected to a bow with the GI-Gun hanging on two chains. An elongated buoy, which stabilized the gun in a horizontal position in a water depth of ~1.5 m, was connected above the bow. The Injector was triggered with a delay of 31 ms with respect to the Generator signal, which basically eliminated the bubble signal.

The second source type was a S15 watergun (Sodera) with a volume of 0.16 l. The watergun was towed by a Meteor rope, that was fixed to the umbilical of the watergun, about 20 m behind the ship's stern. A steel frame held the watergun in a tight position parallel to the elongated buoy in a depth of approximately 0.7 m.

5.3.1.2.3 Streamer

For operation in the shallow water environment of the Gulf of Aqaba only 300 m of the 600 m long streamer were used. The multichannel seismic streamer (Syntron) consisted of a tow-lead, one 50 m long stretch section and three active sections of 100 m length each. A 100 m long Meteor rope with a buoy at the end was connected to the tail swivel. A 30 m long deck cable connected the streamer to the recording system. During operations the streamer (tow lead) was fixed with two Meteor ropes. The distance from the ship's stern to the beginning of the stretch section was 40 m. In order to optimize the frequency response character of the streamer in shallow water and therefore large reflection angles, hydrophone groups consisting of only 2 hydrophones at a distance of 0.32 m were chosen. 24 of those channels with a midpoint distance of 12.5 m have been recorded.

Ship's speed during deployment and retrieval was 3 kn and 2 kn, respectively. Deployment and retrieval lasted around 30 minutes including installation of the 4 Remote Bird Units (RUs; see below).

5.3.1.2.4 MultiTrak Bird Controller

In operation 4 MultiTrak Remote Units (RU) were attached to the streamer. The position of RUs is listed in Tab. 6. Each RU includes a depth and a heading sensor as well as adjustable wings. The MultiTrak controllers in the seismic lab control the RUs. Controller and RUs communicate via communication coils nested within the streamer. A twisted pair wire within the deck cable connects controller and coils. One wire had to be grounded to avoid communication errors. Each shot trigger started a scan (delay 0.5 s, duration 0.2 s) to retrieve values for water depth, heading, water temperature, and battery voltage. The current location of the streamer (depth or heading versus offset) can be displayed on a monitor. All parameters are digitally stored on the controller PC together with shot number, date, and time.

Tab. 6: RU positions along seismic streamer

RU (No.)	Position	Distance to Tow-Lead
1	End of Stretch Section	48 m
2	End of Active Section No. 1	139 m
3	End of Active Section No. 2	239 m
4	End of Active Section No. 3	339 m

There are two ways of controlling the streamer depth. The most common way is to define an operating depth for the RUs, which was in most cases 3 m allowing a deviation of up to 1 m in both directions. The RUs adjust wing angles to force the streamer to the chosen depth. Another option is to set a constant wing angle. Depth and wing angle statistics help to find and set appropriate parameters.

5.3.1.2.5 Data Acquisition System

The recording unit includes a switch box, a seismograph and a single channel recording unit for online plotting. The switch box connects the streamer via deck cable with the seismograph and allows the assignment and optional stacking of streamer hydrophone subgroups to individual recording channels. The configuration during the cruise remained unchanged.

The 48-channel seismograph (BISON) was specially designed for the University of Bremen, which allows a continuous operation mode for very high resolution seismic data. The seismograph allows online data display, online demultiplexing and storing in SEG-Y format. All channels were pre-amplified by a factor of 1000 (60 dB) to keep the incoming signal within the optimum operation voltage. The data were stored on 2 DLT4000 cartridge tapes with 20 GByte uncompressed capacity. The recording delay had to be adjusted according to the current water depth.

For online immediate graphic information about the acquired seismic data, quality control and storing navigation data, the ParaDigMA acquisition system (see chapter 8) with a Hewlett Packard HP 3852 Data Acquisition Unit (DAU) and a PC was modified to display variable area seismic plots on a DesignJet 350 A1 roll paper plotter.

5.3.1.3 Base Maps and First Results

All seismic lines are listed in Tab. 7. Figures 47-53 show base maps from the different working areas. Common offset gathers are presented in the subsequent figures (54-60).

The seismic and PARASOUND lines in **survey area north** (Fig. 47) were measured to investigate the left stepping overstep of the southern prolongation of the Dead Sea Rift to the eastern margin of the northern Gulf of Aqaba. The central seismic line GeoB99-005 (Fig. 54) shows the transition from slope sediments, characterized by slides and slumps intercalated with parallel-layered sediments, to the deposits in the central basin. The West-East striking line GeoB99-014 (Fig. 55) shows a major unconformity that can be traced in the entire area.

The **survey area Ras Burka** (Fig. 48) includes the western marginal block of the Aqaba Deep. Signal penetration is limited due to the small sediment thickness of just a few hundred meters (Fig. 56). A cyclic reflection pattern can be observed on the southern flank of this crustal block.

The dense seismic grid at **survey area Wadi Watir** covers the submarine fan in front of the wadi and the western marginal block of the Aragonese Deep further south (Fig. 49; 50). Lines run parallel and perpendicular to the slope, some lines link the grid to the area Ras Burka. The channels of the fan seem to be correlated with faults (Fig. 57), their location has not changed as it can be observed in submarine fans located at passive margins (e.g., Amazon Fan or Bengal Fan).

Parallel lines cover **survey area Wadi Dahab** (Fig. 51). As at the Watir Fan, channels are connected to faults (Fig. 58). Continuous reflections within the entire cone can hardly be found. A dominant channel at the foot of the southern flank may be filled with brine, which would be a striking result.

The **survey area Conrad Deep** was studied in detail (Fig. 52). The presence of a brine layer was unknown so far (Fig. 59). The aim of this survey was to determine the breakup history of this depression. This was the same goal as for the **Shaban Deep** (Fig. 53), which was surveyed on the western side (Fig. 60).

Tab. 7: List of seismic lines.

Survey area: North
13.03. – 14.03.1999 julian days 72-73

Name	alat	alon	elat	elon	at	et	affn	effn	rem	Length [km]	Length [nm]
GeoB99-001	29°26.41‘n	34°57.38‘e	29°21.95‘n	34°56.27‘e	20:48	22:38	194	843	*13.03*	8.4	4.55
GeoB99-002	29°22.36‘n	34°55.36‘e	29°30.85‘n	34°58.31‘e	00:31	02:23	1317	1989	*14.03*	16.3	8.83
GeoB99-003	29°30.87‘n	34°57.18‘e	29°23.38‘n	34°52.64‘e	02:43	04:26	2109	2727		15.5	8.36
GeoB99-004	29°24.01‘n	34°51.96‘e	29°31.24‘n	34°57.05‘e	04:45	06:30	2841	3471		15.4	8.35
GeoB99-005	29°30.99‘n	34°57.96‘e	29°22.52‘n	34°54.33‘e	06:45	08:36	3561	4227		16.6	8.98
GeoB99-006	29°23.51‘n	34°53.48‘e	29°30.91‘n	34°57.52‘e	09:02	10:45	4383	5001		15.0	8.11
GeoB99-007	29°29.92‘n	34°58.10‘e	29°30.72‘n	34°56.66‘e	11:14	11:38	5175	5319		2.6	1.43
GeoB99-008	29°29.98‘n	34°56.57‘e	29°29.19‘n	34°58.11‘e	11:53	12:14	5409	5535		2.8	1.49
GeoB99-009	29°28.41‘n	34°57.77‘e	29°29.37‘n	34°55.56‘e	12:29	12:58	5625	5799		3.8	2.05
GeoB99-010	29°28.18‘n	34°55.64‘e	29°27.17‘n	34°57.41‘e	13.23	13:47	5948	6092		3.3	1.77
GeoB99-011	29°26.02‘n	34°56.77‘e	29°27.51‘n	34°54.33‘e	14:09	14:41	6224	6416		4.6	2.49
GeoB99-012	29°26.71‘n	34°53.58‘e	29°24.41‘n	34°56.93‘e	15:00	15:45	6530	6800		6.6	3.58
GeoB99-013	29°22.95‘n	34°56.42‘e	29°25.11‘n	34°52.97‘e	16:08	16:54	6338	7214		6.6	3.56
GeoB99-014	29°23.76‘n	34°52.23‘e	29°21.64‘n	34°56.25‘e	17:16	18:06	7346	7646		7.3	3.92
GeoB99-015	29°21.19‘n	34°56.59‘e	29°30.86‘n	34°58.68‘e	18:14	20:07	7694	8371		18.1	9.82

Survey area: Ras el Burka
15.03 – 16.03.1999 julian days 74-75

Name	alat	alon	elat	elon	at	et	affn	effn	rem	Length [km]	Length [nm]
GeoB99-016	29°16.94‘n	34°48.93‘e	29°08.35‘n	34°46.31‘e	18:18	20:04	208	844		16.4	8.85
GeoB99-017	29°08.75‘n	34°44.98‘e	29°17.16‘n	34°47.98‘e	20:22	22:10	951	1599		16.2	8.76
GeoB99-018	29°16.77‘n	34°49.59‘e	29°08.26‘n	34°47.02‘e	22:34	00:24	1743	2403	*15.-16.03*	16.2	8.77
GeoB99-019	29°08.69‘n	34°45.80‘e	29°17.18‘n	34°48.51‘e	00:48	02:38	2547	3207		16.2	8.78
GeoB99-020	29°17.47‘n	34°47.65‘e	29°08.74‘n	34°43.14‘e	02:50	04:46	3279	3975	*Bend!*	17.5	9.48
GeoB99-021	29°08.40‘n	34°43.35‘e	29°14.69‘n	34°47.04‘e	04:52	06:22	4011	4551		12.9	6.98
GeoB99-022	29°15.13‘n	34°47.51‘e	29°15.88‘n	34°49.73‘e	06:30	06:56	4599	4755		3.6	1.97
GeoB99-023	29°13.14‘n	34°49.56‘e	29°13.16‘n	34°46,69‘e	07:38	08:08	5007	5187		4.4	2.35
GeoB99-024	29°11.50‘n	34°45.84‘e	24°10.08‘	34°48.08‘	08:34	09:08	5343	5547		4.3	2.32

Tab. 7: List of seismic lines (continuation).

Survey area: Wadi Watir
16.03.-18.03.1999 julian days 75-77

Name	alat	alon	elat	elon	at	et	affn	effn	rem	Length [km]	Length [nm]
GeoB99-025	29°11.88‘	34°45.76‘	28°41.71‘	34°38.38‘	20:33	03:07	111	1929	*16.03*	72.2	39.04
WP2	29°11.88‘	34°45.76‘			20:33		111				
WP3	29°06.10‘	34°41.91‘			22:07		545				
WP4	28°58.87‘	34°32.10‘			23:35		951				
WP5	28°55.08‘	34°40.82‘			00:23		1172		*17.03*		
WP6	28°45.81‘	34°39.73‘			02:17		1699				
WP7	28°41.71‘	34°38.38‘			03:07		1929				
GeoB99-026	28°42.48‘	34°41.10‘	29°10.48‘	34°49.20	04:15	10:01	2123	3719	*17.03*	53.4	28.87
WP8	28°42.48‘	34°41.10‘			04:15		2123				
WP9	28°49.16‘	34°43.62‘			05:39		2511				
WP10	28°59.56‘	23°45.31‘			07:43		3083				
WP12	28°.04.73‘	34°46.90‘			08:47		3378				
WP13	29°10.48‘	34°49.20			10:01		3719				
GeoB99-027	29°10.48‘	34°49.20	28°51.04‘	34°41.51‘	11:25	15:17	4107	5178		34.7	18.75
WP13	29°09.03‘	34°46.15‘			11:25		4107				
WP14	29°02.70‘	34°42.93‘			12:53		4513				
WP15	28°59.31‘	34°42.92‘			13:35		4707				
WP16	28°57.63‘	34°41.83‘			13:59		4818				
WP17	28°51.04‘	34°41.51‘			15:17		5178				
GeoB99-028	28°52.87‘	34°40.83‘	29°03.10	34°42.78‘	15:56	18:25	227	914		20.8	11.24
WP18	28°52.87‘	34°40.83‘			15:56		227				
WP19	28°58.47‘	34°44.22‘			17:14		587				
WP20	29°01.01	34°44.33‘			17:45		730				
WP21	29°03.10	34°42.78‘			18:25		914				
GeoB99-029	29°03.34‘	34°42.59‘	28°54.96‘	34°41.38‘	18:44	20:31	1002	1496		16.3	8.83
WP22	29°03.34‘	34°42.59‘			18:44		1002				
WP23	28°58.95‘	34°43.56‘			19:38		1251				
WP24	28°54.96‘	34°41.38‘			20:31		1496				
GeoB99-030	28°51.85‘	34°41.18‘	29°04.71‘	34°42.81‘	21:23	00:24	1736	2571		25.9	14.01
WP25	28°51.85‘	34°41.18‘			21:23		1736				
WP26	28°57.24‘	34°44.50‘			22:38		2082				
WP27	29°00.79‘	34°45.18‘			23:25		2299				
WP28	29°04.71‘	34°42.81‘			00:24		2571		*18.03*		

Tab. 7: List of seismic lines (continuation).

Survey area: Ras el Burqa

Name	alat	alon	elat	elon	at	et	affn	effn	rem	Length [km]	Length [nm]
GeoB99-031	29°04.71‘	34°42.81‘	29°08.75‘	34°43.62‘	00:24	01:31	2571	3174		7.6	4.09
GeoB99-032	29°09.46‘	34°44.23	29°09.18‘	34°48.11‘	01:31	02:17	3174	3386		5.9	3.19
GeoB99-033	29°09.84‘	34°48.47‘	29°10.86‘	34°45.61‘	02:30	03:03	3446	3598		4.7	2.56
GeoB99-034	29°12.56‘	34°46.04‘	29°11.76‘	34°48.81‘	03:34	04:05	3741	3884		4.5	2.41
GeoB99-035	29°14.61‘	34°49.09‘	29°14.33‘	34°47.62‘	04:46	05:08	4074	4175		2.3	1.24
GeoB99-036	29°15.48‘	34°46.89‘	29°15.66‘	34°49.48‘	05:28	05:56	4267	4397		3.9	2.13
GeoB99-037	29°16.79‘	34°49.66‘	29°16.60‘	34°47.21‘	06:18	06:44	4498	4618		3.7	2.02
GeoB99-038	29°16.01‘	34°47.15‘	29°07.55‘	34°46.98‘	06:54	08:37	4664	5141		15.6	8.46
GeoB99-039	29°07.57‘	34°47.72‘	29°16.99	34°50.62‘	08:51	10:50	5168	5718		18.0	9.71

Survey area: Wadi Watir
18.03.-20.03.1999 julian days 77-83

Name	alat	alon	elat	elon	at	et	affn	effn	rem	Length [km]	Length [nm]
GeoB99-040	29°10.17‘	34°45.40‘	29°09:54‘	34°48.14‘	19:31	20:01	249	429	*18.03*	4.3	2.33
GeoB99-041	29°08.09‘	34°47.18‘	29°04.33‘	34°42.33‘	20:27	21:37	585	1005		10.1	5.47
GeoB99-041b	29°03.90‘	34°42.17‘	29°01.61‘	34°42.39‘	21:43	22:11	1041	1209		4.2	2.30
GeoB99-042	29°01.18‘	34°43.01‘	29°02.59‘	34°46.16‘	22:25	23:05	1293	1433		5.4	2.94
GeoB99-043	29°03.50‘	34°46.43‘	29°07.51‘	34°43.49‘	23:21	00:19	1630	1977	*19.03*	8.7	4.68
GeoB99-044	29°08.39‘	34°44.00‘	29°04.80‘	34°46.82‘	00:41	01:35	2109	2433		7.9	4.27
GeoB99-045	29°04.20‘	34°46.63‘	29°01.86‘	34°42.37‘	01:45	02:39	2493	2817		7.8	4.20
GeoB99-046	29°00.62‘	34°42.40‘	29°00.42	34°45.54‘	02:57	03:31	2925	3129		4.8	2.58
GeoB99-047	28°58.40‘	34°44.95‘	28°59.10‘	34°42.67‘	04:03	04:29	3321	3477		3.7	1.99
GeoB99-048	28°58.15‘	34°42.29‘	28°55.43‘	34°44.59‘	04:45	05:25	3573	3813		6.1	3.31
GeoB99-049	28°53.17‘	34°43.89‘	28°57.51‘	34°41.60‘	05:59	06:55	4017	4353		8.8	4.73
GeoB99-050	28°58.96‘	34°42.41‘	29°05.37‘	34°41.99‘	07:15	08:33	4473	4941		11.9	6.42
GeoB99-051	29°06.62‘	34°42.64‘	28°44.11‘	34°39.49‘	08:57	14:01	5085	6909		44.3	23.94
WP25	29°06.62‘	34°42.64‘			08:57		5085				
WP26	29°02.17‘	34°45.70‘			10:01		5469				
WP27	28°55.29‘	34°44.32‘			11:29		5997				
WP28	28°44.11‘	34°39.49‘			14:01		6909				
GeoB99-052	28°48.96‘	34°39.14‘	28°42.03‘	34°41.91‘	14:19	14:49	7017	7197		13.5	7.29
GeoB99-053	28°44.67‘	34°42.54‘	28°45.88‘	34°40.05‘	15:25	15:55	7413	7593		4.4	2.37
GeoB99-054	28°48.96‘	34°40.51‘	28°47.72‘	34°43.04	16:33	17:03	7821	8001		4.5	2.42
GeoB99-055	28°50.25‘	34°43.79‘	28°51.97‘	34°40.72‘	17:41	18:19	8230	8457		5.6	3.05
GeoB99-056	28°54.73‘	34°41.20‘	28°52.83‘	34°44.14‘	19:03	19:41	8721	8949		5.7	3.07
GeoB99-057	28°52.45‘	34°42.45‘	28°05.85‘	34°44.06‘	20:19	23:01	9177	10149		86.3	46.62
GeoB99-058	29°04.88‘	34°42.22‘	28°53.74‘	34°41.00‘	23:55	02:31	10473	11409		22.1	11.95
WP4	29°04.88‘	34°42.22‘			23:55		10473				
WP5	29°01.08‘	34°43.94‘			00:51		10809		*20.03*		
WP6	28°58.60‘	34°43.93‘			01:23		11001				
WP7	28°53.74‘	34°41.00‘			02:31		11409				
GeoB99-059	28°53.31‘	34°42.01‘	28°56.02‘	34°43.67‘	02:47	03:23	11505	11721		5.6	3.03

Tab. 7: List of seismic lines (continuation).

Survey area: Wadi Dahab
20.03-23.03.1999 julian days 79-83

Name	alat	alon	elat	elon	at	et	affn	effn	rem	Length [km]	Length [nm]
GeoB99-060	28°39.93‘	34°41.05‘	28°20.44‘	34°33.73‘	14:14	18:46	296	1927	*20.03*	37.7	20.39
GeoB99-061	28°20.40‘	34°31.30‘	28°46.60‘	34°41.72‘	19:18	00:58	2119	4159	*21.03*	51.0	27.56
GeoB99-062	28°45.93‘	34°30.84‘	28°21.27‘	34°33.52‘	01:24	06:34	4315	6175		45.8	24.76
GeoB99-063	28°20.51‘	34°30.84‘	28°36.24‘	34°36.93‘	07:18	10:40	6439	7651		30.5	16.50
GeoB99-064	28°27.40‘	34°35.33‘	28°20.50‘	34°32.65‘	11:10	14:28	7831	9019		13.4	7.24
GeoB99-065	28°20.51‘	34°30.31‘	28°36.25‘	34°36.54‘	14:58	18:16	9199	10387		30.6	16.55
GeoB99-066	28°36.16‘	34°38.01‘	28°20.32‘	34°31.93‘	18:38	22:00	10519	11731		30.7	16.60
GeoB99-067	28°20.73‘	34°29.80‘	28°35.41‘	34°35.78‘	22:28	01:44	11899	13075	*22.03*	28.6	15.48
GeoB99-068	28°36.23‘	34°36.26‘	28°30.13‘	34°38.58‘	02:20	03:36	288	708		11.8	6.39
GeoB99-069	28°29.07‘	34°38.25‘	28°20.87‘	34°28.72‘	03:50	06:12	826	1680		21.2	11.44
WP20	28°29.07‘	34°38.25‘			03:50		826				
WP21	28°24.06‘	34°31.13‘			05:26		1404				
WP22	28°20.87‘	34°28.72‘			06:12		1680				

Survey area: Conrad Deep

Name	alat	alon	elat	elon	at	et	affn	effn	rem	Length [km]	Length [nm]
GeoB99-070	27°07.30‘	34°43.01‘	27°04.56‘	34°47.11‘	21:54	23:04	217	637	22.03	8.0	4.33
GeoB99-071	27°04.55‘	34°46.63‘	27°06.02‘	34°42.92‘	23:12	23:58	685	961		6.3	3.38
GeoB99-072	27°05.23‘	34°42.29‘	27°03.62‘	34°46.27	00:18	01:06	1081	1369	23.03	6.7	3.64
GeoB99-073	27°02.63‘	34°45.78‘	27°04.38‘	34°41.59‘	01:36	02:26	1549	1849		7.1	3.85
GeoB99-074	27°03.48‘	34°41.31‘	27°01.67‘	34°45.55‘	02:40	03:30	1933	2233		7.3	3.92
GeoB99-075	27°00.72‘	34°44.97‘	27°02.36‘	34°40.89‘	03:50	04:38	2353	2641		6.9	3.72
GeoB99-076	27°01.26‘	34°40.55‘	26°59.58‘	34°44.68‘	04:58	05:56	2761	3049		7.0	3.78
GeoB99-077	26°58.59‘	34°44.16‘	27°00.09	34°40.31‘	06:04	06:48	3157	3421		6.5	3.49
GeoB99-078	26°58.06‘	34°40.04‘	26°56.94‘	34°42.08‘	07:20	08:38	3613	4081		3.7	2.01
GeoB99-079	26°57.10‘	34°42.14‘	27°06.19‘	34°46.07‘	08:40	10:36	4094	4789		17.8	9.64
GeoB99-080	27°06.54‘	34°45.00‘	26°57.38	34°41.28‘	11:00	13:02	4933	5665		17.9	9.65
GeoB99-081	26°57.26‘	34°40.40‘	27°07.56‘	34°44.10‘	13:24	15:34	5797	6577		19.9	10.74
GeoB99-082	27°07.52‘	34°43.53‘	26°56.73‘	34°43.11‘	15:52	18:00	6685	7449		20.0	10.80
WP26	27°07.52‘	34°43.53‘			15:52		6685				
WP27	27°02.30‘	34°43.30‘			16:54		7057				
WP28	26°56.73‘	34°43.11‘			18:00		7449				

Tab. 7: List of seismic lines (continuation).

Survey area: Shaban Deep

Name	alat	alon	elat	elon	at	et	affn	effn	rem	Length [km]	Length [nm]
GeoB99-083	26°17.98‘	35°14.92‘	26°16.49‘	35°17.84‘	22:54	23:32	139	314		5.2	2.82
GeoB99-084	26°14.79‘	35°18.88‘	26°08.15‘	35°18.92‘	23:58	01:22	434	729	*24.03*	12.3	6.64
GeoB99-085	26°09.49‘	35°19.89‘	26°17.70‘	35°15.47‘	02:02	03:58	191	873		16.6	8.97
GeoB99-086	26°18.18‘	35°17.03‘	26°10.43‘	35°21.14‘	04:24	06:08	1026	1638		15.6	8.45
GeoB99-087	26°09.19‘	35°19.20‘	26°17.46‘	35°14.66‘	06:44	08:38	1849	2520		16.8	9.07
GeoB99-088	26°18.01‘	35°16.21‘	26°09.60‘	35°20.77‘	09:04	10:58	2674	3344		17.0	9.20
GeoB99-089	26°11.41‘	35°20.64‘	26°16.90‘	35°14.02‘	11:28	13:08	3520	4108		14.3	7.72
SUM:										**1680.9**	**908.58**

alat Latitude Profile Start
alon Longitude Profile Start
at UTC Time Profile Start
affn Shot Number Profile Start
rem Remark

elat Latitude Profile End
elon Longitude Profile End
et UTC Time Profile End
effn Shot Number Profile End
WP waypoint

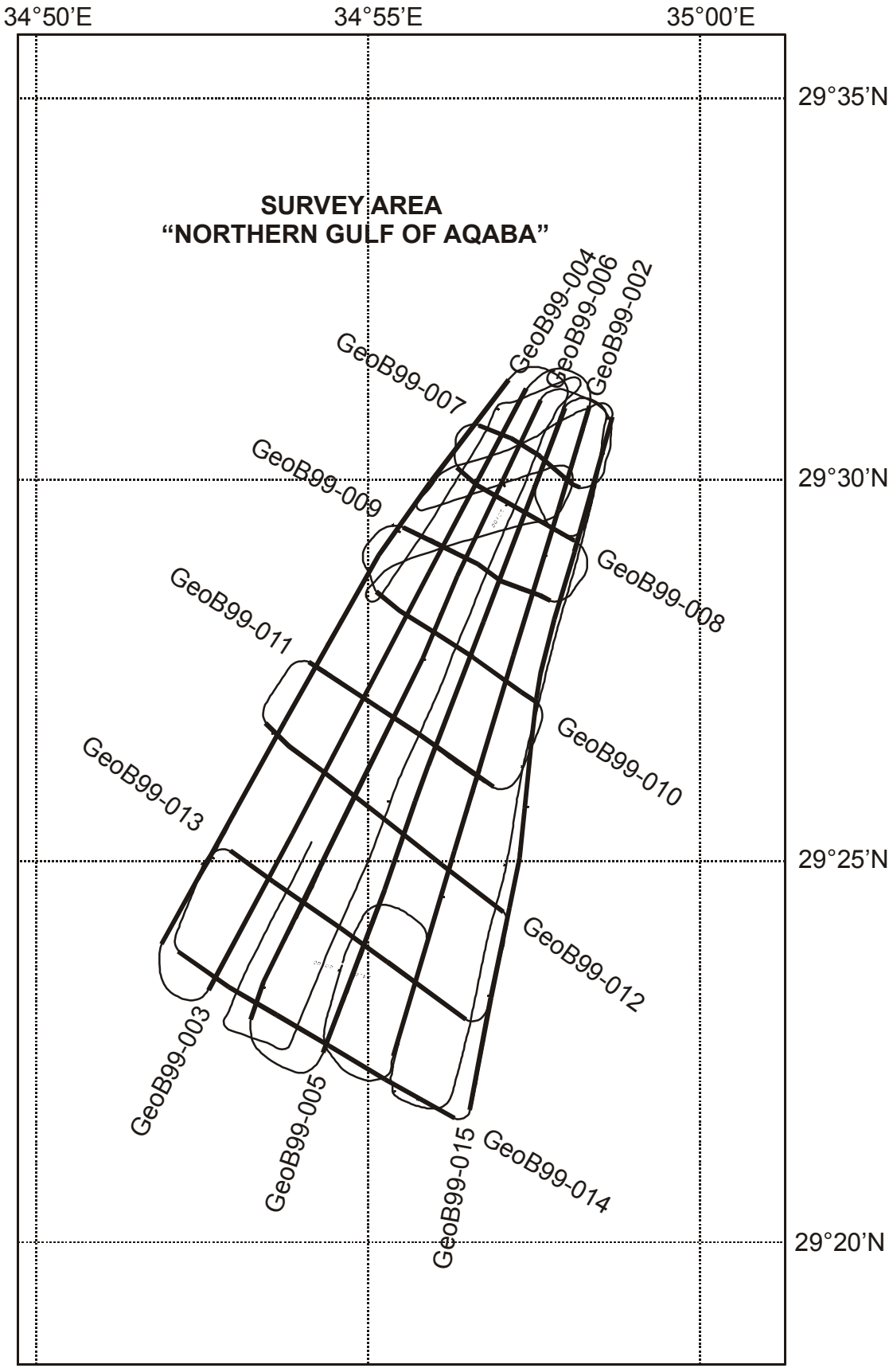

Fig. 47: Base map of the survey area 'Northern Gulf of Aqaba'. Postion of labels is at the end of each line.

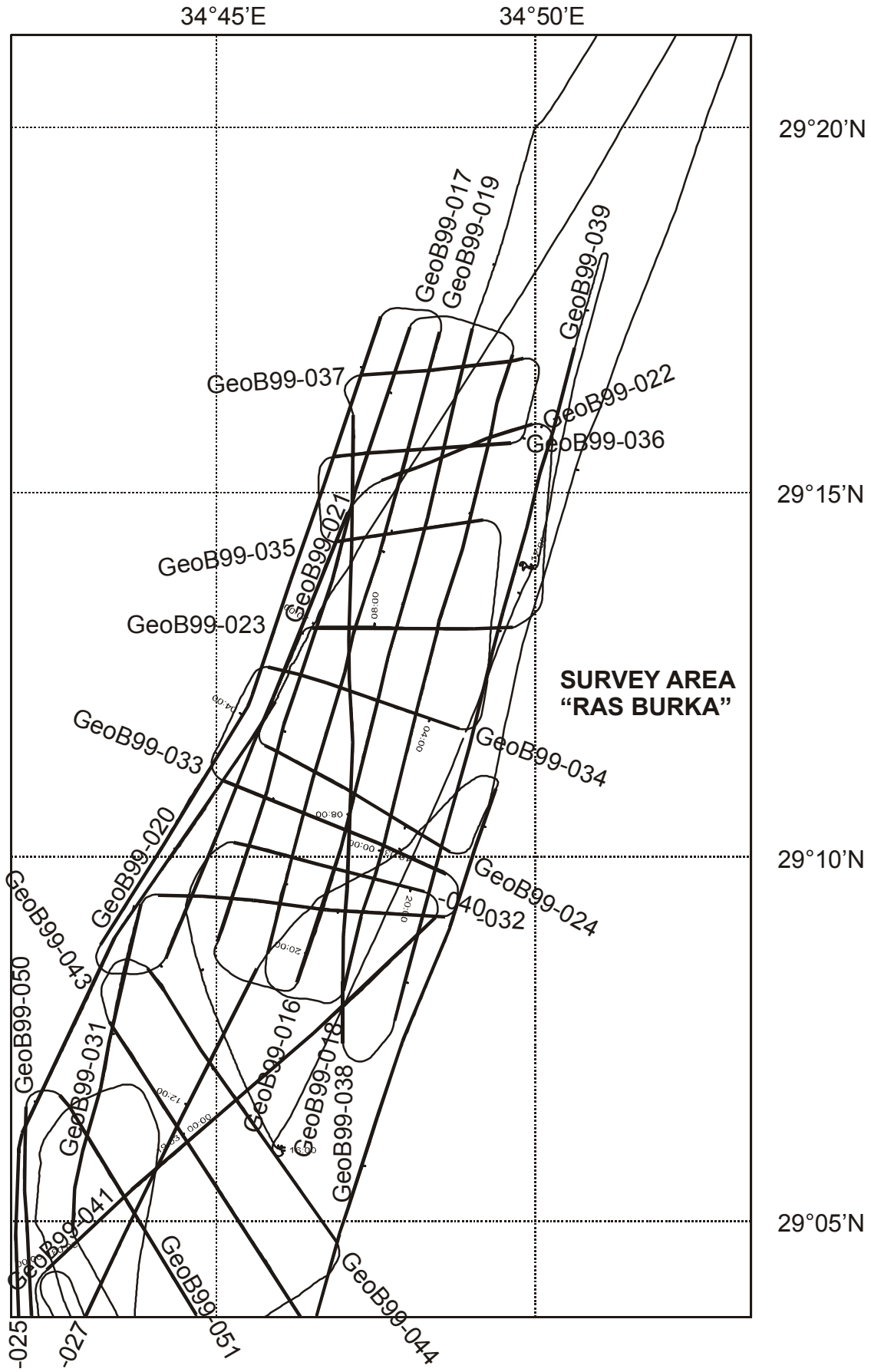

Fig. 48: Base map of the survey area 'Ras Burka'. Postion of labels is at the end of each line.

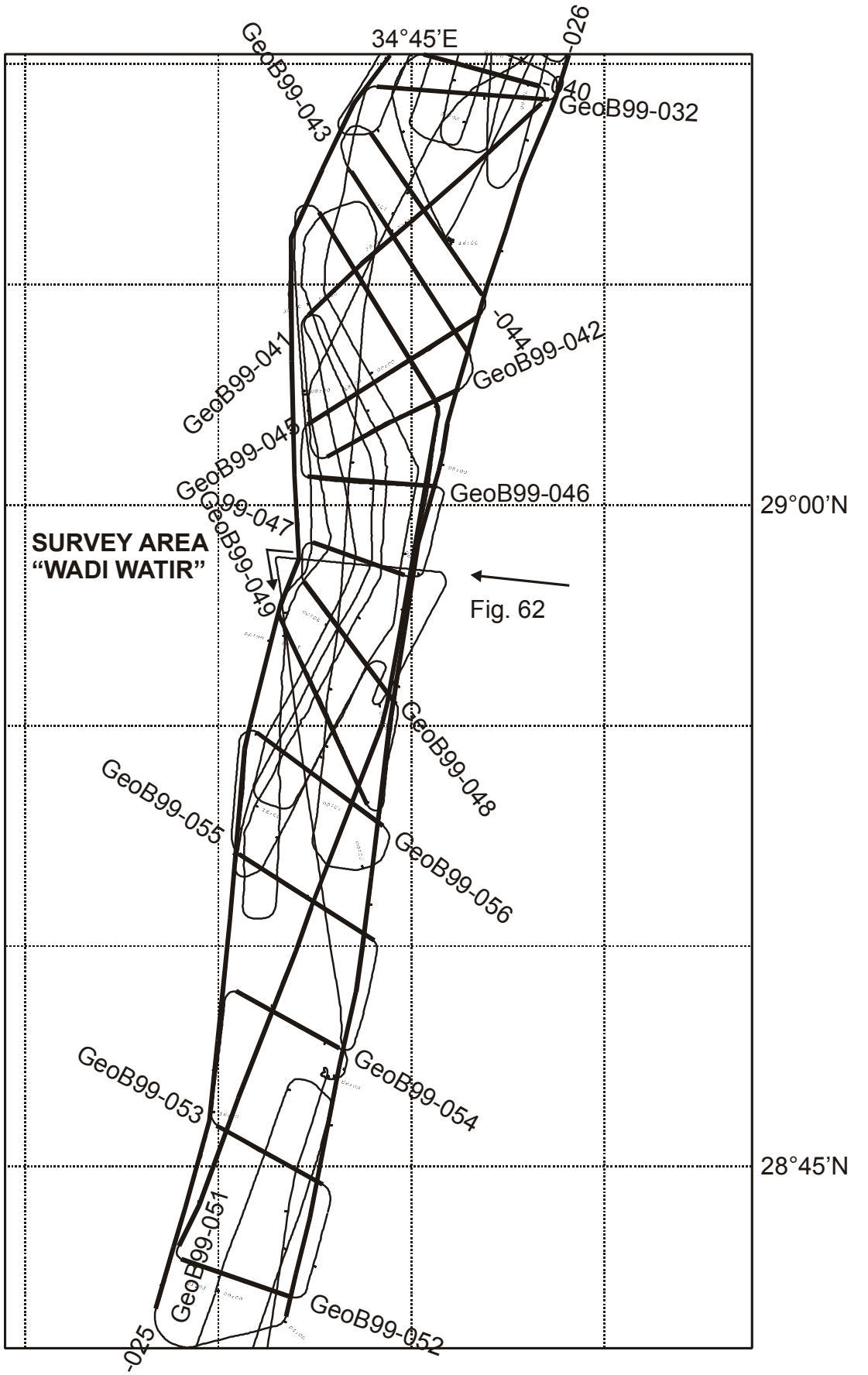

Fig. 49: Base map of the entire survey area 'Wadi Watir'. Postion of labels is at the end of each line. For clarity just some lines are labelled in this figure. The other lines are presented on the next page.

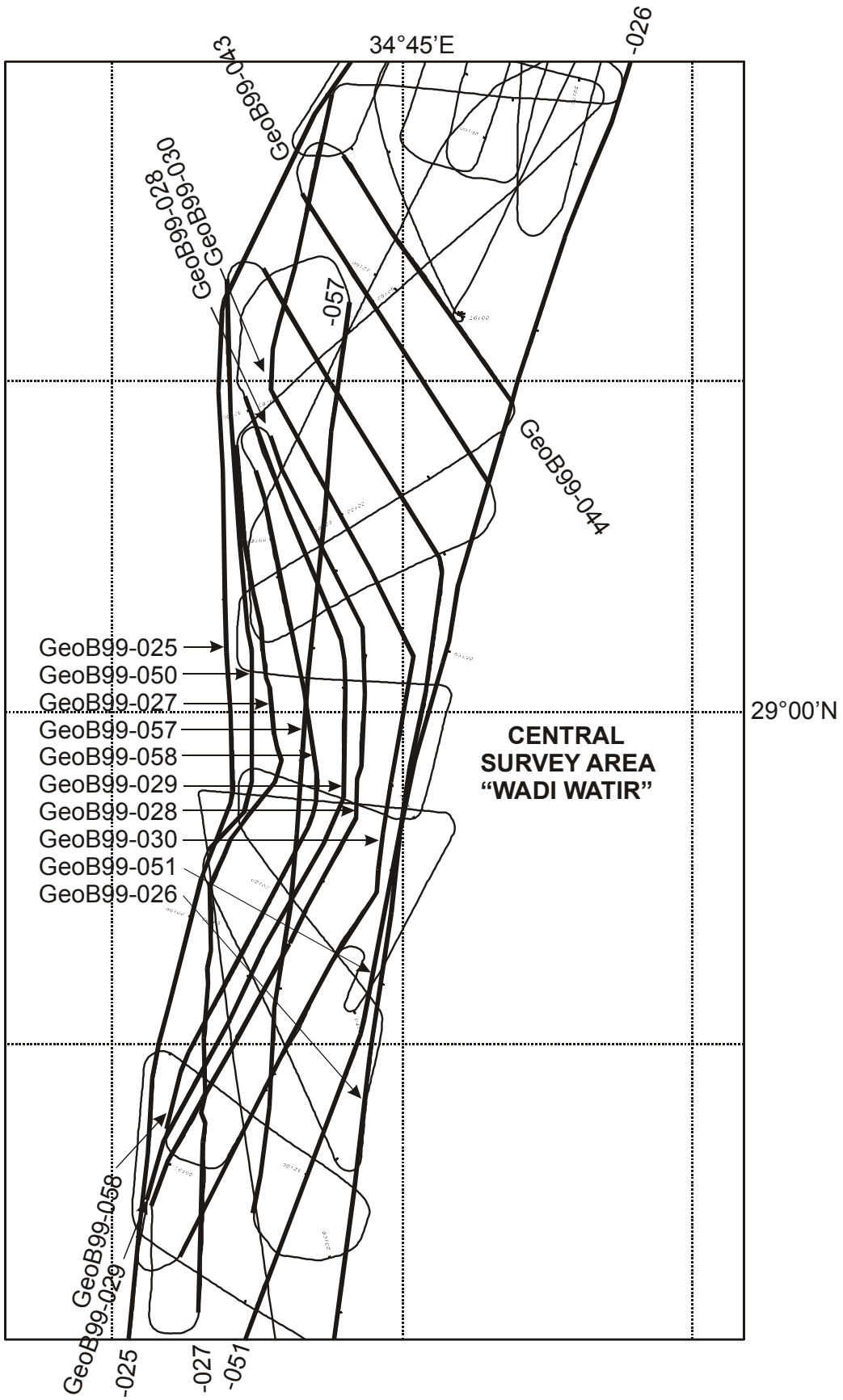

Fig. 50: Base map of the central survey area 'Wadi Watir'. Postion of labels is at the end of each line. For clarity just some lines are labelled in this figure. The other lines are presented on the previous page.

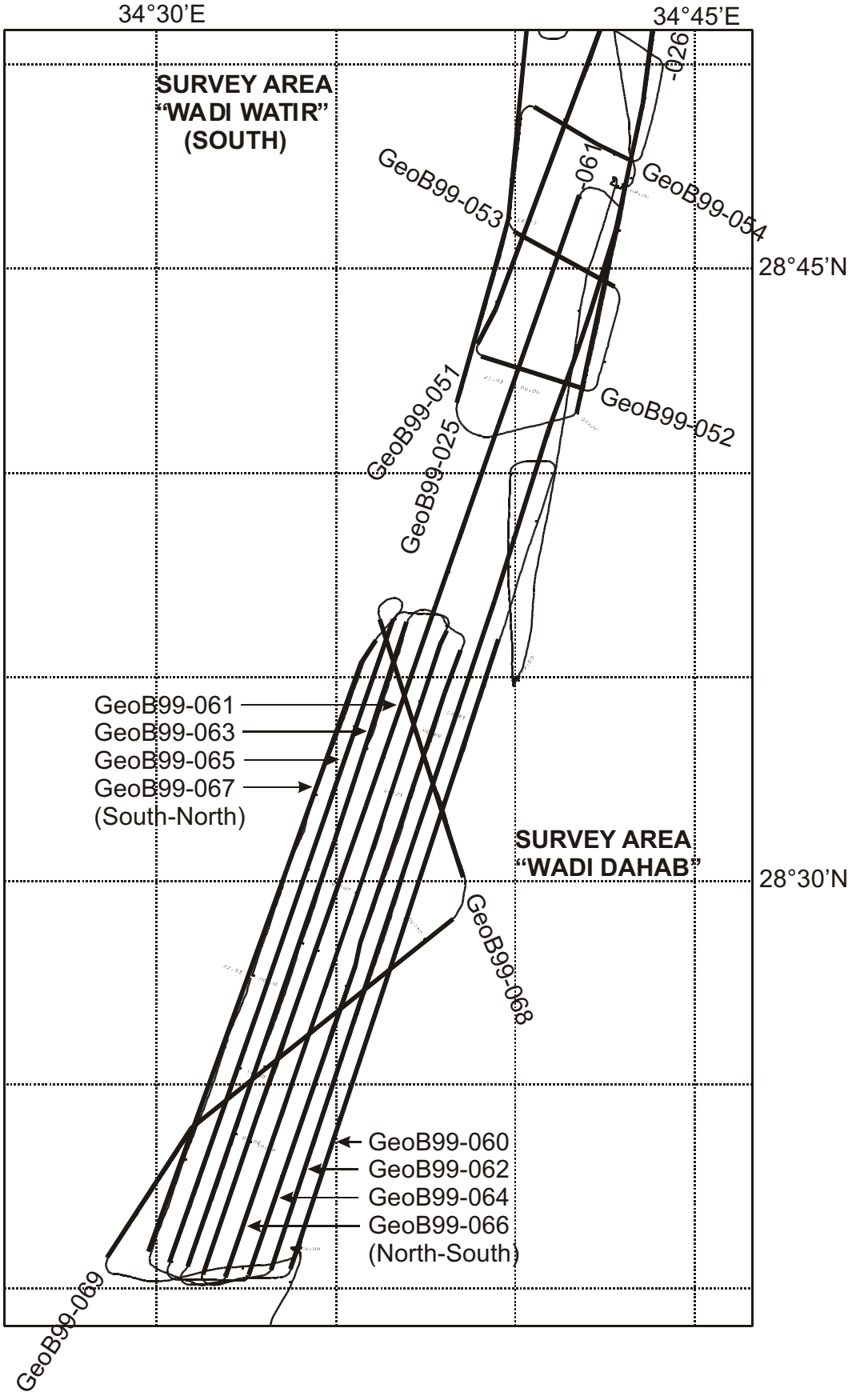

Fig. 51: Base map of the survey area 'Wadi Dahab'. Position of labels is at the end of each line.

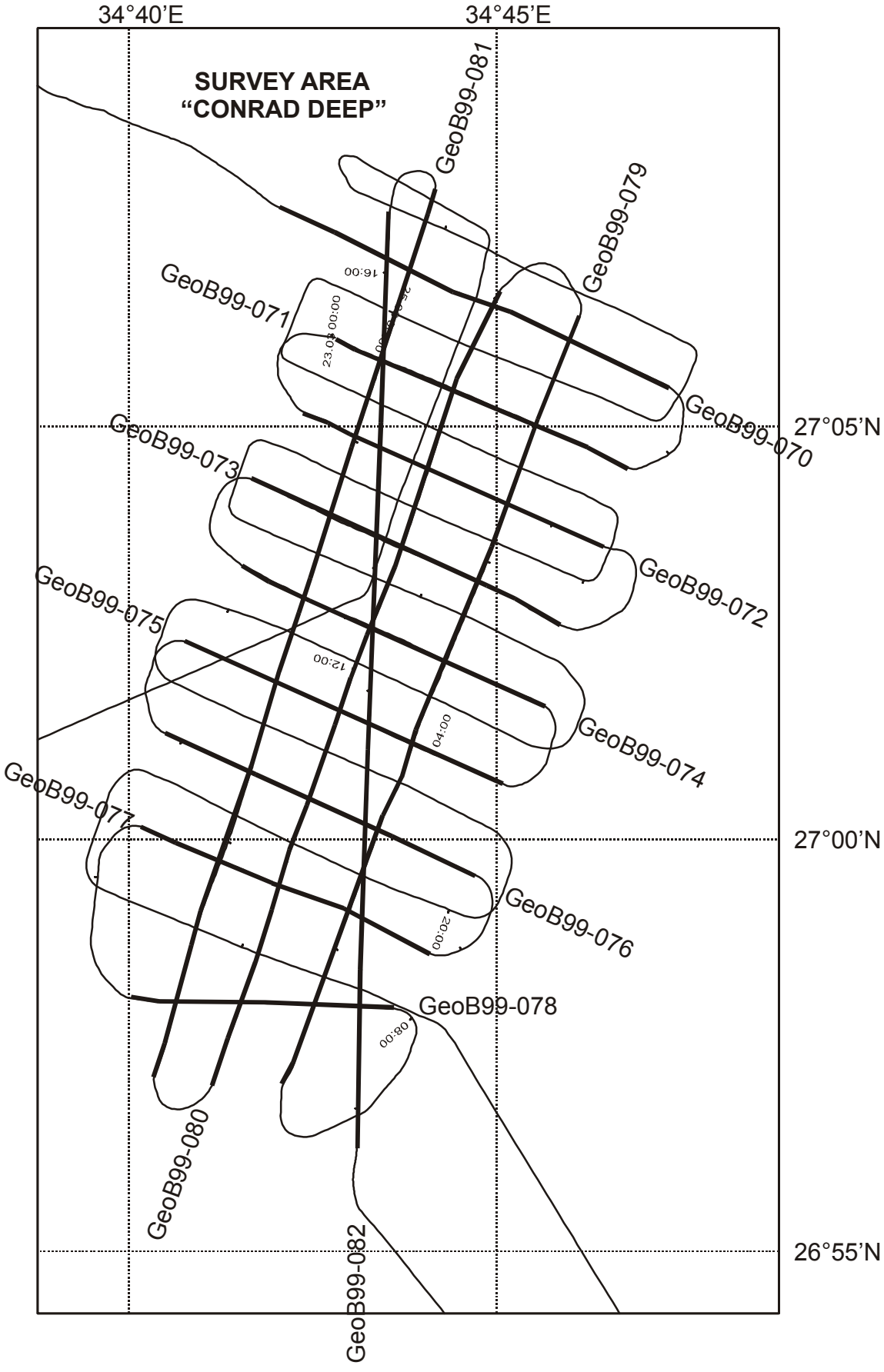

Fig. 52: Base map of the central survey area 'Conrad Deep'. Postion of labels is at the end of each line.

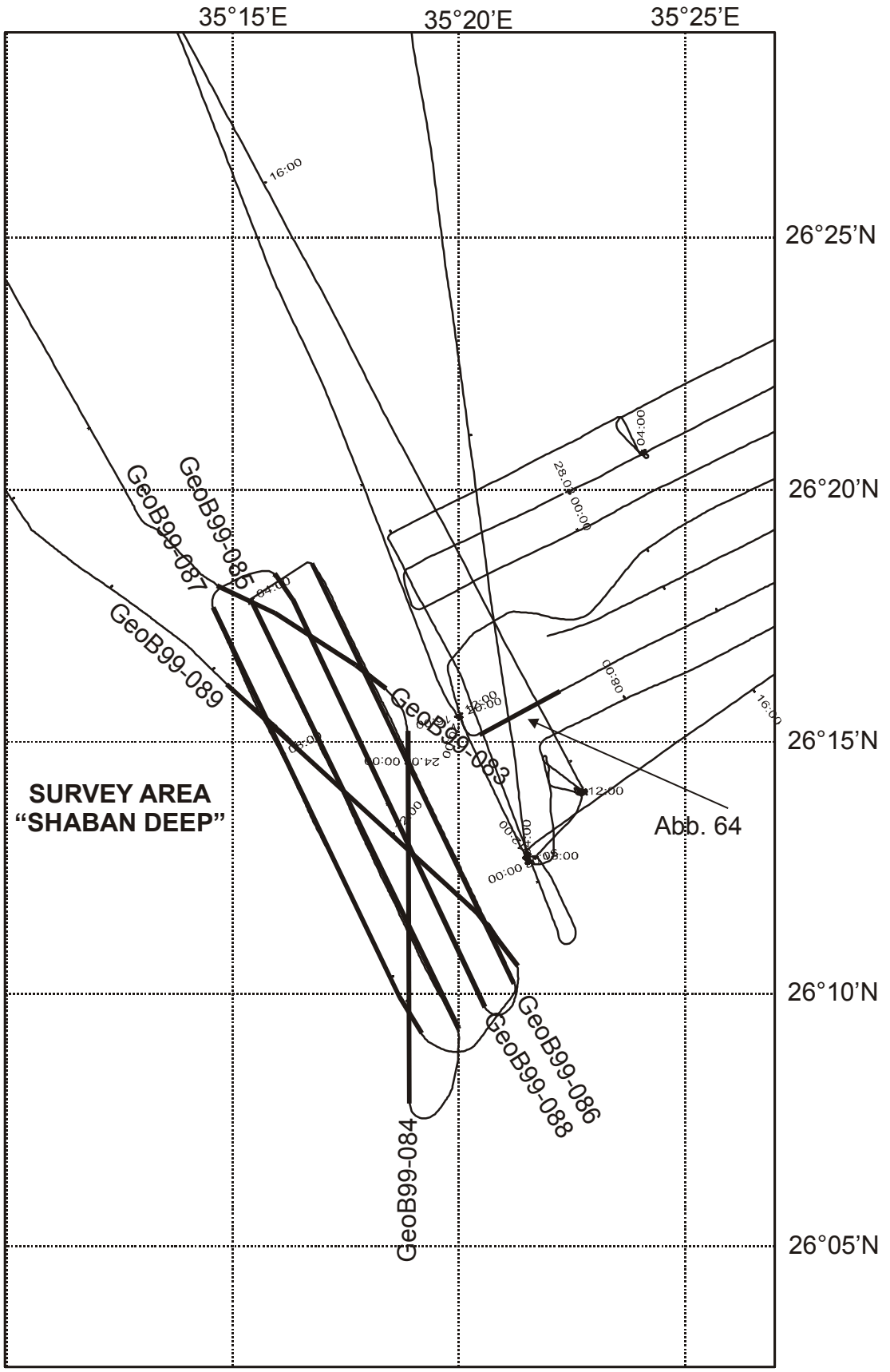

Fig. 53: Base map of the central survey area 'Shaban Deep'. Postion of labels is at the end of each line.

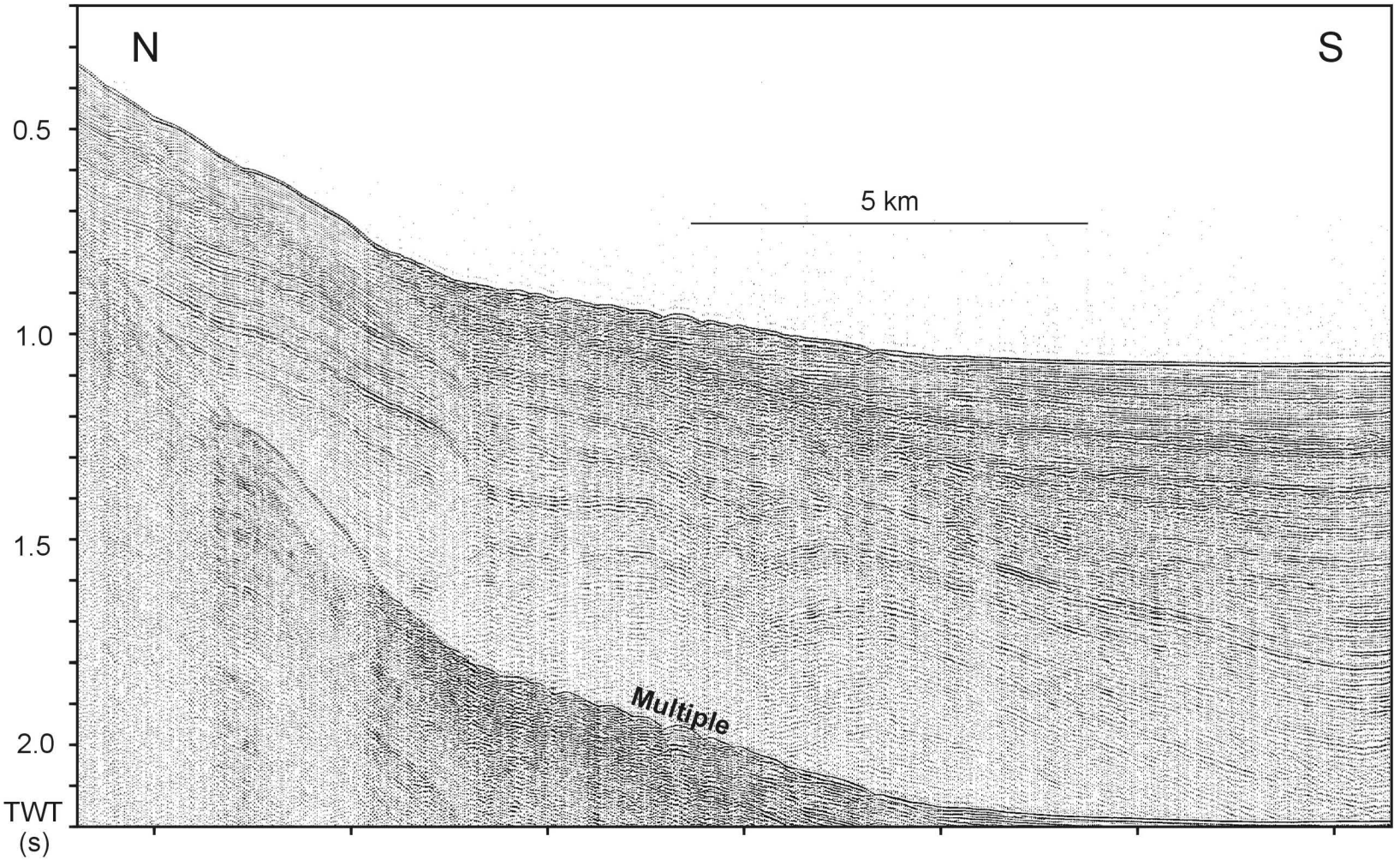

Fig. 54: Line GeoB99-005, GI-Gun. This line represents the central N-S striking line of the survey area 'NorthernGulf of Aqaba'.

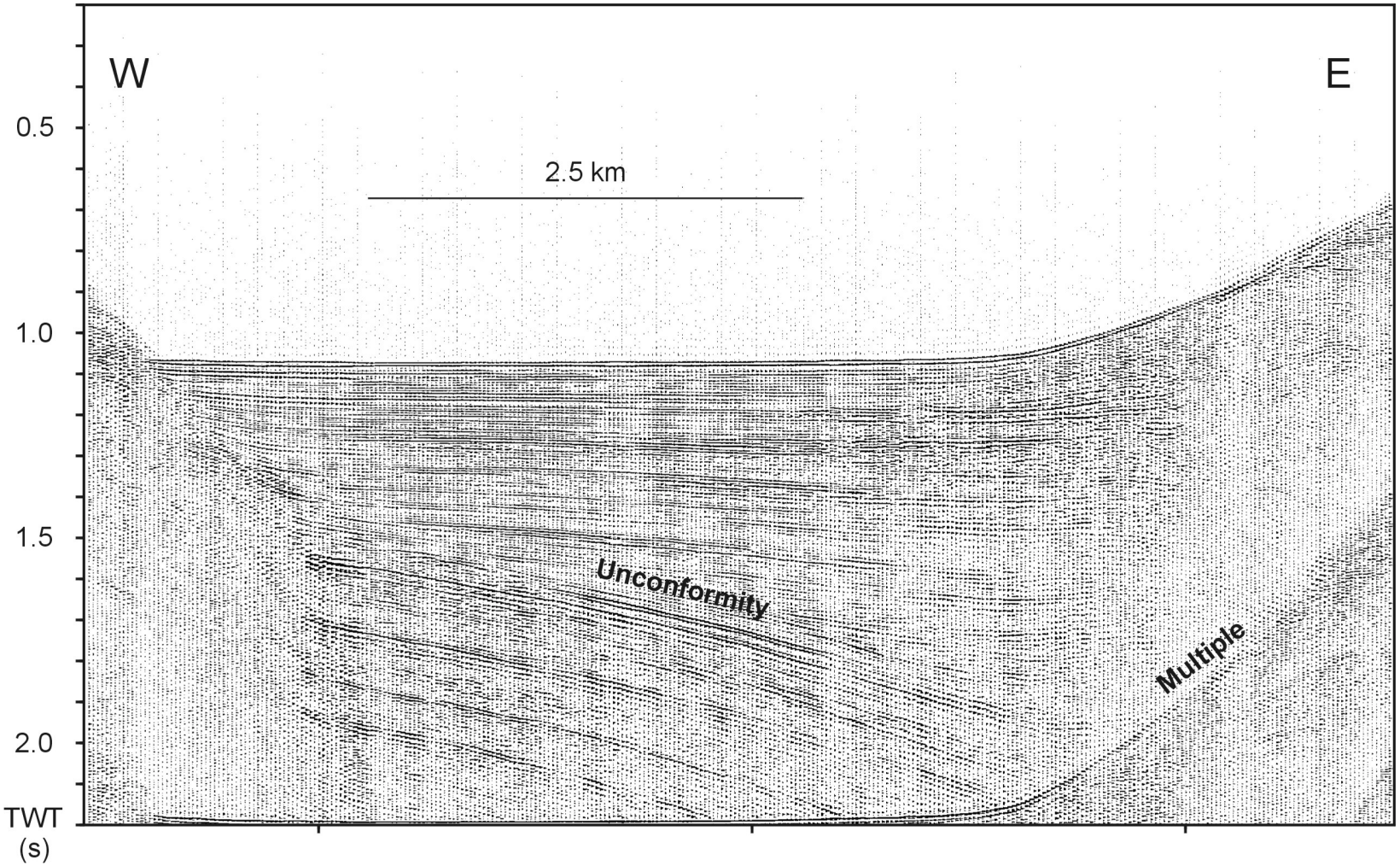

Fig. 55: Line GeoB99-014, GI-Gun. This southernmost W-E trending line of the Northern Gulf of Aqaba area reveals an eastward dipping unconformity within the basin deposits.

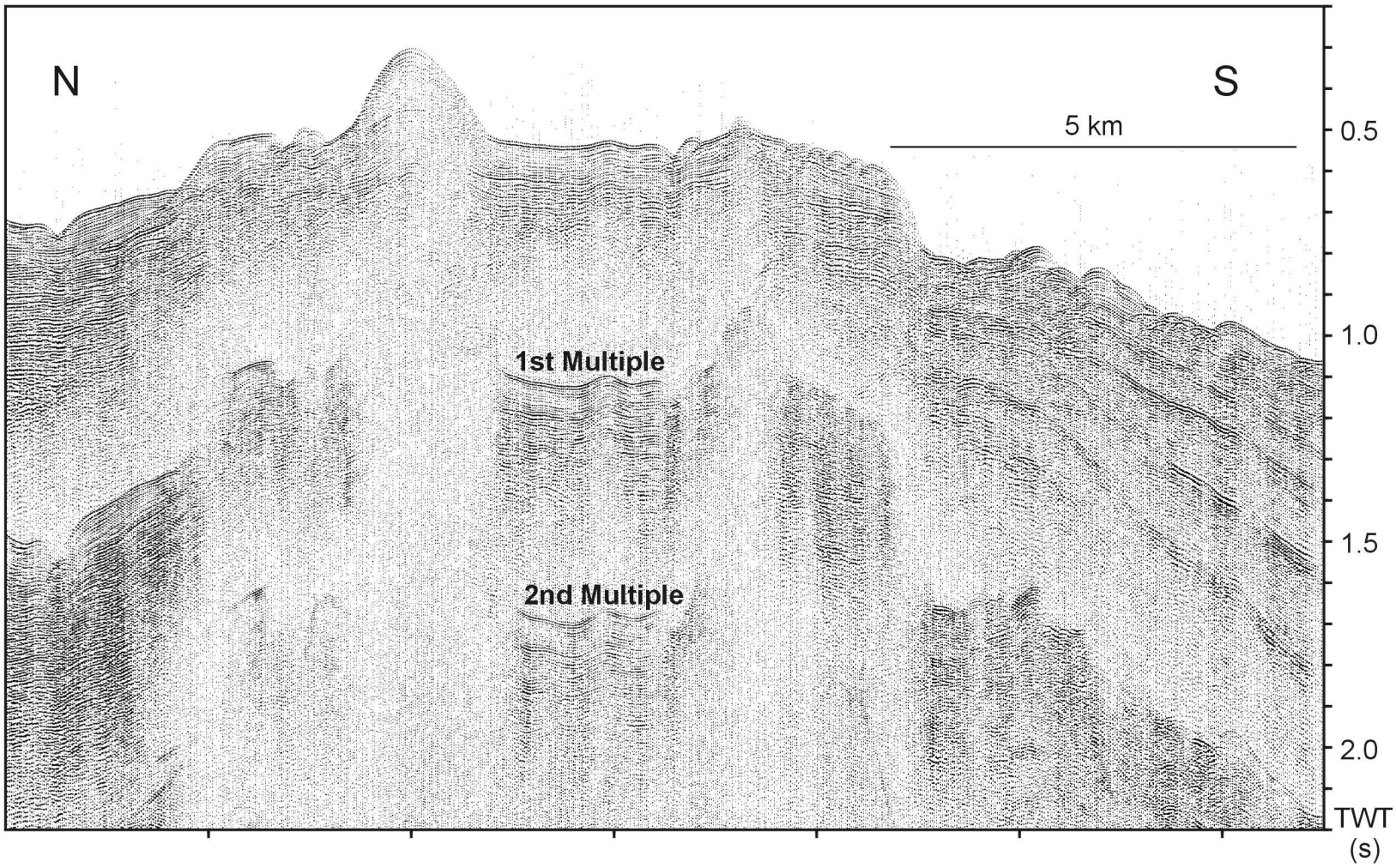

Fig.56: Line GeoB99-017, GI-Gun, Ras Burka area. The southern sediment packages of the rift parallel to the trending line reveal a cyclic reflection pattern.

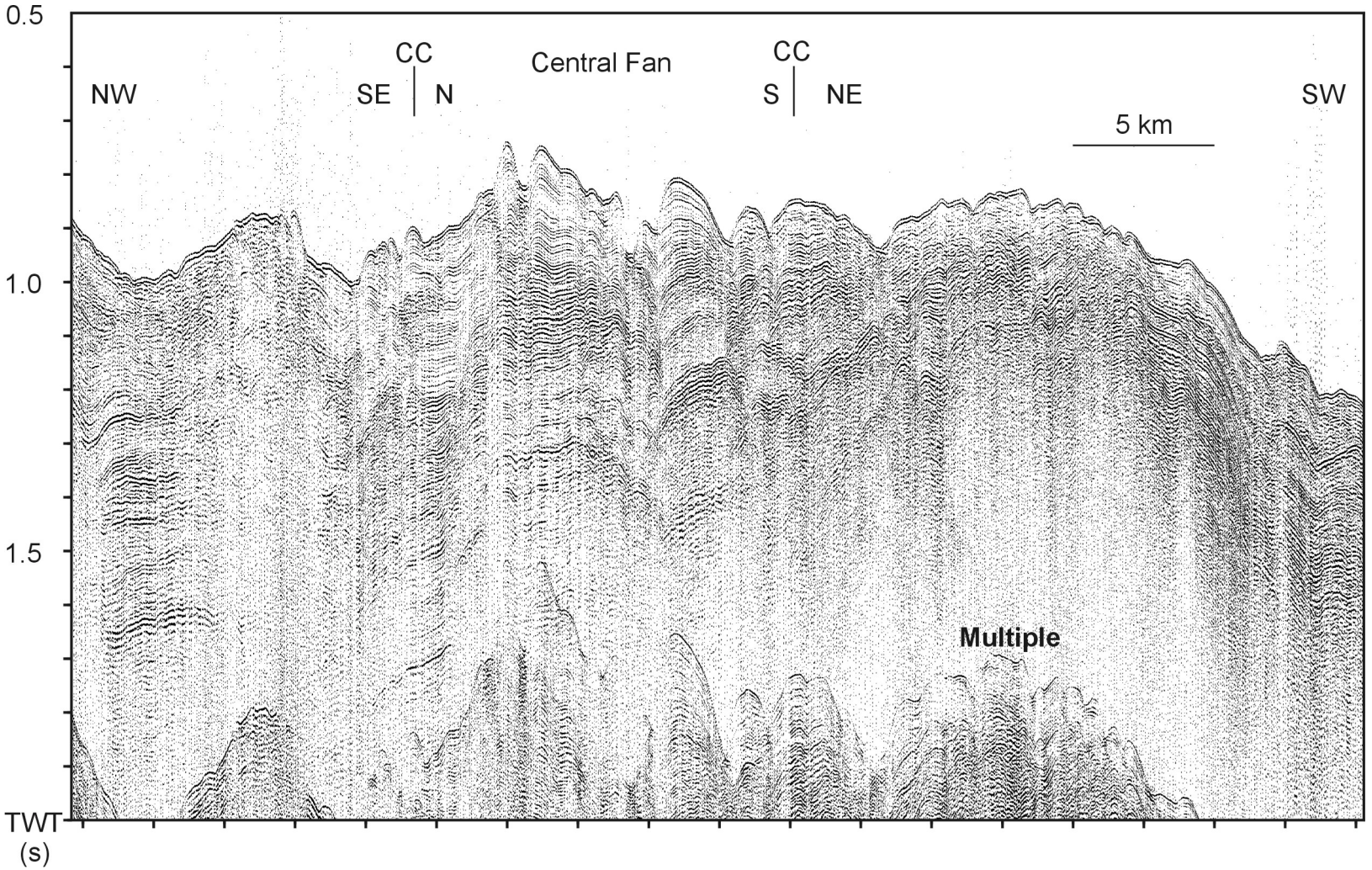

Fig. 57: Line GeoB99-051, GI-Gun, Wadi Watir. This line wraps the Wadi Watir Fan in a water depth between 550 and 750 m.

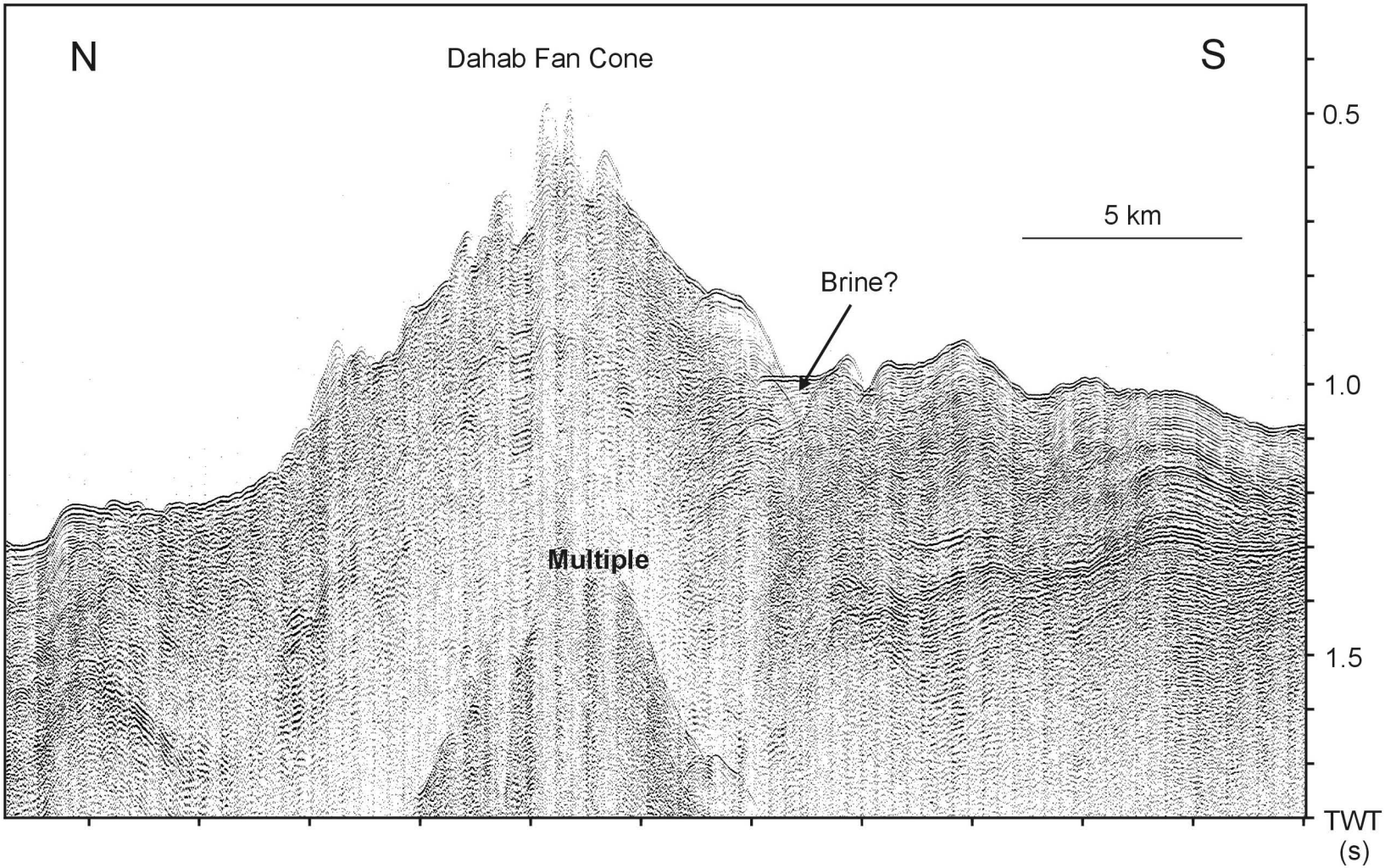

Fig. 58: Line GeoB99-067, GI-Gun, Wadi Dahab. The cone of the Dahab Fan is clearly seen in the central part of the profile. At the southern end of the cone a channel is perhaps filled with a brine layer.

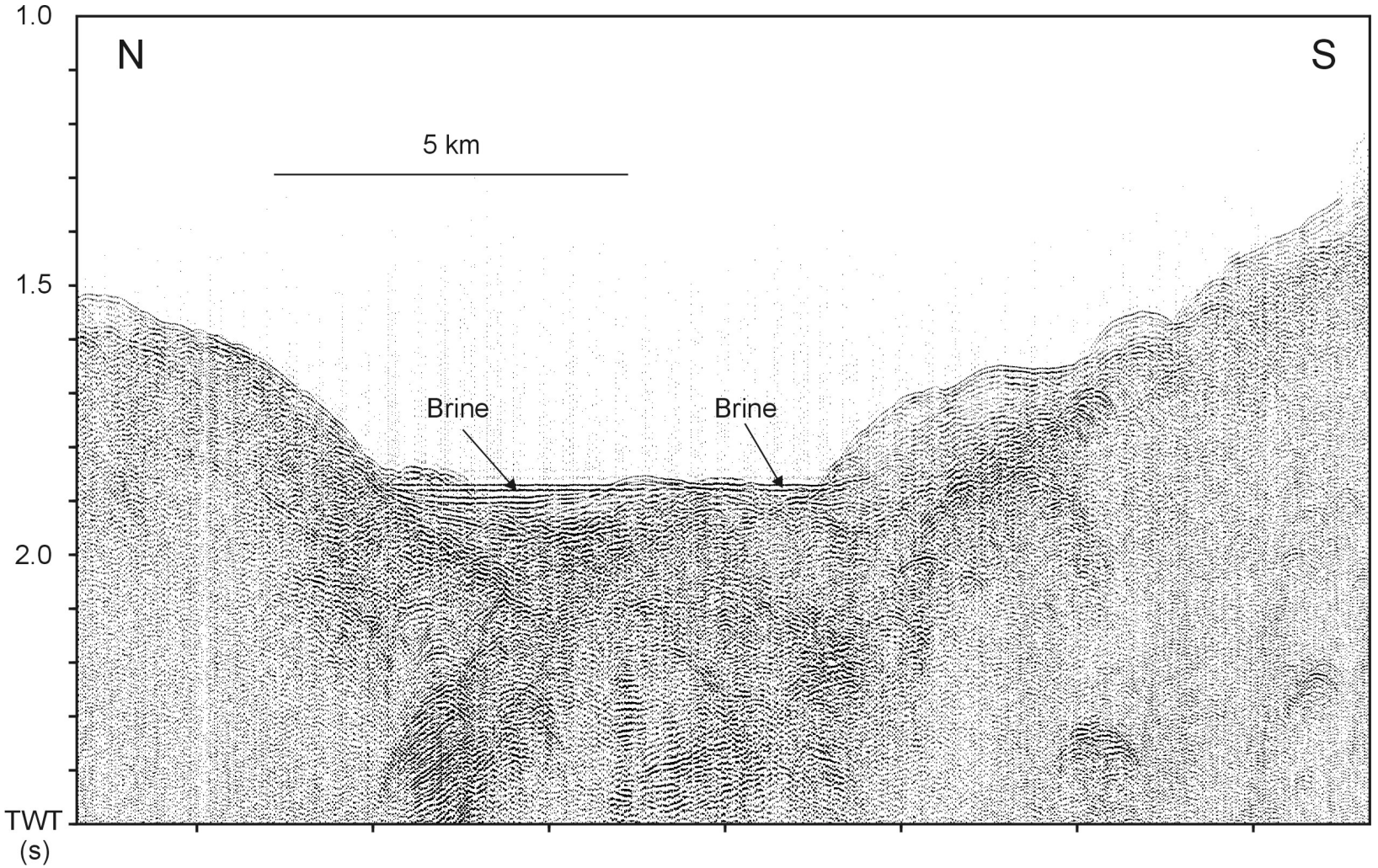

Fig. 59: Line GeoB99-080, GI-Gun, Conrad Deep. The flat reflection clearly indicates a brine layer, which was not recognized during former surveys.

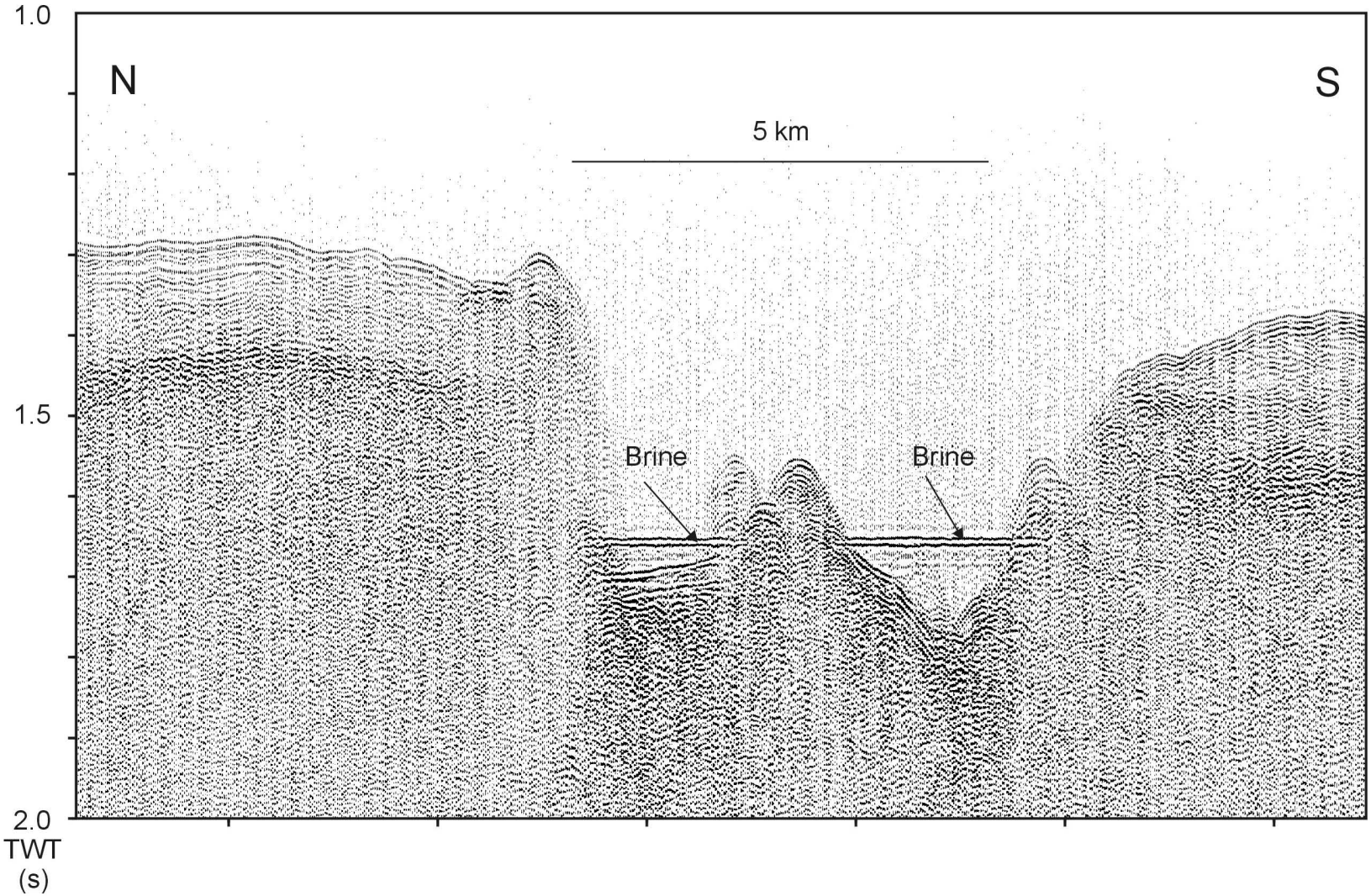

Fig. 60: Line GeoB99-086, GI-Gun, Shaban Deep. The reflection from the brine layer lies well above the basin floor deposits.

5.3.2 PARASOUND and HYDROSWEEP

(C. Hübscher and Shipboard Scientific Party)

5.3.2.1 Introduction

The hydroacoustic systems of R/V METEOR Cruise M44/3 were continuously operated to collect sediment echosounder and swath sounder data from the deposits in the working areas Gulf of Aqaba, the northern Red Sea, and the eastern Mediterranean Sea. The HYDROSWEEP swath sounder and the PARASOUND sediment echosounder are permanently installed on R/V METEOR. The HYDROSWEEP system provides topographic information at a width of twice the water depth. The PARASOUND sediment echosounder uses frequencies around 4 kHz, which allow signal penetration between 10 and 100 m depending on sediment composition and grain size. Digital echosounder data were routinely collected with the help of all scientists onboard by participating in the 24-hour watch duties.

5.3.2.2 Instruments

5.3.2.2.1 PARASOUND

The PARASOUND system works both as a low-frequency sediment echosounder and as a high-frequency narrow beam sounder to determine the water depth. It makes use of the parametric effect, which produces additional frequencies through nonlinear acoustic interaction of finite amplitude waves. If two sound waves of similar frequencies (here 18 kHz and e.g. 22 kHz) are emitted simultaneously, a signal of the difference-frequency (e.g. 4 kHz) is generated for sufficiently high primary amplitudes. The new component is travelling within the emission cone of the original high frequency waves, which are limited to an angle of only 4° for the equipment used. Therefore, the footprint size of 7% of the water depth is much smaller than for conventional systems and both vertical and lateral resolution are significantly improved.

The PARASOUND system is permanently installed on the ship. The hull-mounted transducer array has 128 elements on an area of ~1 m^2. It requires up to 70 kW of electric power due to the low degree of efficiency of the parametric effect. In 2 electronic cabinets, beam forming, signal generation and the separation of primary (18, 22 kHz) and secondary frequencies (4 kHz) is carried out. With the third electronic cabinet in the echosounder control room the system is operated on a 24-hour watch schedule.

Since the two-way travel time in the deep sea is long compared to the length of the reception window of up to 266 ms, the PARASOUND System sends out a burst of pulses at 400 ms intervals, until the first echo returns. The coverage of this discontinuous mode depends on the water depth and produces non-equidistant shot distances between bursts. On average, one seismogram is recorded about every second providing a spatial resolution on the order of a few meters on seismic profiles at 4.9 knots.

The main tasks of the operators are system and quality control and the adjustment of the start of the reception window. Because of the limited penetration of the echosounder signal into the sediment, only a short window close to the sea floor is recorded.

In addition to the analog recording features with the b/w DESO 25 device, the PARASOUND System was equipped with the digital data acquisition system ParaDigMA, which was developed at the University of Bremen (SPIEß , 1993). The data were stored using the standard, industry-compatible

SEGY-format. The 486-processor based PC allows the buffering, transfer, and storage of the digital seismograms at very high repetition rates. From the emitted series of pulses, usually every second pulse could be digitized and stored, resulting in recording intervals of 800 ms within a pulse sequence. The seismograms were sampled at a frequency of 40 kHz, with a typical registration length of 266 ms for a depth window of ~200 m. The source signal was a band limited, 2-6 kHz sinusoidal wavelet of 4 kHz dominant frequency with a duration of 2 periods (~500 □s total length).

Already during the acquisition of the data an online processing was carried out. For all profiles PARASOUND sections were plotted with a vertical scale of several hundred meters. Most of the changes in window depth could thereby be eliminated. From these plots a first impression of variations in sea floor morphology, sediment coverage and sedimentation patterns along the ships track could be gained. To improve the signal-to-noise ratio, the echogram sections were filtered with a wide band pass filter. In addition the data were normalized to a constant value much smaller than the maximum average amplitude, to amplify in particular deeper and weaker reflections.

5.3.2.2.2 HYDROSWEEP

The multibeam echosounder HYDROSWEEP on R/V METEOR was routinely used during the cruise and serviced by the system operator and the electronics engineers. During a 24-hour watch the scientific crew operated continuously both the HYDROSWEEP and the PARASOUND echosounder systems in parallel. The HYDROSWEEP System worked without major technical problems. The multi-beam sounder provided a complete coverage of the sea floor topography with a swath width of twice the water depth. The data quality was generally good with data losses at higher speeds and under high-sea conditions.

5.3.2.3 First Results

As an example PARASOUND sections from different working areas are shown in the following figures. Fig. 61 was selected to show the transition from slope sediments, characterized by diffraction hyperbolae, to the flat lying uppermost sediments. The shallow shelf area off Wadi Watir reveals only a few reflections (Fig. 62; for location see Fig. 49). It is presumably the strong reflection coefficient of the carbonate that prevents signal penetration. Possible indicators for low stands are only seen on the southern flank, where pinnacle shaped features may indicate lowstand reefs. Presumably due to a density gradient over some wavelengths no reflections from the brine layer were observed in the Conrad Deep (Fig. 63). Reflections from the bottom of the depression are diffuse, similar to the Shaban Deep (Fig. 64). Here, the top of the brine causes a sharp signal. The PARASOUND data from the eastern slope of the Red Sea just east of the Shaban Deep elucidates the difficulty to detect appropriate sites for gravity coring (Fig. 65).

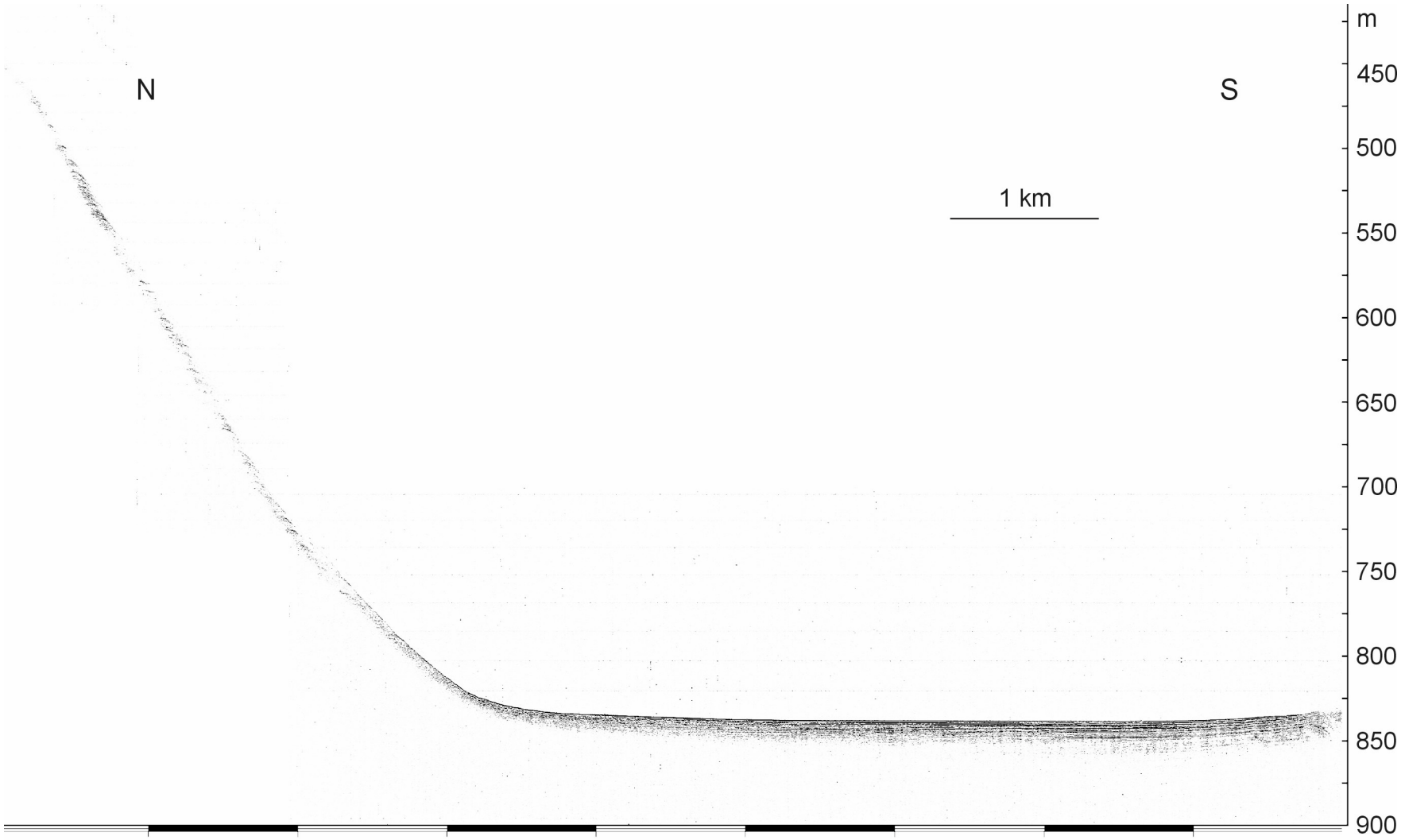

Fig. 61: GeoB99-014. The PARASOUND data from the northern end of the Gulf of Aqaba show the transition from slope sediments to the basin deposits. Seismic data are shown in Fig. 54, location in Fig.47.

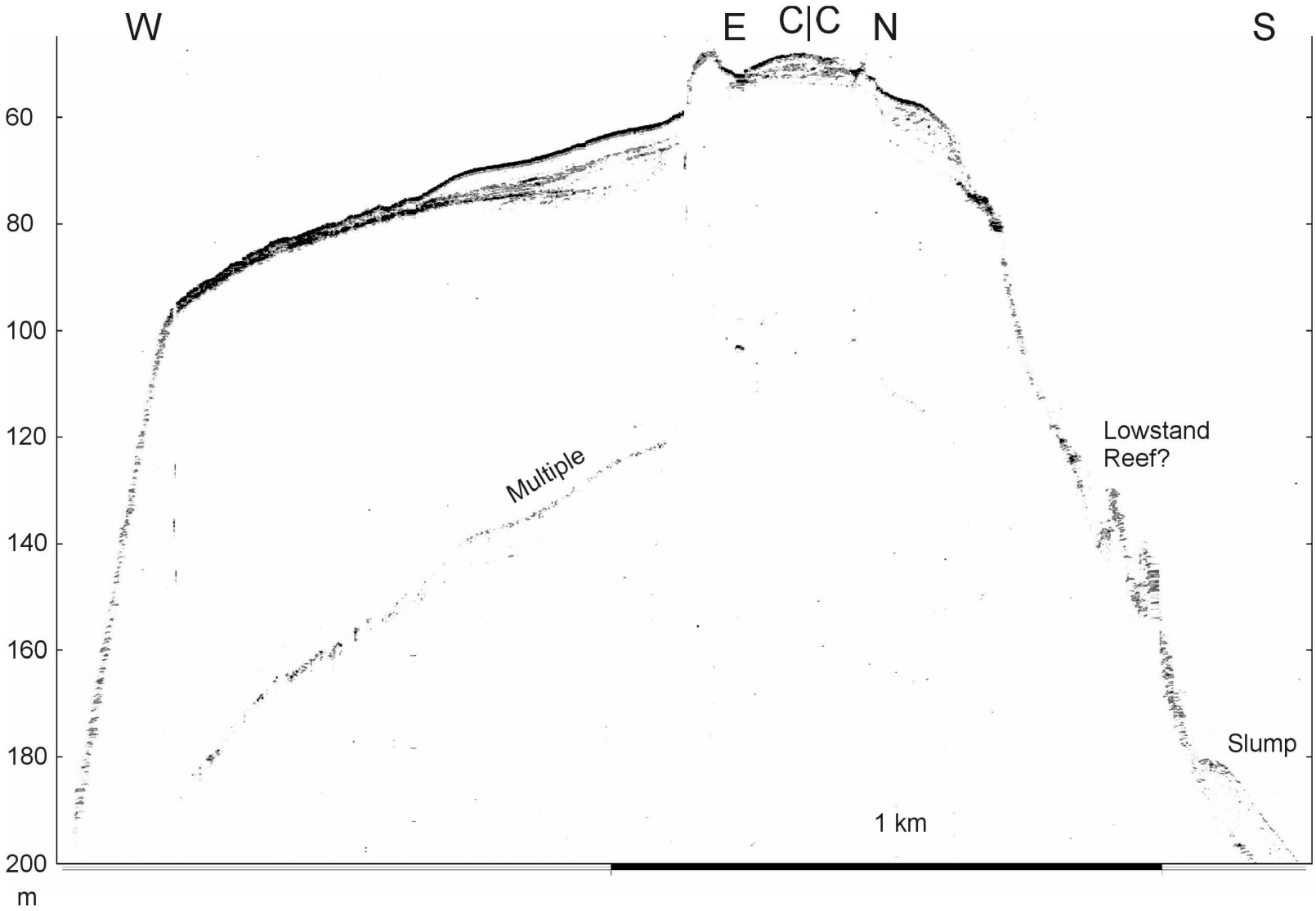

Fig. 62: The shallow shelf area off Wadi Watir reveals only a few reflections. The strong reflection amplitudes from the top of the plateau are presumably caused by the carbonate reef and its detritus. The pinnacles in water depths between 130 and 150 m of the N-S striking part of the profile on the right side of the figure may indicate lowstand reefs. For location see Fig. 49.

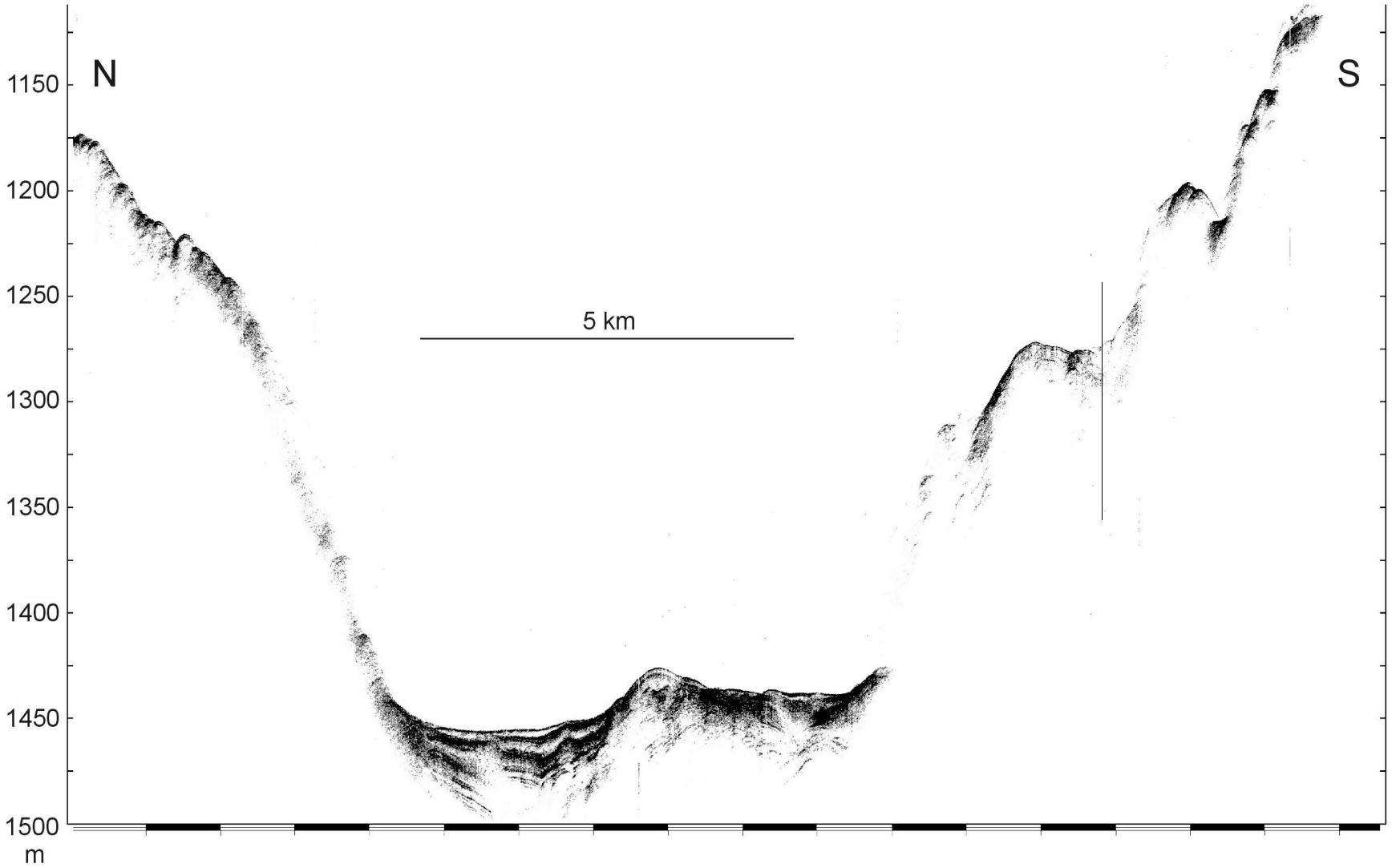

Fig. 63: GeoB99-080, Conrad Deep. The reflection from the top of the brine layer is not resolved in the PARASOUND data. The seismic data are presented in Fig. 59, the location map in Fig.52.

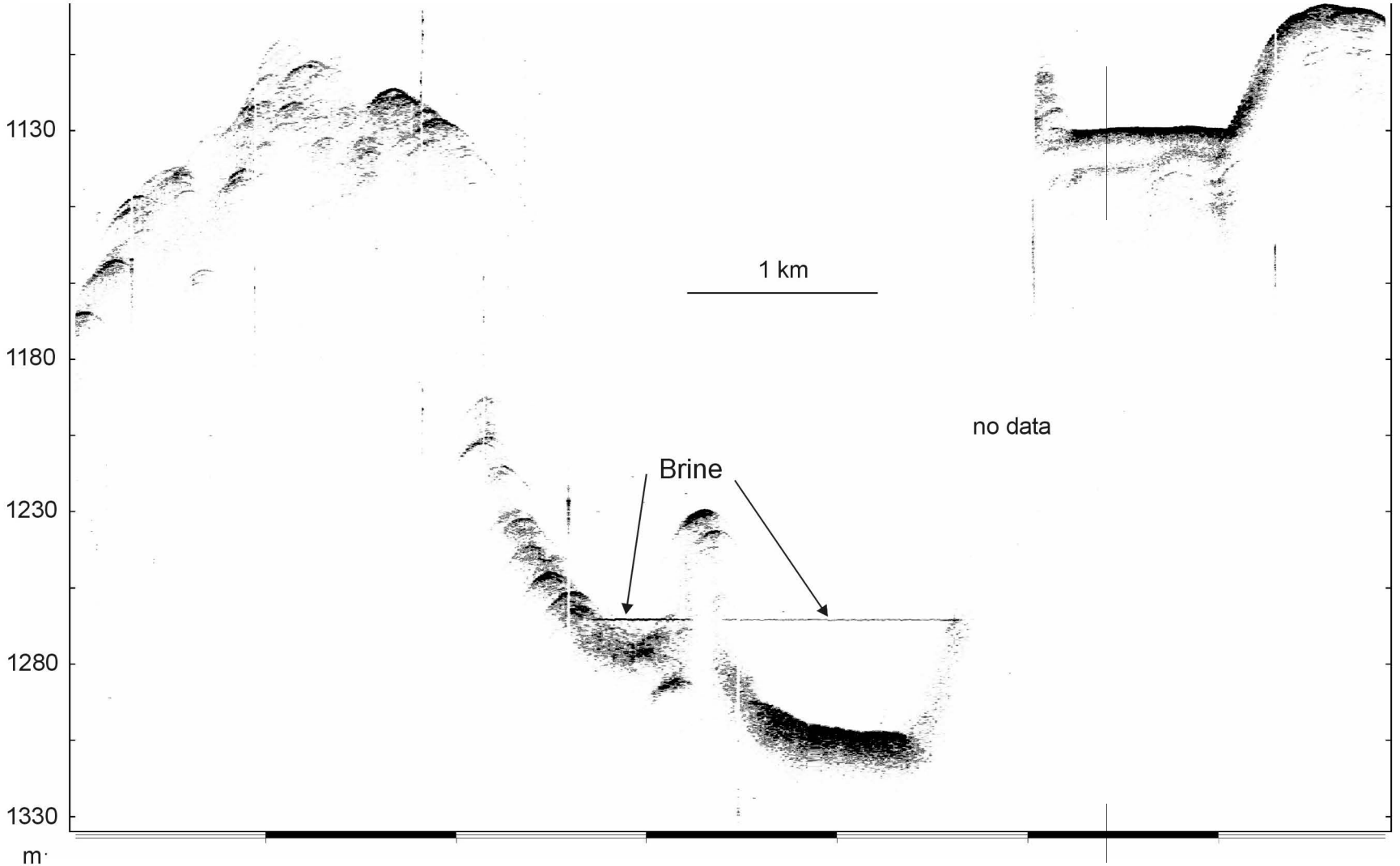

Fig. 64: PARASOUND cross-section through the Shaban Deep. The shoulders of the depression show a hummocky reflection pattern. The brine layer is a sharp reflection. The basin floor deposits reveal no distinct reflections. The location of the line is shown in Fig. 53.

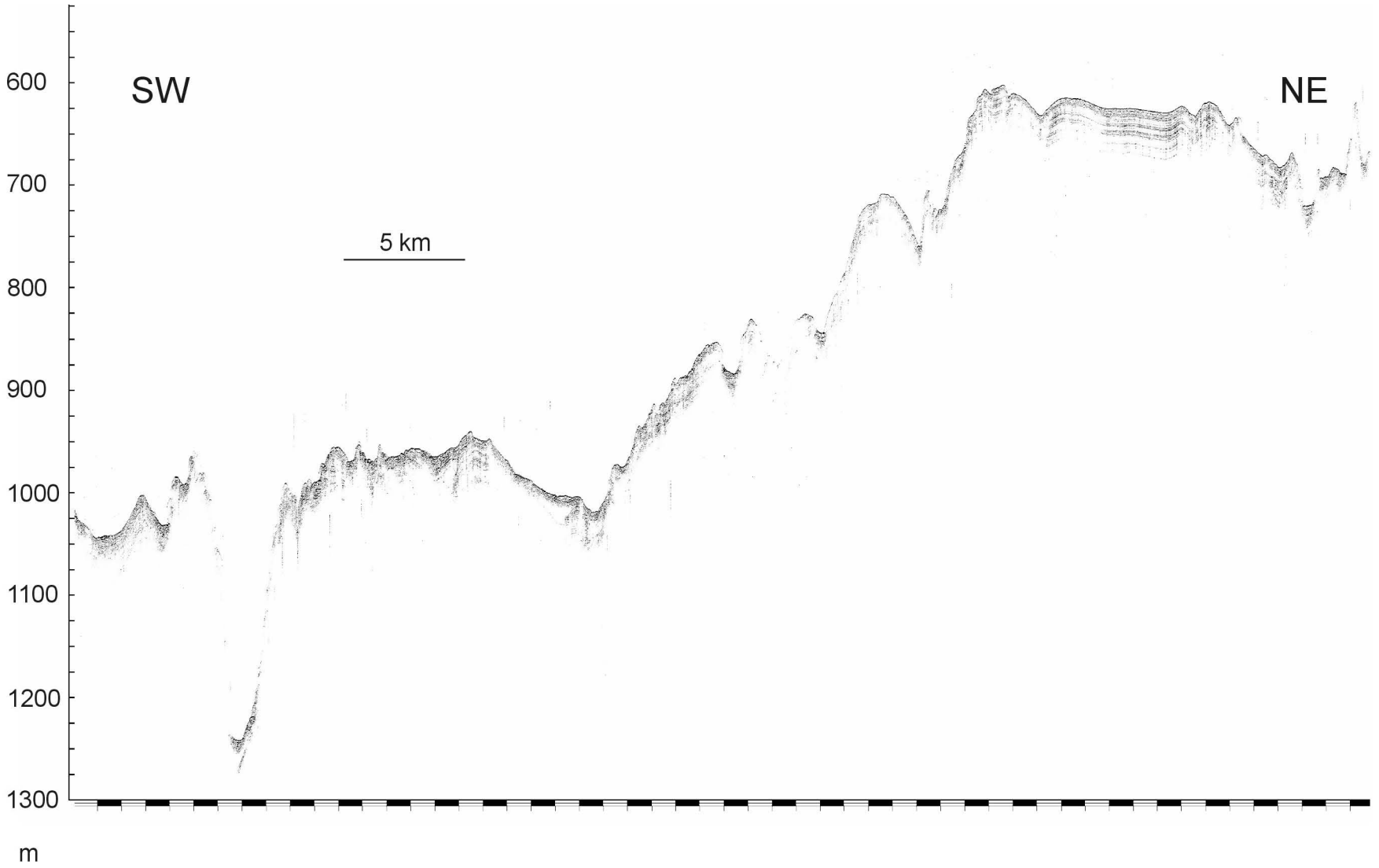

Fig. 65: This PARASOUND transect shows the rough and hummocky sea floor in working area II in the eastern Red Sea. The best site for coring was at the plateau in a water depth of 600 m at the eastern end of the profile

5.3.3 Sediment Sampling

(M. Abu-Ouf, Y. M. Al-Hazmi, S. Al-Rousan, H. W. Arz, B. Donner, T. Felis, K. A. Kadi, H. Kuhlmann, T. Lützeler, M. O. Moammar, C. Moos)

At 37 stations in the northern Gulf of Aqaba, the northern Red Sea, and the eastern Mediterranean Sea we sampled sea floor sediments by means of a giant box corer (GKG), a multicorer (MUC), a gravity corer (SL6, SL12, SL18), and a piston corer (KL12, KL18) from water depths between 135 and 1500 m. All details are given in the station list (Appendix I). In the northern Gulf of Aqaba (Jordan, Israel) one box core-sample, 16 multicores, and 13 gravity cores were retrieved (Fig. 6). Along three profiles extending from the Saudi Arabian coast to the central axis of the northern Red Sea altogether 16 multicores, 18 gravity cores, and 6 piston cores were recovered (Fig. 8). During the last part (III) of Leg M44/3, 4 multicores and 4 piston cores were retrieved in the eastern Mediterranean Sea (Israel) (Fig. 9).

5.3.3.1 Giant Box Corer

In order to sample relatively coarse-grained surface sediment the box corer was used at one station (29°30.64' N, 34°58.98'S, 326 m water depth). With a surface area of 50 x 50 cm the box corer recovers the uppermost max. 50 cm of sediments. Once on board, the overlying water was carefully removed from the box corer and the surface sediments (0-1 cm) were photographed and sampled as follows:

- 3 cores (f =12 cm) as archive,
- 400 cm² for analysis of foraminifera, stained with rose bengal,
- 200 cm² for analysis of organic carbon

The front cover of the box was subsequently removed, the sediment cleaned and photographed. Two series of syringes were taken at a 1 cm depth interval for faunal/stable isotope analysis and organic geochemistry and physical properties analysis. Finally, bulk samples of the uppermost 5 cm and the intervals 5-10 cm, 10-20 cm, and 20 cm to the base of the box were taken in order to collect the macro fauna using a 1 mm mesh sieve.

5.3.3.2 Multicorer

The main tool for the sampling of undisturbed surface sediment and the overlying bottom water was the multicorer (MUC, GeoB) equipped with six large (diameter of 10 cm) and four smaller (diameter of 6 cm) plastic tubes of 60 cm length. During M44/3, part III (the last four stations) a second model, the MUC II (GPITü), with only 8 but large tubes was used. Depending on the working area and the core recovery, the tubes were generally sampled as follows:

-1 large tube, cut into 1 cm thick slices and frozen for organic carbon (TOC) geochemistry,
-1 large tube, cut into 1 cm thick slices for the surveys on dinoflagellates,
-1 small and 2 large tubes, cut into 1 cm thick slices and stained with rose bengal for faunal investigations
- surface of 1 large tube (first cm) for diatom and radiolaria investigations, stained with ethanol/ methanol,

for M44/3 I
-3 large tubes (one without surface) and 3 small tubes were frozen as archive cores,

for M44/3 II
-1 large tube, cut in 0.5 cm thick slices for investigation of foraminiferal composition,
-2 large tubes (one without surface) and 1 small tube were frozen as archive cores,
-1 small tube, cut into 1 cm thick slices for the Saudi Arabian authority as reference sample
-1 small tube, cut into 1 cm thick slices for Dr. Khalid A. Kadi, Saudi Arabia.

50 ml bottom water samples for stable carbon and oxygen isotopes were taken at each station where sediment was recovered.
In total, the multicorer was employed 40 times. More detailed sampling information is given in Table 8.

Tab. 8: Multicorer sampling M44/3

GeoB No.	Latitude N	Longitude E	Water depth (m)	Sediment recovery (cm)	Remarks
M44/3 I, Gulf of Aqaba					
5801-2	29°24.90'	34°54.70'	826 m	40 cm	6 big, 4 small tubes filled
5801-3	29°24.90'	34°54.70'	826 m	40 cm	6 big, 4 small tubes filled
5802-2	29°30.45'	34°57.68'	396 m	43 cm	6 big, 4 small tubes filled
5803-2	29°30.96'	34°58.02'	301 m	7 cm	6 big, 3 small tubes filled
5804-2	29°30.07'	34°57.44'	463 m	41 cm	6 big, 4 small tubes filled
5804-3	29°30.10'	34°57.40'	464 m	40 cm	6 big, 4 small tubes filled
5806-2	29°22.75'	34°53.30'	838 m	40 cm	5 big, 4 small tubes filled
5807-2	29°28.81'	34°56.78'	646 m	39 cm	6 big, 4 small tubes filled
5808-3	29°29.06'	34°56.35'	576 m	43 cm	6 big, 4 small tubes filled
5809-2	29°30.40'	34°57.36'	401 m	41 cm	6 big, 4 small tubes filled
5810-3	29°30.21'	34°57.73'	441 m	35 cm	6 big, 4 small tubes filled
5811-1	29°24.86'	34°54.70'	827 m	39 cm	6 big, 4 small tubes filled
5812-2	29°31.14'	34°57.79'	269 m	15 cm	6 big, 4 small tubes filled
5813-1	29°31.32'	34°57.90'	240 m	19 cm	6 big, 4 small tubes filled
5814-2	29°31.71'	34°58.08'	140 m	-	no core recovery
5814-3	29°31.72'	34°58.09'	135 m	6 cm	6 big, 4 small tubes filled
M44/3 II, Northern Red Sea, Saudi Arabia					
5823-1	26°25.26'	35°40.19'	789 m	33 cm	6 big, 4 small tubes filled
5824-1	26°29.12'	35°49.52'	587 m	33 cm	6 big, 4 small tubes filled
5825-1	26°30.47'	35°56.94'	1031 m	31 cm	5 big, 4 small tubes filled
5827-1	26°19.11'	35°31.20'	959 m	9 cm	4 small tubes filled
5828-1	26°20.78'	35°24.13'	1072 m	11-35 cm	5 big, 4 small tubes filled
5831-1	27°05.30'	35°33.98'	884 m	32 cm	5 big, 4 small tubes filled
5832-1	27°03.20'	35°24.32'	628 m	30 cm	5 big, 4 small tubes filled
5832-3	27°03.18'	35°24.31'	628 m	30 cm	6 big, 4 small tubes filled
5835-4	26°15.49'	35°20.02'	1328 m	-	no surface, no samples
5835-5	26°15.52'	35°19.99'	1328 m	2 kg	6 big, 4 small tubes filled
5835-6	26°15.50'	35°19.99'	1328 m	2 kg	6 big, 4 small tubes filled
5836-1	26°12.60'	35°21.55'	1474 m	-	no surface, no samples
5836-3	26°12.61'	35°21.54'	1475 m	-	no core recovery
5837-1	27°36.69'	34°51.85'	771 m	18 cm	6 big, 4 small tubes filled
5838-1	27°34.54'	34°44.16'	832 m	31 cm	6 big, 4 small tubes filled
5839-2	27°34.84'	34°47.92'	803 m	17 cm	6 big, 3 small tubes filled
5840-1	27°31.66'	34°41.24'	908 m	32 cm	6 big, 4 small tubes filled
5842-1	27°42.70'	35°02.84'	863 m	35 cm	6 big, 4 small tubes filled
5843-2	27°52.69'	34°58.16'	529 m	35 cm	5 big, 4 small tubes filled
5844-1	27°42.81'	34°40.94'	963 m	32 cm	6 big, 4 small tubes filled

M44/3 III, Eastern Mediterranean Sea, Israel (see Table 11)

5.3.3.3 Gravity Corer

5.3.3.3.1 Sampling

To recover deeper sediment sequences, a gravity corer with pipe lengths of alternatively 6, 12 or 18 m and a weight of 1.5 tons was used at 31 stations. Before using the coring tools, the liners had been marked lengthwise with a straight line in order to retain the orientation of the core. Once on board, the sediment core was cut into 1 m sections, closed with caps on both ends and labelled according to a standard scheme (Fig. 66).

Thirty cores were retrieved with recoveries between 0.5 and 16.5 m (Table 9). Altogether some 216 m of sediment cores were recovered with the gravity corer during R/V METEOR Cruise M44/3. At three stations, coring had to be repeated with a longer corer pipe because in a first attempt the very deep penetration of the gravity corer resulted in sediment overflow and high surface-sediment loss (stations GeoB 5824, 5831/34, and 5832/33).

All cores recovered in the northern Gulf of Aqaba (M44/3 I) were cut into an archive and work half. The archive half was used for core description, smear slide sampling, core photography, and color scanning. The work half was sampled with two series of syringes (10 ml) for geochemical and faunal studies, both at 2 or 4 cm intervals. Additionally, syringe samples for an initial shipboard biostratigraphic analysis (10 cm³) were taken at depth intervals of about 50 cm (see chapter 5.3.3.3.3 Stratigraphy). Except for gravity cores GeoB 5828-2, 5843-1, and 5844-2, all work on the sediment cores retrieved during the second part of the cruise in the northern Red Sea M44/3 (II) was carried out at the University of Bremen.

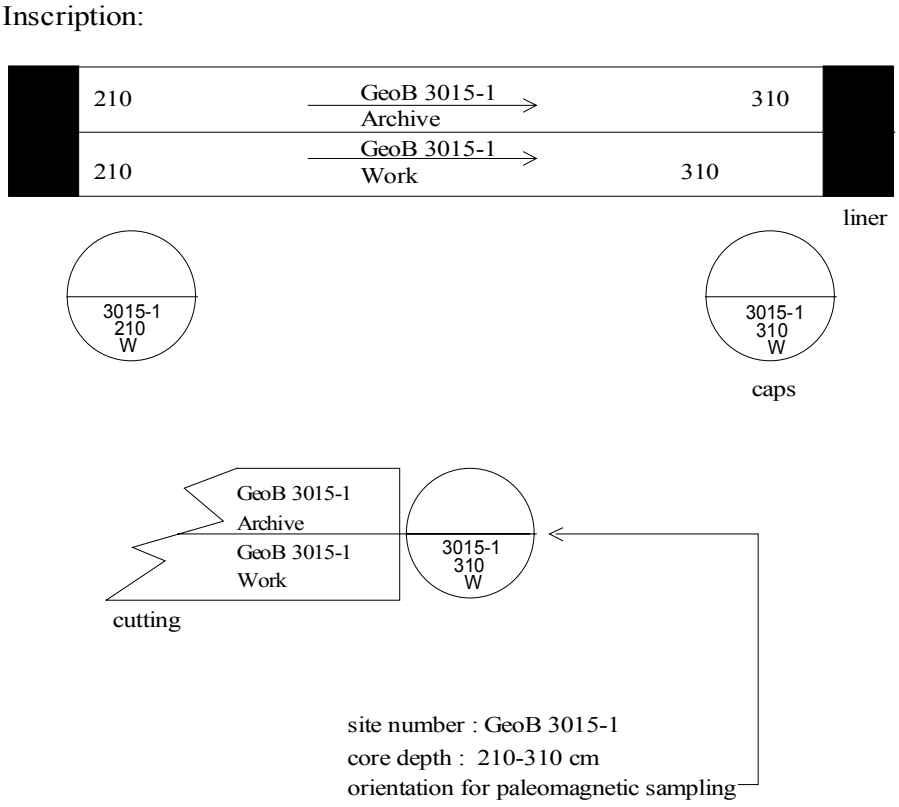

Fig. 66: Scheme of the inscription of gravity core segments.

Tab. 9: List of gravity cores retrieved during R/V METEOR Cruise M44/3.

GeoB No.	Equipment	Latitude N	Longitude E	Water depth (m)	Core length (cm)	Remarks
M44/3 I, Gulf of Aqaba						
5801-4	SL 12	29°24.92'	34°54.71'	824 m	280 cm	
5802-3	SL 6	29°30.42'	34°57.65'	400 m	295 cm	
5803-1	SL 6	29°30.99'	34°58.10'	298 m	97 cm	
5804-4	SL 6	29°30.10'	34°57.40'	464 m	330 cm	
5805-1	SL 6	29°24.90'	34°54.60'	827 m	97 cm	
5806-1	SL 6	29°22.76'	34°53.30'	838 m	39 cm	
5807-3	SL 6	29°28.82'	34°56.76'	644 m	186 cm	
5808-2	SL 6	29°29.03'	34°56.32'	578 m	364 cm	
5809-3	SL 6	29°30.39'	34°57.36'	404 m	304 cm	
5810-2	SL 6	29°30.22'	34°57.73'	440 m	265 cm	
5812-1	SL 6	29°31.19'	34°57.84'	262 m	50 cm	
5813-2	SL 6	29°31.34'	34°57.90'	235 m	247 cm	
5814-1	SL 6	29°31.71'	34°58.09'	138 m	-	cc: fossil corals
M44/3 II, Northern Red Sea, Saudi Arabia						
5823-2	SL 6	26°25.25'	35°40.18'	789 m	410 cm	
5824-2	SL 6	26°29.13'	35°49.49'	591 m	567 cm	
5824-3	SL 12	26°29.12'	35°49.50'	587 m	1016 cm	
5825-2	SL 12	26°30.47'	35°56.92'	1030 m	728 cm	
5828-2	SL 12	26°20.71'	35°24.08'	1057 m	915 cm	
5831-2	SL 12	27°05.29'	35°33.97'	884 m	1146 cm	
5832-2	SL 12	27°03.17'	35°24.29'	628 m	1147 cm	
5833-1	SL 18	27°03.17'	35°24.26'	628 m	-	(same location as 5832) core empty, no samples
5833-2	SL 18	27°03.17'	35°24.26'	628 m	1638 cm	(same location as 5832)
5834-1	SL 18	27°05.27'	35°34.01'	886 m	1661 cm	(same location as 5831)
5835-7	SL 18	26°15.50'	35°20.00'	1328 m	152 cm	70 cm liquid, tube bent
5836-2	SL 12	26°12.61'	35°21.56'	1475 m	790 cm	
5837-2	SL 12	27°36.69'	34°51.87'	770 m	718 cm	
5838-3	SL 18	27°34.67'	34°44.26'	830 m	1618 cm	
5839-1	SL 18	27°34.73'	34°47.91'	802 m	1052 cm	
5840-2	SL 18	27°31.66'	34°41.24'	909 m	1630 cm	
5842-2	SL 18	27°42.74'	35°02.86'	863 m	1337 cm	
5843-1	SL 18	27°52.71'	34°58.16'	529 m	1469 cm	
5844-2	SL 18	27°42.81'	34°40.90'	963 m	1235 cm	

5.3.3.3.2 Core Description, Smear Slide Analysis, and Color-Scanning

(H. W. Arz, T. Felis)

5.3.3.3.2.1 Methods

The core descriptions summarize the most important results of the analysis of each sediment core following ODP convention (Graham and Mazullo, 1988). Core descriptions for all retrieved sediment cores are shown in PÄTZOLD ET AL. (2000: Figs. 4.3.2 to 4.3.28 therein). The "Stratigraphy" column gives the zonation defined by paleontological data (M44/3 I) and profiling color data (M44/3 II). The lithological data, indicated in the "Lithology" column, are based on smear slide analyses. In the structure column the intensity of bioturbation together with individual or special features (slumps, turbidites, lamination, shell fragments etc.) is shown. The hue and chroma attributes of color were determined by comparison with the Munsell soil color charts and are given in the color column in the Munsell notation.

In order to supplement the macroscopic core descriptions, a smear slide analysis was carried out. Smear slides were taken from every described core. Altogether 225 slides were examined using a light microscope at about 125x - 1250x magnification with cross-polarised and transmitted light. Smear slides were primarily taken from all representative lithologies. The sediment classification is also based on ODP-nomenclature.

A Minolta CM - 2002™ hand-held spectrophotometer was used to measure percent reflectance values of sediment color at 31 wavelength channels over the visible light range (400-700 nm). The digital reflectance data of the spectrophotometer readings were routinely obtained from the surface (measured in 0.5 or 1 cm steps) of the splitt cores (archive half). In Pätzold et al. (2000: Figs. 4.3.2 to 4.3.28 therein) the color measurements of each core - representative wavelengths of 400, 550, and 700 nm, and the hue and lightness of the sediment - are shown.

5.3.3.3.2.2 Results

Northern Gulf of Aqaba

Twelve gravity cores were retrieved along a transect close to the central axis of the northern Gulf of Aqaba from water depths between 138 and 838 m (Fig. 6). Core recovery was generally low (39 to 364 cm core length) because of the relatively coarse grained sediments deposited between the morphologically steep outcropping lateral faults which embrace the northern gulf. As tectonic activity in this area often relates to earthquake activity, continuous sedimentation is frequently interrupted by sandy turbidites. Generally, the sediments are a uniform brownish color containing high amounts of terrigenous material and variable amounts of biogenic carbonate. The sediments retrieved from below 500 m water depth (GeoB 5801-4, 5805-1, 5806-1, 5807-3, and 5808-2) much more frequently show erosive sand turbidites than the shallower ones (GeoB 5802-3, 5804-4, 5809-3, and 5810-2). A proper explanation may be the increased accumulation of turbidites in the deeper parts of the basin. The cores from intermediate water depths (around 400 m) are mostly undisturbed. The shallow cores (GeoB 5803-1, 5812-1, and 5813-2) are again highly disturbed because of detrital fore-reef sedimentation and coarse sand deposits. All cores are most probably of Holocene age.

Northern Red Sea, transects C, D, and E

Sixteen gravity cores were retrieved along three profiles extending from the Saudi Arabian coast to the central axis of the northern Red Sea from water depths between 590 and 1060 m (Fig. 8). The cores are between 4.1 and 16.3 m long and consist of alternating white to light gray foraminifer-bearing nannofossil oozes and olive gray clayey nannofossil oozes to nannofossil clays. The variable amount of darker terrigenous material down-core strongly affects sediment color, providing an excellent tool for stratigraphic purposes and core correlation (see chapter 4.3.3.3 Stratigraphy). The sediments are, in general, moderately bioturbated, and except for the proximal cores GeoB 5842-2, 5843-1, 5831-2/5834-1, and 5825-2, the gravity cores represent undisturbed sedimentary records of the past 80 kyrs (GeoB 5823-2) to 500 kyrs (GeoB 5833-2). The carbonate concretion layer of the Last Glacial Maximum (LGM) is exceptionally well documented in all sediment cores. During this period sea-surface salinity in the Red Sea probably exceeded 53‰ (Hemleben et al., 1996), resulting in an almost complete disappearance of planktonic organisms (except for some pteropod species) and anorganic precipitation of carbonate. Comparable concretion layers were found in the deeper sections of the southern-transect cores GeoB 5824-3 and 5828-2, which are obviously related

to the penultimate glacial stage around 140 kyrs (OIS 6). The cores next to the Saudi Arabian coast, cores GeoB 5842-2, 5843-1, 5831-2/5834-1, and 5825-2, are extensively disturbed by turbidites. The admixture of detrital carbonates in many of the turbidite sequences clearly reflects the proximal position to the coastal reef platforms. Stratigraphic information for these cores is therefore very sparse.

Shaban Deep gravity cores GeoB 5835-7 and 5836-2

The two gravity cores GeoB 5835-7 and 5836-2 were retrieved from the NE basin and SW basin of the Shaban Deep from water depths of 1328 and 1475 m, respectively. The cores comprise of partly laminated olive gray to black brine sediments that have a very high content of hypersaline pore water. The individual layers vary in their composition depending on the carbonate, clay, and biogene silica (mainly diatoms) content. Much like the multicorer samples at these stations, about the uppermost 70 cm of the sediment cores were highly liquid and relatively hard to recover. In core GeoB 5835-7 volcanic glass particles were occasionally found in the coarse fraction.

5.3.3.3.3 Stratigraphy

(H. W. Arz, B. Donner, T. Lützeler)

5.3.3.3.3.1 Methods

For a preliminary shipboard biostratigraphic analysis samples were taken in about 50 cm intervals down core of each sediment core from the northern Gulf of Aqaba. Sampling depths coincide with those for smear slide analysis. 8 to 10 ml of the sediment were washed over a 150 µm mesh sieve, dried in an oven at 60°C and finally filled into 5 ml glass tubes. The height of the material column in the glass tube was used as an indicator for the relative sand content of the samples.

Normally at a latitude of 20°-30° N (Atlantic Ocean), the stratigraphical analysis can be done by counting forminifera of the *Globorotalia menardii* complex (ERICSON AND WOLLIN, 1968). They give information about glacial/interglacial cycles. In the Gulf of Aqaba foraminifera of the *G. menardii* complex are very rare, too rare to allow a stratigraphic overview. Instead, the stratigraphic classification was made by determining the abundance of the warm-water surface species *Globigerinoides ruber* and *Globigerinoides sacculifer* - both appearing in the Gulf in high abundances during warmer times.

According to REISS ET AL. (1980) in isotope stages 1 and 5 faunal assemblages are representatives of present-day temperature and salinity conditions in the Gulf of Aqaba/Northern Red Sea. Species of tropical-subtropical character, symbionts bearing and spinose are dominant. Fine-pored, smooth and keeled forms are absent (only southern Red Sea is *Globorotalia*-bearing). Pitted species (*N. pachyderma*, sinistral) are rare, but occurring in intervals of isotope stage 5. In isotope stages 2-4 and 6, faunal assemblages reflect both lower temperatures and particularly higher salinities. Amounts of *G. sacculifer* decrease and *G. ruber* becomes dominant. Probably winter temperatures of <17°C in the Gulf prevent *G. sacculifer* from surviving. The temperature limit of *G. ruber* seems to be about 13°C. Finally, during the Last Glacial Maximum planktonic foraminifera are absent due to high salinities exceeding 50‰ (aplanktic zone). On the basis of the *G. ruber*/(*G. ruber* + *G. sacculifer*) index and especially the identification of the LGM aplanktic zone of the Red Sea and the Gulf of Aqaba area described by e.g. REISS ET AL. (1980), preliminary stratigraphies were established for most of the cores.

The profiling color reflectance values and especially the 700 nm wave length of the visual light spectra of the sediments from the northern Red Sea transects strongly reflect compositional variations of the sediment through time. In general (Mix et al., 1993), but also in this particular case, light colors (high 700 nm reflectance) represent carbonate-rich interglacial sediments and dark colors more terrigenous glacial sediments. It can be clearly demonstrated by comparing an oxygen-isotope record of a sediment core from the central Red Sea (Hemleben et al., 1996) with our color measurements, that sediment color is generally an excellent stratigraphic tool in the Red Sea area (Fig. 68, 69, and 70).

5.3.3.3.3.2 Results

Northern Gulf of Aqaba

The foraminiferal composition in every sediment core indicates that all samples are of Holocene age, and the LGM was not penetrated (Fig. 67). According to the foraminiferal index of Reiss et al. (1980), higher values mark the middle to late Holocene period. Therefore high sedimentation rates of up to 20 cm/kyrs are suggested for most of the cores.

Northern Red Sea, transects C, D, and E

In Figures 68, 69, and 70, the color measurements of the gravity cores along the three transects are compared with the isotopic record of core KL 11 from the central Red Sea (Hemleben et al., 1996). Besides the clearly distinguishable glacial-interglacial shifts in color, a rough age for most of the cores could be assessed. Based on these data, the cores extend back to a maximum of 500 kyrs (GeoB 5833-2) and average sedimentation rates vary between 2.5 and 10 cm. For details see Table 10.

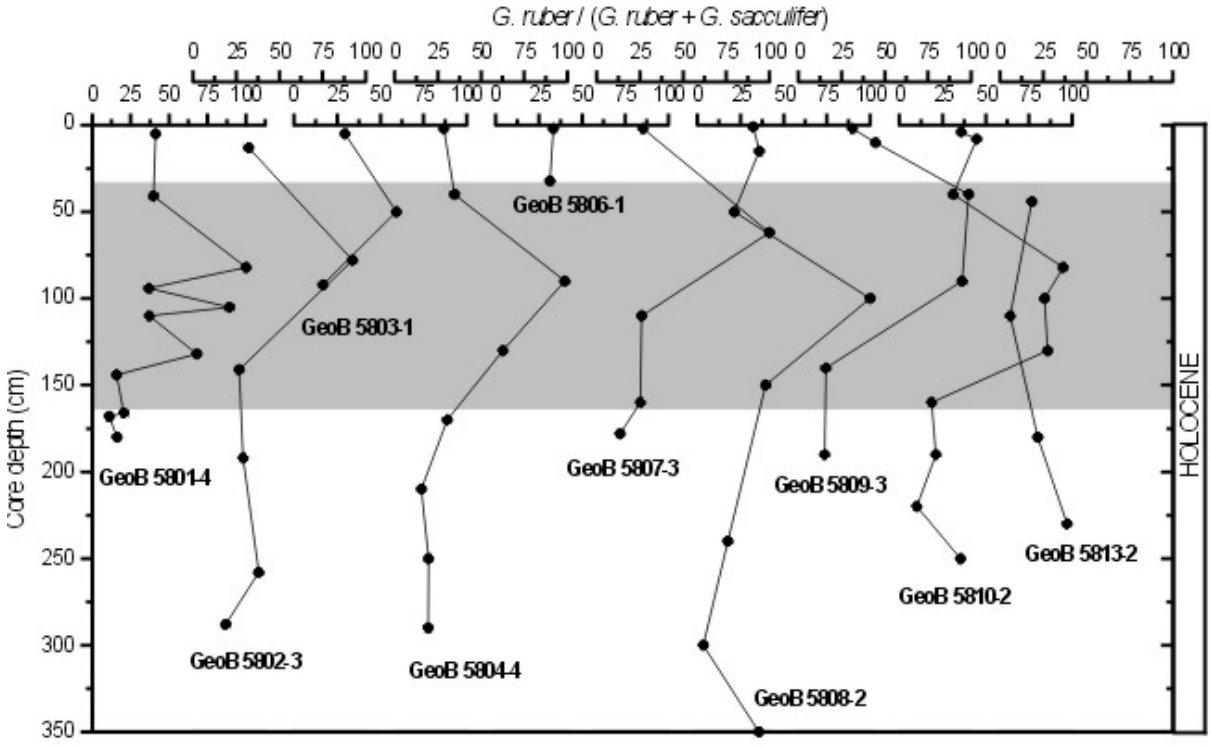

Fig. 67: *G. ruber* / (*G. ruber* + *G. sacculifer*) index of the gravity cores from the northern Gulf of Aqaba. The gray shaded box probably marks the middle to late Holocene period.

Tab. 10: Estimation of age and sedimentation rates of the northern Red Sea gravity cores, based on comparisons of the color measurements with an isotopic record of core KL 11 from the central Red Sea (HEMLEBEN ET AL., 1996).

GeoB core nr.	Approximate age (kyrs)	Average sedimentation rate (cm/kyr)	Core GeoB nr.	Approximate age (kyrs)	Average sedimentation rate (cm/kyr)
5823-2	128	3.3	5835-7	?	-
5824-2	245	3.3	5836-2	?	-
5824-3	360	2.8	5837-2	150	4.8
5825-2	?	-	5838-3	435	2.5
5828-2	375	2.4	5839-1	300	3.5
5831-2	?	-	5840-2	350	4.7
5832-2	350	3.3	5842-2	130	10.3
5833-2	500	3.3	5843-1	?	-
5834-1	?	-	5844-2	210	5.6

5.3.3.4 Piston Corer

(Chr. Hemleben, H. Hübner, S. Themann, S. Weldeab)

During the cruise we retrieved sediment samples at different stations by means of a multicorer and a piston corer. Prior to coring, the site was intensively investigated using PARASOUND and HYDROSWEEP to find the best location. The recovered sediment samples will be investigated for temporal and spatial changes in the composition of planktic and benthic foraminiferal faunas and the chemical signals of the tests. Since we will mainly concentrate on high-resolution studies we expect to gain information not only on long-term glacial to interglacial cycles but also on high frequent fluctuations of the past climate and deep-water circulation.

Tab. 11: List of piston cores retrieved during R/V METEOR Cruise M44/3. Multicorer stations from the Levantine Sea are added.

Station	Latitude N	Longitude E	Water depth (m)	Piston Core	Core recovery (cm)
M44/3 II, Northern Red Sea, Saudi Arabia					
199	27°03,17'	35°24,32'	627	199-1-KL 76	1065
199	27°03,17'	35°24,29'	628	199-2-KL 77	1660
204	27°36,67'	34°51,86'	770	204-1-KL 78	1740
205	27°34,64'	34°44,33'	831	205-1-KL 79	1070
207	27°31,65'	34°41,24'	909	199-1-KL 80	1720
208	27°40,00'	34°48,00'	812	208-1-KL 81	1065
M44/3 III, Eastern Mediterranean Sea (Levantine Sea), Israel					
multicorer					
212	32°19,29'	34°09,93'	1283	MC 604	42
213	32°36,80'	34°08,94'	1432	MC 605	40
214	32°49,23'	34°09,84'	1532	MC 606	40
215	32°36,81'	34°01,62'	1449	MC 607	42
piston corer					
212	32°19,31'	34°09,93'	1284	212-1-KL 82	1065
213	32°36,87'	34°08,89'	1431	213-1-KL 83	1050
214	32°49,23'	34°09,92'	1533	214-1-KL 84	890
215	32°36,81'	34°01,62'	1450	215-1-KL 85	1040

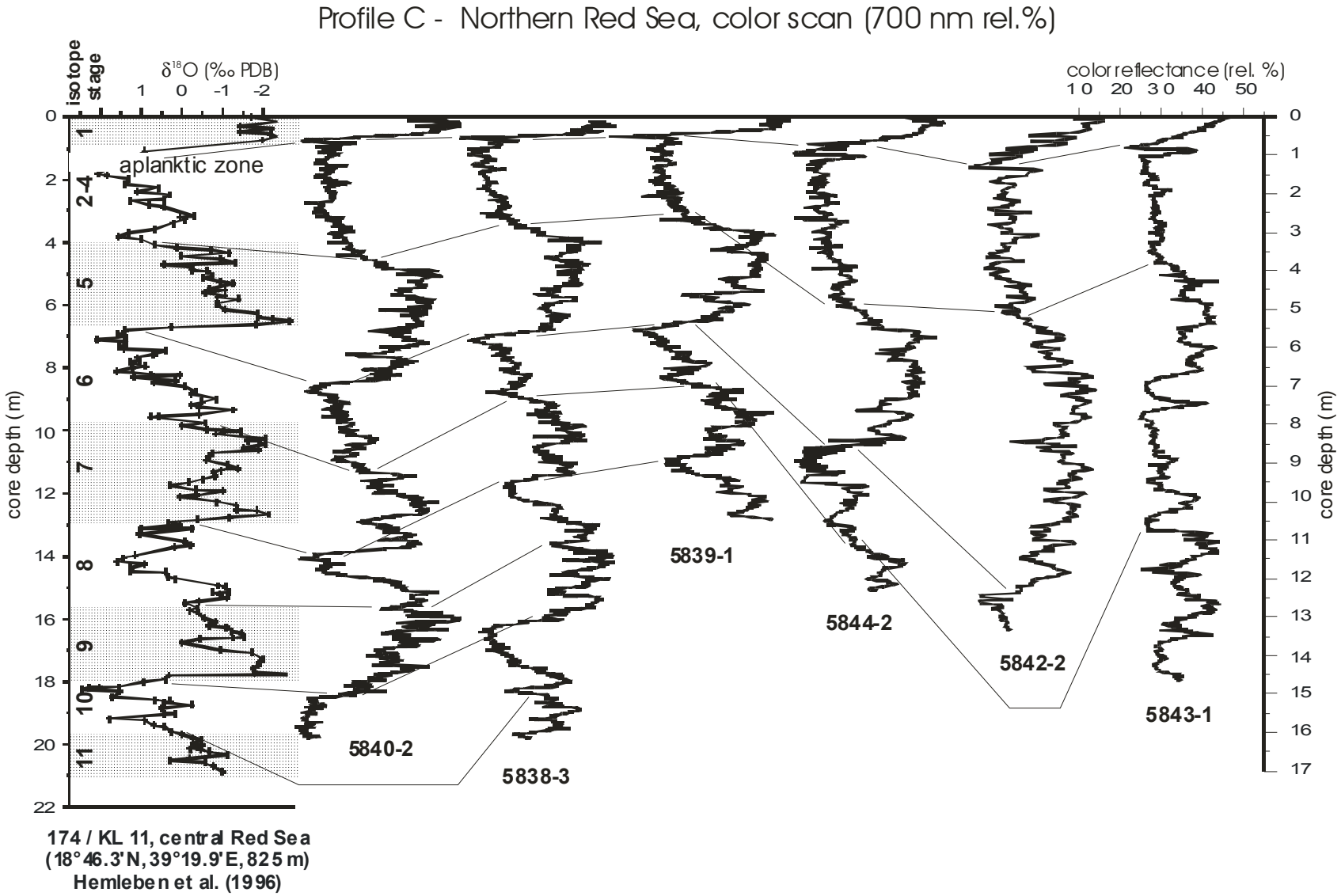

Fig. 68: Comparisons of the sediment color of gravity cores from profile C, northern Red Sea, with the isotopic record of core KL 11 from the central Red Sea (HEMLEBEN ET AL., 1996).

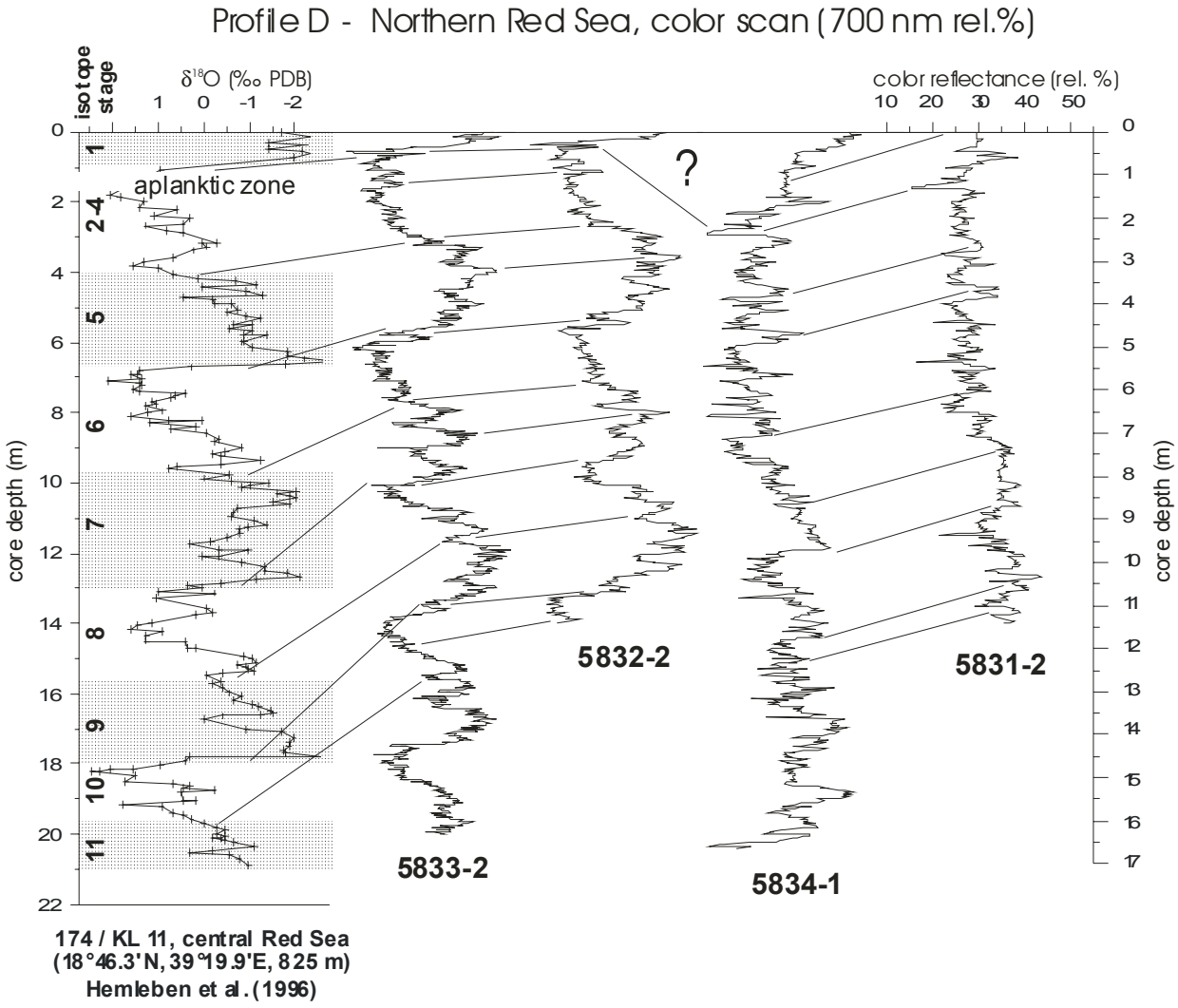

Fig. 69: Comparisons of the sediment color of gravity cores from profile D, northern Red Sea, with the isotopic record of core KL 11 from the central Red Sea (HEMLEBEN ET AL., 1996). Dotted bold lines conect cores retrieved at the same location.

5.3.4 CTD Profiling

(T. Felis, C. Moos)

5.3.4.1 Methods

A self-contained SEABIRD SBE 19 CTD profiler equipped with a conductivity-temperature-depth-sensor, an oxygen probe and a CHELSEA fluorometer for chlorophyll *a* measurements was used at 31 stations in order to study the variability of temperature, salinity, oxygen, and chlorophyll *a* throughout the water column. These data provide important information on water-column stratification and will also support the interpretation of the stable carbon and oxygen isotope ($\delta^{13}C$, $\delta^{18}O$) and nutrient (PO_4) analyses of the water samples recovered from different depths of the water column. All sensors were calibrated by the manufacturer prior to the cruise. The CTD profiler was attached to the wire 50 m above the multicorer or, when no multicorer was used, 50 m above the multinet. Full parameter sets were taken at 0.5 sec intervals both during downcast and retrieval. Immediately after each CTD profiling the data were transfered to a PC and the downcast profiles were displayed in standard plots.

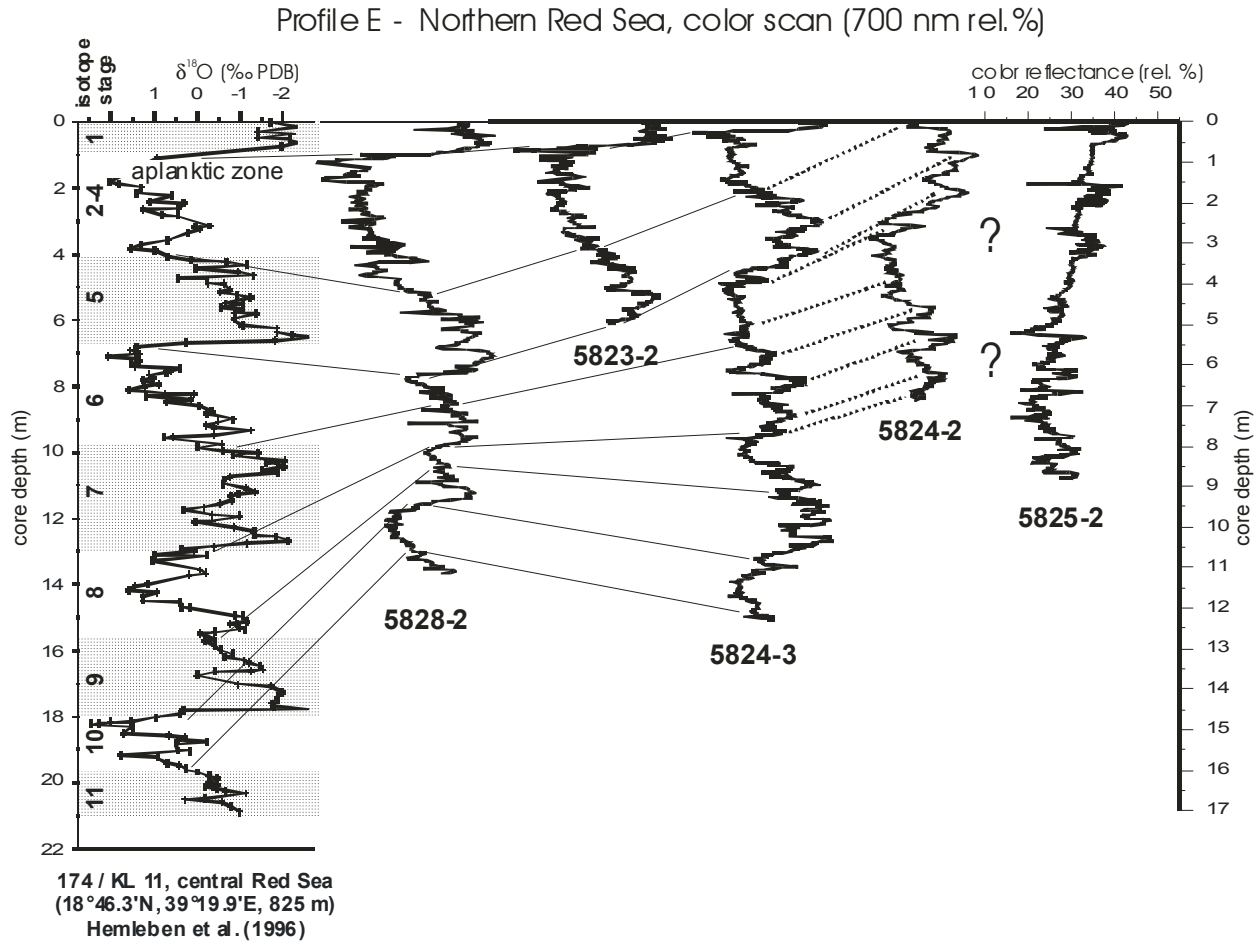

Fig. 70: Comparisons of the sediment color of gravity cores from profile E, northern Red Sea, with the isotopic record of core KL 11 from the central Red Sea (Hemleben et al., 1996). Dotted bold lines connect cores retrieved at the same location.

At some stations the salinity profiles showed an anomalous varibility of 0.1-0.2 and the Chelsea Fluorometer ran out of its range at some stations. At the end of the cruise, the manufacturer checked the CTD profiler but no malfunction could was detected. The CTD-recordings from station GeoB 5802-2 were lost during data upload.

5.3.4.2 Preliminary Results

The temperature/salinity versus depth profiles (Fig. 71) show the unusually weak vertical stratification of the water mass in the Gulf of Aqaba, which is mainly determined by temperature. The contribution of salinity to stratification is negligible (e.g., Reiss and Hottinger, 1984). Deep vertical water mass mixing reached a maximum depth of about 500 m at the northern end of the Gulf during the period of the cruise. Therefore, complete homogeneity between the upper water mass and the deep water was probably not achieved that winter. In the southern part of the Gulf, the upper water mass is more stratified and warmer, probably as a result of the beginning summer stratification and/or the influence of the northward-flowing Red Sea surface waters. The influence of these warmer and less saline waters can be clearly seen at the southernmost station in the Gulf (station 5820-3). In the southern part of the Gulf a slightly warmer and more saline water mass was detected in a depth of

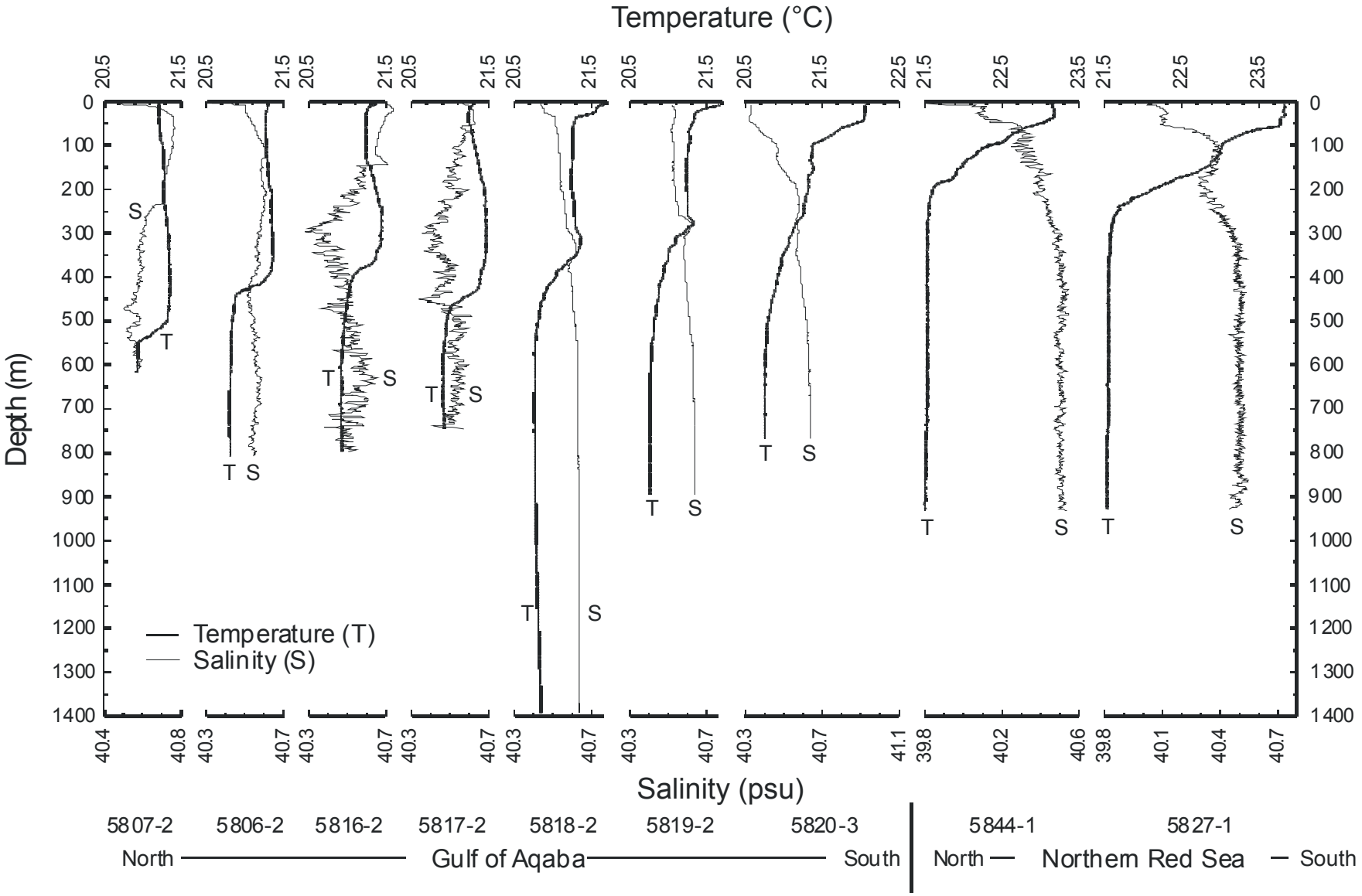

Fig. 71: North-south transect of CTD profiles (temperature and salinity) from the northern Gulf of Aqaba to the northern Red Sea.

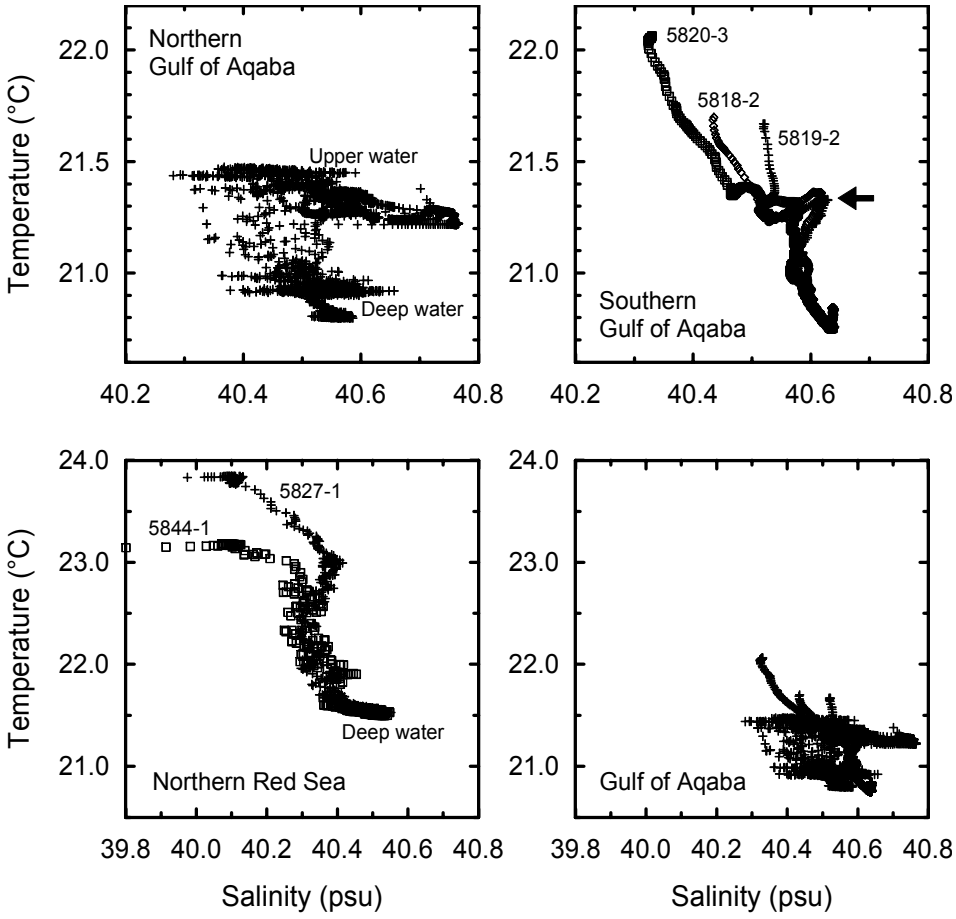

Fig. 72: Temperature-salinity diagrams for the Gulf of Aqaba and the northern Red Sea revealing characteristic water masses. Data used are from the stations shown in Figure 71.

330 m (station 5818-2) and 280 m (station 5819-2), respectively. Compared to the Gulf, the upper water mass of the northern Red Sea is more stratified which is determined by both temperature and salinity.

The temperature-salinity (T-S) diagram for the northern Gulf of Aqaba shows the two characteristic water masses of upper and deep water with their difference mainly determined by temperature (Fig. 72). The T-S diagram for the southern part of the Gulf reveals slightly warmer and more saline water mass (arrow) in a depth of about 300 m. Comparison of the T-S diagrams for the northern Red Sea and the Gulf of Aqaba shows that the deep-water mass of the latter is colder and slightly more saline.

Although the CTD-recorded absolute data for dissolved oxygen are not reliable, a comparison between the northern Red Sea and the Gulf of Aqaba shows the lack of a pronounced oxygen minimum in the latter (e.g., REISS AND HOTTINGER, 1984) (Fig. 73).

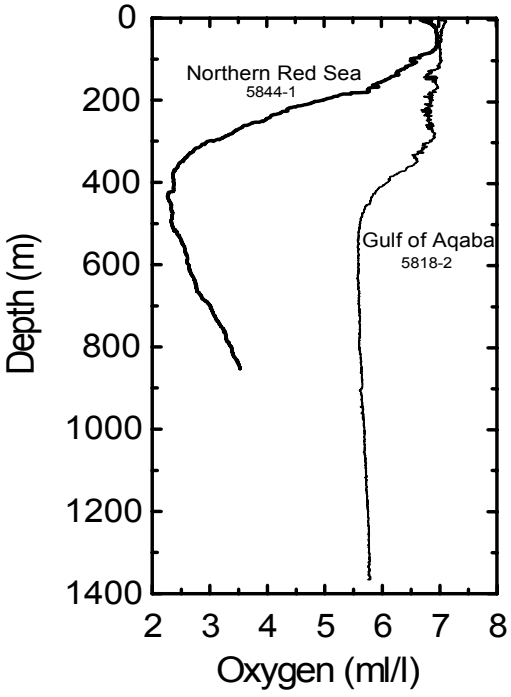

Fig.73: CTD profiles of dissolved oxygen from the Gulf of Aqaba and the northern Red Sea

5.3.5 Sampling of Plankton in the Water Column

5.3.5.1 Dinoflagellate Investigations

(S. Meier)

5.3.5.1.1 Introduction

Dinoflagellates are unicellular, biflagellated algae that are known from most aquatic environments. They are a major group of the marine plankton and can live autotrophically, heterotrophically or even be symbiotic and parasitic. During their life cycle, which can be very complex, they generally pass through a vegetative-thecate stage in which they are able to swim actively with their two flagellae. This stage is followed by the formation of resting cysts, which can be induced by adverse environmental conditions. The cyst material can be organic or calcareous. The only species forming a vegetative-coccoid cyst stage with a calcareous wall is *Thoracosphaera heimii*.

Calcareous dinoflagellate cysts have been overlooked for a long time due to their size between nannoplankton and foraminifera, and because they are dissolved during the preparation of palynological samples. Recent studies showed that they are a useful proxy for palaeoceanographic reconstruction. However, knowledge about their distribution in the water column and in the sediments is still quite limited, especially in the Gulf of Aqaba, the northern Red Sea, and the Levantine Basin, which have never been systematically investigated for calcareous dinoflagellate cysts. Their spatial distribution in combination with environmental parameters such as temperature, salinity, nutrient supply, stratification, etc. may lead to a better understanding of their ecological preferences and help to understand their paleoecological signal. For these purposes, water and sediment samples were taken during the cruise and living calcareous dinoflagellate cysts were isolated from the samples for culturing experiments under controlled laboratory conditions.

5.3.5.1.2 Samples

5.3.5.1.2.1 Water Samples

Water from a depth of about 5 m depth was sampled with the ship's membrane pump during daytime on most transits and geophysical profiles (Tab. 12). The plankton content of a measured amount of liters was concentrated with a two-filter system (100 µm pre-filter and 10 µm end-filter) in a 1 l bottle. In general, three samples were taken per day (ca. 08:00-12:00; 12:00-16:00, 16:00-20:00 board time), but depending on the volume of plankton in the seawater, the filters had to be cleaned every 100 to 600 liters, which means that in regions with higher plankton concentrations, more samples had to be taken. In total, 41 samples were taken (Tab. 12).

The 1 l of concentrated seawater was filtered through a 5 µm polycarbonate filter down to 100 ml. A part of this water was analysed with a light microscope with special notive taken of the calcareous dinoflagellate cysts. Living cysts were isolated and cultured in polyterene Cell Wells containing different culture media (f/2 35‰ and K 35‰ mixed with filtered sea water) at temperatures of about 20°C and using the local day/night cycle. These cultures will be used for laboratory experiments under controlled conditions at the University of Bremen.

The remaining part of the sample was fixed with 37% formaldehyde at a final concentration of 3-4% and stored in the dark at 4°C.

Tab. 12: Water samples from the membrane pump.

Sample No M44/3	Date 1999	Start of filtration			End of filtration			Temperature [°C]	Salinity [‰]	Volume of filtered water [l]	Remarks
		Time UTC	Latitude N	Longitude E	Time UTC	Latitude N	Longitude E				
3/13/b	13.03.	11:45	29°30,04′	34°17,43′	13:11	29°24,89′	34°54,71′	21,8	40,55	121	KP
3/14/a	14.03.	06:22	29°30,76′	34°56,76′	07:49	29°26,11′	34°55,85′	21,7	40,62	112	KP
3/14/b	14.03.	08:13	29°24,22′	34°55,10′	09:49	29°26,92′	34°55,40′	21,7	40,58	94	MP
3/14/c	14.03.	10:10	29°28,41′	34°56,18′	11:39	29°30,71′	34°56,52′	21,7	40,58	151	MP
3/14/d	14.03.	11:52	29°29,98′	34°56,56′	13:33	29°27,73′	34°56,46′	21,8	40,62	199	MP
3/14/e	14.03.	13:47	29°27,13′	34°57,48′	15:57	29°23,43′	34°56,90′	21,8	40,61	174	MP
3/16/a	16.03.	06:07	29°13,68′	34°46,58′	07:39	29°13,15′	34°49,46′	21,8	40,61	160	MP
3/16/b	16.03.	07:58	29°13,15′	34°47,63′	10:18	29°18,96′	34°52,24′	21,8	40,61	196	MP
3/17/a	17.03.	06:00	28°51,08′	34°43,92′	07:54	29°00,56′	34°45,64′	21,7	40,51	204	MP
3/17/b	17.03.	08:09	29°01,75′	34°45,94′	10:39	29°10,73′	34°48,60′	21,7	40,55	219	MP
3/17/c	17.03.	10:54	29°10,20′	34°48,05′	13:21	29°00,38′	34°42,69′	21,8	40,57	229	MP
3/17/d	17.03.	13:39	28°58,94′	34°42,81′	16:11	28°54,03′	34°41,49′	21,9	40,52	177	MP
3/18/a	18.03.	06:15	29°16,83′	34°49,88′	08:28	29°08,26′	34°46,98′	21,7	40,61	227	MP
3/18/b	18.03.	10:10	29°13,96′	34°49,70′	11:36	29°16,67′	34°50,67′	21,8	40,61	106	MP
3/19/a	19.03.	06:01	28°53,44′	34°43,76′	07:42	29°01,18′	34°42,35′	21,8	40,54	146	MP
3/19/b	19.03.	09:47	29°03,07′	34°45,14′	12:05	28°52,58′	34°43,18′	21,9	40,57	94	MP
3/19/c	19.03.	13:21	28°46,98′	34°40,72′	14:44	28°42,13′	34°41,55′	21,8	40,49	109	MP
3/20/b	20.03.	09:44	28°46,92′	34°42,76′	10:56	28°34,97′	34°40,00′	22,2	40,41	123	MP
3/20/c	20.03.	16:01	28°33,78′	34°38,78′	17:39	28°25,79′	34°37,75′	22,0	40,52	132	MP
3/21/a	21.03.	06:17	28°22,59′	34°34,03′	07:32	28°21,66′	34°31,34′	22,5	40,30	174	MP
3/21/b	21.03.	10:12	28°34,28′	34°36,23′	12:13	28°30,97′	34°36,72′	22,2	40,38	233	MP
3/21/c	21.03.	14:27	28°20,55′	34°32,67′	16:32	28°28,06′	34°33,33′	22,8	40,27	268	MP
3/22/b	22.03.	10:58	28°20,38′	34°33,87′	13:04	27°55,97′	34°25,80′	22,5	40,32	300	MP
3/22/c	22.03.	15:01	27°32,22′	34°17,87′	15:50	27°23,98′	34°14,93′	23,2	40,21	166	MP
3/23/a	23.03.	06:21	26°59,24′	34°42,68′	09:15	26°59,94′	34°43,32′	23,0	40,17	382	MP
3/23/b	23.03.	09:28	27°00,97′	34°43,79′	13:26	26°57,47′	34°40,48′	23,0	40,17	468	Mp
3/23/c	23.03.	13:49	26°58,74′	34°40,86′	16:42	27°03,25′	34°43,35′	23,1	40,18	408	MP
3/24/a	24.03.	06:21	26°09,48′	35°20,78′	09:53	26°14,25′	35°18,19′	24,2	39,80	490	MP
3/24/b	24.03.	10:09	26°13,09′	35°18,82′	13:24	26°17,28′	35°13,47′	23,9	39,94	452	MP
3/24/c	24.03.	13:45	26°17,75′	35°12,76′	16:15	26°32,75′	35°01,33′	23,6	40,07	400	MP
3/26/a	26.03.	07:06	26°46,63′	34°16,26′	10:50	26°24,65′	35°02,08′	23,0	40,22	303	MP
3/26/b	26.03.	11:03	26°23,44′	35°04,75′	13:42	26°20,32′	35°29,44′	23,5	40,00	290	MP
3/28/b	28.03.	10:02	26°13,97′	35°22,82′	13:48	26°14,02′	35°22,65′	24,4	39,87	578	MP
3/29/c	29.03.	12:54	27°03,03′	35°24,32′	16:26	27°02,48′	35°24,52′	24,3	39,96	577	MP
3/31/a	31.03.	07:06	26°46,40′	35°16,17′	09:59	27°20,20′	35°10,81′	24,6	39,83	561	MP
3/31/b	31.03.	10:09	27°22,19′	35°10,46′	12:25	27°42,50′	35°03,92′	24,6	39,96	565	MP
3/31/c	31.03.	12:38	27°41,66′	35°02,16′	14:28	27°35,93′	34°51,03′	24,8	40,04	456	MP
4/2/a	02.04.	07:58	27°26,11′	35°33,62′	10:12	27°34,85′	35°13,79′	24,0	40,10	397	MP
4/2/b	02.04.	10:21	27°35,92′	35°12,16′	11:31	27°43,94′	35°02,69′	23,8	40,07	334	MP
4/5/b	05.04.	09:14	32°20,50′	34°09,87′	12:03	32°42,74′	34°09,40′	18,4	38,99	362	MP
4/5/c	05.04.	12:21	32°45,28′	34°09,63′	15:27	32°36,13′	34°27,38′	18,7	39,00	415	MP

MP: membrane pump
KP: wheel pump

5.3.5.1.2.2 Sediment Samples

At 29 stations sediment samples were taken from one core (diameter 9.5 cm) of the multicorer. Fresh material of the upper 1 cm of each core was stored together with some bottom water in polycarbonate flasks at a temperature of 4°C in the dark to prevent living cysts from hatching. These samples will be analysed for living calcareous dinoflagellate cysts to begin the unicellular culture investigations at the University of Bremen.

The remaining segmant of the core was cut into 1 cm scilces and stored in petri dishes at 4°C. These cores will be analysed for their content of calcareous dinoflagellate cysts. The distribution pattern in relation to environmental characteristics of the upper water column are of interest for reconstructing climatic changes reflected in the changes in the associations of calcareous dinoflagellate cysts during the time span represented by the core.

5.3.5.1.3 Preliminary Results

Water samples were taken in three differerent regions: the Gulf of Aqaba, the northern Red Sea and the Levantine Basin. In the Gulf of Aqaba the plankton concentration was higher than in the other regions. In every sample a lot of different dinoflagellate species could be found of which most of them were thecate stages. Four different species of calcareous dinoflagellate cysts could be identified: *Thoracosphaera heimii, ?Sphaerodinella albatrosiana, ?Sphaerodinella tuberosa* and *Scrippsiella regalis* from which the first three could be cultured.

In the northern Red Sea the plankton concentration was lower than in the Gulf of Aqaba and dinoflagellates were less abundant, but still common. Beside the calcareous-cyst-producing dinoflagellate species, which were also found in the Gulf of Aqaba (apart from *S. regalis*), at least three as yet unidentified species were found and cultured.

The calcareous dinoflagellate cyst associations of the Gulf of Aqaba and the northern Red Sea seem to be similar to those of the Atlantic Ocean and the Arabian Sea, which are well known from recent studies at the University of Bremen.

The samples from the Levantine Basin had approximately the same plankton content as the samples from the northern Red Sea and were not used for culturing on board due to shortness of time. Raw material will be examined at the University of Bremen.

5.3.5.2 Plankton and Water Sampling

(B. Donner, C. Moos)

5.3.5.2.1 Multiple Closing Net

Plankton was sampled with a multiple closing net (Fa. HYDROBIOS) with a 0.25 m^2 opening and 63 □m mesh size. It was used for vertical hawls at 17 sites (Tab. 13). Each multinet station comprised one hawl with 5 different depth intervals.

The samples will be used for studies on planktonic foraminifera. The samples containing zooplankton and phytoplankton were carefully rinsed with seawater into KAUTEX bottles, fixed with mercury chloride for the reduction of bacterial degradation, and stored at 4°C.

Tab. 13: Plankton samples using a multiple closing net.

Station GeoB	Depth (m)	Position Latitude / Longitude	Station GeoB	Depth (m)	Position Latitude / Longitude
5801-1	500 - 400	28°24.9´N / 34°54.7´E	5819-1	500 - 400	28°35.0´N / 34°40.11´E
	400 - 300			400 - 300	
	300 - 200			300 - 200	
	200 - 100			200 - 100	
	100 - 0			100 - 0	
5802-1	370 - 300	29°30,5´N / 34°57.7´E	5820-1	500 - 400	28°21.0´N / 34°33.8´E
	300 - 200			400 - 300	
	200 - 100			300 - 200	
	100 – 50			200 - 100	
	50 - 0			100 – 0	
5804-1	400 - 300	29°30.0´N / 34°57.4´E	5820-2*	500 - 400	28°21.0´N / 34°34.0´E
	300 - 200			400 - 300	
	200 - 100			300 - 200	
	100 – 50			200 - 100	
	50 - 0			100 - 0	
5806-3	500 - 400	29°23.7´N / 34°53.6´E	5821-1	500 - 400	27°24.0´N / 34°14.9´E
	400 - 300			400 - 300	
	300 - 200			300 - 200	
	200 - 100			200 - 100	
	100 - 0			100 - 0	
5807-1	500 - 400	29°28.8´N / 34°56.8´E	5821-2*	500 - 400	27°24.0´N / 34°14.9´E
	400 - 300			400 - 300	
	300 - 200			300 - 200	
	200 - 100			200 - 100	
	100 - 0			100 - 0	
5808-1	500 - 400	29°29.1´N / 34°56.3´E	5822-1*	500 - 400	27°24.0´N / 34°14.9´E
	400 - 300			400 - 300	
	300 - 200			300 - 200	
	200 - 100			200 - 100	
	100 - 0			100 - 0	
5809-1	350 – 250	29°30.4´N / 34°57.3´E			
	250 – 150				
	150 – 100				
	100 – 50				
	50 - 0				
5810-1	400 - 300	29°30.2´N / 34°57.8´E			
	300 - 200				
	200 - 100				
	100 – 50				
	50 - 0				
5816-1	500 - 400	29°14.0´N / 34°49.8´E			
	400 - 300				
	300 - 200				
	200 - 100				
	100 - 0				
5817-1	500 - 400	29°06.0´N / 34°46.0´E			
	400 - 300				
	300 - 200				
	200 - 100				
	100 - 0				
5818-1	500 - 400	28°47.1´N / 34°43.0´E			
	400 - 300				
	300 - 200				
	200 - 100				
	100 - 0				

*Samples for H. Gayed (EEAA, Sharm el Sheikh, Egypt)

5.3.5.2.2 Pumped Net Samples

Additionally, marine plankton from surface waters was sampled using the ship's emergency pump system (Tab. 14). A single plankton net (63 µm mesh size) was tied on the main deck and water from 3,5 m depth was filtered for several hours a day.

In order to be able to distinguish between daytime and nocturnal plankton activities - with main emphasis here on pteropods and foraminifera - we took two samples per day: one from sunrise to

Tab. 14: Plankton samples filterted from the emergency pump system.

Sample Nr.	Start of filtration Date 1999	Time UTC	End of filtration Date 1999	Time UTC
FP 1	16.03.	11:00	16.03.	18:00
FP 2	16.03.	18:00	17.03.	6:00
FP 3	17.03.	6:00	17.03.	18:00
FP 4	17.03.	18:00	18.03.	8:00
FP 5	18.03.	6:00	18.03.	18:00
FP 6	18.03.	18:00	19.03.	8:00
FP 7	19.03.	6:00	19.03.	18:00
FP 8	19.03.	18:00	20.03.	6:00
FP 9	20.03.	6:00	20.03.	18:00
FP 10	20.03.	18:00	21.03.	6:00
FP 11	21.03.	6:00	21.03.	18:00
FP 12	22.03.	18:00	22.03.	6:00
FP 13	22.03.	6:00	22.03.	14:00
FP 14	22.03.	14:00	23.03.	6:00
FP 15	23.03.	6:00	24.03.	6:00
FP 16	26.03.	6:00	26.03.	18:00
FP 17	26.03.	18:00	27.03.	06:00
FP 18	27.03.	6:00	27.03.	18:00
FP 19	27.03.	18:00	28.03.	06:00
FP 20	28.03.	6:00	28.03.	18:00
FP 21	28.03	18:00	29.03	06:00
FP 22	29.03	6:00	29.03	18:00
FP 23	29.03	18:00	30.03	06:00
FP 24	30.03	6:00	31.03	06:00

sunset, the 2nd from sunset to sunrise. To obtain information about the stable-isotope compositions of living carbonate-shell-building organisms and their relationships to the regional hydrography, each single pteropod and foraminifer was picked, rinsed in freshwater, dried, and stored.

The samples of the Gulf of Aqaba contained high numbers of copepods, a lot of small bivalvia, a lot of organic material (debris, fecal material), few diatoms, few pteropods and also few foraminifera. Differences in the faunal composition during the day and during the night could not be stated.

Pteropods: As active swimmers and migrators through the water column, they could only be found in very small numbers in these surface samples (less than expected).

Foraminifera: Warm-water surface species (*Globigerinoides ruber, Globigerinoides sacculifer*) were dominant. Additionally, we found species with a wider temperature range (*Orbulina universa, Globigerinella siphonifera, Globigerinella calida*). All these species are spinose and symbiont bearing. According to REISS ET AL. (1980) the spinous species are abundant in the Gulf of Aqaba, but deeper-dwelling nonspinous foraminifera of the genus *Globorotalia* are absent.

But in two samples on the transect in the northern part of the Gulf off Ras Burka we could find three different species of *Globorotalia (menardii, truncatulinoides* and *inflata*). The study of the multinet samples (subsurface water) at home will probably show up to which depths those species are to be found.

5.3.6 Geochemistry in the Brine filled Shaban Deep

(H. Blaschek, S. Klauke, M. O. Moammar, M. Schmidt, M. Schmitt, P. Stoffers)

5.3.6.1 Introduction

The Red Sea is a natural laboratory where the influences of early rifting, spreading, volcanism, and hydrothermal processes on tectonics and sedimentation can be studied. Within the central rift valley of the Red Sea a number of brine-filled depressions occur. The high salinities are due to leaching of subbottom Miocene evaporites.

Our work concentrated on the Shaban Deep in the northern Red Sea at 26°12.66'N and 35°21.47'E. This deep consists of four basins (Shaban-S, -E, -N, -W) filled with high saline brines. The interface between Red Sea Deep Water (RSDW) and the brine occurs at a depth of 1325m (Hartmann et al., 1998) in all four basins. A second interface was found in the southern and eastern basins at a depth of 1459m.

5.3.6.2 Objectives

One of the major goals of cruise M44/3 was the detailed sampling of the brine bodies and the brine interfaces in the Shaban Deep. High-resolution spatial sampling (decimeter to 1 meter sections) should give a better understanding of the geochemical cycles of trace elements and other inorganic compounds in, and between, the convecting brine layers and the overlying RSDW. Besides sampling the brine with a rosette water sampler (+ multiprobe), high-resolution sampling of dissolved and particulate compounds was carried out in the seawater/brine interface with a newly designed (by M. Schmitt, Geochemische Analysen) Interface Water Sampler (IWS, Fig. 74).

The major aim of the trace gas (hydrocarbons, noble gases) studies was to understand the genesis of the gases dissolved in the brine layers of Shaban Deep and their exchange with overlying RSDW. In particular, the stable-isotope compositions of the gases in the brine should give evidence both of thermal degradation mechanisms of organic matter buried in the sediments and mantle-derived fluid input. Furthermore, secondary degradation processes like inorganic or bacterial oxidation of hydrocarbons may be resolved by the stable isotope signature of, e.g., CH_4.

Microbiological and inorganic results of investigations at the seafloor/brine and brine/RSDW interfaces will be linked to the measurements of hydrocarbons. We expect a new clue to formation and degradation mechanisms of organic carbon in this extreme environment, as postulated by Faber et al. (1998).

Additional sediment samples were taken at several core stations in the northern Red Sea. Isotope geochemical investigations of free and adsorbed hydrocarbons in the sediment samples should give information about the hydrocarbon sources (thermal degradation) in deeper sediment layers and/or bacterial processes near the sediment surface.

5.3.6.3 First Results

5.3.6.3.1 Sampling the Sea Water/Brine Interface at Shaban Deep with the Interface-Water-Sampler

5.3.6.3.1.1 Introduction

Water sampling in stratified water bodies, i.e., of brines in the Red Sea, is commonly performed by a rosette sampler equipped with 12 or more Niskin bottles. Sampling is done by lowering the rosette carefully down into the brine layer and closing individual Niskin bottles whilst descending. However, because of the large size of the rosette system and many metal parts, the interface layers can be physically disturbed by mixing, and metal parts may contaminate water samples and influence the chemical redox cycles.

To overcome the mixing effect, to prevent chemical contamination by metals, and to collect water samples at an interval of < 0,5 m simultaneously by only one trigger impulse, we designed a new so-called IWS (Interface Water Sampler, see schematic drawing Fig. 74). The aim of using the IWS is to collect a profile of water samples in only one step from stratified water bodies like brines in the Red Sea. The IWS system was tested for the first time on-board the ship R/V METEOR during cruise M44/3 at the Shaban Deep (R/V METEOR station 202d).

5.3.6.3.1.2 Construction Details

Approximate dimensions of the sampling device are 3m in length and 20 cm in diameter (Fig. 74). About 2.71 m of the sampler length are equipped with 17 water valves in various distances from 8 cm to 24 cm which can be used for water- and gas-sampling (Tab. 15). The sample volume varies from about 1.5 liters to 3 liters. Construction material used is mainly polypropylene, as this material does not contaminate the inorganic and gas chemistry of the water samples. The temperature stability of polypropylene is about > 80°C. The system was triggered by a fall-weight connected to the firing wire and mechanical releaser system from Hydro-Bios.

Tab. 15: Dimensions of IWS-Sampler.

Tube / segment length (cm)	Valve No.	Valve distance (cm)	Total length (cm)
1 / 90	1	33	33
	2	9	42
	3	9	51
	4	14	65
	5	15	80
2 / 84	6	24	104
	7	13	117
	8	19	136
	9	14	150
	10	15	165
3 / 84	11	23	188
	12	9	197
	13	8	205
	14	15	220
	15	15	235
	16	14	249
Head / 45cm	17	22	271

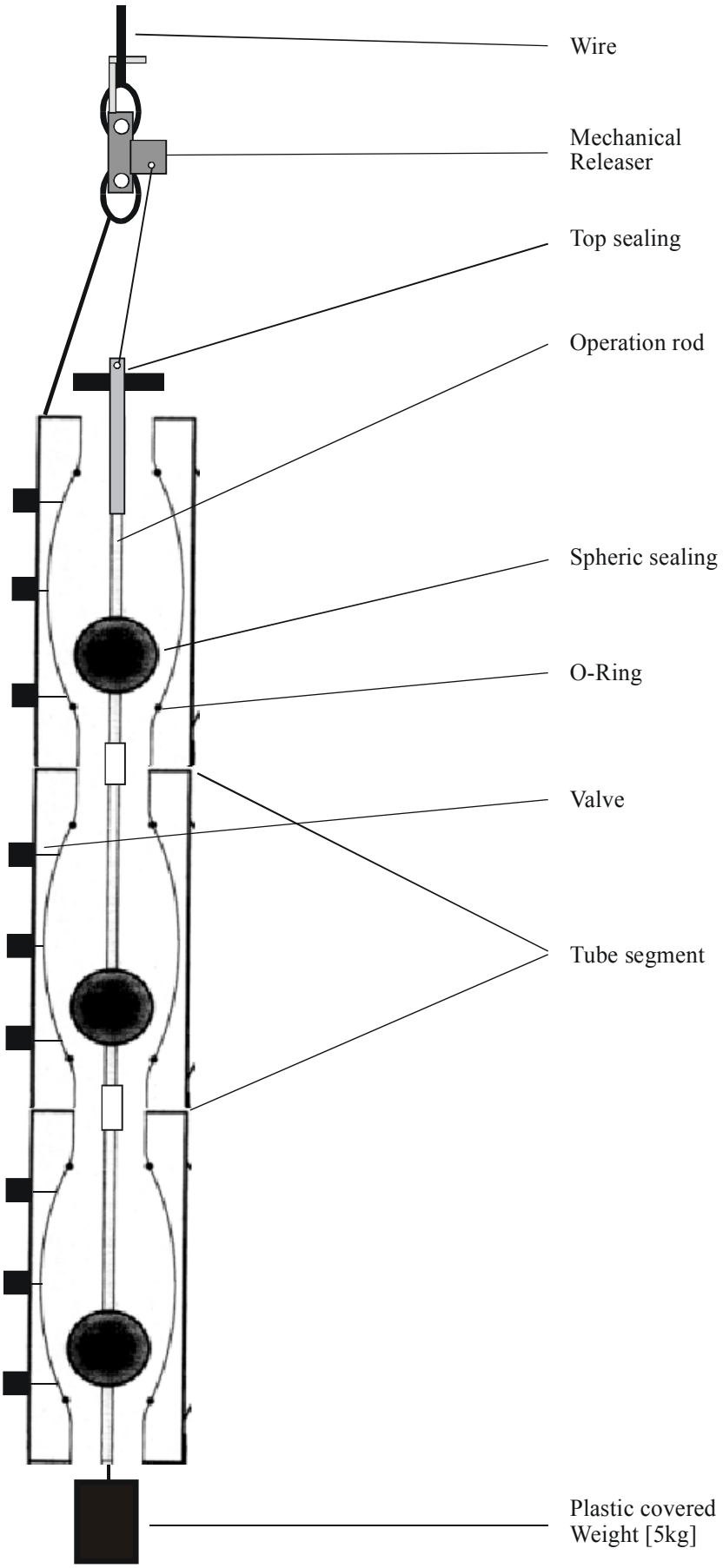

Fig. 74: Schematic drawing of the Interface-Water-Sampler (IWS) @M.Schmitt, GCA

Fig. 75: Echosounding during sampling with the IWS

5.3.6.3.1.3 Handling Onboard the Vessel

The IWS sampler is carefully lowered by a winch down to the beginning of the brine interface. Control of the water depth was established by reading the wire length and additionally by a pinger system, which was installed about 5 m below the end of the IWS. Careful insertion of the lower end of the IWS into the brine body was therefore possible. The sampling procedure was visualized (see Fig. 75) by echosounding. The upper line is the signal from the pinger and the lower line represents the brine surface.

After penetration of the system across the sea-water/ brine interface, the IWS was triggered by the fall weight with a running time of about 10 minutes. After retrieval of the IWS, the sampler was secured outboard and water samples were collected starting at the top of the IWS (valve 1). Salinity and pH measurements were performed immediately after the sampling. A high spatial resolution could be measured (Fig. 76) with the IWS system. The steep gradient of pH and salinity between water depth 1328 m and 1330 m (cable length) defines an interface layer of about 80 cm thickness.

5.3.6.3.2 Water and Sediment Samples from the Northern Red Sea

The shipboard data of 10 hydrocast stations in the southern, eastern, and northern sub-basins of the Shaban Deep and sediment samples of the northern Red Sea are presented in the tables 16-19. Sample locations at the Shaban Deep are plotted in Fig. 77. A temperature and sound-velocity profile, measured with the multi-probe, plotted against water depth (pressure) of the Shaban Deep east basin (Figure 78). Steep temperature, oxygen and sound-velocity (which is related to salinity) gradients were detected at about 1330 m (rope length) for all investigated basins (Fig. 77). A second interface was measured in the southern and eastern basin at about 1365m (rope length).

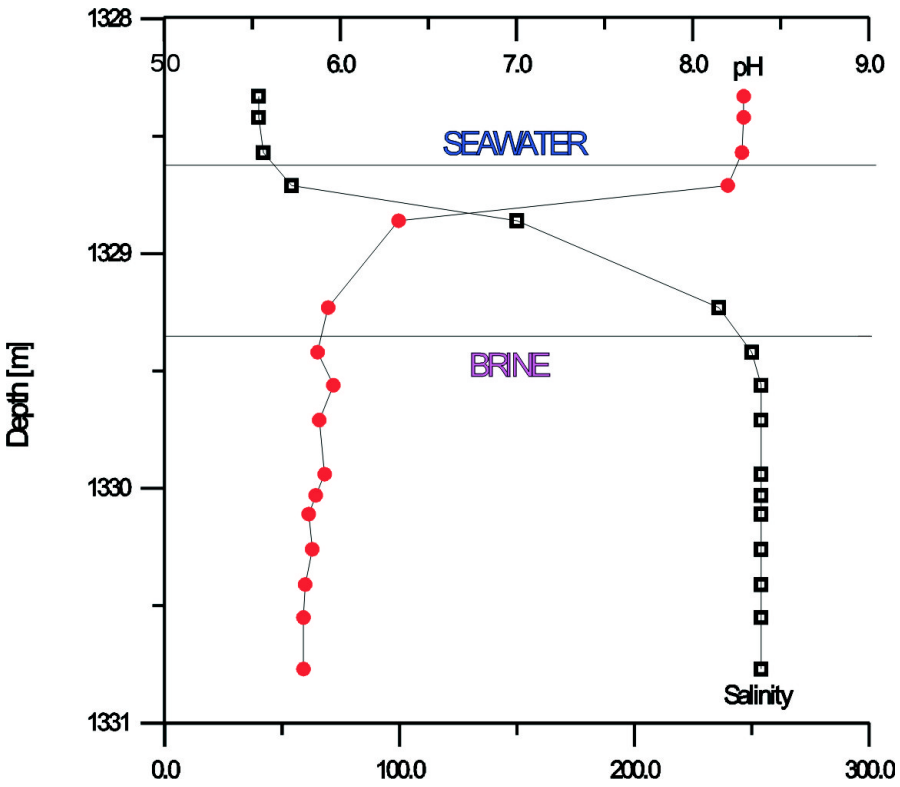

Fig. 76: Salinity and pH-profiles in the seawater/brine-interface of Shaban-N Deep (sampled with Interface-Water-Sampler at R/V METEOR station 202d).

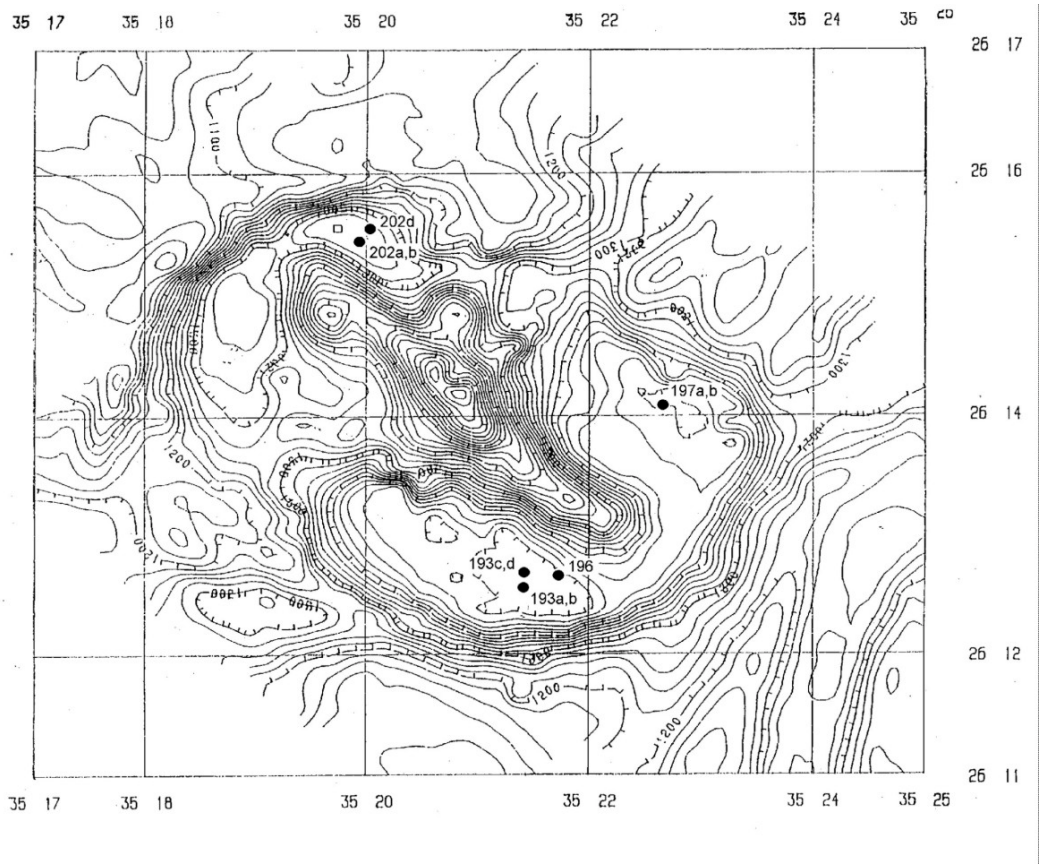

Fig. 77: Sampling stations (·) in the Shaban Deep.

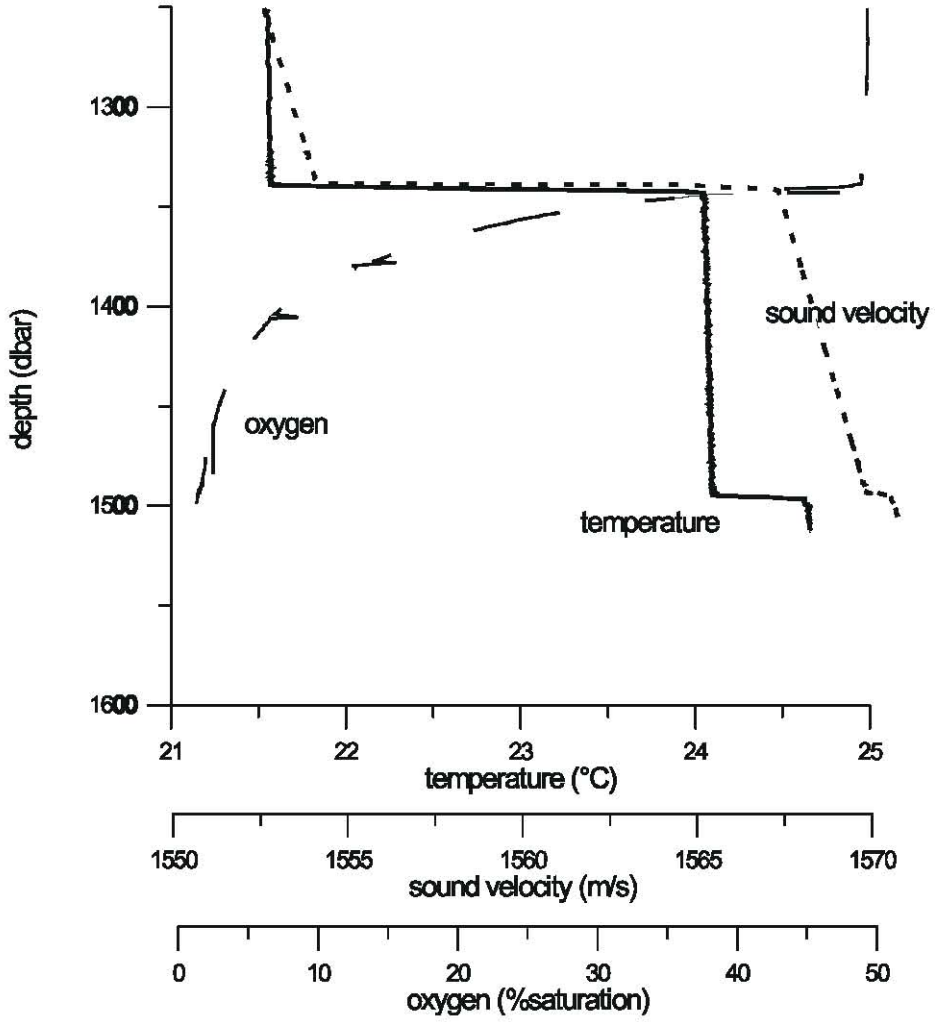

Fig. 78: Multiprobe measurements in the seawater/brine-interface at R/V METEOR station 197b (Shaban-E Deep).

Tab. 16: Water samples for inorganic investigation.

METEOR Station	Bottle No.	Cable length	Latitude N	Longitude E	Temp. (°C)	Salinity Refrakt.	O2 (% / mg/l)	pH	filtr. Vol.	Sulfide sample
Shaban S - Deep										
193 a	3	100	26° 12,66'	35° 21,47'	22,7	---	---	---	---	---
193 a	4	---	26° 12,66'	35° 21,47'	---	---	---	---	---	---
193 a	5	1300	26° 12,66'	35° 21,47'	21,36	---	---	---	---	---
193 a	6	1305	26° 12,66'	35° 21,47'	21,56	40,5	---	---	---	---
193 a	7	1305	26° 12,66'	35° 21,47'	21,56	40,5	38 / 3,4	8,13	600	---
193 a	8	---	26° 12,66'	35° 21,47'	---	---	---	---	---	---
193 a	9	---	26° 12,66'	35° 21,47'	---	---	---	---	---	---
193 a	10	1315	26° 12,66'	35° 21,47'	21,56	40,5	---	---	---	---
193 a	11	1315	26° 12,66'	35° 21,47'	21,56	40,5	---	---	---	---
193 a	12	---	26° 12,66'	35° 21,47'	---	41	39 / 3,3	8,17	700	---
193 b	12	20	26° 12,66'	35° 21,47'	23,8	40	63 / 5,2	8,29	700	---
193 c	4	1300	26° 12,72'	35° 21,50'	21,56	43	---	---	400	---
193 c	5	1315	26° 12,72'	35° 21,50'	21,56	44	---	---	---	---
193 c	6	1318	26° 12,72'	35° 21,50'	21,56	44	40 / 3,6	8,16		
193 c	7	1318	26° 12,72'	35° 21,50'	21,56	44	36 / 3,1	8,18		
193 c	8	1320	26° 12,72'	35° 21,50'	21,56	43	37 / 3,2	8,13		
193 c	9	1321	26° 12,72'	35° 21,50'	21,56	43	37 / 3.1	8,15	500	---
193 c	10	1322	26° 12,72'	35° 21,50'	21,57	42	37 / 3.1	8,14	---	---
193 c	11	1325	26° 12,72'	35° 21,50'	21,56	43	37 / 3.2	8,19	---	---
193 c	12	1328	26° 12,72'	35° 21,50'	21,57	43	39 / 3.2	8,21	650	---
193 d	4	1000	26° 12,72'	35° 21,48'	21,52	41,5	---	8,17	650	---
193 d	7	1330	26° 12,72'	35° 21,48'	21,7	74,5	47 / 4,0	8,18	650	---
193 d	8	1331	26° 12,72'	35° 21,48'	22,5	192	14 / 1,2	6,45	650	---
193 d	9	1332	26° 12,72'	35° 21,48'	23,5	242	10 / 10,8	6,09	750	X
193 d	10	1333	26° 12,72'	35° 21,48'	23,5	256	10 / 1,0	6,04	750	X
193 d	11	1334	26° 12,72'	35° 21,48'	24	254	12 / 0,8	6,03	700	---
193 d	12	1335	26° 12,72'	35° 21,48'	24	258	8 / 0,4	6,01	780	---
193 d	6	1340	26° 12,72'	35° 21,48'	24,06	252,5	11 / 0,8	6,04	750	---
193 d	2	1400	26° 12,72'	35° 21,48'	24,08	260	---	---	800	---
196	12	100	26° 12,71'	35° 21,69'	22,7	40	60 / 5,0	8,24	600	X
196	11	1000	26° 12,71'	35° 21,69'	21,5	42	40 / 3,2	8,12	750	X
196	4	1440	26° 12,71'	35° 21,69'	24,1	254,5	6 / 0,5	6,06	700	X
196	5	1450	26° 12,71'	35° 21,69'	24,5	256	6 / 0,4	6,04	650	X
196	7	1464	26° 12,71'	35° 21,69'	24,5	254	10 / 0,8	6,05	---	X
196	9	1465	26° 12,71'	35° 21,69'	24,6	260	5 / 0,5	6,07	780	X
196	2	1470	26° 12,71'	35° 21,69'	24,6	252	7 / 0,5	6,05	750	X
Shaban-E Deep										
197 a	4	1300	26° 14,01'	35°22,70'	21,5	42	40 / 3,0	8,04	650	---
197 a	5	1320	26° 14,01'	35°22,70'	21,5	42	---	---	---	---
197 a	6	1325	26° 14,01'	35°22,70'	21,5	42	---	---	---	---
197 a	7	1328	26° 14,01'	35°22,70'	21,6	42	---	---	---	---
197 a	9	1330	26° 14,01'	35°22,70'	22,1	136	22 / 1,8	6,91	800	X
197 a	10	1331	26° 14,01'	35°22,70'	23	230	10 / 0.6	6,20	---	X
197 a	11	1332	26° 14,01'	35°22,70'	24	254	8 / 0,6	6,02	650	X
197 a	12	1332	26° 14,01'	35°22,70'	24	256	7 / 0,6	6,01	---	X
197 a	8	1358	26° 14,01'	35°22,70'	24	220	2 /0,1	5,80	700	X
197 b	4	1370	26° 14,01'	35° 22,69'	24,06	254	9 / 0,6	5,86	750	X
197 b	5	1420	26° 14,01'	35° 22,69'	24,08	254	---	---	---	---
197 b	6	1450	26° 14,01'	35° 22,69'	24,09	254	---	---	---	---
197 b	7	1463	26° 14,01'	35° 22,69'	24,1	254	10 / 0,8	5,85	---	---
197 b	9	1465	26° 14,01'	35° 22,69'	24,3	256	8 / 0,6	5,85	700	X
197 b	10	1466	26° 14,01'	35° 22,69'	24,6	260	5 / 0,3	5,83	800	---
197 b	11	1467	26° 14,01'	35° 22,69'	24,6	260	---	---	---	---
197 b	2	1480	26° 14,01'	35° 22,69'	24,6	260	8 / 0,4	5,87	700	X

Tab. 16: Water samples for inorganic investigations (continuation).

METEOR Station	Bottle No.	Cable length	Latitude N	Longitude E	Temp. (°C)	Salinity Refrakt.	O2 (% / mg/l)	pH	filtr. Vol.	Sulfide sample
Shaban-N Deep										
202 a	4	1300	26°15,51'	35° 20,01'	21,56	41	54 / 4,4	8,18	---	---
202 a	6	1320	26°15,51'	35° 20,01'	21,57	41	55 / 4,7	8,17	750	---
202 a	7	1325	26°15,51'	35° 20,01'	21,57	41	54 / 4,6	8,22	---	X
202 a	8	1328	26°15,51'	35° 20,01'	21,57	40	51 / 4,3	8,16	750	X
202 a	9	1330	26°15,51'	35° 20,01'	21,85	200	48 / 4,1	6,97	700	X
202 a	10	1331	26°15,51'	35° 20,01'	22,7	246	5 / 0,3	5,73	800	X
202 a	11	1332	26°15,51'	35° 20,01'	22,8	252	5 / 0,2	5,74	750	X
202 a	12	1333	26°15,51'	35° 20,01'	22,8	250	2 / 0,1	5,71	650	X
202 a	2	1340	26°15,51'	35° 20,01'	22,8	254	4 / 0,2	5,71	650	X
202 b	5	1000	26°15,51'	35° 20,01'	21,5	50	51 / 4,3	8,20	750	---
202 b	12	1310	26°15,51'	35° 20,01'	21,5	50	40 / 4,2	8,02	700	---
202 b	2	1350	26°15,51'	35° 20,01'	22,8	255	4 / 0,4	5,73	750	X
202 d	1	1328,33	26° 15,53'	35° 20,00'	---	40	---	8,29	350	---
202 d	2	1328,42	26° 15,53'	35° 20,00'	---	40	---	8,29	200	---
202 d	3	1328,57	26° 15,53'	35° 20,00'	---	42	---	8,28	150	---
202 d	4	1328,71	26° 15,53'	35° 20,00'	---	54	---	8,20	330	---
202 d	5	1328,86	26° 15,53'	35° 20,00'	---	150	---	6,33	320	---
202 d	6	1329,1	26° 15,53'	35° 20,00'	---	---	---	---	---	---
202 d	7	1329,23	26° 15,53'	35° 20,00'	---	236	---	5,93	250	---
202 d	8	1329,42	26° 15,53'	35° 20,00'	---	250	---	5,87	260	---
202 d	9	1329,56	26° 15,53'	35° 20,00'	---	254	---	5,96	300	---
202 d	10	1329,71	26° 15,53'	35° 20,00'	---	254	---	5,88	350	---
202 d	11	1329,94	26° 15,53'	35° 20,00'	---	254	---	5,91	350	---
202 d	12	1330,03	26° 15,53'	35° 20,00'	---	254	---	5,86	150	---
202 d	13	1330,11	26° 15,53'	35° 20,00'	---	254	---	5,82	250	---
202 d	14	1330,26	26° 15,53'	35° 20,00'	---	254	---	5,84	250	---
202 d	15	1330,41	26° 15,53'	35° 20,00'	---	254	---	5,80	300	---
202 d	16	1330,55	26° 15,53'	35° 20,00'	---	254	---	5,79	300	---
202 d	17	1330,77	26° 15,53'	35° 20,00'	---	254	---	5,79	300	---

Tab. 17: Water samples for gas chemistry.

METEOR Station	Bottle nr.	Cable length mbs	Latitude N	Longitude E	Total gas ml/l	Sample
Shaban-S Deep						
193a	7	1305	26°12,66'	35°21,47'	52,5	GM ohne
193a	12	1312	26°12,66'	35°21,47'	47,5	GM078
193a	12	1312	26°12,66'	35°21,47'	38,2	GM078
193c	4	1300	26°12,66'	35°21,47'	42	GM002
193c	5	1315	26°12,66'	35°21,47'	34,1	GM049
193c	6	1318	26°12,66'	35°21,47'	45	GM070
193c	8	1320	26°12,66'	35°21,47'	42	GM034
193c	10	1322	26°12,66'	35°21,47'	36,2	GM116
193c	11	1325	26°12,66'	35°21,47'	41	GM096
193c	12	1328	26°12,66'	35°21,47'	39,7	GM011
193c	2	1330	26°12,66'	35°21,47'	43,3	GM070
193c	GWS	1330	26°12,66'	35°21,47'	37,4	GM098
193d	4	1000	26°12,66'	35°21,47'	33,2	GM074
193d	7	1330	26°12,66'	35°21,47'	35	GM085
193d	8	1331	26°12,66'	35°21,47'	43	GM002
193d	9	1332	26°12,66'	35°21,47'	47,5	GM056
193d	10	1333	26°12,66'	35°21,47'	51,5	GM096
193d	11	1334	26°12,66'	35°21,47'	49,5	GM010
193d	12	1335	26°12,66'	35°21,47'	66	GM053
193d	6	1340	26°12,66'	35°21,47'	49,5	GM083
193d	2	1400	26°12,66'	35°21,47'	51	GM095
193d	GWS	1400	26°12,66'	35°21,47'	51	GM081

Tab. 17: Water samples for gas chemistry (continuation).

METEOR Station	Bottle nr.	Cable length mbs	Latitude N	Longitude E	Total gas ml/l	Sample
Shaban-S Deep						
196	12	100	26°12,73'	35°21,68'	34,6	GM048
196	11	1000	26°12,73'	35°21,68'	34,5	GM040
196	4	1440	26°12,73'	35°21,68'	45,3	GM ohne
196	5	1450	26°12,73'	35°21,68'	53,1	GM068
196	7	1464	26°12,73'	35°21,68'	58,7	GM033
196	9	1465	26°12,73'	35°21,68'	47,3	GM012
196	2	1470	26°12,73'	35°21,68'	54,6	GM092
196	2	1470	26°12,73'	35°21,68'	51,8	GM019
196	GWS	1470	26°12,73'	35°21,68'	61,4	GM066
Shaban-E Deep						
197a	4	1300	26°14,00'	35°22,67'	41,5	GM025
197a	5	1320	26°14,00'	35°22,67'	37,3	GM027
197a	6	1325	26°14,00'	35°22,67'	69,1	GM075
197a	7	1328	26°14,00'	35°22,67'	42	GM023
197a	9	1330	26°14,00'	35°22,67'	39,6	GM015
197a	10	1331	26°14,00'	35°22,67'	54,5	GM071
197a	11	1332	26°14,00'	35°22,67'	54,5	GM095
197a	12	1333	26°14,00'	35°22,67'	54,5	GM014
197a	2	1338	26°14,00'	35°22,67'	51,5	GM080
197a	8	1358	26°14,00'	35°22,67'	55	GM050
197a	GWS	1358	26°14,00'	35°22,67'	60,4	GM099
197b	4	1370	26°14,00'	35°22,67'	58,4	GM051
197b	5	1420	26°14,00'	35°22,67'	58,8	GM074
197b	6	1450	26°14,00'	35°22,67'	75,5	GM065
197b	7	1463	26°14,00'	35°22,67'	62,6	GM046
197b	9	1465	26°14,00'	35°22,67'	51,4	GM048
197b	10	1466	26°14,00'	35°22,67'	51	GM072
197b	11	1467	26°14,00'	35°22,67'	44,9	leer
197b	12	1469	26°14,00'	35°22,67'	54,2	GM061
197b	2	1480	26°14,00'	35°22,67'	48,9	GM028
Shaban-N Deep						
202a	4	1300	26°15,52'	35°20,01'	30,5	GM093
202a	6	1320	26°15,52'	35°20,01'	43,5	GM035
202a	7	1325	26°15,52'	35°20,01'	29,9	GM017
202a	8	1328	26°15,52'	35°20,01'	30,5	GM022
202a	9	1330	26°15,52'	35°20,01'	61,5	GM077
202a	10	1331	26°15,52'	35°20,01'	135,5	GM064
202a	11	1332	26°15,52'	35°20,01'	135,5	GM100
202a	12	1333	26°15,52'	35°20,01'	146,8	GM058
202a	2	1340	26°15,52'	35°20,01'	134,5	GM045
202b	12	1310	26°15,52'	35°20,01'	36,1	GM024
202b	7	1335	26°15,52'	35°20,01'	145	2xHS
202b	GWS	1360	26°15,52'	35°20,01'	177	4xHS
202d	IWS-6	1328+	26°15,53'	35°20,02'	189	3xHS
202d	IWS-11	1328+	26°15,53'	35°20,02'	134	3xHS
202d	IWS-17	1328+	26°15,53'	35°20,02'	200	3xHS

Tab. 18: Sediment samples for hydrocarbon analyses.

METEOR station	Core length [m]	Sample	Water depth [m]	Latitude N	Longitude E	Degas-Process	Remarks
190	4,19	STA190-CC1	798,0	26°25,23'	35°40,18'	Head-Space	add 1ml NaN3
190	4,19	STA190-CC2	798,0	26°25,23'	35°40,18'	Head-Space	add 1ml NaN3
190	4,19	STA190-CC	798,0	26°25,23'	35°40,18'	<63µm, wash 30L	add 1ml NaN3
191a	5,70	STA191-CC1	586,0	26°29,13'	35°40,18'	Head-Space	add 1ml NaN3
191a	5,70	STA191-CC2	586,0	26°29,13'	35°40,18'	Head-Space	add 1ml NaN3
191a	5,70	STA191-CC	586,0	26°29,13'	35°40,18'	<63µm, wash 30L	add 1ml NaN3
191b	10,15	STA191-CC1	586,0	26°29,11'	35°49,50'	Head-Space	add 1ml NaN3
191b	10,15	STA191-CC2	586,0	26°29,11'	35°49,50'	Head-Space	add 1ml NaN3
191b	10,15	STA191-CC	586,0	26°29,11'	35°49,50'	<63µm, wash 30L	add 1ml NaN3
192	7,33	STA192-CC1	1032,0	26°30,47'	35°56,9'	Head-Space	add 1ml NaN3
192	7,33	STA192-CC2	1032,0	26°30,47'	35°56,9'	Head-Space	add 1ml NaN3
192	7,33	STA192-CC	1032,0	26°30,47'	35°56,9'	<63µm, wash 30L	add 1ml NaN3
198	11,18	STA198-CC1	834,0	27°05,28'	35°33,96'	Head-Space	add 1ml NaN3
198	11,18	STA198-CC2	834,0	27°05,28'	35°33,96'	Head-Space	add 1ml NaN3
198	11,18	STA198-CC	834,0	27°05,28'	35°33,96'	<63µm, wash 30L	add 1ml NaN3
199		STA199-CC1	628,0	27°05,25'	35°24,34'	Head-Space	add 1ml NaN3
199		STA199-CC2	628,0	27°05,25'	35°24,34'	Head-Space	add 1ml NaN3
199		STA199-CC	628,0	27°05,25'	35°24,34'	<63µm, wash 30L	add 1ml NaN3
200	16,31	STA200-CC1	627,5	27°03,19'	35°24,26'	Head-Space	add 1ml NaN3
200	16,31	STA200-CC2	627,5	27°03,19'	35°24,26'	Head-Space	add 1ml NaN3
200	16,31	STA200-CC	627,5	27°03,19'	35°24,26'	<63µm, wash 30L	add 1ml NaN3
201	16,60	STA201-CC1	883,5	27°05,28'	35°94,01'	Head-Space	add 1ml NaN3
201	16,60	STA201-CC2	883,5	27°05,28'	35°94,01'	Head-Space	add 1ml NaN3
201	16,60	STA201-CC	883,5	27°05,28'	35°94,01'	<63µm, wash 30L	add 1ml NaN3
203	8,03	STA203-CC1	1474,0	26°12,61'	35°21,55'	Head-Space	add 1ml NaN3
203	8,03	STA203-CC2	1474,0	26°12,61'	35°21,55'	Head-Space	add 1ml NaN3
203	8,03	STA203-CC	1474,0	26°12,61'	35°21,55'	<63µm, wash 30L	add 1ml NaN3, sample contains darkbrown Sulfids
204		STA204-CC1	771,2	27°36,69'	34°51,87'	Head-Space	add 1ml NaN3
204		STA204-CC2	771,2	27°36,69'	34°51,87'	Head-Space	add 1ml NaN3
204		STA204-CC	771,2	27°36,69'	34°51,87'	<63µm, wash 30L	add 1ml NaN3
204	17,80	STA204-CC1	770,6	27°36,66'	34°51,88'	Head-Space	add 1ml NaN3
204	17,80	STA204-CC2	770,6	27°36,66'	34°51,88'	Head-Space	add 1ml NaN3
204	17,80	STA204-CC	770,6	27°36,66'	34°51,88'	<63µm, wash 30L	add 1ml NaN3

Tab. 19: Water samples for Rare Gas (He) and $\delta^{18}O$-analyses.

METEOR station	Bottle nr.	Water depth mbs (cable length)	Sample	METEOR station	Bottle nr.	Water depth mbs (cable length)	Sample
193c	2	1330	$\delta^{18}O$	197a	2(IS)	1338	He
193c	8	1320	$\delta^{18}O$		2	1338	He, $\delta^{18}O$
					9	1330	$\delta^{18}O$
193d	1(GWS)	1400	$\delta^{18}O$				
193d	2	1400	He, $\delta^{18}O$	197b	2(IS)	1480	He
				197b	2	1480	He, $\delta^{18}O$
196	11	1000	He, $\delta^{18}O$	197b	9	1465	He, $\delta^{18}O$
196	2	1470	He, $\delta^{18}O$				
196	2(IS)	1470	He	202a	4	1300	He, $\delta^{18}O$
				202a	9	1330	He, $\delta^{18}O$

5.3.7 Microbiology of the Highly Saline Brine Sediments of the Shaban Deep

(W. Eder)

5.3.7.1 Introduction

To date, the microbial communities of extreme saline, anaerobic brine pools and brine sediments of the Red Sea have been only sparsely investigated. In a first phylogenetic approach, a brine sediment sample (transition zone sediment-brine) of the Kebrit Deep showed the existence of 16S rRNA gene sequences, suggesting the presence of novel *Bacteria* and *Archaea* (EDER ET AL., 1999; EDER AND HUBER, 1999; STOFFERS ET AL., 1998). For comparative phylogenetic studies, sediment samples of the Shaban Deep should be taken at the transition zone, sediment-brine. Furthermore, potential extremophiles should be identified in a polyphasic approach (e.g. enrichment and isolation, phylogenetic staining).

5.3.7.2 Sampling

Together with the team of Dr. J. Pätzold (University of Bremen) we tried to obtain sediment samples from the interface between sediment and brine in the north and south basins of the Shaban Deep by the use of a multicorer. Multicorer samples were obtained from 5 stations, but the sample material was not convincing. Nevertheless, still best and most useable sample was still 3 kg of sediment taken from the multicorer METEOR station #202g (Tab. 20), but the depth of the sampling site is unknown. There was no evidence that the sediment-brine transition zone was sampled. No brine overlying the sediment surface could be obtained at any stations.

5.3.7.3 Sample Treatment

The brine sediment sample #202g was filled into argon-flushed 1 l Sovirel bottles, and sealed with rubber stoppers. An aliquot of the sample was reduced by the addition of sodium dithionite (0.05 g/ 100 ml), in order to remove oxygen. The samples were stored at 4°C.

5.3.7.4 Enrichment Attempts and First Results

About 20 enrichment attempts were carried out to look for the existence of potential extremophiles in the original sample while still on board RV METEOR (sediment sample: #202g). Brine taken from the east basin during the water-sampling program of Prof. P. Stoffers and his colleages (University

Tab. 20: Multicorer stations for microbial studies taken in the Shaban Deep.

METEOR station	Basin	Coring device	Sampling
202e	north	multicorer	no surface sediment, no sample
202f	north	multicorer	no surface sediment, no sample
202g	north	multicorer	surface sediment (?)
203a	south	multicorer	no surface sediment, no sample
203c	south	multicorer	no surface sediment, no sample

of Kiel) was used as basal medium with CH_4-CO_2 (95:5; v/v) and H_2-CO_2 (80:20;v/v) as gas phase. For anaerobic conditions, the media were reduced with 1 ml of 50% (w/v) H_2S. In order to create conditions resembling those of the natural environment, the basal medium was supplemented with various organic and inorganic substrates (e.g., CH_4, Fe^{3+}, bacterial cell extracts) as carbon and energy sources. The media were inoculated with 0.5 ml of the original sample ST-51 and were incubated at 25°C. Further enrichment attempts were carried out in the laboratory in Regensburg. No enrichment cultures were obtained from the sediment sample after an incubation time of 60 to 75 days, in contrast to the results of the Kebrit Deep, where halophilic procaryotes could be enriched and isolated by the use of "optical tweezers" (HUBER, 1999).

The same sediment sample was used for nucleic acid extraction and phylogenetic analyses. From about 100 g of sediment material, small amounts of nucleic acids could be extracted and should be used subsequently for 16S rRNA gene sequence analyses.

5.3.8 Organic Matter Remineralization in Carbonate and Quartz Sands of the Gulf of Aqaba, Red Sea, Jordan

(M. Rasheed)

Below, we present the results obtained on the METEOR Cruise with multicores retrieved at station GeoB 5801-2 and 5811-1.

5.3.8.1 Summary

Degradation of organic matter was studied in 'deep' muddy sediments in the Gulf of Aqaba. The goal of the project was to clarify the role of the sediment-matrix-characteristics on organic-matter-decomposition in the seabed. Sediment cores retrieved at station GeoB 5801 and GeoB 5811 were incubated in laboratory flux chambers and observed over time for oxygen consumption and nutrient generation. These spectrophotometric determinations of nutrient concentrations, oxygen, and redox potential measurements were combined in order to quantify the decomposition of algae in the different sediments. *Spirulina* was used as algal organic material for this study. The different sediments were incubated in flux-chambers under controlled conditions, and the observed changes in water and pore water were used to quantify the mineralization capacities of the sediments.

5.3.8.2 Introduction

The role of sediment in the degradation of organic matter and the recycling processes of nutrients in the coastal zone has been studied intensively (e.g. ENTCH ET AL., 1983). NIXON ET AL. (1980) suggested that mineralization of organic material in the sediment can be a controlling factor for nutrient availability. Through their activities, macrobenthos organisms that live in the sediment play an important role in mediating both physical and chemical processes near the sediment-water interface and interstitial water including the organic matter degradation processes. In deep oceanic waters a large fraction of the organic matter can decompose in the water column. In contrast, in shallow coastal waters large proportions of the organic input survive settlement through the water column, and reach to the bottom. Ensuing decomposition of organic matter in marine sediments can be both aerobic in the surface oxic layer and anaerobic in the anoxic deeper layer.

Sediments in coastal coral reef environments of tropical and subtropical zones are composed mainly of coarse biogenic carbonates. However, coarse terrigeneous silicate sediment can also be found in certain parts of the reef, such as valleys and troughs. Deep-water sediments are finer and composed mainly of silts and smaller particles. Rouband et al. (1996) found that the sediments of the Tikehau lagoon were sources of dissolved ammonia, phosphate, and silica resulting from biogeochemical processes. According to Fuentes and Espino (1990) and Rouband et al. (1996) a high percentage of the ammonia and phosphate requirement for the coral reef is supplied by remineralization and recycling processes.

The aim of this study is to investigate whether carbonate sediments, due to their structure, composition, and bacterial colonization, possess different remineralization and degradation rates for organic compounds in comparison with quartz sediments and deep muddy sediments.

5.3.8.3 Material and Methods

During the cruise, sediment cores of up to 40cm length were collected from two sites at the Jordanian side of the Gulf of Aqaba (GeoB 5801-2 from 827 m water depth, 34°54.7'E/29°24.9'N and GeoB 5811-1 from 410 m water depth, 34°54.7'/29°24.9') using a multicorer system. The incubation of the sediment was carried out onboard RV Meteor within half an hour of sample collection. The core liners of the multicorer were used as incubation chambers. The core liners were cylindrical acrylic tubes (60cm high, 9.5cm diameter), the length of the sediment in the core was 40cm and the length of the water column above the sediment was 18cm. The cores were covered with a plastic lid with two holes. The water above the sediment was agitated using a rotating disk of 7cm diameter placed 10cm above the sediment surface (18rpm). 0.2 g dried *Spirulina* were added to two of the incubated cores. Another two cores were not spiked to serve as controls. After starting the stirrer motors (12v motors), dissolved oxygen was measured in the chamber water at different intervals by a Clark type microelectrode. For nutrient analysis, 50ml of the supernatant water was withdrawn at different intervals using a syringe; the volume of water withdrawn was replaced by 50ml of the sea-water. Nutrient analyses were made in duplicates following methods developed by Strickland and Parsons (1968), IOC Manuals and Guides (1983). Absorption was measured in a 1 cm cell. The incubation extended over 150 hours. After the incubation period, the water above the sediment was removed and sediment subcores were taken and analyzed for pore water constituents. The cores were cut into slices as thin as 1cm in the first 10cm of the sediment, and 2cm subsequently to 20cm depth of the sediment. To extract the pore water, pieces of the sliced sediment were centrifuged individually at 10000rpm and 4°C. 5ml of the extracted water was filtered through 0.45µm syringe filters. Cut-off syringes were used to remove 1ml of every sliced sediment layer for bacteria counting, 5ml was taken for pigment analysis and 2ml for C-N analysis. Samples for bacteria counts, pigments and C-N analyses were frozen at -80°C.

5.3.8.4 Results

The course of dissolved oxygen concentration during incubation in both the spiked and control chambers with the 800 m depth sediment is shown in Fig 79. Oxygen content decreased gradually in the two control chambers and sharply in the *Spirulina*-spiked chambers. Within the first 55 hours of incubation the dissolved oxygen concentration went down to zero and anaerobic condition prevailed.

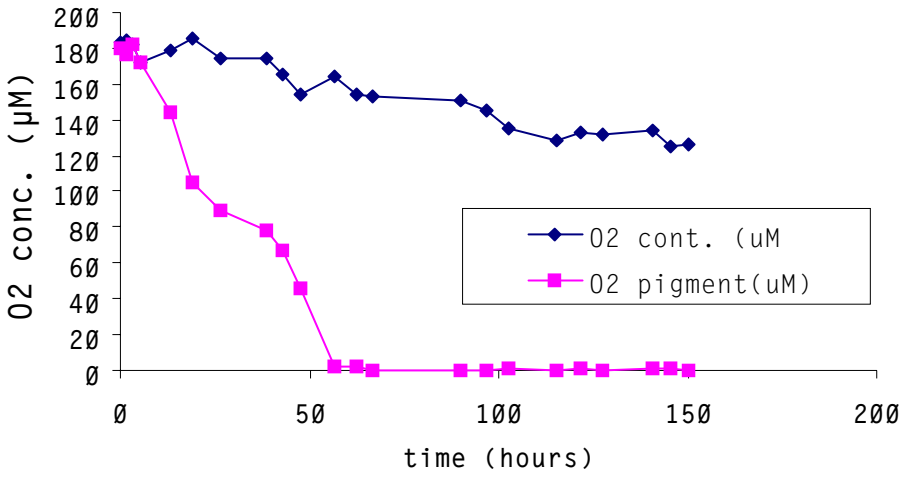

Fig. 79: Evolution of the oxygen concentrations in the control chamber (diamonds) without any additions and the chamber with organic matter (squares, 0.2 mg *Spirulina*) added.

In the control chamber there was no significant increase or decrease in any of the nutrient concentrations throughout the incubation period (Fig. 80a). At the same time, nitrite and nitrate concentrations in the chamber with organic matter approached zero. For the other nutrients, ammonia, phosphate and silicate, the concentrations increased gradually with time to reach a maximum by the end of the incubation.

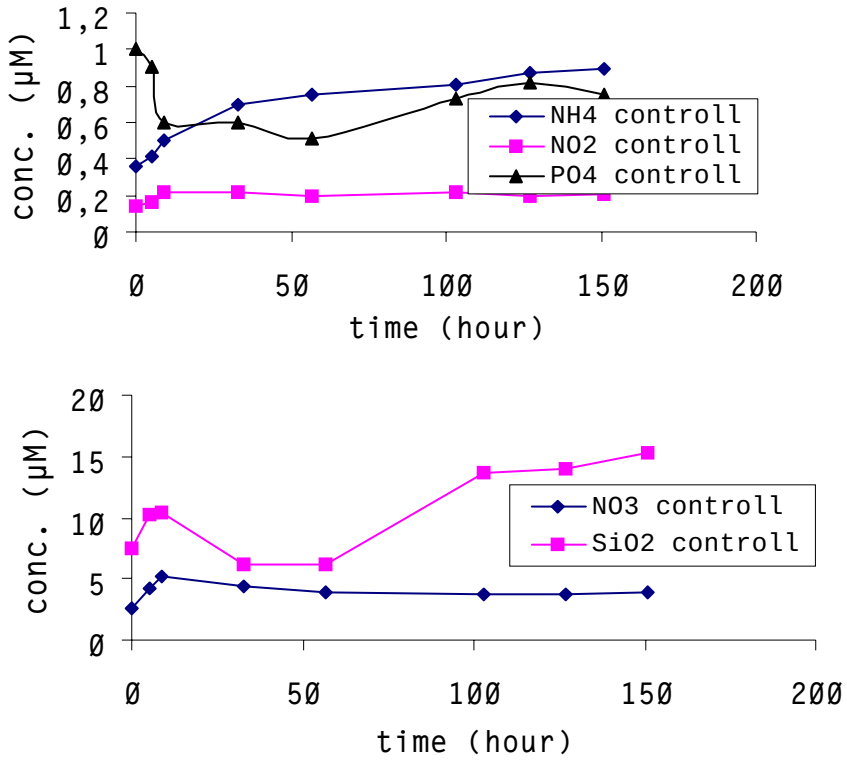

Fig. 80a: Evolution of the nutrient concentrations in the control chambers without organic matter added.

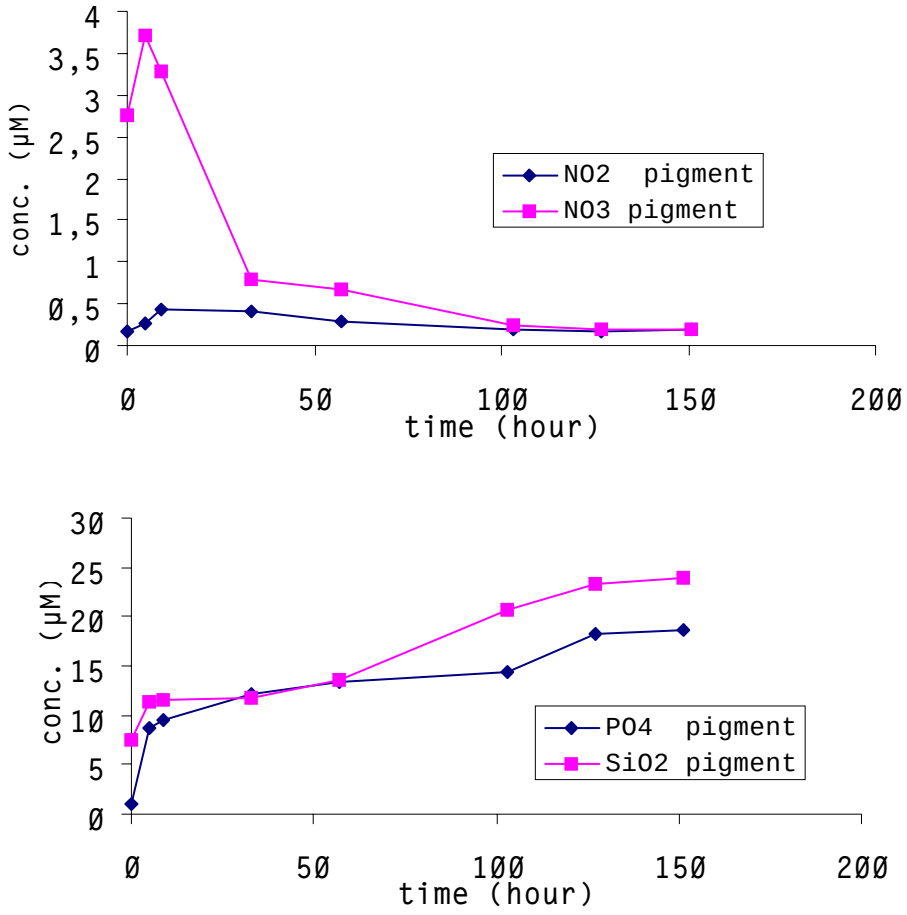

Fig. 80b: Evolution of the nutrient concentrations in the chambers with organic matter added.

Pore water profiles (Fig. 81) for all the spiked and non spiked chambers show no significant change in nitrite concentrations. Nitrate concentration decreased sharply in the upper 3cm of the sediment in the control chamber accompanied by an increase in ammonia, phosphate, and silicate concentrations. In the spiked chambers nitrate and nitrite concentrations were very low in the entire sediment column. Ammonia concentrations were very high at the surface of the sediment (150 µM) and decreased gradually with sediment depth. Silicate and phosphate concentrations increased gradually with depth.

5.3.8.5 Discussion

5.3.8.5.1 Incubation Experiments

Aerobic oxidation of organic matter at the beginning of the incubation occurred mainly in the water overlaying the sediment, at the sediment surface and the uppermost sediment layer. Oxygen may diffuse from the water to the sediment and aerobic oxidation of organic matter might also occur in the sediment. The aerobic oxidation of the organic matter exists in the water, or the sediment produces ammonia, nitrate and phosphate according to the following reaction

(1) $(CH_2O)–(NH_3)_y(H_3PO_4)_z + (x+2y)O_2 = xCO_2 + (x+y)H_2O + yHNO_3 + 2H_3PO_4$

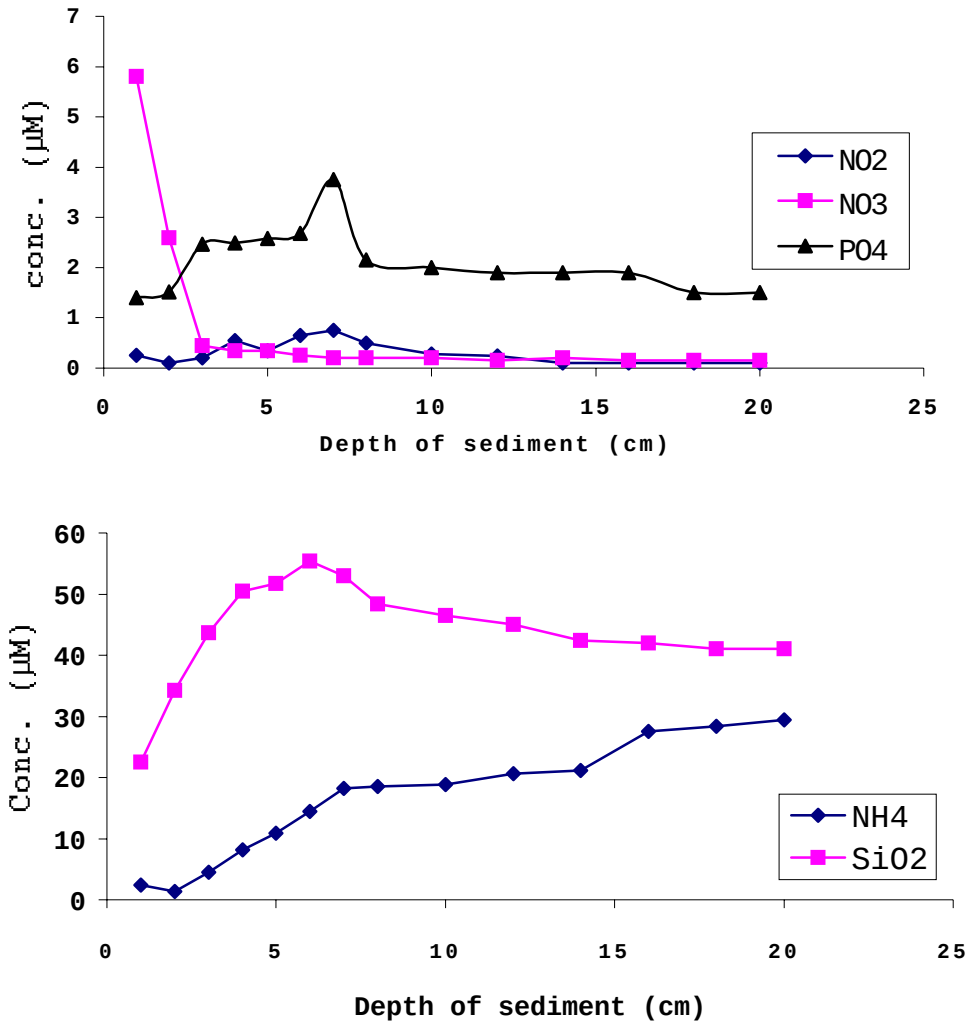

Fig. 81: Evolution of the pore water nutrient concentrations in the chambers with the control cores.

By nitrate reduction, ammonia could be produced according to the following reaction

$$(2)\quad 5(CH_2O)–(NH_3)_y(H_3PO_4)_z + 4NO_3 = xHCO_3 + 2N_2 + 5yNH_3 + 5zH_3PO_4$$

The measurements of oxygen (Fig. 4.8.1) indicate that anaerobic conditions began after different times depending on the experimental conditions. Anaerobic conditions create favorable conditions for NH_4^+ release from the sediment by anaerobic oxidation of organic matter (FUENTES AND ESPINO, 1990) according to reaction 2 and the following reaction

$$(3)\quad (CH_2O)–(NH_3)_y(H_3PO_4)_z + (x/2)SO_4^{-2} + xH^+ = \\ = x/2H_2S + xCO_2 + yNH_3 + xH_2O + H_3PO_4$$

Further, mineralization of organic compounds under these anaerobic conditions would result in additional ammonia at the expense of nitrate and nitrite. The results of all incubation experiments showed that sediments released phosphate under anaerobic conditions (equation 2 and 3).

By the end of the incubation period, ammonia, phosphate, and silicate became stable. This might have resulted from the degradation of all organic matter during the incubation period.

5.3.8.5.2 Pore Water Analysis

Higher pore water concentration of all nutrients compared with the overlaying water indicates that most of the organic matter mineralization occurs in the sediment, rather than in the overlaying water (Blackburn et al., 1988). Microbial activity in the sediment causes decomposition of organic matter and produces high concentrations of nutrient in the pore water. Oxygen depletion in the silicate sediments was faster than in the carbonate sediments, which may point out the importance of the difference in composition and diffusion rate in the two sediment types. The gradient in the pore water in the control chambers in all nutrient concentrations other than nitrate and nitrite from bottom water into the sediment might be attributed to the organic matter degradation and dissolution under anoxic condition. The low concentrations of nitrate and nitrite in the core with added pigment are due to anaerobic nitrate reduction (see equation 2 above). The relatively higher ammonia concentrations in the first 2cm depth of the sediments in the cruise sediment incubation can be attributed to the liberation of ammonia from the water column in addition to the sediment liberation. Performing complementary experiments with different methods will help to explore other features of organic carbon decomposition in both carbonate and silicate sediments. Our long-term objective is to model the organic carbon and nutrient flux in different types of marine sediments.

5.4 Preliminary Results of Leg M44/4

5.4.1 Physics and Air-Sea Interface Parameters

(B. B. Manca, D. Deponte)

Introduction

The participation of the OGS to the cruise M44/4 was carried out in the framework of an international scientific co-operation aimed to evaluate the status of the transient in the Eastern Mediterranean, which affects the deep and intermediate thermohaline circulation, and its impact on the marine ecosystem. The recently evidenced change in the deep circulation of the Eastern Mediterranean, where the Adriatic Deep Water (ADW) was found to be replaced by the denser waters of Aegean origin (ROETHER ET AL., 1996), open the questions of possible impact of this change to the biochemical status and to the ecosystem of the entire Mediterranean. It is important to remark that the signal associated with these changes should also be considered to understand whether the closed thermohaline cell circulation is definitely switched from the previous steady-state to a new equilibrium status characterised by two deep water formation sites, as recently observed.

Main Objectives

The basic hydrographic and physical data collected during the cruise aim in obtaining the following specific objectives:

- to assess the basin-wide surface, intermediate and deep thermohaline circulation;
- to quantify the year-to-year variations in distribution of the thermohaline properties of the different water masses;
- to estimate the relative importance and the effects of the transient on thermohaline properties and bio-chemical parameters distributions;
- to monitor and correlate the Aegean dense water outflow properties in the adjacent investigated basins (i.e. Levantine Basin, Cretan passage, Ionian Sea) as well as through the Sicily Straits and into the Western Mediterranean.

Material and Methods

The parameters which were measured at each station position were: temperature, salinity, dissolved oxygen, light transmission, light scattering and fluorescence. Continuous current measurements and air-sea interface parameters (i.e. meteorological data and data from thermo-salinograph) along the ship track were obtained by means of ship-mounted ADCP vertical profiler (Acoustic Doppler Current Profiler, 75 kHz) and from the navigation system to which the meteorological station is interfaced, respectively.

The basic physical measurements were performed by the SBE 911 plus CTD (Conductivity, Temperature and Depth) vertical profiler, manufactured by SEA-BIRD ELECTRONICS INC., and equipped with the following sensors:

- Paroscientific digiquartz pressure transducer (0 ÷10000 psia, 0.015 % F.S.);
- Oceanographic thermometer, primary (-5 ÷ 35 °C, ± 0.002 °C);
- Electrical Conductivity sensor, primary (0 ÷ 7 Siemens/m, ± 0.001 S/m);
- Oceanographic thermometer, secondary (-5 ÷ 35 °C, ± 0.002 °C);
- Electrical Conductivity sensor, secondary (0 ÷ 7 Siemens/m, ± 0.001 S/m);
- BECKMAN dissolved oxygen sensor (0 ÷ 15 ml/l, ± 0.1 ml/l);

- Chelsea Alphatracka transmissometer, 25 cm water path (0 ÷ 100 %, <0.3 % F.S.);
- Chelsea, MK III Aquatracka Fluorometer (0-96 g/l of Chl, ± 3% of reading);
- Sea Tech light scattering (0 ÷ 100 %, <0.3 % F.S);
- Tilt sensor, set to reveal a distance of 10 m from the sea bottom.

A 24-bottles SBE Carousel sampler was used in combination with the CTD to collect water samples with 10-12 liters Niskin bottles at desired depth during the up-cast. Additional independent measurements of pressure, temperature and salinity, for calibration purposes, were obtained from two SIS digital reversing pressure meters (± 1 dbar resolution), two SIS digital thermometers (± 0.001 resolution), while the salinity determination was obtained by a 8400A Guildline Autosal salinometer (± 0.001 pss).

The high resolution CTD profiles, with the complete dataset, were sampled at 24 Hz when the CTD was lowered a nominal winch-speed of 1 m/s. All the CTD data were processed on board by visual inspection of the vertical profiles, eliminating the obvious erroneous data by retaining the down cast, exclusively. The up-cast was used to extract the data in correspondence of the water samples, which were collected by firing the bottles at desired depth for bio-chemical and tracer measurements. The final quality controlled data were averaged over 1 dbar pressure interval. The salinity determination of the water samples was performed on board after the samples stabilised at the environment temperature, while the bath of the salinometer was maintained at 24 °C.

The data were converted into physical units. The water temperature was expressed following the IPTS-68 thermometer scale, the salinity following the practical salinity scale (UNESCO, 1983), while the dissolved oxygen (derived from temperature and current data of the Beckman sensor) was computed by using the standard procedures implemented in the Seasoft package of SBE. The additional data of light transmission and light scattering were expressed in % giving a measurement of the beam attenuation coefficient, and the Fluorometer data were expressed in arbitrary units. The intercomparison with the chlorophyll data will be performed as soon as this data will be made available from the responsible scientist.

The preliminary analysis of temperature and salinity data was concerned with the data quality control. The differences of temperature and salinity values between the primary and secondary sensors have been revealed to be extremely stable along the water column, within the instrumental accuracy of ± 0.001 units. Nevertheless, whereas the comparison of temperature values exhibits zero-offset (within the accuracy of the instrument), the comparison of salinity shows an offset of about 0.012. This discrepancy was verified to be stable during the course of the cruise and a correction of -0.007 units was applied to the primary sensor data, after the comparison with salinity determinations obtained from the salinometer water samples analysis. The data of dissolved oxygen content (D.O.) has been quality controlled by the comparison with the data obtained on board from Nurit Kress (IOLR, Haifa, Israel) by the Carpenter-Winkler titration procedure conducted on the water samples (the precision is contained within the ± 0.3 % of the measurement). The discrepancy between the two measurements has been best-fitted with a quadratic function vs. the pressure (x) and the final corrected high resolution vertical profiles have been corrected as follows:

$$\text{D.O. (ml/l) corr.} = \text{D.O. meas} - (1.5106\text{E-}08x^2 + 3.3022\text{E-}05x + 1.951\text{ E-}01)$$

The current profiles obtained by ship-mounted ADCP along the ship track, have been monitored contemporarily to the ship movement with a differential GPS. Due to the impossibility to operate in bottom tracking (the instrumental range is limited to about 400-500 m of the water column), the bias due to the velocity ship was minimised by averaging 230 ping data over an interval time of 5

minutes. The final vertical resolution was set to obtain 40 cells, which represent the current speed averaged over 16 m bin intervals. As the ADCP data analysis is not trivial, the complete data set will be analysed in the lab. A preliminary analysis performed on board revealed that current data will be available in correspondence of fishing towing (velocity ship ≈ 2 kn) and at hydrological stations.

During the oceanographic survey 59 CTD casts were performed at 35 different station positions in the Eastern Mediterranean (Fig. 82, Table 21), and one profile was obtained in the Thyrrenian Sea. A total of 43 deep casts were performed down to the bottom, whereas 16 casts were shallow to obtain additional water samples in the 0-200 m layer for biological parameters determination. Moreover a 26-hour time series experiment was conducted at the station position 219 (see Fig. 82), lowering the CTD to the intermediate-transitional layer (down to 1000 m) every three hours. The measurements were performed in combination with water sampling in the upper thermocline for pico-phytoplankton determinations. The aim of this intensive experiment was to evaluate the fluctuation of the water masses and the short-time scale variability in the upper and intermediate layers due to the propagation of the internal waves.

Preliminary Results

The complexity of the temperature, salinity and density profiles, considering the deep casts exclusively, is shown in Figure 83. The vertical variability of the hydrographic characteristics encountered in the Eastern Mediterranean is related to the different water masses distribution. Fig. 83 clearly shows that in the Eastern Mediterranean, as a result of the transient status, a four-layer system may be recognised. The surface layer (0-150 m) is characterised by the alternate presence of two water masses: the LSW (Levantine Surface Water) with S>39.0 which dominates in the Eastern Levantine, and the MAW (Modified Atlantic Water) that flows through the Sicily Straits (S ≅ 37.5) and after successive modification enters the Levantine Basin, where it was transformed to S @ 38.9 at the stations 219-234. The intermediate layer (150-500 m) is dominated by the LIW (Levantine Intermediate Water), which exhibits the maximum core salinity of about 39.06 at 250 m in the Levantine Basin. The LIW spreads through the Cretan passage into the southern Ionian, along a meridional path close to the African coast, and reaches the Sicily Straits with core properties S < 38.80. There the LIW is subjected to further transformation and finally it intrudes the Western Mediterranean with a core salinity value of about 38.76. The transitional layer (500-1500 m), i.e. below the LIW and above the bottom layer, has core properties of $\theta \cong 13.5$ and $S \cong 38.74$ quite similar to those of the EMDW (Eastern Mediterranean Deep Water) of Adriatic origin, now uplifted to this layer. In the bottom layer (1500-bottom) an increase of both temperature and salinity, as moving from the west to the east, confirms the presence of the saline and dense waters of Aegean origin.

A comparison with the data obtained during the METEOR cruise M31/1, conducted in January 1995, shows that the Western Levantine Basin (st. 217) is affected by an increase of temperature and salinity in the bottom layer (from 2000 m to the bottom) of about 0.23 °C and 0.10, respectively; while a substantial decrease of temperature and salinity ($\theta \cong 13.85$-13.74 °C and $S \cong 38.87$-38.83) have been documented at station 249 located close to the Eastern Cretan Arc Straits. The maximum potential density of about 29.22 kg/m^3 was documented in the very deep profiles carried out in the Hellenic Trench (Ierapetra-Deep Basin). Similar variations were encountered also in the Ionian Sea. The temperature and salinity decreased at the stations located close to the Western Cretan Arc Straits ($\theta \cong 14.25$-14.15 °C, $S \cong 38.85$-38.81, and σ_θ 29.21 kg/m^3), while a general increase of salt content was documented in the transitional and deep layers in the Western Ionian. The Ionian

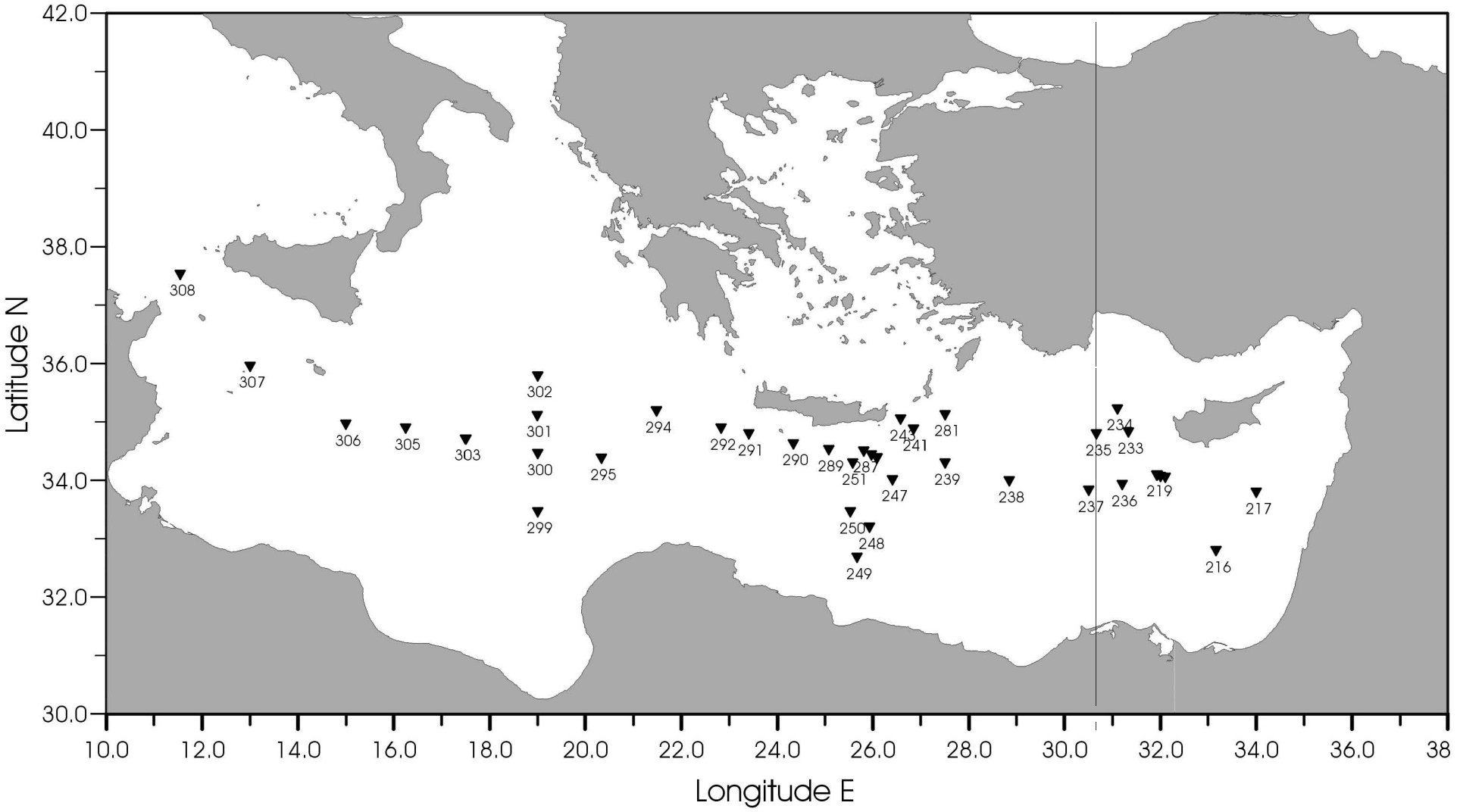

Fig.82: Station map for the hydrological station occupied during the R/V METEOR cruise, M44/4.

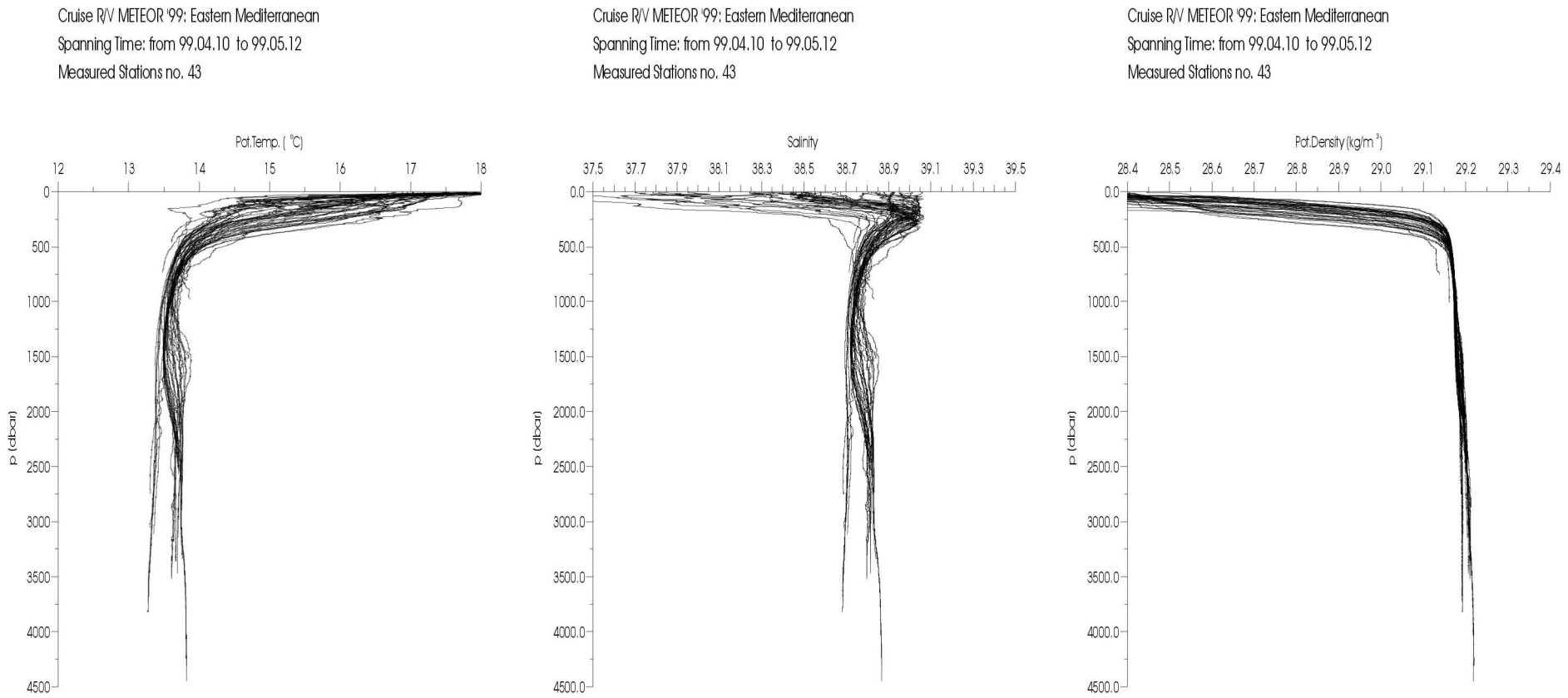

Fig. 83: Superimposed vertical profiles of potential temperature, salinity and potential density.

abyssal plain is occupied by dense water of Adriatic origin, the EMDW, which has properties of about $\theta \cong 13.4$ °C and $\cong$ S 38.70.

A special CTD cast was performed in the Urania Basin, filled with high saline brines. The interface between the deep water and the brines occurs at a depth of 3472 m. Accidentally, the CTD was immersed into the brine for about 3 m (cast performed to max depth of 3475 m) and promptly recovered without apparent effects on the calibration of temperature and conductivity sensors, which were verified by the intercomparison with the data collected during the up-cast.

T-S properties are plotted in Figure 84 separately for the stations in the Eastern Levantine (st. 216-219), in the Central Levantine (st. 233-238), in the Western Levantine (st. 239-287), and in Figure 85 for the stations in the Cretan passage (st. 289-292), in the Eastern Ionian (st. 293-302), and finally in the Western Ionian and Sicily Straits (st. 303-308). All the diagrams show relatively fresh Atlantic Water which is transformed from S $\cong$ 37.2 in the Sicily Straits to S $\cong$ 38.9 into the eastern part of the Levantine Basin, where it may be distinguished from the more saline LSW (S $\cong$ 39.0). The LIW, with a salinity maximum S > 39.0, is characterised by a temperature of about 16.0-15.5 °C as moving to the western Levantine Basin. In the Cretan passage and Ionian Sea it seems that a different saline water mass occupies the intermediate layer ($\theta \cong 14.0$-15.0 °C and S $\cong$ 38.90). The source is recognised to be close to the Western Cretan Arc straits, thus confirming the dominant role of the Cretan Intermediate Water (CIW) in filling the intermediate layer in the Ionian, first discovered by Malanotte-Rizzoli et al. (1999) from the POEM-BC data collected during the October 1991 cruise. A substantial difference between the two group of diagrams emerges in the deep water range. The profiles in the eastern part of the basin show the inversion in temperature and salinity in the deepest layers ($\sigma_\theta > 29.2$ kg/m^3) clearly connected with the presence of dense water of Aegean origin. In the Ionian the signal is evident close to the source, the Western Cretan Arc Straits. However, the western part of the Ionian has been subjected to advective and mixing processes, and a general increase of the salinity in the deep layer was documented.

Vertical sections of temperature and salinity were prepared from the CTD data, for interpretation of the main dynamical features encountered along the ship track. The features appearing in the long section through the Eastern Mediterranean are shown in Figures 86 and 87 for temperature and salinity, respectively. The distributions in the upper layer down to 500 dbar provide evidence of the intense dynamics and complexity of the regional hydrography. The main dynamical features, mostly evident in the temperature sections, from right to left are (for the nomenclature see for example the paper of the POEM GROUP, 1992): (i) the dome bordering the West Cyprus cyclonic gyre; (ii) the large anticyclone dominating the southern part of the Levantine Basin culminating in the Ierapetra anticyclone in correspondence of the stations 251-239; (iii) the doming in correspondence of the western tip of Crete (st. 292) indicates the Cretan cyclone; (iv) the very strong Pelops anticyclone which was detected at station 294 in the Eastern Ionian. The salinity section is mostly indicative of the core of the LIW, which seems entrained in the Ierapetra anticyclone without spreading into the Eastern Ionian, where a secondary core of salinity maximum is located in correspondence of the Western Cretan Arc Straits. Finally, the front formed by the fresh MAW at the left side of the section seems to extend deeply until the eastern part of the Cretan passage. Transformed water patches of MAW are detected in the central part of the Levantine Basin.

Property sections in the deep layer demonstrate the change in the vertical structure caused by the addition of warmer and saline Cretan Dense Water (CDW). In the past this deep range was influenced by the EMDW of Adriatic origin, new dense waters prevail in the new situation while the old EMDW, which is visible in the well established tongue of temperature and salinity minima, are

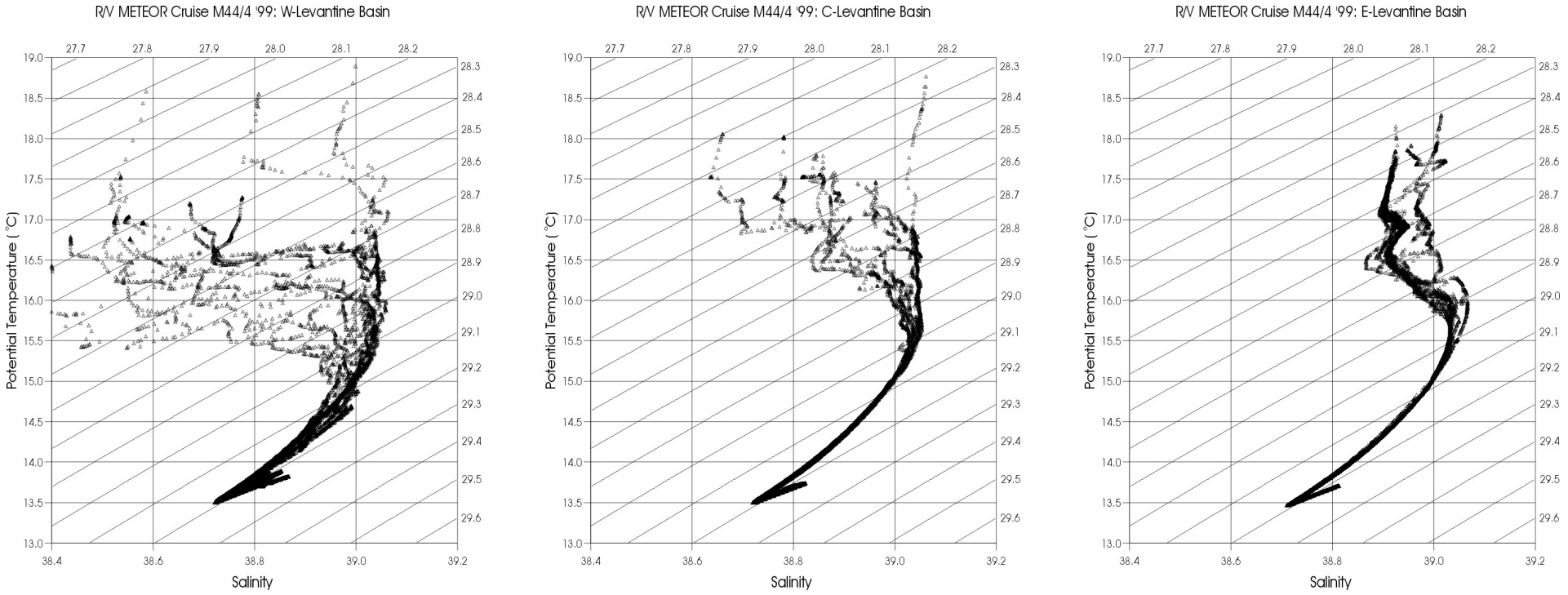

Fig. 84: Potential temperature-salinity relationships in the different regions of the Levantine Basin.

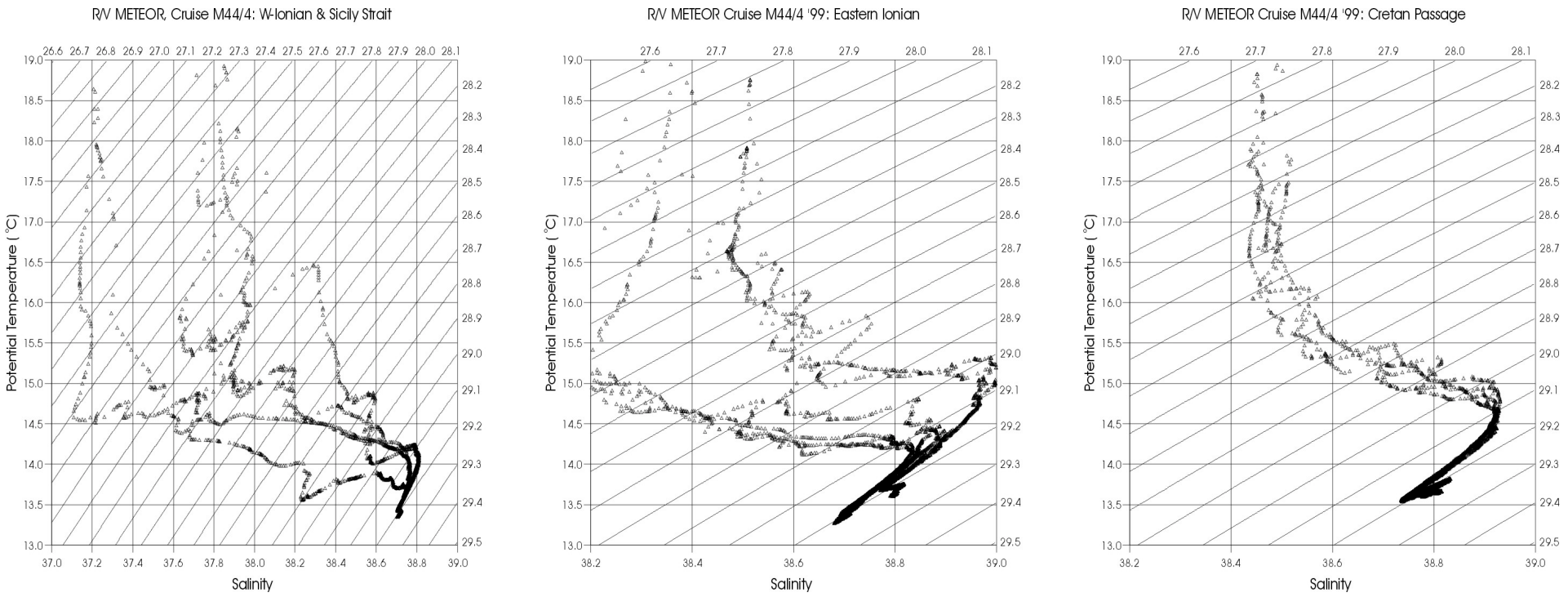

Fig. 85: Potential temperature-salinity relationships in the different regions of the Cretan passage and Ionian Sea.

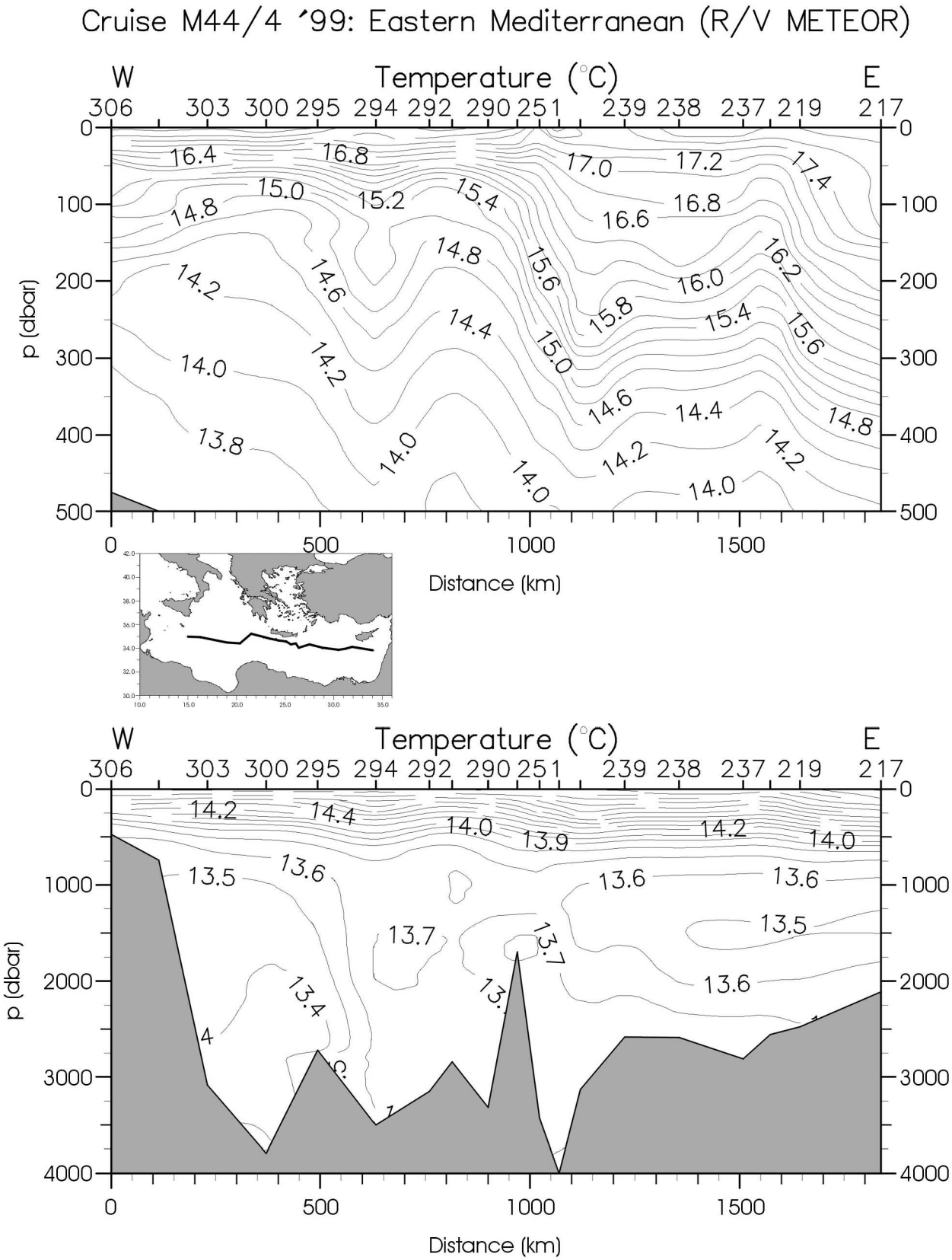

Fig. 86: Vertical distribution of temperature down to 500 dbar (upper panel) and for the whole vater column (lower panel). The position of the stations is indicated at the top. The section is denoted in the insert map.

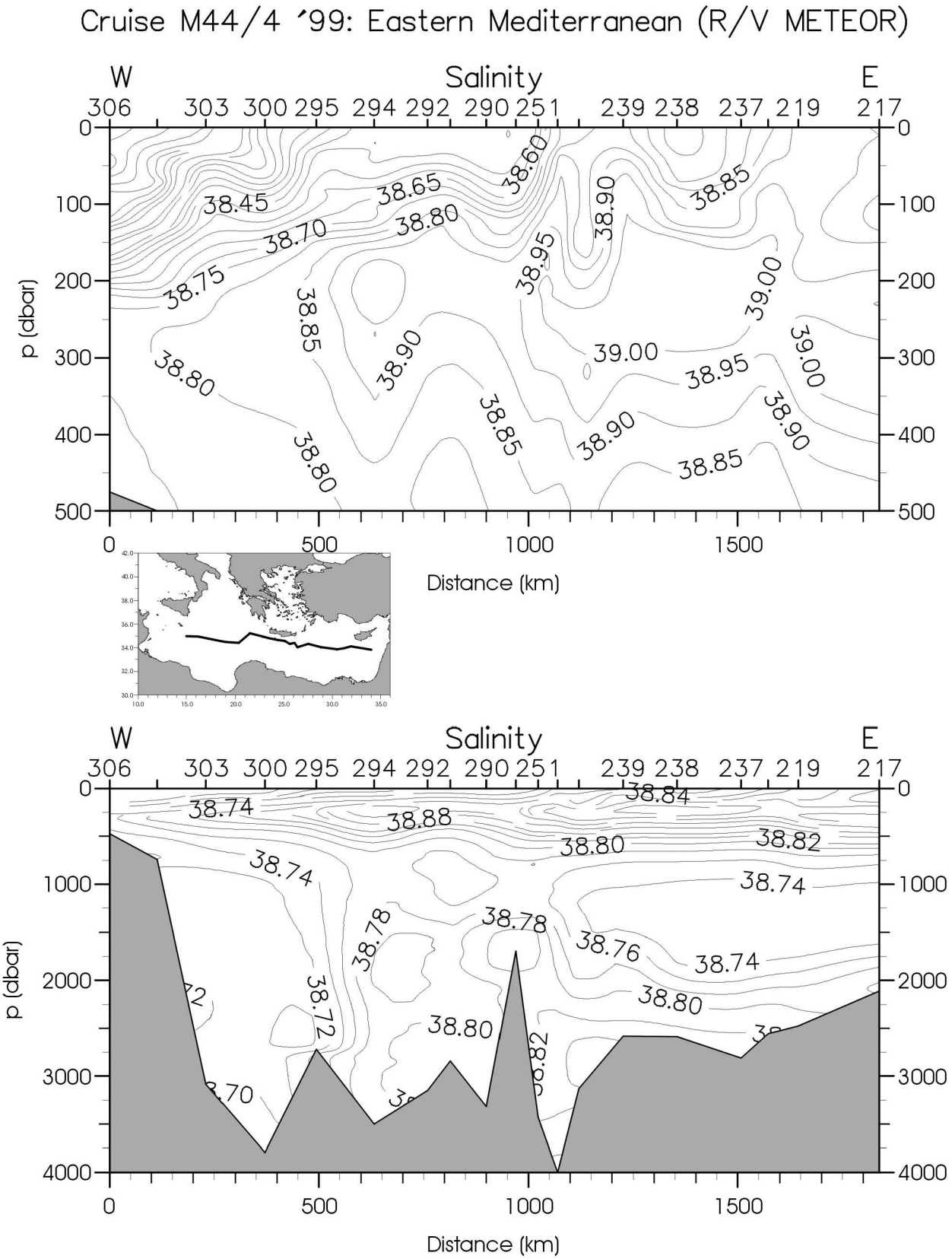

Fig. 87: As for Fig. 86, but for salinity.

lifted to 1200 m. Moreover, the influence of CDW is now extended to the Eastern Levantine, where temperature and salinity have been increased considerably compared to the past. A clear indication of westward spreading of CDW is still missing in the present situation, apart from the general increase of temperature and salinity in the transition and deep layers of the Western Ionian.

Tab. 21: CTD casts and measured objects from the mounted Rosette sampler (Niskin water bottles)

Station Id.	Cast	Date dd/mm/ 1999	Time hh.mm (UTC)	Lat N dd mm.th	Lon E dd mm.th	Depth (m)	Bottle nos.	Data File-name	Subject
216	S	10.04.	20:49	32° 49.96	33° 10.04	1396	14	S216	CTD cast, pico-phytoplankton
216	D	10.04.	21:25	32° 49.94	33° 10.01	1396	24	D216	CTD cast, D.O., nutrients, bacterial diversity/abundance, aggregates/microbial food web
217	D	11.04.	05:04	33° 50.07	34° 00.08	2109	24	D217	CTD cast, D.O., nutrients
219	D	11.04.	23:06	34° 07.96	31° 55.85	2476	0	D219	CTD cast
219	S	12.04.	01:00	34° 07.93	31° 55.85	2476	9	S2191	CTD cast, pico-phytoplankton
219	S	12.04.	02:18	34° 07.91	31° 55.79	2475	12	S2192	CTD cast, primary production, bacterial heterotrophic production/abundance, chlorophyll a
219	S	12.04.	04:11	34° 07.87	31° 55.7	2476	9	S2193	CTD cast, pico-phytoplankton,
219	D	12.04.	05:06	34° 07.92	31° 55.76	2504	21	D2191	CTD cast, pico-phytoplankton, primary production, aggregates/microbial food web
219	S	12.04.	09:05	34° 07.12	31° 58.14	2456	11	S2194	CTD cast, pico-phytoplankton
219	S	12.04.	11:54	34° 07.89	31° 55.87	2475	9	S2195	CTD cast, pico-phytoplankton
219	S	12.04.	14:51	34° 07.92	31° 55.86	2475	9	S2196	CTD cast, pico-phytoplankton
219	S	12.04.	17:54	34° 07.92	31° 55.83	2476	12	S2197	CTD cast, pico-phytoplankton
219	S	12.04.	20:54	34° 07.9	31° 55.89	2476	13	S2198	CTD cast, pico-phytoplankton
219	S	12.04.	23:54	34° 07.86	31° 55.89	2477	10	S2199	CTD cast, pico-phytoplankton
219	S	13.04.	02:51	34° 08	31° 55.81	2475	14	S219A	CTD cast, pico-phytoplankton
219	D	13.04.	03:33	34° 07.95	31° 55.82	2490	14	D2192	CTD cast, D.O., nutrients, tracers
226	D	15.04.	0:00	34° 05.5	32° 06.07	2443	24	D226	CTD cast, D.O., nutrients, tracers, primary production, bacterial heterotrophic production/abundance, chlorophyll a
230	D	16.04.	13:34	34° 06.29	32° 00	2537	24	D230	CTD cast, D.O., intercalibration with CTD R/V ARGONAUT from Cyprus
233	D	17.04.	10:24	34° 52.01	31° 20.13	2271	24	D233	CTD cast, D.O., nutrients, tracers, pico-phytoplankton
234	D	17.04.	14:49	35° 16.01	31° 06	2254	24	D234	CTD cast, D.O., nutrients, tracers, pico-phytoplankton, bacterial diversity/abundance, aggregates/microbial food web
235	D	17.04.	19:55	34° 50.01	30° 39.96	2362	24	D235	CTD cast, D.O., nutrients, tracers, pico-phytoplankton
236	D	18.04.	03:02	33° 58	31° 12	2555	24	D236	CTD cast, D.O., nutrients, tracers, pico-phytoplankton, bacterial diversity/abundance, aggregates/microbial food web
237	D	18.04.	08:16	33° 52.07	30° 30.03	2841	24	D237	CTD cast, D.O., nutrients, tracers, pico-phytoplankton
238	D	18.04.	17:44	34° 02	28° 51	2600	24	D238	CTD cast, D.O., nutrients, tracers, pico-phytoplankton, bacterial diversity/abundance
239	S	19.04.	02:08	34° 19.84	27° 30.16	2582	24	S239	CTD cast, pico-phytoplankton, primary production, bacterial heterotrophic production/abundance, chlorophyll a, bacterial diversity/abundance

Tab. 21: continued

239	D	19.04.	03:34	34° 20	27° 30	2619	24	D239	CTD cast, D.O., nutrients, tracers, bacterial diversity/abundance, aggregates/microbial food web
241	D	19.04.	22:34	34° 55	26° 51.07	1555	24	D241	CTD cast, D.O., nutrients, tracers
243	D	20.04.	05:04	35° 05.55	26° 34.97	971	24	D243	CTD cast, D.O., nutrients, tracers, pico-phytoplankton, bacterial diversity/abundance, aggregates/microbial food web
246	D	20.04.	23:55	34° 28.5	25° 58.53	3310	24	D246	CTD cast, D.O., nutrients, pico-phytoplankton
247	D	21.04.	05:04	34° 03.04	26° 24.96	3128	24	D247	CTD cast, D.O., nutrients, tracers, pico-phytoplankton
248	D	21.04.	12:51	33° 14.04	25° 56.08	2369	24	D248	CTD cast, D.O., nutrients, tracers, pico-phytoplankton
249	D	21.04.	17:57	32° 42.94	25° 40	2560	24	D249	CTD cast, D.O., nutrients, tracers, pico-phytoplankton, bacterial diversity/abundance, aggregates/microbial food web
250	D	22.04.	04:03	33° 30	25° 32	2435	24	D250	CTD cast, D.O., nutrients, tracers, pico-phytoplankton
251	D	22.04.	10:53	34° 20.01	25° 35.03	3428	24	D251	CTD cast, D.O., nutrients, tracers, pico-phytoplankton
254	D	22.04.	23:02	34° 25.52	26° 05.34	4260	24	D254	CTD cast, primary production, bacterial heterotrophic production/abundance, chlorophyll a, bacterial diversity/abundance, aggregates/microbial food web
265	S	26.04.	02:35	34° 21.19	25° 51.64	3167	12	S265	CTD cast, primary production, bacterial heterotrophic production/abundance, chlorophyll a
265	D	26.04.	04:52	34° 25.23	26° 04.96	4376	24	D265	CTD cast, tracers, bacterial heterotrophic production/abundance, chlorophyll a, bacterial diversity/abundance (same position as 254)
273	S	29.04.	02:25	34° 25.49	26° 05.16	4261	12	S273	CTD cast, primary production, bacterial heterotrophic production/abundance, chlorophyll a,
273	D	29.04.	03:48	34° 25.51	26° 05.19	4261	24	D273	CTD cast, water samples at 1000m for tracers intercalibration exercise
281	D	02.05.	08:58	35° 10.08	27° 30	1127	24	D281	CTD cast, D.O., nutrients, tracers, pico-phytoplankton, bacterial diversity/abundance, aggregates/microbial food web
287	D	04.05.	14:16	34° 32.76	25° 48.34	1529	24	D287	CTD cast, D.O., nutrients, tracers, pico-phytoplankton
289	D	05.05.	05:54	34° 34	25° 04.93	1694	24	D289	CTD cast, D.O., nutrients, tracers, pico-phytoplankton
290	D	05.05.	10:49	34° 40.02	24° 19.98	3316	24	D290	CTD cast, D.O., nutrients, tracers, pico-phytoplankton
291	D	05.05.	17:37	34° 50.08	23° 25.01	2842	24	D291	CTD cast, D.O., nutrients, tracers, pico-phytoplankton, aggregates/microbial food web
292	D	05.05.	22:27	34° 55.96	22° 49.98	3150	24	D292	CTD cast, D.O., nutrients, tracers, pico-phytoplankton
293	D	06.05.	07:14	35° 13.76	21° 28.7	3500	23	D293	CTD cast, bacterial diversity/abundance
293	U	06.05.	07:14	35° 13.76	21° 28.7	3500	23	D293	CTD up-cast, intercomparison with the down-cast after brine immersion
294	S	07.05.	02:42	35° 13.75	21° 28.66	3500	18	S294	CTD cast, pico-phytoplankton, primary production
294	D	07.05.	04:41	35° 13.77	21° 28.75	3500	24	D294	CTD cast, D.O., nutrients, tracers, bacterial heterotrophic production/abundance, chlorophyll a, aggregates/microbial food web
294	D	07.05.	16:48	35° 13.76	21° 28.71	3500			Rosette without CTD, nutrients, bacterial heterotrophic production/abundance, chlorophyll a, bacterial diversity

Tab. 21: continued

295	D	08.05.	14:58	34° 24.93	20° 20.14	2717	24	D295	CTD cast, D.O., nutrients, tracers, pico-phytoplankton, bacterial diversity/abundance, aggregates/microbial food web
299	D	09.05.	14:11	33° 30.02	19° 00.07	3023	24	D299	CTD cast, D.O., nutrients, tracers, pico-phytoplankton
300	D	09.05.	21:22	34° 30	19° 00.03	3794	24	D300	CTD cast, D.O., nutrients, tracers, pico-phytoplankton, bacterial diversity/abundance, aggregates/microbial food web
301	D	10.05.	03:35	35° 09.08	18° 59.92	3686	24	D301	CTD cast, D.O., nutrients, tracers, pico-phytoplankton
302	D	10.05.	10:18	35° 50.03	19° 00.02	3700	24	D302	CTD cast, D.O., nutrients, tracers, pico-phytoplankton
303	D	10.05.	21:05	34° 44.94	17° 29.92	3086	24	D303	CTD cast, D.O., nutrients, tracers, pico-phytoplankton, bacterial diversity/abundance, aggregates/microbial food web
305	D	11.05.	08:06	34° 56.09	16° 14.96	744	24	D305	CTD cast, D.O., nutrients, tracers, pico-phytoplankton
306	D	11.05.	14:32	34° 59.98	14° 59.96	475	24	D306	CTD cast, D.O., nutrients, tracers, pico-phytoplankton, bacterial diversity/abundance, aggregates/microbial food web
307	D	12.05.	01:09	35° 59.94	12° 59.87	1011	24	D307	CTD cast, D.O., nutrients, tracers, pico-phytoplankton, bacterial diversity/abundance, aggregates/microbial food web
308	D	13.05.	13:13	37° 34.02	11° 31.99	767	24	D308	CTD cast, D.O., nutrients, tracers, pico-phytoplankton, bacterial diversity/abundance, aggregates/microbial food web
310	D	12.05.	03:07	39° 00.04	10° 30	2677	24	D310	CTD cast, D.O., nutrients, tracers, pico-phytoplankton, bacterial diversity/abundance, aggregates/microbial food web

Note: D means „Deep cast“, i.e. down to the bottom
S means „Shallow cast“, i.e, down to the upper/intermediate layer for additional bio-chemical water samples
D.O. means „dissolved oxygen“

5.4.2 Tracer Measurements

(K. Bulsiwiecz, S. Kämper, B. Klein and W. Plep)

Material and Methods

During M44/4 water samples have been collected for the analysis of helium and neon isotopes, tritium and chlorofluorocarbons (CFC-11, CFC-12 and CFC-113). Measurements of the CFC concentrations in the water samples have been performed on board by means of gas chromatography. Helium/neon samples have been collected into copper tubes which are clamped off to prevent air exchange. These samples will be measured with a specially designed noble gas mass spectrometer after the cruise at the laboratory in Bremen. Tritium samples have been collected in 1 l glas bottles. After the cruise the water samples will be de-gased and the gas free samples will be stored in sealed glas containers to allow ingrowth of the helium isotope ^{3}He from the radioactive decay of the tritium contained in the water sample. After a storage time of about 6 month, to obtain sufficient amounts of ^{3}He from the radioactive decay of tritium, the 3He concentrations will be measured with the noble gas mass spectrometer. Helium/neon, tritium and CFC sampling has been performed on 38 stations (see chapter 5.4.1, table 21), a total of 674 CFC data, and 535 helium/neon and tritium data have been obtained. An additional station was only sampled for helium/neon and tritium to gather samples for an international intercalibration experiment. These samples will be distributed among institutes in Germany, England and the United States.

The anthropogenic compounds CFC-11, CFC-12 and CFC-113 have been released into the environment since several decades. The atmospheric release of CFC12 and CFC11 started in the 1930s and showed initially exponential increase, since the 1980s the increase is slowing down. CFC113 has been released into the atmosphere much later than the other two compounds and showed measureable concentrations since the 1960s. Because of their transient nature the CFCs provide time information on the ventilation of water masses. Despite a small natural background the major part of the tritium found in ocean waters stems from the atomic weapon tests in the mid 60s. Tritium is radioactive and decays to ^{3}He. Measurements of tritium and helium in a water sample therefore provide another dating mechanism. The main source of helium in the ocean is the atmosphere but interior sources also exist. One is the above mentioned ^{3}He production from radioactive decay of tritium. Helium is also released from the ocean bottom either through a-decay of uranium and thorium or through volcanism and hydrothermal vents. Helium provides a good indicator of bottom water movements.

Preliminary Results

The tracer investigations in the Eastern Mediterranean during M44/4 continue earlier investigations in 1987 and 1995. The main purpose of the sampling was to follow the development of the bottom water layer which had changed thoroughly by the discharge of a new bottom water type from the Aegean in the early 1990s. In the past the dense bottom water of the Eastern Mediterranean had been produced entirely by the Adriatic Sea from which it was discharged through the Strait of Otranto and spreaded eastward through the Ionian and Levantine Basin. In the early 1990s a second deep water source was established in the Aegean Sea which produced a saltier, warmer but still denser deep water type than the Adriatic. The signature of this deep water type from the Aegean could be traced through the eastern half of the Ionian Basin and the western half of the Levantine Basin in 1995.

Figure 88 shows a section of the chlorofluorocarbon F12. The section basically runs east/west along approximately 34°N from the Strait of Sicily towards Cyprus. The highest concentrations are found at the surface where the mixed layer is in direct contact with the atmosphere and an equilibrium between the CFC concentrations in air and water is reached. Below the mixed layer the contentrations decrease towards a minimum layer which is found at depth between 500-1500 m in the Ionian Basin and 700-1700 m in the Levantine Basin indicating poor ventilation of this layer. Lowest values of the minimum layer (<0.3 pmol/kg) are found in the Levantine Basin. The distributions rise towards the bottom and depict the presence of a more recently ventilated bottom water mass. Highest bottom water concentrations are found in the Cretan Passage (St.290-294) and in the Ierapetra Deep (St. 265). This is the signature of the deep water discharged from the Aegean. Compared to the distributions in 1995 (not shown) the Aegean Deep water has advanced towards the east in the Levantine Basin and is now covering the entire Levantine Basin, while in 1995 this water mass was not found in the eastern half (approximately east of St. 238). The advancing Aegean Deep Water has produced an uplifting of the minimum layer in the Levantine Basin by about 300 m as was noted previously for the Ionian Basin. In the Ionian Basin the situation is more complicated. In the west a clear sign of the dense water produced in the Adriatic is no longer identifiable. At the western end of the Ionian Basin (St. 303) the bottom concentrations are close ot 0.6 pmol/kg. Compared to 1995 no increase in bottom water concentrations can be noted in this area. This could either be due to the fact that not much new bottom water had been produced in the Adriatic after 1995 or could indicate that these bottom water did not reach sufficient densities to sink to the bottom and settled above the bottom layer. The large distance between the 0.5 pmol/kg and 0.6 pmol/kg isoline could be a sign of the latter effect. From the comparison of the 1995 and 1999 distributions it also seems that the deep water from the Aegean in the bottom layer did not advance further into the Ionian Basin probably blocked by topography.

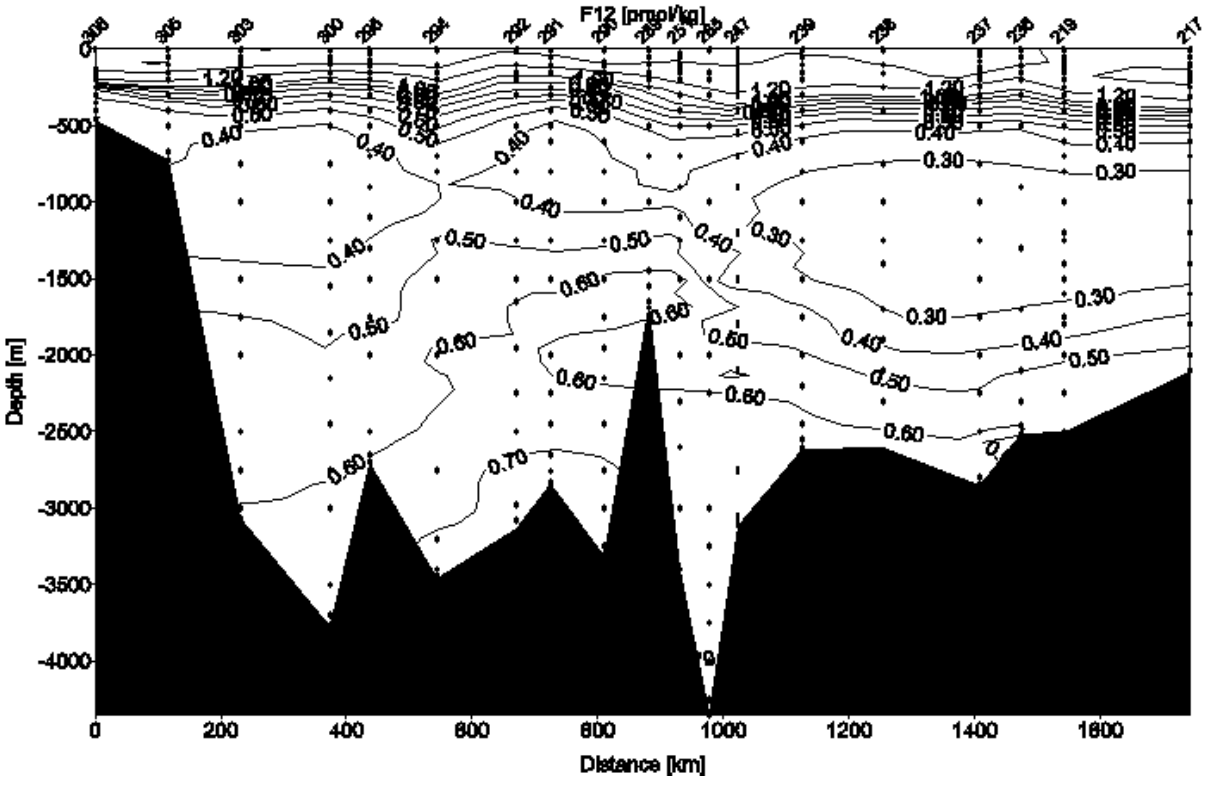

Fig. 88: Section of the chlorofluorocarbon F12.

5.4.3 Dissolved Oxygen and Nutrients (o-phosphate, nitrate, nitrite, silicic acid)

(N. Kress)

Introduction and Scope

The objectives of the dissolved oxygen and nutrient determinations are to describe their basinwide distribution, in conjunction with the physical forcing and to characterize the chemical properties of the different water masses. Together with the physical parameters and the tracer analysis they will help to follow the evolution of the changes in the circulation of the Eastern Mediterranean first observed by Roether et al. (1996) during Meteor cruise M31/1.

Material and Methods

Water samples were collected at 38 stations with a Seabird Rosette equipped with twenty-four 10-12 liters Niskin bottles (chapter 5.4.1, table 21). Water was sampled at 14-24 depths, from 10 meters above the sea bottom to the surface, the number of samples depending on the station's water depth. Water samples for dissolved oxygen were sampled after the sampling for tracers and pickled. Duplicate samples for nutrient analysis were collected in 15-ml acid washed plastic scintillation vials and immediately frozen. Dissolved oxygen was measured at sea using the Carpenter-Winkler titration procedure (Carpenter, 1965) and a Radiometer automatic titrator (TTT80), equipped with a dual platinum electrode, in the dead-stop end point mode. The precision was 0.3%. Nutrients will be shipped to IOLR, Haifa, and determined using a segmented flow Technicon AutoAnalyser II (AA-II) system by the methods described by Krom et al. (1991, 1993). The precision for nitrate+nitrate, phosphate and silicic acid is 0.02, 0.003 and 0.06 µM, respectively. The limit of detection (2 times the standard deviation of the blank) for the procedures is 0.075 µM for nitrate+nitrite, 0.018 µM for phosphate and 0.03 µM for silicic acid.

Intercalibration will be performed with the Italian colleagues by comparing depth profiles at two mutual stations occupied by the R/V Meteor and the Italian R/V Urania. In addition, frozen nutrient samples will be exchanged between IOLR and The Statione Zoologica, Naples.

Preliminary results

The results of the bottle's oxygen (Winkler titration) were used to calibrate the oxygen sensor of the CTD, resulting on calibrated continuous depth profiles of oxygen. These profiles show the fine structure of dissolved oxygen that is not possible to resolve with the bottle's data alone. Bruno Manca (from OGS) plotted two vertical sections of dissolved oxygen with the calibrated CTD data: a) from the Eastern Levantine to Crete (Fig. 89), and b) Around the Cretan Arc (Fig. 90). The vertical section from the Eastern Levantine to Crete (Fig. 89) showed an oxygen minimum layer at intermediate level (900-1000 m) in the whole basin, with more oxygenated waters at the bottom. This implies that the new, younger, transient deep waters reached the easternmost part of the Levantine Basin and lifted the older deep water to intermediate level. The eastern Levantine Basin did not have an oxygen minimum layer until 1995 and the oxygen concentration was constant from ca. 800 m down to the bottom. The section around the Cretan Arc (Fig. 90) showed an oxygen minimum layer centered at 500 m south west of Crete and at ca. 900 m south west of Crete. The bottom layer was well oxygenated. It was possible to discern the influence of the anticyclonic Ierapetra gyre at station 241 by the depression of the oxygen isolines, as well as the influence of the cyclonic Cretan gyre at station 291, lifting the oxygen isolines.

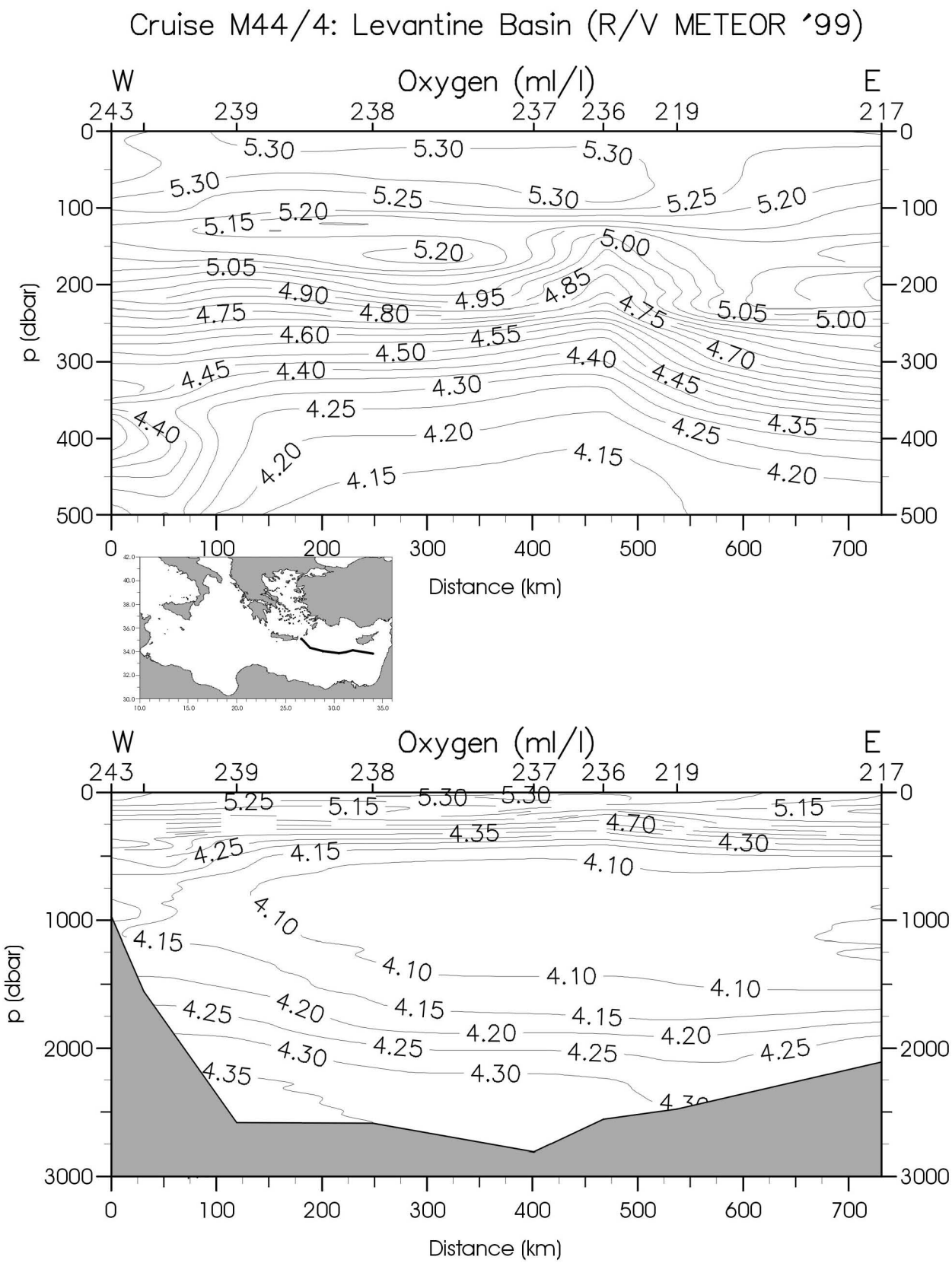

Fig. 89: Vertical section of dissolved oxygen from the Eastern Levantine Basin to Crete.

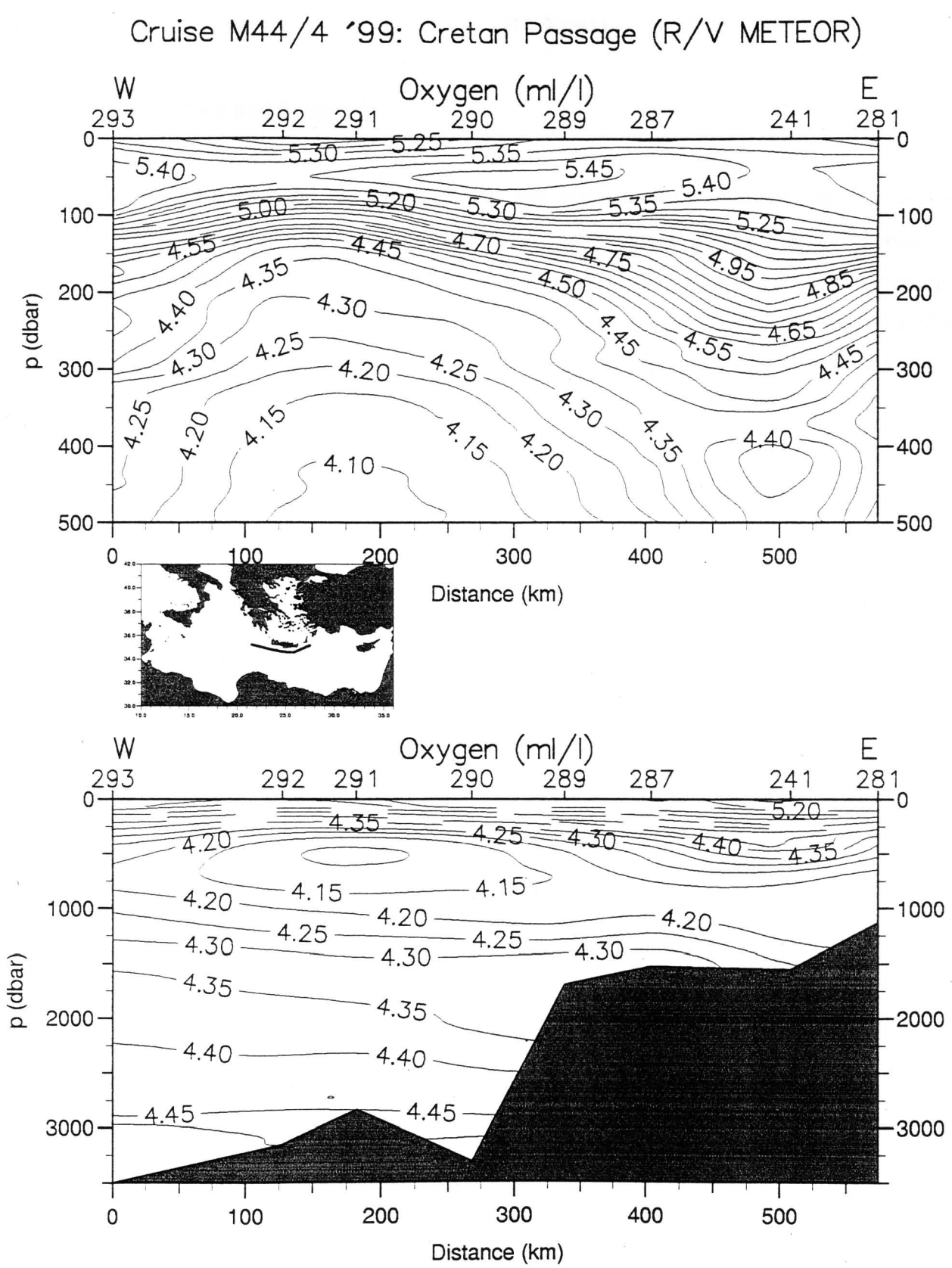

Fig. 90: Vertical section of dissolved oxygen around the Cretan Arc.

5.4.4 Diversity and Abundances of Bacteria in the Oligotrophic Eastern Mediterranean Sea

(G. Karsten, J. Süling, M. Blümel, S. Walter)

Introduction

Bacteria play an important role in the food webs of oligotrophic warm marine environments. About half of the organic matter which originates from primary production in these areas is turned over by bacteria (AZAM ET AL., 1983). Nonetheless, only little is known about bacterial communities in these habitats.

Results from former METEOR cruises in the Eastern Mediterranean Sea (M25/2, 12 May - 20 August 93; M40/3, 28 December 97 - 18 January 98) showed that bacterial abundances in the water column of the Eastern Mediterranean Sea were relatively low. During M40/3, total cell counts in the Ierapetra Basin lay between $1.4 \cdot 10^4$ and $1.9 \cdot 10^5$ per ml (DAPI staining), depending on water depth (KARSTEN AND IMHOFF, 1999). Even though low in number, the bacteria revealed a relative high diversity (determined by fluorescence-*in-situ*-hybridization (FISH) and denaturing gradient gel electrophoresis (DGGE)), both in the water column and the sediment.

Main Objectives

The main objectives of the microbial diversity group during METEOR cruise 44/4 were:

- bacterial abundances in the water column and comparison of these data with the respective data from METEOR cruises 25/2 and 40/3;
- bacterial diversity in water columns and sediment profiles and comparison of these data with the respective data from cruise M40/3;
- comparison of bacterial communities in defined water masses at different stations;
- enrichment and isolation of bacteria which are adapted to life under extreme oligotrophic conditions;
- effect of pressure onto bacterial communities in the water column of the deep sea;
- effect of nutrient input onto bacterial communities in the water column;
- microbial examination of the brine at the Urania Basin: bacterial abundances and diversity, enrichment and isolation of bacteria.

Material and Methods

Bacterial diversity

In order to describe the bacterial diversity, three different molecular biological methods will be employed: fluorescence-*in-situ*-hybridization (FISH), denaturing gradient gel electrophoresis (DGGE), and membrane fatty acid analysis.

- **FISH** gives quantitative information on the composition of bacterial communities (AMANN ET AL., 1995). Phylogenetic groups or species which make up at least 1% of the total community can be visualized and quantified. Bacteria from water samples were concentrated on polycarbonate filters (1 l water per filter). Seawater was incubated with chloramphenicol prior to filtration in order to increase the number of ribosomes per cell (OUVERNEY AND FUHRMAN, 1997). Bacteria on the filters were fixed with paraformaldehyde and frozen at -20°C (KARSTEN ET AL., in press). The FISH itself will be performed in the home lab: The filters will be incubated together with fluorescently labelled oligonucleotide probes which are complementary

to certain sequences of the 16S rRNA and specific for certain phylogenetic groups or species. If a bacterium belongs to the group which can be detected with a certain probe, the probe will hybridize with the respective 16S rRNA in the ribosomes. Cells thus labelled can be counted and quantified *via* epifluorescence microscopy.

- **DGGE** is a method to separate amplificates of 16S rDNA from different species (Muyzer and Smalla, 1998). In general, each band in a DGGE gel is derived from a different bacterium. Therefore, the DGGE band pattern gives information about the number and kind of different bacterial species in a community. Single bands can be excised from the gel and used for the determination of the DNA sequence. Using 16S rRNA data bases, the bacterium from which this sequence was obtained can be identified or - if this bacterium is still unknown - the phylogenetic group to which it belongs can be identified. DGGE and FISH together can give a qualitative and quantitative description of bacterial communities. For DGGE, bacteria from water samples (at least 3 l) were collected on polycarbonate filters and frozen at -20°C. In the home lab, DNA from these bacteria will be extracted and utilized for polymerase chain reaction (PCR) followed by DGGE and DNA sequencing.

Bacterial membranes consist of different and usually specific fatty acids. **Membrane fatty acids** can be extracted from bacterial communities and identified by gas chromatography. The composition of this mixture can give a fast overview over the bacterial groups present in the community. Bacteria were collected on polycarbonate filters with an *in-situ*-pump (bacteria from approximately 240 l water on one filter with a diameter of 142 mm). Bacteria were conserved with formaldehyde. Fatty acid analysis will be performed in the home lab.

For FISH and DGGE, water samples were taken with the CTD/rosette (Sea Bird, CTD model 911 plus, rosette model "Carrousel" fitted with 24 10- and 12-l-Niskin bottles) at 19 stations in the Eastern Mediterranean Sea (stations #: 216, 219 [south west off Cyprus], 234, 235, 238, 239, 243, 249, 254 [Ierapetra Basin], 281, 291, 293 [Urania Basin], 295, 300, 303, 306, 307, 308, 310; for positions cf. station list). At each station, a profile of 12 samples was taken. The water sampled with the rosette will also be used for the determination of bacterial abundances and biomass by the acridine orange method in the home lab (250 ml of each sample were fixed with formaldehyde) and for nutrient measurements in the home lab *via* ion chromatography (5 ml of each sample were filter sterilized and frozen at -20°C).

For membrane fatty acid analysis, samples were taken south west off Cyprus (station # 228) and in the Ierapetra Basin (station # 263).

Effect of nutrient input onto microbial communities

At the three main biological stations (stations # 224, 226, 228 south west off Cyprus, # 263, 277 in the Ierapetra Basin, # 294 in the Urania Basin) water samples were taken with sterile bag samplers („butterfly samplers", GENERAL OCEANICS, Miami, Florida, USA) from 12 depths each. The depths were the same as for the samples for FISH and DGGE.

For batch cultures, the water was transfered into several incubation bottles under sterile conditions. Each bottle was supplemented with certain substrates in different concentrations:

- Tryptic Soy Broth (TSB, final concentrations: 2.75 g/l, 0.275 g/l, 0.0275 g/l, 0.00275 g/l),
- Carbon-source-mixture (C-Mix, final concentrations: 10 ml/l, 1 ml/l, 0.1 ml/l, 0.01 ml/l).

Semi-continuous cultures were prepared similar as batch cultures except that substrates were added every 24 hours (10 times 0.00275 g/l TSB and 10 times 0.01 ml/l C-Mix, respectively).

All cultures were incubated under *in-situ* temperature (13.5°C) in the dark. After bacterial growth was visible by turbidity, (i) the cultures were transfered to fresh media, (ii) part of the culture was harvested for further cultures in the home lab, and (iii) the rest of the cultures was fixed with formaldehyde for further examinations in the home lab (DNA extraction and DGGE).

For the isolation of bacteria, solidified media containing 0.0275 g/l TSB were used. Colonies from these plates were transfered to new plates. This procedure will be continued in the home lab, until pure cultures will be gained. The isolates will be characterized for their physiological properties and identified by their 16S rDNA sequence.

The effect of nutrient input onto bacterial communities under *in-situ* pressure was examined with water samples from 4000 m and 4250 m depth in the Ierapetra Basin. Subsamples were supplemented with TSB to yield final concentrations of 0.0275 g/l, 0.1375 g/l, and 0.6875 g/l, respectively. The cultures were incubated under *in-situ* pressure (400 bar) and *in-situ* temperature (13.5°C) in special pressure incubation devices. After growth was observed, the cultures were fixed with formaldehyde and will be examined by DGGE in the home lab.

Effect of pressure onto microbial communities from the deep sea

Water samples from the Ierapetra Basin (station # 265, depths: 10 m, 1000 m, 2000 m, 3000 m, 4000 m, 4250 m) were supplemented with TSB (final concentration 1.375 g/l). Cultures from each depth were incubated under *in-situ* temperature (13.5°C) at the following pressures in special pressure incubation devices: atmospheric pressure, 100 bar, 200 bar, 300 bar, 400 bar, 425 bar. After growth was observerd, the cultures were fixed with formaldehyde and will be examined by DGGE in the home lab.

Enrichment cultures from the brine of the Urania Basin

Additional to enrichments with regard to the substrate concentration (see above), enrichment cultures were set up in order to examine the influence of salinity on bacterial communities from the brine and the brine/seawater interface at the Urania Basin. Two different media were utilized. One contained TSB (0.275 g/l) as carbon source, the second contained C-Mix (5ml/l) and different sulfur compounds. Of each media there were 4 varieties with different NaCl-concentrations (5%, 10%, 15%, 20%). From each media, parallell cultures were incubated under anoxic and oxic conditions, respectively. The cultures will be utilized for the isolation of bacteria and diversity analysis.

Sediment samples

Bacterial diversity in the sediment will be examined by DGGE and membrane fatty acid analysis. Sediment samples were taken with a multiple corer at the three main biological stations south west off Cyprus (station # 221), in the Ierapetra Basin (stations # 284 and 285), and in the Urania Basin (station # 294). The sediment samples will also be utilized for enrichment cultures, the measurement of chlorophyll, the determination of total bacterial counts and bacterial biomass, and measurement of nutrients in the pore water.

Tab. 22: Sampling for bacterial diversity.

Station No.	Position	Date 1999	Time (UTC)	Sampling Device	Depths sampled [m]	Applications
216	32°49.97'N, 33°09.92'E	10.04.	21:25	CTD/Rosette	10/50/100/150 250/400/600 800/1000/1200 1300/1390	DNA extraction, fluorescence-*in-situ*-hybridisation (FISH), total bacterial counts (TBC), bacterial biomass, nutrients
	SW-Cyprus					
219	34°07.92'N, 31°55.76'E	12.04.	05:00	CTD/Rosette	10/100/200/250 300/500/750 1000/1300/2000 2300/2500	DNA extraction, FISH, TBC, bacterial biomass, nutrients
221	34°04.81'N, 31°59.67'E (bottom contact)	13.04.	12:30	Multiple Corer	0-0.5 cm 0.5-1 cm -2 -3 -4 -6 -8 -10 -12 -14 -16 -18 -20 -24 -28 -32 -36 -40	DNA extraction, fatty acid analysis, TBC, bacterial biomass, enrichment cultures, chlorophyll, nutrients
221	34°05.64'N, 31°57.92'E	13.04.	14:00	In-situ-pump	(2500)	-
224	33°57.11'N, 31°50.29'E	14.04.	14:00	Sterile Bag Samplers	300/500	enrichment cultures
226	34°05.46'N, 32°05.93'E	15.04.	03:30	Sterile Bag Samplers	10/100/200/250 750/1000/1300	enrichment cultures
228	34°05.73'N, 31°45.84'E	15./16. 04.	19:30	*In-situ*-pump + Sterile Bag Samplers	2425 (ISP) 2400 (SBS) 2250 (SBS)	DNA extraction (ISP), fatty acid analysis (ISP), enrichment cultures (ISP + SBS)
234	35°16.00'N, 31°06.00'E	17.04.	14:43	CTD/Rosette	10/50/75/100 130/300/600 900/1300/1700 2100/2250	DNA extraction, FISH, TBC, bacterial biomass, nutrients
236	33°58.01'N, 31°11.98'E	18.04.	03:00	CTD/Rosette	10/30/115/150 400/700/900 1300/1700/2100 2460/2519	DNA extraction, FISH, TBC, bacterial biomass, nutrients
238	34°01.99' N, 28°51.04' E	18.04.	17:45	CTD/Rosette	10/50/100/200 550/750/1000 1400/1700/1900 2300/2580	DNA extraction, TBC, bacterial biomass, nutrients
239	34°20.00'N, 27°30.00'E	19.04.	02:00	CTD/Rosette	10/75/130/150 300/600/900	DNA extraction, FISH, TBC, bacterial biomass, nutrients
239	34°19.85'N, 27°30.15'E	19.04.	03:35	CTD/Rosette	1200/1500/2000 2500/2610	DNA extraction, FISH, TBC, bacterial biomass, nutrients

Tab. 22: continued

243	35°05.54'N, 26°34.98'E	20.04.	05:00-05:45	CTD/Rosette	10/60/100/150 200/230/330 350/370/500 700/970	DNA extraction, FISH, TBC, bacterial biomass, nutrients
249	32°42.96'N, 25°39.97'E	21.04.	18:00	CTD/Rosette	10/100/200/350 500/900/1100 1300/1700/2100 2300/(2500) 2554	DNA extraction, FISH, TBC, bacterial biomass, nutrients
	Ierapetra Basin					
254	34°25.48'N, 26°05.39'E	22.04.	23:15	CTD/Rosette	10/50/100/200 500/1000/1500 2000/2500/3000 4000/4250	DNA extraction, FISH, TBC, bacterial biomass, nutrients
263	34°26.16'N, 26°06.78'E	25.04.	01:15	*In-situ*-pump + Sterile Bag Samplers	4250 (ISP) 4230 (SBS) 4000 (SBS)	DNA extraction (ISP), fatty acid analysis (ISP), enrichment cultures (ISP + SBS)
263	34°26.16'N, 26°06.78'E	25.04.	10:15	Sterile Bag Samplers	10/50/100/200 500/1000	enrichment cultures
265	34°25.20'N, 26°04.93'E	26.04.	05:00	CTD/Rosette	10/1000/2000 3000/4000/4250	DNA extraction, FISH (substrate preincubation), pressure incubations (pressure series, substrate concentration series)
277	34°26.45'N, 26°07.86'E	30.04.	18:30	*In-situ*-pump + Sterile Bag Samplers	4230 (ISP) 3000 (SBS) 2500 (SBS) 2000 (SBS) 1500 (SBS)	enrichment cultures (SBS)
281	35°10.08'N, 27°29.99'E	02.05.	08:50	CTD/Rosette	10/50/110/150 200/250/400 600/800/1000 1100/1125	DNA extraction, FISH, TBC, bacterial biomass, nutrients
284	34°24.79'N, 26°05.81'E (bottom contact)	03.05.	14:54	Multiple Corer	0-0.5 -1 -2 -3 -4 -6 -8 -10 -12 -14 -15 -16 -18 -20 -24 -28 -32 -36 -40	DNA extraction, fatty acid analysis, TBC, bacterial biomass, chlorophyll, enrichment cultures, nutrients

Tab. 22: continued

285	34°25.90'N, 26°10.76'E (bottom contact)	03.05.	18:00	Multiple Corer	0-0.5 -1 -2 -3 -4 -6 -8 -10 -12 -14 -15 -16 -18	DNA extraction, fatty acid analysis, TBC, bacterial biomass, chlorophyll, enrichment cultures, nutrients
291	34°50.06'N, 23°25.00'E	05.05.	17:30	CTD/Rosette	10/50/100/200 400/800/1000 1500/2000/2650 2760/2830	DNA extraction, FISH, TBC, bacterial biomass, nutrients
	Urania Basin					
293	35°13.76'N, 21°28.70'E	06.05.	07:10	CTD/Rosette	10/100/200 1000/1840/2250 3380/3429	DNA extraction, FISH, TBC, bacterial biomass, nutrients
294	35°14.00'N, 21°28.60'E	06.05.	16:00	Multiple Corer	not defined	DNA extraction, fatty acid analysis, enrichment cultures
294	35°13.75'N, 21°28.73'E	06.05.	18:00	*In-situ*-pump + Sterile Bag Samplers	3490 (ISP) 3429 (SBS) 3380 (SBS) 2250 (SBS)	enrichment cultures (SBS)
294	35°13.77'N, 21°28.65'E	07.05.	07:15	Sterile Bag Samplers	15 m above sed. 40 m above sed. 50 m above sed. 60 m above sed.	enrichment cultures, electron microscopy, DNA extraction
294	35°13.76'N, 21°28.71'E	07.05.	16:50	Rosette (without CTD)	20 m above sed. 30 m above sed. 40 m above sed. 50 m above sed. 60 m above sed. 70 m above sed.	DNA extraction, TBC, bacterial biomass, nutrients
294	35°13.76'N, 21°28.72'E	07.05.	19:21	Sterile Bag Samplers	100/200/1000 1840	enrichment cultures
294	35°13.76'N, 21°28.74'E	07.05.	21:50	Sterile Bag Samplers	10	enrichment cultures
295	34°24.98'N, 20°20.12'E	08.05.	15:00	CTD/Rosette	(10)/50/100/200 300/ (400)/500 900/1500/2000 2500/2650 (2750)	DNA extraction, FISH, TBC, bacterial biomass, nutrients
300	34°30.02'N, 18°59.98'E	09.05.	21:20	CTD/Rosette	10/50/90/300 500/1000/1550 2150/2750/3250 3700/3765	DNA extraction, FISH, TBC, bacterial biomass, nutrients
303	34°44.99'N, 17°29.97'E	10.05.	22:05	CTD/Rosette	10/50/105/200 300/600/1000 1500/2000/2500 3000/3066	DNA extraction, FISH, TBC, bacterial biomass, nutrients
306	34°59.98'N, 14°59.96'E	11.05.	14:30	CTD/Rosette	0/10/50/90/110 140/180/200 250/300/400 460	DNA extraction, FISH, TBC, bacterial biomass, nutrients
307	35°59.95'N,	12.05.	01:00	CTD/Rosette	10/60/70/100	DNA extraction, FISH, TBC, bacterial

Tab. 22: continued

	12°59.87'E				200/220/300 450/650/850 950/1000	biomass, nutrients
308	37°34.05'N, 11°32.02'E	12.05.	13:10	CTD/Rosette	10/30/50/100 150/250/300 400/500/600 700/750	DNA extraction, FISH, TBC, bacterial biomass, nutrients
310	38°59.99'N, 10°30.00'E	13.05.	03:10	CTD/Rosette	10/55/90/110 300/600/900 1500/2000/2400 2600/2666	DNA extraction, FISH, TBC, bacterial biomass, nutrients

5.4.5 Interrelationship Between Primary Production and Microbial Activity in the Eastern Mediterranean Sea

(D. Hoffmann, P. Krischker, F. Lappe)

Introduction

Due to the special hydrological situation the concentration of nutrients in the Mediterranean Sea is remarkably low compared with the North Atlantic. On the way to the east the Atlantic water flowing into the Mediterranean looses a considerable part of its already low content due to nutrient consumption by planctonic algae and mixing with nutrient exhausted Mediterranean surface water, thus leading to an extremely nutrient-poor euphotic layer in the Easter Mediterranean Sea. The Levantine Sea, therefore, belongs to the most oligotrophic areas of the world ocean, where a close coupling between production and mineralization processes is of utmost importance for the formation of organic material.

Main Objectives

Our research work focussed on the functional relationship between phytoplancton as primary producers and heterotrophic microorganisms, mainly bacteria, as decomposers of organic matter. The work included

- spatial distribution (both regional and vertical) of phytoplankton abundance and primary production, and
- concomitant spatial distribution of bacterial abundance and activity.

The results should be compared to similar earlier studies made during METEOR cruises 25/2 (1993) and 40/3 (1998).

Another important question of the recent cruise dealt with bacterial abundance and activity around the interphase between "normal" Mediterranean deep water and the brine solution encountered in the deep layer of the Urania Basin west off Crete.

Material and Methods

Sampling strategy

For regional distribution of Chlorophyll *a*, total bacterial number and bacterial secondary production surface samples were obtained using a stainless steel bucket. Sampling started off Haifa (Israel) and ended in the Strait of Sicily thus giving a roughly latitudinal transect through the whole Eastern Mediterranean.

For the determination of primary production and concomitant bacterial variables water samples were taken by means of a Rosette sampler equipped with 12 l-Niskin bottels at 7 stations. The bottles were non-sterile, but thoroughly cleaned. Water samples were obtained from 0, 10, 20, 30, 40, 50, 60, 70, 80, 90, 100 and 120 m depths.

Samples for the distribution of bacterial abundance and activity below the euphotic zone were taken with the above mentioned Rosette at 3 stations.

Sampling and processing for measuring bacterial numbers, bacterial primary production by chemosynthesis and bacterial secondary production around the interphase between the extremely dense anoxic deep water layer of the Urania Basin and the overlying oxic Mediterranean water was done with special care. This is important in order to avoid changes in the natural O_2/H_2S-concentration, which is a controlling factor for the rate of bacterial activity.

Sample information is listed in Table 23.

Chlorophyll *a*-concentration

1 l of water (3 replicates) were filtered through glassfibre filters (Whatman GF/F) shortly after sampling. The pigments were extracted with 96% ethanol and measured with a Turner fluorimeter, which was calibrated with pure chlorophyll *a*.

Primary productivity

Water samples were taken before sunrise. From each of the 12 depth between surface and 120 m two clear glass bottles (100 ml nominal volume) were filled and inoculated with 10 µCi of $NaH^{14}CO_3$ solution. Incubation was done "in situ" with a drifting buoy usually from sunrise to local noon. Additionally one dark bottle from 4 depths was inoculated and incubated at in situ-temperature. Radioactivity incorporated by the algae was measured using the liquid scintillation technique.

Abundance of bacteria

Subsamples were preserved with 2 ml of filtered, buffered formalin per 100 ml of water and stored in the dark till filtration, which will be done at the home laboratory. Volumes of 10 and 40 ml (from surface down to 600 m depth) and of 50 and 100 ml (from 1000 m down to the sediment) will be filtered through black polycarbonate filters of 0.2 µm pore size (Nuclepore) and stained with Acridine Orange (Zimmermann, 1977). Bacteria will be counted and size measured with a Zeiss epifluorescence microscope equipped with a Petterson grid. Bacteria volumes will be converted into bacterial carbon using a conversion factor of 0.25 x 10^6 µg C per μm^3 of bacteria volume.

Secondary production of bacteria

Bacterial protein production was measured with the ^3H -leucine incorporation technique (Simon and Azam, 1989). The technique was performed as follows: Immediately after having taken the samples with the rosette four 20 ml subsamples per sample were filled into clean (but not sterilized) plastic scintillation vials. Prior to this the vials received 10 µlCi of ^3H-Leucine and non-labelled leucine. The combined final concentration was 33.3 nmol l^{-1}. One vial per set served as blank and received 0.1 ml of formalin. The vials from samples down to 120 m were incubated at in situ temperature (+/- 1°C) for two and from deeper samples for four hours. After incubation and fixing, the samples were filtered through polycarbonate filters (0.2 µm pore size), washed 10 times with 1 ml of ice cold 5% TCA and radioassayed with a scintillation counter. Protein production was calculated using a CF of 3595 pg protein/pmol leucine.

Tab. 23: Sampling for phytoplankton and bacterial productivity studies.

Station No.	Internal Stat.No.	Position	Date 1999	Local Time	Sampling Device	Depths sampled [m]	Applications
-	2	32°51.25'N 33°50.82'E	10.04.	15:35	Surface Sampler	0	^{3}H-Leucine incorporation (TLI), total bacterial counts (TBC), chlorophyll a
-	3	32°51.45'N 33°10.20'E	10.04.	19:15	Surface Sampler	0	TLI, TBC, chlorophyll a
217	4	33°50.01'N 34°00.07'E	11.04.	08:26	Surface Sampler	0	TLI, TBC, chlorophyll a
	5	33°49.95'N 32°49.98'E	11.04.	14:10	Surface Sampler	0	TLI, TBC, chlorophyll a
219	6a	34°07.90'N 31°55.83'E	12.04.	05:09	CTD/Rosette	0/10/20/30/4 50/60/70/80 90/100/120	Salinity, oxygen, temperature, fluorimeter; TLI, TBC, chlorophyll a
219	6a	34°07.90'N 31°55.83'E	12.04.	05:00	Deployment of drifting unit		Primary Production
219	6a	34°05.98'N 31°59.28'E	12.04.	12:00	Secchi disk		Secchi Depth
219	6a	34°05.98'N 31°59.28'E	12.04.	12:15	Recovery of drifting unit		Primary Production
220	6b	34°04.84'N 32°00.38'E	13.04.	12:51	Surface Sampler	0	TLI, TBC, chlorophyll a
226	6c	34°05.60'N 32°05.94'E	15.04.	03:43	CTD/Rosette	0/10/20/30/40 50/60/70/80 90/100/120 150/200/250 300/500/800 1250/1500 1750/2000 2250/2430	Salinity, oxygen, temperature, fluorimeter; TLI, TBC, chlorophyll a
226	6c	34°05.60'N 32°05.94'E	15.04.	05:15	Deployment of drifting unit		Primary Production
226	6c	34°02.00'N 32°07.01'E	15.04.	11:30	Secchi disk		Secchi Depth
226	6c	34°02.00'N 32°07.01'E	15.04.	12:15	Recovery of drifting unit		Primary Production
-	7a	34°33.27'N 31°33.95' E	17.04.	10:30	Surface Sampler	0	TLI, TBC, chlorophyll a
-	7b	34°52.00'N 31°20.08'E	17.04.	14:00	Surface Sampler	0	TLI, TBC, chlorophyll a
-	8	35°16.00'N 31°05.99'E	17.04.	17:08	Surface Sampler	0	TLI, TBC, chlorophyll a
-	9	34°50.02'N 30°39.94'E	17.04.	22:00	Surface Sampler	0	TLI, TBC, chlorophyll a
-	10	33°52.05'N 30°30.03'E	18.04.	10:25	Surface Sampler	0	TLI, TBC, chlorophyll a
-	11	34°01.99'N 28°51.04'E	18.04.	20:00	Surface Sampler	0	TLI, TBC, chlorophyll a

Tab. 23: continued

239	12	34°20.00'N 27°30.03'E	19.04.	05:00	CTD/Rosette	0/10/20/30/40 50/60/70/80 90/100/120	Salinity, oxygen, temperature, fluorimeter; TLI, TBC, chlorophyll a
239	12	34°20.00'N 27°30.03'E	19.04.	07:50	Deployment of drifting unit		Primary Production
239	12	34°10.80'N 27°31.33'E	19.04.	14:30	Secchi disk		Secchi Depth
239	12	34°10.80'N 27°31.33'E	19.04.	14:00	Recovery of drifting unit		Primary Production
-	12b	34°55.00'N 26°51.06'E	20.04.	00:33	Surface Sampler	0	TLI, TBC, chlorophyll a
-	13	34°03.01'N 26°24.95'E	21.04.	08:20	Surface Sampler	0	TLI, TBC, chlorophyll a
-	14	33°21.56'N 26°00.48'E	21.04.	14:01	Surface Sampler	0	TLI, TBC, chlorophyll a
-	15	32°42.98'N 25°40.01'E	21.04.	20:55	Surface Sampler	0	TLI, TBC, chlorophyll a
250	16	33°30.00'N 25°32.00'E	22.04.	07:00	Surface Sampler	0	TLI, TBC, chlorophyll a
-	17a	34°19.93'N 25°35.27'E	22.04.	13:12	Surface Sampler	0	TLI, TBC, chlorophyll a
254	17b	34°25.49'N 26°05.15'E	23.04.	04:10	CTD/Rosette	0/10/20/30/40 50/60/70/80 90/100/120	Salinity, oxygen, temperature, fluorimeter; TLI, TBC, chlorophyll a
254	17b	34°25.49'N 26°05,15'E	23.04.	05:40	Deployment of drifting unit		Primary Production
254	17b	34°27.12'N 26°06.23'E	23.04.	12:30	Secchi disk		Secchi Depth
254	17b	34°27.12'N 26°06.23'E	23.04.	12:05	Recovery of drifting unit		Primary Production
265	17c	34°21.18'N 25°51.65'E	26.04.	04:54	CTD/Rosette	0/10/20/3/40 50(60/70/80 90/100/120	Salinity, oxygen, temperature, fluorimeter; TLI, TBC, chlorophyll a
265	17c	34°25.20'N 26°04.93'E	26.04.	06:45	Deployment of drifting unit		Primary Production
265	17c	34°25.20'N 26°04.97'E	26.04.	09:45	CTD/Rosette	150/200/300 500/1000 1500/2000 2500/3000 3500/4000 4250	Salinity, oxygen, temperature, fluorimeter; TLI, TBC, chlorophyll a
265	17c	34°26.90'N 26°04.48'E	26.04.	12:45	Secchi disk		Secchi Depth
265	17c	34°26.90'N 26°04.48'E	26.04.	12:37	Recovery of drifting unit		Primary Production
273	17d	34°25.49'N 26°05.14'E	29.04.	04:42	CTD/Rosette	0/10/20/30/40 50/60/70(80 90/100/120	Salinity, oxygen, temperature, fluorimeter; TLI, TBC, chlorophyll a
273	17d	34°21.18'N 25°51.65'E	29.04.	05:38	Deployment of drifting unit		Primary Production
273	17d	34°29.43'N 26°06.25'E	29.04.	13:30	Secchi disk		Secchi Depth
273	17d	34°29.43'N 26°06.25'E	29.04.	13:20	Recovery of drifting unit		Primary Production
289	18	34°34.00'N 25°04.96'E	05.05.	08:22	Surface Sampler	0	TLI, TBC, chlorophyll a

Tab. 23: continued

290	19	34°40.02'N 24°20.01'E	05.05.	13:12	Surface Sampler	0	TLI, TBC, chlorophyll a
291	20	34°50.01'N 23°24.99'E	05.05.	19:54	Surface Sampler	0	TLI, TBC, chlorophyll a
292	21	34°55.97'N 22°49.92'E	06.05.	00:32	Surface Sampler	0	TLI, TBC, chlorophyll a
293	22	35°13.76'N 21°28.73'E	06.05.	11:06	Surface Sampler	0	TLI, TBC, chlorophyll a
294	22	35°13.77'N 21°28.54'E	07.05.	05:40	CTD/Rosette	0/10/20/30/40 50/60/70/80 90/100/120	Salinity, oxygen, temperature, fluorimeter;
294	22	35°13.79'N 21°28.07' E	07.05.	06:10	Deployment of drifting unit		Primary Production
294	22	35°13.79'N 21°28.07'E	07.05.	09:05	CTD/Rosette	200/1000 2000/3000 3440	TLI, TBC, chlorophyll a
294	22	35°19.56'N 21°13.65'E	07.05.	16:40	Recovery of drifting unit		Primary Production
294	22	35°13.79'N 21°28.7'E	07.05.	21:15	Rosette without CTD	3450/3460 3470/3480 3490/3500	TLI, TBC, chlorophyll a
295	23	34°24.99'N 20°20.18'E	08.05.	17:36	Surface Sampler	0	TLI, TBC, chlorophyll a
299	24	33°30.02'N 19°00.03'E	09.05.	16:21	Surface Sampler	0	TLI, TBC, chlorophyll a
300	25	34°20.02'N 19°00.03'E	09.05.	23:30	Surface Sampler	0	TLI, TBC, chlorophyll a
302	26	35°49.97'N 18°59.98'E	10.05.	14:35	Surface Sampler	0	TLI, TBC, chlorophyll a
-	27	35°17.45'N 18°14.73'E	10.05.	18:55	Surface Sampler	0	TLI, TBC, chlorophyll a
303	28	34°44.91'N 17°29.91'E	10.05.	23:02	Surface Sampler	0	TLI, TBC, chlorophyll a
305	29	34°56.10'N 16°14.98'E	11.05.	10:03	Surface Sampler	0	TLI, TBC, chlorophyll a
306	30	34°59.98'N 14°60.00'E	11.05.	17:02	Surface Sampler	0	TLI, TBC, chlorophyll a
-	31	35°30.26'N 13°59.93'E	11.05.	22:17	Surface Sampler	0	TLI, TBC, chlorophyll a
307	32	35°59.94'N 12°59.92'E	12.5.99	03:28	Surface Sampler	0	TLI, TBC, chlorophyll a
-	33	36°47.17'N 12°16.34'E	12.05.	09:56	Surface Sampler	0	TLI, TBC, chlorophyll a
308	34	37°34.03'N 11°32.01'E	12.05.	15:17	Surface Sampler	0	TLI, TBC, chlorophyll a
-	35	38°17.00'N 11°01.10'E	12.05.	20:37	Surface Sampler	0	TLI, TBC, chlorophyll a
310	36	38°59.09'N 10°30.00'E	13.05.	06:12	Surface Sampler	0	TLI, TBC, chlorophyll a

Preliminary results

As already mentioned, the final processing and calculations of most of the variables still requires some time at the home laboratory. Therefore, most of results are not yet available.

Regarding the incorporation of leucine as a relative measure for bacterial activity some data are already available. The roughly latitudinal transect from the most eastern part of the Mediterranean to the Strait of Sicily revealed a remarable increase in bacterial activity. Lowest values were found in the Levantine Sea. From south of Crete to the west values began to increase significantly (Fig. 91). This might be an indication for increasing productivity in the Mediterranean from est to west.

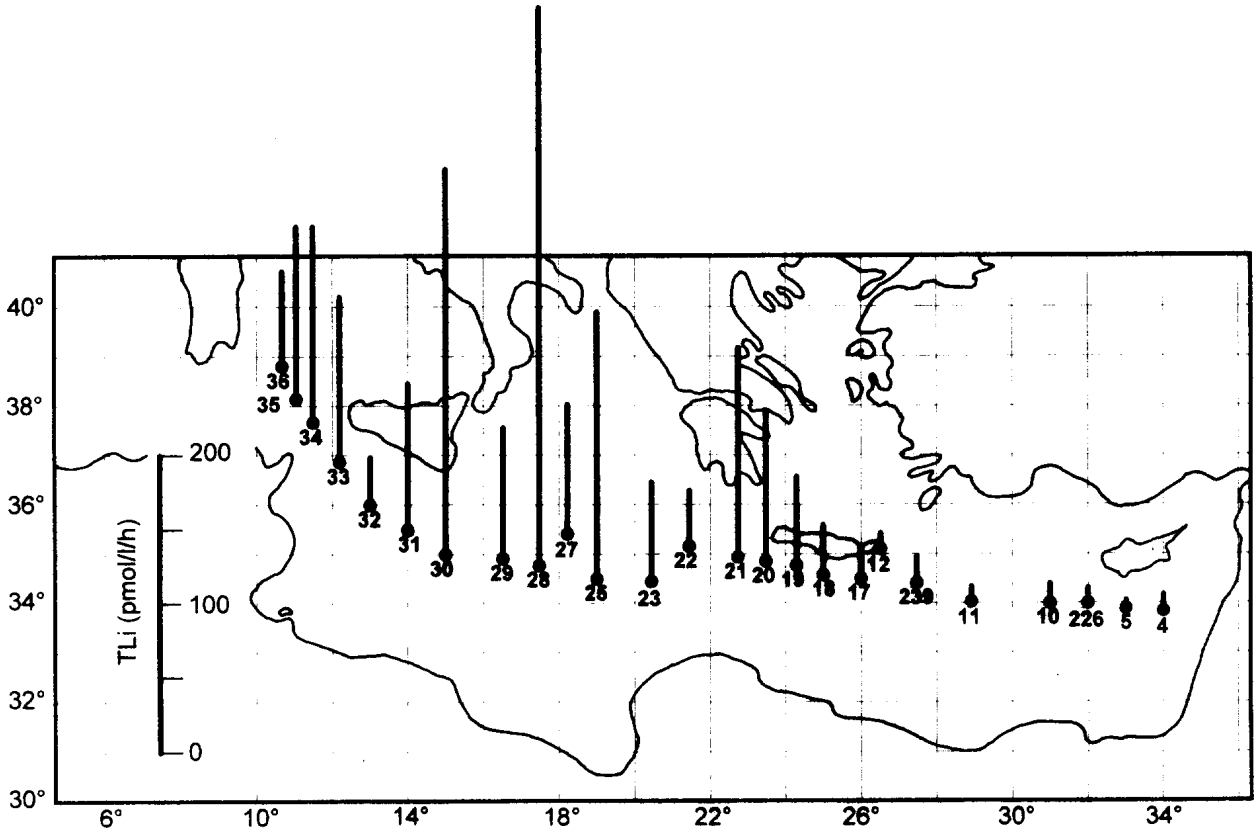

Fig. 91: Bacterial activity in the surface layer of the eastern part of the Mediterranean Sea.

5.4.6 Ultraplankton

(E. Montella)

Introduction and Scope

The objectives of the research are twofold, to assess (i) the concentration and fluorescence of ultraplankton (cyanobacteria,prochlorophytes and picoeukaryotes) and (ii) the concentration of heterotrophic bacteria. Samples from a diel cycle will be analysed to determine the proportion of cells of the different groups which are at different stages of the cell cycle, in order to estimate in situ growth rates. Samples were taken from the whole euphotic zone, since ultraplankton is known to develop at very low light levels. In the oligotrophic Mediterranean, ultraplankton often contributes significatively to the observed deep fluorescence maximum.

Material and Methods

Sea water samples were collected from Niskin bottles closed in the euphotic zone until a depth of 250 m. The sampling depths were chosen according to the continuous fluorescence profile from the CTD. In detail, samples were taken at the depths of maximum fluorescence as well as 10 m above and 10 m below. Additional samples were collected at standard depths starting from the surface down to 250 m (Table 24). Subsequentely, 2 ml of water were split into two cryovials containing paraformaldehyde and glutaraldehyde to obtain a final concentration of 1% paraformaldehyde and 0.05% glutaraldehyde. Vials were immediately immersed and stored in liquid nitrogen. They will be analysed in the Laboratory of Biological Oceanography of the Stazione Zoologica „A.Dohrn“, 80121 Naples, by Raffaella Casotti with a BECTON-DICKINSON FACSCALIBUR flow cytometer. One replicate will be run unstained in order to asses the concentration and fluorescence of ultraplankton (cyanobacteria, prochlorophytes and picoeukaryotes). The second will be stained with the fluorescent DNA marker SYBR Green II in order to assess the concentration of heterotrophic bacteria.

Water samples were collected at 35 stations obtaining 22 samples from each station (two for each Niskin bottle). At station 219 a special 26 hours experiment consisting of 10 casts was conducted to follow a daily cycle. Sampling was performed every 3 hours.

5.4.7 Genesis of Aggregates and Structure, Function and Ecology of Protozooplankton in the Oligotrophic Eastern Mediterranean Sea

(H. Zimmermann-Timm, H. Weikert)

Introduction

Planktonic protozoans constitute an important part of the microbial food web (POMEROY, 1974, AZAM ET AL., 1983) and play two principal roles in the aquatic system. They are the intermediate organisms that link phytoplankton and bacteria with higher trophic levels (VERITY, 1991), and they are important sources of remineralised nutrients (CARON, 1991). However, the information about the microbial community and their importance in the pelagic food web in the oligotrophic warm marine environment with high water temperature and high rates of irradiation is very scarce (GOCKE AND KOPPE, 1994, HAUSMANN ET AL., 1994, HAUSMANN ET AL., 1999, LENZ ET AL., 1994).

Aggregates are of special interest for the enrichment of microbial populations in oligotrophic systems since they are nutrient reach environments or „hot spots“ of the microbial life (CARON ET AL., 1986). They are ubiquitous in aquatic environments (SUZUKI AND KATO, 1957) and their size ranges from a few micrometer to many centimeters, depending on the environment in which they

Tab. 24: Stations of ultraplankton sampling.

Station No.	Depths of Sampling (m)	No. of Depths
216	250/200/150/130/120/110/100/80/60/50/30/20/10/0	14
217	250/210/200/190/150/110/100/90/50/10/0	11
219-01	150/130/120/110/80/50/30/15/0	09
219-02	150/125/115/105/80/50/30/15/0	09
219-03	150/120/110/100/80/50/30/15/0	09
219-04	150/135/125/110/100/90/70/50/30/15/0	11
219-05	150/130/120/110/80/50/30/10/0	09
219-06	150/130/120/110/80/50/30/15/0	09
219-07	200/190/180/150/130/120/110/80/50/30/5	11
219-08	200/190/180/175/150/140/120/100/80/50/30/15/5	13
219-09	200/180/150/130/110/90/50/30/15/5	09
219-10	250/230/210/200/180/150/120/100/80/50/40/15/5	13
233	200/160/150/140/110/100/90/50/30/10/0	11
234	200/170/140/130/115/100/75/50/30/10/0	11
235	200/180/150/120/100/85/70/60/30/10/0	11
236	200/180/150/125/115/105/90/50/30/10/0	11
237	200/185/170/140/130/120/80/40/10/0	10
238	250/220/200/160/140/120/100/90/50/10/0	11
239	250/230/200/170/150/130/120/100/90/80/50/30/10/0	14
241	250/220/200/150/130/120/110/90/60/40/20/0	12
246	200/150/130/115/105/95/50/30/10/0	10
247	300/250/200/170/150/130/105/95/85/40/10/0	12
248	200/185/175/165/130/110/100/90/60/30/10/0	12
249	250/200/150/120/110/100/90/60/30/10/0	11
250	250/200/150/120/105/95/85/60/30/10/0	11
251	200/150/120/100/90/80/70/50/30/10/0	11
281	200/150/130/120/110/80/50/30/10/0	10
287	200/175/150/130/105/95/85/50/30/10/0	11

occur, their composition and the shere forces which determine aggregate formation (Alldredge and Silver, 1988). Many investigations about possible causes and consequences of „marine snow“ exist for a shallow ecosystem in the Adriatic Sea (Bochdansky and Herndl, 1992a, 1992b, Herndl, 1988, 1992, HerndL and Peduzzi, 1988, Müller-Nicklas et al., 1994). There is, however, little information about aggregates in other basins of the oligotrophic Eastern Mediteranean Sea, and no micro- and macroaggregates were observed during the cruise.

Main Objectives

In an experiment the mechanisms of the genesis of aggregates in the oligotrophic environment were tested. The main objectives during Meteor cruise 44/4 were:

- Protozoan diversity in the water column and comparison of these spring data with other protozoan data from the Mediterranean Sea,
- Protozoan abundances in the water column and comparison of these spring data with other protozoan data from the Mediterranean Sea,
- Comparision of protozoan communities at different stations in the Levantine Sea,
- Protozoan grazing on microbial food web components,
- Interactions between planktonic protozoans and metazoans,
- Genesis of aggregates.

Material and Methods

Protozoan diversity and abundances in the water columns will be examined in samples from 18 stations in the Eastern Mediterranean Sea (station 216, 219 [south west off Cyprus], 234, 236, 239, 243, 249, 254 [Ierapetra Basin], 281, 291, 294 [Urania Basin], 295, 300, 303, 306, 307, 308, 310; for positions cf. station list). At each station, a depth-profile of 12 samples was taken with the rosette water sampler fitted with 24 10- or 12-l-Niskin bottles. 500 ml of each sample were fixed in 1.5 % formaldeyhd, 500 ml with Bouin's fixative (Lynn, 1992) and 200 ml were used for life examinations.

Protozoan diversity

In order to describe the protozoan diversity three different methods will be employed: life observations for ciliates and flagellates, observation of fixed samples with phase- and Normarski optics or epifluorescence microscopy and use of special staining methods (see Zimmermann-Timm, 1999) and determing cells under the phase- and Normarski optics.

- Life observations: A few ml water were given on a slide. An Olympus microscope with phase contrast and Normarski optics allowed the investigation of specimens.
- Observations of fixed samples: A few ml of water, fixed with Bouin's fixative, were given on a slide and observed with an Olympus microscope with phase contrast and Normarski optics.
- Exact species determinations with the Bouin's fixative will be done later, after using special staining techniques (see Zimmermann-Timm, 1999).

Protozoan abundance

- Ciliates: Samples of 0.01 l, fixed with the Bouin's fixative, will be allowed to settle for 24 h; then the entire surface of the settling chamber will be examind at 200 x magnification (Utermöhl, 1958). Ciliates will be determined in most cases to the level of genus and sorted according to their size groups.
- Flagellates: Samples for determination of flagellate abundance, fixed with formalin, will be stained with the fluorochrome, 4'6-diamidino-2-phenylindole (DAPI), according to Porter and Feig (1980) and counted under an epifluorescence microscope.

Tab. 25: Aggregate and microbial food web sampling with the CTD/Rosette assambly.

Station No	Date 1999	Time (UTC)	GPS Latitude (°N)	GPS Longitude (°E)	Water Depth [m]	Sampled Depths [m]
216	10.04.	21:25	32°49.97‘	33° 09.92‘	1397	10/50/100/150/250/400/600 800/1000/1200/1300/1390
219	12.04.	05:00	34° 07.92‘	31° 55.76‘	2475	10/100/200/250/300/500/750 1000/1300/2000/2300/2500
234	17.04.	14:43	35° 16.01‘	31° 05.99‘	2477	10/50/75/100/130/300/600 900/1300/1700/2100/2250
236	18.04.	03:00	33° 57.99‘	31° 12.00‘	2494	10/30/115/150/400/700/900 1300/1700/2100/2460/2519
239	19.04.	02:00	34° 19.86‘	27° 30.15‘	2583	10/75/130/150/300/600/900
239	19.04.	03:35	34° 20.00‘	27° 30.00‘	2580	1200/1500/2000/2500/2610
243	20.04.	05:27	35° 05.54‘	26° 34.98‘	971	10/60/100/150/200/230/330 350/370/500/700/970
249	21.04.	18:00	32° 42.96‘	25° 39.97‘	2517	10/100/200/350/500/900/1100 1300/1700/2100/2300/2554
254	22.04.	23:11	34° 25.47‘	26° 05.39‘	4261	10/50/100/200/500/1000/1500 2000/2500/3000/3985/4250
281	02.05.	08:50	35°10.08‘	27°29.99‘	1361	10/50/110/150/200/250/400 600/800/1100/1125
291	05.05.	17:32	34°50.06‘	23°25.00‘	2850	10/50/100/200/400/80071000 1500/200072650/2760/2830
294	07.05.	04:42	35°13.77‘	21°28.75‘	3440	10/50/100/150/200/250/300 400/500/600/700/800/1000 1250/1500/2000/2250/2500 2750/3000/3400/3440
295	08.05.	15:01	34°25.00‘	20°20.15‘	2671	10/50/100/200/400/500/900 1500/2000/2500/2650/2700
300	09.05.	21:22	34°30.02‘	18°59.98‘	3785	10/50/90/300/500/1000/1550 2150/2750/3250/3700/3765
303	10.05.	22:05	34°45.00‘	17°29.98‘	3067	10/50/105/200/300/600/1000 1500/2000/2500/3000/3066
306	11.05.	14.26	35° 59.98‘	14°59.97‘	508	0/10/50/90/110/140/180/200 250/300/400/460
307	12.05.	01:00	35° 59.95‘	12° 59.87‘	1013	10/60/70/100/200/220/300 450/650/850/950/1000
308	12.05.	13:10	37° 34.05‘	11°32.02‘	770	10/30/50/100/150/250/300 400/500/600/700/750
310	13.05.	03:10	39°00.00‘	10°30.00‘	2667	10/55/90/110/300/600/900 1500/2000/2400/2600/2666

Comparision of protozoan communities in defined water masses at different stations
Considering other abiotic and biotic parameters such as temperature, salimity, oxygen, chlorophyll *a*, bacteria and metazooplankton abundance this analysis will be done after qualitative and quantitative examinations of the protozooplankton.

Protozoan grazing on microbial food web components
Protozoan grazing was measured in short-term direct-uptake experiments on fluorescently labelled particles (FLP, Zimmermann-Timm and Barkmann, submitted) at two different stations (SE off Cyprus, station 219 and Ierapetra Basin, station 254). Grazing experiments were performed on each sampling date using 100 ml of a sample in 250 ml acid - washed glass bottles. Two sets of experiments were carried out to calculate selectivity independently for FLP’s. To calculate ingestion rates prefiltered sea water was enriched with fluorescently stained particles. After the samples had been allowed a 15 min adaption period at *in situ* temperature, food was added at a concentration of 30 % of the natural abundance of picoplankton. Subsamples of 0.005 l were taken after 5, 10, 20, 30, 40, 50 and 60 min and fixed in alkaline Lugol’s solution (0.5 % final concentration) and placed in borate buffered formalin, previously filtered through a 0.2 mm membrane at a final concentration

of 3 %. Subsamples will be stained with DAPI, filtered through a 1 mm black filter from Poretics and examind using an epifluorescence microscope. About 50 ciliates will be checked for tracer uptake in each sample. As a measure of seletivity between the different kinds of food, we will choose the relative difference in the mortality rates of two kinds of prey according to Jacobs (1974). Besides this, feeding rates and clearance rates will be calculated (Peters, 1984).

Interactions between planktonic protozoans and metazoans in the food web

To study the growth rates, grazing impact, and energy fluxes from the picoplankton to the metazoans, the size fractionation technique (Arndt, 1990, Landry, 1994, Zimmermann, 1996) was used at two different stations (SW off Cyprus, station 219 and Ierapetra Basin, station 254). To separate the species at the higher trophic levels in the plankton, the water was filtered through 150, 44 and 15 mm sieves. Filtered and unfiltered water (UF) as well as water enriched with zooplankton (3 x 1 litres $\geq$ 150 mm and unfiltered water, ZP) was placed in 1 l glass bottles. All procedures were performed on triplicate samples. The bottles were exposed on a rotating wheel under ambient conditions. Abundance and biomass of the autotrophic picoplankton (APP), bacteria, algae and protozoa were detemined at the beginning of the experiment and after incubation periods of 12, 24 and 48 h. The protozoa were separated into several groups: nanoflagellates (NF), flagellates smaller than 20 mm, large heterotrophic flagellates (LF), ciliates smaller than 20 mm (NC), and ciliates larger than 20 mm (LC). Metazoans were counted at the start and at the end of the experiments. The phytoplankton and ciliates will be identified in samples fixed in Lugol's solution as desribed above. The abundance of bacteria, APP and NF will be determined after staining with DAPI on black membrane filters under the epifluorescence microscope (Porter and Feig, 1980). Metazoans will be determined under an inverted microscope. The size of the bacteria, APP and NF will be measured using an image analysis system. The sizes of the algae and ciliates will be measured under the microscope, and the volume will be calculated using appropriate formulas (Padisák and Adrian, 1999). Crustacean abundance will be converted to biomass according to known relationhips between body length and dry weight. The number of cells and their biovolume will be used to calculate the amount of carbon using the following conversion factors: for bacteria 15 fg C $cell^{-1}$ (Simon and Tilzer, 1987), NF 220 fg C mm^{-3} (Børsheim and Bratbak, 1987), ciliates 110 fg C m^{-3} (Turley et al., 1986) and metazoans (Cushing et al., 1958). For a rough calculation of total phytoplankton, chlorophyll *a* values will be converted to C, assuming a C : Chlorophyll *a* ratio of 25 : 1 (Bell and Kuparinen, 1984). Protozoan production will be estimated from the mean cell concentrations and the calculated size specific growth rates. The production of metazooplankton will be derived from the calculated community ingestion rates, assuming a growth efficiency of 25 % (Bosselmann and Riemann, 1986). To determine the food supply of the protozoa, their ingestion rates were calculated, assuming that 200 % of the body weight per day must be ingested by individuals in the size class from 5 to 50 x 103 mm^{-3}, when their production efficiency is 50 %. An ingestion rate greater than 300 % of the body weight is assumed for smaller individuals, and 150 % for larger ones (Laybourn-Parry, 1984).

Genesis of aggregates

Aggregates were produced in the laboratory from natural water at three different stations. Each experiment was carried out over a period of 48 h. The environmental temperature and illumination at each station was maintained in a climate room. Water for the laboratory experiment was taken at the surface using a bucket. Within an hour after collection, the water was delivered to the laboratory

and unfiltered water (UF) and water enriched with metazooplankton (3 x 1 l ≥ 150 mm and unfiltered water, ZP) was placed in sterile 1 l screw-cap glass bottles. Three replicates were made. Aggregates were generated using a rotating wheel. They were rolled at 2.50 r.p.m. Samples were taken at 12 hours intervals in order to determine aggregate abundance and volume. At the begin and at the end of the experiment zooplankton abundance was determined. To characterise the colonization single aggregates were collected using a narrow Pasteur pipette and observed under the microscope. Single aggregates were also fixed with formaldehyd in vials at an 8 % final concentration (Wörner et al. submitted) to characterise their content using different staining techniques under a light microscope (Zimmermann-Timm, 1999).

First Results

I. Exact determinations of the protozoans will be done later, using on protargol stained material prepared in the laboratory.

It was visible that the protozoan community was represented by auto- and heterotrophic flagellates, by rhizopds and by ciliates. *Mesodinium rubrum*, a mixotrophic ciliate, was present at all station, but mostly in low concentrations. Other mixotrophic ciliates, until now not qualitatively characterised, harbouring incorporated chloroplasts, were also present. The most important group with a pronounced peak at the depth of the deep chlorophyll maximum were the heterotrohic oligotrichs. Tintinnids which were the only well-preserving specimens because of their lorica, were only of minor importance (see also Lenz et al., 1994).

Bacteria grazing species like some flagellates, small-sized amoebae and ciliates were observed. Predatory activities against bacterial feeders were not visible till now (see Hausmann et al., 1994). Algae ingesting protozoa were represented by the ciliate *Chilodonella* sp. and the rhizopod *Hyalodiscus* sp.. As described in Hausmann et al. (1994), numbers of species and abundance of individuals decreased with increasing depth. In general, only a few individuals have been found in the fresh samples. But at depths below 4000 m and in the presence of resuspended organic matter, a high protozoan activity was observed during this cruise. Exact abundances will be determined in the laboratory.

It has to be taken into account, that a certain amount of organisms is not able to survive after sampling for a longer period of time. Normally those protozoa died during the first 60 minutes after the beginning of the observations, in all, likelihood due to the pressure change as well as the strong illumination for microscopy rather than due to the temperature difference between the water and the labortory.

Experiments about the importance of protozoans in the microbial food web were done successfully, detailed results will follow after further analysis in the laboratory.

II. Experiments about the genesis of the aggegates showed, that micro- and macroaggregates were prepared after one day if higher concentrations of metazooplankton were present. The importance of their motility, excretion products etc has now to be examined in detailed studies in the lab.

5.4.8 Copepod Gut Fluorescence and Egg Production Rates

(S. Zervoudaki)

Introduction and Scope

A common and increasingly popular approach for the estimation of ingestion rates of herbivores and predators is based on use of gut contents and estimated gut passages times. The instantaneous gut content of an animal is a function of its ingestion rate, its gut evacuation rate and the amount of food destroyed or undedected in the gut. The ingestion rate (amount of food animal^{-1}.time^{-1}) is given by the product of the gut content (amount of food animal^{-1}) and the gut evacuation rate constant which is reciprocal of gut passage time.

Over the past decade the gut fluorescence method has frequently been used to investigate herbivorous feeding by copepods. The method makes use of the fact that copepods convert chlorophyll a into a-type phaeopigments during digestion, so that concentrations of phaeopigments in copepods' guts are taken to be indices of levels of feeding activity. The major objective of this study is to estimate the ingestion rates of dominant copepods of the epipelagic and mesopelagic layers and their relative and total contribution to the grazing of primary producers in the Eastern Mediterranean Sea.

Material and Methods

The focus of the analysis was on three main stations in the Eastern Mediterranean Sea, situated SW off Cyprus, above the Urania Basin and above the Ierapetra-Deep. At the latter site, an extended period of 14.5 days was available for sampling. Intermediate stations were also occupied but for shorter periods. Table 26 presents the stations, the positions, the dates as well as the dominant copepod species in each sample.

Zooplankton samples for gut fluorescence were collected with a Double-Mocness (0.333 mm mesh size). Immediately after retrieval of the net, only the cod end content was sieved through a 0.200 mm mesh size, stored in petri dishes and frozen (-20^{o}C). These treatments were performed with minimal light exposure in order not to affect the pigments measurements.

The gut fluorescence analyses included picking a number of 10-30 individuals of selected copepod species from the filters with tweezers, under a low light microscope. Extract in 90% analytical aceton will be measured for fluoroscence in a Turner fluorometer in the home lab, before and after acidification. Results will be expressed as the sum of chlorophyll and phaeopigments (as chlorophyll *a* equivalents).

During the cruise, we also attempted to estimate the production of the copepod community. This study was carried out at the three main stations (Table 27) where at one of them (Ierapetra Basin) eight experiments were performed. Copepod egg production rates were determined by bottle incubations for numerically dominant calanoid copepods: *Acartia sp.*, *Nannocalanus minor*, *Neocalanus gracilis*, *Centropages violaceus*, *Lucicutia sp*.. Copepods were collected with a 0.300 mm mesh-size net with oblique haul from 30 m depth until the surface. Adult females were removed and incubated for 24h in 500 ml screwcap bottles. Three to eight bottles, each containing 3-5 females were set up for each species. Photoperiod and temperature were kept similar to field conditions. The incubation medium was 0.060 mm screened surface water.

Tab. 26 : Copepod gut fluorescence information.

Sample no 1

Date	Station	Position	Net	Depth (m)	Time
13/4/99	220	34°05.10N 32°10.20E-	MOC-D-03	450-0	13.15
		34°04.80N 31°59.87E	0.333 mm		

Dominant copepod species:

Neocalanus gracilis, Mesocalanus tenuicornis, Pleuromamma gracilis, Pleuromamma abdominalis, Lucicutia flavicornis, Lucicutia gemina, Lucicutia clausi, Lucicutia ovalis, Eucalanus monachus, Clausocalanus furcatus, Clausocalanus parapergens, Clausocalanus pergens (paululus), Oncaea sp., Corycaeus sp..

Sample no 2

Date	Station	Position	Net	Depth (m)	Time
14/4/99	220	34°04.50N 31°48.40E-	MOC-D-05	450-0	15.30
		33°57.12N 31°50.21E	0.333 mm		

Dominant copepod species:

Neocalanus gracilis, Mesocalanus tenuicornis, Haloptilus longicornis, Pleuromamma gracilis, Pleuromamma abdominalis, Lucicutia flavicornis, Lucicutia gemina, Lucicutia clausi, Lucicutia ovalis, Eucalanus monachus, Clausocalanus furcatus, Clausocalanus parapergens, Clausocalanus pergens (paululus), Oncaea sp., Corycaeus sp..

Sample no 3

Date	Station	Position	Net	Depth (m)	Time
14/4/99	220	33°57.00N 31°50.10E-	MOC-D-06	450-0	23.15
		33°48.53N 31°42.66E	0.333 mm		

Dominant copepod species:

Neocalanus gracilis, Haloptilus longicornis, Pleuromamma gracilis, Pleuromamma abdominalis, Lucicutia flavicornis, Lucicutia gemina, Lucicutia clausi, Lucicutia ovalis, Eucalanus monachus, Clausocalanus furcatus, Clausocalanus parapergens, Clausocalanus pergens (paululus), Oithona plumifera (setigera), Oncaea sp., Corycaeus sp., Euchaeta sp., Euaetideus giesbrechti.

Tab. 26 : continued

Sample no 4

Date	Station	Position	Net	Depth (m)	Time
19/4/99	239	34°23.76N 27°26.19E-	MOC-D-09	450-0	12.00
		34°25.13N 27°25.13E	0.333 mm		

Dominant copepod species:

Haloptilus longicornis, Neocalanus gracilis, Eucalanus monachus, Clausocalanus sp., Oithona plumifera (setigera), Scaphocalanus sp., Lucicutia flavicornis, Lucicutia gemina, Lucicutia clausi, Lucicutia ovalis, Scolesithricella sp., Pleuromamma gracilis, Pleuromamma abdominalis, Oncaea sp., Corycaeus sp., Euchaeta sp., Euaetideus giesbrechti.

Sample no 5

Date	Station	Position	Net	Depth (m)	Time
20/4/99	242	35°03.13N 26°48.57E-	MOC-D-11	450-0	06.00
		35°03.65N 26°47.10E	0.333 mm		

Dominant copepod species:

Haloptilus longicornis, Neocalanus gracilis, Eucalanus monachus, Clausocalanus sp., Oithona plumifera (setigera), Scaphocalanus sp., Temora stylifera, Lucicutia flavicornis, Lucicutia gemina, Lucicutia clausi, Lucicutia ovalis, Scolesithricella sp., Pleuromamma gracilis, Pleuromamma abdominalis, Oncaea sp., Corycaeus sp., Euchaeta sp., Euaetideus giesbrechti.

Sample no 6

Date	Station	Position	Net	Depth (m)	Time
22/4/99	249	32°51.0N 25°38.2E	MOC-D-13	900-0	03.15
			0.333 mm		

Dominant copepod species:

Eucalanus monachus, Haloptilus longicornis, Neocalanus gracilis, Mesocalanus tenuicornis, Oithona plumifera (setigera), Clausocalanus sp., Lucicutia gemina, Lucicutia flavicornis, Lucicutia ovalis, Acartia sp., Spinocalanus sp., Pleuromamma gracilis, Pleuromamma abdominalis, Scolesithricella sp., Scaphocalanus sp..

Tab. 26 : continued

Sample no 7

Date	Station	Position	Net	Depth (m)	Time
27/4/99	268	34°30.52N 26°08.83E-	MOC-D-17	450-0	15.30
	Ierapetra	34°29.15N 26°08.40E	0.333 mm		

Dominant copepod species:

Haloptilus longicornis, Eucalanus monachus, E. crassus, E. elongatus, Neocalanus gracilis, Mesocalanus tenuicornis, Nanocalanus minor, Oithona plumifera (setigera), Clausocalanus lividus, C.furcatus, Lucicutia gemina, Lucicutia flavicornis, Lucicutia ovalis, Lucicutia clausi, Acartia sp., Spinocalanus sp., Pleuromamma gracilis, Pleuromamma abdominalis, Scolesithricella sp., Scaphocalanus sp..

Sample no 8

Date	Station	Position	Net	Depth (m)	Time
29/4/99	272	34°25.53N 26°05.13E-	MOC-D-21	450-0	02.00
	Ierapetra	34°25.55N 26°07.45E	0.333 mm		

Dominant copepod species:

Haloptilus longicornis, Eucalanus monachus, E. crassus, E. elongatus, Neocalanus gracilis, Mesocalanus tenuicornis, Nanocalanus minor, Oithona plumifera (setigera), Clausocalanus lividus, C.furcatus, Lucicutia gemina, Lucicutia flavicornis, Lucicutia ovalis, Lucicutia clausi, Acartia sp., Temora sp., Centropages violaceus, Spinocalanus sp., Pleuromamma gracilis, Pleuromamma abdominalis, Scolesithricella sp., Scaphocalanus sp..

Sample no 9

Date	Station	Position	Net	Depth (m)	Time
29/4/99	273	34°28.95N 26°12.81E-	MOC-D-22	450-0	12.15
	Ierapetra	34°29.63N 26°14.28E	0.333 mm		

Dominant copepod species:

Haloptilus longicornis, Eucalanus monachus, E. crassus, E. elongatus, Neocalanus gracilis, Mesocalanus tenuicornis, Nanocalanus minor, Oithona plumifera (setigera), Clausocalanus lividus, C.furcatus, Lucicutia gemina, Lucicutia flavicornis, Lucicutia ovalis, Lucicutia clausi, Acartia sp., Temora sp., Centropages violaceus, Spinocalanus sp., Pleuromamma gracilis, Pleuromamma abdominalis, Scolesithricella sp., Scaphocalanus sp..

Tab. 26 : continued

Sample no 10

Date	Station	Position	Net	Depth (m)	Time
2/5/99	280	34°25.69N 26°05.49E-	MOC-D-24	450-0	01.00
	Ierapetra	34°24.92N 26°03.48E	0.333 mm		

Dominant copepod species:

Haloptilus longicornis, Eucalanus monachus, E. crassus, E. elongatus, Neocalanus gracilis, Mesocalanus tenuicornis, Nanocalanus minor, Oithona plumifera (setigera), Clausocalanus lividus, C.furcatus, Lucicutia gemina, Lucicutia flavicornis, Lucicutia ovalis, Lucicutia clausi, Acartia sp., Temora sp., Centropages violaceus, Spinocalanus sp., Pleuromamma gracilis, Pleuromamma abdominalis, Scolesithricella sp., Scaphocalanus sp..

Sample no 11

Date	Station	Position	Net	Depth (m)	Time
2/5/99	281	35°10.69N 27°21.02E-	MOC-D-25	300-0	15.30
		35°10.18N 27°19.98E	0.333 mm		

Dominant copepod species:

Temora sp., Haloptilus longicornis, Oithona plumifera (setigera), Acartia sp., Neocalanus gracilis, Calocalanus pavo, Calocalanus sp., Clausocalanus sp., Lucicutia flavicornis, L. gemina, Eucalanus monachus, E. attenuatus, Mecynocera clausi, Centropages violaceus, Sapphirina sp., Corycaeus sp., Scaphocalanus sp., Oncaea sp., Euaetideus giesbrechtii.

Preliminary Results

The first results on calanoid copepod egg production are shown in Figures 92-97. Above the Ierapetra Basin, during the eight days experiments, the mean values of egg production of Acartia sp. ranged between 3.5-6.8 eggs/female/day (Fig. 92). Similar mean values (Fig.93) were abtained for Nannocalanus minor (3.5-6.5 eggs/female/day). For Neocalanus gracilis (Fig.94) the experiment was run only three days, and the egg production rate varied from 2.8 to 7.2 eggs/female/day. Centropages violaceus (Fig.95) was dominant in the samples only the 4th and 5th days, and it presented higher egg production rates than the previous species (7.4-21.5 eggs/female/day). On the last day, Lucicutia sp. was dominant, too. Also this copepod presented a high egg production rate (21.9 eggs/female/day). Figure 96 presents the mean values of the dominant copepods egg production in the Ierapetra Basin. Figure 97 shows the mean values of the Acartia sp. at all the stations. The maximum mean value of egg production was observed at station St. 296 whereas the minimum value was noticed at the station above the Urania Basin.

Tab. 27: Copepod egg production.

Experiment No	Date 1999	Station	Depth (m), Oblique haul	Species
01	22-23.04.	Ierapetra Basin	0-30	*Acartia sp.*
02	24-25.04	Ierapetra Basin	0-30	*Acartia sp.*
03	25-26.04.	Ierapetra Basin	0-30	*Nannocalanus minor*
04	26-27.05.	Ierapetra Basin	0-30	*Acartia sp., Nannocalanus minor, Centropages violaceus*
05	28-29.04.	Ierapetra Basin	0-30	*Acartia sp., Centropages violaceus*
06	29-30.04.	Ierapetra Basin	0-30	*Acartia sp., Nannocalanus minor, Neocalanus gracilis*
07	01-02.05.	Ierapetra Basin	0-30	*Acartia sp., Nannocalanus minor, Neocalanus gracilis*
08	04-05.05.	Ierapetra Basin	0-30	*Neocalanus gracilis, Nannocalanus minor, Acartia sp., Lucicutia sp.*
09	06-07.05.	Urania Deep	0-30	*Acartia sp.*
10	09-10.05.	296 (off Libya)	0-30	*Acartia sp., Nannocalanus minor, Centropages typicus*
11	11-12.05.	304	0-30	*Centropages typicus*

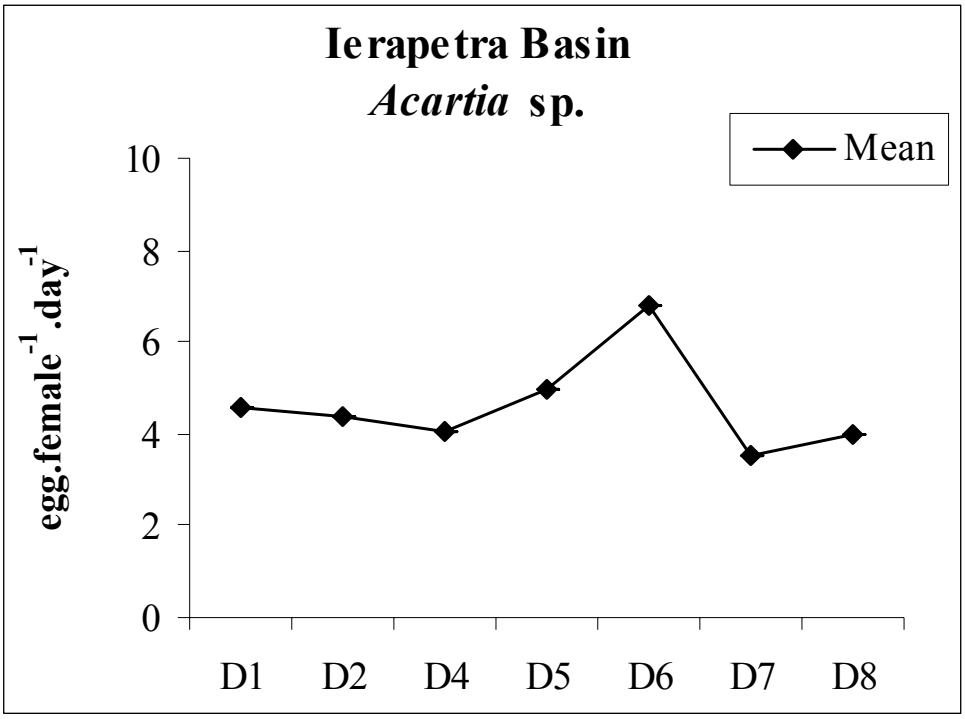

Fig. 92: Mean values of *Acartia sp.* egg production in the Ierapetra Basin.

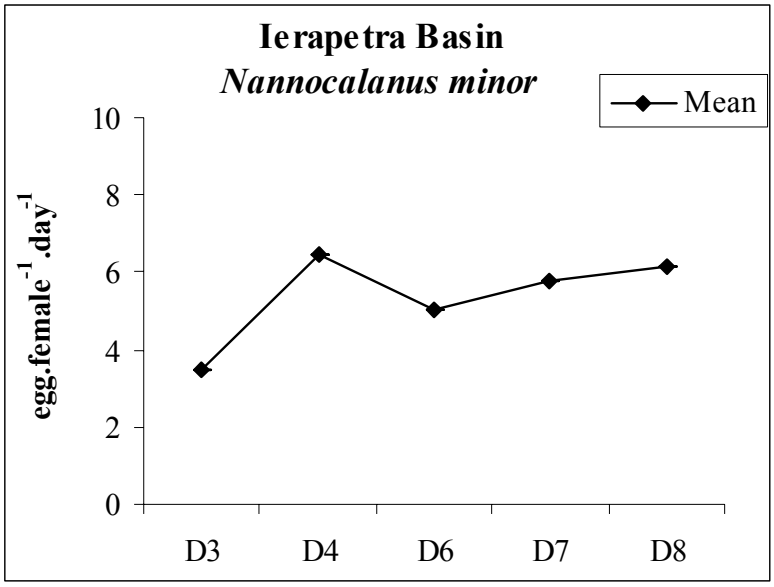

Fig. 93: Mean values of *Nannocalanus minor* egg production in the Ierapetra Basin.

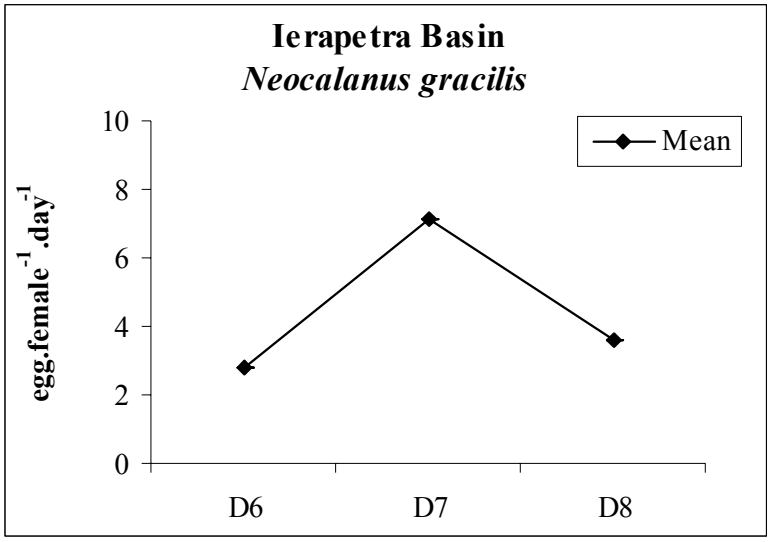

Fig. 94: Mean values of *Neocalanus gracilis* egg production in the Ierapetra Basin.

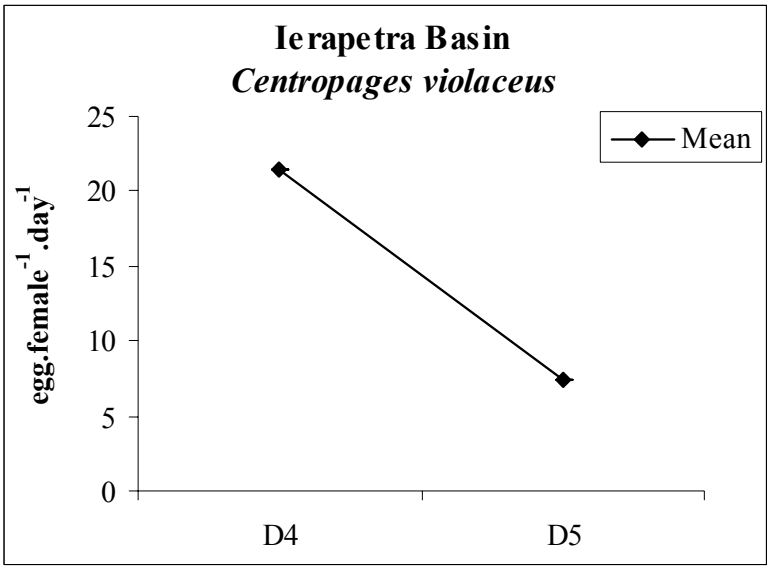

Fig. 95: Mean values of *Centropages violaceus* egg production in the Ierapetra Basin.

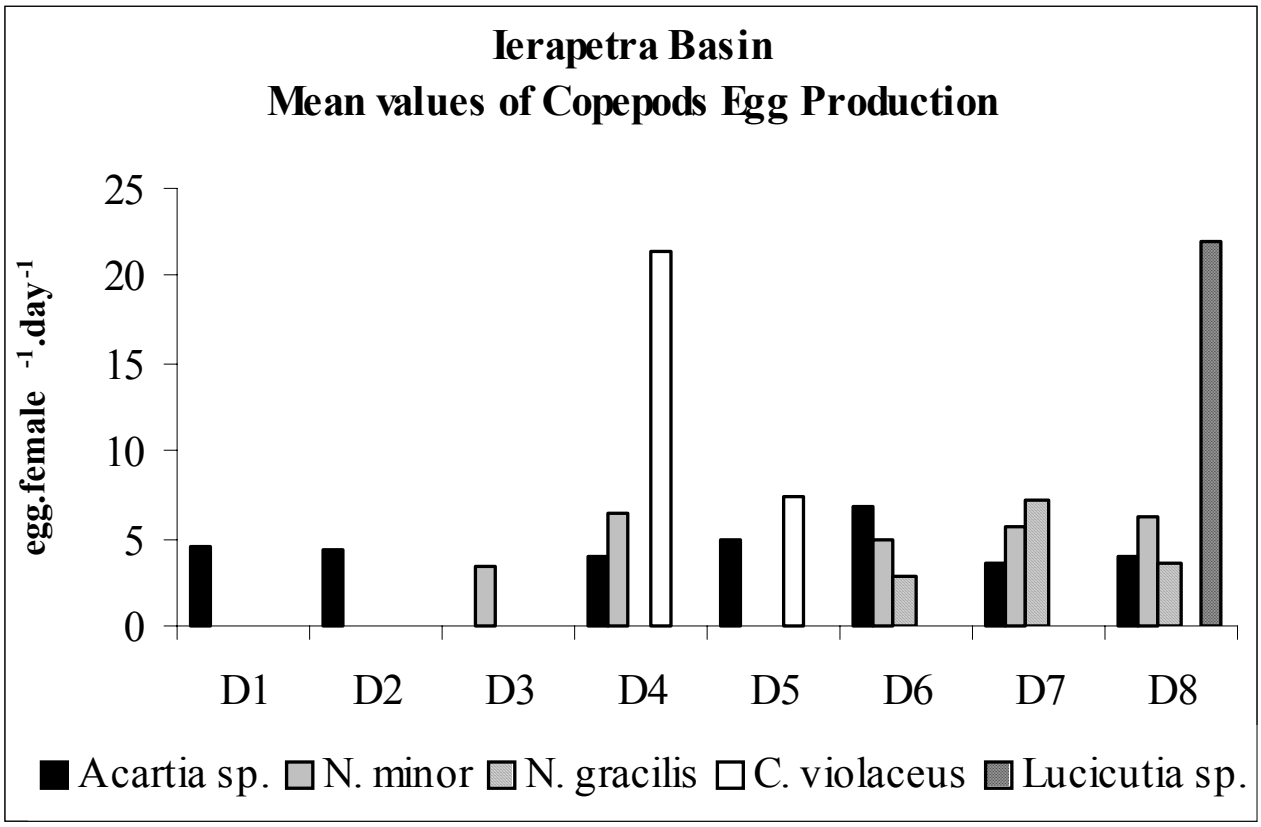

Fig. 96: Mean values of copepod egg production during the eight days experiments in the Ierapetra Basin.

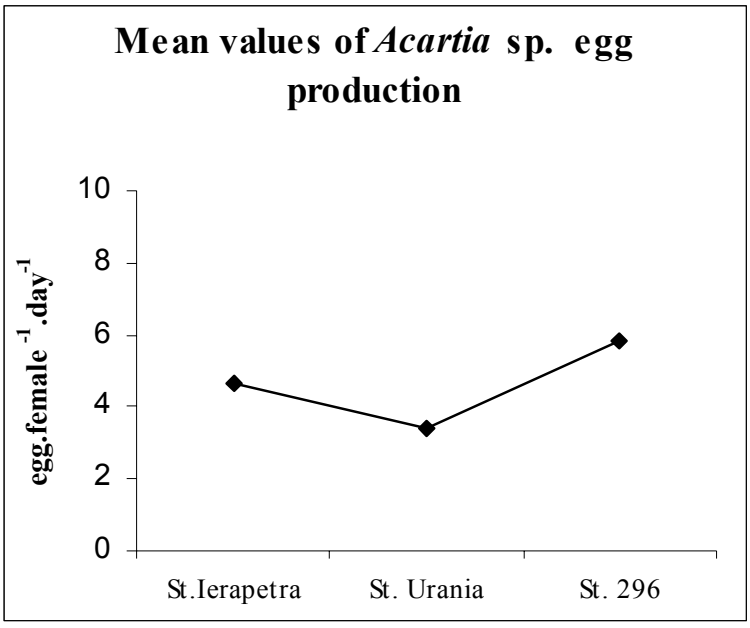

Fig. 97: Mean values of *Acartia sp.* egg production in the three stations.

5.4.9 Changes in Deep-Sea Zooplankton and Micronekton

(H. Weikert, M. Abel, B. Blume, H. Fabian, R. Gollembiewsky, S. Grabbert
R. Koppelmann, L. Neugebohrn, V. Miske, H. Zimmermann-Timm)

Introduction

The traditional view that the deep-sea communities are constant in their abundances and species composition has been challenged in the last two decades. In the NE-Atlantic, spring bloom settlements have been documented to produce significant changes in the abundance and structure of the benthic community (GOODAY AND TURLEY, 1990), particularly its microbial component (LOCHTE AND TURLEY, 1988). A respective response of bathypelagic zooplankton has been reported recently (KOPPELMANN AND WEIKERT, 1999). Changes over long periods were revealed by the European (MAST III) funded project BENGAL (High resolution temporal and spatial study of the BENthic biology and Geochemistry of a north-eastern Atlantic abyssal Locality). The significant increase in the abundance of the benthic invertebrate megafauna and in a number of its species at a depth of nearly 5000 m in the NE-Atlantic (Final BENGAL report, 1999) may be stochastic or more likely, linked with pulses of food supply, which, however, show a high inter-annual variability.

While the causes of this long-term variability in the NE-Atlantic are unknown, the conspicuous faunal alterations in the Levantine Basin of the Eastern Mediterranean can be analysed on the sound knowledge of the Eastern Mediterranean Transient which has been triggered by the Aegean deep-water inflow since about 1990 (ROETHER ET AL., 1996; KLEIN ET AL., 1999). Also in contrast to the situation in the Atlantic, the change in the Levantine Sea is most obvious in the deep-sea zooplankton (WEIKERT, 1995). A dramatic increase of organisms below 1000 m by two orders of magnitude in both numbers and biomass were detected down to 4300 m by comparison of samples which were collected in January 1987 and June 1993 using identical methods. Two calanoid copepods carried the transformation: *Eucalanus monachus* and *Calanus helgolandicus*, the latter was reported for the first time in the western Levantine Sea. First results from repeated sampling in January 1998 confirm this long-term faunal shift. However similar to the NE-Atlantic, the shift appears to be overlain by a high seasonal variability in abundance (WEIKERT, unpublished data). This result is in concordance with findings on microbial activity and amounts of chloroplastic pigments which were increased in the deep-sea sediment in June 1993 (BOETIUS ET AL., 1996), indicating a solitary phytodetrital influx from the overlying euphotic zone.

Main objectives

The changes in the concentration, size structure and taxonomic composition as well as in the vertical distribution pattern of zooplankton imply changes in functional diversity and the modes of vertical flux. To get a first insight into these topics the program aimed at

- quantitative sampling the pelagic and near-bottom faunas to estimate their composition and standing crop,
- determinating the variability of zooplankton and micronekton on different scales in space and time,
- analysing ontogenetical and size structures,
- assessing and analysing trophic levels,
- estimating the carbon demands of the pelagic deep-sea metazoan faunas and selected components.

Material and Methods

Quantitative sampling of pelagic metazoans was performed with three types of Mocness nets (Multiple opening/closing net and environmental sensing system, Wiebe et al., 1985). Zooplankton and micronekton were collected by stratified oblique tows with the use of a 1 m^2-Double-Mocness equipped with twenty 0.333 mm-nets and a 10 m^2-Mocness with six 1.600 mm-nets, respectively, all dark coloured. The sampled standard intervals increased with depth, from 50 m in the top 450 m to a maximum spacing of 250 m at depths greater than 2250 m (Weikert, 1994). Information on depth of device, net angle, flow counts, net number, temperature and conductivity is transmitted via conducting cable to a shipboard unit and logged on to a computer. To investigate diel migrations, the hauls were intended to sample symmetrically around midday and midnight. For the collection of the benthopelagic faunas both Mocness devices were equipped with a near-bottom-echo-sounding device (altimeter, SIMRAD MESOTECH). While the 10 m^2-Mocness fished the layer 10 mab (metres above bottom) only, the 1 m^2-Double-Mocness was towed horizontally at 10 mab, 50 mab and 100 mab. For each depth layer, two consecutive nets were used and, in addition, two nets during transition between depth layers. Benthopelagic sampling was completed by horizontal tows with a supraepibenthic sledge. The device is equipped with a flow meter and five nets (mouth opening 0.8m^2, mesh size 0.333 mm). Like the Mocness, the nets can be opened and closed on command via a conducting cable. They fish consecutively a 0.5 to 1.5 m-stratum off the bottom. An epibenthic net at the rear end of the sledge catches epibenthic megafauna. The towing speed of the devices was about 2 knots.

Concomitantly to the above devices, neuston was caught with a catamaran which fished the 0-10 cm surface layer and the contiguous 15-30 cm. Additional sampling was carried out along the course track just before and/or after the CTD stations. In total, 67 pairs of samples were obtained. Net tow information on all devices employed has been listed in Tables 28 - 30.

Repeated sampling of zooplankton in fine-spaced depth intervals throughout the water column was centred at two main sites, SW off Cyprus and SE off Crete above the Ierapetra-Deep (Fig. 98). Special emphasis was given to the deep water column below 1000 m, the bathypelagic zone. Both sites had been intensively investigated during M5/1, M25/2, and M40/3. Like on these previous cruises, four full depth profiles were obtained from each site with the 1 m^2-Double-Mocness. This allows for statistical treatment of the data sets to study seasonal and long-term changes of mesozooplankton and micronekton. Two full depth profiles with the 10 m^2-Mocness above the 4300 m Ierapetra-Deep provided respective information for larger and/or rare micronekton faunas and their contribution to the monitored deep-scattering layer (33 kHz). Of the Mocness hauls (10 m^2-Mocness: 14, 1 m^2-Double-Mocness: 33) only haul no. 30 of the small-sized device failed by malfunction of 10 nets, due to inproper handling.

For the first time faunal elements living near the sediment contact zone in the deep Eastern Mediterranean could be quantitatively sampled and addressed to the pelagic realm by the use of the supraepibenthic sledge (SBT). Traditional catches by non-closing epibenthic trawls do not allow for a discrimination between metazoans living on the bottom or in the water overlying the sediment. In this respect, the SBT tows were successful, though of the five nets only the first three nets could be operated successfully except of tow no. 3 in the Ierapetra-Basin which was perfectly completed. Here, five tows were performed, but tow no. 6 failed due to problems with the deep-sea whinch (see chapter 4.4). Two tows were run SW off Cyprus.

Previous investigations in the Levantine and Ionian Seas on deep-living zooplankton have been small in scale. There has not been a study sampling on a large-scale good enough to 1) detect spatial

changes within and among subbasins of the Eastern Med and 2) set them in context with a detailled basin-wide analysis of water masses (see chapter 5.4.1). To fill this void single profiles were performed with the 1 m^2-Double-Mocness. By region, they fell into waters off Africa and Israel, which are preferred by Lessepsian immigrants (POR, 1978), and into the northern part of the aforementioned basins (Fig. 10). Here, a „cluster" of profiles, including those from above the Ierapetra-Deep, was lain south of the Caso Strait which, by its shallow sill, sets the border between the Aegean and Levantine basins. The data may provide information on the yet unknown pathways of transport of *Calanus helgolandicus*, either from the Aegean Sea or the eutrophic area of the Rhodes cyclone in the Levantine Sea.

For trophical studies, two profiles with the 1 m^2-Double-Mocness were designed partitioning the water column in the Ierapetra-Deep by parallel sampling into nine coarser depth intervals. The zooplankton was fractionated by sieves into five to six size classes which will be analysed for the stable nitrogen isotope ratio $^{15}N/^{14}N$. Additionally, individuals of common zooplankton taxa and of copepod species, separated according to their developmental stages, were selected from the above fine-spaced profiles and prepared for the determination of carbon, nitrogen and lipids.

From the fine-spaced profiles in the Ierapetra-Deep, samples were taken at defined depths (400-450 m, 1250-1450 m, 2750 m, 4250 m) for an ETS assay (WEIKERT ET AL., 1999). Due of operational reasons, the respective nets of 0.333 and 0.100 mm mesh size were towed horizontally or in an undulating manner. While the ETS activity measurements were carried out on board, related parameters of zooplankton (wet, dry and ash-free dry weight, C, N) will be determined from subsamples in the home lab. The ETSA data which were supplemented by measurements from the deep-sea sediment taken by the multiple corer will be used to estimate the carbon demands of the deep-living zooplankton and benthic communities. These data can be compared to the carbon input measured by the sediment trap at 2700 m in order to establish a balance sheet for the carbon budget of the abyssal zone.

Preliminary Results

The abundance of zooplankton increased along the transect from east to west. In accord with this trend, zooplankton was well-conditioned and owned oil droplets except at the easternmost stations off Israel and SW-Cyprus. On a subbasin-scale, the profile off Karpathos-Island in the eutrophic waters of the Rhodes cyclon was against the trend and yielded exceptionally rich samples. Along the north-south traverses, the Mocness and neuston net samples indicated increased zooplankton numbers and biomass towards the Libyan coast. Hydrographically, the stations were affected by the inflow of Atlantic Surface Water which also could be traced biologically as far as SW off Cyprus by means of the neustonic copepod *Pontella atlantica*.

Zooplankton and micronekton decreased with increasing depth. By this feature and the concentrations at any depth, the vertical profiles in April/June 1999 were similar to the patterns encountered in January 1987 and 1998, respectively. In consequence, they showed a clear contrast to the situation in June 1993, when there were high zooplankton concentrations throughout the bathypelagic zone. At all stations and depths, calanoid copepods were most numerous in the 0.333 mm-net plankton collections. No marked faunistic differences were obvious by a superficial examination, neither between the depths layers 10, 50, and 100 mab nor between these layers and samples taken in the bathypelagic zone at greater distances from the bottom. Calanoid copepods of the genus *Lucicutia*, possibly *L. longiserrata*, predominated. There was, however, a distinct faunal

change in the immediate vicinity of the sea bed. In the SBT samples, decapod crustaceans were a conspicuous micronekton element which was virtually absent at greater depths in the bathypelagic water column. Due to the large body size of the decapods, biomass of metazoans in the 0.50-1.50 m-layer appeared to be significantly increased as compared to contiguous layers.

Tab. 28: 1 m²-Double-Mocness haul information; period of quantitative interval sampling.

Haul No.	Station No.	Start Date	Start Time (UTC)	End Time (UTC)	Start Position				End Position				Water Depth (m)		Depth Range of Sampling (m)	Type	Remarks
					°N	'N	°E	'E	°N	'N	°E	'E	min.	max.			
MOC-D-01	216	10.04.99	17:09	19:18	32	53.20	33	10.19	32	57.53	33	09.75	1442	1505	1370-0	17 O	test sampling
MOC-D-02	218	11.04.99	19:58	22:46	34	02.96	31	59.72	34	07.87	31	55.89	2437	2510	1850-0	17 O	
MOC-D-03	220	13.04.99	08:27	11:07	34	05.03	32	06.16	34	04.80	31	59.87	2466	2509	1850-0	17 O	
MOC-D-04	222	14.04.99	02:12	06:10	34	05.60	31	59.08	34	05.76	31	49.70	2431	2532	10 mab-100 mab	3 HB (10 mab), 4 HB (20 mab), 2 HB (50 mab), 2 HB (100 mab), 3 O (10 mab-20 mab, 20 mab-50 mab, 50 mab-100 mab), 4 O (100 mab-0)	altimeter failed (partly no response)
MOC-D-05	223	14.04.99	10:49	13:21	34	01.99	31	48.71	33	57.12	31	50.21	2486	2663	1850-0	17 O	
MOC-D-06	225	14.04.99	17:45	20:53	33	53.12	31	47.47	33	48.53	31	42.66	2441	2565	1850-0	17 O	
MOC-D-07	227	15.04.99	13:31	17:32	34	05.64	32	00.02	34	05.72	31	50.15	2428	2530	10 mab-100 mab	3 HB (10 mab), 4 HB (50 mab), 5 HB (100 mab), 2 O (10 mab-50 mab, 50 mab-100 mab) 4 O (100 mab-0)	
MOC-D-08	229	16.04.99	08:25	09:53	34	06.59	31	54.54	34	07.68	31	51.35	2452	2515	10 mab-100 mab	2 HB (10 mab), 2 HB (50 mab), 2 HB (100 mab), 4 O (10 mab-50 mab, 50 mab-100 mab) 8 O (100 mab-0)	parallel sampling; R9 failed
MOC-D-09	239	19.04.99	07:22	09:58	34	31.09	27	28.30	34	25.13	27	25.13	2467	2628	1450-0	17 O	
MOC-D-10	240	19.04.99	15:38	18:49	34	21.15	27	27.34	34	26.91	27	23.38	2434	2673	2500-0	17 O	
MOC-D-11	242	20.04.99	01:53	03:49	35	00.76	26	50.47	35	03.65	26	47.10	1580	2895	1450-0	17 O	system problems
MOC-D-12	245	20.04.99	17:21	21:18	34	26.51	25	58.94	34	31.37	25	50.43	1588	4966	4100-750	17 O	
MOC-D-13	249	21.04.99	22:02	00:59	32	47.61	25	39.70	32	53.40	25	38.20	2352	2526	2500-0	17 O	
MOC-D-14	264	25.04.99	18:14	20:24	34	25.16	26	04.45	34	23.69	25	59.41	4045	4261	10 mab-100 mab	4 HB (10 mab), 4 HB (50 mab), 4 HB (100 mab), 2 O (10 mab-50 mab) 2 O (50 mab-100 mab); parallel sampling	
MOC-D-15	266	26.04.99	16:06	20:40	34	24.95	26	03.97	34	21.52	25	53.38	3412	4260	4250-1450	2 HC (4250; 100 µm, 300 µm), 6 O (4250-2750), 2 HC (2750; 100 µm, 300 µm), 6 O (2750-1450); bio-chemistry sampling	

Tab. 28: continued

Haul No.	Station No.	Start Date	Start Time (UTC)	End Time (UTC)	Start Position				End Position				Water Depth (m)		Depth Range of Sampling (m)	Type	Remarks
					°N	'N	°E	'E	°N	'N	°E	'E	min.	max.			
MOC-D-16	267	27.04.99	04:02	08:05	34	26.30	26	06.90	34	33.40	26	10.30	3632	4255	4250-1450	2 HC (4250; 100 µm, 300 µm), 6 O (4250-2750), 2 HC (2750; 100 µm, 300 µm), 6 O (2750-1450); bio-chemistry sampling	
MOC-D-17	268	27.04.99	11:06	13:26	34	33.61	26	19.90	34	29.15	26	08.40	3429	4045	1450-0	1 ZZ (1450-1250-1450; 100 µm, 300 µm), 6 O (1450-450), 1 ZZ (450-400-450; 100 µm, 300 µm), 9 O (450-0); biochemistry sampling	
MOC-D-18	269	27.04.99	18:22	22:33	34	24.95	26	04.43	34	21.40	25	54.59	3699	4262	4250-0	9 O; parallel sampling; isotope sampling	
MOC-D-19	270	28.04.99	03:32	07:21	34	26.20	26	07.10	34	29.46	26	15.69	3498	4258	4250-1450	2 HC (4250; 100 µm, 300 µm), 6 O (4250-2750), 2 HC (2750; 100 µm, 300 µm), 6 O (2750-1450); bio-chemistry sampling	
MOC-D-20	271	28.04.99	14:13	15:57	34	25.19	26	02.71	34	25.37	25	58.41	3620	4210	10 mab-100 mab	4 HB (50 mab), 4 HB (10 mab), 4 HB (100 mab), 2 O (50 mab-10 mab) 2 O (10 mab-100 mab); parallel sampling	
MOC-D-21	272	28.04.99	21:41	00:03	34	25.44	26	01.30	34	25.60	26	07.50	4150	4891	1450-0	1 ZZ (1450-1250-1450; 100 µm, 300 µm), 6 O (1450-450), 1 ZZ (450-400-450; 100 µm, 300 µm), 9 O (450-0); biochemistry sampling	
MOC-D-22	273	29.04.99	07:47	10:16	34	26.88	26	08.53	34	29.58	26	14.16	3595	4891	1450-0	1 ZZ (1450-1250-1450; 100 µm, 300 µm), 6 O (1450-450), 1 ZZ (450-400-450; 100 µm, 300 µm), 9 O (450-0); biochemistry sampling	
MOC-D-23	274	29.04.99	16:08	19:57	34	25.03	26	04.50	34	19.54	25	59.03	3463	4261	4250-0	9 O; parallel sampling; isotope sampling	
MOC-D-24	280	01.05.99	20:02	22:48	34	27.18	26	09.71	34	24.92	26	03.46	3972	4261	1450-0	1 ZZ (1450-1250-1450; 100 µm, 300 µm), 6 O (1450-450), 1 ZZ (450-400-450; 100 µm, 300 µm), 9 O (450-0); biochemistry sampling	
MOC-D-25	281	02.05.99	11:50	13:42	35	12.22	27	23.96	35	10.18	27	19.97	1463	1743	1250-0	14 O; partly parallel sampling	

Tab. 28: continued

Haul No.	Station No.	Start Date	Start Time (UTC)	End Time (UTC)	Start Position				End Position				Water Depth (m)		Depth Range of Sampling (m)	Type	Remarks
					°N	'N	°E	'E	°N	'N	°E	'E	min.	max.			
MOC-D-26	286	04.05.99	01:40	03:14	34	22.94	26	07.48	34	20.48	26	05.25	3769	4192	10 mab-100 mab	6 HB (10 mab), 4 HB (50 mab), 2 HB (100 mab), 2 O (10 mab-50 mab), 2 O (50 mab-100 mab), parallel sampling	
MOC-D-27	293	06.05.99	11:15	13:42	35	14.46	21	24.72	35	15.67	21	18.73	3298	3737	1450-0	8 O (1450-400), 1 ZZ (400-350-400), 8 O (400-0)	
MOC-D-28	294	08.05.99	01:49	06:30	35	14.80	21	38.10	35	16.40	21	49.80	3214	3291	3250-600	15 O	
MOC-D-29	296	09.05.99	02:09	05:38	33	36.09	19	10.50	33	32.53	19	03.80	3014	3291	3250-600	15 O	
MOC-D-30	297	09.05.99	08:40	10:50	33	33.09	19	04.51	33	30.23	19	00.45	2973	3047	1450-0	8 O (1450-400), 1 ZZ (400-350-400), 8 O (400-0)	L1-L10 failed
MOC-D-31	298	09.05.99	12:28	13:46	33	32.03	19	02.95	33	30.37	19	00.59	2981	2999	750-0	17 O	
MOC-D-32	304	11.05.99	05:02	07:13	34	54.40	16	25.70	34	55.37	16	20.32	1255	1738	1450-0	15 O	
MOC-D-33	309	12.05.99	23:48	23:00	38	53.40	10	34.90	38	58.38	10	31.20	2585	2629	1850-0	17 O	

HB: horizontal near-bottom
HC: horizontal for chemistry
O: depth intervals
ZZ: zig-zag- tow
Local Time: UTC + 2 hrs.

Tab. 29: 10 m²-Mocness haul information; period of quantitative interval sampling.

Haul No.	Station No.	Start Date	Start Time (UTC)	End Time (UTC)	Start Position				End Position				Water Depth (m)		Depth Range of Sampling (m)	Type	Remarks
					°N	'N	°E	'E	°N	'N	°E	'E	min.	max.			
MOC-10-01	252	22.04.99	17:45	18:53	34	25.02	26	03.84	34	25.94	26	06.51	4260	4261	2500-1450	O 5	computer problems (data savings)
MOC-10-02	253	22.04.99	21:51	22:23	34	24.41	26	01.12	34	24.81	26	02.28	4099	4199	600-250	O 5	flow counter failed, net damages
MOC-10-03	254	23.04.99	06:21	07:55	34	27.60	26	10.73	34	30.40	26	11.20	3730	4891	2500-1450	O 5	flow counter failed partly
MOC-10-04	255	23.04.99	11:00	11:25	34	27.67	26	06.39	34	27.15	26	07.07	4051	4096	250-0	O 5	
MOC-10-05	256	23.04.99	17:40	19:07	34	23.04	26	06.73	34	20.20	26	06.58	3312	4185	10 mab-3750	2 HB (10 mab), 3 O (10 mab-3750 mab)	
MOC-10-06	257	23.04.99	22:53	23:14	34	19.18	26	06.20	34	20.00	26	06.20	3057	3376	250-0	O 5	
MOC-10-07	258	24.04.99	04:08	05:42	34	26.10	26	06.78	34	22.94	26	06.72	4195	4265	3750-2500	O 5	
MOC-10-08	259	24.04.99	09:57	10:56	34	25.62	26	07.04	34	27.63	26	07.11	4030	4264	1450-600	O 5	
MOC-10-09	260	24.04.99	12:49	13:23	34	25.63	26	07.09	34	24.48	26	07.10	4264	4265	600-250	O 5	
MOC-10-10	261	24.04.99	18:01	19:31	34	24.43	26	02.27	34	23.35	25	58.77	4031	4183	3750-2500	O 5	
MOC-10-11	262	24.04.99	23:33	00:36	34	25.00	26	03.18	34	25.67	26	05.40	4196	4256	1450-600	O 5	bucket V suspect
MOC-10-12	278	01.05.99	08:06	09:31	34	25.31	26	05.07	34	24.21	26	01.95	4149	4262	3750-2500	O 5	sal., temp. measure-ments failed
MOC-10-13	279	01.05.99	14:22	15:19	34	25.09	26	06.13	34	26.44	26	08.31	4240	4262	2500-1450	O 5	
MOC-10-14	282	02.05.99	21:41	23:09	34	27.11	26	09.80	34	26.00	26	06.60	3886	4260	1450-600	O 5	winch problems
HB: horizontal near-bottom O: depth intervals Local Time: UTC + 2 hrs.																	

Tab. 30: Suprabenthos trawl information; period of strata sampling.

Haul No.	Station No.	Start Date	Start Time (UTC)	End Time (UTC)	Start Position				End Position				Water Depth (m)		Remarks
					°N	'N	°E	'E	°N	'N	°E	'E	min.	max.	
SBT-01	231	16.04.99	20:38	21:45	34	04.21	32	01.76	34	03.99	32	04.13	2483	2520	net 4 and 5 failed
SBT-02	232	17.04.99	03:02	04:17	34	05.92	31	57.06	34	06.42	31	54.21	2437	2507	partly no response, net 5 failed
SBT-03	275	30.04.99	02:03	03:06	34	23.95	26	08.36	34	23.31	26	10.64	3532	4231	
SBT-04	276	30.04.99	11:29	12:38	34	25.26	26	04.94	34	24.45	26	02.56	4181	4262	nets 3-5 failed
SBT-05	283	03.05.99	05:01	05:46	34	24.89	26	03.80	34	24.34	26	02.07	4174	4260	end of sampling after net 4
SBT-06	287	04.05.99	08:23	09:43	34	28.10	26	12.80	34	28.23	26	12.36			no sampling (winch problems)
SBT-07	288	04.05.99	21:42	22:37	34	24.56	26	03.15	34	24.08	26	01.71	4126	4180	nets 4 and 5 failed
Local Time: UTC + 2 hrs.															

Tab. 31: List of neuston hauls.

Haul No.	Station No.	Start Date	Start Time (UTC)	End Time (UTC)	Start Position				End Position				Flow Counts	Remarks
					°N	'N	°E	'E	°N	'N	°E	'E		
Neu-01	229	16.04.99	07:02	07:18	34	06.05	31	56.70	34	06.22	31	56.13	170	test sampling
Neu-02	229	16.04.99	07:27	07:41	34	06.09	31	56.56	34	06.28	31	55.91	1772	
Neu-03	229	16.04.99	10:23	10:38	34	87.18	31	50.23	34	08.48	31	49.60	3090	
Neu-04	229	16.04.99	10:40	10:55	34	08.48	31	49.60	34	08.80	31	48.85	3080	
Neu-05	233	17.04.99	12:10	12:25	34	52.22	31	19.95	34	52.76	31	19.62	2216	
Neu-06	234	17.04.99	16:37	16:52	35	15.90	31	05.85	35	15.27	31	05.27	81	
Neu-07	235	17.04.99	21:43	21:58	34	49.97	30	40.03	34	49.59	30	40.27	80	
Neu-08	236	18.04.99	04:56	05:11	33	58.02	31	11.84	33	57.86	31	11.10	82	
Neu-09	238	18.04.99	19:33	19:48	34	00.11	28	50.99	34	02.06	28	50.53	950	
Neu-10	239	19.04.99	10:07	10:23	34	25.14	27	25.09	34	25.56	27	24.81	2406	very windy
Neu-11	240	19.04.99	13:53	14:08	34	18.08	27	29.43	34	18.60	27	29.11	3017	very windy
Neu-12	246	21.04.99	02:17	02:31	34	28.50	25	58.50	34	28.00	25	59.00	2708	
Neu-13	247	21.04.99	09:50	10:05	34	02.90	26	24.80	34	02.50	26	24.60	2090	
Neu-14	248	21.04.99	14:37	14:52	33	13,90	25	56,17	33	13.30	25	56.13	4050	
Neu-15	249	21.04.99	20:19	20:34	32	44.17	25	39.86	32	44,74	25	39,77	2571	
Neu-16	249	21.04.99	20:36	20:51	32	44.76	25	39.79	32	45.24	25	39.74	2226	
Neu-17	250	22.04.99	06:13	06:29	33	30.06	25	31.99	33	30.49	25	23.13	3228	
Neu-18	256	23.04.99	13:35	13:50	34	30.89	26	06.79	34	30.50	26	06.80	2594	
Neu-19	256	23.04.99	13:52	14:07	34	30.40	26	06.79	34	29.89	26	06.78	2774	
Neu-20	258	24.04.99	00:56	00:11	34	32.17	26	06.80	34	31.65	26	06.80	3525	
Neu-21	261	24.04.99	14:58	15:17	34	26.74	26	08.89	34	26.48	26	08.13	3781	
Neu-22	261	24.04.99	15:17	15:25	34	26.48	26	08.13	34	26.37	26	07.80	3513	
Neu-23	264	25.04.99	16:55	17:10	34	26.17	26	07.40	34	25.26	26	06.76	13763	
Neu-24	266	26.04.99	13:19	13:34	34	27.09	26	09.97	34	26.90	26	09.40	3234	
Neu-25	266	26.04.99	13:36	13:51	34	26.90	26	09.40	34	26.69	26	08.85	3682	

Tab. 31: continued

Haul No.	Station No.	Start Date	Start Time (UTC)	End Time (UTC)	Start Position				End Position				Flow Counts	Remarks
					°N	'N	°E	'E	°N	'N	°E	'E		
Neu-26	267	27.04.99	00:10	00:25	34	23.22	25	59.04	34	23.40	25	59.52	2928	
Neu-27	269	27.04.99	18:05	18:20	34	25.17	26	05.00	34	24.93	26	04.39	3721	
Neu-28	270	27.04.99	23:40	23:55	34	23.30	25	58.85	34	23.50	25	59.45	3633	
Neu-29	270	28.04.99	07:44	07:58	34	29.90	26	16.60	34	30.20	26	17.20	2585	
Neu-30	271	28.04.99	13:21	13:36	34	25.13	26	04.51	34	25.15	26	03.88	3492	
Neu-31	272	28.04.99	21:15	21:30	34	25.44	26	00.33	34	25.44	26	01.01	3120	
Neu-32	275	29.04.99	23:32	22:47	34	26.20	26	01.00	34	26.00	26	01.50	3626	
Neu-33	275	30.04.99	04:59	05:14	34	22.60	26	12.84	34	22.48	26	13.36		flow count failed
Neu-34	275	30.04.99	04:37	04:52	34	22.23	26	14.31	34	22.05	26	14.93	4110	
Neu-35	276	30.04.99	15:24	15:39	34	22.14	25	56.15	34	21.90	25	55.47	4025	
Neu-36	279	01.05.99	12:39	12:54	34	24.39	26	02.32	34	24.61	26	02.98	3277	
Neu-37	281	02.05.99	10:43	10:58	35	13.46	27	26.32	35	13.18	27	25.82	3381	
Neu-38	281	02.05.99	11:00	11:15	35	13.18	27	25.82	35	12.82	27	25.10	3383	
Neu-39	281	02.05.99	11:18	11:33	35	12.82	27	25.10	35	12.49	27	24.49	3050	
Neu-40	288	04.05.99	19:02	19:17	34	26.66	26	08.93	34	26.43	26	08.37	3022	
Neu-41	288	04.05.99	22:23	22:38	34	24.06	26	01.64	34	23.87	26	01.09	3658	
Neu-42	289	05.04.99	07:15	07:30	34	34.00	25	04.83	34	34.23	25	04.26	3514	
Neu-43	290	05.04.99	13:08	13:23	34	40.07	24	19.68	34	40.21	24	18.90	4317	
Neu-44	290	05.05.99	13:27	13:40	34	40.21	24	18.90	34	40.34	24	18.18	3837	
Neu-45	291	05.05.99	19:35	19:50	34	49.98	23	24.89	34	49.85	23	24.14	3996	
Neu-46	292	06.05.99	00:42	00:57	34	56.02	22	49.91	34	56.10	22	49.17	2496	
Neu-47	293	06.05.99	10:27	10:42	35	14.10	21	26.64	35	14.21	21	25.97	2419	
Neu-48	293	06.05.99	10:45	11:00	35	14.21	21	25.97	35	14.36	21	25.24	2490	
Neu-49	295	08.05.99	16:50	17:05	34	24.92	20	20.04	34	24.47	20	19.44	3188	

Tab. 31: continued

Haul No.	Station No.	Start Date	Start Time (UTC)	End Time (UTC)	Start Position				End Position				Flow Counts	Remarks
					°N	'N	°E	'E	°N	'N	°E	'E		
Neu-50	296	08.05.99	22:58	23:13									4344	estim. positions 33°40'N 19°15'E (no data print possible)
Neu-51	296	08.05.99	23:20	23:35										estim. positions 33°40'N 19°15'E (no data print possible)
Neu-52	297	09.05.99	07:13	07:27	33	34.90	19	07.10	33	34.60	19	07.70	3847	
Neu-53	297	09.05.99	08:26	08:41	33	33.36	19	04.91	33	33.01	19	04.40	3845	
Neu-54	300	10.05.99	00:02	00:16	34	30.10	19	00.00	34	30.70	18	59.97	3951	
Neu-55	301	10.05.99	06:03	06:18	35	09.18	19	00.04	35	09.80	19	00.00	3531	
Neu-56	302	10.05.99	14:40	14:55	35	49.91	18	59.95	35	49.41	18	59.22	4334	
Neu-57	303	10.05.99	23:08	23:22	34	45.10	17	29.90	34	45.20	17	29.00	4039	
Neu-58	304	11.05.99	04:57	05:12	34	54.42	16	25.81	34	54.50	16	25.10	3711	
Neu-59	304	11.05.99	05:15	05:30	34	54.52	16	25.13	34	54.62	16	24.39	3688	
Neu-60	306	11.05.99	15:13	15:28	35	00.01	14	60.00	35	00.51	14	59.35	3448	
Neu-61	306	11.05.99	15:30	15:45	35	00.51	14	59.34	35	00.85	14	58.71	3468	
Neu-62	307	12.05.99	02:28	02:43	36	00.00	12	59.70	36	00.60	12	59.10	3745	
Neu-63	307	12.05.99	02:46	03:01	36	00.56	12	59.12	36	01.04	12	58.75	3821	
Neu-64	308	12.05.99	14:00	14:15	37	34.05	11	31.92	37	34.57	11	31.57	3507	
Neu-65	309	12.05.99	14:18	14:33	37	34.57	11	31.57	37	35.22	11	31.18	3799	
Neu-66	309	12.05.99	22:56	23:11	38	51.90	10	36.00	38	52.30	10	35.70	3441	
Neu-67	309	12.05.99	23:15	23:30	38	52.40	10	35.60	38	53.00	10	35.10	3613	
Local Time: UTC + 2 hrs.														

5.4.10 Taxonomic Composition and Vertical Distribution of Planktonic and Micronektonic Cephalopoda in the Levantine Sea (Eastern Mediterranean)

(V. Ch. Miske)

Introduction and Scope

Information concerning species composition and abundance of pelagic cephalopods especially of the deeper layers of the Levantine Sea is very sparse. The main purpose of the present study was to add new data concerning the taxonomic composition and vertical distribution of the poorly known planktonic and micronektonic teuthofauna of the deep-water body of the oligotrophic Levantine Sea, which is in comparison to the deep open ocean warmer and more saline (MALANOTTE-RIZZOLI AND HECHT, 1988 and literature cited therein).

Material and Methods

During the cruise there were carried out 33 hauls with the 1m^2-Double- Mocness (20 nets of 0.333 mm mesh size) and 14 hauls with the 10m^2- Mocness (5 nets with 1.6 mm mesh size). The closing net systems were used to subsample the water column by day and night starting the deepest hauls some meters above the abyssal sea floor. Immediately after the end of each haul and before the standard fixation and preservation procedure of the plankton and micronekton samples the content of each net bucket was searched for cephalopods as carefully as time allowed it. The material sorted out was fixed and preserved in 70% ethanol.

In addition, planktonic and micronektonic animals from different depth zones of the pelagic zone and of the benthic deep-sea macro- and megafauna were photographed. If the collected animals were still alive and in good condition also digital video documentations were made. More than 60 objects belonging e. g. to the taxa Siphonophora, Crustacea, Pteropoda, Heteropoda, Cephalopoda, Tunicata and Pisces were documented for educational purposes.

First results and discussion

The superficial examination of the samples on board yielded only 17 cephalopod specimens, despite the relatively large amount of Mocness tows made at all depths.

More than one-half of the specimens (9 individuals) belonged to the genus *Heteroteuthis* GRAY, 1849 of the Decabrachia family Sepiolidae. Of these, five *Heteroteuthis* were found in a single 10m^2-Mocness tow SE off Crete (34°18'N to 34°20'N, 26°06'E; total depth about 3200 m) at depths between 150 m and 250 m shortly after midnight. The rest of the specimens was caught with the 1m^2-Double-Mocness: one individual SE off Crete (34°19'N, 27°30'E to 34°25'N, 27°25'E; total depth ca 2500 m) at 450-500 m in the morning, one specimen E off Crete (35°14'N, 27°27'E to 35°10'N, 27°20'E; total depth about 1600 m) at 300-350 m in the afternoon, and one specimen SE off Crete (34°17'N, 27°30'E to 34°27'N, 27°23'E; total depth ca 2500 m) at 200-250 m in the evening. The remaining *Heteroteuthis* specimen was captured SW off Cyprus (34°06'N, 32°06'E to 31°46'E; total depth ca 2500 m). It was found in an integrated haul (0-1850 m) allowing no precise determination of capture depth.

Heteroteuthis is one of the most common pelagic cephalopods in the Mediterranean Sea (NESIS, 1982/87). It inhabits the water column from a few meters to ca 500 m depth, mostly between 25 and 150 m (LU ET AL., 1992). The depth range of the up to the present proved *Heteroteuthis* captures of the cruise M 44/4 reaches from 150 m to 500 m, which is within the range given by the authors. Five of the eight up to now found specimens with precise depth information (62,5%) were caught at depths between 150 m and 250 m.

According to Roper (1974) *Heteroteuthis* from the Mediterranean migrates towards the surface at night. Roper and Young (1975) reported on *Heteroteuthis* caught in that sea: During the day four specimens were taken in 150-250 m depth and 10 specimens at depths of 400-500 m, while 16 specimens were captured between 50 m and 300 m at night. Although in amount very limited, the proved *Heteroteuthis* captures of the present study also indicate a stay of the specimens in shallower depths (150-250 m) at night and in greater depths (200-500 m) during daytime.

The other cephalopods found were members of the Decabrachia families Cranchiidae (three specimens collected at 100-150 m, 550-600 m and 0-1850 m depth, respectively), Enoplo-teuthididae (one specimen from 0-450 m and one from 0-1850 m) and Pyroteuthididae (one individual from 0-700 m) and of the Octopoda (one specimen caught in 100-150 m depth) as well. A very small ontogenetic stage of a decabrachian from 0-1850 m depth could not yet be determined.

The Cranchiidae found were collected within the range mentioned by Voss et al. (1992). Members of this family live in the water column from the surface to unknown depths below 2000 m. While the adults of the Enoploteuthididae and Pyroteuthididae live at mesopelagic depths, the juveniles occupy the upper 200 m. Probably all members of these families undergo extensive vertical migrations (Young et al., 1992, Young15.03.1998, Young et al. 15.03.1998). The depth ranges of the up to now found specimens of M 44/4 match the quoted habitat range (except the individual, which came from the deep integrated haul).

Based on the provisional examination of the material, no individual was captured for sure in the bathypelagic zone (the deepest capture excluding integrated hauls took place in 550-600 m). This matches in part the finding of Weickert (1990) that micronekton is absent from the deeper bathypelagic zone of the Levantine Sea.

In conclusion, the results of this preliminary study may suggest that the oligotrophic Levantine Sea does not harbour many planktonic and micronektonic cephalopods. The deeper layers seem to lack them. The findings need to be confirmed by a detailed taxonomic and quantitative examination of the samples.

5.4.11 Biogeochemical Fluxes in the Deep Water

(K. Neumann, G. Schroll)

Introduction and Scope

The objective of the IBMC-group during the cruise M44/4 in the Mediterranean was to recover a sediment trap system deployed during M44/1 and to participate in sediment sampling. Major goal of the project is to investigate externally forced material fluxes to the deep Mediterranean and their relevance for deep sea biology. In detail, our project aims to study the biogeochemical composition of settling particles and sediments, the variation of fluxes to the deep sea sediment in space and time and to obtain information on the sources, transport pathways and transport processes of organic matter.

Material and Methods

A sediment trap system collecting settling particles from January 30, 1999 to April 13, 1999 was recovered from the Ierapetra-Deep SE of Crete. This mooring consisted of two traps at the depths of 700 m and 2700 m (Fig. 98). The sampling interval was 3.5 days for each cup for a period of 73,5 days. 21 trap samples were collected from the deep trap. Due to electronic problems the sediment

trap in 700 m depth collected two samples. The obtained samples were stored at 4 °C. In the laboratory in Hamburg all samples were filtered and dried for further biogeochemical analyses.

Four sediment cores (19-59 cm length) were taken with a multicorer. The cores were opened immediately and samples were taken from the following intervals: 0-0.5 cm, 0.5-1 cm, 1-1.5 cm, 1.5-2 cm, 2.5-3 cm, 3-4 cm, 4-5 cm, 6.5-7.5 cm, 9-10 cm, 14-15 cm, 19-20 cm, 24-25 cm, 29-30 cm and 34-35. Two subsamples of 5 ml volume were taken from each depth horizon. Altogether 82 sub-samples were taken. The sediments were filled into 30 ml glass vials (pre-combusted at 550 °C). 41 samples were dried at 60 °C for 3-6 days and 41 samples were stored cool at 4 °C, respectively. Both sediment trap and sediment samples will be analysed for Corg, nitrogen, carbonate, biogenic silica, amino acids, hexosamines, carbohydrates and nitrogen isotopes.

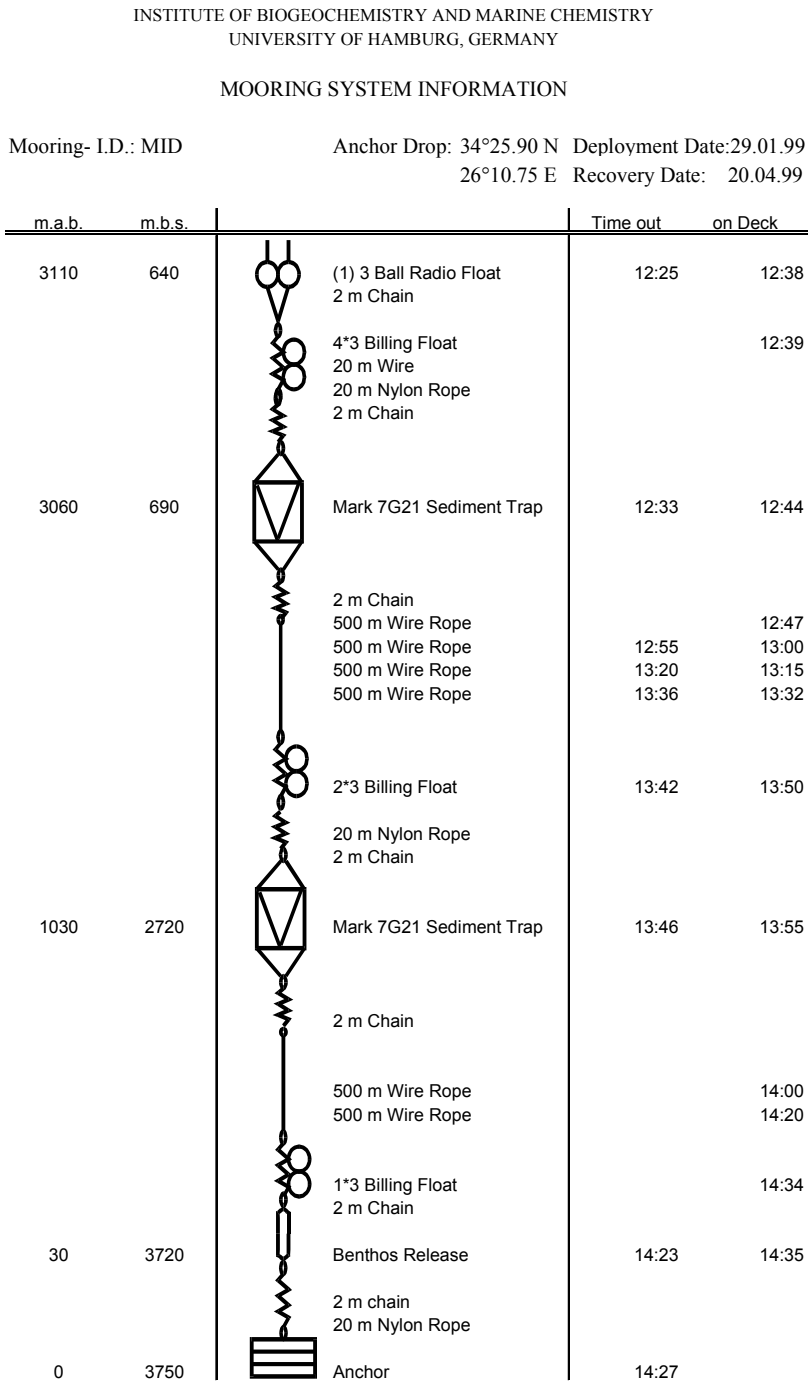

Fig. 98: Moored particle interceptor trap.

6 Ship's Meteorological Station

6.1 Weather and Meteorological Conditions during Leg M 44/1

(D. Behr)

R/V Meteor left the port of Cádiz on January 22, 1998 morning steering on an easterly course to her first working position at 35°14'N/21°30'E (Urania-Basin). During her transit there were northerly winds force 4 Bft shifting to north-westerly direction soon after. A small but intense gale centre developing near Cape Finisterre followed R/V Meteor and reached her first working area at the same time. In the vicinity of Crete Island there were south-westerly winds force 8 Bft and a swell of up to 4 m making the station work troublesome. After finishing station work R/V Meteor sailed with southerly winds force 4 to 5 to the Port of Çanakkale for picking up a large group of scientists at January, 31.

R/V Meteor started in the Sea of Marmara with a bathymetric-profile-transect (see 4.1). Due to increasing north-easterly winds force 7 causing a swell of nearly 3 m the transect was hold up. Station work was done leeward of a peninsula in the meantime. After the passage of a cold front the wedge of a central European high expanded to the Sea of Marmara. Due to this there were westerly to south-westerly winds between force 3 and 5 Bft.

At February 5 a storm centre moved from Scotland to southern Finland. Its cold-front swung southwards across eastern Europe and passed the Sea of Marmara at February 6. In the vicinity of this front there were in the working area of R/V Meteor light and variable winds and poor visibility.

New lows developed at this cold-front and moved from France over the Ionian Sea and Aegean Sea to the Sea of Marmara since then up to the end of the cruise. They cause a steady change between south-westerly winds force 5 to 6 Bft. (the low was approaching to the working area of R/V Meteor), light and variable winds combined with rainy periods (the low was passing the working area), and north-westerly winds force 7 to 8 combined with showersqualls (passage of the cold-front). R/V Meteor reached Istanbul on February 13, 1999 noon.

The following short statistics of wind force in Beaufort and sea heights in m during the leg M44/1 illustrates the statements given above. They are given in % of all measurements.

Tab. 32: Statistics about wind force and sea hights during M 44/1

0	1	2	3	4	5	6	7	8	9	Windforce in Bft
0.6	2.8	7.5	18.2	22.8	16.8	19.2	10.5	1.6	-	% of all measurements

0-1	1-2	2-3	3-4	4-5	5-6	6-7	7-8	8-9	Swell and sea in m
55.3	30.9	13.8	-	-	-	-	-	-	% of all measurements

Activities of the Ship's Weather Watch

a) A weather report was compiled and published twice a day. Comments on this report were given to the ship's command and the chief scientist regularly. The other participants of the cruise were informed by a bulletin or on special request. Special advice was given if necessary. The records needed for preparing the weather report were received as synoptic observations and weather maps from the wireless stations Pinneberg and Rome, as satellite pictures from METEOSAT 7, and as forecast charts from Deutscher Wetterdienst, Hamburg and Offenbach (Main).
   The forecasts of weather conditions and height of sea and swell were based essentially on surface analyses charts of the Northern Atlantic Ocean (east of 30°W) and the Mediterranean Sea. Surface observations of European and Northern African weather-stations and voluntary merchant ships were compiled by hand drawing in these charts. They were analyzed by hand afterwards twice every day.
b) Meteorological parameters have been measured and recorded continuously and were transferred to the ship's data collecting system. By this every participant could retrieve the necessary data into his computer system afterwards. Sensors and meteorological equipment were maintained regularly, some repairs were done.
c) Every hour a World Meteorological Organization (WMO) standard weather observation was carried out. 8 of them were transmitted into the WMO Global Telecommunication System (GTS) including eye observations done by meteorological staff.
d) Every day at 12 UTC a radar-wind sound was launched with the ASAP-System, determining a vertical profile of pressure, temperature, moisture, and horizontal wind up to an altitude of 20 to 25 km. The evaluated data (temps) were transmitted into the GTS of the WMO.

Determination of the atmospheric turbidity at sea

Information about the spatial and temporal distribution of the net total radiation and its components at the sea surface as well as atmospheric turbidity are one of the most important parameters in resolving numerous meteorological and oceanographic questions. Therefore during the cruise the following radiation components were recorded: direct solar radiation, sunshine duration, global solar radiation and UV-B global solar radiation as well as longwave thermal radiation of the atmosphere. Additional components necessary to establish a radiation balance: reflected solar radiation and ocean surface radiation are computed using numerical models successfully tested on former research cruises in the Atlantic (BEHR, 1990).

As atmospheric turbidity influences global solar radiation on its way through the atmosphere, the knowledge of this quantity is essential. Atmospheric turbidity is expressed by turbidity coefficients as follows:

T_L: Linke-turbidity-coefficient, describing all radiative processes in the whole solar spectrum,
T_s: turbidity-coefficient, describing all radiative processes in the **s**hort-range part of the solar spectrum ($0\ \mu m < \lambda < 0.63\ \mu m$), giving information about the dust in the atmosphere,
T_r: turbidity-coefficient, describing all radiative processes in the **r**ed part of the solar spectrum ($0.62\ \mu m < \lambda < 2.8\ \mu m$), giving information about the water-vapour-content in the atmosphere.

The coefficients T_L, T_s, and $T_r \equiv T_x$ can be computed by:

$$I_x = I_{0x} \exp(-T_x \cdot m \cdot \delta) \qquad (1)$$

with:
I_{0x}: extraterrestrial solar radiation received from a surface normal to the beam of the sun. Its quantity depends on the distance sun - earth only,
I_x: direct solar radiation received from a surface normal to the beam of the sun, e.g. measured with a Linke-Feussner-Actinometer,
m: optical pathlength, dependent on the solar elevation angle.
δ: optical thickness of the atmosphere.

Simply spoken T_x equals the number of clear Rayleigh-atmospheres which had to stack up one on the top of the other in order to correspond to the atmsphere in which measurements were done.

The data set of numerous measurements of direct solar radiation I done with a Linke-Feussner-Actinometer revealed the spatial and temporal variation of the atmospheric turbidity during the cruise. As a first result the daily courses of T_L, T_s, and T_r at February, 3 will be shown here.
R/V Meteor worked the whole day in cold and cloudless air originating from the eastern parts of Central Europe. There were weak northerly winds with 5 to 10 knots. At this day the horizontal visibility decreased from 20 km at sunrise to 5 km after sunset remarkably (Fig. 99). The alteration of the atmospheric transparency can be explained by the measurements of atmospheric turbidity done on this day very frequently.

In Figs. 99 and 100 the time-scale used is True Solar Time (TST) in order to make the daily courses of the meteorological quantities more clear. The decrease of the horizontal visibility cannot not be explained by the daily course of the direct solar radiation (Fig. 100, thin line) as it is nearly symmetric to noon, neither by the Linke-turbidity coefficient T_L (Fig. 100, dotted line) as it is nearly constant the whole day. The value of about 4 represents a Central Europe air in spring loaded with dust particles from an larger city. But the spectral turbidity coefficients show a striking different behaviour: decreasing of T_r (Fig. 100, triangles) and an increase of T_s (Fig 100, crosses). These effects show: the drying of the atmosphere (decrease of T_r) is overcompensated by the transport of loaded air from eastern Central Europe (increase of T_s). The transport took place in the lower layers of the atmosphere (surface up to 1 km) according to the backwards-trajectories computed for this day. The new air-masses reduce the horizontal visibility as shown in Fig. 100.

These findings correspond to former results found by Behr (1990, 1992).

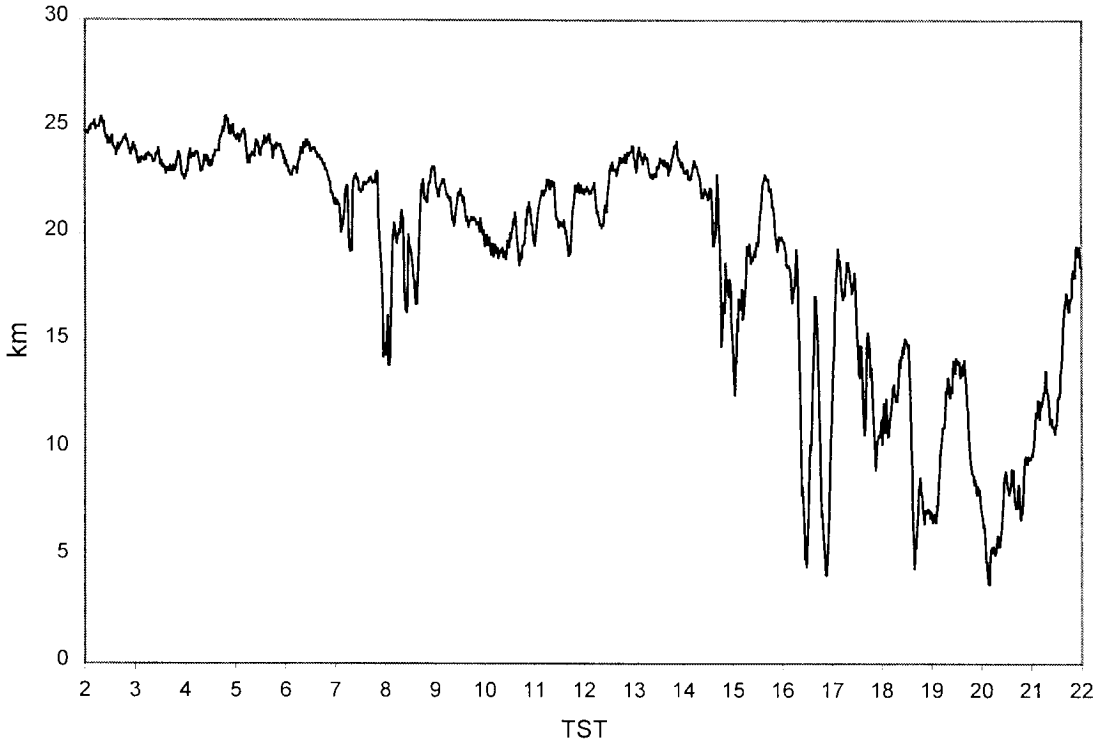

Fig. 99: Horizontal visibility on February, 3 1999. Time used is true solar time (TST).

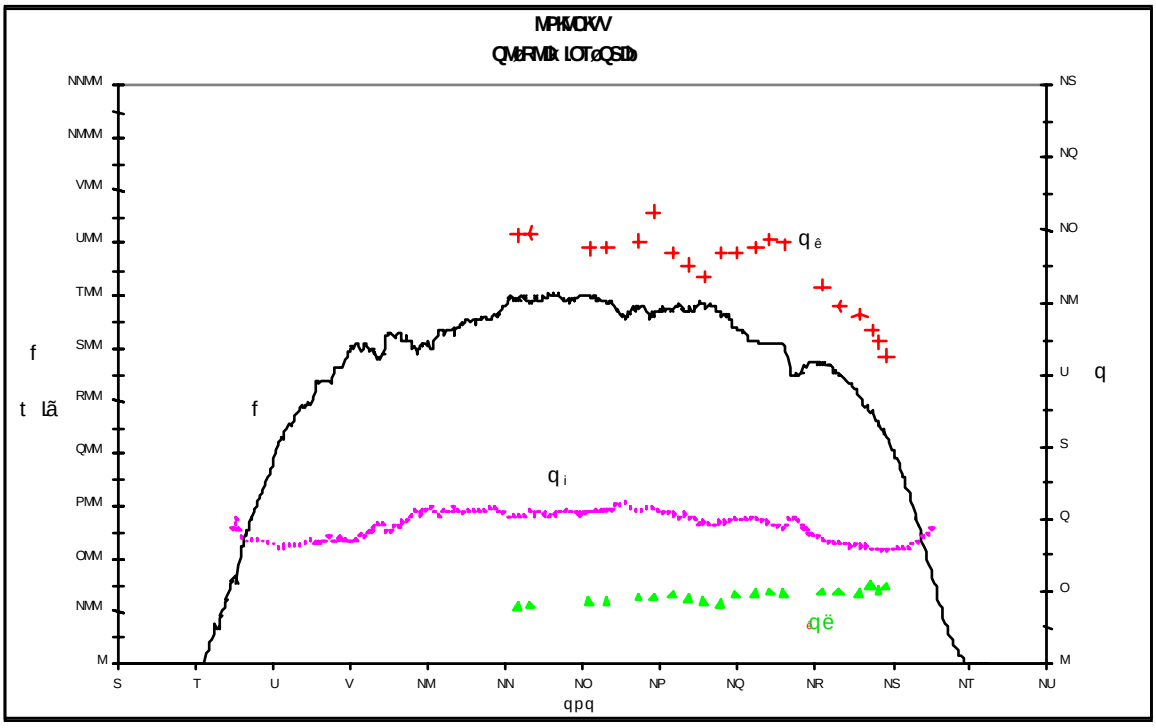

Fig. 100: Daily courses of direct solar radiation (I), Linke-Turbidity-coefficient (T_L), short-range-turbidity-coefficient (T_s), and red-part-turbidity-coefficient (T_r) on February, 3 1999. Time used is true solar time (TST).

6.2 Weather and Meteorological Conditions during Leg M 44/2

(R. Brauner)

R/V Meteor left Istanbul on the 16th of January at 19:00 hours with light southerly winds and a temperature of about 8°C. When Meteor reached the Aegean Sea northwesterly winds increased up to 28 Knots due to a low pressure system moving slowly from the Ionian Sea to thesouthwestern part of Turkey. This low pressure sytems with winds from northwest- to westerly directions dominated the weather on the cruise to Port Said. Because of the low temperature of the airmass in comparison to sea surface temperature rainshowers developed during day and night and forced the wind additionally by gusts. Due to the strong northwesterly winds windsea and swell increased to 2.5 meter.

Cruising from Port Said to Aqaba and also for scientific work in the Gulf of Aqaba was done under good weather conditions and a poorcloudiness. The winds blowed daily from northerly directions with windspeeds between 18 and 26 knots. Additionally orographic- and katabatic effects forced the windspeed up to 40 knots in some regions of the Gulf of Aqaba, especially in the Street of Tiran. The average wind speed during the cruise was about 20 knots from northerly directions with a frequency of 92 %. Due to the short fetch of about 100 km, the maximum windsea was about 1.5 meter. The temperatures cooled to 13°C in the morning and rised up to 22°C in the afternoon. Only in the last three days of the cruise the wind became calm because of a low pressure gradient in the area. Therefore seebreeze developed in the afternoon with windspeeds up to 8 knots from southerly directions.

The cruise M 44-2 ended in the morning of the 11th of March 1999 in Aqaba.

6.3 Weather and Meteorological Conditions during Leg M 44/3

(D. Bassek)

R/V Meteor left Aqaba on the 12th of March at 10:00 hours with moderate northerly winds and a temperature of about 20°C. The scientific work in the Gulf of Aqaba was done under good weather conditions and a poor cloudiness. The winds blowed daily from northerly directions with windspeeds between 0.5 and 26 knots. The average wind speed during the cruise in Gulf of Aqaba was about 20 knots from northerly directions. Due to the short fetch of about 100 km, the maximum windsea was about 1.5 meter. The temperatures cooled to 13°C in the morning and rose up to 22°C in the afternoon.

In the area of the Red Sea, the scientific work was also performed under good weather conditions and with windspeeds between 0 and 40 knots. The average wind speed during this cruise was about 20 knots from northwesterly to northerly directions. Only on one day did the wind reach velocities of 40 to 43 knots. The maximum wind sea was about 2 meters. To be precise, it was 16% 0 Meter, 55% 1 Meter, 29% 2 Meter. The temperatures were between 24°C and 26°C during the whole day with humidity from 30% to 90%. The visibility was good most of the time good, on other days it was dusty. Scientific work in the Eastern Mediterranean Sea onr the last 2 days was also done under weather conditions.

Synoptic situation during Leg M44/3: After starting this leg at Aqaba, the anticyclone over the eastern part of the Mediterranean Sea caused mostly northerly winds in the Gulf of Aqaba. The strongest winds were noticed in the morning hour's bft 5 to 6 with gusts up to bft 7 sometimes. Because of sunny conditions, sea breeze effects took place during the afternoon. On 18.03.99 a low passed the eastern Mediterranean Sea from west to east. Therefore winds in the Gulf of Aqaba turned right to SE but very weak in force. On 22.03.99 the anticyclone influence west of Aqaba increased again. Winds from NW to NE Bft 4 to 6 were recorded onboard. On 30.03.99 light winds were registered due to small pressure gradients in the operating area. On 31.03.99 heavy northwesterly winds were noticed enroute at the rear of a low with maximum winds near bft 9 for some hours. After leaving Port Said, winds from NW to E took place mostly moderate to strong in force.

6.3 Weather and Meteorological Conditions during Leg M 44/4

(R. Strüfing)

In spring time the weather situation over the Mediterranean Sea changes from the wintry cyclonic activities over relatively warm waters to prevailing high pressure mainly due to temperatures over sea being considerably lower than over the surrounding continents. The weather during M44/4 followed this development.

For the first three weeks an anticyclone over Crete and the Levantine Sea held the low pressure systems at bay which developed over the western parts of the Mediterranean Sea. Though these lows moved to the northeast and thus never penetrated into the Levantine Sea, the short passage of their cold fronts caused the winds to rise up to force 6. Since these few rainless weather events lasted a few hours only, the first part of M44/4 was dominated by weak winds and an abundance of sunshine.

When 'RV Meteor moved on to the Urania Basin, on 5th May a strong pressure gradient between an anticyclone over Bulgaria and a low over the asiatic parts of Turkey lead to northeasterly winds force 7 in the Agean Sea stretching out into the Ionian Sea through the Kithira Strait. This single event of strong winds persisted for 36 hours causing waves up to 3 meters. Later on high pressure over the Ionian Sea combined with weak winds ruled the weather again.

Until the beginning of May the weather over western parts of the Mediterranean Sea had been dominated by strong cyclogenisis but on 12th May hardly any pressure gradient could be found over this area. Due to the low windspeed and the relatively cold water RV Meteor experienced large fog patches on entering the Straits of Sicily (12th May).

During the transfer to Malaga westerly winds up to force 5 to 6 prevailed. Since these intervals of moderate to strong winds never lasted long the cruise M44/4 ended as smooth as it had begun. And the many hours of sunshine will be remembered as well as the lack of rain.

7 Lists
7.1 Leg M44/1
7.1.1 Station Lists

Table 7.1.1: Station list of Leg M44/1

Meteor No. 1999	FU Berlin No.	Date	Equipment	Latitude N	Longitude E	Water Depth (m)	Samples/ Sediment recovery	Remarks
Mediterranean								
29	3 KG	28.1.99	BC	35°13.74'	21°28.40'	3514 m	-	
30	4 KG	28.1.99	BC	35°14.21'	21°28.52'	3435 m	0.65 m	
31	5 KG	28.1.99	BC	35°13.82'	21°28.34'	3520 m	-	
32	6 KL	28.1.99	BC	35°48.71'	22°40.51'	1000 m	7.20 m	
33	7 ST	29.1.99	ST	34°25.90	26°10.75'	4300 m		
Sea of Marmara								
34	9 MC	1.2.99	MUC	40°50.63‘	27°40.20‘	1087 m		
34	10 KL	1.2.99	PC	40°50.60‘	27°40.18‘	1087 m	8.15 m	
34	11 KLG	1.2.99	PCG	40°50.60‘	27°40.17‘	1087 m	11.34 m	
35	12 KLG	2.2.99	PCG	40°50.21‘	27°40.77‘	1078 m	12.76 m	
36	13 MC	2.2.99	MUC	40°50.21‘	27°40.86‘	1077 m		
37	14 MC	2.2.99	MUC	40°51.11‘	27°40.84'	1079 m		
38	15 KL	2.2.99	PC	40°51.08‘	27°40.86‘	1079 m	10.47 m	
39	16 CTD	3.2.99	CTD	40°51.08‘	27°40.85‘	1079 m		
40	17 KL	3.2.99	PC	40°49.42‘	27°43.90‘	426 m	3.20 m	banana
41	18 KL	3.2.99	PC	40°49.43‘	27°43.88‘	420 m	2.20 m	
42	19 MC	3.2.99	MUC	40°50.50‘	27°45.79‘	567 m		
43	20 KLG	3.2.99	PCG	40°50.51‘	27°45.79‘	566 m	10.61 m	
44	21 KL	3.2.99	PC	40°50.50‘	27°45.77‘	566 m	7.20 m	
45	22 CTD	3.2.99	CTD	40°48.87‘	27°44.00‘	730 m		
46	23 KL	3.2.99	PC	40°48.83‘	27°43.99‘	731 m	9.35 m	
47	25 MC	3.2.99	MUC	40°48.91‘	27°44.05‘	727 m		
48	26 CTD	3.2.99	CTD	40°48.67‘	27°57.45‘	1216 m		
49	28 CTD	4.2.99	CTD	40°48.25‘	28°01.02‘	1235 m		
50	29 KL	4.2.99	PC	40°48.22‘	28°01.12‘	1222 m	12 m	
51	30 MC	4.2.99	MUC	40°48.20‘	28°01.12‘	1227 m		
52	31 MC	4.2.99	MUC	40°48.94‘	27°44.13‘	723 m		
53	32 MC	4.2.99	MUC	40°45.61‘	27°44.94‘	711 m		
54	33 KL	4.2.99	PC	40°45.64‘	27°44.90‘	712 m	6 m	
55	34 CTD	4.2.99	CTD	40°48.82'	27°42.49‘	771 m		
56	35 CTD	4.2.99	CTD	40°48.83‘	27°43.28‘	727 m		
57	36 CTD	4.2.99	CTD	40°48.84'	27°43.67‘	730 m		
58	37 CTD	5.2.99	CTD	40°48.85‘	27°44.28‘	727 m		
59	38 CTD	5.2.99	CTD	40°48.78‘	27°44.93‘	668 m		
60	39 CTD	5.2.99	CTD	40°48.75‘	27°45.74‘	647 m		
61	40 KL	5.2.99	PC	40°47.12	27°46.31‘	702 m	9 m	
62	43 CTD	6.2.99	CTD	40°48.94‘	27°46.01‘	642 m		
63	44 CTD	6.2.99	CTD	40°49.34‘	27°42.20‘	709 m		
64	45 CTD	6.2.99	CTD	40°48.96‘	27°43.48‘	714 m		

Table 7.1.1: continued

Meteor No. 1999	FU Berlin No.	Date	Equipment	Latitude N	Longitude E	Water Depth (m)	Samples/ Sediment recovery	Remarks
65	46 CTD	6.2.99	CTD	40°48.71‘	27°43.97‘	691 m		
66	47 CTD	6.2.99	CTD	40°48.22‘	27°44.80‘	593 m		
67	48 HBS	6.2.99	HBS	40°48.70‘	27°43.97‘	691 m		(rope length)
				40°48.70‘	27°43.96‘			
68	49 HBS	6.2.99	HBS	40°48.72‘	27°43.93‘	721 m		(rope length)
69	51 SM	7.2.99	FCM	40°48.83‘	27°44.08‘	727 m		
70	52 HBS	7.2.99	HBS	40°48.73‘	27°43.96‘	719 m		(rope length)
				40°48.72‘	27°43.96‘			
71	53 HBS	7.2.99	HBS	40°48.69‘	27°45.81‘	647 m		(rope length)
				40°49.05‘	27°43.56‘			
72	54 HBS	7.2.99	HBS	40°49.31‘	27°43.41‘	718 m		(rope length)
				40°48.94‘	27°44.39‘			
73	55 SM	7.2.99	WCM	40°48.70‘	27°48.31‘	715 m		
74	56 CTD	8.2.99	CTD	40°48.67‘	27°48.38‘	724 m		
75	57 CTD	8.2.99	CTD	40°49.13‘	27°55.94‘	1175 m		
76	58 HBS	8.2.99	HBS	40°48.99‘	27°43.82‘	724 m		(rope length)
				40°48.88‘	27°44.61‘			
77	59 HBS	8.2.99	HBS	40°48.89‘	27°44.42‘	706 m		(rope length)
				40°49.10‘	27°43.70‘			
78	60 HBS	8.2.99	HBS	40°49.50‘	27°45.49‘	596 m		(rope length)
				40°48.33‘	27°43.90‘			
79	61 HBS	8.2.99	HBS	40°49.00‘	27°43.79‘	722 m		
80	62 HBS	8.2.99	HBS	40°49.00‘	27°43.79‘	722 m		
81	63 SM	8.2.99	WCM	40°48.83‘	27°44.78‘	678 m		
82	64 CTD	9.2.99	CTD	40°49.27‘	27°55.33‘	1076 m		
83	65 CTD	9.2.99	CTD	40°49.17‘	27°56.19‘	1190 m		
84	66 HBS	9.2.99	HBS	40°49.30‘	27°54.95‘	1047 m		
85	67 HBS	9.2.99	HBS	40°49.06‘	27°44.38‘	695 m		
86	68 KL	9.2.99	PC	40°48.98‘	27°43.80‘	724 m	8 m	
87	69 MC	9.2.99	MUC	40°48.98‘	27°43.80‘	723 m		
88	70 MC	9.2.99	MUC	40°49.00‘	27°43.81‘	725 m		
89	71 MC	9.2.99	MUC	40°48.83‘	27°43.98‘	727 m		
90	72 KLG	9.2.99	PCG	40°48.84‘	27°43.99‘	728 m		
91	73 KL	9.2.99	PC	40°49.22‘	27°55.25‘	1072 m	8.90 m	
92	74 MC	9.2.99	MUC	40°49.21‘	27°55.30‘	1078 m		
93	75 MC	10.2.99	MUC	40°49.27‘	27°55.30‘	1074 m		
94	76 MC	10.2.99	MUC	40°48.96‘	27°43.80‘	730 m		
95	77 MC	10.2.99	MUC	40°48.95‘	27°43.78‘	731 m		
96	78 MC	10.2.99	MUC	40°48.89‘	27°43.79‘	733 m		
97	79 KL	10.2.99	PC	40°48.93‘	27°43.83‘	732 m	8.65 m	
98	80 SM	10.2.99	WCM	40°49.27‘	27°55.32‘	1078 m		
99	81 CTD	10.2.99	CTD	40°45.50‘	27°43.97‘	681 m		
100	82 KL	10.2.99	PC	40°45.50‘	27°44.03‘	684 m	4.50 m	banana
101	83 MC	10.2.99	MUC	40°49.00‘	27°43.91‘	721 m		
102	84 KL	10.2.99	PC	40°49.02‘	27°43.95‘	717 m	0.20 m	
103	85 KL	10.2.99	PC	40°48.85‘	27°43.96‘	730 m	8.35 m	
104	86 KL	10.2.99	PC	40°51.38‘	27°57.33‘	1194 m		
105	88 KLG	10.2.99	PCG	40°45.39‘	28°46.45‘	1175 m	14.85 m	
106	89 KL	11.2.99	PC	40°45.40‘	28°46.36‘	1169 m	7.30 m	
107	90 MC	11.2.99	MUC	40°45.41‘	28°46.28‘	1168 m		
108	91 CTD	11.2.99	CTD	40°45.46‘	28°46.33‘	1169 m		
109	92 SM	11.2.99	WCM	40°45.45‘	28°46.33‘	1168 m		

Table 7.1.1: continued

Meteor No. 1999	FU Berlin No.	Date	Equipment	Latitude N	Longitude E	Water Depth (m)	Samples/ Sediment recovery	Remarks
110	93 MC	12.2.99	MUC	40°46.95‘	28°46.45‘	1143 m		
111	94 KL	12.2.99	PC	40°47.02‘	28°46.37‘	1151 m	no core	
112	95 KL	12.2.99	PC	40°47.00‘	28°46.40‘	1143 m	8.80 m	
113	96 KLG	12.2.99	PCG	40°47.02‘	28°46.50‘	1142 m	10.26 m	
114	97 KL	12.2.99	PC	40°46.53‘	28°46.53‘	1094 m	5.40 m	

BC: Box Corer
HBS: Hydro Bottom Station
MUC: Multicorer
PC: Piston Corer (Göttingen)
PCG: Piston Corer (FU Berlin)
ST: Sediment Trap
WCM: Water Current Meter

7.1.2 Fluid samples with Mn^{2+} and S^{2-} data

Table 7.1.2: Fluid samples with Mn^{2+} and S^{2-} data

Station	Location	depth (m)	Mn^{2+} (ppb)	S^{2-} (ppb)
22 CTD	40°48.82' N, 27°44.62' W	13.5	1.5	
		307	0.6	
		559	1.4	
		609	1.2	
		658	0.7	
		698	2.2	
		729	0.6	
26 CTD	40°48.67' N, 27°57.47' W	5	2.2	
		706	2.3	
		1134	3	
		1184	5.9	
28 CTD	40°48.25' N, 28°01.02' W	4.5	0.5	
		1203	1.7	
		1249	4.5	
34 CTD	40°48.83' N, 27°42.48' W	503	1.8	
		602	3.8	
		702	3.3	
		771	1.7	
35 CTD	40°48.85' N, 27°43.27' W	504	1.4	
		604	1.2	
		703	1.6	
		734	2.8	
36 CTD	40°48.85' N, 27°43.69' W	504	1	
		604	5.3	
		694	5.1	
		736	3.6	
37 CTD	40°48.85' N, 27°44.28' W	504	0.7	
		603	2.5	
		702	5.5	
		731	2.8	
38 CTD	40°48.77' N, 27°44.90' W	314	1.7	
		504	2.3	
		604	2.3	
		653	2.9	
39 CTD	40°48.75' N, 27°45.73' W	505	1.6	
		604	1.8	
		650	3.7	
43 CTD	40°49.32' N, 27°42.28' W	605	1.7	
		653	3.9	
56 CTD	40°48.66' N, 27°48.36' W	604	1.6	
		634	0.8	
		683	1.9	
		731	1.9	
57 CTD	40°49.17' N, 27°55.93' W	606	0.5	
		706	0.7	
		806	0.7	
		906	0.5	
		1030	0.4	
		1124	0.6	
		1174	2	

Table 7.1.2: continued

Station	Location	depth (m)	Mn^{2+} (ppb)	S^{2-} (ppb)
64 CTD	40°49.24' N, 27°55.40' W	297	0.4	
		895	1.1	
		944	0.5	
		994	1.4	
		1044	0.9	
		1094	3.2	
65 CTD	40°49.17' N, 27°56.20' W	34	0.1	
		415	0.6	
		1016	0.2	
		1065	0.2	
		1114	0.7	
		1164	1.1	
		1214	1.7	
9 MC	40°50.63' N, 27°40.20' W	-5	34.4	< 10
		1.5	42.1	< 10
		11	1260	< 10
		21	1520	< 10
		31	1080	< 10
		52	1160	< 10
14 MC	40°51.11' N, 27°40.84' W	-5	6.3	< 10
		1	47	< 10
		6	193	< 10
		8	429	< 10
		12	1234	< 10
		17	1696	< 10
		24	2593	< 10
		33	2174	< 10
		41	1530	< 10
		51	1225	< 10
25 MC	40°48.91' N, 27°44.05' W	-5	11	< 10
		1	58.8	< 10
		9	2148	< 10
		15	1095	< 10
		24	1285	< 10
		36	1285	< 10
		51	1168	< 10
30 MC	40°48.20' N, 28°01.12' W	-5	2.1	< 10
		1	101	< 10
		9	157	< 10
		15	1444	< 10
		22	1632	< 10
		41	1404	< 10
31 MC	40°48.94' N, 27°44.13' W	-5		< 10
		1	33.6	< 10
		7	693	< 10
		15	795	< 10
		22	1820	< 10
		27	1198	< 10
		41	568	< 10
10 KL	40°50.61' N, 27°40.18' W	150	1208	6.3
		400	477	19.9
		750	187	24.3
		905	82	23800

Table 7.1.2: continued

Station	Location	depth (m)	Mn^{2+} (ppb)	S^{2-} (ppb)
23 KL	40°48.85' N, 27°43.99' W	17	507	1
		57	358	1
		95	964	1
		170	413	1
		256	298	53
		340	331	1
		370	275	1
		459	47	949
		469	130	540
		501	23.4	610
		530	51	4240
		557	53	57600
		590	27	28600
		630	33.8	2322
		670	99.9	748
		720	288	2150
		756	197	361
		801	28.4	206
		856	55	146
40 KL	40°47.06' N, 27°46.34' W	217	1006	0.3
		275	899	0.1
		455	446	3.2
		772	500	2.6
72 KL	40°48.84 N, 27°43.99' W	35	10	1
		65	11	1
		120	550	1
		150	352	1
		190	319	1
		220	171	1
		262	175	1
		282	120	10
		302	81	69
		322	139	1480
		342	66	7410
		362	23	38630
		382	17	26170
		402	33	17210
		422	19	108990
		442	8	215650
		462	14	72046
		482	40	38780
		502	14	104500
		522	15	1053
		542	15	8887
		562	27	5604
		582	39	1
		602	12	62
		622	18	1

Table 7.1.2: continued

Station	Location	depth (m)	Mn^{2+} (ppb)	S^{2-} (ppb)
72 KL	40°48.84 N, 27°43.99' W	662	23	1
		695		101
		745		20
		810		14
		860		179
		913	48	776
		973	36	361
		1011	63	436
		1061	45	365

7.2 Leg M44/2

7.2.1 Station Lists

Meteor No. 1999	Profile No.	Date 1999	Equipment	Time (UTC)	Latitude N	Longitude E	Water Depth (m)
117	3	21.02	CTD/Ro, MN maxi 2x LS MER	13:58	28°20.22'	34°33.06'	865
118	4		CTD/Ro	19:32	28°34.92'	34°39.06'	1175
119	5		CTD/Ro	22:25	28°49.98'	34°44.04'	1283
120	6	22.02	CTD/Ro	01:11	29°05.04'	34°46.08'	820
121	7		CTD/Ro, HLN 2x	03:30	29°16.98'	34°48.96'	827
122	8		CTD/Ro, MPS, MN maxi	07:19	29°29.52'	34°57.00'	591
	9		CTD/Ro , MN maxi 2x, LS PAR, LS MER 2x	08:52	29°29.52'	34°57.00'	591
123	10		CTD/Ro, MN maxi 2x, MPS	14:33	29°17.04'	34°48.90'	831
	11		CTD/Ro	18:12	29°17.04'	34°49.02'	831
124	12		CTD/Ro, MN maxi 2x	20:00	29°04.98'	34°45.96'	824
125	13	23.02	CTD/Ro, HLN, MN maxi 2x, LS PAR, LS MER	02:00	28°49.98'	34°44.04'	1410
126	14		CTD/Ro, MN maxi 3x, MPS, LS PAR, LS MER 2x	09:56	28°35.04'	34°39.00'	1176
	15		CTD/Ro	16:27	28°35.10'	34°39.00'	1176
127	16		CTD/Ro	19:11	28°20.04'	34°33.00'	859
128	17		CTD/Ro	23:51	27°53.04'	34°40.02'	623
129	18	24.02	CTD/Ro, HLN	02:06	27°38.94'	34°40.14'	910
130	19		CTD/Ro	05:34	27°25.08'	34°40.08'	885
131	20		CTD/Ro, MN maxi 2x, LS PAR, LS MER 2x	08:20	27°11.04'	34°39.96'	1121
132	21		CTD/Ro	16:07	27°17.88'	34°22.08'	1291
	22		CTD/Ro, MPS	17:00	27°17.88'	34°22.02'	1291
133	23		CTD/Ro, MN maxi 2x, MPS	21:45	27°25.02'	34°04.92'	808
134	24	25.02	CTD/Ro, LS MER 3x, MPS, MOCNESS	07:20	28°20.04'	34°33.00'	872
135	25		LS MER 2x, CTD/Ro, MPS, MOCNESS	14:05	28°34.92'	34°39.00'	1182
136	26		CTD/Ro, MN maxi, MPS	19:47	28°50.04'	34°43.98'	1347
137	27	26.02	CTD/Ro, MOCNESS, LS MER 3x	01:49	29°05.04'	34°46.02'	885
138	28		LS MER 2x, LS PAR, CTD/Ro, MPS, MOCNESS	08:15	29°17.04'	34°49.02'	848
139	29		CTD/Ro, LSPAR, LS MER 2x	12:56	29°29.52'	34°57.00'	587
	30		CTD/Ro, MN maxi	14:18	29°29.52'	34°57.06'	587
140	31		CTD/Ro	16:52	29°31.02'	34°58.68'	311
141	32		CTD/Ro	17:56	29°27.60'	34°56.34'	731
142	33		CTD/Ro	19:06	29°27.60'	34°54.84'	751
143	34		CTD/Ro	20:26	29°23.70'	34°53.22'	838
144	35	27.02	LS MER 3x, CTD/Ro, MN maxi 2x	08:35	27°52.80'	34°39.96'	651
145	36		LS PAR, LS MER 2x, CTD/Ro, MN maxi, MOC	13:54	27°39.24'	34°40.08'	953
	37		CTD/Ro	18:03	27°41.70'	34°40.20'	953
146	38		CTD/Ro, MN maxi	20:07	27°24.96'	34°39.96'	897
147	39	28.02	CTD/Ro, Nansen-Netz	01:56	27°10.98'	34°39.96'	1123
	40		CTD/Ro	03:22	27°10.92'	34°39.90'	1123
148	41		LS MER + PAR 2x, LS MER, CTD/Ro, MN maxi, MOC	07:53	27°23.82'	34°22.08'	1086
149	42		LS MER, CTD/Ro	13:31	27°25.02'	34°05.04'	797
150	43	01.03	CTD/Ro	04:39	29°29.46'	34°57.00'	585
151	44		LS PAR, LS MER 2x, MN mini 3x, CTD/Ro	16:48	29°29.46'	34°57.18'	599

7.2.1 continued

Meteor No. 1999	Profile No.	Date 1999	Equipment	Time (UTC)	Latitude N	Longitude E	Water Depth (m)
152	45	02.03	CTD/Ro, Nansen-Netz, LS MER 2x, LS PAR	01:57	28°20.04'	34°33.06'	866
	46		CTD/Ro 2x, MN maxi, LS MER 2x	06:00	28°20.04'	34°33.00'	866
	47		CTD/Ro, LS PAR, LS MER 2x, MN maxi	09:54	28°20.10'	34°33.06'	866
	48		CTD/Ro Jo-Jo, Nansen-Netz 2x	13:28	28°20.04'	34°33.06'	866
	49		CTD/RO, MN maxi	18:03	28°20.04'	34°33.00'	866
	50		CTD/Ro Jo-Jo, MN maxi	21:03	28°20.10'	34°33.06'	866
	51	03.03	CTD/Ro, LS PAR, LS MER 3x, MN mini 2x	01:52	28°20.04'	34°33.06'	866
153	52		CTD/Ro, MN-Mini,Schl.eins. 1x4 NDR, 2x5, 1x7 Pers.	12:03	27°53.04'	34°39.96'	646
154	53		CTD/Ro, MN- maxi	17:56	27°25.08'	34°40.38'	891
155	54	04.03	CTD/Ro, Nansen-Netz2x, LS PAR, LS MER 2x	03:00	27°24.00'	34°22.14'	1079
156	55		CTD/Ro, MN mini 4x, LS PAR, LS MER 2x	08:05	27°24.96'	34°04.98'	826
157	56	05.03	CTD/Ro, Nansen-Netz, LS PAR, LS MER 2x,	02:09	29°29.46'	34°57.06'	590
	57		CTD/Ro, MN Maxi, LS PAR, LS MER 3x	06:18	29°29.52'	34°57.00'	590
	58		CTD/Ro, LS PAR, LS MER 3x, MN maxi	09:58	29°29.52'	34°56.88'	590
	59		CTD/Ro? Jo-Jo, BO, Nansen-Netz	13:09	29°29.58'	34°57.24'	590
	60		CTD/Ro Jo-Jo, MN maxi	16:55	29°29.64'	34°57.12'	590
	61		CTD/Ro	21:42	29°29.52'	34°57.12'	590
158	62	06.03	MN maxi, CTD/Ro, Nansen-Netz	02:00	29°24.60'	34°54.30'	829
159	63		CTD/Ro, MN maxi, LS MER	04:30	29°24.66'	34°51.66'	446
160	64		CTD/Ro, MN maxi	06:32	29°24.60'	34°52.62'	650
161	65		CTD/Ro, MN maxi	08:39	29°24.60'	34°54.36'	829
162	66		CTD/Ro, MN maxi	11:00	29°24.66'	34°56.16'	798
163	67		CTD/Ro, MN maxi, LS MER 2x	13:15	29°24.60'	34°57.06'	521
	68		CTD/Ro	16:00	29°24.54'	34°57.00'	521
164	69		CTD/Ro, MN Mini 3x	18:56	29°04.98'	34°45.96'	822
165	70	07.03	CTD/Ro, Nansen-Netz, MN maxi, MPS, LS PAR, LS MER 3x	03:13	28°49.92'	34°44.04'	1402
166	71		CTD/Ro, LS PAR 2X, LS MER 2x	11:26	28°34.98'	34°39.00'	1174
167	72		CTD/Ro, MN maxi	15:43	28°19.80'	34°32.82'	849

CTD/Ro	Rosette with CTD
MN maxi	MultiNet maxi
MN mini	MultiNet mini
MOC	MocNess
BO	Bongo Net
HLN	Helgoländer Larvae Net
Nansen-Netz	Nansen Net
MPS	Multipara Probe
LS MER	Light Probe
LS PAR	Light Probe

7.3 Leg M44/3

7.3.1 Station Lists

Table 7.3.1: Station list of Leg M44/3

Meteor No. 1999	GeoB No.	Date 1999	Equipment	Time Seafloor (UTC)	Latitude N	Longitude E	Water Depth (m)	Samples/ Sediment recovery (cm)	Remarks
Gulf of Aqaba, Jordan									
168	5801-1	12.03.	MN	14:32	29°24.89'	34°54.72'	827 m	5x1.5 l 5xNet	500, 400, 300, 200, 100 m ($2x\delta^{13}C, 1x\delta^{18}O$, $1xPO_4$)
	5801-2		MUC	15:18	29°24.90'	34°54.70'	826 m	40 cm	6 big, 4 small tubes filled,
	5801-3		MUC/ CTD	16:27	29°24.90'	34°54.70'	826 m	40 cm	6 big, 4 small tubes filled,
	5801-4		SL 12	17:39	29°24.92'	34°54.71'	824 m	280 cm	
169	5802-1	13.03.	MN	05:10	29°30.47'	34°59.68'	396 m	5x1.5 l 5xNet	370, 300, 200, 100, 50 m ($2x\delta^{13}C, 1x\delta^{18}O$, $1xPO_4$)
	5802-2		MUC/ CTD	05:49	29°30.45'	34°57.68'	396 m	43 cm	6 big, 4 small tubes filled,
	5802-3		SL 6	06:42	29°30.42'	34°57.65'	400 m	295 cm	
170	5803-1	13.03.	SL 6	07:31	29°30.99'	34°58.10'	298 m	97 cm	
	5803-2		MUC/ CTD	08:05	29°30.96'	34°58.02'	301 m	7 cm	6 big, 3 small tubes filled,
171	5804-1	13.03.	MN	09:14	29°30.12'	34°57.42'	456 m	5x1.5 l 5xNet	400, 300, 200, 100, 50 m ($2x\delta^{13}C, 1x\delta^{18}O$, $1xPO_4$)
	5804-2		MUC/ CTD	09:46	29°30.07'	34°57.44'	463 m	41 cm	6 big, 4 small tubes filled,
	5804-3		MUC	10:32	29°30.10'	34°57.40'	464 m	40 cm	6 big, 4 small tubes filled,
	5804-4		SL 6	11:23	29°30.10'	34°57.40'	464 m	330 cm	
172	5805-1	13.03.	SL 6	12:55	29°24.90'	34°54.60'	827 m	97 cm	
173	5806-1	13.03.	SL 6	14:58	29°22.76'	34°53.30'	838 m	39 cm	
	5806-2		MUC/ CTD	15:51	29°22.75'	34°53.30'	838 m	40 cm	5 big, 4 small tubes filled,
	5806-2		MN	17:01	29°23.26'	34°53.54'	838 m	5x1.5 l 5xNet	500, 400, 300, 200, 100 m ($2x\delta^{13}C, 1x\delta^{18}O$, $1xPO_4$)
174	5807-1	15.03.	MN	04:31	29°28.81'	34°56.78'	644 m	5x1.5 l 5xNet	500, 400, 300, 200, 100 m ($2x\delta^{13}C, 1x\delta^{18}O$, $1xPO_4$)
	5807-2		MUC/ CTD	05:15	29°28.81'	34°56.78'	646 m	39 cm	6 big, 4 small tubes filled,
	5807-3		SL 6	06:12	29°28.82'	34°56.76'	644 m	186 cm	
Gulf of Aqaba, Israel									
175	5808-1	15.03.	MN	07:46	29°29.06'	34°56.32'	573 m	5x1.5 l 5xNet	500, 400, 300, 200, 100 m ($2x\delta^{13}C, 1x\delta^{18}O$, $1xPO_4$)
	5808-2		SL 6	09:00	29°29.03'	34°56.32'	578 m	364 cm	
	5808-3		MUC/ CTD	11:10	29°29.06'	34°56.35'	576 m	43 cm	6 big, 4 small tubes filled,
176	5809-1	15.03.	MN	12:21	29°30.41'	34°57.42'	397 m	5x1.5 l 5xNet	350, 250, 150, 100, 50 m ($2x\delta^{13}C, 1x\delta^{18}O$, $1xPO_4$)
	5809-2		MUC/ CTD	12:56	29°30.40'	34°57.36'	401 m	41 cm	6 big, 4 small tubes filled,
	5809-3		SL 6	13:41	29°30.39'	34°57.36'	404 m	304 cm	
Gulf of Aqaba, Jordan									
177	5810-1	15.03.	MN	14:31	29°30.23'	34°57.73'	442 m	5x1.5 l 5xNet	400, 300, 200, 100, 50 m ($2x\delta^{13}C, 1x\delta^{18}O$, $1xPO_4$)
	5810-2		SL 6	15:01	29°30.22'	34°57.73'	440 m	265 cm	
	5810-3		MUC/ CTD	15:43	29°30.21'	34°57.73'	441 m	35 cm	6 big, 4 small tubes filled,
178	5811-1	16.03.	MUC/ CTD	11:21	29°24.86'	34°54.70'	827 m	39 cm	6 big, 4 small tubes filled,

Table 7.3.1: continued

Meteor No. 1999	GeoB No.	Date 1999	Equipment	Time Seafloor (UTC)	Latitude N	Longitude E	Water Depth (m)	Samples/ Sediment recovery (cm)	Remarks
Gulf of Aqaba, Israel									
179	5812-1	16.03.	SL 6	13:04	29°31.19'	34°57.84'	262 m	50 cm	
	5812-2		MUC	13:34	29°31.14'	34°57.79'	269 m	15 cm	6 big, 4 small tubes filled,
180	5813-1	16.03.	MUC	14:07	29°31.32'	34°57.90'	240 m	19 cm	6 big, 4 small tubes filled,
	5813-2		SL 6	14:43	29°31.34'	34°57.90'	235 m	247 cm	
181	5814-1	16.03.	SL 6	15:20	29°31.71'	34°58.09'	138 m	0 cm	cc: fossil corals
	5814-2		MUC	15:43	29°31.71'	34°58.08'	140 m	0 cm	did not close, no core recovery
	5814-3		MUC	15:57	29°31.72'	34°58.09'	135 m	6 cm	6 big, 4 small tubes filled
Gulf of Aqaba, Jordan									
182	5815-1	16.03.	GKG	17:42	29°30.64'	34°58.98'	326 m	24 cm	sandy mud, yellowish brown
Gulf of Aqaba, Egypt									
183	5816-1	18.03.	MN	12:31	29°14.00'	34°49.85'	891 m	5x1.5 l 5xNet	Station "B" 500, 400, 300, 200, 100 m ($1x\delta^{13}C$,$1x\delta^{18}O$, $1xPO_4$,)
	5816-2		MN without net/ CTD	14:00	29°14.00'	34°50.00'	892 m	5x1.5 l	Station "B" 850, 800, 700, 600, 50 m ($1x\delta^{13}C$,$1x\delta^{18}O$, $1xPO_4$, Neodym)
184	5817-1	18.03.	MN	16:14	29°06.00'	34°46.01'	857 m	5x1.5 l 5xNet	Station "B1 500, 400, 300, 200, 100 m ($1x\delta^{13}C$,$1x\delta^{18}O$, $1xPO_4$)
	5817-2		MN without net/ CTD	17:27	29°06.00'	34°46.00'	856 m	5x1.5 l	Station "B1 800, 750, 700, 600, 50 m ($1x\delta^{13}C$,$1x\delta^{18}O$, $1xPO_4$, Neodym)
185	5818-1	20.03.	MN	07:30	28°47.02'	34°43.02'	1467 m	5x1.5 l 5xNet	Station "M" 500, 400, 300, 200, 100 m ($1x\delta^{13}C$,$1x\delta^{18}O$, $1xPO_4$)
	5818-2		MN without net/ CTD	08:55	28°47.00'	34°43.00'	1467 m	5x1.5 l	Station "M" 1450, 1200, 1000, 750, 50 m ($1x\delta^{13}C$,$1x\delta^{18}O$, $1xPO_4$, Neodym)
186	5819-1	20.03.	MN	11:30	28°35.00'	34°40.00'	1018 m	5x1.5 l 5xNet	Station "K" 500, 400, 300, 200, 100 m ($1x\delta^{13}C$,$1x\delta^{18}O$, $1xPO_4$)
	5819-2		MN without net/ CTD	12:38	28°35.00'	34°00.00'	1042 m	4x1.5 l	Station "K" 950, 800, 700, 600 m ($1x\delta^{13}C$,$1x\delta^{18}O$, $1xPO_4$, Neodym)
187	5820-1	22.03.	MN	07:50	28°20.98'	34°33.78'	886 m	3x1.5 l 5xNet	Station "F" 500, 400,300*, 200*,100m * no water samples ($1x\delta^{13}C$,$1x\delta^{18}O$, $1xPO_4$)
	5820-2		MN	09:22	28°21.02'	34°33.99'	888 m	2x1.5 l 5xNet	Station "F" 500*,400*,300, 200,100*m * no water samples ($1x\delta^{13}C$,$1x\delta^{18}O$, $1xPO_4$, Neodym)
	5820-3		MN without net/ CTD	10:22	28°20.99'	34°33.96'	888 m	5x1.5 l	Station "F" 820, 700, 600, 450, 50 m ($1x\delta^{13}C$,$1x\delta^{18}O$, $1xPO_4$)

Table 7.3.1: continued

Meteor No. 1999	GeoB No.	Date 1999	Equipment	Time Seafloor (UTC)	Latitude N	Longitude E	Water Depth (m)	Samples/ Sediment recovery (cm)	Remarks
Northern Red Sea, Egypt									
188	5821-1	22.03.	MN	16:22	27°23.97'	34°14.88'	1118 m	4x1.5 l 5xNet	500, 400*, 300, 200, 100m * no water samples ($1x\delta^{13}C$,$1x\delta^{18}O$, $1xPO_4$)
	5821-2		MN	17:16	27°23.98'	34°14.90'	1119 m	5x1.5 l 5xNet	500*,400,300*,200*,100*m * no water samples ($1x\delta^{13}C$,$1x\delta^{18}O$, $1xPO_4$ Neodym)
	5821-3		MN without net/ CTD	18:19	27°24.00'	34°14.96'	1119 m	5x1.5 l 5xNet	1050, 900, 750, 600, 50 m ($1x\delta^{13}C$,$1x\delta^{18}O$, $1xPO_4$)
189	5822-1	25.03.	MN/CTD	05:44	26°49.46'	34°08.10'	609 m	5xNet	500, 400, 300, 200, 100 m no water samples
Northern Red Sea, Saudi Arabia									
190	5823-1	26.03.	MUC/ CTD	16:19	26°25.26'	35°40.19'	789 m	33 cm	6 big, 4 small tubes filled
	5823-2		SL 6	17:24	26°25.25'	35°40.18'	789 m	410 cm	
191	5824-1	26.03.	MUC/ CTD	20:35	26°29.12'	35°49.52'	587 m	33 cm	6 big, 4 small tubes filled
	5824-2		SL 6	21:23	26°29.13'	35°49.49'	591 m	567 cm	
	5824-3		SL 12	22:40	26°29.12'	35°49.50'	587 m	1016 cm	
192	5825-1	27.03.	MUC/ CTD	01:19	26°30.47'	35°56.94'	1031 m	31 cm	5 big, 4 small tubes filled
	5825-2		SL 12	02:35	26°30.47'	35°56.92'	1030 m	728 cm	
193	5826-1	27.03.	CTD/Ro.	09:29	26°12.70'	35°21.50'	1474 m	3x10 l	
	5826-2		CTD/Ro.	11:07	26°12.71'	35°21.51'	1475 m	3x10 l	
	5826-3		CTD/Ro.	12:49	26°12.71'	35°21.51'	1474 m	10x10 l	
	5826-4		CTD/Ro.	14:45	26°12.72'	35°21.78'	1474 m	10x10 l	
194	5827-1	27.03.	MUC/ CTD	17:10	26°19.11'	35°31.20'	959 m	9 cm	4 small tubes filled
195	5828-1	28.03.	MUC/ CTD	02:19	26°20.78'	35°24.13'	1072 m	11-35 cm	5 big, 4 small tubes filled
	5828-2		SL 12	03:39	26°20.71'	35°24.08'	1057 m	915 cm	
196	5829-1	28.03.	CTD/Ro.	07:23	26°12.73'	35°21.68'	1472 m	10x10 l	
197	5830-1	28.03.	CTD/Ro.	11:34	26°14.00'	35°22.70'	1444 m	10x10 l	
	5830-2	.	CTD/Ro.	14:20	26°14.00'	35°22.70'	1445 m	10x10 l	
198	5831-1	29.03.	MUC/ CTD	01:25	27°05.30'	35°33.98'	884 m	32 cm	5 big, 4 small tubes filled
	5831-2		SL 12	02:33	27°05.29'	35°33.97'	884 m	1146 cm	
199	5832-1	29.03.	MUC/ CTD	04:49	27°03.20'	35°24.32'	628 m	30 cm	5 big, 4 small tubes filled
	5832-2		SL 12	05:43	27°03.17'	35°24.29'	628 m	1147 cm	
	5832-3		MUC	07:09	27°03.18'	35°24.31'	628 m	30 cm	6 big, 4 small tubes filled
	5832-4		KL 12	09:30	27°03.18'	35°24.32'	627 m	1090 cm	
	5832-5		KL 18	11:49	27°03.18'	35°24.30'	628 m	1660 cm	
200	5833-1	29.03.	SL 18	16:59	27°03.17'	35°24.26'	628 m	-	(same location as 5832) core empty, no samples
	5833-2		SL 18	17:46	27°03.17'	35°24.26'	628 m	1638 cm	(same location as 5832)
201	5834-1	29.03.	SL 18	19:43	27°05.27'	35°34.01'	886 m	1661 cm	(same location as 5831)
202	5835-1	30.03.	CTD/Ro.	10:25	26°15.51'	35°20.00'	1327 m	10x10 l	
	5835-2		CTD/Ro.	12:38	26°15.52'	35°20.00'	1327 m	10x10 l	
	5835-3		IWS 3 m	16:47	26°15.51'	35°20.00'	1328 m	17x0.5 l	
	5835-4		MUC	18:17	26°15.49'	35°20.02'	1328 m	-	no surface, no samples
	5835-5		MUC	19:41	26°15.52'	35°19.99'	1328 m	2 kg	6 big, 4 small tubes filled
	5835-6		MUC	21:03	26°15.50'	35°19.99'	1328 m	2 kg	6 big, 4 small tubes filled
	5835-7		SL 18	22:34	26°15.50'	35°20.00'	1328 m	152 cm	70 cm liquid, tube bent
203	5836-1	31.03.	MUC	00:32	26°12.60'	35°21.55'	1474 m	-	no surface, no samples
	5836-2		SL 12	02:09	26°12.61'	35°21.56'	1475 m	790 cm	
	5836-3		MUC	03:13	26°12.61'	35°21.54'	1475 m	-	tubes empty, no samples
204	5837-1	31.03.	MUC/ CTD	15:01	27°36.69'	34°51.85'	771 m	18 cm	6 big, 4 small tubes filled
	5837-2		SL 12	15:51	27°36.69'	34°51.87'	770 m	718 cm	
	5837-3		KL 18	18:02	27°36.67'	34°51.86'	770 m	1740 cm	

Table 7.3.1: continued

Meteor No. 1999	GeoB No.	Date 1999	Equipment	Time Seafloor (UTC)	Latitude N	Longitude E	Water Depth (m)	Samples/ Sediment recovery (cm)	Remarks
205	5838-1	01.04.	MUC/ CTD	07:24	27°34.54'	34°44.16'	832 m	31 cm	6 big, 4 small tubes filled
	5838-2		KL 12	08:37	27°32.76'	34°44.33'	830 m	1070 cm	
	5838-3		SL 18	10:37	27°34.67'	34°44.26'	830 m	1618 cm	
206	5839-1	01.04.	SL 18	12:06	27°34.73'	34°47.91'	802 m	1052 cm	
	5839-2		MUC/ CTD	12:55	27°34.84'	34°47.92'	803 m	17 cm	6 big, 3 small tubes filled
207	5840-1	01.04.	MUC/ CTD	15:01	27°31.66'	34°41.24'	908 m	32 cm	6 big, 4 small tubes filled
	5840-2		SL 18	16:08	27°31.66'	34°41.24'	909 m	1630 cm	
	5840-3		KL 18	18:21	27°31.65'	34°41.24'	908 m	1720 cm	
208	5841-1	01.04.	KL 12	20:55	27°40.52'	34°48.00'	813 m	1065 cm	
209	5842-1	02.04.	MUC/ CTD	12:14	27°42.70'	35°02.84'	863 m	35 cm	6 big, 4 small tubes filled
	5842-2		SL 18	13:21	27°42.74'	35°02.86'	863 m	1337 cm	
210	5843-1	02.04.	SL 18	16:34	27°52.71'	34°58.16'	529 m	1469 cm	
	5843-2		MUC/ CTD	17:15	27°52.69'	34°58.16'	529 m	35 cm	5 big, 4 small tubes filled
211	5844-1	02.04.	MUC/ CTD	20:00	27°42.81'	34°40.94'	963 m	32 cm	6 big, 4 small tubes filled
	5844-2		SL 18	20:53	27°42.81'	34°40.90'	963 m	1235 cm	
Eastern Mediterranean Sea, Israel									
212	5845-1	05.04.	MUCII	06:30	32°19.29'	34°09.90'	1284 m	42 cm	2 big tubes filled
	5845-2		KL 12	07:55	32°19.30'	34°09.96'	1283 m	1065 cm	
213	5846-1	06.04.	KL 12	04:59	32°36.87'	34°08.89'	1433 m	1050 cm	
	5846-2		MUCII	06:04	32°36.80'	34°08.94'	1432 m	50 cm	3 big tubes filled
214	5847-1	06.04.	MUCII	08:48	32°49.23'	34°09.84'	1532 m	40 cm	3 big tubes filled
	5847-2		KL 12	10:27	32°49.23'	34°09.92'	1533 m	893 cm	
215	5848-1	06.04.	KL 12	13:20	32°36.82'	34°01.62'	1449 m	1042 cm	
	5848-2		MUCII	14:32	32°36.81'	34°01.62'	1449 m	40 cm	3 big tubes filled

CTD	Conductivity-temperature-depth profiler
CTD/Ro.	CTD/Rosette water sampler (10 NISKIN bottles with 10 l each)
GKG	Large box corer
IWS 3m	Interface water sampler, 3 m length (17x0.5 l)
KL	Piston corer (with 12 or 18 m pipe)
MN	Multinet (5 nets)
MUC	Multicorer (with 6 big and 4 small tubes, GeoB)
MUCII	Multicorer (with 8 big tubes, GPITü)
SL	Gravity corer (with 6, 12, or 18 m pipe)

7.4 Leg M44/4

7.4.1 Station Lists

Table 7.4.1: Station list of Leg M44/4

Abbreviation of devices		Deployments
CTD/Ro	= CTD/Rosette (with pinger)	60
BYP	= Butterfly sampler	13
D-MOC	= Double-Mocness, 1 sqm mouth opening	33
Go-Flo-WS	= water sampler (Niskin) cast	01
HN	= Handnet	34
ISP	= *In-situ*-pump	05
MOC-10	= Mocness, 10 sqm mouth opening	14
MUC	= Multiple corer	05
NBT	= Near Bottom Trawl (supraepibenthic sledge)	07
NEU	= Neustonnet	61
OFS	= Surface water sampler	35
PP-Drifter	= *In-situ*-production assambly	07
SD	= Secchi-Disc	06
ST	= Sediment trap	01

HYDROSWEEP/PARASOUND (HS/PN): 35 nm; ADCP and thermosalinograph continuously between 10.4. and 13.05.1999, i.e. begin and end of the station program.

a.b. = above bottom

Station No	Date 1999	Local Time (UTC+2 hrs)	Device	Start-Position	End-Position	Working Depth (m) remarks
	10.04.	1535	OFS	32°51.25N 033°50.82E		0
216		1735-2140	D-MOC	32°50.06N 033°10.02E	32°57.56N 033°09.73E	0-1370
		1915	OFS	32°51.45N 033°10.20E		0
		2228-2308	CTD/Ro	32°49.97N 033°10.05E		0-200
	10./11.04.	2321-0031	CTD/Ro	32°49.94N 033°10.01E		wc (water column)
217	11.04.	0704-0856	CTD/Ro	33°50.07N 034°00.08E		wc
		0826	OFS	33°50.01N 034°00.07E		0
		1410	OFS	33°49.95N 032°49.98E		0
		1700-1855	HS/PN	33 50.00N 032 10.00E	34°08.00N 031°55.80E	
218	11./12.04	20:08-0048	D-MOC	33°59.64N 032°02.38E	34°07.87N 031°55.89E	0-1850
219	12.04.	0102-0230	CTD/Ro	34°07.96N 031°55.85E		wc
		0300-0319	CTD/Ro	34°07.93N 031°55.85E		0-200
		0410-0509	CTD/Ro	34 07.90N 031°55.82E		0-1000
		0546-1242	PP-Drifter	34°07.88N 031°55.84E	34°05.98N 031°59.28E	
		0611-0634	CTD/Ro	34°07.87N 031°55.73E		0-200
		0705-0853	CTD/Ro	34°07.93N 031°55.76E		wc
		0904-0912	HN	34°07.90N 031°55.80E		0-ca 30
		0932-0948	HN	34°07.91N 031°55.81E		0-ca 30
		1105-1151	CTD/Ro	34°07.15N 031°58.10E		0-1000
		1157-1202	SD	34°06.79N 031°58.26E		0-20
		1355-1444	CTD/Ro	34°07.89N 031°55.87E		0-1000
		1650-1734	CTD/Ro	34°07.89N 031°55.85E		0-1000
		1953-2037	CTD/Ro	34°07.91N 031°55.82E		0-1000
		2038-2053	HN	34°07.88N 031°55.89E		0-ca 30
		2252-2337	CTD/Ro	34°07.90N 031°55.87E		0-1000
	13.04.	0152-0235	CTD/Ro	34°07.86N 031°55.89E		0-1000
		0451-0518	CTD/Ro	34°07.99N 031°55.82E		0-300
		0533-0723	CTD/Ro	34°07.95N 031°55.82E		wc
		0724-0831	HS/PN	34°07.82N 031°55.76E	34°05.00N 032°10.00E	
220		0836-1312	D-MOC	34°05.10N 032°10.22E	34°04.80N 031°59.61E	0-1850
		1251	OFS	34°04.84N 032°00.38E		0
221		1335-1511	MUC	34°04.81N 031°59.67E		2483
	13./14.04.	1555-0030	ISP	34°05.65N 031°57.92E		2500

Table 7.4.1: continued

222	14.04.	0126-0952	D-MOC	34°05.57N 032°06.15E	34°04.32N 031°47.75E	near bottom
		10:00-10:21	HN	34°04.27N 031°47.75E	34°04.35N 031°47.94E	0-ca 30
223		1117-1518	D-MOC	34°04.64N 031°48.44E	33°57.13N 031°50.21E	0-1850
224		1552-1729	BYP	33°57.10N 031°50.28E		300-500
225		1741-2255	D-MOC	33°56.94N 031°50.12E	33°48.49N 031°42.62E	0-1850
226	15.04.	0157-0343	CTD/Ro	34°05.51N 032°06.06E		wc
		0512-1218	PP-Drifter	34°05.47N 032°06.05E	34°02.00N 032°07.01E	
		0531-0817	BYP	34°05.52N 032°05.90E		0-2400
		0832-0908	BYP	34°05.21N 032°06.02E		0-253
		0918-1045	BYP	34°05.11N 032°06.12E		0-1000
		1132-1142	SD	34°02.15N 032°07.37E		0-28
227		1302-2110	D-MOC	34°05.56N 032°05.82E	34°05.74N 031°46.03E	near bottom
228	15./16.04.	2131-0634	ISP+BYP	34°05.73N 031°45.85E		2250-2425
229	16.04.	0754-1328	D-MOC	34°05.25N 032°00.21E	34°09.29N 031°47.52E	near bottom
		0904-0921	NEU	34°05.86N 031°57.44E	34°06.01N 031°56.83E	0-ca 30 cm
		0935-0943	NEU	34°06.15N 031°56.40E	34°06.29N 031°55.88E	0-ca 30 cm
		1224-1240	NEU	34°08.18N 031°50.20E	34°08.50N 031°49.54E	0-ca 30 cm
		1242-1258	NEU	34°08.53N 031°49.47E	34°08.83N 031°48.76E	0-ca 30 cm
230		1533-1719	CTD/Ro intercalibration with RV „EDT Argonaut“	34°06.30N 031°55.99E		wc
231	16./17.04.	2000-0132	NBT	34°06.30N 031°56.00E	34°02.76N 032°08.89E	0.5-1.5 a.b.
232	17.04.	0236-0810	NBT	34°05.03N 032°02.47E	34°08.81N 031°51.83E	0.5-1.5 a.b.
		1030	OFS	34°33.27N 031°33.95E		0
233		1224-1357	CTD/Ro	34°52.01N 031°20.09E		wc
		1400	OFS			0
		1409-1427	NEU	34°52.21N 031°19.95E	34°52.83N 031°19.57E	0-ca 30 cm
234		1643-1823	CTD/Ro	35°16.00N 031°06.00E		wc
		1708	OFS	35°16.00N 031°05.99E		0
		1833-1850	NEU	35°16.00N 031°06.00E	35°15.36N 031°05.35E	0-ca 30 cm
235		2146-2334	CTD/Ro	34°50.01N 030°40.00E		wc
		2200	OFS	34°50.02N 030°39.94E		0
		2342-2400	NEU	34°50.00N 030°40.02E	34°49.55N 030°40.29E	0-ca 30 cm
236	18.04.	0500-0649	CTD/Ro	33°57.99N 031°12.00E		wc
		0655-0713	NEU	33°58.01N 031°11.85E	33°57.85N 031°11.06E	0-ca 30 cm
237		1015-1210	CTD/Ro	33°52.07N 030°30.03E	33°52.05N 030°30.01E	wc
		1025	OFS	33°52.05N 030°30.03E		0
238		1940-2129	CTD/Ro	34°01.99N 028°51.00E		wc
		2000	OFS	34°01.99N 028°51.04E		0
		2133-2152	NEU	34°02.01N 028°51.10E	34°02.07N 028°50.45E	0-ca 30 cm
239	19.04.	0405-0500	CTD/Ro	34°19.85N 027°30.15E		0-1000
		0535-0724	CTD/Ro	34°20.00N 027°30.00E		wc
		0730-1401	PP-Drifter	34°19.00N 027°30.00E	34°10.80N 027°31.33E	
		0802-1200	D-MOC	34°19.20N 027°29.82E	34°25.12N 027°25.13E	0-1450
		1206-1222	NEU	34°25.13N 027°25.09E	34°25.54N 027°24.82E	0-ca 30 cm
		1406-1410	SD	34°10.74N 027°31.32E		0-24
240		1514-2055	MOC	34°17.04N 027°30.19E	34°26.81N 027°23.37E	0-2500
		1553-1610	NEU	34°18.09N 027°29.42E	3418.62°N 027°29.10E	0-ca 30 cm
241	20.04.	0033	OFS	34°55.00N 026°51.06E		0
		0034-0150	CTD/Ro	34°55.00N 026°51.06E		wc
242		0225-0551	D-MOC	34°58.11N 026°52.02E	35°03.66N 026°47.05E	0-1450
243		0704-0800	CTD/Ro	35°05.55N 026°34.97E		wc
244		1211-1356	ST	34°25.78N 026°11.32E	34°25.98N 026°11.97E	release/ recov. trap
		1435	ST	34°25.78N 026°12.70E		end station
245	20./21.04.	1524-0023	D-MOC	34°22.03N 026°06.54E	34°32.56N 025°48.03E	0-4100
246	21.04.	0149-0408	CTD/Ro	34°28.47N 025°58.60E		wc
		0417-0436	NEU	34°28.48N 025°58.55E	34°28.00N 025°58.96E	0-ca 30 cm
247		0741-0944	CTD/Ro	34°03.04N 026°25.00E		wc

Table 7.4.1: continued

		0820	OFS	34°03.01N 024°95.00E		0
		0951-1010	NEU	34°02.85N 026°24.87E	34°02.38N 026°24.51E	0-ca 30 cm
-		1401	OFS	33°21.56N 026°00.48E		0
248		1452-1631	CTD/Ro	33°14.05N 025°56.10E		wc
		1637-1654	NEU	33°13.93N 025°56.17E	33°13.22N 025°56.12E	0-ca 30 cm
249		1952-2143	CTD/Ro	32°42.94N 025°40.00E		wc
		2055	OFS	32°42.98N 025°40.01E		0
	21./22.04.	2147-0303	D-MOC	32°43.13N 025°39.93E	32°53.96N 025°38.15E	0-2500
		2220-2254	NEU	32°44.19N 025°39.86E	32°45.33N 025°39.73E	0-ca 30 cm
250	22.04.	0630-0810	CTD/Ro	33°29.99N 025°32.00E		wc
		0700	OFS	33°30.00N 025°32.00E		0
		0813-0831	NEU	33°30.03N 02531.99°E	33°30.58N 025°32.17E	0-ca 30 cm
251		1252-1512	CTD/Ro	34°20.01N 025°35.01E		wc
		1312	OFS	34°19.93N 025°35.27E		0
		1515-1524	HN	34°19.63N 025°35.10E		0-ca 30
		1528-1534	HN	34°19.53N 025°35.03E		0-ca 30
252		1718-2200	MOC-10	34°23.03N 025°58.19E	34°26.87N 026°09.20E	1450-2500
253	22./23.04.	2307-0047	MOC-10	34°23.64N 025°59.50E	34°25.16N 026°03.34E	250-600
254	23.04.	0112-0411	CTD/Ro	34°25.51N 026°05.11E		wc
		0530-1207	PP-drifter	34°25.54N 026°05.21E	34°27.12N 026°06.28E	
		0557-1100	MOC-10	34°25.57N 026°05.57E	34°32.37N 026°09.95E	1450-2500
		1209-1217	SD	34°27.15N 026°06.30E		0-36
255		1239-1330	MOC-10	34°28.19N 026°05.77E	34°27.04N 026°07.22E	0-250
256		1442-2400	MOC-10	34°32.73N 026°06.78E	34°14.36N 026°06.09E	3750 - near bottom
		1536-1552	NEU	34°30.91N 026°06.79E	34°30.43N 026°06.79E	0-ca 30 cm
		1553-1610	NEU	34°30.39N 026°06.79E	34°29.95N 026°06.78E	0-ca 30 cm
257	24.04.	0030-0122	MOC-10	34°18.24N 026°06.15E	34°20.29N 026°06.25E	0-250
258		0238-0939	MOC-10	34°32.80N 026°06.84E	34°18.80N 026°06.71E	2500-3750
		0257-0314	NEU	34°32.16N 026°06.80E	34°31.57N 026°06.79E	0-ca 30 cm
		0941-0958	HN	34°18.78N 026°06.71E	34°18.73N 026°06.64E	0-ca 30
259		1032-1333	MOC-10	34°22.78N 026°06.76E	34°28.97N 026°07.09E	600-1450
260		1410-1546	MOC-10	34°26.90N 026°07.08E	34°23.84N 026°07.14E	250-600
261		1635-2325	MOC-10	34°27.05N 026°09.80E	34°21.76N 025°54.29E	2500-3750
		1658-1733	NEU	34°26.75N 026°08.90E	34°26.27N 026°07.48E	0-ca 30 cm
262	25.04	0013-0309	MOC-10	34°24.03N 026°00.10E	34°26.13N 026°06.75E	600-1450
263		0322-1252	ISP+BYP	34°26.20N 026°06.82E		4000-4250
		1259-1435	BYP+GoFo-Sampler	34°26.20N 026°06.82E		0-1000
		1437-1453	BYP	34°26.20N 026°06.81E		0-54
264	25./26.04.	1540-0147	D-MOC	34°28.53N 026°14.41E	34°21.17N 025°51.62E	near bottom
		1855-1912	NEU	34°26.17N 026°07.41E	34°25.95N 026°06.72E	0-ca 30 cm
		2012-2040	HN	34°25.19N 026°04.54E	34°24.83N 026°03.40E	0-ca 30
265	26.04.	0434-0454	CTD/Ro	34°21.19N 025°51.64E		0-150
		0646-1237	PP-drifter	34°25.32N 026°05.02E	34°26.90N 026°04.48E	
		0655-0943	CTD/Ro	34°25.21N 026°04.96E		wc
		1240-1245	SD	34°26.92N 026°04.45E		0-31
266		1341-2345	D-MOC	34°28.24N 026°13.33E	34°20.70N 025°51.23E	0-4250
		1521-1535	NEU	34°27.08N 026°09.96E	34°26.92N 026°09.46E	0-ca 30 cm
		1538-1553	NEU	34°26.89N 026°09.38E	34°26.68N 026°08.83E	0-ca 30 cm
		1906-1932	HN	34°24.15N 026°01.72E	34°23.80N 026°00.75E	0-ca 30
		2144-2201	HN	34°22.17N 025°56.65E	34°22.00N 025°54.97E	0-ca 30
267	27.04.	0144-1105	D-MOC	34°22.89N 025°58.04E	34°35.69N 026°10.56E	1450-4250
		0211-0228	NEU	34°23.22N 025°59.04E	34°23.44N 025°59.62E	0-ca 30 cm
268		1148-1534	D-MOC	34°35.96N 026°10.65E	34°29.10N 026°08.43E	0-1450
269	27./28.04.	1624-0043	D-MOC	34°28.00N 026°12.84E	34°21.30N 025°54.41E	0-4250
	27.04.	1915-1940	HN	34°25.67N 026°06.43E	34°25.51N 026°06.00E	0-ca 30
		2009-2025	NEU	34°25.11N 026°04.83E	34°24.90N 026°04.30E	0-ca 30 cm
		2146-2226	HN	34°23.64N 026°01.28E	34°23.11N 025°59.74E	0-ca 30
270	28.04.	0122-1030	D-MOC	34°23.04N 025°58.12E	34°30.76N 026°18.45E	1450-4250

Table 7.4.1: continued

		0139-0157	NEU	34°23.30N 025°58.88E	34°23.53N 025°54.54E	0-ca 30 cm
		0929-0942	HN	34°29.63N 026°16.01E	34°29.88N 026°16.50E	0-ca 30
		0945-1001	NEU	34°29.94N 026°16.64E	34°30.27N 026°17.36E	0-ca 30 cm
		1032-1052	HN	34°30.88N 026°18.67E	34°31.13N 026°19.11E	0-ca 30
271		1204-2108	D-MOC	34°24.64N 026°12.42E	34°25.50N 025°50.02E	near bottom
		1526-1542	NEU	34°25.13N 026°04.49E	34°25.15N 026°03.88E	0-ca 30 cm
272	28./29.04.	2206-0213	D-MOC	34°25.51N 025°57.41E	34°25.60N 026°07.76E	0-1450
	28.04.	2240-2254	HN	34°25.42N 025°58.91E	34°25.42N 025°59.45E	0-ca 30
	28.04.	2315-2332	NEU	34°25.44N 026°00.31E	34°25.44N 026°00.96E	0-ca 30 cm
273	29.04.	0423-0442	CTD/Ro	34°25.49N 026°05.16E		0-150
		0538-1323	PP-Drifter	34°25.58N 026°05.24E	34°29.43N 026°06.25E	
		0548-0800	CTD/Ro	34°25.51N 026°05.19E		wc
		0826-1220	D-MOC	34°25.56N 026°05.93E	34°29.67N 026°14.36E	0-1450
		1324-1328	SD	34°29.45N 026°06.26E		0-28
		1325-1332	HN	34°29.45N 026°06.26E		0-ca 30
274		1415-2200	D-MOC	34°28.04N 026°12.91E	34°19.54N 025°59.03E	0-4250
		2100-2150	HN	34°21.59N 025°59.33E	34°19.74N 025°59.06E	0-ca 30
275	30.04.	0000-0830	NBT	34°26.50N 025°59.58E	34°21.06N 026°18.67E	0.5-1.5 a.b.
		0032-0049	NEU	34°26.17N 026°01.04E	34°26.00N 026°01.64E	0-ca 30 cm
		0600-0618	NEU	34°22.60N 026°12.86E	34°22.43N 026°13.56E	0-ca 30 cm
		0639-0655	NEU	34°22.21N 026°14.38E	34°22.02N 026°15.08E	0-ca 30 cm
276		0927-1804	NBT	34°28.13N 026°13.24E	34°21.57N 025°54.50E	0.5-1.5 a.b.
		1724-1741	NEU	34°22.13N 025°56.14E	34°21.89N 025°55.44E	0-ca 30 cm
277	30.04./ 01.05.	2031-0552	ISP+BYP	34°26.43N 026°07.86E		2000-4230
278	01.05.	0631-1327	MOC-10	34°28.14N 026°12.82E	34°22.60N 025°57.15E	2500-3750
279		1407-1910	MOC-10	34°23.93N 026°00.95E	34°28.00N 026°12.40E	600-1450
		1439-1456	NEU	34°24.40N 026°02.34E	34°24.62N 026°02.99E	0-ca 30 cm
280	01./02.05.	2030-0102	D-MOC	34°28.30N 026°13.02E	34°24.88N 026°03.15E	0-1450
	01.05.	2140-2155	HN	34°27.66N 026°11.22E	34°27.26N 026°09.96E	0-ca 30
281	02.05.	1050-1150	CTD/Ro	35°10.08N 027°30.00E		wc
		1229-1547	D-MOC	35°13.75N 027°26.92E	35°10.18N 027°19.93E	0-1250
		1244-1300	NEU	35°13.50N 027°26.38E	35°13.15N 027°25.77E	0-ca 30 cm
		1301-1316	NEU	35°13.14N 027°25.74E	35°12.87N 027°25.16E	0-ca 30 cm
		1318-1335	NEU	35°12.81N 027°25.09E	35°12.49N 027°24.49E	0-ca 30 cm
282	02./03.05.	2208-0156	MOC-10	34°28.26N 026°13.19E	34°25.43N 026°04.84E	600-1450
283	03.05.	0249-1130	NBT	34°28.03N 026°12.90E	34°21.55N 025°53.67E	0.5-1.5 a.b.
284		1235-1517	MUC	34°24.88N 026°05.81E		failure
		1532-1807	MUC	34°24.88N 026°05.79E		4263
285		1848-2112	MUC	34°25.90N 026°10.76E		3702
286	04.05.	0000-0844	D-MOC	34°29.72N 026°10.17E	34°15.51N 026°00.06E	near bottom
287		1021-1142	NBT	34°28.12N 026°12.91E	34°28.05N 026°12.35E	winch failure
		1226-1314	HN	34°28.30N 026°13.20E		0-ca 30
		1611-1722	CTD/Ro	34°32.76N 025°48.35E		wc
288	04./05.05.	1919-0422	NBT	34°27.99N 026°12.82E		0.5-1.5 a.b.
	04.05.	2039-2101	HN	34°27.99N 026°12.82E	34°26.68N 026°09.83E	0-ca 30
	04.05.	2105-2122	NEU	34°26.63N 026°08.85E	34°26.44N 026°08.26E	0-ca 30 cm
	05.05.	0023-0040	NEU	34°24.05N 026°01.62E	34°20.46N 025°51.61E	0-ca 30 cm
289		0753-0910	CTD/Ro	34°34.00N 025°04.93E		wc
		0822	OFS	34°34.00N 025°04.96E		0
		0915-0935	NEU	34°34.01N 025°04.81E	34°34.31N 025°03.99E	0-ca 30 cm
290		1249-1458	CTD/Ro	34°40.02N 024°19.98E		wc
		1312	OFS	34°40.02N 024°20.01E		0
		1509-1524	NEU	34°40.07N 024°19.66E	34°40.20N 024°18.92E	0-ca 30 cm
		1526-1541	NEU	34°40.22N 024°18.84E	34°40.34N 024°18.19E	0-ca 30 cm
291		1932-2129	CTD/Ro	34°50.06N 023°25.00E		wc
		1954	OFS	34°50.01N 023°24.99E		0
		2135-2154	NEU	34°49.98N 023°24.87E	34°49.84N 023°24.08E	0-ca 30 cm
292	06.05.	0028-0237	CTD/Ro	34°55.96N 022°49.92E		wc

Table 7.4.1: continued

		0032	OFS	34°55.97N 022°49.92E		0
		0243-0300	NEU	34°56.03N 022°49.78E	34°56.11N 022°49.08E	0-ca 30 cm
293		0911-1133	CTD/Ro	35°13.76N 021°28.70E		wc
		1106	OFS	35°13.76N 021°28.73E		0
		1145-1545	D-MOC	35°13.77N 021°28.56E	35°15.67N 021°18.68E	0-1450
		1227-1243	NEU	35°14.36N 021°25.24E	35°14.20N 021°26.01E	0-ca 30 cm
		1245-1302	NEU	35°14.22N 021°25.90E	35°14.36N 021°25.24E	0-ca 30 cm
		1305-1314	HN	35°14.38N 021°25.11E	35°14.44N 021°24.78E	0-ca 30
		1315-1324	HN	35°14.46N 021°24.70E	35°14.52N 021°24.39E	0-ca 30
294		1649-1911	MUC	35°14.00N 021°28.53E		3457
	06./07.5.	1956-0430	ISP+BYP	35°13.74N 021°28.69E		2250-3490
	07.5.	0442-0537	CTD/Ro	35°13.75N 021°28.66E		0-250
		0614-1323	PP-Drifter	35°13.86N 021°28.46E	35°19.56N 021°13.65E	
		0642-0859	CTD/Ro	35°13.77N 021°28.76E		wc
		0914-1323	BYP	35°13.77N 021°28.65E		near bottom
		1837-1842	Ro	35°13.77N 021°28.67E		30; test
		1848-2115	Ro	35°13.76N 021°28.69E		near bottom
		2121-2347	BYP	35°13.75N 021°28.72E		100-1840
		2350-2400	BYP	35°13.76N 021°28.74E		10
	08.5.	0006-0906	D-MOC	35°13.76N 021°28.88E	35°16.58N 021°51.15E	600-3250
295		1655-1846	CTD/Ro	34°25.00N 020°20.15E		wc
		1736	OFS	34°24.99N 020°20.18E		0
		1851-1907	NEU	34°25.00N 020°20.00E	34°24.48N 020°19.45E	0-ca 30 cm
296	09.5.	0045-0820	D-MOC	33°41.31N 019°16.58E	33°31.80N 019°02.67E	600-3250
		0059-0114	NEU	33°40.96N 019°16.06E	33°40.56N 019°15.49E	0-ca 30 cm
		0119-0137	NEU	33°40.44N 019°15.36E	33°40.06N 019°14.88E	0-ca 30 cm
		0405-0430	HN	33°36.99N 019°10.60E	33°36.51N 019°09.88E	0-ca 30
297		0905-1254	D-MOC	33°35.08N 019°07.46E	33°30.14N 019°00.35E	0-1450
		0914-0931	NEU	33°34.84N 019°07.12E	33°34.47N 019°06.59E	0-ca 30 cm
		1026-1043	NEU	33°33.37N 019°04.91E	33°33.01N 019°04.40E	0-ca 30 cm
		1040-1103	HN	33°33.04N 019°04.43E	33°32.61N 019°03.79E	0-ca 30
		1212-1218	HN	33°31.01N 019°01.64E	33°30.86N 019°01.43E	0-ca 30
		1220-1227	HN	33°30.83N 019°01.38E	33°30.67N 019°01.14E	0-ca 30
298		1338-1551	D-MOC	33°33.18N 019°04.54E	33°30.28N 019°00.45E	0-750
299		1605-1809	CTD/Ro	33°30.02N 019°00.05E		wc
		1621	OFS	33°30.02N 019°00.03E		0
300	09./10.5.	2317-0156	CTD/Ro	34°30.00N 019°00.03E		wc
	09.05.	2330	OFS	34°30.02N 019°00.03E		0
	10.5.	0202-0217	NEU	34°30.12N 018°59.99E	34°30.82N 018°59.97E	0-ca 30 cm
301		0531-0800	CTD/Ro	35°09.05N 019°00.00E		wc
		0804-0822	NEU	35°09.18N 019°00.04E	35°09.99N 018°59.98E	0-ca 30 cm
302		1213-1435	CTD/Ro	35°50.04N 019°00.02E		wc
		1435	OFS	35°49.97N 018°59.98E		0
		1440-1458	NEU	35°49.90N 018°59.93E	35°49.27N 018°59.03E	0-ca 30 cm
-		1855	OFS	35°17.45N 018°14.73E		0
303		2302	OFS	34°44.91N 017°29.91E		0
	10./11.5.	2303-0059	CTD/Ro	34°44.96N 017°29.95E		wc
	11.5.	0107-0124	NEU	34°45.09N 017°29.83E	34°45.21N 017°28.86E	0-ca 30 cm
304		0531-0918	D-MOC	34°53.88N 016°29.31E	34°55.43N 016°20.17E	0-1450
		0658-0732	NEU	34°54.43N 016°25.76E	34°54.61N 016°24.45E	0-ca 30 cm
		0820-0837	HN	34°55.00N 016°22.20E	34°55.08N 016°21.75E	0-ca 30
		0845-0858	HN	34°55.13N 016°21.41E	34°55.23N 016°20.91E	0-ca 30
305		1003-1053	CTD/Ro	34°56.08N 016°14.85E		wc
		1003	OFS	34°56.08N 016°14.85E		0
306		1626-1710	CTD/Ro	34°56.10N 016°14.98E		wc
		1702	OFS	34°59.98N 016°60.00E		0
		1714-1747	NEU	35°00.10N 014°59.98E	35°00.85N 014°58.72E	0-ca 30 cm
-		2217	OFS	35°30.26N 013°59.93E		0
307	12.05.	0305-0422	CTD/Ro	35°59.94N 012°59.87E		wc
		0328	OFS	35°59.94N 012°59.92E		0

		0427-0459	NEU	35°59.96N 012°59.66E	36°00.99N 012°58.72E	0-ca 30 cm
-		0956	OFS	36°47.17N 012°16.34E		0
308		1508-1555	CTD/Ro	37°34.02N 011°31.98E		wc
		1517	OFS	37°34.03N 011°32.01E		0
		1601-1633	NEU	37°34.08N 011°31.90E	37°35.09N 011°31.26E	0-ca 30 cm
-		2037	OFS	38°17.00N 011°01.10E		0
309	12./13.05.	2347-0440	D-MOC	38°49.61N 010°37.63E	38°58.74N 010°30.95E	0-1850
	13.05.	0056-0111	NEU	38°51.88N 010°35.95E	38°52.32N 010°35.62E	0-ca 30 cm
		0114-0132	NEU	38°52.40N 010°35.56E	38°52.93N 010°35.18E	0-ca 30 cm
310		0505-0700	CTD/Ro	39°00.04N 010°30.00E		wc
	13.05.	0612	OFS	38°59.09N 010°30.00E		0

8 Concluding Remarks

The scientific parties aboard R/V Meteor gratefully acknowledge the fruitful cooperation and efficient technical assistence of captian M. Kull and captain S. Bülow, their officers and crews, who substancially contributed to the overall success of this cruise.

We are indepted to the Federal Foreign Office in Bonn and the German diplomatic representatives in various countries surrounding the Mediterranean and the northern Red Sea, who helped to clear necessary allowances from national authorities. Special thanks go to the German Ambassies at Cairo, at Riad, at Amman, and at Tel Aviv for the support to achieve permissions to carry out research in Egyptian, Saudi Arabian, Jordanian, and Israeli waters in the Red Sea.

We very much appreciate the most valuable help of captain H. Schmickler at the Leitstelle Meteor, Hamburg and the ship´s managing owner, the RF "Reederei Forschungsgemeinschaft GmbH", Bremen during planning and implementation of the cruise.

Financial support for the cruise was supplied by the Deutsche Forschungsgemeinschaft (DFG PA 492/2-1).

9 References

Aksu, A.E., R.N. Hiscott, and D. Yasar (1999). Oscillating Quaternary water levels of the Marmara Sea and vigorous outflow into the Aegean Sea from the Marmara Sea-Black Sea drainage corridor. Mar. Geol., 153, 275-302.

Alavi, S.N. (1988). Late Holocene deep-sea benthic foraminifera from the Sea of Marmara. Mar. Micropaleontol., 13, 213-237.

Alldredge, A. L. and N.W. Silver (1988). Characteristics, dynamics and significance of marine snow.Prog. Oceanog., 20, 41-82.

Amann, R.I., W. Ludwig and K.-H. Schleifer (1995). Phylogenetic identification and in situ detection of individual microbial cells without cultivation. Microbiol. Rev., 59, 143-169.

Arndt, H. (1990). Das pelagische "microbial web" in einem eutrophen Flachsee: Jahreszeitliche Unterschiede in der Wechselwirkung zwischen Proto- und Metazooplankton.- Deutsche Gesellschaft für Limnologie, Erweiterte Zusammenfasung der Jahrestagung in Essen, 112-116.

Azam, F., T. Fenchel, J.G. Field, J.S. Gray, L.-A. Meyer-Reil and T.F. Thingstad (1983). The ecological role of water-column microbes in the sea. Mar. Ecol. Prog. Ser., 10, 257-263.

Barka, A.A. and Kadinsky-Cade, K. (1988). Strike-slip Fault Geometry in Turkey and its influence on earthquake activity. Tectonics, 7, 663-684.

Bau, M. and Dulski, P. (1996). Anthropogenic origin of positive gadolinium anomalies in river waters. Earth and Planet. Sci. Lett., 143, 245-255

Behr, H. D. (1990). Radiation Balance at the Sea Surface in the Atlantic Ocean Region between 40°S and 40°N, J. Geophys. Res., D95, 20633-20640.

Behr, H. D. (1992). Net total and UV-B Radiation at the Sea Surface, Journal of Atmospheric Chemistry, 15, 299-314.

Bell, R.T. and A..J. Kuparinen (1984). Assessing phytoplankton and bacterioplankton production during early spring in lake Erken, Sweden. Appl. Environ. Microbial., 48, 1221-1230.

BENGAL (1999). High resolution temporal and spatial study of the BENthic biology and Geochemistry of a north-eastern Atlantic abyssal Locality (BENGAL). Contract No MAS3 - CT950018. 1 February 1996-31 January 1999. Final Report.

Blackburn, T. H. B. Lund, Aa., Korm, M. D. (1988). C- and N-mineralization in the sediments of earthen marine fishponds. Mar. Ecol. Progr. Ser., 44, 221-227.

Bochdansky, A.B. and G. J. Herndl (1992a). Ecology of amorphous aggregations (marine snow) in the Northern Adriatic Sea: III. Zooplankton interactions with marine snow.- Mar. Ecol. Prog. Ser., 87, 135-146.

Bochdansky, A.B. and G. J. Herndl (1992b). Ecology of amorphous aggregations (marine snow) in the Northern Adriatic Sea: V. Role of zooplankon fecal pellets in marine snow.- Mar. Ecol. Prog. Ser., 89, 297-303.

Boetius, A., S. Scheibe, A. Tselepides, and H. Thiel (1996). Microbial biomass and activities in deep-sea sediments of the Eastern Mediterranean: trenches are benthic hotspots. Deep-Sea Res., I, 43, 1439-1460.

Børsheim, K.Y. and G. Bratbak (1987). Cell volume to carbon conversion factor for a bacteriovorous Monas sp. enriched from seawater. Mar. Ecol. Prog. Ser., 36, 171-175.

Bosselmann, S. and B. Riemann (1986). Zooplankton. In: Riemann, B. and M. Sondergaard, (eds.). Carbondynamics in eutrophic temperate lakes. Elsevier, 199-236.

Cagatay, M.N., Görür, N., Alpar, B., Saatcilar, R. Akkök, R. Sakinç, M. Yuce, H., Yaltirak, C. and Kuscu, I. (1998). Geological evolution of the Gulf of saros. Geo-Marine Letters, 18, 1-9.

Cagatay, M.N., Görür, N., Algan, O., Eastoe, C., Tchapalyga, A., Ongan, D., Kuhn, T., and Kuscu, I.: Late glacial-Holocene palaeoceanography of the Sea of Marmara: timing of the last connections with the Mediterranean and the Black Sea. Marine Geology (submitted).

Caron, D.A. (1991). Evolving role of Protozoa in aquatic nutrient cycles. In: Reid, P.C., C.M. Turley and P.H. Burkill (eds.). Protozoa and their role in marine processes. Springer-Verlg, Berlin, Heidelberg. NATO/ASI Series G, Ecological Science, 25, 387-415.

Caron, D.A., Davis, P.G., Madin, L.P. and Sieburth, Y.McN. (1986). Enrichment of microbial populations in macroaggregetes (marine snow)from surface water of the North Atlantic.- Journal of MarineResearch, 44, 543-565.

Carpenter, J.H. (1965). The Chesapeake Bay Institute technique for the Winkler dissolved oxygen method. Limnol. Oceanogr., 10, 141-143.

CUSHING, D.H., G.F. HUMPRHEY, K. BANSE and T. LAEVASTU (1958). Report of the Committee on Terms and Equivalents.- In: Conseil permanent International Mer (Ed. P.-V. Rapports), 144, 15-16.

DEWEY, J.F. and SENGÖR, A.M.C. (1979). Aegean and surrounding regions: complex multiplate and continuum tectonics in a convergent zone. Geol. Soc. Am. Bull., Part I, 90, 84-92.

DULSKI, P. (1994). Interferences of oxode, hydroxide and chloride analyte species in the determination of rare earth elements in geological samples by inductively coupled plasma-mass spectrometry. Fresenius'Journal of Analytical Chemistry, 350, 194-203.

EDER, W., and HUBER, R. (1999). Recovery of novel procaryotic rRNA sequences from low-temperature, saline brine sediments of Kebrit Deep, Red Sea. Meeresforschung mit FS Sonne, Statusseminar 10.-12.03.99 in Freiberg, Bundesministerium für Bildung und Forschung, Rostock-Warnemünde, Germany.

EDER, W., LUDWIG, W., and HUBER, R. (1999). Novel 16S rRNA gene sequences retrieved from highly saline brine sediments of Kebrit Deep, Red Sea. Arch. Microbiol., 172, 213-218.

EIE (Elektrik Isleri Etud Idaresi Genel Mudurlugu) (1993). Sediment data and sediment transport amount for Surface Waters in Turkey. Publication No. 93-59, 615 pp.

ENTCH B., BOTO, K. G., SIM, R. G., and WELLINGTON, J. T. (1983). Phosphorous and nitrogen in coral reef sediments. Limnol. Oceanogr. 28, 465-467.

ERICSON, D. B., and WOLLIN, G. (1968). Pleistocene climates and chronology in deep-sea sediments. Science, 162, 1227-1234.

FABER, E., BOTZ, R., POGGENBURG, J. SCHMIDT, M., STOFFERS, P., and HARTMANN, M. (1998). Methane in Red Sea brines. Organic Geochemistry 29, 363-379.

FUENTES, A, and ESPINO, L. (1990). Metabolism as determination of nutrient exchange in organic-rich sediments of a coastal lagoon. Ciencias Marinas, 16(3), 45-62.

GOCKE, K. and R. KOPPE (1994). Abundance and Secondary Production of Bacteria in an Extreme Oligotrophic Marine Environment.- In: HIEKE, W., P. HALBACH, M. TÜRKAY and H. WEIKERT, (eds.). Mittelmeer 1993. METEOR-Berichte 94-3, Leitstelle METEOR, Universität Hamburg, 89-91.

GOODAY, A.J. and C.M TURLEY (1990). Response by benthic organisms to input of organic material to the ocean floor. Phil. trans. R. Soc. Lond., 331, 119-138.

GÖRÜR, N., CAGATAY, M.N., SAKINÇ, M., SÜMENGEN, M., GENTÜRK, K., YALTIRAK, C. and TCHAPALYGA, A. (1997). Origin of the Sea of Marmara from Neogene to Quaternary paleogeographic evolution of its frame. International Geology Review, 39, 342-352.

GRAHAM, G., and MAZZULLO, J. (1988). Handbook for Shipboard Sedimentologists. ODP Technical Note Nr. 9.

GRASSHOFF, K., EHRHARDT, M., and KREMLING, K. (1983). Methods of Seawater Analysis. Verlag Chemie, Weinheim, 419 pp.

HALBACH, P., KUHN, T., SCHMIEDL, G., SEIFERT, R., PEKDEGER, A. und MOCHE, R. (1999). Untersuchung des Feststoff- und Fluid-Haushalts im tiefen Marmarameer sowie der regionalen quartären paläozeanographischen Entwicklung. Kurzbericht zur Forschungsfahrt M 44/1. FU Berlin, 22 S.

HARTMANN, M., SCHOLTEN, J., STOFFERS, P., and WEHNER, F. (1998). Hydrographic structure of brine-filled deeps in the Red Sea – new results from the Shaban, Kebrit, Atlantis II, and Discovery Deep. Marine Geology, 144, 311-330.

HAUSMANN, K, N. HÜLSEMANN and S. SCHADE (1994). Protozoology.- In: HIEKE, W., P. HALBACH, M. TÜRKAY and H. WEIKERT, (eds.). Mittelmeer 1993. METEOR-Berichte 94-3, Leitstelle METEOR, Universität Hamburg, 46-47.

HAUSMANN, K., H. ARNDT and M. WOLF (1999). Protozoology. In: HIEKE, W., Ch. HEMLEBEN, P. LINKE, M. TÜRKAY and H. WEIKERT (eds.). Mittelmeer 1997/98, Cruise No. 40, 28 October 1997 - 10 February 1998. METEOR-Berichte, Universität Hamburg, 99-2, 117-119.

HEMLEBEN, C., MEISCHNER, D., ZAHN, R., ALMOGI-LABIN, A., ERLENKEUSER, H., and HILLER, B. (1996). Three hundred eighty thousand year long stable isotope and faunal records from the Red Sea: Influence of global sea level change on hydrography. Paleoceanography, 11, 147-156.

HERNDL, G.J. (1988). Ecology of amorphous aggregations (marine snow) in the Northern Adriatic Sea. II. Microbial density and activity in marine snow and its implication to overall pelagic processes.- Mar. Ecol. Prog. Ser., 48, 265-275.

HERNDL, G.J. (1992). Marine snow in the Northern Adriatic Sea: possible causes and consequences for a shallow ecosystem. Mar. Microb. Food Webs, 6, 149-172.

Herndl, G.J. and P. Peduzzi (1988). Ecology of amorphous aggregations (marine snow) in the Northern Adriatic Sea: I. General considerations. Mar. Ecol., 9, 79-90.

Huber, R. (1999). Die Laserpinzette als Basis für Einzelzellkultivierung. Biospektrum, 4, 289-291.

IOC Manuals and Guides (1983). Chemical methods for use in marine environmental monitoring, UNESCO, 12, pp. 53.

Jacobs, J. (1974). Quantitative Measurement of Food Selection. Oecologia, 31, 420-426.

Karsten, G. and J.F. Imhoff (1999). Analysis of the microbial diversity in the oligotrophic Eastern Mediterranean Sea by fluorescence-in-situ-hybridization. Annual Meeting of the "Vereinigung für Allgemeine und Angewandte Mikrobiologie", 7.3.-10.3.99, Göttingen, Germany. Poster abstract No. P-K 17, Biospektrum Sonderdruck, p. 104.

Karsten, G., J. Süling, F. Lappe and C. Begler. (1999). Abundance, activity and diversity of bacteria in the extreme oligotrophic Eastern Mediterranean. In: W. Hieke, CH. Hemleben, P. Linke, M. Türkay and H. Weikert (eds.). Mittelmeer 1997/98, Cruise No. 40, 28 October 1997 - 10 February 1998. Meteor-Berichte, Universität Hamburg, 99-2, 132-136.

Keller, J., Ryan, W.B.F., Ninkovich, D. and Altherr, R. (1978). Explosive volcanic activity in the Mediterranean over the past 200,000 yr as recorded in deep-sea sediments. Geol. Soc. Am. bull., v89, p 591-606.

Klein, B., W. Roether, B.B. Manca, D. Bregant, V. Beitzel, V. Kovacevic and A. Luchetta (1999). The large deep water transient in the Eastern Mediterranean. Deep-Sea Res. I, 46, 371-414.

Koppelmann, R. and H. Weikert (1999). Temporal changes of deep-sea mesozooplankton abundance in the temperate NE Atlantic and estimates of the carbon budget. Mar. Ecol. Prog. Ser., 179, 27-40.

Krom, M.D., N. Kress, S. Brenner and L.I. Gordon (1991). Phosphorus limitation of primary productivity in the E. Mediterranean Sea. Limnol. Oceanogr., 36, 424-432.

Krom, M.D., S. Brenner, N. Kress, A. Neori and L.I. Gordon (1993). Nutrient distributions during an annual cycle across a warm-core eddy from the eastern Mediterranean Sea. Deep-Sea Res., 40, 805-825.

Landry, M.J. (1994). Methods and controls for measuring the grazing impact of planktonic protists. Mar. Microb. Food Webs, 8, 37-57.

Landry, M.R. and Hassett, R.P. (1982). Estimating the grazing impact of marine mocrozooplankton. Mar. Biol., 67, 283-288.

Landry, M.R., Kirshtein, J. and Constantinou, L. (1995) A refined dilution technique for measuring the community grazing impact of microzooplankton with experimental tests in the Central Equatorial Pacific. Mar. Ecol. Prog. Ser., 120, 53-63.

Laybourn-Parry, J. (1984). A Functional Biology of Free-Living Protozoa. Croom Helm, Australia.

Li, H., Veldhuis, M.J.W. and Post, A.F. (1998). Alkaline phosphatase activities among planktonic communities in the northern Red Sea. Mar. Ecol. Prog. Series.

Lindell, D. and Post, A.F. (1995). Deep mixing triggers a succession among ultraphytoplankton in the Gulf of Aqaba (Eilat), Red Sea. Limnol. Oceanogr, 40, 1130-1140.

Lindell, D., Padan, E. and Post, A.F. (1998). ntcA expression and nitrite uptake in the marine Synechococcus sp. strain WH7803. J. Bacteriol., 180, 1878-1886.

Lenz, J., H. auf dem Venne, A. Detmer, P. Fritsche, U. Junghans, I. Kirsch, T. Luetkebohle and R. Turnewitsch (1994). Primary Production and Microbial Loop in the Mixed Surface Layer.- In: Hieke, W., P. Halbach, M. Türkay and H. Weikert, (eds.). Mittelmeer 1993. Meteor-Berichte 94-3, Leitstelle Meteor, Universität Hamburg, 81-89.

Lochte, K. and C.M Turley (1988). Bacteria and cyanobacteria associated with phytodetritus in the deep sea. Nature, 333, 67-69.

Lu, C.C., A. Guerra, F. Palumbo and W.C. Summers (1992). Order Sepioidea Naef, 1916. In: Sweeney, M.J., C.F.E. Roper, K.M. Mangold, M.R. Clarke, and S. von Boletzky (eds.). "Larval" and juvenile cephalopods: a manual for their identification. Smithson. Contrib. Zool., 513, 21-36.

Lynn, D.H. (1992). Protargol staining, B-4.1-C-4.8.- In: Lee, J.J. and A.T. Saldo (eds.). Protocols in Protozoology. Published by the Society of Protozoologists.

Malanotte-Rizzoli, P. and A. Hecht (1988). Large-scale properties of the eastern Mediter-ranean: a review. Oceanologica Acta, 11, 323-335.

Malanotte-Rizzoli, P., B.B. Manca., M. Ribera d'AlcalÀ, A. Theocharis, S. Brenner, G. Budillon and E. Ozsoy (1999). The Eastern Mediterranean in the 80'S and in the 90'S: the big transition in the intermediate and deep circulation. Dyn. Atm. and Oceans, (accepted).

McKenzie, D.P., (1972). Active tectonics of the Mediterranean region, Geophys. J.R. Astr. Soc., 30, 109-185.

Mix, A. C., Rugh, W., Pisias, N. G., and Veirs, S. (1992). Color reflectance spectroscopy: A tool for rapid characterization of deep-sea sediment. In "Proceedings of the Ocean Drilling Project, Initial Report 138." (I. Mayer, N. G. Pisias, and T. e. a. Janecek, Eds.).

Mulineaux, L.S., and G.P. Lohmann (1981). Late Quaternary stagnations and recirculation of the eastern Mediterranean: Changes in the deep water recorded by fossil benthic foraminifera. J. Foraminiferal Res., 11, 20-39.

Müller-Nicklas, G., S. Schuster, E. Kaltenböck and G. Herndl (1994). Organic content and bacteria metabolism in amorphous aggregations of the northern Adriatic Sea. Limnol. Oceanogr., 39, 58-68.

Murray, J.W. (1991). Ecology and palaeoecology of benthic foraminifera. Longman Scientific & Technical, London, 397 pp.

Muyzer, G. and K. Smalla (1998). Application of denaturing gradient gel electrophoresis (DGGE) and temperature gradient gel electrophoresis (TGGE) in microbial ecology. Antonie van Leeuwenhoek 73, 127-141.

Nesis, K.N. (1982). Abridged key to the cephalopod mollusks of the World Ocean. In Burgess, L.A. (ed.). Cephalopods of the world. Light and Food Industry Publishing House, Moscow: 385+ii pp (In Russian.). Translated into English by Levitov, B.S. 1987. T. F. H. Publications, Neptune City: 351 pp.

Niewöhner, C., Hensen, C., Kasten, S., Zabel, M., and Schulz, H.D. (1998). Deep sulfate reduction completely mediated by anaerobic methane oxidation in sediments of the upwelling area off Namibia. Geochim. Cosmochim. Acta, 62, 455-464.

Nixon, S. W., Kelly, J. R., Purnas, B. N., Oviatte, C. A., and Hale, S. S. (1980). Phosphorus regeneration and the metabolism of coastal marine bottom communities. In: K.R. Tenore and B.C Coull (eds). Marine Benthic Dynamics, University of South Carolina Press, Columbia, pp. 219-242.

Okay, A.I., Demirbag, E., Kurt, H., Okay, N. and Kuscu, I. (1999). An active, deep marine strike-slip basin along the north Anatolian Fault in Turkey. Tectonics, 18, 129-147.

Ouverney, C. C. and J.A. Fuhrman (1997). Increase in fluorescence intensity of 16S rRNA in situ hybridization in natural samples treated with chloramphenicol. Appl. Environ. Microbiol., 63, 2735-2740.

Padisák, J. and R. Adrian (1999). In: von Tümpling, W. and G. Friedrich, (eds.). Biovolumen. Biologische Gewässeruntersuchung, Methoden der Biologischen Wasseruntersuchung, 2, Gustav Fischer Verlag, 334-368.

Pätzold, J., and cruise participants (2000). Report and preliminary results of Meteor cruise M44/3, Aqaba (Jordan)- Safaga (Egypt)- Dubá (Saudi Arabia)- Suez (Egypt)- Haifa (Israel), 12.03. - 07.04.99. Berichte aus dem Fachbereich Geowissenschaften der Universität Bremen 149, pp. 135.

Peters, R.H. (1984). Methods for the study of feeding, grazing and assimilation by zooplankton. In: Downing, J.A. and F.H. Rigler (eds.). A Manual on Methods for the Assessment of Secondary Production in Freshwaters. Blackwell, Oxford IBP Handbook, 17, 336-412.

POEM Group, The (1992). General circulation of the Eastern Mediterranean, Earth-Science Rev., 32, 285-239.

Pomeroy, L.R. (1974). The ocean's food web, a changing paradigm. Bioscience, 24, 499-504.

Por, F. D. (1978). Lessepsian migration. Ecological Studies 23, Springer, Heidelberg.

Porter, K.G. and Y.S. Feig (1980). The use of DAPI for identifying and counting aquatic microflora.- Limnol. Oceanogr., 25, 943-948.

Reiss, Z., and Hottinger, L. (1984). "The Gulf of Aqaba (Elat)." Springer-Verlag, Berlin, 330 p.

Reiss, Z., Luz, B., Almogi-Labin, A., Halicz, E., Winter, A., and Wolf, M. (1980). Late quaternary paleoceanography of the Gulf of Aqaba (Elat), Red Sea. Quaternary Research 14, 294-308.

Rickard, D. (1997). Kinetics of pyrite formation by the H_2S oxidation of iron (II) monosulfide in aqueous solutions between 25 and 125 °C: The rate equation. Geochimica et Cosmochimica Acta, 61, 115-134

Roether, W., B.B. Manca, B. Klein, D. Bregant, D. Georgopoulos, V. Beitzel, V. Kovacevic, and A. Luchetta (1996). Recent changes in the Eastern Mediterranean deep water. Science, 271, 333-335.

Roper, C.F.E. (1974). Vertical and seasonal distribution of pelagic cephalopods in the Mediterranean. Preliminary report. Bull. Am. Malacol. Union, May 1974, 27-30.

Roper, C.F.E. and Young, R.E. (1975). Vertical distribution of pelagic cephalopods. Smithson. Contrib. Zool., 209, 51 pp.

ROUBAUD, C., CHARPY, L., and SARAZIN., G. (1996). Diffusional nutrient fluxes at the sediment-water interface and organic matter mineralization in an atoll lagoon (Tihehau, Tuamotu archipelago, French Polynesia). Mar. Ecol. Progr. Ser., 132, 181-190.

SAROGLU, F. (1988). Age and Offset of the North Anatolian fault. In: Melih Tokay Symposium: Spec. Publ. of the Middle East Technical University, Ankara, p. 65-79.

SCHLÜTER, M. (1990). Zur Frühdiagenese von organischem Kohlenstoff und Opal in Sedimenten des südlichen und östlichen Wedellmeeres. Geochemische Analyse und Modellierung. Ber. Polarforsch., 73, 156 pp.

SCHMIEDL, G., C. HEMLEBEN, J. KELLER, and M. SEGL (1998). Impact of climatic changes on the benthic foraminiferal fauna in the Ionian Sea during the last 330,000 years. Paleoceanography, 13, 447-458.

SEIFERT, R., DELLING, N., RICHNOW, H. H., KEMPE, S., HEFTER, J., and MICHAELIS, W. (1999). Ethylene and methane in the upper water column of the subtropical Atlantic. Biogeochemistry 44, 73-91.

SENGÖR, A.M.C. (1979). The North Anatolian Transform Fault: its age, offset and tectonic significance. J. Geol. Soc. London, 136, 269-282.

SENGÖR, A.M.C., GÖRÜR, N. and SAROGLU, F. (1985). Strike slip faulting and related basin formation in zones of tectonic escape. In: Turkey as a case study. In: Strike-slip Deformation, Basin Formation and Sedimentation. Biddle, K.T. and Christie-Blick, N. Soc. Econ. Palent. Min. Spec. Publ., 37, 227-264.

SIMON, M. and M.M. TILZER (1987). Bacterial response to seasonal changes in primary production and phytoplankton biomass in Lake Constance. J. Plankton Res., 9, 535-553.

SIMON, M. and F. AZAM (1989). Protein content and protein synthesis rates of planktonic bacteria. Mar. Ecol. Prog. Ser., 51, 201-213.

SMITH, A.D., TAYMAZ, T., OKTAY, F., YUCE, H., ALPAR, B.,BASARAN, H., JACKSON, J.A., KARA, S.and SIMSEK, M. (1995). High resolution seismic profiling in the Sea of Marmara (nortwest Turkey). Late Quaternary sedimentation and sea level changes. Geol. Soc. Am. Bull., 107, 923-936.

SPIEß , V. (1993). Digitale Sedimentechographie - Neue Wege zu einer hochauflösenden Akustostratigraphie. Berichte, Fachbereich Geowissenschaften, Universität Bremen 35, 199 p.

STOFFERS, P., and cruise participants (1998). Cruise report SONNE 121, Red Sea. Hydrography, hydrothermalism, and palaeoceanography in the Red Sea. Nr. 88. Geologisch-Paläontologisches Institut der Universität Kiel, Kiel, Germany.

STRAUB, C. and KAHLE, H.-G. (1997). Recent crustal deformation and strain accumulation in the Marmara Sea region, NW Anatolia, inferrred from repeated GPS measurements, in Active tectonics of Northwest Anatolia. In: The Marmara Poly-project. Schindler, C. and Pfister, M. (eds.), Hochschulverlag AG an der ETH, Zürich, pp. 417-447.

STRICKLAND., J., and PARSONS, T. (1968). A particular hand book of sea water analysis. pp. 67-311.

SUZUKI, N. and K. KATO (1957). Studies on suspended material. Marine snow in the sea. 1. Sources of marine snow. Bull. Fac. Fish. Hokkaido Univ., 4, 132-135.

TAYMAZ, T., JACKSON, J.A. and MCKENZIE, D. (1991). Active Tectonics of the North and central Aegean Sea. Geophys. J. Int., 106, 433-490.

TURLEY, C., R.C. NEWELL and D.B. ROBINS (1986). Survival strategies of two small marine ciliates and their role in regulating bacterial community structure under experimental conditions. Mar. Ecol. Progr. Ser., 33, 57-70.

UNESCO (1983). Algorithm for the computation of the standard properties of seawater. Unesco TP in Marine Science 44.

UTERMÖHL, H. (1958). Zur Vervollkommnung der quantitativen Phytoplankton-Methodik.- Internat. Verein. Limnol., 9, 1-39.

VERITY, P.G. (1991). Feeding in planktonic protozoans: Evidence for non-random acquisition of prey. J. Protozool., 83, 69-76.

VOSS, N.A., S.J. STEPHEN and Zh. DONG (1992). Family Cranchiidae Prosch, 1849. In: SWEENEY, M.J., C.F.E. ROPER, K.M. MANGOLD, M.R. CLARKE, and S. VON BOLETZKY (eds.). "Larval" and juvenile cephalopods: a manual for their identification. Smithson. Contrib. Zool., 513, 187-210.

WEIKERT, H. (1990). A proposed vertical distribution pattern of micronekton in the deep Levantine Sea, Eastern Mediterranean, and its applicability to the Red Sea. Bull. Inst. OcÈanogr. Monaco, no spècial, 7, 39-50.

Weikert, H. (1994). Structure and ecology of mesozooplankton and micronekton. In: Hieke, W., P. Halbach, M. Türkay and H. Weikert (eds.). Mittelmeer 1993, Cruise No. 25, 12 May - 20 August 1993. Meteor-Berichte, Universität Hamburg, 94-3, 72-76.

Weikert, H. (1995). Strong variability of bathypelagic zooplankton at a site in the Levantine Sea - a signal of seasonality in a low-latitude deep-sea? Rapp. Comm. int. Mer Médit., 34, 218.

Weikert, H., B. Christiansen and L. Neugebohrn (1999). Zooplankton studies in the deep Eastern Mediterranean Sea. Temporal changes in deep-sea zooplankton. In: Hieke, W., CH. Hemleben, P. Linke, M. Türkay and H. Weikert (eds.). Mittelmeer 1997/98, Cruise No. 40, 28 October 1997 - 10 February 1998. Meteor-Berichte, Universität Hamburg, 99-2, 145-147.

Wiebe, P.H., A.W. Morton, A.M. Bradley, R.H. Backus, J.E. Craddock, V. Barber, T.J. Cowles and G.R. Flierl (1985). New developments in the MOCNESS, an apparatus for sampling zooplankton and micronekton. Mar. Biol., 60, 179-187.

Wong, H.K., Ludman, T., Ulug, A. and Gorur, N. (1995). The Sea of Marmara: a plate boundary sea in an escape tectonic regime. Tectonophysics, 244, 231-250.

Wörner, U., H. Zimmermann-Timm and H. Kausch (submitted). Succession of bacteria and protists on laboratory-made aggregates during winter and spring. Mirob. Ecol.

Yahel, G., Fabricius, K., Post, A.F., Marie, D., Vaulot, D. and Genin, A. (1998). Phytoplankton grazing near coral reefs. Limnol. Oceanogr., 43, 551-563.

Young, R.E. (15.03.1998). Enoploteuthididae Pfeffer, 1900. In: Young, R.E., M. Vecchione and K.M. Mangold (eds.). The tree of life – Cephalopoda. Internet: http://www.soest.hawaii.edu/ tree/cephalopoda/cephalopoda.html

Young, R.E., K.M. Mangold and M. Vecchione (1992). The enoploteuthid group of families. In: Sweeney, M.J., C.F.E. Roper, K.M. Mangold, M.R. Clarke, and S. von Boletzky (eds.). "Larval" and juvenile cephalopods: a manual for their identification. Smithson. Contrib. Zool., 513, 55-66.

Young, R.E., K.M. Mangold and M. Vecchione (15.03.1998). Pyroteuthididae Pfeffer, 1912. In: Young, R.E., M. Vecchione and K.M. Mangold (eds.). The tree of life – Cephalopoda. Internet: http://www.soest.hawaii.edu/tree/cephalopoda/cephalopoda.html

Zimmermann, R. (1977). Estimation of bacterial number and biomass by epifluorescence microscopy and scanning electron microscopy. In: Rheinheimer G. (ed.). Microbial ecology of a brackish water environment. Ecological Studies 25, Springer, Berlin, 103-120.

Zimmermann, H. (1996). Interactions between Planktonic Protozoans and Metazoans after the Spring Bloom of Phytoplankton in a Eutrophic Lake, the Belauer See, in the Bornhöveder Seenkette, North Germany. Acta Protozoologica, 35, 215-221.

Zimmermannn-Timm, H. (1999). In: von Tümpling, W. and G. Friedrich, (eds.). Zooplankton-Protozooplankton. Biologische Gewässeruntersuchung, Methoden der Biologischen Wasseruntersuchung, 2, Gustav Fischer Verlag, 76-97.

Zimmermannn-Timm, H. (1999). In: von Tümpling, W. and G. Friedrich, (eds.). Ästuare. Biologische Gewässeruntersuchung, Methoden der Biologischen Wasseruntersuchung, 2, Gustav Fischer Verlag, 482-534.

Zimmermannn-Timm, H. and S. Barkmann (submitted). Feeding behaviour of two planktonic freshwater ciliates coexisting during spring time in the eutrophic Belauer See (Bornhöveder Seenkette, North Germany).- Limnologica

Publications from METEOR expeditions
in other reports

Gerlach, S.A., J. Thiede, G. Graf und F. Werner (1986): Forschungsschiff Meteor, Reise 2 vom 19. Juni bis 16. Juli 1986. Forschungsschiff Poseidon, Reise 128 vom 7. Mai bis 8. Juni 1986. Ber. Sonderforschungsbereich 313, Univ. Kiel, 4, 140 S.

Siedler, G., H. Schmickler, T.J. Müller, H.-W. Schenke und W. Zenk (1987): Forschungsschiff Meteor, Reise Nr. 4, Kapverden - Expedition, Oktober - Dezember 1986. Ber. Inst. f. Meeresk., 173, Kiel, 123 S.

Wefer, G., G.F. Lutze, T.J. Müller, O. Pfannkuche, W. Schenke, G. Siedler und W. Zenk (1988): Kurzbericht über die Meteor - Expedition Nr. 6, Hamburg - Hamburg, 28. Oktober 1987 - 19. Mai 1988. Berichte, Fachbereich Geowissenschaften, Universität Bremen, 4, 29 S.

Müller T.J., G. Siedler und W. Zenk (1988): Forschungsschiff Meteor, Reise Nr. 6, Atlantik 87/88, Fahrtabschnitte Nr. 1 - 3, Oktober - Dezember 1987. Ber. Inst. f. Meeresk., 184, Kiel, 77 S.

Lutze, G.F., C.O.C. Agwu, A. Altenbach, U. Henken-Mellies, C. Kothe, N. Mühlhan, U. Pflaumann, C. Samtleben, M. Sarnthein, M. Segl, Th. Soltwedel, U. Stute, R. Tiedemann und P. Weinholz (1988): Bericht über die ”Meteor” -Fahrt 6-5, Dakar - Libreville, 15.1.-16.2.1988.Berichte - Reports, Geol. Paläont. Inst., Univ. Kiel, 22, 60 S.

Wefer, G., U. Bleil, P.J. Müller, H.D. Schulz, W.H.Berger, U. Brathauer, L. Brück, A. Dahmke, K. Dehning, M.L. Durate-Morais, F. Fürsich, S. Hinrichs, K. Klockgeter, A. Kölling, C. Kothe, J.F. Makaya, H. Oberhänsli, W. Oschmann, J. Posny, F. Rostek, H. Schmidt, R. Schneider, M. Segl, M. Sobiesiak, T. Soltwedel und V. Spieß (1988): Bericht über die Meteor - Fahrt M 6-6, Libreville - Las Palmas, 18.2.1988 - 23.2.1988. Berichte, Fachbereich Geowissenschaften, Universität Bremen, 3, 97 S.

Hirschleber, H., F. Theilen, W. Balzer, B. v. Bodungen und J. Thiede (1988): Forschungsschiff Meteor, Reise 7, vom 1. Juni bis 28. September 1988, Ber. Sonderforschungsbereich 313, Univ. Kiel, 10, 358 S.

METEOR-Berichte
List of publications

89-1	(1989) Meincke, J., Quadfasel, D.	GRÖNLANDSEE 1988-Expedition, Reise Nr. 8, 27. Oktober 1988 - 18. Dezember 1988. Universität Hamburg, 40 S.
89-2	(1989) Zenk, W., Müller, T.J., Wefer, G.	BARLAVENTO-Expedition, Reise Nr. 9, 29. Dezember 1988 - 17. März 1989. Universität Hamburg, 238 S.
90-1	(1990) Zeitschel, B., Lenz, J., Thiel, H., Boje, R., Stuhr, A., Passow, U.	PLANKTON´89 - BENTHOS´89, Reise Nr. 10, 19. März - 31. August 1989. Universität Hamburg, 216 S.
90-2	(1990) Roether, W., Sarnthein, M., Müller, T.J., Nellen, W., Sahrhage, D.	SÜDATLANTIK-ZIRKUMPOLARSTROM, Reise Nr. 11, 3. Oktober 1989 - 11. März 1990. Universität Hamburg, 169 S.
91-1	(1991) Wefer, G., Weigel, W., Pfannkuche	OSTATLANTIK 90 - EXPEDITION, Reise Nr. 12, 13. März - 30. Juni 1990. Universität Hamburg, 166 S.
91-2	(1991) Gerlach, S.A., Graf, G.	EUROPÄISCHES NORDMEER, Reise Nr. 13, 6. Juli - 24. August 1990. Universität Hamburg, 217 S.
91-3	(1991) Hinz, K., Hasse, L., Schott, F.	SUBTROPISCHER & TROPISCHER ATLANTIK, Reise Nr. 14/1-3, Maritime Meteorologie und Physikalische Ozeanographie, 17. September - 30. Dezember 1990. Universität Hamburg, 58 S.
91-4	(1991) Hinz, K.	SUBTROPISCHER & TROPISCHER ATLANTIK, Reise Nr. 14/3, Geophysik, 31. Oktober - 30. Dezember 1990. Universität Hamburg, 94 S.
92-1	(1992) Siedler, G., Zenk, W.	WOCE Südatlantik 1991, Reise Nr. 15, 30. Dezember 1990 - 23. März 1991. Universität Hamburg, 126 S.
92-2	(1992) Wefer, G., Schulz, H.D., Schott, F., Hirschleber, H. B.	ATLANTIK 91 - EXPEDITION, Reise Nr. 16, 27. März - 8. Juli 1991. Universität Hamburg, 288 S.

92-3	(1992)	Suess, E., Altenbach, A.V.	EUROPÄISCHES NORDMEER, Reise Nr. 17, 15. Juli - 29. August 1991. Universität Hamburg, 164 S.
93-1	(1993)	Meincke, J., Becker, G.	WOCE-NORD, Cruise No. 18, 2. September - 26. September 1991. NORDSEE, Cruise No. 19, 30 September - 12 October 1991. Universität Hamburg, 105 pp.
93-2	(1993)	Wefer, G., Schulz, H.D.	OSTATLANTIK 91/92 - EXPEDITION, Reise Nr. 20, M 20/1 und M 20/2, 18. November 1991 - 3. Februar 1992. Universität Hamburg, 248 S.
93-3	(1993)	Wefer, G., Hinz, K., Roeser, H.A.	OSTATLANTIK 91/92 - EXPEDITION, Reise Nr. 20, M 20/3, 4. Februar - 13. März 1992. Universität Hamburg, 145 S.
93-4	(1993)	Pfannkuche, O., Duinker, J.C., Graf, G., Henrich, R., Thiel, H., Zeitschel, B.	NORDATLANTIK 92, Reise Nr. 21, 16. März - 31. August 1992. Universität Hamburg, 281 S.
93-5	(1993)	Siedler, G., Balzer, W., Müller, T.J., Rhein, M., Onken, R., Zenk, W.	WOCE South Atlantic 1992, Cruise No. 22, 22 September 1992 - 31 January 1993. Universität Hamburg, 131 pp.
94-1	(1994)	Bleil, U., Spieß, V., Wefer, G.	Geo Bremen SOUTH ATLANTIC 1993, Cruise No. 23, 4 February - 12 April 1993. Universität Hamburg, 261 pp.
94-2	(1994)	Schmincke, H.-U., Rihm, O.	OZEANVULKAN 1993, Cruise No. 24, 15 April - 9 May 1993. Universität Hamburg, 88 pp.
94-3	(1994)	Hieke, W., Halbach, P., Türkay, M., Weikert, H.	MITTELMEER 1993, Cruise No. 25, 12 May - 20 August 1993. Universität Hamburg, 243 pp.
94-4	(1994)	Suess, E., Kremling, K., Mienert, J.	NORDATLANTIK 1993, Cruise No. 26, 24 August - 26 November 1993. Universität Hamburg, 256 pp.

94-5	(1994)	Bröckel, K. von, Thiel, H., Krause, G.	ÜBERFÜHRUNGSFAHRT, Reise Nr. 0, 15. März - 15. Mai 1986. ERPROBUNGSFAHRT, Reise Nr. 1, 16. Mai - 14. Juni 1986. BIOTRANS IV, Skagerrak 86, Reise Nr. 3, 21. Juli - 28. August 1986. Universität Hamburg, 126 S.
94-6	(1994)	Pfannkuche, O., Balzer, W., Schott, F.	CARBON CYCLE AND TRANSPORT OF WATER MASSES IN THE NORTH ATLANTIC - THE WINTER SITUATION, Cruise No. 27, 29 December - 26 March 1994. Universität Hamburg, 134 pp.
95-1	(1995)	Zenk, W., Müller, T.J.	WOCE Studies in the South Atlantic, Cruise No. 28, 29 March - 14 June 1994. Universität Hamburg, 193 pp.
95-2	(1995)	Schulz, H., Bleil, U., Henrich, R., Segl, M.	Geo Bremen SOUTH ATLANTIC 1994, Cruise No. 29, 17 June - 5 September 1994. Universität Hamburg, 323 pp.
96-1	(1996)	Nellen, W., Bettac, W., Roether, W., Schnack, D., Thiel, H., Weikert, H., Zeitschel, B.	MINDIK (Band I), Reise Nr. 5, 2. Januar - 24. September 1987. Universität Hamburg, 275 S.
96-2	(1996)	Nellen, W., Bettac, W., Roether, W., Schnack, D., Thiel, H., Weikert, H., Zeitschel, B.	MINDIK (Band II), Reise Nr. 5, 2. Januar - 24. September 1987. Universität Hamburg, 179 S.
96-3	(1996)	Koltermann, K.P., Pfannkuche, O., Meincke, J.	JGOFS, OMEX and WOCE in the North Atlantic 1994, Cruise No. 30, 7 September - 22 December 1994. Universität Hamburg, 148 pp.
96-4	(1996)	Hemleben, Ch., Roether, W., Stoffers, P.	Östliches Mittelmeer, Rotes Meer, Arabisches Meer, Cruise No. 31, 30 December 1994 - 22 March 1995. Universität Hamburg, 282 pp.
96-5	(1996)	Lochte, K., Halbach, P., Flemming, B.W.	Biogeochemical Fluxes in the Deep-Sea and Investigations of Geological Structures in the Indian Ocean, Cruise No. 33, 22 September - 30 December 1995. Universität Hamburg, 160 pp.

96-6	(1996)	Schott, F., Pollehne, F., Quadfasel, D., Stramma, L., Wiesner, M., Zeitzschel, B.	ARABIAN SEA 1995, Cruise No. 32, 23 March - 19 September 1995. Universität Hamburg, 163 pp
97-1	(1997)	Wefer, G. Bleil, U. Schulz, H. Fischer, G.	Geo Bremen SOUTH ATLANTIC 1996 (Volume I), Cruise No. 34, 3 January - 18 February 1996. Universität Hamburg, 254 pp.
97-2	(1997)	Wefer, G. Bleil, U. Schulz, H. Fischer, G.	Geo Bremen SOUTH ATLANTIC 1996 (Volume II), Cruise No. 34, 21 February - 15 April 1996. Universität Hamburg, 268 pp.
97-3	(1997)	Wefer, G.	10 Jahre Forschungsschiff METEOR (1986 - 1996) - Dokumentation der Fahrten M0 - M34 (Volume I), Cruise No. 0-17. Universität Hamburg, 269 pp.
97-4	(1997)	Wefer, G.	10 Jahre Forschungsschiff METEOR (1986 - 1996) - Dokumentation der Fahrten M0 - M34 (Volume II), Cruise No. 18-34. Universität Hamburg, 236 pp.
98-1	(1998)	Wefer, G. Müller, T.J.	Canary Islands 1996/97, Cruise No. 37, 4 December 1996 - 22 January 1997. Universität Hamburg, 134 pp.
98-2	(1998)	Mienert, J. Graf, G. Hemleben, C. Kremling, K. Pfannkuche, O. Schulz-Bull, D.	Nordatlantik 1996, Cruise No. 36, 6 June 1996 - 4 November 1996. Universität Hamburg, 302 pp.
98-3	(1998)	Hemleben, C. Zahn, R. Meischner, D.	Karibik 1996, Cruise No. 35, 18 April - 3 June 1996. Universität Hamburg, 208 pp.
98-4	(1998)	Bleil, U. Fischer, G.	Geo Bremen South Atlantic 1997, Cruise No. 38, 25 January - 14 April 1997. Universität Hamburg, 244 pp.
99-1	(1999)	Schott, F. Koltermann, K.-P. Stramma, L. Sy, A. Zahn, R. Zenk, W.	North Atlantic 1997, Cruise No. 39, 18 April - 14 September 1997. Universität Hamburg, 197 pp.

99-2	(1999)	Hieke,W. Hemleben, Ch. Linke, P. Türkay, M. Weikert, H.	Mittelmeer 1997/98, Cruise No. 40, 28 October 1997-10 February 1998. Universität Hamburg, 286 pp.
99-3	(1999)	Schulz, H.D. Devey, C.W. Pätzold, J. Fischer, G.	Geo Bremen / GPI Kiel South Atlantic 1998, Cruise No. 41, 13 February - 13 June 1998. Universität Hamburg, 341 pp.
00-1	(2000)	Pfannkuche, O. Müller, T.J. Nellen, W. Wefer, G.	Ostatlantik 1998, Cruise No. 42, 16 June - 26 October 1998. Universität Hamburg, 259 pp.
00-2	(2000)	Schmincke, H.-U. Graf, G., Krastel, S.	DECOS / OMEX II, Cruise No. 43, 25 November 1998-14 January 1999, Universität Hamburg, 103 pp.
00-3	(2000)	Pätzold, J. Halbach, P.E. Hempel, G. Weikert, H.	Östliches Mittelmeer - Nördliches Rotes Meer 1999, Cruise No. 44, 22 January - 16 May 1999, Universität Hamburg, 240 pp.